

**-The Functional Renormalization Group-
&
applications to gauge theories and gravity**

J. M. Pawłowski, J. A. Bonnet, S. Rechenberger, M. Reichert, N. Wink

Contents

I. Functional Renormalisation Group	9
1. Euclidean Quantum Field Theory	11
1.1. Correlation functions and generating functionals	11
1.2. Effective action	13
1.3. Dyson-Schwinger equations	16
2. Functional Renormalisation Group	25
2.1. Flow equations for generating functionals	25
2.2. Properties of the Wetterich equation	32
2.2.1. Diagrammatics, DSEs, and the 1PI property	32
2.2.2. Full effective action and RG-consistency	34
2.2.3. UV & IR finiteness and momentum locality of RG-steps	36
2.3. Systematic expansion schemes	38
2.3.1. Perturbative expansion	39
2.3.2. Complete resummations [*]	48
2.3.3. Vertex expansion	50
2.3.4. Derivative expansion	58
2.4. Flows for Fermi-Bose mixtures	72
2.4.1. Yukawa theory	72
2.4.2. Flow equation for Fermi-Bose mixtures	74
2.4.3. Condensed notation [*]	76
2.4.4. Flow for Fermi-Bose mixtures in LPA	77
3. Critical Phenomena	83
3.1. Phase transitions	83
3.1.1. Spontaneous symmetry breaking and the Goldstone theorem	83
3.1.2. Spontaneous symmetry breaking, quantum fluctuations and masses	85
3.1.3. Little reminder on the Higgs mechanism [*]	87
3.1.4. Low energy effective theory for QCD & chiral symmetry breaking	88
3.1.5. LPA Flow for the effective potential in the quark meson model	91
3.2. Phase structure	95
3.2.1. Density and chemical potential	95
3.2.2. Finite temperature QFT	98
3.2.3. Flows at finite temperature and density	104
3.2.4. Phase structure of the two flavour Quark Meson Model	107
3.3. Fixed points	114
II. Quantum Chromodynamics from an FRG perspective	119
4. Introduction	121

5. Non-Abelian gauge theories	122
5.1. Basics of Yang-Mills theories	122
5.1.1. Classical action of Yang-Mills theory	123
5.2. Quantization and gauge fixing	124
5.3. QCD	127
5.4. Flow equations for QCD	129
5.4.1. Flow equation for the effective action	129
5.4.2. Flow equation for correlation functions	131
5.5. Functional Renormalisation for QCD in the Landau gauge	134
5.5.1. Closed functional relations for purely transversal correlation functions	135
5.5.2. Non-renormalisation theorem for the ghost-gluon vertex	136
5.6. Yang-Mills correlation functions in the Landau gauge	138
5.6.1. Yang-Mills propagators in the Landau gauge	138
5.6.2. Solution and interpretation	140
5.7. Quantum gauge symmetry & modified Slavnov-Taylor identities	144
5.7.1. Gauge transformations and Slavnov-Taylor identities	144
5.7.2. BRST symmetry	146
5.7.3. Slavnov-Taylor Identities for the Effective Action	149
5.7.4. Modified Slavnov-Taylor identities	150
5.7.5. modified STI at work	151
6. Chiral symmetry breaking in QCD	153
6.1. Apparent convergence	153
6.1.1. Success & failure	153
6.1.2. Resonant interactions and large densities in QCD	153
6.1.3. Off-shell fluctuations and on-shell expansions	154
6.2. Dynamical hadronisation	154
6.2.1. Flows with composite operators	154
6.2.2. BRST Master equation with composite fields	158
6.2.3. Dynamical hadronisation at work	159
7. QCD at finite temperature	160
7.1. Confinement	160
7.1.1. Order parameters for confinement	161
7.2. Confinement-deconfinement phase transition at finite temperature	163
7.2.1. Polyakov loop and Polyakov loop potential	163
7.2.2. Background field formalism	168
7.2.3. Polyakov loop potential in functional approaches	169
8. A glimpse at the phase structure of QCD	178
III. Quantum Gravity from an FRG perspective	181
9. Introduction	183
9.1. Classical general relativity	183
9.2. Failure of Perturbative Quantisation	186
10. RG approach to quantum gravity	193
10.1. Flow equations for quantum gravity	193

10.2.	Background independence in quantum gravity	195
10.2.1.	Approaches to fluctuation and background correlation functions	195
10.3.	General framework	195
10.3.1.	FRG and Nielsen identities for gravity	196
10.3.2.	Background independence in non-perturbative expansion schemes	198
10.4.	Einstein-Hilbert Truncation	199
10.5.	Correlation functions of the fluctuation field	203
10.5.1.	Covariant expansion	203
10.6.	Flows of correlation functions	204
10.6.1.	Covariant tensors and uniformity	204
10.6.2.	Projection onto n -point functions	206
10.6.3.	Momentum dependence of the graviton n -point functions	207
10.6.4.	Higher-order vertices and the background effective action	209
10.6.5.	Flow equations for the couplings	210
10.6.6.	Disentangling R and R^2 tensor structures	210
10.6.7.	Computational details	211
10.7.	Asymptotic safety	211
10.7.1.	UV fixed point	212
10.7.2.	Stability	213
10.7.3.	Importance of the R^2 tensor structure	214
10.8.	IR behaviour	215
10.9.	Towards apparent convergence	217
11. Gravity and matter		219
11.1.	Gravity-matter systems	219
11.2.	Yang-Mills–gravity system with the FRG	223
11.3.	Graviton contributions to Yang-Mills	227
11.3.1.	Background observables	228
11.3.2.	Gravity supports asymptotic freedom	229
11.4.	Yang-Mills contributions to gravity	231
11.4.1.	General structure	232
11.4.2.	Contributions to the graviton propagator	233
11.4.3.	Contributions to the three-point function	234
11.4.4.	Mixed graviton-gluon coupling	234
11.4.5.	Momentum locality	235
11.5.	Asymptotic safety of Yang-Mills–gravity	235
11.5.1.	Finite N_c	236
11.5.2.	Large N_c scaling	236
11.5.3.	Decoupling of gravity-induced gluon self-interactions	237
11.6.	UV dominance of gravity	239
11.6.1.	Dynamical scale fixing	239
11.6.2.	Results in the extended approximation	242
11.6.3.	Resumé: Signatures of asymptotic safety of Yang-Mills–gravity systems	243
11.7.	Effective universality	244
11.7.1.	Beta functions	245
11.7.2.	Sources of deviations from effective universality	247
11.7.3.	Modified Slavnov-Taylor identities	248
11.7.4.	Implications	249

11.8. Asymptotically safe Standard Model	249
11.8.1. Ultraviolet fixed point	251
11.8.2. RG flow at transplanckian scales	252
11.8.3. RG flow between the Planck and the electroweak scale	253
11.8.4. Exploring the gravitational parameter space	254
11.8.5. Three observations	255
12. Asymptotically safe black holes and cosmology	258
12.1. Quantum Improved Schwarzschild-(A)dS and Kerr-(A)dS Space-times	261
12.2. Asymptotic Safe Quantum Gravity	262
12.3. Investigated Geometries	264
12.3.1. Schwarzschild-(A)dS	264
12.3.2. Kerr-(A)dS	264
12.4. Scale Identification	265
12.5. Lapse Function and Number of Horizons	266
12.5.1. Schwarzschild-AdS	266
12.5.2. Kerr-AdS	268
12.5.3. Asymptotically de Sitter spaces	268
12.6. Global Structure, Penrose Diagrams and Particle Trajectories	273
12.6.1. Asymptotically anti-de Sitter space-times	273
12.6.2. Asymptotically de Sitter space-times	273
12.6.3. Particle Trajectories	273
12.7. Curvature Singularity & Effective Energy-momentum Tensor	280
12.8. Horizon Temperatures and Black Hole Evaporation	281
12.9. Summary	284
IV. Appendix	287
A. Fourier Conventions	289
B. Saddle point expansion of the effective action	290
C. Calculation of Matsubara sums	291
D. Grassmann variables: Reminder	293
E. Low energy effective theories of QCD	294
F. Quantisation & gauge fixing	300
F.1. Feynman rules for QCD in the covariant gauge	300
F.2. Faddeev-Popov quantisation & Gribov copies within a toy model	301
F.2.1. Faddeev-Popov quantisation	301
F.2.2. Gribov Ambiguity within a toy model	302
F.3. Flow equations for Yang-Mills propagators	302
F.4. Regulators	306
F.4.1. BRST transformation of the cutoff term	308
F.5. Wegner-Wilson loop	308
F.6. Wegner-Wilson loop in QED	310
F.7. Details on the background field approach	311
F.8. Perturbative Polyakov loop potential	312

G. Quantum Gravity appendices	316
G.1. Heat-Kernel techniques	316
G.2. Graviton propagator	317
G.2.1. York decomposition & curved background	318
G.2.2. Stelle decomposition & flat background	320
G.3. Details of the fluctuation computation in pure gravity	321
G.4. Approximations of the stability matrix	321
G.5. Background couplings	321
G.6. Identification scheme	324
G.7. Local momentum projection	324
G.8. Derivation of flow equations	325
G.9. Analytic flow equations	328
G.10. From asymptotic freedom to asymptotic safety	330
G.10.1. Yang-Mills coupled to gravity: the setup	330
G.10.2. Asymptotic freedom in Yang-Mills with gravity	331
G.10.3. Asymptotic safety in gravity with Yang-Mills	334
G.11. Computational Details for Yang-Mills gravity	335
G.11.1. Regulators	335
G.11.2. Regulator dependence of the gluon contribution to the graviton mass parameter .	336
G.11.3. Inhomogeneous Fredholm integral equations of the second kind	336
G.11.4. Sign of the gluon anomalous dimension	339
G.11.5. Derivative at vanishing momentum	340
G.11.6. Derivative at non-vanishing momentum	340
G.11.7. Finite differences	341
G.11.8. Scaling equations	341
G.11.9. Flow equations	343
G.11.10. Coefficients in the scaling equations	344
G.12. Quantum Improved Schwarzschild-(A)dS and Kerr-(A)dS Space-times	345
G.12.1. Choice of Scale Identification	346
G.12.2. Killing Horizons	346
G.12.3. Other Matchings	348
G.12.4. Shape and Divergences of Proper Distances	350
G.12.5. UV-limits of $D(r)$	352
G.12.6. Eigentime of an Inflating Observer in a Schwarzschild-(A)dS Geometry	354
G.12.7. Eigentime of an Inflating Observer in a Kerr-(A)dS Geometry	355

Part I.

Functional Renormalisation Group

1. Euclidean Quantum Field Theory

In this chapter we lay the foundations of functional approaches to quantum field theories (QFT). The results and derivations presented here are typically covered in (advanced) QFT books or lecture notes, where it is based on the path or functional integral point of view. While most of the material is standard, some aspects go beyond that covered in QFT books or are presented slightly differently, for being suited or adapted to the functional renormalisation group approach we aim at.

A general quantum field theory (QFT) is fully determined by its complete set of correlation functions. A prototypical but simple example is a QFT with one real scalar field $\varphi(x)$ in d dimensions. This theory is used frequently throughout this chapter for illustrative purposes. While we are finally interested in strongly correlated relativistic gauge theories, most of the numerical computations are done after a Wick rotation in d -dimensional Euclidean spacetime with the $O(d)$ -symmetric dispersion $p^2 = p_0^2 + \vec{p}^2$. In a Euclidean setup QFTs are given by quantum statistical theories. While the derivations in this chapter hold for general quantum field theories our explicit examples are worked out in a ϕ^4 -theory with the classical action

$$S[\varphi] = \int_x \left[\frac{1}{2} \partial_\mu \varphi(x) \partial_\mu \varphi(x) + \frac{m^2}{2} \varphi(x)^2 + \frac{\lambda}{4!} \varphi(x)^4 \right] \quad \text{where} \quad \int_x = \int d^d x. \quad (1.1)$$

1.1. Correlation functions and generating functionals

The low order correlation or Green functions in a statistical approach in Euclidean spacetime are summarised in [Table 1.1](#). These correlation functions of the fundamental quantum field φ are the moments of the central quantity in quantum statistical field theory, the generating functional $\mathcal{Z}[J]$. The latter is the analogue of the partition function in classical statistics and contains all information of the physical system under consideration. We obtain the correlation function in terms of the generating functional via functional derivatives as

$$\langle \varphi(x_1) \dots \varphi(x_n) \rangle_J = \frac{1}{\mathcal{Z}[J]} \frac{\delta^n \mathcal{Z}[J]}{\delta J(x_1) \dots \delta J(x_n)}, \quad (1.2)$$

n	n -point correlation function			interpretation
0	$\langle 1 \rangle$	=	1	normalisation
1	$\langle \varphi(x) \rangle$	=	$\phi(x)$	mean field
2	$\langle \varphi(x_1) \varphi(x_2) \rangle$	=	$\langle \varphi(x_1) \varphi(x_2) \rangle_c + \phi(x_1) \phi(x_2)$	propagator
3	$\langle \varphi(x_1) \varphi(x_2) \varphi(x_3) \rangle$	=	$\langle \varphi(x_1) \varphi(x_2) \varphi(x_3) \rangle_c + \dots$	three-point vertex
\vdots	\vdots		\vdots	\vdots

Table 1.1.: The finite n -point correlation functions $\langle \varphi(x_1) \dots \varphi(x_n) \rangle$ ($n \in \mathbb{N}_0$) of a real scalar field theory with one scalar field $\varphi(x)$. The $\langle \varphi(x_1) \dots \varphi(x_n) \rangle_c$ denote connected correlation functions.

The subscript J at the correlation function marks its dependence on the source $J(x)$ that determines the background. The generating functional $\mathcal{Z}[J]$ is defined by its derivatives in (1.2). Hence, strictly speaking the following considerations and derivations do not need an explicit representation for $\mathcal{Z}[J]$ but only the existence of its derivatives. However, it is convenient for some of the arguments to link them to an explicit path integral representation of $\mathcal{Z}[J]$. It is given by

$$\mathcal{Z}[J] = \frac{1}{N} \int [d\varphi]_{\text{ren}} \exp \left\{ -S[\varphi] + \int_x J(x) \varphi(x) \right\}, \quad (1.3)$$

with an exponential statistical damping factor $\exp(-S[\varphi])$ with classical action $S[\varphi]$, e.g. that of the ϕ^4 -theory defined in (1.1), and a flat functional measure $\int [d\varphi]_{\text{ren}}$. *Flat* means that the measure is translation invariant under space-time dependent shifts $d(x)$ of the field $\phi(x) \rightarrow \phi(x) + d(x)$. This important symmetry is used later for the derivation of the quantum equations of motion, the Dyson-Schwinger equations (DSE) in Section 1.3. The subscript ren at the measure denotes the fact that in general such a path integral has to be regularized and renormalised. Note that the normalisation $1/N$ in front of the path integral is irrelevant for the normalised correlation functions as is clear from their definition (1.2). In summary the correlation functions (1.2) are simply the normalised moments of the statistical integral (1.3).

The normalised correlation functions in Table 1.1, e.g. the two-point function with $n = 2$, are decomposed in the connected part, $\langle \varphi(x_1) \varphi(x_2) \rangle_c$ for $n = 2$, and a disconnected part $\phi(x_1) \phi(x_2) = \langle \varphi(x_1) \rangle \langle \varphi(x_2) \rangle$. Here "connected" and "disconnected" refer to the connectivity of the Feynman diagram representation of the correlation functions: All external lines of connected diagrams are connected through a path in the diagram. In turn, at least two external lines in a disconnected diagram are not connected. For example, the disconnected part of the two-point correlation function, see Table 1.1, consists of the product of the mean fields at the positions x_1 and x_2 . Accordingly, the information of its disconnected part is already stored in the one-point correlation function. The same holds true for a general n -point correlation function whose disconnected part can be constructed from the connected parts of the lower m -point correlation functions with $m < n$. In this general case the disconnected parts describe that parts of scattering processes where only a subset of the fields or particles involves scatter which each other.

Consequently, while the disconnected processes are relevant for observables such as cross sections, in terms of a generating functional they carry redundant information already encoded in the lower order correlation functions. The disconnected parts are removed if considering the logarithm of $\mathcal{Z}[J]$, the *Schwinger functional*,

$$\mathcal{W}[J] = \ln \mathcal{Z}[J]. \quad (1.4)$$

It is the generating functional for the connected correlation functions. This is evident for the two-point function discussed above,

$$G(x_1, x_2) = \frac{\delta^2 \mathcal{W}[J]}{\delta J(x_1) \delta J(x_2)} = \langle \varphi(x_1) \varphi(x_2) \rangle - \langle \varphi(x_1) \rangle \langle \varphi(x_2) \rangle = \langle \varphi(x_1) \varphi(x_2) \rangle_c. \quad (1.5)$$

Equation (1.5) defines the quantum propagator $G(x_1, x_2)$ which encodes the quantum dispersion of the QFT at hand. It is the key object in functional approaches and depends on the chosen background via J . For the sake of completeness we remark that the propagator in a Euclidean QFT is necessarily positive semi-definite, its spectrum is positive including zero for all backgrounds. This signals the Schwinger functional as a convex functional, which can be proven with Hölder's inequality, see e.g. [1].

The higher order correlation functions derived from $\mathcal{W}[J]$ are also connected correlation functions,

$$\langle \varphi(x_1) \cdots \varphi(x_n) \rangle_c = W^{(n)}(x_1, \dots, x_n), \quad \text{with} \quad \mathcal{W}^{(n)}(x_1, \dots, x_n) := \frac{\delta^n \mathcal{W}[J]}{\delta J(x_1) \cdots \delta J(x_n)}. \quad (1.6)$$

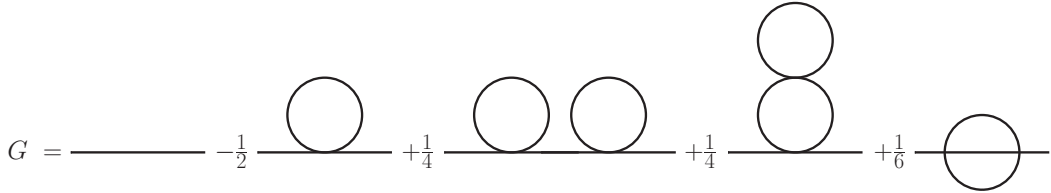


Figure 1.1.: The propagator $G(x_1, x_2)$, see (1.5), schematically up to two-loop.

This property follows within a very simple proof by induction directly from the functional renormalisation group equation (FRG), or the Dyson-Schwinger equation (DSE), for $\mathcal{W}[J]$. Hence we postpone the related discussion.

From the definition (1.4) it also follows that the normalisation $1/\mathcal{N}$ in (1.3) is an additive constant to $\mathcal{W}[J]$, which drops out from all correlation functions except the zero-point function. The latter is related to the free energy in the system or better its additive normalisation. While this is not measurable, differences of free energies are. This is relevant when changing external parameters of a QFT such as volume, temperature or chemical potential/density, where it is linked to thermodynamical quantities such as the volume or thermal pressure or the density and density fluctuations. It also is relevant in quantum gravity where such a term is linked to the cosmological constant. However, for now we are interested in correlation functions with $n > 0$ and drop this term.

1.2. Effective action

The Schwinger functional (1.4) still contains redundant information, as connected correlation functions can be separated into one-particle irreducible (1PI) and one-particle reducible ones. 1PI diagrams are those, which can not be separated into two disconnected ones by cutting one internal line. Within our basic example, the (connected) two-point function or propagator, this is easily seen from its two loop diagrams, see Figure 1.1. Evidently the first two loop diagram in Figure 1.1 is the square of the one-loop contribution, the tadpole. Trivially, this construction principle holds true for all connected not-1PI diagrams. Accordingly, the 1PI correlation functions already contain all information about the QFT under consideration. The respective generating functional of 1PI correlation functions, the *effective action* $\Gamma[\phi]$, is the Legendre transform of the Schwinger functional,

$$\Gamma[\phi] = \sup_J \left\{ \int_x J(x) \phi(x) - \mathcal{W}[J] \right\} = \int_x J_{\text{sub}}(x) \phi(x) - \mathcal{W}[J_{\text{sub}}], \quad (1.7)$$

where J_{sub} has to be understood as a field-dependent current, $J_{\text{sub}}[\phi]$. Typically, in the literature one finds the form on the right hand side of (1.7) without any reference to either the supremum nor the field-dependence of the current. The supremum or maximum is then implicitly understood. The 1PI property of the effective action is very simple to prove from its functional renormalisation group equation FRG, or its Dyson-Schwinger equation, and we defer the proof to this point. From its definition (1.7) as a Legendre transform it also follows that Γ is convex, as is the Schwinger functional. The physics interpretation of the effective action is that of the quantum analogue of the classical action. The field ϕ in the effective action is indeed the mean field in a given background current J . This is seen by taking the

derivative with respect to J of (1.7) and restricting ourselves to differentiable situations with a maximum at J_{sup} . We find

$$\phi(x) = \frac{\delta W[J]}{\delta J(x)} \Big|_{J_{\text{sup}}} = \frac{1}{Z[J]} \frac{\delta Z[J]}{\delta J(x)} \Big|_{J_{\text{sup}}} \quad \rightarrow \quad \phi(x) = \langle \varphi(x) \rangle, \quad (1.8)$$

where we have dropped the superscript J of the expectation value. In (1.8) we have inserted (1.4) and used the definition of the mean field as the one-point correlation function in eq. (1.2). Analogously, the one-point function $\delta\Gamma/\delta\phi$ can be obtained by taking the functional derivative of eq. (1.7) with respect to ϕ . We find

$$\frac{\delta\Gamma[\phi]}{\delta\phi(x)} = J(x), \quad (1.9)$$

where again the subscript sub is implicitly understood, $J = J_{\text{sup}}[\phi]$. For the derivation of (1.9) we have used that the terms originating in the field dependence of the current $J_{\text{sup}} = J_{\text{sup}}[\phi]$ cancel out,

$$\int_y \frac{\delta J_{\text{sup}}(y)}{\delta\phi(x)} \left(\phi(y) - \frac{\delta W[J]}{\delta J(y)} \Big|_{J_{\text{sup}}} \right) = 0. \quad (1.10)$$

In (1.10) we have used (1.8), and the cancellation is due to the fact that we work at a maximum of the functional in terms of J . While it is instructive to go through this explicitly once we shall drop these terms directly from now on.

Equation (1.9) are the quantum equations of motion (EoM) in a given background specified by J_{sup} . For vanishing J_{sup} , they reduce to the quantum analogue of the classical equations of motion in the vacuum and the effective action Γ reduces to the vacuum free energy $\Gamma[\phi_{\text{EoM}}] = -W[J=0]$. In the following we will suppress the supremum index for convenience and the evaluation at the supremum is understood implicitly unless stated otherwise.

In functional approaches to quantum field theories, the two-point function or propagator G defined in (1.5) is the central quantity. For example, the functional renormalisation group equation for the effective action will take a simple form in terms of $G[\phi]$, see (2.27). Indeed, in terms of the effective action the propagator is simply the inverse of $\Gamma^{(2)}[\phi]$, the second derivative of Γ w.r.t. to the mean field. General vertices or moments of the effective action $\Gamma[\phi]$ will be noted by

$$\Gamma^{(n)}(x_1, \dots, x_n) = \frac{\delta^n \Gamma}{\delta\phi(x_1) \dots \delta\phi(x_n)}. \quad (1.11)$$

For a general conversion of connected correlation functions to 1PI correlation functions we simply have to convert J -derivatives to ϕ -derivatives. This is encoded in

$$\frac{\delta}{J(x)} = \int_y \frac{\delta\phi(y)}{\delta J(x)} \frac{\delta}{\phi(y)} = \int_y G(x, y) \frac{\delta}{\phi(y)}, \quad (1.12)$$

where we have used that $\phi = W^{(1)}[J]$ and hence $\delta\phi/\delta J = W^{(2)}[J] = G$. Equation (1.12) also highlightens the pivotal rôle of the propagator. Let us now already anticipate the result $W^{(2)} = 1/\Gamma^{(2)}$ and simply evaluate the product of the two two-point functions,

$$\begin{aligned} \int_y \frac{\delta^2 W}{\delta J(x_1) \delta J(y)} \frac{\delta^2 \Gamma}{\delta\phi(y) \delta\phi(x_2)} &= \int_y \frac{\delta}{\delta J(x_1)} \left[\frac{\delta W}{\delta J(y)} \right] \frac{\delta}{\delta\phi(y)} \left[\frac{\delta \Gamma}{\delta\phi(x_2)} \right] = \int_y \frac{\delta\phi(y)}{\delta J(x_1)} \frac{\delta}{\delta\phi(y)} J(x_2) \\ &= \delta(x_1 - x_2), \end{aligned} \quad (1.13)$$

[Equation \(1.13\)](#) proves that the connected two-point function, the full propagator $G(x_1, x_2) = \langle \varphi(x_1)\varphi(x_2) \rangle_c$, is the inverse of the 1PI two-point function. We summarise this important finding as

$$\mathcal{W}^{(2)}(x_1, x_2) = G(x_1, x_2) = \frac{1}{\Gamma^{(2)}}(x_1, x_2). \quad (1.14)$$

With the results obtained so far we are now in the position to provide a diagrammatic representation of general correlation functions in terms of the propagator G and n -point vertices $\Gamma^{(n)}$. Such a representation is the basis for the skeleton expansion. To that end we start with our initial expression for the correlation functions, [\(1.2\)](#), and pull out one J -derivative of the generating functional $\mathcal{Z}[J]$. As this derivative also hits the normalisation $1/\mathcal{Z}[J]$ in [\(1.2\)](#), it has to be compensated for,

$$\frac{1}{\mathcal{Z}[J]} \frac{\delta^n \mathcal{Z}[J]}{\delta J(x_1) \dots \delta J(x_n)} = \left(\frac{\delta}{\delta J(x_1)} + \phi(x_1) \right) \frac{1}{\mathcal{Z}[J]} \frac{\delta^{n-1} \mathcal{Z}[J]}{\delta J(x_2) \dots \delta J(x_n)}, \quad (1.15)$$

where the mean field $\phi(x_1) = \langle \varphi(x_1) \rangle_J$ compensates for the derivative of the normalisation. In terms of correlation functions this reads

$$\begin{aligned} \langle \varphi(x_1) \dots \varphi(x_n) \rangle_J &= \left(\frac{\delta}{\delta J(x_1)} + \phi(x_1) \right) \langle \varphi(x_2) \dots \varphi(x_n) \rangle_J \\ &= \left(\frac{\delta}{\delta J(x_1)} + \phi(x_1) \right) \dots \left(\frac{\delta}{\delta J(x_n)} + \phi(x_n) \right). \end{aligned} \quad (1.16)$$

Here we used the first step of pulling out a J -derivative recursively to find the result in the second line. Finally we are interested in an expression in terms of 1PI quantities, that is in terms of field derivatives of the effective action. With [\(1.12\)](#) this leads us to our final result, the full n -point function in terms of the propagator G , the mean field ϕ and the 1PI vertices $\Gamma^{(n)}$,

$$\langle \varphi(x_1) \dots \varphi(x_n) \rangle = \prod_{i=1}^n \left(\int_{x'_i} G(x_i, x'_i) \frac{\delta}{\delta \phi(x'_i)} + \phi(x_i) \right), \quad (1.17)$$

where we also dropped the subscript J for the expectation values. The 1PI-vertices are still hidden in the representation [\(1.17\)](#). They can be made explicit by performing the ϕ -derivatives. It follows from the definition of the ϕ -dependent propagator, [\(1.14\)](#),

$$\frac{\delta}{\delta \phi(x_1)} G(x_2, x_3) = - \int_{x'_2, x'_3} G(x_2, x'_2) \Gamma^{(3)}(x'_2, x_1, x'_3) G(x'_3, x_3), \quad (1.18)$$

where all quantities in [\(1.18\)](#) are ϕ -dependent. Naturally the field-derivative of an n -point 1PI vertex is an $n+1$ -point function, $\delta/\delta \phi \Gamma^{(n)} = \Gamma^{(n+1)}$. With this rule and [\(1.18\)](#) we can turn [\(1.17\)](#) into a diagrammatic expression in terms of propagators and 1PI vertices. [Equation \(1.17\)](#) generalises straightforwardly to any expectation value $\langle \mathcal{O}[\varphi] \rangle$ of an operator $\mathcal{O}[\varphi]$, that has a well-defined series representation in terms of n -point functions. Then, the expectation value of \mathcal{O} has the functional representation

$$\langle \mathcal{O}[\varphi] \rangle = \mathcal{O} \left[\varphi = G \cdot \frac{\delta}{\delta \phi} + \phi \right], \quad (1.19)$$

with the short hand notation

$$G \cdot \frac{\delta}{\delta \phi} = \int_y G(x, y) \frac{\delta}{\delta \phi(y)}. \quad (1.20)$$

We close this chapter with two simple examples that illustrate the content of (1.17). The first, trivial one, is the two-point function with $n = 2$. The last term in (1.17) always reduces to the mean field as the derivative hits no field-dependence and vanishes. This leaves us with

$$\langle \varphi(x_1)\varphi(x_2) \rangle = \left(\int_{x'_i} G(x_1, x'_1) \frac{\delta}{\delta\phi(x'_1)} + \phi(x_1) \right) \phi(x_2) = G(x_1, x_2) + \phi(x_1)\phi(x_2), \quad (1.21)$$

which is nothing but the representation of the full two-point function in terms of its connected part, the propagator $G = \mathcal{W}^{(2)}$, and the disconnected part $\phi(x_1)\phi(x_2)$, see Table 1.1.

The disconnected part in (1.21) stems from the normalisation $1/\mathcal{Z}[J]$ leading to the compensation of the mean field in (1.15). For the connected n -point functions this term is missing as they are directly defined as the n th derivative of the Schwinger functional, $\mathcal{W}^{(n)}$. Accordingly, this leads us straightforwardly to a similar, even simpler, representation of connected correlation functions,

$$\langle \varphi(x_1) \cdots \varphi(x_n) \rangle_{\text{con}} = W^{(n)}(x_1, \dots, x_n) = \prod_{i=1}^{n-1} \left(\int_{x'_i} G(x_i, x'_i) \frac{\delta}{\delta\phi(x'_i)} \right) \phi(x_n), \quad n > 0. \quad (1.22)$$

The connected one-point function is simply the mean field, the two-point function is the propagator, while the higher connected correlation functions are obviously connected. Our final example if the three-point function. It reads

$$\begin{aligned} \langle \varphi(x_1)\varphi(x_2)\varphi(x_3) \rangle &= - \left(\prod_{i=1}^3 \int_{x'_i} G(x_i, x'_i) \right) \Gamma^{(3)}(x'_1, x'_2, x'_3) \\ &\quad + G(x_1, x_2)\phi(x_3) + G(x_1, x_3)\phi(x_2) + G(x_2, x_3)\phi(x_1) + \phi(x_1)\phi(x_2)\phi(x_3). \end{aligned} \quad (1.23)$$

The second line comprises the different disconnected terms. The on the right hand side in the first line is the connected part of the three-point function. It is simply $W^{(3)}$ as can be shown from (1.22). It also signals the fact that the n -point vertices $\Gamma^{(n)}$ are necessarily amputated correlation functions, they lack the propagators attached to the external lines in the full correlation functions and the connected correlation functions.

1.3. Dyson-Schwinger equations

So far we have refrained from using the path integral representation of correlation functions and generating functionals. However, this representation is convenient for example when it comes to the discussion of symmetries on the quantum level as well as the discussion of systematic approximation schemes. In this chapter we provide a closed path integral representation and derive the Dyson-Schwinger equation that encodes the translation invariance of the path integral measure. As mentioned before, such an explicit representation is not required for the following derivations but it provides some further physics and structural insight. Utilising the path integral representation of $\mathcal{Z}[J]$, (1.3), and its relation to the Schwinger functional, (1.4) and hence the effective action (1.7) we are led to

$$e^{-\Gamma[\phi]} = \int [d\varphi']_{\text{ren}} \exp \left\{ -S[\phi + \varphi'] + \int_x \varphi'(x) \frac{\delta\Gamma[\phi]}{\delta\phi(x)} \right\}. \quad (1.24)$$

In the derivation of (1.24) we have shifted the integration field φ by the mean field, $\varphi = \phi + \varphi'$, as being obvious from the argument of the classical action. We have used in (1.24) that the flat path integral measure is invariant under this shift,

$$[d(\phi + \varphi')]_{\text{ren}} = [d\varphi']_{\text{ren}}. \quad (1.25)$$

Note that this property is less trivial than it seems as we buried the details of the renormalisation of the path integral in the path integral measure. Note also that the expectation value of the new integration field vanishes,

$$\phi = \langle \varphi \rangle, \quad \rightarrow \quad \langle \varphi' \rangle = 0, \quad (1.26)$$

φ' it is a 'true' fluctuation. The quantum equations of motion now follow from taking a ϕ derivative of (1.24) and multiplying by $\exp \Gamma[\phi]$ in order to cancel the exponential factor. This leads us to

$$\frac{\delta \Gamma[\phi]}{\delta \phi} = \left\langle \frac{\delta S[\phi + \varphi']}{\delta \phi(x)} \right\rangle_J. \quad (1.27)$$

Evidently, the quantum equation of motion is simply given the expectation value of the classical EoM. Still, for a closed form we have to rewrite the right hand side of eq. (1.27) in terms of Γ . This is done with the help of (1.19), which certainly covers generic classical actions and in particular that of our example theory, (1.1). This leads us to the functional Dyson-Schwinger equation

$$\frac{\delta \Gamma}{\delta \phi(x)} = \frac{\delta S}{\delta \varphi(x)} \left[\varphi = G \cdot \frac{\delta}{\delta \phi} + \phi \right], \quad (1.28)$$

Dyson-Schwinger Equation (DSE)

with the abbreviation $G \cdot \delta/\delta\phi$ introduced in (1.20). Equation (1.28) is the master DSE for 1PI correlation functions in its final form. It is a closed equation for the first field derivative of the effective action, $\Gamma^{(1)}[\phi]$. All n -point correlation function with $n < 0$ can be obtained via the $(n - 1)$ st functional derivative with respect to the mean field ϕ . In turn, the zero-point function cannot be obtained from the DSE (1.28), it has to be determined differently. Accordingly, the DSE does not comprise directly thermodynamical information.

Note that equivalent master DSEs can be derived for the correlation functions (1.2) and the connected correlation functions obtained from the Schwinger functional. Moreover, the derivation of the DSE from the path integral representation (1.24) has hidden the fact that the DSE is the symmetry identity following from the translation invariance of the path integral measure. This symmetry was used in the derivation of (1.24). The DSE Equation (1.28) can be also derived from

$$\frac{1}{Z[J]} \int [d\varphi]_{\text{ren}} \frac{\delta}{\delta \varphi(x)} \left[\exp \left\{ -S[\varphi] + \int_y J(y) \varphi(y) \right\} \right] = 0, \quad (1.29)$$

which makes apparent the connection to the translation invariance of the path integral measure. This concludes our derivation of the DSEs, more details and applications can be found in e.g. [2, 3, 4, 5, 6, 7]. We close this chapter with an application of the DSE to the simple scalar example theory with the ϕ^4 action defined in (1.1). For this theory the right hand side of the master DSE (1.28) reads

$$\frac{\delta S}{\delta \varphi(x)} \left[\varphi = G \cdot \frac{\delta}{\delta \phi} + \phi \right] = -\partial_\mu^2 \phi(x) + m^2 \phi(x) + \frac{\lambda}{3!} \phi(x)^3 + \frac{\lambda}{3!} \left[\left(G \cdot \frac{\delta}{\delta \phi} + \phi \right)^3 - \phi^3 \right](x), \quad (1.30)$$

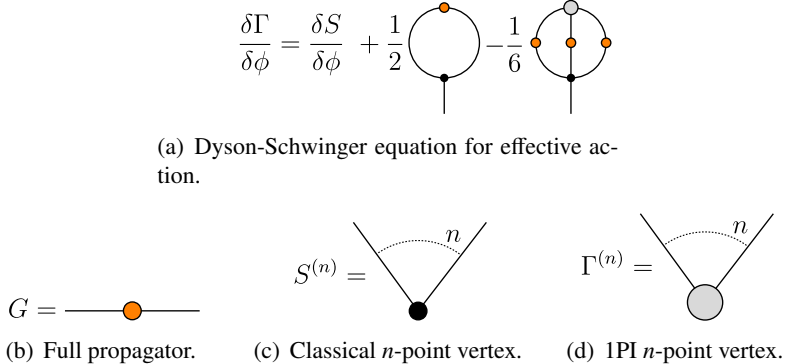


Figure 1.2.: Functional Dyson-Schwinger equation

where the overall argument x in the last term indicates that all fields and products $G \cdot \delta/\delta\phi$ are evaluated at x . While the first term is nothing but the first derivative of the classical action evaluated on the mean field, $S^{(1)}[\phi]$, the last term has already been computed in (1.23). We identify $x_i = x$ in (1.23) and subtract the mean field term ϕ^3 in (1.23) as in (1.30). Then we are led to

$$\left(G \cdot \frac{\delta}{\delta\phi} + \phi \right)^3 - \phi^3 = -G \cdot (G \cdot \Gamma^{(3)} \cdot G) + 3\phi G, \quad (1.31)$$

where all space-time arguments are x . In summary, the final closed form of the master DSE for the φ^4 theory in terms of the effective action Γ is given by

$$\frac{\delta\Gamma}{\delta\phi} = \frac{\delta S}{\delta\phi} + \frac{\lambda}{2} \phi G - \frac{\lambda}{3!} G^3 \cdot \Gamma^{(3)} \quad (1.32)$$

where in the last term, all G couple to both, $\Gamma^{(3)}$ and λ . Equation (1.32) makes the structure very apparent. Restoring all space-time dependence leads us to

$$\frac{\delta\Gamma[\phi]}{\delta\phi(x)} = \frac{\delta S[\phi]}{\delta\phi(x)} + \frac{\lambda}{2} \phi(x) G(x, x) - \frac{\lambda}{3!} \int_{x_1, x_2, x_3} \left(\prod_{i=1}^3 G(x, x_i) \right) \Gamma^{(3)}(x_1, x_2, x_3), \quad (1.33)$$

where both, the G 's and $\Gamma^{(3)}$ are ϕ -dependent. The full loop structure of the equation is apparent in its diagrammatic representation. The pictorial master DSE is then given in Figure 1.2(a), while in Figure 1.2(b) and Figure 1.2(d) a transcription of the propagator and a general n -point vertex into the diagrammatic language is given.

Typically functional relations are evaluated in momentum space. The diagonal part of the propagator, $G(x, x)$, is given by

$$G(x, x) = \int_{p,q} G(q, p) e^{i(p+q)x}, \quad \text{where} \quad \int_q = \int \frac{d^d q}{(2\pi)^d}. \quad (1.34)$$

and we have used the conventions for Fourier transformations in Appendix A. The full propagator $G[\phi]$ is not diagonal in momentum space as it depends on a general field $\phi(x)$. For constant or vanishing fields

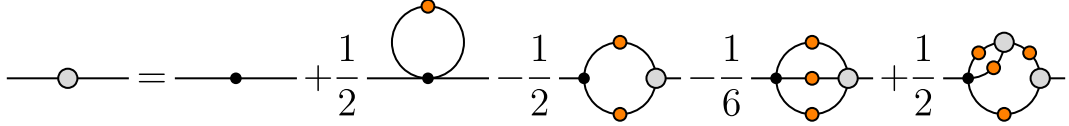


Figure 1.3.: Dyson-Schwinger equation for the full inverse propagator, for the notation see [Figure 1.2\(a\)](#).

the propagator is diagonal with

$$G(q, p) = G(q)(2\pi)^d \delta(p + q), \quad \rightarrow \quad G(x, x) = \int_q G(q). \quad (1.35)$$

The δ -function in the propagator in (1.35) carries momentum conservation and the homogeneity of the background. Using (1.35) in (1.33) makes explicit the tadpole nature of the one loop term in the DSE. The simple ϕ^4 example here already allows us to discuss the structure of DSEs in general theories: a classical n -point vertex leads to diagrams up to $n - 1$ loops in full propagators and full vertices with one classical vertex being present. This follows already from the right hand side of (1.28). Consequently, for QCD the DSEs are of one- (for quark and ghost) or two-loop (for the gauge field) form depending on which field derivative is taken. For quantum gravity the DSE is an infinite loop equation as the classical action of general relativity, the Einstein-Hilbert action, already contains vertices to any order of the field. The functional DSE in (1.28) also allows us to prove the 1PI property of the effective action as well as the property that the Schwinger functional $\mathcal{W}[J]$ generates connected correlation functions. Here we only present a sketch of these proofs: Let us insert the classical action $S[\phi]$ on the right hand side which is trivially 1PI. As the right hand side only contains 1PI diagrams, this produces a left hand side $\Gamma^{(1)}$ which also is 1PI, as are its further derivatives $\Gamma^{(n)}$. Re-inserting these 1PI- $\Gamma^{(n)}$ again leads to a 1PI right hand side. Assuming its convergence, this iteration leads to a solution of (1.28) with classical part $S[\phi]$. With the representation (1.22) of the $\mathcal{W}^{(n)}$ in terms of the propagator G and the (proven) 1PI vertices $\Gamma^{(n)}$ it follows directly that the $\mathcal{W}^{(n)}$ are connected correlation functions.

The DSEs for general n -point functions follow from further derivatives with respect to the classical field $\phi(x)$ in [eq. \(1.32\)](#), as already mentioned above. The simplest example is the scalar propagator. Its DSE, the gap equation, can be obtained from the master DSE, [eq. \(1.28\)](#), by one derivative with respect to ϕ , for the diagrammatic representation see [Figure 1.3](#). The next step would be to solve [eq. \(1.32\)](#) for a generic n -point function. However, a closer look at the diagrams in [Figure 1.2](#) shows that for the solution of the n -point function we need to know at least the $(n + 2)$ -point function. Consequently, we are dealing with an infinite tower of coupled equations that are not always analytically solvable. Therefore, the equations have to be truncated in a physically reasonable way, i.e. with paying attention to e.g. gauge invariance, multiplicative renormalizability etc. One common technique to truncate the set of coupled equations would be by employing a specially designed vertex ansatz. For further details we refer the interested reader to DSE reviews and literature therein, [2, 3, 4, 5, 6, 7].

As a simple final application of the DSE (1.28) we formally derive the one loop effective action without paying attention to the necessary renormalisation. We restrict ourselves to the classical and one loop term of the DSE,

$$\left. \frac{\delta \Gamma[\phi]}{\delta \phi(x)} \right|_{1\text{-loop}} = \frac{\delta S[\phi]}{\delta \phi(x)} + \frac{\lambda}{2} \phi(x) \frac{1}{\Gamma^{(2)}[\phi]}(x, x) \Big|_{1\text{-loop}} = \frac{\delta S[\phi]}{\delta \phi(x)} + \frac{\lambda}{2} \phi(x) \frac{1}{S^{(2)}[\phi]}(x, x). \quad (1.36)$$

The difference of $\Gamma^{(2)}$ and $S^{(2)}$ is at least of one loop nature. Inserted into a one-loop diagram it contributes only to at least two-loop diagrams. Hence we could restrict ourselves to the classical, but ϕ -dependent propagator. The factor in front of the classical propagator is nothing but the third derivative of the classical action, $1/2 S^{(3)}[\phi]$. Hence we arrive at

$$\frac{\delta\Gamma[\phi]}{\delta\phi(x)} \Big|_{\text{1-loop}} = \frac{\delta S[\phi]}{\delta\phi(x)} + \frac{\delta}{\delta\phi(x)} \text{Tr} \ln S^{(2)}[\phi], \quad (1.37)$$

where the trace Tr stands for an integral over the diagonal part of $\ln S^{(2)}[\phi]$. [Equation \(1.37\)](#) can be integrated straightforwardly and we arrive at the standard expression for the one-loop effective action,

$$\Gamma^{\text{1-loop}}[\phi] = S[\phi] + \frac{1}{2} \text{Tr} \ln S^{(2)}[\phi], \quad (1.38)$$

where we have set the integration constant to zero. This result can also be derived from a saddle point expansion of the path integral which is done for comparison in [Appendix B](#). The expression [\(1.37\)](#) requires renormalisation in $d \geq 2$ dimensions. The related discussion is deferred to the exercises.

We close this chapter with a remark on general DSEs including that for quantum symmetries. For this purpose we reconsider the derivation of the DSE from a total derivative of the integrand in the path integral, [\(1.29\)](#). This is easily generalised by inserting a generic function $\Psi[\varphi]$, to wit

$$\frac{1}{Z[J]} \int [d\varphi]_{\text{ren}} \frac{\delta}{\delta\varphi(x)} \left[\Psi[\varphi] \exp \left\{ -S[\varphi] + \int_y J(y) \varphi(y) \right\} \right] = 0, \quad (1.39)$$

This leads to the general DSE

$$\langle \Psi[\varphi] \rangle \frac{\delta\Gamma[\phi]}{\delta\phi(x)} = \left\langle \Psi[\varphi] \frac{\delta S[\varphi]}{\delta\varphi(x)} \right\rangle - \left\langle \frac{\delta\Psi[\varphi]}{\delta\varphi(x)} \right\rangle. \quad (1.40)$$

For example, $\Psi = 1$ we recover the standard DSE [\(1.28\)](#), for a symmetry transformation of the classical action, $\Psi[\varphi]\delta S/\delta\phi = 0$ we get a symmetry identity of the effective action. Note that such a transformation could also be a total scale transformation in which case the generic DSE provides a functional renormalisation group equation. For more details on general DSEs and their connection to FRGs see e.g. [\[8, 9, 10\]](#). The DSE approach is a very versatile approach which has been very successfully applied to various problems in QFTs including its application to strongly correlated infrared QCD, for more details we again refer to DSE reviews and literature therein, [\[2, 3, 4, 5, 6, 7\]](#).

Exercises

For this set of exercises we are mostly considering a scalar theory in the framework of Dyson-Schwinger Equations. The Lagrangian for this theory is given by

$$\mathcal{L}[\phi] = \frac{1}{2}(p^2 + m^2)\phi^2 + \frac{\lambda}{4!}\phi^4, \quad (1.41)$$

which is Z_2 -symmetric. Nevertheless, it can dynamically acquire a finite expectation value $\phi = \langle\phi\rangle$, spontaneously breaking the symmetry. Additionally, we assume the ground-state $\langle\phi\rangle$ to be space-time independent throughout this set of exercises.

Exercise 1: Effective potential from Dyson-Schwinger Equations

In the following we are going to calculate a differential equation for the effective potential in two space-time for a scalar ϕ^4 -theory with classical action (1.1) in two space-time dimensions, $d = 2$. In order to truncate the infinite tower of equations we work in a derivative expansion, i.e. full correlation functions at vanishing momentum are given derivatives of the effective potential. Practically this reduces the full two and three-point functions to

$$\begin{aligned} \Gamma_{\phi\phi}^{(2)}(p) &= p^2 + V^{(2)}(\phi), \\ \Gamma_{\phi\phi\phi}^{(3)} &= V^{(3)}(\phi), \end{aligned} \quad (1.42)$$

where we have dropped the momentum dependence for all correlation functions $n \geq 3$, since they are momentum independent in leading order.

- a) Recollect the derivation of the master equation for this theory.

You should arrive at the following expression, for the graphical representation see [Figure 1.2](#)

$$V^{(1)}(\phi) = \frac{\delta S}{\delta \phi} + \frac{\lambda}{2}\phi \int_p G_{\phi\phi}(p) - \frac{\lambda}{3!} \int_{p,q} G_{\phi\phi}(p)G_{\phi\phi}(q)G_{\phi\phi}(p+q)\Gamma_{\phi\phi\phi}^{(3)}. \quad (1.43)$$

- b) Calculate the one-loop term in (1.43).

The integral is not finite and requires regularisation, split the mass term in the classical action into a renormalised mass and counter term

$$\bar{m}^2 = m^2 - \frac{\lambda}{2} \int_p \frac{1}{p^2 + m_{\text{ren}}^2}, \quad (1.44)$$

which renders the integral finite.

- c) Calculate the two-loop term in (1.43).

The integral is finite, but not entirely straightforward to calculate:

- Introduce Feynman parameters

$$\frac{1}{A_1 \dots A_n} = (n-1)! \int_0^1 du_1 \dots \int_0^1 du_n \frac{\delta(1 - \sum_{k=1}^n u_k)}{\left(\sum_{k=1}^n u_k A_k\right)^n}. \quad (1.45)$$

- Complete the square first for q and p consecutively , introducing two new momentum variables k_1, k_2 that decouple the momentum integrations.

- Rewrite in the denominator as an exponential

$$\frac{1}{D^3} = \frac{1}{2} \int_0^\infty dt t^2 e^{-Dt} \quad (1.46)$$

and carry out the momentum integrations over k_1 and k_2 .

- Only the integral over the Feynman parameters is left, the result is given by:

$$\int_0^1 dx_i \frac{\delta(1 - \sum x_i)}{x_1 x_2 + x_1 x_3 + x_2 x_3} = \frac{1}{18} (\psi^{(1)}(1/6) + \psi^{(1)}(1/3) - \psi^{(1)}(2/3) - \psi^{(1)}(5/6)) \approx 2.3439, \quad (1.47)$$

where $\psi^{(n)}(z)$ is the n-th derivative of the digamma function, $\psi^{(0)}(z) = \Gamma'(z)/\Gamma(z)$.

The result you have derived is a differential equation for the effective potential. In order to solve it the initial condition is the classical potential at a large field value, where all quantum fluctuations are suppressed. Solving the differential equation is however in almost all cases analytically not possible.

Exercise 2: Dyson-Schwinger Equation for the two-point function

Derive the Dyson-Schwinger Equation of the two-point function for the same theory as in [Exercise 1](#).

Remark: *Solving [Exercise 3](#) renders this exercise trivial.*

Exercise 3: Dyson-Schwinger Equations for general theories

Derive the Dyson-Schwinger Equation for the two-point function in the superfield formalism.

The superfield formalism collects all fields in a single superfield, where the field-space metric accounts for possible minus signs for fermions. For example, in Yang-Mills theory we have $\Phi = (A, c, \bar{c})^T$ and the metric reads

$$(\gamma^{ab}) = \begin{pmatrix} 1 & 0 & 0 \\ 0 & 0 & 1 \\ 0 & -1 & 0 \end{pmatrix}, \quad (1.48)$$

which results from the requirement $\Phi^a \Phi_a = A^2 + 2\bar{c}c$, where the delta-distribution in space is implicitly contained in the metric γ and integration on the right-hand side is implied. By our convention indices are always raised from the left and lowered from the right, e.g. $\Phi^a = \gamma^{ab} \Phi_b = \Phi_b \gamma^{ab} = (A, \bar{c}, -c)$. This immediately implies the following identities

$$\begin{aligned} \gamma_a^b &= \gamma^{bc} \gamma_{ac} = \gamma^{cb} \gamma_{ca} = \delta_a^b \\ \gamma^a_b &= \gamma^{ac} \gamma_{cb} = \gamma^{ca} \gamma_{bc} = (-1)^{ab} \delta_b^a, \end{aligned} \quad (1.49)$$

where $(-1)^{ab}$ is -1 iff a and b are fermionic and 1 else. For completeness we do not set the fields in the end to zero, but to a finite, arbitrary value. As we cannot go to arbitrary order in the classical action we will restrict ourselves to a polynomial up to order 4, i.e.

$$S[\Phi] = \frac{1}{2!} S^{ij} \Phi_i \Phi_j + \frac{1}{3!} S^{ijk} \Phi_i \Phi_j \Phi_k + \frac{1}{4!} S^{ijkl} \Phi_i \Phi_j \Phi_k \Phi_l, \quad (1.50)$$

where integration is again implied.

Derive the Dyson-Schwinger equation for a two point function starting from

$$\frac{\delta\Gamma}{\delta\Phi_i} = \frac{\delta S}{\delta\varphi_i} \left[\varphi_i = G_{ij} \frac{\delta}{\delta\Phi_j} + \Phi_i \right]. \quad (1.51)$$

2. Functional Renormalisation Group

In [Chapter 1](#) we have introduced the basic setting for functional approaches to QFT cumulating finally in the derivation of the quantum equations of motion for the effective action, the functional Dyson-Schwinger equations, [\(1.28\)](#). In the following we pursue a different, though related, functional approach, the functional renormalisation group (FRG). It can be viewed as a differential DSE, its prominent feature being its inherent finiteness. No regularisation and renormalisation procedure has to be applied, and the latter simply is a self-consistency condition of the approach which is systematically implemented.

Heuristically, the FRG is based on a continuous version of the Kadanoff block spinning idea, [\[11\]](#), on the lattice as introduced by Wilson in [\[12, 13\]](#). In its momentum space version used in the present work it amounts to solving the theory successively momentum shell for momentum shell. It is very illuminating to discuss this idea in a path integral setting. To that end we reconsider the path integral representation [\(1.3\)](#) in more detail for explaining the heuristic idea. In theories such as QCD it is the low energy regime with $p^2/\Lambda_{\text{gap}}^2$ that is strongly correlated. Here, Λ_{gap} is the physical, intrinsic, scale in the theory below which the strong correlations take place. This can be a scale where a phase transition takes place or simply a dynamical scale such as Λ_{QCD} in QCD. Accordingly, if we do not include momentum modes with $p^2 \lesssim \Lambda_{\text{gap}}^2$ in our path integral, we are dealing with a path integral that is perturbatively accessible.

2.1. Flow equations for generating functionals

In order to achieve such a setup we introduce an infrared cutoff scale k , below which the momentum modes are not integrated out. The related infrared regularised path integral is given by

$$\mathcal{Z}_k[J] = \int [d\varphi]_{\text{ren}, p^2 \geq k^2} \exp \left\{ -S[\varphi] + \int_x J(x) \varphi(x) \right\}, \quad (2.1)$$

where the modified path integral measure in [\(2.1\)](#) has a simple representation in momentum space,

$$[d\varphi]_{p^2 \geq k^2} = \prod_{p^2 \geq k^2} d\varphi_p. \quad (2.2)$$

In [\(2.2\)](#), the momentum modes $\varphi_p(q)$ only have support at the momentum p : $\varphi_p(q) \propto \delta(q^2 - p^2)$, for illustration and later use we depict a soft version of such a function in [Figure 2.1](#). The measure [\(2.2\)](#) implements a sharp infrared momentum cutoff: the infrared momenta $p^2 < k^2$ are completely suppressed as they are not integrated out. From the infrared regularised generating functional $Z_k[J]$ one can deduce an infrared regularised effective action $\Gamma_k[\phi]$ along the same line discussed in [Chapter 1](#). The effective action satisfies a functional renormalisation group equation, the Wegner-Houghton (WH) equation [\[14\]](#). The WH equation will be discussed as a special case of the more general setup discussed below, so no more details are given here.

A more general and more versatile way for introducing such a mode regularisation is a soft cutoff procedure. Then the infrared modes are still suppressed, but not infinitely strong as in [\(2.2\)](#). One of its advantages lies in the explicit form in terms of a modification of the classical action. The scale-dependent integration measure is defined as

$$\int [d\varphi]_{\text{ren}, p^2 \gtrsim k^2} = \int [d\varphi]_{\text{ren}} \exp(-\Delta S_k[\varphi]), \quad (2.3)$$

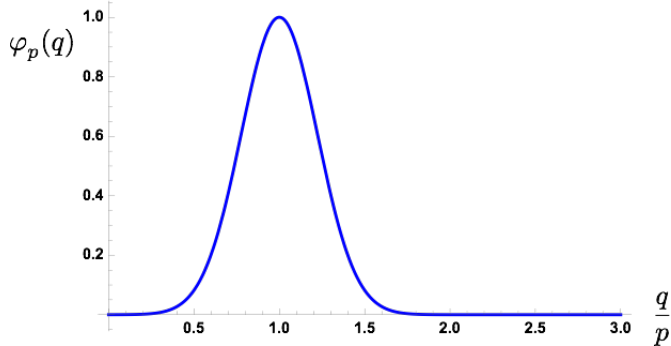


Figure 2.1.: Smeared momentum mode $\varphi_p(q)$

with an infrared cutoff term

$$\Delta S_k[\varphi] = \frac{1}{2} \int_p \varphi(p) R_k(p^2) \varphi(-p). \quad (2.4)$$

The regulator function $R_k(p^2)$ is chosen such that it suppresses the propagation of momentum modes for momenta $p^2 \lesssim k^2$ and does not modify the propagation of momenta $p^2 \gtrsim k^2$. This is achieved with a momentum-dependent mass function $R_k(p^2)$ with the properties

(i) Suppression of IR modes

$$\lim_{p^2 \rightarrow 0} R_k(p^2) > 0 \quad (2.5a)$$

(ii) Physical limit

$$\lim_{k \rightarrow 0} R_k(p^2) = 0 \quad (2.5b)$$

(iii) UV limit

$$\lim_{k \rightarrow \Lambda \rightarrow \infty} R_k(p^2) = \infty. \quad (2.5c)$$

In [Figure 2.2](#) we depict some suitable regulator functions. Note that the choice of $R_k(p)$ is by no means unique. Finally the cutoff is removed, $k \rightarrow 0$ and the resulting generating functional, $\mathcal{Z}_{k=0}[J] = \mathcal{Z}[J]$, is the full generating functional, independent of the choice of the intermediate infrared regularisation procedure. Hence, general functions that satisfy the conditions (i), (ii) and (iii) in [2.5](#) are legitimate, though not all choices work equally well. This important topic is discussed later in [??](#). For convenience, the regulator is often adapted to the kinetic term of the field under investigation. A convenient and standard parameterisation for regulator functions is

$$R_k(p^2) = p^2 r(y), \quad \text{with} \quad y = \frac{p^2}{k^2}, \quad (2.6)$$

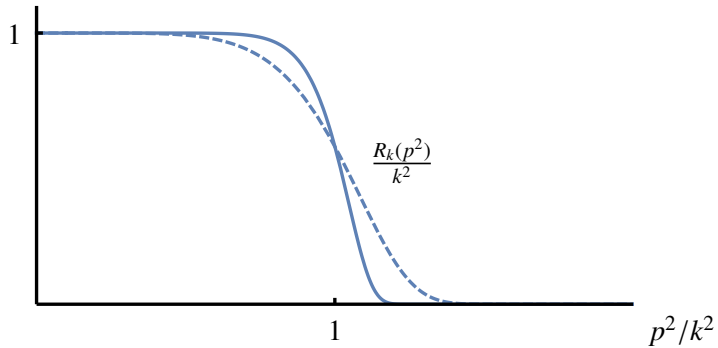


Figure 2.2.: Infrared regulator functions. The depicted regulators are exponential regulators 2.9b with $c = 1$: $R_k/k^2 = y^{n-1}/(e^{y^n} - 1)$ with $n = 6(12)$ and $y = p^2/k^2$ for the dashed (solid) curve.

where r is a dimensionless regulator shape function, only depending on the dimensionless momentum argument $y = p^2/k^2$. We have dropped the subscript k for the shape function. Even though in general it might carry a k -dependence but in most cases it is simply a k -independent function of y . Note also that an additional k -dependence of r requires another scale as r is dimensionless. For no explicit k -dependence we conclude that

$$k\partial_k R_k(p^2) = p^2 \partial_y r(y) = -2p^2 y r'(y), \quad (2.7)$$

with $r'(y) = \partial_y r(y)$. With (2.7) we have turned the scale derivative in a p^2 -derivative. Moreover, the scale dependence of the full regulator function $R_k(p)$ is entirely encoded in the shape function $r(y)$. Within this parameterisation it is obvious that the conditions (i), (ii), (iii) in 2.5 above can be combined into two conditions (i') and (ii'). In a compact form we write

(i') IR regularisation

$$\lim_{\frac{p^2}{k^2} \rightarrow 0} \frac{R_k(p^2)}{k^2} > 0, \quad (2.8a)$$

(ii') Physical limit

$$\lim_{\substack{\frac{k^2}{p^2} \rightarrow 0 \\ p^2}} \frac{R_k(p^2)}{k^2} = 0. \quad (2.8b)$$

Evidently 2.8a leads to an additional mass for the field φ for low momenta, while 2.5c ensures that the cutoff term vanishes identically in the limit $k \rightarrow 0$. It also ensures, that for a fixed cutoff scale k , momenta larger than the cutoff scale k are not affected by the infrared regularisation. Let us now specify

some standard, and frequently used, choices for regulator or sets of regulator functions:

$$\text{Litim regulator: } r(y) = \begin{cases} 1 & y < 1 \\ 0 & y \geq 1 \end{cases}, \quad (2.9a)$$

$$\text{Exponential regulator: } r(y) = \frac{cy^{b-1}}{\exp(y^b) - 1}, \quad (2.9b)$$

$$\text{Sharp regulator: } r(y) = \frac{1}{\theta(y-1)} - 1, \quad (2.9c)$$

with $\theta(x)$ being the Heaviside step function and c, b being parameters to be chosen by hand. All these regulators have an effective infrared cutoff scale of about k but have different shapes as well as different decay behaviours and infrared limits. While the Litim regulator and sharp regulator lead to analytic flow equations in simple approximations, the set of exponential regulators is well suited for numerical implementations. Note also that the exponential regulator tends towards the sharp regulator for $b \rightarrow \infty$. More details on different choices of regulators and the subject of optimisation and error control is discussed in ??, see also [15, 16, 9, 17, 18, 19].

With the properties 2.8 for the regulator functions it is simple to see that (2.3) is a soft version of the sharp cutoff measure (2.2): For momentum modes $\varphi_p(q)$ with $p^2 \ll k^2$ we have

$$\lim_{\frac{p^2}{k^2} \rightarrow 0} \Delta S_k[\varphi_p] = \frac{1}{2} \int_q \varphi_p(q) R_k(q^2) \varphi_p(-q) \rightarrow \frac{k^2}{2} \int_q \varphi_p(q) \varphi_p(-q), \quad (2.10)$$

where we have taken the standard limit $R_k(q^2 \rightarrow 0) = k^2$. In turn, for momentum modes $\varphi_p(q)$ with $p^2 \gg k^2$ we have

$$\lim_{\frac{p^2}{k^2} \rightarrow \infty} \Delta S_k[\varphi_p] = \frac{1}{2} \int_q \varphi_p(q) R_k(q^2) \varphi_p(-q) \rightarrow 0. \quad (2.11)$$

The limits (2.10), (2.11) can be explicitly investigated with the regulator choices in 2.9. Moreover, with the sharp regulator the measure (2.3) reduces to the sharp momentum cutoff measure (2.2). With this we conclude our discussion of the infrared cutoff procedure we shall use throughout these lecture notes. Substituting the flat measure $[d\varphi]_{\text{ren}}$ in (1.3) with that in (2.3) leads to scale-dependent generating functional \mathcal{Z}_k with

$$\mathcal{Z}_k[J] = \int [d\varphi]_{\text{ren}} \exp \left[-S[\varphi] - \Delta S_k[\varphi] + \int d^d x J(x) \varphi(x) \right]. \quad (2.12)$$

As the regulator $R_k(p^2)$ decays rapidly in the ultraviolet it does not affect the UV renormalisation. Accordingly, if the original generating functional $\mathcal{Z}[J]$ defined by (1.2) was finite, so is the infrared regularised one in (2.12). For large infrared cutoff scales, relying on the assumption of a weakly interacting UV limit of the theory (asymptotic freedom), (2.12) provides a well defined starting point for solving our theory. The latter is then achieved by lowering the cutoff infinitesimally and successively integrating out momentum shells of momentum modes $\varphi_{p \approx k}$. This procedure is encoded in the flow equation for $\mathcal{Z}_k[J]$ which can be read off from (2.12) as

$$k \partial_k \mathcal{Z}_k[J] = -\langle k \partial_k \Delta S_k[\varphi] \rangle \mathcal{Z}_k[J]. \quad (2.13)$$

The $k \partial_k$ -derivative is used for convenience as it does not change the dimension of the generating functional. This leads us to the definition of (minus) the RG time, $t = \ln k/\Lambda$, with a fixed reference scale Λ , typically the ultraviolet cutoff scale where the flow is initiated. In the latter case the flow runs from the

initial RG-times $t = 1$ to $t = -\infty$ with $k = 0$. Total derivatives with respect to this RG time shall be abbreviated in the following by ∂_t or even shorter, in the style of a time derivative, by a dot,

$$\dot{f} = \partial_t f \quad \text{with} \quad t = \ln \frac{k}{\Lambda}. \quad (2.14)$$

Equation (2.13) can be readily rewritten in a functional form by using **(1.19)** for $\langle k \partial_k \Delta S_k[\varphi] \rangle$. Here we will not pursue this path as we want to provide a derivation of the flow equation without any reference to the path integral. Instead, the -functional- derivation will be only based on the assumption of dealing with a theory that admits finite correlation functions. In other words, this is the -highly non-trivial- assumption that the theory at hand exists.

For the derivation we rewrite the infrared regularised generating functional $\mathcal{Z}_k[J]$ as follows,

$$\mathcal{Z}_k[J] := e^{-\Delta S_k[\frac{\delta}{\delta J}]} \mathcal{Z}[J]. \quad (2.15)$$

As promised, **(2.15)** only relies on the existence of $\mathcal{Z}[J]$, or rather its J -derivatives. The latter, however, simply provide the definition of $\mathcal{Z}[J]$ via **(1.2)**. Also, the exponential of ΔS_k provides an infrared suppression of momentum modes. The definition **(2.12)** is obtained via

$$f \left[\frac{\delta}{\delta J} \right] e^{\int_x J(x) \varphi(x)} = f[\varphi] e^{\int_x J(x) \varphi(x)}. \quad (2.16)$$

Hence, moving $\exp\{-\Delta S_k[\delta/\delta J]\}$ into the φ -integral of the path integral representation of $\mathcal{Z}[J]$ in **(1.3)** and then applying **(2.16)** leads us from **(2.15)** to **(2.12)**. In the latter case we have to discuss the renormalisation procedure of the path integral, in the former we may get away with the self-consistent assumption of the existence of finite correlation functions. We shall see that this indeed holds true.

Applying a $\partial_t = k \partial_k$ -derivative to **(2.15)** leads us to the flow equation

$$\begin{aligned} \partial_t \mathcal{Z}_k[J] &= -\partial_t \Delta S_k \left[\frac{\delta}{\delta J} \right] e^{-\Delta S_k[\frac{\delta}{\delta J}]} \mathcal{Z}[J] \\ &= -\partial_t \Delta S_k \left[\frac{\delta}{\delta J} \right] \mathcal{Z}_k[J], \end{aligned} \quad (2.17)$$

where we have used that $k \partial_k \Delta S_k[\delta/\delta J]$ commutes with $\Delta S_k[\delta/\delta J]$ in the first line. For the second line we identified $\mathcal{Z}_k[J]$ from its defintion **(2.15)**. More explicitly we have

$$\partial_t \mathcal{Z}_k[J] = -\frac{1}{2} \int_p \frac{\delta^2 \mathcal{Z}_k[J]}{\delta J(p) \delta J(-p)} \partial_t R_k(p^2), \quad \text{with} \quad t = \ln \frac{k}{\Lambda}. \quad (2.18)$$

Equation (2.18) is the functional flow equation for the generating functional $\mathcal{Z}[J]$ with similarities to a functional heat equation. Given a finite two-point correlation function $\delta^2 \mathcal{Z}_k[J]/\delta J^2$, as an input, **(2.18)** is finite, subject to a sufficiently strong decay of $\partial_t R_k(p^2)$ for large momenta.

For illustration we depict in **Figure 2.3** we depict the momentum behaviour of the regulator function $R_k(p^2)$ and its scale derivative $\dot{R}_k(p) = \partial_t R_k(p^2)$. The flow equation **(2.18)** is easily rewritten for the Schwinger functional $\mathcal{W}[J] = \ln \mathcal{Z}[J]$. The relation of the two point functions has been already discussed in **(1.5)** and reads in terms of derivatives of \mathcal{Z} and \mathcal{W}

$$\frac{1}{\mathcal{Z}[J]} \mathcal{Z}^{(2)}[J](x_1, x_2) = \mathcal{W}^{(2)}(x_1, x_2) + \mathcal{W}^{(1)}(x_1) \mathcal{W}^{(1)}(x_2) = G(x_1, x_2) + \phi(x_1) \phi(x_2). \quad (2.19)$$

Multiplying the flow equation for the generating functional $\mathcal{Z}[J]$ with $1/\mathcal{Z}[J]$ and inserting the relation **(2.19)** leads us to the flow equation for the Schwinger functional,

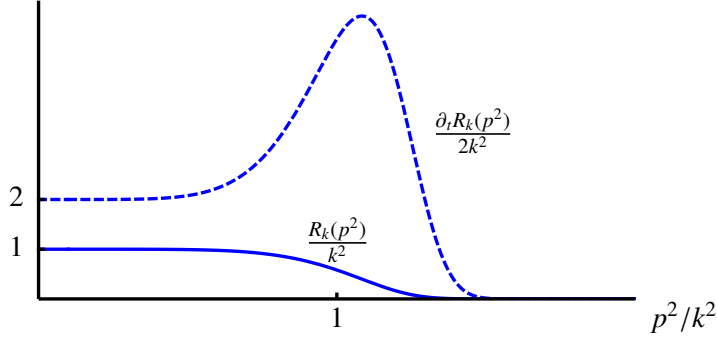


Figure 2.3.: The regulator function depicted in [Figure 2.2](#) and its derivative with respect to the RG time $t = \ln k/\Lambda$.

$$\partial_t \mathcal{W}_k[J] = -\frac{1}{2} \int_p \left[\mathcal{W}_k^{(2)}[J] + (\mathcal{W}_k^{(1)}[J])^2 \right] (p, -p) \partial_t R_k(p^2), \quad (2.20)$$

where $t = \ln k/\Lambda$. Upon n th derivatives w.r.t. J , [\(2.20\)](#) provides the scale dependence of connected correlation functions. As already discussed before, these correlation functions have propagators attached to their external legs. These propagators can be removed via an appropriate redefinition of the currents. We also can subtract the -classical- free Gaussian part of the infrared regularised theory, as its flow is trivial. Note also that the structure of the equation does not change if we consider an ultraviolet (UV) regulator function instead of an infrared one. Combining all these modifications, we are led to the Polchinski equation [20], the flow equation for *amputated* connected correlation function. It has been introduced for simplifying proofs of perturbative renormalisability (hence the UV cutoff), a purpose the Polchinski equation is very well suited for. Moreover, for the derivation and discussion of functional symmetry relations it is very well-suited due to its algebraic form. Its structure is the same as [\(2.20\)](#), and we do not discuss it any further here, but will reconsider it for the discussion of gauge symmetries and diffeomorphism invariance later.

Our final interest applies to the flow equation for the effective action. It follows straightforwardly from the functional flows for \mathcal{Z} or \mathcal{W} by using the relations between connected n -point functions $\mathcal{W}^{(n)}[J]$ and 1PI n -point functions $\Gamma^{(n)}[\phi]$. Before doing so it is worth to study the structure of [\(2.20\)](#) more closely. The term with the connected one-point functions $\mathcal{W}^{(1)}$ is simply the derivative of the cutoff term $\Delta S_k[\phi]$ evaluated on the mean field. More explicitly we have

$$\frac{1}{2} \int_p \mathcal{W}_k^{(1)}[J](p) \mathcal{W}_k^{(1)}[J](-p) \partial_t R_k(p^2) = \frac{1}{2} \int_p \phi(p) \phi(-p) \partial_t R_k(p^2) = \partial_t \Delta S_k[\phi]. \quad (2.21)$$

[Equation \(2.21\)](#) marks this term in the flow equation for \mathcal{W} as a trivial one in terms of the mean field. This suggests to subtract it from the effective action for the sake of convenience. Accordingly we define the scale-dependent or flowing effective action $\Gamma_k[\phi]$ as a modified Legendre transformation of $\mathcal{W}_k[J]$,

which reduces to the standard expression (1.7) in the limit $k \rightarrow 0$.

$$\Gamma_k[\phi] = \int_x J(x) \phi(x) - \mathcal{W}_k[J] - \Delta S_k[\phi], \quad (2.22)$$

where it is understood that $J = J_k[\phi]$ maximises (2.22). Note that the Legendre transformation of $\mathcal{W}_k[J]$ simply is $\Gamma_k[\phi] + \Delta S_k[\phi]$. Hence, the relations derived in Section 1.2 and Section 1.3 between the Schwinger functional and its Legendre transformation apply to $\Gamma_k + \Delta S_k$. This implies the relations

$$\frac{\delta(\Gamma_k[\phi] + \Delta S_k[\phi])}{\delta\phi(x)} = J(x), \quad \frac{\delta\mathcal{W}_k[J]}{\delta J(x)} = \phi(x). \quad (2.23)$$

which reduce to (1.9) and (1.8) in the limit $k \rightarrow 0$. In order to provide a further insight in the definition of $\Gamma_k[\phi]$ we discuss the integro-differential path integral representation for the scale dependent effective action analogously to (1.24). It reads

$$e^{-\Gamma_k[\phi]} = \int [d\varphi]_{\text{ren}} \exp \left\{ -S[\varphi + \phi] - \Delta S_k[\varphi] + \int_x \varphi(x) \frac{\delta\Gamma_k[\phi]}{\delta\phi(x)} \right\}. \quad (2.24)$$

Equation (2.24) allows us in particular to study the limit $k \rightarrow \infty$ in a concise way: the infrared cutoff term dominates the path integral and all other dependences on the fluctuation field can be neglected as subleading terms in an expansion in powers of k . Then, in leading order, the source term proportional to $\delta\Gamma_k/\delta\phi$ drops out, and we have $S[\phi + \varphi] \rightarrow S[\phi]$. Accordingly, the effective action Γ_k reduces to the classical action. Note however, that we have neglected potential intricacies due to the necessary renormalisation of the path integral. A fully satisfactory discussion of the UV limit with $k \rightarrow \infty$ is given later on the basis of the flow equation for the effective action $\Gamma_k[\phi]$.

After this interlude we continue with the derivation of this flow. Taking all t -dependences into account including that of the current into account we are led to

$$\begin{aligned} \partial_t \Gamma_k[\phi] &= -\partial_t \mathcal{W}_k[J] - \partial_t \Delta S_k[\phi] - \int_x \partial_t J(x) \left[\phi(x) - \frac{\mathcal{W}_k[J]}{\delta J(x)} \right] \\ &= \frac{1}{2} \text{Tr} W^{(2)}[J] \partial_t R_k + \partial_t \Delta S_k[\phi] - \partial_t \Delta S_k[\phi] \\ &= \frac{1}{2} \text{Tr} G_k[\phi] \partial_t R_k. \end{aligned} \quad (2.25)$$

From the first to the second line in (2.25) we have used that the expression in the square bracket in the last term vanishes due to (2.23). For the $\mathcal{W}^{(1)}$ -term in the flow of the Schwinger functional we have used (2.21), which leads us to the last line. The propagator $G_k[\phi]$ is the inverse of the two point function of the Legendre transformation of $\mathcal{W}_k[J]$, see (1.14). With (2.22) this is $\Gamma_k^{(2)} + \Delta S_k^{(2)}$ leading to

$$\mathcal{W}_k^{(2)}[J[\phi]] = G_k[\phi] = \frac{1}{\Gamma_k^{(2)}[\phi] + R_k}. \quad (2.26)$$

With (2.26) of the propagator we arrive at the Wetterich equation [21], the functional renormalisation group equation (ERGE) or flow equation for the effective action,

$$\partial_t \Gamma_k[\phi] = \frac{1}{2} \text{Tr} \frac{1}{\Gamma_k^{(2)}[\phi] + R_k} \partial_t R_k = \frac{1}{2} \int_p \frac{1}{\Gamma_k^{(2)}[\phi] + R_k}(p, -p) \partial_t R_k(p^2), \quad (2.27)$$

Wetterich Equation

Figure 2.4.: Diagrammatic representation of the Wetterich equation (2.27). The circled cross stands for the insertion of the regulator, $\otimes = \partial_t R_k$.

where $t = \ln k/\Lambda$. The first account of such a functional renormalisation group equation has been given by Symanzik in his seminal papers on the -functional- Callan-Symanzik equation [22, 23]. While derived with a mass cutoff, $R_k = k^2$, the option of more general, momentum-dependent cutoff functions is mentioned. As already discussed above, the Wetterich equation can be structurally understood as a modified Legendre transform of the Polchinski equation [20] while also changing from an ultraviolet to an infrared cutoff. Note that the latter substitution is a seemingly trivial step but is crucially important for applications. The Polchinski equation was introduced for facilitating proofs of perturbative renormalisability. In this context (2.27) has been also used in the work of Bonini, D'Attanasio and Marchesini [24]. Its relation to the Polchinski equation and further initial development have been achieved by Ellwanger [25] and Morris [26]. Becchi has given an account of (2.27) (with an UV cutoff) in lecture notes published in [27]. Inserting the sharp cutoff given in eq. (2.9) the Wetterich equation becomes the Wegner-Houghton equation of the seminal paper [14]. For more structural developments and details we defer the interested reader to [9] and references therein.

2.2. Properties of the Wetterich equation

Equation (2.27) is the central result of this chapter and is the master equation from which flows for correlation functions are computed in the remainder of this work. Hence we close with a discussion of some important properties and its generality. In Section 2.2.1 and Section 2.2.2 we discuss the functional structure of the Wetterich equation and its renormalisation group properties. For this analysis we will simply assume the finiteness of all expressions, which is then proven in Section 2.2.3.

2.2.1. Diagrammatics, DSEs, and the 1PI property

The Wetterich equation (2.27) has a simple one loop exact form, see also Figure 2.4. Another appealing property is its sole dependence on $\Gamma^{(2)}[\phi]$, no classical vertices $S^{(n)}[\phi]$ are involved. The latter are present in the DSE, see (1.28) and Figure 1.2(a). They are also present in other functional equations such as two-particle or even n -particle irreducible approaches. The latter even lack the closed form, they have infinite loop representations. This combination of one loop exactness and the occurrence of only $\Gamma^{(n)}$ is paid for with the necessity of a further integration, namely that over the RG-time t , for more details see [28]. Whether or not this is a price to be paid gladly depends on the problem under investigation. Moreover, solving for correlation functions in a theory also allows for a combined use of functional equations, which allows for more flexibility.

For an optimal use of functional relations it is necessary to understand their diagrammatic structure. For a better comparison of the Wetterich equation with the functional DSE for $\Gamma^{(1)} = \delta\Gamma/\delta\phi$ we take one

Figure 2.5.: Diagrammatic representation of the flow of $\Gamma^{(1)}[\phi]$ in 2.28.

field-derivative of the flow equation. This leads us to

$$\partial_t \Gamma_k^{(1)}[\phi] = -\frac{1}{2} \text{Tr} \left[\Gamma_k^{(3)}[\phi] \cdot (G_k[\phi] \cdot \partial_t R_k \cdot G_k[\phi]) \right], \quad (2.28)$$

for the diagrammatic representation see Figure 2.5. The term in parenthesis represents a line with the regulator or cutoff insertion. Taking field derivatives of the Wetterich equation will lead to one loop diagrams with full vertices and propagator, where one line has the cutoff insertion. The left hand side of (2.28) is nothing but the scale-derivative of the left hand side of the DSE, (1.28), see also Figure 1.2(a). In comparison, (2.28) lacks the higher loop terms present in the DSE if the classical action has four-point vertices or even higher order vertices. The FRG for $\partial_t \Gamma^{(1)}[\phi]$ only features a one loop term for general theories. However, instead the classical three-point vertex $S^{(3)}[\phi]$ it depends on the full three-point function $\Gamma^{(3)}[\phi]$. This entails that both exact functional equations comprise different resummation schemes. Moreover, FRG and DSE for the same correlation function $\Gamma^{(n)}$ require different vertices $\{\Gamma^{(m)}\}$ as an input. Hence, depending on the different complexity of the input for the one or the other functional relation either FRG or DSE may be better adapted. We will discuss this property again within QCD applications.

As in the case of the DSE, the Wetterich equation allows for a simple proof of the fact, that the effective action Γ generates 1PI correlation functions. For that purpose it is sufficient to show that a 1PI input on the right hand side of the flow equation only generates 1PI diagrams. Then this property will persist upon integration of the flow. For this discussion we only require a formal solution of the flow equation (2.27): Its right hand side only depends on the two-point function $\Gamma^{(2)}[\phi]$ only. Its flow is obtained by another derivative of (2.28),

$$\partial_t \Gamma_k^{(2)}[\phi] = \frac{1}{2} \text{Tr} \left[\left(-\Gamma_k^{(4)}[\phi] + 2 \Gamma_k^{(3)}[\phi] \cdot G_k[\phi] \cdot \Gamma_k^{(3)}[\phi] \right) \cdot (G_k[\phi] \cdot \partial_t R_k \cdot G_k[\phi]) \right], \quad (2.29)$$

with the diagrammatic representation Figure 2.6. Note that the contribution with the three-point function represents the sum of two terms. In one of them the cutted line ($G \cdot \partial_t R_k \cdot G$) is the upper one as in Figure 2.6, in the other diagram the cutted line is the lower one. The diagrams give identical contributions which leads to (2.29). Now we assume that the input $\Gamma_k[\phi]$ is 1PI. Then, the flow (2.29) contains only 1PI diagrams: First we notice that if we insert a 1PI diagram for a three or four point function into a one loop diagram, we only generate 1PI diagrams. The same holds true for loop contributions of the propagator. More concisely we state that a one loop diagram in full 1PI vertices and (inverse) two-point functions is 1PI. This concludes our proof. Note that we have assumed that the input is 1PI which holds for the classical action. Strictly speaking we still have to prove that the classical action is a valid input for $k \rightarrow \infty$, where all quantum fluctuations are suppressed. This is discussed in Section 2.2.2.

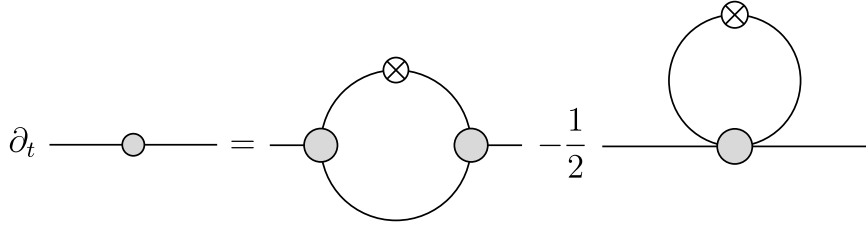


Figure 2.6.: Diagrammatic representation of the flow equation for the two-point function.

We close this chapter with a remark on possible solutions of the flow equation. All flow equations so far are full functional equations and solving either of them solves the QFT at hand. For example, if we solve the flow for the two-point function in (2.29), we can simply integrate the flow equation for the effective action $\Gamma_k[\phi]$ or that for $\Gamma_k^{(1)}[\phi]$. However, a solution for either of these functional integro-differential equations is usually not possible, at least for sufficiently rich theories. Hence, we have to expand the flow equation in a given systematic expansion scheme. Various schemes will be discussed in Section 2.3. Here, we simply notice that the flow for $\Gamma_k[\phi]$, evaluated at some field configuration ϕ_0 , for example $\phi = 0$, depends on the three- and four-point vertices $\Gamma^{(3)}[\phi_0]$ and $\Gamma^{(4)}[\phi_0]$. The related flows are obtained from (2.29) with one or two further field derivatives. The structure of the flows makes it apparent, that the term with the highest correlation function in $\partial_t \Gamma^{(n)}$ is the tadpole with $\Gamma^{(n+2)}$,

$$\partial_t \Gamma_k^{(n)}[\phi] = -\frac{1}{2} \text{Tr} \left[\Gamma_k^{(n+2)}[\phi] \cdot (G_k[\phi] \cdot \partial_t R_k \cdot G_k[\phi]) + \Gamma^{(m < n+2)} - \text{terms} \right]. \quad (2.30)$$

see also (2.104) in Section 2.3.3. Evaluated at ϕ_0 this results in an infinite hierarchy of coupled integro-differential equations. As mentioned above, systematic expansion schemes, truncations and systematic error control will be discussed in Section 2.3 and ??.

2.2.2. Full effective action and RG-consistency

Finally we are interested in full correlation functions at $k = 0$ with a vanishing cutoff $\Delta S_{k=0}[\phi] \equiv 0$. Initialising the flow at a large cutoff scale $k \rightarrow \Lambda$ leads to a well-defined initial condition where perturbation theory can be applied, at least in asymptotically free theories. The picture we have for infrared regulators satisfying the regulator conditions 2.8 is that of a successive integration of momentum shells with momenta. This appealing picture is depicted in Figure 2.7. This picture suggests that the flow equation is indeed UV & IR finite, which will be shown in detail in Section 2.2.3. For now we simply assume this which leads us to a representation of the full effective action $\Gamma[\phi] = \Gamma_{k=0}[\phi]$ in terms of the integrated flow,

$$\Gamma[\phi] = \int_{\Lambda}^0 \frac{dk}{k} \partial_t \Gamma_k[\phi] + \Gamma_{\Lambda}[\phi]. \quad (2.31)$$

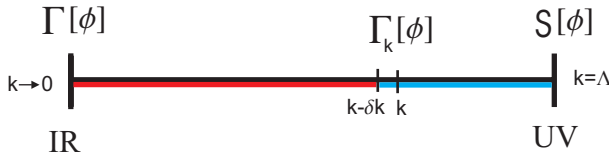


Figure 2.7.: Scale-dependent or flowing effective action $\Gamma_k[\phi]$: It is the full quantum effective action for physics with momenta $p^2 \gtrsim k^2$ (blue interval). The quantum physics of momenta $p^2 \lesssim k^2$ is not included in $\Gamma_k[\phi]$, which serves as an effective classical for this regime (red interval).

In (2.31) the effective action $\Gamma_\Lambda[\phi]$ specifies the theory and the physical parameters such as masses and couplings. In our ϕ^4 -theory example the theory is determined by three parameters

$$\Gamma_\Lambda[\phi] = \Gamma_\Lambda[\phi; Z_\phi, m_\Lambda^2, \lambda_\Lambda], \quad (2.32)$$

which are the parameters of the three different operators in the classical action, $[(\partial_\mu \phi)^2]$, $[\phi^2]$ and $[\phi^4]$. In the following we will also use the terminology that all parameters of a theory (except for the wave function renormalisation) are called couplings including the mass parameters.

Heuristically we expect that the effective action tends towards the classical action in the ultraviolet. This holds indeed true in a slightly generalised meaning,

$$\lim_{k \rightarrow \infty} \Gamma_\Lambda[\phi] = S_{\text{UV}}[\phi, R_\Lambda]. \quad (2.33)$$

where $S_{\text{UV}}[\phi, R_\Lambda]$ contains all UV-relevant terms in the theory that are allowed by the symmetries (or breaking of symmetries) of the theory in the presence of ΔS_k . In the setting with (2.27) all UV-relevant terms of the UV action run according to their dimension which can be easily seen by a Λ -derivative of (2.31). We use that the left hand side, the effective action at vanishing cutoff, $\Gamma[\phi]$, knows nothing about Λ . More generally it does not even depend on the chose regulator $R_k(p^2)$,

$$\frac{\delta}{\delta R_k(p^2)} \Gamma[\phi] \equiv 0. \quad (2.34)$$

Equation (2.34) entails the *RG-consistency* of the renormalisation procedure, for more details see [9, 19]. Note that substituting Γ by $\Gamma_{k'}$ for a general cutoff scale k' in (2.34), this does not vanish but describes the regulator-dependence of the theory. Equation (2.34) is nothing but the independence of the full theory on the UV cutoff as well as on the regularisation procedure. Assuming this property we arrive at

$$\Lambda \partial_\Lambda \Gamma_\Lambda[\phi] = \frac{1}{2} \text{Tr} \frac{1}{\Gamma_\Lambda^{(2)}[\phi] + R_\Lambda} \Lambda \partial_\Lambda R_\Lambda, \quad (2.35)$$

Hence, the UV-effective action $S_{\text{UV}}[\phi, R_\Lambda]$ runs according to (2.35). This will be discussed in detail at the example of one and two loop perturbation theory in Section 2.3.1. It also follows from the form of the flow equation that all UV-relevant terms will be generated that are not forbidden by the symmetries of $S[\phi] + \Delta S_k$. We will come back to this point later in ??.

For the flowing UV action with a few UV-relevant terms it is possible to absorb the Λ -running in the fields and couplings of the theory in a *finite* re-normalisation procedure. This finally leads to a renormalised UV action with $\lim_\Lambda \Lambda \partial_\Lambda S_{\text{UV,ren}}[\phi, R_\Lambda] \rightarrow 0$. Such a setting has the appealing property that the renormalised flow only describes the integration of physical fluctuations in contrast to reparameterisations of the theory. More details can be found in [9, 10].

The above discussion clarifies the rôle of the initial effective action $\Gamma_\Lambda[\phi] \propto S[\phi]$ as the classical UV action that specifies the theory. The structure of the flow equation entails that within the first RG step with $\Lambda \rightarrow \Lambda - \Delta k$ we generate all order interaction terms. This can be seen easily with $S^{(2)}[\phi] = S^{(2)}[0] + S_{\text{int}}[\phi]$ with the interacting part $S_{\text{int}}[\phi] = S^{(2)}[\phi] - S^{(2)}[0]$ and an expansion of the propagator about that with $S^{(2)}[0]$. In summary the flow generates all terms that are not forbidden by the symmetry of the flow equation itself and the input $\Gamma_\Lambda[\phi]$. The important topic of the fate of symmetries, and in particular gauge symmetries is discussed in ??.

2.2.3. UV & IR finiteness and momentum locality of RG-steps

Now we come back to the important question of the UV and IR finiteness of the Wetterich equation (2.27). This finiteness is indeed an immediate consequence of the properties 2.8 of the regulator function $R_k(p^2)$. With these properties the UV and IR finiteness of the flow equation follows from the respective limits $p^2/k^2 \rightarrow 0, \infty$. For the ultraviolet limit $p^2/k^2 \rightarrow \infty$ the right hand side of the flow equation satisfies

$$p^d \frac{1}{\Gamma_k^{(2)}[\phi] + R_k}(p, -p) \partial_t R_k(p^2) \xrightarrow{p^2/k^2 \rightarrow \infty} 0, \quad (2.36)$$

for sufficiently fast decaying regulator functions $R_k(p^2)$. Here, the prefactor p^d comes from the momentum integration in (2.27). All the examples given in 2.9 decay at least exponentially for large momenta or even vanish identically for momenta $p^2 > k^2$. In turn, regulators with an algebraic decay should at least compensate the momentum integration divided by the dispersion $\Gamma^{(2)}(p, -p)$. Standard bosonic relativistic theories have a dispersion p^2 for large momenta. This leads to

$$p^{d-2} R_k(p^2) \xrightarrow{p^2/k^2 \rightarrow \infty} 0. \quad (2.37)$$

This bound can be reduced further by p^2 if taking one ϕ -derivative in theories with momentum-independent couplings. This leads us to the flow of the one-point function in (2.28), depicted in Figure 2.5. Taking the ϕ -derivative removes the field-independent part of the flow of effective action, which is the most divergent part. For momentum-independent classical couplings it can be shown that $\Gamma_k[\phi]$ does not rise with powers of momentum for large momenta. Hence, the additional propagator leads to an additional $1/p^2$ decay for $p^2 \rightarrow \infty$. Assuming diagonal propagators in momentum space for asymptotically large momenta we are led to

$$p^d \left[\frac{1}{\Gamma_k^{(2)}[\phi] + R_k}(p, -p) \right]^2 \partial_t R_k(p^2) \xrightarrow{p^2/k^2 \rightarrow \infty} p^{d-4} R_k(p^2) \rightarrow 0. \quad (2.38)$$

Note that even the weaker bound excludes the Callan-Symanzik (CS) regulator $R_k(p^2) = k^2$ in dimensions $d \geq 4$.

However, even though the CS flow is finite in lower dimensions, CS flows are conceptually different from flows with a decaying regulator choice. This originates in the fact that the mass m or better the respective field operator $[\phi(x)^2]$ is a relevant operator in the QFTs under investigation. Hence, the CS flow is a flow in the space of theories. In turn, a decaying regulator function with the property (2.28) relates to the operator $[\phi(x)R_k(-\partial_x^2)\phi(x)]$ which is not a relevant operator in the QFTs under investigation. It can be seen as a perturbation of a fixed QFT. Then, the UV-finiteness of the flow for decaying regulators with (2.28) reflects this property. Note that the converse does not hold as is proven by the Callan-Symanzik example in lower dimensions.

This consideration leads us to a necessary property for functional renormalisation group flows that supposedly integrate out momentum shells in a fixed physical QFT. Such an FRG should lead to subleading

changes of the ultraviolet relevant correlation functions, an example being the mass. This *momentum locality* can be summarised in a relative decay of the flow $\partial_t \Gamma^{(n)}$ in comparison to the correlation function itself, $\Gamma^{(n)}$ at the symmetric point, see [29],

$$\left[\frac{\partial_t \Gamma_k^{(n)}[p_1, \dots, p_n]}{\Gamma_k[p_1, \dots, p_n]} \right]_{p_i^2 = p^2} \xrightarrow{p^2/k^2 \rightarrow \infty} 0. \quad (2.39)$$

Note that (2.39) cannot hold for general momentum configurations with $p_i^2 \rightarrow \infty$ as one has to guarantee that also all momentum transfers diverge. Equation (2.39) has been put forward in the context of quantum gravity where the momentum dependence of the classical vertices make it a highly non-trivial statement even for decaying regulators. We also emphasise that (2.39) is a necessary but not a sufficient property for a local RG procedure.

We close this discussion with the remark that even with the momentum locality of the RG-step (and hence the UV finiteness of the flow) finite re-normalisations of the relevant parameters of the theory are still necessary as can be seen from RG-consistency with (2.35).

The infrared finiteness of the flow equation for $p^2 \rightarrow 0$ follows from the fact that the regulator functions act as a mass for low momenta. Without loss of generality we take regulators with $R_k(0) = k^2$. For the sake of simplicity we also restrict ourselves to constant fields and arrive at

$$\frac{1}{\Gamma_k^{(2)}[\phi] + R_k}(p, -p) \partial_t R_k(p) \xrightarrow{p^2/k^2 \rightarrow 0} \frac{2k^2}{\Gamma_k^{(2)}[\phi] + k^2} \quad (2.40)$$

Equation (2.40) makes explicit that for low momenta the regulator function leads to an additional mass Δm^2 , in most cases normalised to k^2 . For the sharp cutoff case, 2.9c, this mass is even infinite. Hence, even if the classical theory was massless, the infrared regularised theory is not. Note however, that this argument, as it stands, has to be taken with a grain of salt. $\Gamma_k^{(2)}[\phi]$ can be and is in many cases negative for small momenta and small fields. In our example this property signals a non-trivial minimum of the effective action for a non-vanishing field value related to spontaneous symmetry breaking. Still, in these cases $\Gamma_k^{(2)} + R_k > 0$. Strictly speaking the latter is loose notation as $\Gamma_k^{(2)} + R_k$ is an operator. What is meant are positive spectral values or eigenvalues: $\Gamma_k^{(2)} + R_k$ is the Hessian of $\Gamma_k + \Delta S_k$, which is the legendre transformation of the Schwinger functional \mathcal{W}_k . Hence it is convex with a positive semi-definite Hessian. Indeed one can show that the flow equation has convexity-restoring properties, and a pole in the propagator cannot be reached, for more details see [30]. This property will be illustrated explicitly within the derivative expansion, see Section 2.3.4 and ??.

2.3. Systematic expansion schemes

In the last two chapters, [Section 2.1](#) and [Section 2.2](#), we have introduced the flow equation for the effective action, [\(2.27\)](#) as well as discussing in details its general properties and finiteness. In this approach the flow equation interpolates between a well-controlled initial condition, $\Gamma_\Lambda[\phi] \simeq S[\phi]$ in the ultraviolet for $k \rightarrow \infty$ and the full quantum effective action in the infrared for $k \rightarrow 0$. We have also seen that already one RG step $k \rightarrow k - \Delta k$ generates all (infinitely many) new interaction terms due to the resummation structure of the flow. These terms have to obey the underlying symmetries constraints of the underlying theory realised in the input effective action $\Gamma_\Lambda[\phi]$ as well as that of the flow equation. This intertwined structure makes it very important to discuss the symmetry identities of the theory in the presence of the cutoff term, which will be done in details in [??](#).

In summary the effective action consists of all combinations of the fields and their derivatives which satisfy the underlying symmetries of the theory. We write schematically

$$\Gamma_k[\phi] = \sum_{n \in \mathbb{N}} g_n \cdot O_n[\phi] \quad (2.41)$$

where g_n are the coupling constants or expansion coefficients for the functional basis $\{O_n[\phi]\}$. Note that schematic form [\(2.41\)](#) covers general expansion schemes. For example, the $O_n[\phi]$ could simply be monomials in the field,

$$O_n[\phi](x_1, \dots, x_n) = \prod_{i=1}^n \phi(x_i), \quad (2.42)$$

in which case we have

$$g_n \cdot O_n[\phi] = \int_{x_1, \dots, x_n} g_n(x_1, \dots, x_n) O_n[\phi](x_1, \dots, x_n), \quad \text{where} \quad g_n = \frac{1}{n!} \Gamma^{(n)}[\phi = 0]. \quad (2.43)$$

[Equation \(2.42\)](#) with [\(2.43\)](#) describe a vertex expansion of the effective action. Then the flow equation for $\Gamma_k[\phi]$ is written in terms of $\partial_t \Gamma_k^{(n)}[\phi = 0]$, or more generally in terms of $\partial_t \Gamma_k^{(n)}[\phi_0]$ with a background ϕ_0 . This approximation will be used in QCD and is described in more detail in [Section 2.3.3](#).

Another well known expansion is the loop expansion where the O_n are simply the n -loop contribution to the effective action,

$$g_n \cdot O_n[\phi] = \Delta \Gamma_{k,n}[\phi], \quad (2.44)$$

with the n -loop contributions $\Delta \Gamma_{k,n}[\phi]$ to the effective action. This expansion scheme reproduces perturbation theory. We discuss it in details in the next [Section 2.3.1](#) as it illuminates the implicit renormalisation procedure contained in the flow equation approach, as well as providing a simple example for the discussion of optimisation and systematic error control in [??](#). Moreover, it is a show case for expansion schemes that implement full systematic (re-) summations in the flow equation. Other examples are 2PI, n PI schemes as well as Parquet schemes. They are also discussed in [Section 2.3.1](#).

A further expansion scheme is the derivative expansion, where one systematically increases the number of derivatives of the fields in the effective action. This scheme is described in [Section 2.3.4](#).

Finally, these and other schemes can be combined into mixed schemes, such as the Blaizot-Mendez-Wschebor (BMW) scheme, [31, 32, 33] which combines the vertex expansion and derivative expansion. In practice, most applications use such mixed schemes implicitly or explicitly. On the one hand this makes it difficult to work out the systematics, and hence the systematic error. On the other hand a mixed scheme combines in most cases the advantages of both approaches and minimises the combined systematic error. The latter question as well as that of optimal regulators and the important one of convergence of a given scheme is discussed in a separate [??](#), after discussion a few examples before in [??](#).

2.3.1. Perturbative expansion

Renormalised perturbation theory to any order can be easily computed from the flow equation within an iterative procedure: Inserting the perturbative N -loop result for $\Gamma_k^{(2),N\text{-loop}}$ into the right hand side of the flow equation leads to the complete $N + 1$ -loop order of perturbation theory as well as higher loop contribution. Evidently, such an iterative approach is also amiable towards computer-algebra implementation and is a simple way to generate perturbative 1PI diagrams to any order including the combinatorial factors. Here we illustrate this at one-loop and two-loop perturbation theory, where we follow [34]. Perturbative results have been discussed e.g. in [35, 36, 37, 38, 34, 9, 10, 39, 40].

Iterative structure of perturbation theory

First, we write the scale-dependent effective action within a loop expansion as discussed in (2.44),

$$\Gamma_k^{N\text{-loop}} = S + \sum_{n=1}^N \Delta\Gamma_{k,n}, \quad \Gamma_k = \lim_{N \rightarrow \infty} \Gamma_k^{N\text{-loop}} \quad (2.45)$$

where S is the classical action and $\Delta\Gamma_{k,n}$ comprises the quantum corrections at n -th loop order. Now we want to show that the flow equation with the N -loop approximation of $\Gamma_k^{(2)}$,

$$\frac{1}{2} \text{Tr} \frac{1}{\Gamma_k^{(2),N\text{-loop}}[\phi] + R_k} = \partial_t \Gamma_k^{(N+1)\text{-loop}}[\phi] + O((N+2) - \text{loop}), \quad (2.46)$$

comprises all N -loop diagrams. If (2.46) holds true, the difference of (2.46) has to be of $N + 2$ -loop order. Note also that the flow in (2.46) contains perturbative loops to any order, as $1/(\Gamma_k^{(2),N\text{-loop}} + R_k)$ can be expanded in a series of perturbative loops. This is related to the resummation structure of the flow diagram. This argument is valid for any $N > 0$, while for $N = 0$ we have $\Gamma_k^{(2),0\text{-loop}} = S^{(2)}$ which does not contain any loop contribution, hence the expansion of the propagator terminates immediately.

Now we continue with our proof, and subtract the full flow from the flow (2.46), to wit,

$$\begin{aligned} \frac{1}{2} \text{Tr} \left[\frac{1}{\Gamma_k^{(2),N\text{-loop}} + R_k} - \frac{1}{\Gamma_k^{(2)} + R_k} \right] &= \frac{1}{2} \text{Tr} \left[\frac{1}{\Gamma_k^{(2)} + R_k} (\Gamma_k^{(2)} - \Gamma_k^{(2),N\text{-loop}}) \frac{1}{\Gamma_k^{(2),N\text{-loop}} + R_k} \right] \\ &= \frac{1}{2} \text{Tr} \left[\frac{1}{\Gamma_k^{(2)} + R_k} \left(\sum_{n>N} \Delta\Gamma_{k,n}^{(2)} \right) \frac{1}{\Gamma_k^{(2),N\text{-loop}} + R_k} \right] \\ &= + O((N+2) - \text{loop}). \end{aligned} \quad (2.47)$$

The step from the penultimate line to the last line comes from the fact, that the insertion in parenthesis, $\sum_{n>N} \Delta\Gamma_{k,n}^{(2)}$, is already of perturbative $N + 1$ -loop. It is inserted in the loop of the flow, which adds to the total perturbative loop number $N + 2$. This concludes our proof. In summary, starting at $N = 0$ with the classical two point function $S^{(2)}[\phi]$ we can iteratively generated full perturbation theory. This defines the systematic *Perturbative Expansion* in the FRG.

We emphasise that the flow generates the renormalised, finite perturbation series due to the finiteness of the flow equation, see Section 2.2.3. In the remainder of this chapter we discuss how the FRG regularisation and renormalisation procedure works at the example of the perturbative one-loop and two-loop effective action, and discuss the consequences for practical computations.

One loop perturbation theory

From the above argument we know that the one-loop effective action is obtained by evaluating the flow with the classical two-point function with $N = 1$. As already mentioned below (2.46), this is the only

order where only the next order, $N = 1$ and no higher loops are generated. Inserting eq. (2.45) with $N = 0$ into the Wetterich equation we find

$$\partial_t \Gamma_k^{1\text{-loop}}[\phi] = \frac{1}{2} \text{Tr} \frac{1}{S^{(2)}[\phi] + R_k} \partial_t R_k = \frac{1}{2} \text{Tr} [\partial_t \ln(S^{(2)}[\phi] + R_k)]. \quad (2.48)$$

The right hand side of (2.48) is already the t -derivative of the one-loop result we have already obtained from the DSE, see (1.38). In both cases it was a simple one line computation starting from the functional relation. Moreover, in both cases no reference to the specific theory has been made and the result is general.

An important difference concerns the renormalisation. While (1.38) is not finite and has to be renormalised, (2.48) is finite. This comes from the t -derivative which cannot be moved outside the trace. To see this more clearly we rewrite the formal expression for our ϕ^4 -theory example,

$$\partial_t \Gamma_k^{1\text{-loop}}[\phi] = \frac{1}{2} \int_p \partial_t \ln(S^{(2)}[\phi] + R_k)(p, -p). \quad (2.49)$$

Without the t -derivative the momentum integral in (2.49) diverges with Λ^d , if a UV momentum cutoff with $p^2 \leq \Lambda^2$ is applied. If we take field derivatives of (2.49) the degree of divergence is reduced by the additional powers of the propagators. Now we integrate (2.48) from a fixed UV cutoff Λ to an intermediate cutoff scale k with

$$\Gamma_k^{1\text{-loop}}[\phi] = \frac{1}{2} \text{Tr} \{\ln(S^{(2)}[\phi] + R_k) - \ln(S^{(2)}[\phi] + R_\Lambda)\} + \Gamma_\Lambda^{1\text{-loop}}[\phi]. \quad (2.50)$$

As for the t -derivative, only the trace of the difference in (2.50) is finite. Indeed, the second term at $k = \Lambda$ in the trace is nothing but the subtraction term that renders the effective action finite. The initial effective action is initiated at a sufficiently large cutoff scale and hence only includes the Λ -dependent classical action, while higher order terms are suppressed with inverse powers of the initial cutoff Λ . We have

$$\Gamma_\Lambda[\phi] = \int_x \left(\frac{1}{2} Z_{\phi,\Lambda} (\partial_\mu \phi)^2 + \frac{1}{2} m_\Lambda^2 \phi^2 + \frac{\lambda_\Lambda}{4!} \phi^4 \right) + \mathcal{O}(\Lambda^{-1}), \quad (2.51)$$

where the Λ -dependence of the relevant parameters $Z_{\phi,\Lambda}$, m_Λ^2 , λ_Λ is determined by RG-consistency, (2.35), which renders $\Gamma_k[\phi]$ Λ -independent.

The present simple one loop example already elucidates how the FRG-renormalisation and renormalisation works in general. The regularisation is done by discussion only soft momentum shells in the flow equation. The renormalisation is a renormalisation by subtraction. As such it is very reminiscent of the Pauli-Villars regularization where a divergent diagram is made finite by subtracting the same diagram with the particle's propagator replaced by the one of a fictitious heavy particle. It also relates to the Bogoliubov, Parasiuk, Hepp and Zimmermann (BPHZ) scheme allowing for rigorous proofs of perturbative renormalisability. Finally, it is a generalised version of the standard UV-cutoff procedure in momenta. We will come back to these relations in our two loop example where we can also discuss the cancellation of sub-divergencies and the iterative emergence of the Zimmermann forest formula. Note also that this structure is common to all FRGs discussed so far, in particular also to the Polchinski RG, which is very amiable towards facilitating proof of perturbative renormalisability.

With the regularisation and renormalisation procedure clarified, we are left with the question for the renormalisation conditions. This discussion will again bring up all parts of the renormalisation procedure in an even more obvious way. We evaluate (2.50) at $k = 0$, which gives us the full perturbative one loop effective action,

$$\Gamma^{1\text{-loop}}[\phi] = \frac{1}{2} \text{Tr} \{\ln(S^{(2)}[\phi]) - \ln(S^{(2)}[\phi] + R_\Lambda)\} + \Gamma_\Lambda^{1\text{-loop}}[\phi]. \quad (2.52)$$

It is left to fix the initial effective action $\Gamma_\Lambda[\phi; Z_\phi, m_\Lambda^2, \lambda_\Lambda]$ or rather the three relevant parameters in the theory, $(Z_\phi, m_\Lambda^2, \lambda_\Lambda)$. These parameters carry the cutoff dependence on Λ as well as fixing the physics. We expand them in a loop expansion,

$$m_\Lambda^2 = m^2 + c_{1,m^2} \lambda \Lambda^{d-2} + O(\lambda^2), \quad \lambda_\Lambda = \lambda + c_{1,\lambda} \lambda^2 \Lambda^{d-4} + O(\lambda^2), \quad (2.53)$$

with finite, dimensionless expansion coefficients $c_{n,m^2}(m^2/\Lambda^2)$ and $c_{n,\lambda}(m^2/\Lambda^2)$. Here, the n labels the loop level. For $d = 2$ and $d = 4$ respectively it is understood that $\Lambda^{d-2} \rightarrow \ln \Lambda^2/m^2$ and $\Lambda^{d-4} \rightarrow \ln \Lambda^2/m^2$, where the reference scale m has been chosen for the sake of convenience. The wave function renormalisation only receives contributions from two loop on,

$$Z_{\phi,\Lambda} = 1 + Z_{2,\phi} (\lambda \Lambda^{d-4})^2 + O(\lambda^3), \quad (2.54)$$

with $Z_{1,\phi} = 0$. The vanishing of the one loop contribution comes from the fact that the only diagram at one loop is the momentum-independent tadpole. This is discussed below (2.62). In ?? the Z_n 's are the coefficients of the n -loop contribution to the wave function renormalisation. We also used the standard normalisation to unity at tree level and a logarithmic running at $d = 4$. The cutoff dependence of the couplings $m_\Lambda^2, \lambda_\Lambda$ in (2.53) at one loop is given by

$$\begin{aligned} \Lambda \partial_\Lambda m_\Lambda^2 &= \left([(d-2) + 2\delta_{d,2}] c_{1,m^2} - 2 \frac{m^2}{\Lambda^2} c'_{1,m^2} \right) \lambda \Lambda^{d-2}, \\ \Lambda \partial_\Lambda \lambda_\Lambda &= \left([(4-d) + 2\delta_{d,4}] c_{1,\lambda} - 2 \frac{m^2}{\Lambda^2} c'_{1,\lambda} \right) \lambda^2 \Lambda^{d-4}, \end{aligned} \quad (2.55)$$

with $c'(x) = \partial_x c(x)$ and $x = m^2/\Lambda^2$. It is left to compute the coefficients c_{1,m^2} and $c_{1,\lambda}$. They are fixed by RG-consistency, as discussed in Section 2.2.2: the full effective action $\Gamma[\phi]$ does not depend on Λ leading to (2.35): $\Gamma_\Lambda[\phi]$ satisfies the flow equation. At one loop we have

$$\Lambda \partial_\Lambda \Gamma_\Lambda^{1\text{-loop}} = \frac{1}{2} \text{Tr} \frac{1}{S^{(2)} + R_\Lambda} \Lambda \partial_\Lambda R_\Lambda. \quad (2.56)$$

Inserting the initial effective action Γ_Λ in (2.51) into the flow (2.56) we can extract the flows of the wave function renormalisation $Z_{\phi,\Lambda}$ and couplings m_Λ^2 and λ_Λ by appropriate field and momentum derivatives at vanishing field and momentum. More explicitly we consider the following second and fourth order ϕ -derivatives of (2.56) at $\phi = 0$ and external momentum $p = 0$,

$$\begin{aligned} \Lambda \partial_\Lambda Z_{\phi,\Lambda} &= \partial_p^2 \Lambda \partial_\Lambda \Gamma_\Lambda^{(2)} \Big|_{\phi=0,p=0}, \\ \Lambda \partial_\Lambda m_\Lambda^2 &= \Lambda \partial_\Lambda \Gamma_\Lambda^{(2)} \Big|_{\phi=0,p=0}, \\ \Lambda \partial_\Lambda \lambda_\Lambda &= \Lambda \partial_\Lambda \Gamma_\Lambda^{(4)} \Big|_{\phi=0,p=0}. \end{aligned} \quad (2.57)$$

As this is the first of many projections of this type we will perform this computation step by step: we first take the second and fourth derivatives of $\Gamma_\Lambda[\phi]$ in (2.51) in space-time,

$$\begin{aligned} \Gamma_\Lambda^{(2)}[\phi](x_1, x_2) &= \left[-Z_{\phi,\Lambda} \partial_\mu^2 + m_\Lambda^2 + \frac{1}{2} \lambda_\Lambda \phi^2(x_1) \right] \delta(x_1 - x_2), \\ \Gamma_\Lambda^{(4)}(x_1, x_2, x_3, x_4) &= \lambda_\Lambda \delta(x_1 - x_2) \delta(x_1 - x_3) \delta(x_1 - x_4). \end{aligned} \quad (2.58)$$

In (2.58) the space-time argument of ∂_μ has been dropped as it can be either x_1 or x_2 . While $\Gamma_\Lambda^{(2)}$ has a field-dependence, $\Gamma_\Lambda^{(4)}$ has none as Γ_Λ only contains local terms up to the ϕ^4 -term. It is also

straightforward to extend the equations above the more general actions and higher correlation functions. Local actions in terms of the field and its derivatives as the classical one will always generate $n - 1$ δ -functions and expressions that are local in space-time. Naturally, the flow also generated interactions that are spread in space time, for example $\Gamma_k^{(2)}(x_1, x_2)$ will have parts proportional to the δ -function $\delta(x_1 - x_2)$ and its derivatives as in (2.58), but also has regular parts. However, these regular parts are non-local and hence should vanish for $\Lambda \rightarrow \infty$ where the effective action reduces to its local -classical- counterpart.

After the Fourier transformation to momentum space the above expressions read

$$\begin{aligned}\Gamma_{\Lambda}^{(2)}[\phi](p_1, p_2) &= [Z_{\phi, \Lambda} p_1^2 + m_{\Lambda}^2] (2\pi)^d \delta(p_1 + p_2) + \frac{1}{2} \lambda_{\Lambda} \int_q \phi(q) \phi(p_1 + p_2 - q), \\ \Gamma_{\Lambda}^{(4)}(p_1, p_2, p_3, p_4) &= \lambda_{\Lambda} (2\pi)^d \delta(p_1 + p_2 + p_3 + p_4).\end{aligned}\quad (2.59)$$

The momentum integral in the two-point functions originates in the fact that products of functions in position space turn into convolutions in momentum space. However, in case we restrict ourselves to constant fields ϕ_c in space-time, their Fourier transformation is given by

$$\phi(p) = \phi_c (2\pi)^d \delta(p). \quad (2.60)$$

Then, the two-point function in (2.59) reads

$$\Gamma_{\Lambda}^{(2)}(p, q) = \Gamma_{\Lambda}^{(2)}(p) (2\pi)^d \delta(p + q), \quad \text{with} \quad \Gamma_{\Lambda}^{(2)}(p) = \left[Z_{\phi, \Lambda} p^2 + m_{\Lambda}^2 + \frac{1}{2} \lambda_{\Lambda} \phi_c^2 \right], \quad (2.61)$$

where we have defined the local part $\Gamma_{\Lambda}^{(2)}(p)$ without the δ -function. This is a common notation which we shall use from now on. Equation (2.61) facilitates the projection on higher correlation functions at vanishing momenta, one only takes further standard derivatives with respect to the constant field, $\partial_{\phi_c}^n$.

Applying $n = 2$ derivatives to $\Gamma_{\Lambda}^{(2)}[\phi_c]$ we arrive at $\Gamma_{\Lambda}^{(4)}$ in (2.59).

With (2.59) the flows in (2.57) follow by inserting. The right hand sides of the respective flow equations follow by applying the same field- and momentum derivatives to the right hand side of the flow equation (2.27). For the flow of the wave function renormalisation $Z_{\phi, k}$ and the mass parameter m_{Λ}^2 we resort to the full flow for $\Gamma_k^{(2)}$ at $k = \Lambda$ in (2.29), see also Figure 2.6. As the current analysis applies to general local actions we keep the general scale k . The diagram with $\Gamma_k^{(3)}$ vanishes as $\Gamma_k^{(3)}[\phi = 0] \equiv 0$. We are left with the tapole diagram,

$$\partial_t \Gamma_k^{(2)}[\phi = 0](p_1, p_2) = -\frac{1}{2} \text{Tr} \Gamma_k^{(4)} \cdot (G_k \partial_t R_k G_k). \quad (2.62)$$

Equation (2.62) carries no dependence on the external momenta due to momentum conversation and the momentum independence of classical coupling, see (2.59). Hence, $\partial_{p_1}^2 \Gamma_k^{(2)} = 0$ leading to

$$Z_{1, \phi} = 0. \quad (2.63)$$

Note also that $\Gamma^{(2)}[\phi = 0]$ has the diagonal form (2.61), and often the δ -function that carries the total momentum conversation, here $(2\pi)^d \delta(p_1 + p_2)$ is dropped on both sides in a slight abuse of notation.

The flow of the coupling is derived from that of the four point functions. At vanishing fields $\phi = 0$ and vanishing momenta we have

$$\partial_t \Gamma_k^{(4)}[\phi = 0](0, 0, 0) = 3 \text{Tr} [\Gamma_k^{(4)} \cdot G_k \cdot \Gamma_k^{(4)}] \cdot (G_k \partial_t R_k G_k), \quad (2.64)$$

where we have dropped the δ -function that carries the total momentum conversation, $(2\pi)^d \delta(p_1 + \dots + p_4)$. The momentum dependence of this flow and its momentum channels is discussed in more detail in Section 2.3.3 below (2.108).

The right hand sides of (2.62) and (2.64) have to be evaluated in momentum space. To that end we use the momentum representation of the propagators,

$$G_k(p, q) = G_k(q) (2\pi)^d \delta(p + q), \quad \text{with} \quad G_k(q) = \frac{1}{q^2 + m_k^2 + R_k(q)}, \quad (2.65)$$

for a k -dependent action of the form (2.51) with $\Lambda \rightarrow k$. As for the two-point function we have defined the local part $G_k(q)$. Evidently, (2.65) is the inverse of $\Gamma_k^{(2)}(p, q) + R_k(q)(2\pi)^d \delta(p + q)$ with $\Gamma_k^{(2)}(p, q)$ in (2.61) at $\phi_c = 0$ and $k = \Lambda$, which can be shown by insertion,

$$\int_q G(p_1, q) (\Gamma_k^{(2)} + R_k)(q, p_2) = (2\pi)^d \delta(p_1 + p_2). \quad (2.66)$$

Inserting (2.61) and (2.65) into (2.62) we arrive at

$$\partial_t \Gamma_k^{(2)}(p) = -\frac{\lambda}{2} \int_q G_k(q) \partial_t R_k(q) G_k(q) = -\frac{\lambda}{2} \int_q G_k(q)^2 \partial_t R_k(q). \quad (2.67)$$

At $p = 0$ this is simply the flow $\partial_t m_k^2$. The same steps as above can be applied to the flow of $\partial_t \Gamma_k^{(4)}(0, 0, 0)$ in (2.68), leading us to

$$\partial_t \Gamma_k^{(4)}(0, 0, 0) = 3\lambda^2 \int_q [G_k(q)] (\Gamma_k^{(2)}(q) \partial_t R_k(q) G_k(q)) = 3\lambda^2 \int_q G_k(q)^3 \partial_t R_k(q). \quad (2.68)$$

The structure of the two equations, even though at present purely perturbative, occurs very often in applications of flow equations: flows of correlation function at vanishing external momenta have one cutted line $G_k \partial_t R_k G_k(q)$, and a product of further $(n - 1)$ propagators $G_k(q)$, where n counts the number of vertices in the diagram. Neglecting the q -dependence of the vertices we are led to integrals such as in (2.67) and (2.68). It is straightforward to see that in the presence of mass scales m_k^2 in the propagators G_k the integrals vanish for $k \rightarrow 0$ with powers of k^2/m_k^2 . In turn, above this threshold they are non-vanishings. Hence they are called *Threshold Functions*, and flows are often written in terms of these threshold functions.

We proceed with the explicit computation of the flows for m_k^2 and λ_k . The diagrams are rewritten in a manifestly dimensionless way with

$$k^2 G_k(q) = \frac{1}{y} \frac{1}{1 + \frac{\bar{m}^2}{y} + r}, \quad \frac{1}{k^2} \partial_t R_k(q) = -2y^2 r'(y), \quad \text{where} \quad \bar{m}^2 = \frac{m^2}{k^2} \quad y = \frac{q^2}{k^2}. \quad (2.69)$$

with $R_k(q) = q^2 r(q^2/k^2)$ defined (2.6) which leads to (2.7) used in 11.25. With 11.25 we derive immediately from (2.56) and (2.67) the flows $\partial_t m_k^2$ and $\partial_t \lambda_k$. We also see that we have a uniform $1/y$ -dependence in the propagator G_k that carries the momentum dependence of the classical propagator. This uniformity is only spoiled by \bar{m}^2/y which introduces the mass threshold to the flows. For the sake of simplicity we first restrict ourselves to $\bar{m}^2 = 0$. Solving the flows for the one loop coefficients c_{1,m^2} and $c_{1,\lambda}$ leads us to

$$\begin{aligned} c_{1,m^2} &= \frac{1}{[(d-2) + 2\delta_{2,d}]} \frac{\Omega_d}{2(2\pi)^d} \int_0^\infty dy y^{\frac{d}{2}-1} \frac{y^2 r'(y)}{[y(1+r(y))]^2}, \\ c_{1,\lambda} &= -\frac{1}{[(d-4) + 2\delta_{4,d}]} \frac{3\Omega_d}{(2\pi)^d} \int_0^\infty dy y^{\frac{d}{2}-1} \frac{y^2 r'(y)}{[y(1+r(y))]^3}, \end{aligned} \quad (2.70)$$

where Ω_d is the angular volume in d dimensions,

$$\frac{1}{k^d} \int \frac{d^d q}{(2\pi)^d} = \frac{\Omega_d}{2(2\pi)^d} \int_0^\infty dy y^{\frac{d}{2}-1}, \quad \text{with} \quad \Omega_d = \frac{2\pi^{\frac{d}{2}}}{\Gamma\left(\frac{d}{2}\right)}. \quad (2.71)$$

and the Gamma function $\Gamma(x)$. In general, the coefficients c_1 depend on the shape function, as the integrals in (2.70) do. Hence we have $c = c[r]$. This is part of the scheme dependence of the FRG renormalisation scheme. The proportionality to powers of Λ makes clear that the c_n -terms with $n > 0$ do not play a rôle in the full effective action $\Gamma_{k=0}$, which does not depend on Λ . It is the zeroth order parameters m^2, λ that carry the physics of the theory. In summary with the trivial wave function renormalisation at one loop, $Z_\lambda^{(1\text{-loop})} = 1$, the initial effective action $\Gamma_\Lambda[\phi]$ in $d = 4$ at one loop is given by

$$\begin{aligned} \Gamma_\Lambda[\phi; 1, m_\Lambda^2, \lambda_\Lambda] &= S[\phi; 1, m^2, \lambda] + \Delta\Gamma_{\Lambda,1}[\phi], \\ \Delta\Gamma_{\Lambda,1}[\phi] &= \lambda \int_x \left\{ \frac{1}{2} c_{1,\Lambda} \Lambda^2 \phi^2 + \frac{1}{4!} c_{1,\lambda} \lambda \ln \frac{\Lambda^2}{\mu^2} \phi^4 \right\}. \end{aligned} \quad (2.72)$$

which is nothing but $S[\phi; 1, m_\Lambda^2, \lambda_\Lambda]$. In (2.72) the scale μ is some reference scale. Evidently, a change in μ can be absorbed in λ in $S[\phi; 1, m^2, \lambda]$, the two are not independent. In terms of derivatives this relation reads

$$\mu \partial_\mu \lambda = 2c_{1,\lambda} \lambda^2, \quad (2.73)$$

which is nothing but the definition of the standard β -function. In summary we have recovered the standard result for the one loop effective action within a completely finite setup. The different parts of the perturbative renormalisation program, regularisation and re-normalisation, are easily identified.

We proceed with discussing one-loop universality of logarithmically running couplings in the current setup. To that end we restrict ourselves to $d = 4$ and compute the flow $\partial_t \lambda_k$. From (2.55) we get the one loop flow in $d = 4$ with $\partial_t \lambda = 2c_{1,\lambda}[r]$. The coefficient $2c_{1,\lambda}[r]$ is read off from (2.70) with $\Lambda \rightarrow k$. With $\beta_\lambda = \partial_t \lambda_k$ we get for the one loop β -function

$$\beta_\lambda^{1\text{-loop}} = 2c_{1,\lambda}[r]\lambda^2 = -\frac{3\Omega_4}{(2\pi)^4} \lambda^2 \int_0^\infty dy \frac{r'(y)}{[1+r(y)]^3} = \frac{3\lambda^2}{8\pi^2} \int_0^\infty dy \partial_y \left[\frac{1}{[1+r(y)]^2} - 1 \right] = \frac{3}{16\pi^2} \lambda^2, \quad (2.74)$$

the well-known universal result. The r -independence of the result comes from the fact that the flow is dimensionless. For dimensionless flow diagrams at one loop with vanishing external momenta the integrand can be written in general form, ($d \neq 2$),

$$\int_0^\infty dy \frac{r'(y)}{(1+r)^{d-1}} = \frac{1}{d-2}, \quad (2.75)$$

independent of the shape function r . In turn, dimensionful flows explicitly depend on the shape function, see e.g. $\partial_t m_k^2$ with the coefficient $c_{1,m^2}[r]$ in (2.70). This can be made explicit by taking a functional $r(x)$ -derivative of the coefficients c_1 with $x = p^2/k^2$. We restrict ourself to $d = 4$ dimensions and obtain

$$\frac{\delta c_{1,m^2}[r]}{\delta r(x)} = \frac{1}{32\pi^2} \int_0^\infty dy \left(\partial_y \delta(y-x) \frac{y}{[1+r(y)]^2} - 2\delta(y-x) \frac{y r'(y)}{[1+r(y)]^3} \right) = -\frac{1}{32\pi^2} \frac{1}{[1+r(x)]^2}. \quad (2.76)$$

[Equation \(2.76\)](#) again contains implicitly the universality of the dimensionless couplings. The only term left after inserting the δ -function and its derivatives comes from the derivative of y in the denominator of the term with r' . For a coupling g with momentum dimension d_g we have a y^{d_g} -dependence. Hence, for $d_g = 0$ the variation in [\(2.76\)](#) vanishes. Note also that this argument relies on the absense of further mass scales.

Let us now reinstate the mass m^2 in the expression [\(2.72\)](#) originating in the propagators, see [11.25](#). Now we re-evaluatate the one loop β -function. Instead of its computation we apply a $r(x)$ derivative in $d = 4$ dimensions as done for c_{1,m^2} in [\(2.76\)](#).

$$\frac{\delta c_{1,\lambda}[r]}{\delta r(x)} = -\frac{3}{16\pi^2} \int_0^\infty dy \left(\frac{\partial_y \delta(y-x)}{[1 + \frac{\bar{m}^2}{y} + r(y)]^3} - 3 \frac{\delta(y-x) r'(y)}{[1 + \frac{\bar{m}^2}{y} + r(y)]^4} \right) = \frac{9}{16\pi^2} \frac{\bar{m}^2}{x^2} \frac{1}{[1 + r(x)]^4}. \quad (2.77)$$

[Equation \(2.77\)](#) vanishes in both asymptotic momentum regimes: a change of the shape function for $x \gg 1$ does not change $c_{1,\lambda}$. All mass scales are suppressed in the UV and we arrive back at the universal result [\(2.74\)](#). In turn, in the IR for $x/\bar{m}^2 \rightarrow 0$ the gapping with the explicit mass scale \bar{m}^2 suppresses all effects from changing the shape function. In summary, for $m^2 \neq 0$ and finite k the β -function w.r.t. the k -scaling is not universal as the factors $c(m^2/k^2)$ depend on the shape function r . This is related to the fact that the k -dependence encodes the full momentum dependence of physics, while the standard β -functions encode the asymptotic scaling. At one loop it is simple to disentangle the different scalings. From two loop on this starts becoming more difficult. For example, two loop universality is only present for mass-independent RG schemes. The standard FRG scheme is not mass-independent and it would not bring any advantages to fix such a scheme. Nonetheless, two-loop universal β -functions have been computed from the FRG, see e.g. [\[35, 38\]](#). For more details on mapping the FRG scheme to standard perturbative schemes see e.g. [\[35, 36, 37, 38, 34, 9, 10, 39, 40\]](#).

An important final remark concerns the symmetries in the flow. Most of the analysis above has been done for $m^2 = 0$. Nonetheless the flow for the mass does not vanish at $m^2 = 0$ in contradistinction to the situation in dimensional regularisation. Accordingly, the flow does not preserve the presence of massless modes. This comes as no surprise as the cutoff term itself is a momentum-dependent mass term and as such lifts the mass of fields. The fate of symmetries during the flow will be discussed in [??](#).

Two loop perturbation theory

We close this chapter with the formal discussion of the two-loop effective action. This sheets some light in the subtraction procedure at higher order. For the two-loop complete effective action we have to use the one loop two point function $\Gamma_k^{(2),1\text{-loop}}[\phi] = S^{(2)}[\phi] + \Delta\Gamma_{k,1}^{(2)}[\phi]$ in the flow equation and expand the flow up to two loop, see also the discussion below [\(2.47\)](#). This leads us to

$$\begin{aligned} \partial_t \Gamma_k^{2\text{-loop}}[\phi] &= \frac{1}{2} \text{Tr} \frac{1}{S^{(2)}[\phi] + \Delta\Gamma_{k,1}^{(2)}[\phi] + R_k} \partial_t R_k \Big|_{2\text{-loop}} \\ &= \frac{1}{2} \text{Tr} \frac{1}{S^{(2)}[\phi] + R_k} \partial_t R_k - \frac{1}{2} \text{Tr} \frac{1}{S^{(2)}[\phi] + R_k} \Delta\Gamma_{k,1}^{(2)}[\phi] \frac{1}{S^{(2)}[\phi] + R_k} \partial_t R_k. \end{aligned} \quad (2.78)$$

The first part in the last line of [\(2.78\)](#) comprises $\partial_t \Gamma_k^{1\text{-loop}}$, while the second part contains the two-loop term. For the computation of the latter we need $\Delta\Gamma_{k,1}^{(2)}$ which can be derived from [\(2.50\)](#) by taking two field derivatives,

$$\Delta\Gamma_{k,1}^{(2)} = \frac{1}{2} \left[\text{Tr} \frac{1}{S^{(2)} + R_k} S^{(4)} - \text{Tr} \frac{1}{S^{(2)} + R_k} S^{(3)} \frac{1}{S^{(2)} + R_k} S^{(3)} \right]_\Lambda^k + \Delta\Gamma_{\Lambda,1}^{(2)}. \quad (2.79)$$

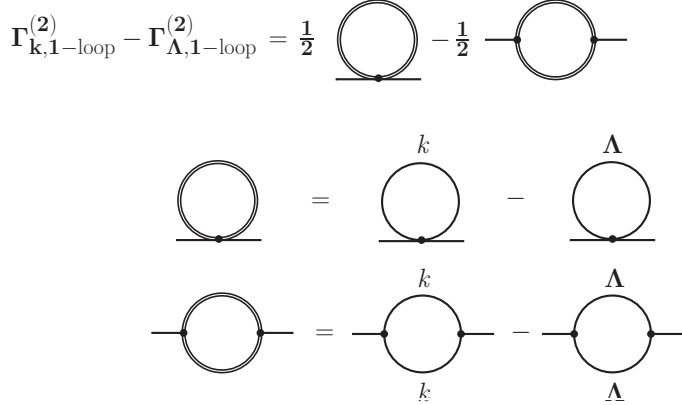


Figure 2.8.: Upper panel: Graphical representation of (2.79).

Lower panel: Graphical representation of the subtracted diagrams (double lines). The scale dependence of the perturbative propagator (full line) is due to the regulator term R_k , hence the index k or Λ .

The graphical representation of (2.79) is depicted in Figure 2.8. The double line loops stand for loops at k with the subtraction at $k = \Lambda$. The rest of the computation is either followed in terms of diagrams or one has to resort to a more concise notation. Here we offer both. The concise notation is given by de Witt's condensed notation, where all indices such as momentum p (or space-time x), Lorentz indices μ and internal indices are summarised with indices i, j, \dots . The propagator of the scalar field is then given by

$$G_k(p, p') = G_{k,ij}, \quad \text{with} \quad i = p, j = p'. \quad (2.80)$$

With this short hand notation the flow equation has the simple form

$$\partial_t \Gamma[\phi] = \frac{1}{2} G_{k,ij} \partial_t R_{k,ji}. \quad (2.81)$$

Reducing the explicit indices even more we get a concise expression for the one loop two-point function in (2.79),

$$(\Delta \Gamma_{k,1}^{(2)})_{ij} = \frac{1}{2} \left[(G_k \cdot S^{(4)})_{ij} - (G_k \cdot S^{(3)} \cdot G_k \cdot S^{(3)})_{ij} \right]_{\Lambda}^k + (\Delta \Gamma_{\Lambda,1}^{(2)})_{ij}, \quad (2.82)$$

where the propagator $G_k = 1/(S^{(2)} + R_k)$ in (2.82) is the classical propagator. Inserting (2.82) in (2.78) leads us to

$$\partial_t \Delta \Gamma_{k,2} = -\frac{1}{2} \left(\frac{1}{2} \left[G_k \cdot S^{(4)} - G_k \cdot S^{(3)} \cdot G_k \cdot S^{(3)} \right]_{\Lambda}^k + \Delta \Gamma_{\Lambda,1}^{(2)} \right)_{ij} (G \cdot \partial_t R_k \cdot G)_{ji}, \quad (2.83)$$

see also Figure 2.9. The expression in (2.83) is manifestly finite and Λ -independent, as the one-loop insertion is Λ -independent. Equation (2.83) is also a total derivative with respect to t . For the proof of this property we have to use that

$$\partial_t G_k|_{\Gamma_k^{(2)} = S^{(2)}} = -G_k \cdot \partial_t R_k \cdot G_k. \quad (2.84)$$

$\frac{1}{4} \left[- \begin{array}{c} \text{Diagram 1} \\ \otimes \end{array} + \begin{array}{c} \text{Diagram 2} \\ \otimes \end{array} \right]$

Figure 2.9.: Two loop contribution to the flow of the effective action, (2.83).

Now we discuss separately the different classes of diagrams in (2.83). The first diagram is the vacuum 'eight', while the second diagram is the vacuum 'sunset'. The last part is proportional to the one loop part of the two-point function $\Delta\Gamma_{\Lambda,1}^{(2)}$ of the initial effective action, inserted into the loop of the flow equation. This part removes all the Λ -dependencies in (2.83). We first discuss the vacuum 'eight',

$$-\frac{1}{4} (G_k \cdot S^{(4)} - G_\Lambda \cdot S^{(4)})_{ij} (G_k \cdot \partial_t R_k \cdot G_k)_{ji} = \frac{1}{8} \partial_t [(G_k - G_\Lambda) \cdot S^{(4)} \cdot (G_k - G_\Lambda)]. \quad (2.85)$$

For convenience we have added a term without k -dependence, $1/8(G_\Lambda \cdot S^{(4)} \cdot G_\Lambda)$, in the square bracket. This term does not give any contribution after the t -derivative is applied. However, it leads to a finite expression already in the square bracket. Upon integration from $k = \Lambda$ to $k = 0$ and with $G_{k=0} = G$ we are led to

$$\Delta\Gamma_2^{\text{eight}} = \frac{1}{8} (G - G_\Lambda) \cdot S^{(4)} \cdot (G - G_\Lambda), \quad (2.86)$$

the finite vacuum 'eight', renormalised by subtraction. Note that (2.86) is symmetric under $k \leftrightarrow \Lambda$, but the total expression is anti-symmetric under $k \leftrightarrow \Lambda$. However, this symmetry is only present for the full term including the vacuum 'sunset' and the initial two-point function piece. Now we turn to the vacuum 'sunset'. Similarly we have

$$\begin{aligned} & \frac{1}{4} (G_k \cdot S^{(3)} \cdot G_k \cdot S^{(3)} - G_\Lambda \cdot S^{(3)} \cdot G_\Lambda \cdot S^{(3)})_{ij} (G_k \cdot \partial_t R_k \cdot G_k)_{ji} \\ &= -\frac{1}{12} \partial_t [(G_k - G_\Lambda) \cdot S^{(3)} \cdot (G_k - G_\Lambda) \cdot S^{(3)} \cdot (G_k + 2G_\Lambda)], \end{aligned} \quad (2.87)$$

where we have added a k -independent term in the square bracket, $1/6(G_\Lambda \cdot S^{(3)} \cdot G_\Lambda \cdot S^{(3)})$, in order to render it finite, similarly to the situation in the vacuum 'eight'. As for the vacuum eight, we are led to a finite result upon integration from $k = \Lambda$ to $k = 0$,

$$\Delta\Gamma_2^{\text{sunset}} = -\frac{1}{12} (G - G_\Lambda) \cdot S^{(3)} \cdot (G - G_\Lambda) \cdot S^{(3)} \cdot (G + 2G_\Lambda). \quad (2.88)$$

As in the case of the vacuum 'eight', (2.88) is not anti-symmetric under $k \leftrightarrow \Lambda$. Note that the only antisymmetric combination at a finite cutoff scale k is proportional to $(G_k - G_\Lambda)^3$. It can be easily shown e.g. with mixed scale derivatives $\Lambda\partial_\Lambda \partial_t \Gamma_k = 0$, that this cannot hold true.

In conclusion, only the full combination including that proportional to the insertion $\Delta\Gamma_{\Lambda,1}^{(2)}$ has this symmetry, in which case it will not be apparent. For the insertion term we simply quote the result of the analysis similar to that above for the vacuum 'eight' and 'sunset' diagrams,

$$\Delta\Gamma_2^{\text{insert}} = \frac{1}{2} (G - G_\Lambda) \cdot \Delta\Gamma_{\Lambda,1}^{(2)}. \quad (2.89)$$

Figure 2.10.: Two loop contribution to the effective action, (2.90).

Summing up all terms, (2.86), (2.88), (2.89), we are led to the final result

$$\Delta\Gamma_2 = \Delta\Gamma_2^{\text{eight}} + \Delta\Gamma_2^{\text{subset}} + \Delta\Gamma_2^{\text{insert}} + \Delta\Gamma_{\Lambda,2}, \quad (2.90)$$

see also Figure 2.10. The last term is the two loop contribution of the initial effective action. RG-consistency fixed the Λ -dependence of this term via (2.35),

$$\Lambda\partial_\Lambda\Delta\Gamma_{\Lambda,2} = \frac{1}{2}\text{Tr}\left.\frac{1}{\Gamma_\lambda^{(2)} + R_\Lambda}\right|_{2\text{-loop}}\Lambda\partial_\Lambda R_\Lambda, \quad (2.91)$$

which can be evaluated similarly to the one loop case. This provides the Λ -independence of $\Delta\Gamma_2$. We remark, that with (2.91) the symmetry under $k \leftrightarrow \Lambda$ is apparent. The higher loops follow straightforwardly, all expressions are finite as well as Λ -independent. Note that this result trivially implies the independence on the choice of the shape function $r(p^2/k^2)$.

We have already mentioned in the beginning of this chapter, that the FRG renormalisation procedure bears some similarity to the Pauli-Villars schemes due to the subtraction of heavy fictitious particles, to Bogoliubov, Parasiuk, Hepp and Zimmermann due to the organisation of the subtractions as well as to momentum cutoff schemes such as e.g. used in DSE applications. We close this chapter with a brief discussion of the latter resemblance. To that end we re-visit the one loop two point function (2.79) and insert a sharp regulator function 2.9c. Now we evaluate the loops at vanishing field, $\phi = 0$, and vanishing external momentum, $p = 0$. The diagrams are either proportional to $G(q) - G_\Lambda(q)$ or $[G(q) - G_\Lambda(q)]^2$. For the sharp cutoff the tree level propagator $G_\Lambda(q) = 1/(S^{(2)} + R_\Lambda)$ has the property

$$G_\Lambda(q) = G(q)\theta(q^2 - \Lambda^2). \quad (2.92)$$

Accordingly the loops vanish for momenta $q^2 > \Lambda^2$ and we arrive at the result

$$\Delta\Gamma_1^{(2)}(0) = \int_q \left[\frac{1}{2}G(q)S^{(4)}(q, -q, 0, 0) - G(q)S^{(3)}(q, 0, -q)G(q)S^{(3)}(q, 0, -q) \right] \theta(\Lambda^2 - q^2) + \Delta\Gamma_{1,\Lambda}^{(2)}(0). \quad (2.93)$$

This is reminiscent of the standard momentum cutoff for loop momenta. Note however, that for non-vanishing external momenta the Heaviside θ -functions also depend on the external momenta, and the consistent cutoff procedure does not simply consist in $q^2 \leq \Lambda^2$ for the loop momenta q .

2.3.2. Complete resummations*

The perturbative expansion discussed in the last chapter is but one expansion scheme that rely on the systematic diagrammatic expansion. In the case of perturbation theory it is an expansion in terms of

the classical (tree level) propagator and the tree level vertices. There are many different diagrammatic expansion schemes that are not based on the tree level quantities.

Important and very useful ones are two-particle irreducible (2PI) expansion schemes (also called Kadanoff-Baym or Φ -derivable) based on the 2PI effective action. In the context of the FRG the 2PI and nPI effective actions are discussed in [9] including a derivation of the 1PI flow equation from the 2PI effective action as well as the discussion of genuine 2PI flows. A lucid introduction to the 2PI approach and non-equilibrium applications is given in [41].

The 2PI approach is based on a further reduction of the diagrammatics going from 1PI diagrams to 2PI diagrams. The respective generating functional is the 2PI effective action. Practically it depends on the mean field and on the propagator as variable. Accordingly it is derived from the Schwinger functional with currents for $\varphi(x)$ and for $\varphi(x)\varphi(y)$. Note that the regulator function $R_k(p^2)$ is nothing but a restricted current for the latter, we simply have to generalise the cutoff term to regulator functions $R(x, y)$ with

$$\Delta S[\phi; R] = \frac{1}{2} \int_{x,y} \phi(x) R(x, y) \phi(y). \quad (2.94)$$

The 2PI Schwinger functional then depends on J and R , $\mathcal{W} = \mathcal{W}[J, R]$ with the path integral representation

$$e^{\mathcal{W}[J, R]} = \int [d\varphi]_{\text{ren}} e^{-S[\varphi] - \frac{1}{2} \int_{x,y} R(x, y) \varphi(x) \varphi(y) + \int_x J(x) \varphi(x)}. \quad (2.95)$$

The 2PI effective action $\Gamma[\phi, G]$ is now defined via a double Legendre transformation with respect to J and R ,

$$\Gamma[\phi, G] = \int_x J(x) \phi(x) - \frac{1}{2} \int_{x,y} R(x, y) [G(x, y) + \phi(x) \phi(y)] - \mathcal{W}[J, R], \quad (2.96)$$

where the suprema of J, R as in the definition of the 1PI effective action, (1.7), are implicitly understood. This leads us immediately to the relations

$$\frac{\delta \mathcal{W}[J, R]}{\delta J(x)} = \phi(x), \quad \frac{\delta \mathcal{W}[J, R]}{\delta R(x, y)} = -\frac{1}{2} [G(x, y) + \phi(x) \phi(y)], \quad (2.97)$$

and

$$\frac{\delta \Gamma[\phi, G]}{\delta \phi(x)} = J(x) - \int_y R(x, y) \phi(y), \quad \frac{\delta \Gamma[\phi, G]}{\delta G(x, y)} = -\frac{1}{2} R(x, y). \quad (2.98)$$

Equation (2.97) signifies $\phi(x)$ as the mean field and $G(x, y)$ as the propagator. The 1PI effective action is obtained from the 2PI effective action if evaluating the latter on the EoM for the propagator, the gap equation. This reads

$$\Gamma[\phi] = \Gamma[\phi, G_{\text{EoM}}[\phi]], \quad \text{with} \quad \left. \frac{\delta \Gamma[\phi, G]}{\delta G(x, y)} \right|_{G=G_{\text{EoM}}} = 0. \quad (2.99)$$

The EoM for the propagator implies that $R(x, y)$ vanishes for which (2.95) reduces to the standard Schwinger functional. Moreover, for $R(x, y) = 0$ the Legendre transformation in (2.96) reduces to the 1PI Legendre transformation for the 1PI effective action, (1.7).

With this setup the derivation of the 1PI flow equation is a one-liner: First we realise that the first three terms on the right hand side of (2.96) are $\Gamma_k[\phi]$ for $R(x, y) = R_k(x, y)$ with $R_k(x, y) = R_k(-\partial^2) \delta(x - y)$.

Accordingly this implies that the 1PI effective action in the presence of the infrared cutoff term is given by

$$\Gamma_k[\phi] = \Gamma[\phi, G_k] + \frac{1}{2} \int_{x,y} R(x,y) G_k(x,y), \quad (2.100a)$$

where $G_k(x,y)$ is defined by the modified equations of motion,

$$\left. \frac{\delta \Gamma[\phi, G]}{\delta G(x,y)} \right|_{G=G_k} = -\frac{1}{2} R_k(x,y). \quad (2.100b)$$

The flow equation (2.27) follows from 2.100 as

$$\begin{aligned} \partial_t \Gamma[\phi] &= \int_{x,y} \partial_t G_k \left(\frac{\delta \Gamma[\phi, G_k]}{\delta G_k} + \frac{1}{2} R_k(x,y) \right) + \frac{1}{2} \int_{x,y} G_k(x,y) \partial_t R_k(x,y) \\ &= \frac{1}{2} \text{Tr } G_k \partial_t R_k. \end{aligned} \quad (2.101)$$

Similarly to the derivation of the flow equation for the 1PI effective action from that of \mathcal{W}_k , the derivation in (2.101) used even more explicitly, that dependencies on the variable in the Legendre transformation drops out. In the present case this variable is G_k .

The above is a simple derivation of the flow equation, even though its simplicity is certainly in the eye of the beholder. In turn, the flow equation can be also of use in the 2PI approach. In this approach systematic expansion schemes with the full propagators are used for the 1PI effective action based on the gap equation (2.99), the most prominent ones being 2PI perturbation theory in the full propagator and perturbative vertices, and the $1/N$ -expansion for a large number N of fields, e.g. [41]. These loop expansions have to be renormalised which is a notoriously difficult problem. Hence, expansion schemes for the flow equation that generate the above mentioned 2PI expansion schemes solve the renormalisation task in the 2PI approach in a systematic and self-consistent way. This was put forward in [42] and extended in [43, 44, 45, 46]. As in perturbation theory the resulting flows lead upon integration to regulator-independent results for the effective action: they constitute total derivatives with respect to t and the result has no dependence on the initial scale due to RG-consistency (2.35). For more details we refer to [9, 42, 43, 44, 45, 46] and references therein.

Another interesting resummation scheme is the Parquet resummation with and without combination of 2PI techniques, for this and further related schemes we refer the interested reader to e.g. [47, 48, 49, 50, 51], and literature therein.

In summary systematic *resummation schemes* implement complete resummations obtained within other functional methods in a manifestly and consistently renormalised way in the FRG. The regulator dependence drops out at any order of such an expansion. The simplest example is the perturbative expansion, which has been discussed in Section 2.3.1.

2.3.3. Vertex expansion

In the last two chapters, Section 2.3.1 and Section 2.3.2 we have discussed how to recover complete diagrammatic expansion schemes within the FRG in a systematic and finite way. In non-perturbative numerical application such a setup can cure potential problems with non-perturbative loop divergencies. The diagrammatic expansion is reflected in the missing regulator dependence of the integrated flow in any order of the expansion, if RG-consistency is taken into account. This relates to the fact that the flow can be represented as a total derivative with respect to t and has explicitly shown at one and two loop perturbation theory in Section 2.3.1.

In the present chapter we discuss the first expansion scheme that is 'inherently' an FRG scheme. Within such a scheme the flow equation loses its total derivative nature in a given order N of the expansion scheme. The necessary regulator independence is then recovered for $N \rightarrow \infty$ assuming the convergence of the expansion. The regulator independence of physical observables is an important self-consistency check for 'inherent' FRG schemes such as the vertex expansion. It is discussed in more detail in the context of optimisation in ??.

The vertex expansion is used in particular in QCD, [52, 53, 54, 55, 56, 57] and quantum gravity, [58, 59, 29, 60, 61, 62, 63, 64, 65]. In this scheme the scale-dependent effective average action Γ_k is expanded in the power of fields, as already sketched in the introduction to Section 2.3 in (2.42) and (2.43) for an expansion about a vanishing background. In general the background $\bar{\phi}$, can be non-vanishing, for example a non-trivial (monimal) solution to the equation of motion. In this case we expect a better convergence of the expansion scheme as we expand about the physical saddle point. In the ϕ^4 -theory this leads us to

$$\Gamma_k[\phi] = \sum_{n=0}^{\infty} \frac{1}{n!} \int_{x_1, \dots, x_n} \Gamma_k^{(n)}[\bar{\phi}](x_1, \dots, x_n) [\phi(x_1) - \bar{\phi}(x_1)] \cdots [\phi(x_n) - \bar{\phi}(x_n)], \quad (2.102)$$

with the 1PI vertices $\Gamma_k^{(n)}[\bar{\phi}]$. Note that the ϕ^4 -theory is invariant under $\phi \rightarrow -\phi$. This Z_2 -symmetry implies for the effective action,

$$\Gamma_k[-\phi] = \Gamma_k[\phi]. \quad (2.103)$$

Accordingly, all odd vertices vanish identically in the vanishing background $\bar{\phi} = 0$ and $\phi = 0$ is a solution to the EoM. The property (2.103) can be also proven from the flow equation: with a Z_2 -symmetric input $\Gamma_k[\phi]$ the flow maintains the symmetry. It only depends on $\Gamma_k^{(2)}[\phi]$ which is Z_2 -symmetric if $\Gamma_k[\phi]$ is. More details on symmetries and flow equations can be found in ??.

In the vertex series eq. (2.102) the information in the effective action is comprised in the set the expansion coefficients, $\{\Gamma_k^{(n)}[\bar{\phi}]\}$, the set of 1PI correlation functions or 1PI vertices. The theory is solved if these vertices are known. The flow equation for the $\Gamma_k^{(n)}[\bar{\phi}]$ is obtained by the n th derivative of the master flow equation (2.27) for the effective action. Schematically this leads us to

$$\begin{aligned} \partial_t \Gamma[\bar{\phi}] &= \frac{1}{2} \text{Tr} G_k \partial_t R_k, \\ \partial_t \Gamma^{(1)}[\bar{\phi}] &= -\frac{1}{2} \text{Tr} \Gamma_k^{(3)} (G_k \partial_t R_k G_k), \\ \partial_t \Gamma^{(2)}[\bar{\phi}] &= -\frac{1}{2} \text{Tr} [\Gamma_k^{(4)} - 2 \Gamma_k^{(3)} G_k \Gamma_k^{(3)}] (G_k \partial_t R_k G_k), \\ \partial_t \Gamma^{(3)}[\bar{\phi}] &= -\frac{1}{2} \text{Tr} [\Gamma_k^{(5)} - 6 \Gamma_k^{(4)} G_k \Gamma_k^{(3)} + 6 \Gamma_k^{(3)} G_k \Gamma_k^{(3)} G_k \Gamma_k^{(3)}] (G_k \partial_t R_k G_k), \\ \partial_t \Gamma^{(4)}[\bar{\phi}] &= -\frac{1}{2} \text{Tr} [\Gamma_k^{(6)} - 8 \Gamma_k^{(5)} G_k \Gamma_k^{(3)} - 6 \Gamma_k^{(4)} G_k \Gamma_k^{(4)} + 18 \Gamma_k^{(4)} G_k \Gamma_k^{(3)} G_k \Gamma_k^{(3)} \\ &\quad + 12 \Gamma_k^{(3)} G_k \Gamma_k^{(4)} G_k \Gamma_k^{(3)} - 24 G_k \Gamma_k^{(3)} G_k \Gamma_k^{(3)} G_k \Gamma_k^{(3)} \cdot G_k \Gamma_k^{(3)}] (G_k \partial_t R_k G_k), \\ &\vdots && \vdots \end{aligned} \quad (2.104)$$

where $G_k = G_k[\bar{\phi}]$, the propagator in the given background $\bar{\phi}$ and $(G_k \partial_t R_k G_k)$ is the line with the regulator insertion. From (2.104) we immediately conclude that the zero- and one-point function do

not enter the flow of the higher correlation functions. The two-point function $\Gamma_k^{(2)}$ is the lowest order correlation function that enters the fully coupled subset of flows via the propagator. This already suggests to use the flow equation for $\Gamma_k^{(2)}[\phi]$ for general fields as the master equation instead of the flow equation for the effective action: the two-point function flow already generates the set of all correlation function $\{\Gamma_k^{(n \geq 2)}\}$. The effective action and one-point function can then be computed from this set, see their flows in (2.104).

We also clearly see in (2.104) that the diagram in the flow for $\Gamma_k^{(n)}$ with the highest order vertex is the tadpole with $\Gamma_k^{(n+2)}$ as discussed around (2.30). Note also that the flow equations for $\Gamma_k^{(2n+1)}$ vanishes at $\bar{\phi} = 0$, as to the contributions on the right hand side from these vertices. We have chosen a general background in (2.104) in order to provide some insight in the general structure: Equation (2.104) elucidates the quick growth of the number of diagrams as well as the simple systematics behind it. However, for the following discussion it is also convenient to have a look at the simpler system at $\bar{\phi} = 0$, where all vertices $\Gamma_k^{(2n+1)}$ and flows vanish. Then the above system reduces to

$$\begin{aligned}\partial_t \Gamma[0] &= \frac{1}{2} \text{Tr } G_k \partial_t R_k , \\ \partial_t \Gamma^{(2)}[0] &= -\frac{1}{2} \text{Tr } \Gamma_k^{(4)} (G_k \partial_t R_k G_k) , \\ \partial_t \Gamma^{(4)}[0] &= -\frac{1}{2} \text{Tr } [\Gamma_k^{(6)} - 6 \Gamma_k^{(4)} G_k \Gamma_k^{(4)}] (G_k \partial_t R_k G_k) , \\ &\vdots \quad \vdots \end{aligned}\tag{2.105}$$

This very impressive reduction bases on a fundamental symmetry of the theory already points at the importance of using the underlying symmetries of the theory within given expansion schemes. First, at higher orders of a given scheme it may decide about the algebraic and numerical accessibility of the computations. Second, for gauge symmetries such as the non-Abelian symmetry in QCD and diffeomorphism invariance in quantum gravity it may additionally be important for the conceptual reliability of the setup, see ??.

For the current discussion of the vertex expansion scheme it is more important to realise that in both cases, with and without non-vanishing background, the towers of equations do not close. This property is shared by a vertex expansion of the functional DSE.

Now we set up the systematic *Vertex Expansion*: we consider the series (2.102) up to a highest order N_V on the right hand side of the flow equations in (2.104),

$$\Gamma_k[\phi; N_V] = \sum_{n=0}^{N_V} \frac{1}{n!} \int_{x_1, \dots, x_n} \Gamma_k^{(n)}[\bar{\phi}](x_1, \dots, x_n) [\phi(x_1) - \bar{\phi}(x_1)] \cdots [\phi(x_n) - \bar{\phi}(x_n)] ,\tag{2.106}$$

with

$$\lim_{N_V \rightarrow \infty} \Gamma_k[\phi; N_V] = \Gamma_k[\phi] .\tag{2.107}$$

This expansion converges quickly, if the higher order vertices give subleading contributions to the flows of all the $\Gamma^{(n)}$. For the computation of the lower order $\Gamma_k^{(n)}$ it is already sufficient, if the contribution of the higher order vertices give subleading contributions to their flow. In any case, even though the flow of all vertices is in general non-vanishing for a given finite $N_V > 2$, $\partial_t \Gamma_k^{(n)} \neq 0$ for all n , the vertices with $n > N_V$ do not couple back to the flow.

As an example we consider $N_V = 4$ in (2.104) or (2.105). Then the algebraic form of the flows $\partial_t \Gamma_k^{(n \leq 2)}$ does not change as they only depend on $\Gamma_k^{(n>4)}$. In turn, the flows $\partial_t \Gamma_k^{(3)}$ and $\partial_t \Gamma_k^{(4)}$ loose the diagrams

with $\Gamma_k^{(5)}$ and $\Gamma_k^{(6)}$ respectively. Here we show the flow for $\Gamma_k^{(4)}[0]$, that is in a vanishing background,

$$\partial_t \Gamma_k^{(4)}[0] = 3 \text{Tr} \left[\Gamma_k^{(4)} G_k \Gamma_k^{(4)} \right] \cdot \left(G_k \partial_t R_k G_k \right), \quad (2.108)$$

as already discussed at vanishing momentum in one loop perturbation theory, see (2.64), (2.68). Only one diagram class is left (the fish diagram), the tapole with $\Gamma_k^{(6)}$ is dropped. We rush to add that even though the algebraic form of the flows $\partial_t \Gamma_k^{(n \leq 2)}$ does not change, their result does. The flows depend on $\Gamma^{(3)}$, $\Gamma^{(4)}$, whose flows change, hence do they. This is already one of the technical reasons why the results for the lower order vertices converges rather quickly in a derivative expansion under certain well-defined circumstances discussed below.

Before we come to this we want to discuss the four-point function flow (2.108) in more detail. First we note that the prefactor three in (2.108) stands for the three different classes of diagrams depending on which two of the four external legs, related to the $\phi(x_i), \phi(x_2)$, or $\phi(p_i), \phi(x_2)$ in momentum space, share the same vertex. We continue the discussion in momentum space as also most of the computations will be done there. In the current example the (inverse) two- and four-point functions are required,

$$\begin{aligned} \Gamma_k^{(2)}(p_1, p_2) &= \Gamma_k^{(2)}(p_1) (2\pi)^d \delta(p_1 + p_2), \\ \Gamma_k^{(4)}(p_1, p_2, p_3, p_4) &= \Gamma_k^{(4)}(p_1, p_2, p_3) (2\pi)^d \delta(p_1 + p_2 + p_3 + p_4). \end{aligned} \quad (2.109)$$

where we pulled out the respective δ -functions that entail momentum conservation. Note also that all momenta are counted as incoming. General n -point functions $\Gamma^{(n)}$, momentum conservation are proportional to $\delta(p_1 + \dots + p_n)$ and hence depends on $(n - 1)$ momenta,

$$\Gamma_k^{(n)}(p_1, \dots, p_n) = \Gamma_k^{(n)}(p_1, \dots, p_{n-1}) (2\pi)^d \delta(p_1 + \dots + p_n). \quad (2.110)$$

Now we use that in momentum space diagrams can be classified the momentum flow through the diagram in terms of the Mandelstam variables

$$s = (p_1 + p_2)^2, \quad t = (p_1 + p_3)^2 \quad u = (p_1 + p_4)^2, \quad (2.111)$$

defining the s , t , and u channels. In momentum space each of the vertices in (2.108) carries two of the four external momenta p_1, \dots, p_4 , for example the 'incoming' momenta p_1 and p_2 . These momenta have to flow through the diagram, and the respective momentum channel is the s -channel. Let us now consider the s channel diagram in (2.108). It reads

$$\partial_t \Gamma_k^{(4)} \Big|_{s\text{-channel}} = \int_q \Gamma_k^{(4)}(p_1, p_2, q) \left[G_k(q + p_1 + p_2) (G_k \partial_t R_k G_k)(q) \right] \Gamma_k^{(4)}(-q, p_3, p_4), \quad (2.112)$$

with $p_4 = -(p_1 + p_2 + p_3)$, see the first diagram in ??, where the sum of all channels is depicted. The expression in the square bracket contains the propagators in the loop, one of which has the cutoff insertion, $G_k \partial_t R_k G_k$. Within the standard notation the line with the cutoff insertion carries only the loop momentum. This is particularly convenient if applying derivatives with respect to external moment in the presence of non-analytic regulators such as the Litim or the sharp regulators, 2.9.

In the current order of the vertex expansion scheme, $N_V = 4$, the only other non-trivial flow is that of the two-point function. For $\bar{\phi} = 0$ there is only one diagram, the tapole. We conclude

$$\partial_t \Gamma_k^{(2)}(p) = -\frac{1}{2} \int_q \Gamma_k^{(4)}(p, -p, q) \left[(G_k \partial_t R_k G_k)(q) \right], \quad (2.113)$$

where, as in (2.112), the square bracket contains the propagator in the loop. For the tadpole there is only the one with the cutoff insertion. Note that (2.113) is the exact equation for the two-point function at $\bar{\phi} =$

0 as already mentioned before. If the full non-perturbative four-point function $\Gamma^{(4)}(p_1, p_2, q)$ is given, the solution of (2.113) would be the exact two-point function. We also deduce from (2.113) that a constant vertex approximation leads to a momentum independent self-energy correction, $\partial_t \Gamma_k^{(2)}(p) = \partial_t m_k^2$. This renders the quantum dispersion trivial.

In the rest of this chapter we want to lay the foundation for the practical solution of flow equations in the vertex expansion scheme. The present, relatively simple approximation allows us to already discuss some of the most important standard choices and technicalities. More details follow in ?? where the present system is solved within some further approximation.

To begin with, we introduce dressing functions that take care of the renormalisation group properties of the correlation functions. In the current case we then have the parameterisation

$$\begin{aligned} \Gamma_k^{(2)}(p) &= Z_{\phi,k}(p^2) (p^2 + m_k^2), \\ \Gamma_k^{(4)}(p_1, p_2, p_3) &= \left[\prod_{i=1}^4 \sqrt{Z_{\phi,k}(p_i^2)} \right] \lambda_k(p_1, p_2, p_3), \end{aligned} \quad (2.114)$$

with $p_4^2 = (p_1 + p_2 + p_3)^2$. The multiplicative function $Z_{\phi,k}$ is the FRG-analogue of the wave function renormalisation. In the present formalism it carries, together with the mass m_k^2 , the full information about the propagator. The parameterisation is chosen such that the function $Z_{\phi,k}$ carries the anomalous scaling of the (inverse) propagator with the anomalous dimension

$$\eta_{\phi,k}(p^2) = -\frac{\partial_t Z_{\phi,k}(p^2)}{Z_{\phi,k}(p^2)}. \quad (2.115)$$

The four-point vertex is also parameterised such that the $Z_{\pi,k}$ -parts carry the anomalous scaling of the vertex. The vertex function $\lambda_k(p_1, p_2, p_3)$ carries the momentum-dependence of the scattering process of two fields. In the present order of the vertex expansion this is the full dynamics of the theory.

It is left to extract the three k and momentum dependent quantities, $Z_{\phi,k}(p^2)$, m_k^2 and $\lambda_k(p_1, p_2, p_3)$ from the flows of two- and four point function. The anomalous dimension (2.115) is obtained from the following flow,

$$\eta_{\phi,k}(p^2) = -\frac{\frac{\partial_t \Gamma_k^{(2)}(p^2)}{Z_{\phi,k}(p^2)} - \frac{\partial_t \Gamma_k^{(2)}(0)}{Z_{\phi,k}} - \eta_{\phi,k} m_k^2}{p^2 + m_k^2}, \quad \text{with} \quad Z_{\phi,k} = Z_{\phi,k}(0), \quad \eta_{\phi,k} = \eta_{\phi,k}(0). \quad (2.116)$$

while that of the mass function m_k^2 is simply given by

$$(\partial_t + \eta_{\phi,k}) m_k^2 = \frac{\partial_t \Gamma_k^{(2)}(0)}{Z_{\phi,k}}. \quad (2.117)$$

Finally, the flow of the momentum dependent coupling $\lambda_k(p_1, p_2, p_3)$ is given by

$$\left(\partial_t - \frac{1}{2} \sum_{i=1}^4 \eta_{\phi,k}(p_i^2) \right) \lambda_k(p_1, p_2, p_3) = \frac{\partial_t \Gamma_k^{(4)}(p_1, p_2, p_3)}{\prod_{i=1}^4 \sqrt{Z_{\phi,k}(p_i^2)}}. \quad (2.118)$$

Equation (2.116), (2.117) for the two-point function and (2.118) for the four-point function allow us to determine the full system. However, the parameterisation for the two-point function contains a splitting of $\Gamma_k^{(2)}(p^2)$ into two parts which was only done for convenience and is not necessary to solve the system. A natural distribution of the k -dependence in $\Gamma_k^{(2)}$ into $Z_k(p^2)$ and m_k^2 would be

$$\Gamma_k^{(2)}(p^2 = -m_{k,\text{pole}}^2) = 0, \quad (2.119)$$

which defines the mass function m_k^2 as the pole mass at a given cutoff scale k . However, our setup is Euclidean and (2.119) is not easily accessible. Another definition is tightly related to the standard renormalisation condition at vanishing momentum,

$$\eta_{\phi,k} = - \left. \frac{\partial_{p^2} \partial_t \Gamma_k^{(2)}(p^2)}{\Gamma_k^{(2)}(p^2)} \right|_{p^2=0}. \quad (2.120)$$

Equation (2.120) as well as related choices have been used in the literature. We emphasise again that such a choice is a matter of convenience and does not change the results. We close the discussion of the vertex expansion scheme by the explicit flows in the present $N_V = 0$ approximation with the regulator

$$\bar{R}_k(p^2) = Z_{\phi,k}(p^2) R_k(p^2), \quad \text{with} \quad R_k(p^2) = p^2 r(p^2/k^2). \quad (2.121)$$

The class of regulators defined in (2.121) share the anomalous scaling of the two-point function and hence do not change the scaling of the theory. Apart from facilitating the computations by particularly simple loop integrals it also can be shown to -partly- optimise the choice of the regulator within a given approximation, see ??.

In summary the flow equation of the two-point function $\Gamma_k^{(2)}(p)$ reduces to that for $\eta_{\phi,k}$, m_k^2 with

$$\eta_{\phi,k}(p^2) (p^2 + m_k^2) - \partial_t m_k^2 = \frac{1}{2} \int_q \lambda_k(p_1, p_2, q) \frac{(\partial_t - \eta_{\phi,k}(q^2)) R_k}{(q^2 + m_k^2)^2}, \quad (2.122a)$$

where the definition of $\eta_{\phi,k}(0)$ disentangles the flow of $Z_{\phi,k}(p^2)$ and the constant m_k^2 . We emphasise again that the relation in 2.122 is exact in the vertex expansion: If $\lambda_k(p_1, p_2, q)$ is known, the solution for η_ϕ and m^2 are that of the full theory without any approximation. It is the approximate flow of the four-point vertex and hence its approximate solution that introduces the approximation implicitly in 2.122. The flow of the coupling $\lambda_k(p_1, p_2, p_3)$ is given by

$$\begin{aligned} & \left(\partial_t - \frac{1}{2} \sum_{i=1}^4 \eta_{\phi,k}(p_i^2) \right) \lambda_k(p_1, p_2, p_3) \\ &= \int_q \lambda_k(p_1, p_2, q) \lambda_k(p_3, p_4, -q) \frac{1}{(q + p_1 + p_2)^2 + m_k^2} \frac{(\partial_t - \eta_{\phi,k}(q^2)) R_k}{(q^2 + m_k^2)^2} + \text{permut..} \end{aligned} \quad (2.122b)$$

The permutations lead to the t, u momentum channel diagrams with $p_1 + p_2 \rightarrow p_1 + p_3, p_1 + p_4$. For practical purposes it is helpful to parameterise the six-dimensional function $\lambda_k(p_1, p_2, p_3)$ in terms of Lorentz invariants, the radial momenta squared, p_i^2 , and angular dependencies. This leads us to the set of variables

$$p_i^2, \quad \Theta_{ij} = \frac{p_i p_j}{|p_i| |p_j|}, \quad \text{with} \quad i < j \in 1, \dots, n. \quad (2.123)$$

Equation (2.123) is a complete set of momentum and angular variables. In the present example of the four point function we have $3 + 3 = 6$ variables, three radial momentum ones, (p_1^2, p_2^2, p_3^2) , and three angular ones, $(\Theta_{12}, \Theta_{13}, \Theta_{23})$.

s-channel approximation

We elucidate the vertex expansion within two further approximations that are applied often: the s -channel approximation, as well as within a reduction of the full momentum dependences to the symmetric point.

In the s -channel approximation we compute the four point vertex only in the s -channel and use this approximation consistently in the other diagrams. The flow of $\Gamma_k^{(4)}(p_1, \dots, p_4)$ is thus evaluated in the momentum configuration $p_1 = p_2 = p$ with $s = 4p^2$ and both $t, u = 0$. This implies with total momentum conservation

$$p_1 = p_2 = p, \quad p_3 = p_4 = -p, \quad \leftrightarrow \quad s = 4p^2, \quad t = u = 0. \quad (2.124)$$

For the momentum configuration (2.124) the flow of $\Gamma_k^{(4)}$ simplifies considerably. For the symmetry argument that follows we also introduce a commonly used short hand notation,

$$\tilde{\partial}_t = \partial_t|_{\{\Gamma_k^{(n)}\}} \quad \rightarrow \quad G_k \partial_t G_k = -\tilde{\partial}_t G_k. \quad (2.125)$$

Then we conclude

$$\begin{aligned} \partial_t \Gamma_k^{(4)}(p, p, -p) &= -\frac{1}{2} \int_q \tilde{\partial}_t \left(\Gamma_k^{(4)}(p, p, q-p) [G_k(q+p) G_k(q-p)] \Gamma_k^{(4)}(-q+p, -p, -p) \right. \\ &\quad \left. + 2 \Gamma_k^{(4)}(p, -p, q) [G_k(q) G_k(q)] \Gamma_k^{(4)}(-q, p, -p) \right). \end{aligned} \quad (2.126)$$

The $\tilde{\partial}_t$ -derivative only hits the R_k -dependence in the propagators and thus generates all diagrams with cutted lines. Accordingly, the loop integration is finite. Note also that none of the vertices on the right hand side is in the momentum configuration on the right hand side. This leaves us with some freedom to close the present approximation.

Let us first discuss the diagram in the first line of (2.126), the s -channel diagram. We use that for external momenta p smaller than the cutoff scale, the flow so far will not have generated a sizable momentum to $\Gamma^{(4)}$: the vertices are constant at the initial scale Λ and the momentum dependence of the vertices will then be generated from that of the propagators. However, for small $p^2 \lesssim k^2$ the propagators are rather flat due to the regulator. This argument supports constant vertices for $p^2 \lesssim k^2$. In turn, for $p^2 \gtrsim k^2$ the external momenta dominate in the vertices and we can drop the loop momenta in the vertex. In summary we are led to

$$\Gamma_k^{(4)}(p, p, q-p) \Gamma_k^{(4)}(-q+p, -p, -p) \rightarrow \Gamma_k^{(4)}(p, p, -p) \Gamma_k^{(4)}(p, -p, -p) = [\Gamma_k^{(4)}(p, p, -p)]^2, \quad (2.127)$$

and the first line in (2.126) reduces to

$$[\Gamma_k^{(4)}(p, p, -p)]^2 \int_q G_k(q+2p) (G_k \partial_t R_k G_k)(q), \quad (2.128)$$

which only depends on the s -channel vertex. The situation with the other two momentum channels summarised in the second line of (2.126) is less clear. For small external momenta $p^2 \lesssim k^2$ also the vertices in the second line will be well-approximated with constant vertices. However, for large $p^2 \gtrsim k^2$ the vertices will have an s -channel contribution with the s -channel momentum $s = (p \pm q)^2 \approx p^2$ if dropping the q -dependence. Hence, this suggests approximations with either

$$[\Gamma_k^{(4)}(0, 0, 0)]^2, \quad \left[\Gamma_k^{(4)}\left(\frac{p}{2}, \frac{p}{2}, -\frac{p}{2}\right) \right]^2. \quad (2.129)$$

Both approximations close the flow for the four point function on the s -channel vertex. Her we shall also consider a third approximation for its analytic properties: we take simply take the s -channel vertex squared as in the first, s -channel, diagram. Then, the t and u channel contributions approach their

asymptotic momentum form quicker. Within this approximation we can simply pull out the vertex factor $[\Gamma_k(p, p, -p)]^2$ in front of all diagrams and divide by it,

$$\partial_t \frac{1}{\Gamma_k^{(4)}(p, p, -p)} = \int_q \left[G_k(q + 2p) (G_k \partial_t R_k G_k)(q) + 2G_k(q) (G_k \partial_t R_k G_k)(q) \right]. \quad (2.130)$$

This leads us to the resummed form of the vertex

$$\Gamma_k^{(4)}(p, p, -p) = \frac{\lambda_\Lambda}{1 + \lambda_\Lambda \int_\Lambda^k \frac{dk'}{k'} \int_q [G_k(q + 2p) (G_{k'} \partial_t R_k G_{k'})(q) + 2G_{k'}(q) (G_{k'} \partial_t R_{k'} G_{k'})(q)]}. \quad (2.131)$$

In summary we are led to a four-point vertex $\Gamma_k^{(4)}$ solely as a function of the propagators and the coupling λ_Λ at the initial scale. From its structure (2.131) is very similar to NLO 2PI approximation in a $1/N$ expansion in the number of fields and the Parquet resummation as well as other approximate solutions to Bethe-Salpether equations.

Average momentum approximation

In the last chapter we have seen that reducing the momentum dependence to specific channels or configurations leaves us with an ambiguity of how to close the flows. In all these cases the respective arguments at their root rely on a relatively small angular dependence of the vertices or the complete dominance of specific channels or configurations.

In these cases it is sufficient to consider an average momentum dependence, reducing the vertex to

$$\Gamma_k^{(4)}(p_1, \dots, p_4) = \gamma_k(\bar{p}^2)(2\pi)^d \delta(p_1 + p_2 + p_3 + p_4), \quad \text{with} \quad \bar{p}^2 = \frac{1}{4} \sum_{i=1}^4 p_i^2. \quad (2.132a)$$

Note that the average momentum vertex $\gamma_k(\bar{p})$ is not a coupling, it also carries the momentum and RG scaling of the four legs. It is convenient so separate this scaling, in approximation schemes that also is part a derivative expansion as introduced in the next Section 2.3.4 it even leads to significant improvements. Accordingly we define

$$\gamma_k(\bar{p}^2) = Z_{\phi,k}^2(\bar{p}^2) \lambda_k(\bar{p}^2), \quad (2.132b)$$

where $\lambda_k(\bar{p}^2)$ has the momentum and RG properties of a running coupling. In diagrams the $Z_{\phi,k}$ -factors are either matched by $1/Z_{\phi,k}$ from the propagators in the loops or they carry -part of the- RG-scaling of the external legs.

It is left to determine the flow of $\lambda_{n,k}(\bar{p}^2)$ on a specific momentum configuration. A *symmetric point*

$$p_i^2 = \bar{p}^2, \quad \Theta_{ij} = \Theta, \quad (2.133)$$

is best suited for the evaluation as it carries the full symmetry of the approximation. This concludes the introduction of the *Average Momentum Approximation*.

Note however, that the $Z_{\phi,k}(\bar{p}^2)$ in 2.132b carry the average momentum scaling, and hence the momentum scaling does not match. This suggests an upgrade of 2.132a as follows:

$$\Gamma_k^{(n)}(p_1, \dots, p_n) = \left[\prod_{i=1}^n Z_{\phi,k}^{1/2}(p_i^2) \right] \bar{\Gamma}_k^{(n)}(p_1, \dots, p_n), \quad (2.134a)$$

with the RG-invariant vertex function $\bar{\Gamma}_k(p_1, \dots, p_n)$. For the latter we employ the average momentum approximation

$$\bar{\Gamma}_k^{(n)}(p_1, \dots, p_n) = \lambda_{n,k}(\bar{p}^2)(2\pi)^d \delta(p_1 + \dots + p_n) \quad (2.134b)$$

with the running coupling $\lambda_{n,k}(\bar{p}^2)$ and $\lambda_k = \lambda_{4,k}$. The approximation 2.134 has the very convenient property that the $Z_{\phi,k}$ drop out from all flows, only the anomalous dimension $\eta_{\phi,k}$, (2.115) remains in the cutted line with

$$G_k(q) \left(\partial_t - \eta_{\phi,k}(q^2) \right) R_k(q^2) G_k(q). \quad (2.135)$$

The integrands in the loops are peaked at momenta $q^2 \approx k^2$ and drops rapidly for $q^2 \gtrsim k^2$. For $q^2 \rightarrow 0$ is vanishes at least with q^{d-1} due to the radial momentum integration. This suggests an additional apprtoximation with

$$\eta_{\phi,k}(q^2) R_k(q^2) \rightarrow \eta_{\phi,k}(k^2) R_k(q^2), \quad (2.136)$$

in the loop integral. Equation (2.136) typically works at the percent level, and its accuracy can be always checked on the results of the flow. With (2.136) the non-trivial momentum-dependence in the flow diagrams solely comes from the couplings. Still, the momentum dependence of the propagators is fully encoded in the $\eta_{\phi,k}(p^2)$ on the left hand side of the flow as

$$\begin{aligned} \frac{1}{\prod_{i=1}^n Z_{\phi,k}^{1/2}(p_i^2)} \partial_t \Gamma_k^{(n)}(p_1, \dots, p_{n-1}) &= \partial_t \bar{\Gamma}_k^{(n)}(p_1, \dots, p_{n-1}) - \frac{1}{2} \sum_{i=1}^n \eta_{\phi,k}(p_i^2) \\ &= \partial_t \lambda_k(\bar{p}^2) - \frac{1}{2} \sum_{i=1}^n \eta_{\phi,k}(p_i^2). \end{aligned} \quad (2.137)$$

Both average momentum schemes reduce the computational effort significantly. The second one carries the additional simplifying feature that the propagators in the loop diagrams carry the classical dispersion. Whether the one or the other is the method of choice can be evlauated in a self-consistency check: The full momentum-dependence of the vertex functions $\lambda_{n,k}(p_1, \dots, p_n)$ can be simply integrated on the solutions of 2.132 or 2.134. Then the approximations leading to $\lambda_{n,k}(\bar{p}^2)$ can be checked both on the solutions and in the flow.

2.3.4. Derivative expansion

The derivative expansion is a standard, and very well-working, expansion scheme for low energy effective theories. Assume for a moment that we deal with a fundamental theory with an intrinsic mass scale m_{gap} , such as Λ_{QCD} in Yang theory or Λ_{QCD} and the pion mass m_π in QCD. Note however that on the other hand the Planck mass M_{Planck} is no such mass scale as general relativity at vanishing cosmological constant is massless. The same holds true for QCD with massless quarks. In the latter Λ_{QCD} is still present, but the pion is massless.

In the presence of such a infrared mass scale m_{gap} we can expand the low energy effective theory with a classical action $S_{\text{low}}[\phi]$, which describes long range phenomena with $r \gtrsim 1/m_{\text{gap}}$, in powers of p^2/m_{gap} . As long as the physics momentum scales of interest p^2 satisfy

$$\frac{p^2}{m_{\text{gap}}^2} \ll 1, \quad (2.138)$$

an expansion of the quantum corrections about $p^2/m_{\text{gap}}^2 = 0$ is well-defined and should show good convergence properties. Such a systematic expansion scheme for quantum corrections, $\Gamma[\phi] - S[\phi]$, is called the *Derivative Expansion*.

For our present approach the situation is even bettered at least for finite cutoff scale k as heuristically the regulator increases the mass gap of the theory by

$$m_{\text{gap}}^2 \rightarrow m_{\text{gap}}^2 + k^2. \quad (2.139)$$

This idea can be made even more precise within an investigation of the flow equation. A first hint at the improved convergence properties of the derivative expansion within the flow equation comes from the flow equation (2.27) itself. In view of the expansion about $p^2/(m_{\text{gap}}^2 + k^2)$ we write

$$\partial_t \Gamma_k[\phi] = \frac{1}{2} \int_{p^2 \lesssim k^2} \frac{1}{\Gamma_k^{(2)}[\phi] + R_k} \partial_t R_k + \frac{1}{2} \int_{p^2 \gtrsim k^2} \frac{1}{\Gamma_k^{(2)}[\phi] + R_k} \partial_t R_k \approx \frac{1}{2} \int_{p^2 \lesssim k^2} \frac{1}{\Gamma_k^{(2)}[\phi] + R_k} \partial_t R_k, \quad (2.140)$$

for sufficiently fast decaying regulator, see 2.9 and Figure 2.3. In the infrared loop with loop momenta $p^2 \lesssim k^2$ the condition

$$\frac{p^2}{k^2} \lesssim 1. \quad (2.141)$$

justifies the derivative expansion in the flow equation. We emphasise that (2.141) does not even require the existence of a physical mass gap m_{gap}^2 , it also works for massless theories. Apparently this analysis also suggests using rapidly decaying propagators which lead to smaller momentum tails in the flow. In turn, however, the Taylor expansion coefficients of rapidly decaying propagators $R_k(p^2)$ increase more rapidly with the order of the number of the derivatives and hence with the order of the derivative expansion. These two conflicting properties have to be optimised for optimising the derivative expansion. A *functional optimisation criterion* for any systematic expansion scheme, and in particular for general orders of the derivative expansion, has been put forward in [9]. Functional optimisation in terms of an optimisation criterion for the regulator has first been suggested by Litim in [16, 15], where it led to the Litim regulator as the optimal choice for the zeroth order of the derivative expansion. This will be discussed in more detail in ??.

ϕ^4 -theory

For the remainder of this chapter we want to discuss the general properties of the derivative expansion within the ϕ^4 -theory also in comparison to the vertex expansion. At the zeroth order of the derivative expansion the quantum fluctuations $\Gamma[\phi] - S[\phi]$ carry no momentum dependence. This leaves us with a k -dependent function of the field.

$$\Gamma_k[\phi] = \int d^d x \left(\frac{1}{2} \partial_\mu \phi \partial_\mu \phi + V_k(\rho) + O(\partial^2) \right), \quad \rho = \frac{\phi^2}{2}. \quad (2.142)$$

This approximation is also called the *Local Potential Approximation* (LPA). Note that in (2.142) $O(\partial^2)$ only applies to the quantum fluctuations. The classical kinetic term is not dropped. The *Effective Potential* $V_k(\rho)$ contains all powers in the field including a mass term and a ϕ^4 term. It is a function of $\rho = \phi^2/2$ due to the Z_2 -symmetry of the theory under $\phi \rightarrow -\phi$. In a polynomial expansion it reads

$$V(\rho) = \sum_{n=0}^{\infty} \frac{\lambda_n}{n!} (\rho - \kappa)^n, \quad (2.143)$$

where κ is a conveniently chosen expansion point. In many applications it is the cutoff-dependent minimum, $\kappa = \phi_{0,k}^2/2$ of the effective potential,

$$\left. \frac{\partial V_k(\rho)}{\partial \phi} \right|_{\phi=\phi_{0,k}} = 0. \quad (2.144)$$

Note also that for a polynomial action up to the order $n = 2$ the parameters in the classical ϕ^4 action (1.1) translate into $m^2 = \lambda_1 - \lambda_2 \kappa$ and $\lambda = 6\lambda_2$.

Within the LPA approximation the flow equation takes a very simple form: we evaluate the flow equation for constant fields ϕ , since we are only interested in momentum-independent quantum corrections. Then the left hand side of the flow reduces to

$$\partial_t \Gamma[\phi] = \text{Vol}_d \partial_t V_k(\rho), \quad \text{Vol}_d = \int d^d x. \quad (2.145)$$

For the right hand side of the flow we need the second derivative of (2.142). It is given by

$$\Gamma_k^{(2)}[\phi](p, q) = \Gamma_k^{(2)}[\phi](p)(2\pi)^d \delta(p + q), \quad \Gamma_k^{(2)}[\phi](p) = p^2 + V'_k(\rho) + 2\rho V''_k(\rho), \quad (2.146)$$

where $V'_k = \partial_\rho V_k$ and $V''_k = \partial_\rho^2 V_k$. Note that (2.146) is the generalised version of (2.61) with the simple substitution $\lambda/2\phi^2 \rightarrow V'_k(\rho) + 2\rho V''_k(\rho)$. The propagator is given by $G(p, q) = G(p)(2\pi)^d \delta(p + q)$, and the cutoff derivative of the regulator is given by $\partial_t R_k(p^2)(2\pi)^d \delta(p + q)$. Then we get

$$\partial_t V_k(\rho) = \frac{1}{2} \int_p G_k(p) \partial_t R_k(p) \left[\frac{1}{\text{Vol}_d} (2\pi)^d \delta(0) \right]. \quad (2.147)$$

Now we use that $(2\pi)^d \delta(0) = \int_x \exp(iqx)$ at vanishing q . This is nothing but the volume and the expression in the square bracket in (2.147) is unity. With (2.146) we are finally led to the simple partial differential equation

$$\partial_t V_k(\rho) = \frac{1}{2} \int_p \frac{1}{p^2 + V'_k(\rho) + 2\rho V''_k(\rho) + R_k(p^2)} \partial_t R_k(p^2). \quad (2.148)$$

Equation (2.148) already allows us to discuss general properties of flows at the example of the ϕ^4 -theory. For example, the convexity-restoring property of the flow, [30] is easily deduced from (2.148). This analysis is done below and will also reveal that the flow in the ϕ^4 -theory is symmetry restoring in the presence of spontaneous symmetry breaking.

The structure of the flow underlying the following arguments is even more apparent within the flow equation (2.148) with the Litim or flat regulator

$$R_{k,\text{flat}}(p^2) = p^2 r_{\text{flat}}(p^2/k^2), \quad r_{\text{flat}}(y) = \left(\frac{1}{y} - 1 \right) \theta(1-y), \quad y = \frac{p^2}{k^2}, \quad (2.149)$$

see also 2.9a. With (2.149) the momentum integration in (2.148) can be performed. Another regulator which allows for an analytic expression for the flow is the sharp regulator, 2.9c. However, while the LPA flow is *optimised* with the Litim regulator in terms of the convergence of the expansion scheme, see [16, 15], the convergence is very slow for the latter. For more details see ??.

With (2.149) the derivative of the cutoff function reads in its dimensionless form

$$\frac{1}{k^2} \partial_t R_{k,\text{flat}}(p^2) = -2y^2 r'_{\text{flat}}(y) = 2\theta(1-y). \quad (2.150)$$

Accordingly, we only need the propagator in (2.148) for momenta $q^2 \leq k^2$ with

$$G_k(q)\theta(k^2 - q^2) = \frac{1}{k^2 + V'_k(\rho) + 2\rho V''_k(\rho)}. \quad (2.151)$$

Putting all the pieces together leads us to a simple and optimised analytic flow equation for the effective potential in LPA with the regulator (2.149),

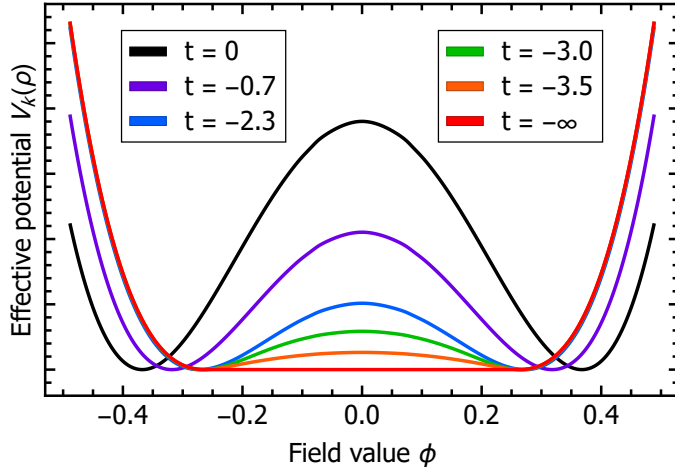


Figure 2.11.: The effective potential $V_k(\rho)$ for an $O(N)$ -theory with $N \rightarrow \infty$ for $k \in [0, \Lambda]$ with the initial scale Λ . Here $t = \ln k/\Lambda$ and $t \in [0, -\infty]$.

$$\partial_t V_k(\rho) = \frac{\Omega_d}{(2\pi)^d} \frac{k^{d+2}}{d} \frac{1}{k^2 + V'_k(\rho) + 2\rho V''_k(\rho)}. \quad (2.152)$$

with Ω_d defined in (2.71). The flow equation (2.152) for the ϕ^4 -theory and the analogue for N scalar fields with $O(N)$ -symmetry, (2.164), are very simple but also powerful approximation to the full flow equations in these scalar theories. Equation (2.148) and (2.152) allow us already to discuss generic properties of the solution. Its numerical solution for N -scalar fields and the analytic one in for $N \rightarrow \infty$ is evaluated subsequently.

The effective potential and its flow are sketched in Figure 2.11 for $N \rightarrow \infty$. For Figure 2.11 we have used that subtracting a k -dependent constant from the flow only changes the total normalisation of the effective potential $V_k(\phi)$. For the present purpose it is convenient to have a vanishing effective potential in the k -dependent minimum. Then the flow reads

$$\partial_t V_k(\rho) = \frac{\Omega_d}{(2\pi)^d} \frac{k^{d+2}}{d} \left[\frac{1}{k^2 + V'_k(\rho) + 2\rho V''_k(\rho)} - \frac{1}{k^2 + V'_k(\rho_{\min,k}) + 2\rho_{\min,k} V''_k(\rho_{\min,k})} \right]. \quad (2.153)$$

Then, the flow is negative for $\rho > \rho_{\min,k}$ and positive for $\rho < \rho_{\min,k}$. The shear force on the minimum drives it towards smaller values when lowering k , that is $\partial_t \rho_{\min,k} > 0$. This can be made more precise when evaluating the flow of the EoM,

$$\partial_t [V'_k(\rho_{\min,k})] = \dot{\rho}_{\min,k} V''_k(\rho_{\min,k}) + \dot{V}_k(\rho_{\min,k}) \quad \rightarrow \quad \partial_t \rho_{\min,k} = -\frac{\dot{V}'_k(\rho_{\min,k})}{V''_k(\rho_{\min,k})} > 0. \quad (2.154)$$

The inequality in (2.154) is deduced from $\dot{V}'_k(\rho_{\min,k}) < 0$, see Figure 2.11 as well as $V''_k(\rho_{\min,k}) > 0$ following from $\rho_{\min,k}$ being a minimum. This property entails that the flow in the ϕ^4 -theory is symmetry

restoring. Accordingly, if we want to have spontaneous symmetry breaking at $k = 0$ we need to start with a initial effective potential V_Λ which shows a sufficiently large non-trivial minimum $\rho_{\min,\Lambda} \neq 0$ such that the flow does not turn it into a vanishing expectation value at $k = 0$. This is sometimes called *microscopic spontaneous symmetry breaking*. We emphasise that this physical interpretation of the initial effective action has to be taken with a grain of salt. The dominant effect triggering these non-trivial minima can be clearly attributed to a regularisation artefact as the negative mass runs with positive powers of the cutoff scale. Note also that even though the flow is symmetry-restoring this does not necessarily imply that the quantum fluctuations are: the flow sums up both, the quantum fluctuations and the flow of the renormalisation scheme. The latter can be already understood from the fact that $\lim_{k \rightarrow \infty} \Gamma_k$ runs towards the bare action at infinite scale, not the renormalised one, for more details see [9, 10]. This point of view is further supported by the fact that the DSE solved in LPA leads to lmore symmetry breaking for the full potential, see [66].

We also already see the importance of the space-time dimension for this argument. The flow $\partial_t \rho_{\min,k}$ in (2.154) is proportional to $\dot{V}_k(\rho_{\min,k})$ that can be derived from (2.148) or (2.152) by a field derivative. For $V''(\rho_{\min,k}) > 0$ it vanishes with k^{d+2} for $k \rightarrow 0$: the higher the dimension, the quicker does it vanishes. This property will be discussed in much more detail in the following example of an $O(N)$ -theory with N scalar fields.

In case the minimum freezes in as in Figure 2.11, the curvature of the potential, $V^{(2)}[\phi]$ is negative for $\rho < \rho_{\text{turn}}$. Here, ρ_{turn} is the turning point of the potential with vanishing curvature,

$$V_k^{(2)}(\phi) = V'_k(\rho) + 2V''_k(\rho) < 0, \quad \text{for } \rho < \rho_{\text{turn}} \quad \text{with} \quad V'_k(\rho_{\text{turn}}) + 2V''_k(\rho_{\text{turn}}) = 0. \quad (2.155)$$

Note that for more general theories it is the inverse of $V_k^{(2)}(\phi) + R_k(p)$ which has to be discussed, see also in the $O(N)$ example discussed below. For the discussion and without loss of generality we restrict ourselves to regulators with $\min[p^2 + R_k(p^2)] = k^2$. In the regime $\rho < \rho_{\text{turn}}$ the flow grows large if $V^{(2)}(\phi) \rightarrow -k^2$. However, in this regime the flow of the effective potential flattens the potential with a strength proportional to $1/(V^{(2)}(\phi) + k^2) \rightarrow \infty$ independent of the value of k . In short, the closer the flow is to the singularity $V^{(2)}(\phi) = -k^2$, the stronger is the flow away from it. This argument can be made precise also beyond LPA, see [30]. In summary one can show that the full flow is *convexity-restoring*: the full curvature $V_k^{(2)}(\phi) + R_k(p) > 0$ for all k .

Here we have argued that the LPA approximation sustains this formal property of the full flow. It is simple to see that this does not hold true for all approximation schemes. Consider for example the one loop effective potential in perturbation theory, the Coleman-Weinberg potential. The latter is not convex even though the full potential has to be convex. Seemingly even worse, the tunneling phenomena derived from the Coleman-Weinberg potential are usually linked to the height and width of the non-convex part of the potential, which is an artefact of the approximation. However, width and hight can be linked to correlation functions evaluated in the minimum of the Coleman-Weinberg potential, and hence carry physics.

Another relevant example, in which the convexity-restoring property is globally lost, is given by a further approximation to the LPA, if one expands the effective potential in a Taylor expansion. This additional approximation is often used as it simplifies the computations. It also shows very good convergence properties about well-chosen expansion points, see e.g. [67] for a detailed investigation. Still, the global properties of the potential are potentially lost in such a local epansion. This is reflected by the potential loss of convexity in the regime not covered by the convergence radius of the expansion.

The above evaluation of the LPA flow of the effective potential allows us to study spontaneous symmetry breaking and phase transitions in a very concise way beyond mean field level. To that end let us consider a classical potential with a positive or negative mass term m_Λ^2 and a positive ϕ^4 -coupling λ_Λ ,

$$V_\Lambda(\rho) = m_\Lambda^2 \rho + \frac{\lambda_\Lambda}{3!} \rho^2, \quad m_\Lambda^2 > 0 \quad \text{or} \quad m_\Lambda^2 < 0, \quad \lambda_\Lambda > 0. \quad (2.156)$$

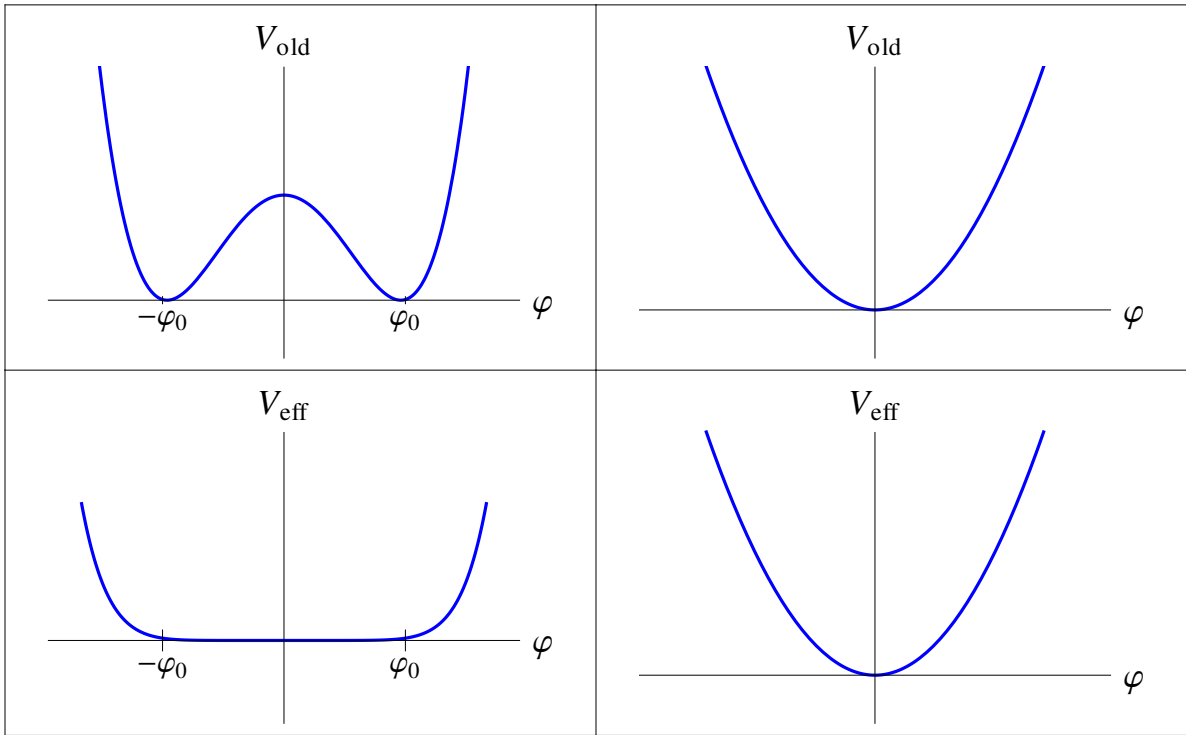


Figure 2.12.: The classical potential (upper panel) and the associated effective potential (lower panel) for a spontaneously broken symmetry (left hand side) and for unbroken symmetry (right hand side).

We know already that for $m_\Lambda^2 > 0$ in the symmetric regime, the full effective potential at vanishing k , $V_{\text{eff}}(\rho) = V_{k=0}(\rho)$ is also in the symmetric regime, the minimum will be at $\rho_{\min} = 0$, see the left hand side of Figure 2.12. Also, for $m_\Lambda^2 < 0$, but $|m_\Lambda^2|$ too small, quantum fluctuations drive the effective potential into the symmetry phase. In turn, if the absolute value of the initial negative mass, $|m_\Lambda^2|$, is too big, then the non-trivial minimum will persist at $k = 0$, $\rho_{\min} > 0$. Then, as discussed before, convexity of the potential at $k = 0$ requires that the flow flattens it in between the non-trivial minima. This situation is depicted in the left plot in Figure 2.12. The whole structure will be explained in much more detail in the example in Section 2.3.4. However, the present analysis already shows that the flow equation within derivative expansion is a powerful tool for investigating symmetry breaking mechanisms and critical phenomena. This will be used in Part II in particular for the discussion of spontaneous chiral symmetry breaking.

Let us now briefly discuss the next order in the derivative expansion. The respective scale dependent effective action is parameterise as

$$\Gamma_k[\phi] = \int d^d x \left(\frac{1}{2} Z_{\phi,k}(\rho) \partial_\mu \phi \partial^\mu \phi + V_k(\rho) + O(\partial^4) \right). \quad (2.157)$$

Equation (2.157) contains all first order terms in derivatives. The new function $Z_{\phi,k}(\rho)$ only depends on ρ due to Z_2 symmetry, which already restricted the ϕ -dependence of V_k to a ρ -dependence, $V_k = V_k(\rho)$. Even though this corrections are written in terms of a field-dependent wave function renormalisation, it also carries momentum dependent couplings. The flow equations for $Z_{\phi,k}$ and V_k are schematically

obtained from the Wetterich equation as

$$\begin{aligned}\partial_t V_k(\rho) &= \frac{1}{2\text{Vol}_d} \text{Tr} \frac{1}{\Gamma_k^{(2)}[\phi] + R_k} \partial_t R_k, \\ \partial_t Z_k(\rho) &= \frac{1}{2\text{Vol}_d} \frac{\partial}{\partial p^2} \left[\frac{\delta^2}{\delta\phi(p)\delta\phi(q)} \text{Tr} \frac{1}{\Gamma_k^{(2)}[\phi] + R_k} \partial_t R_k \right]_{p=q=0},\end{aligned}\quad (2.158)$$

with constant ρ . Note that this system is coupled as well since $\Gamma_k^{(2)}$ on the right hand side depends on both $Z_k(\rho)$ and $V'_k(\rho)$ and their derivatives. Higher orders of the derivative expansion are systematically derived with defining the respective effective action and projections such as used for the first order in (2.158). We emphasise that the projection via momentum derivatives at vanishing momentum, $p^2 = 0$, is a canonical choice that is in line with the setup of the derivative expansion as an expansion about $p^2 = 0$. Still, the projection can be done differently. In particular one can easily show that the integrand in generic flow equations is peaked at radial momenta $p^2 \approx k^2$ and vanishes with $p^{2(d/2-1)}$ for $p^2 \rightarrow 0$. This property suggests an expansion about $p^2 = k^2$, which is also used often. Finally, the above full first order of the derivative expansion is often reduced by only considering a field-independent wave function renormalisation,

$$Z_{\phi,k}(\rho) \rightarrow Z_{\phi,k}, \quad \text{with} \quad \partial_\phi Z_{\phi,k} = 0. \quad (2.159)$$

This approximation is called LPA' and reduces the computational effort significantly.

We close this chapter with a brief comparison of the (low orders of the) derivative expansion, (2.148) with the (lowest order of the) vertex expansion in the last chapter, [Section 2.3.3](#), given in ???. In the latter the two-point function has a full momentum dependence as does the four-point function, this comprises a non-trivial quantum dispersion and the momentum dependence of scatterings. In comparison, the momentum dependence is lacking completely in LPA, see (2.148) and is reduced to p^2 -terms in the first order, see (2.158). In turn, in LPA and higher orders of the derivative expansion the full field-dependence on constant fields is included, this comprises all order low momentum scattering processes. Depending on the physics under investigation the one or the other property is more important. Obviously, the structure of the equations ?? and (2.148) also allows us to mix the two schemes.

O(N)-theory

In this section we are extending the previous example in [Section 2.3.4](#) of a ϕ^4 -theory to a N component scalar theory with an $O(N)$ symmetry. We stay within LPA and the effective average action of the ϕ^4 -theory (2.142) is easily adapted,

$$\Gamma_k[\phi] = \int_x \left\{ \frac{1}{2} (\partial_\mu \phi_a)^2 + V_k(\rho) \right\}, \quad (2.160)$$

which is O(N)-symmetric. The effective potential $V_k(\rho)$ depends only on the invariant $\rho = \frac{1}{2} \phi_a \phi^a$, where $a \in \{1, \dots, N\}$, respecting the $O(N)$ symmetry of the theory. The evaluation of the right-hand side of the flow equation (2.27) requires the second derivative of the effective action (2.160) with respect to the field ϕ_a , here we pass directly to the two-point function in momentum space

$$\Gamma_{k,ab}^{(2)}(p) = (p^2 + V'_k(\rho)) \delta_{ab} + \phi_a \phi_b V''_k(\rho), \quad (2.161)$$

where $V'_k(\rho) = \partial_\rho V_k(\rho)$ and $V''_k(\rho) = \partial_\rho^2 V_k(\rho)$, for details recall the discussion around (2.146). We now make an explicit choice for the parametrisation of the expectation value of the field. To be more precise, we single out the direction for which the field can acquire a finite value. We choose the N th component,

while the expectation value of the others is zero. This results in the following field configuration $\phi_a = (0 \dots, 0, \sigma)$, with the conventional choice from high-energy physics to label this direction σ and collect the others in a vector $\vec{\pi}$, which corresponds to the sigma meson and pions in effective models of QCD. With this choice the two-point function (2.161) takes the following form

$$\Gamma_{k,ab}^{(2)} = \delta_{ab} \left(p^2 + V'_k(\rho) \right) + 2\rho V''_k(\rho) \delta_{aN} \delta_{bN}, \quad (2.162)$$

With (2.162) at hand we can immediately write down the flow equation

$$\partial_t V_k(\rho) = \frac{1}{2} \int_q \left[\frac{N-1}{q^2 + V'_k(\rho) + R_k(q)} + \frac{1}{q^2 + V'_k(\rho) + 2\rho V''_k(\rho) + R_k(q)} \right] \partial_t R_k(q). \quad (2.163)$$

As in the $O(1)$ case discussed before we use the Litim regulator, (2.149). The integral is easy to carry out and the resulting flow equation reads

$$\partial_t V_k(\rho) = \frac{\Omega_d}{(2\pi)^d} \frac{k^{d+2}}{d} \left(\frac{N-1}{k^2 + V'_k(\rho)} + \frac{1}{k^2 + V'_k(\rho) + 2\rho V''_k(\rho)} \right), \quad (2.164)$$

which reduces to the $O(1)$ case in (2.152) for $N = 1$. Then, the contribution from the Goldstone modes is missing. The angular part Ω_d is defined in (2.71). The first term on the right-hand side of (2.164) shows the contribution of the $N-1$ Goldstone modes, which become massless in the limit of vanishing RG scale $k \rightarrow 0$ and evaluated on the solution of the equation of motion, i.e. $V'(\rho_{\min}) = 0$. Correspondingly, the second term is the contribution of the massive mode, which only becomes massless at phase transitions or similar phenomena. The flow equation (2.164) can be solved numerically in the current form, for which it is sometimes beneficial to take a derivative with respect to the invariant ρ of (2.164). For further applications it is beneficial to go to a dimensionless version of (2.164). This amounts to rescaling the potential and the invariant by appropriate powers of k

$$\begin{aligned} \bar{\rho} &= k^{2-d} \rho, \\ u_k(\bar{\rho}) &= k^{-d} V_k(k^{d-2} \bar{\rho}). \end{aligned} \quad (2.165)$$

Please note that the dimensionless invariant is now also a k dependent quantity. After a few algebraic manipulations one finds the following identities, relating the original to the dimensionless quantities

$$\begin{aligned} \partial_t x &= (2-d)\bar{\rho}, \\ k^{-d} \partial_t V_k(\rho) &= \partial_t u_k(\bar{\rho}) + d u_k(\bar{\rho}), \\ \partial_t u_k(\bar{\rho}) &= \partial_t|_{\bar{\rho}} u_k(\bar{\rho}) + (2-d)\bar{\rho} u'_k(\bar{\rho}), \end{aligned} \quad (2.166)$$

where the derivative at fixed $\bar{\rho}$ is required for actual calculations. In the following we will assume RG-time derivatives to be evaluated at fixed $\bar{\rho}$. With these quantities we can rewrite the flow equation (2.164)

$$\partial_t u_k(\bar{\rho}) + d u_k(\bar{\rho}) + (2-d)\bar{\rho} u'_k(\bar{\rho}) = \frac{1}{d} \frac{\Omega_d}{(2\pi)^d} \left(\frac{N-1}{1 + u'_k(\bar{\rho})} + \frac{1}{1 + u'_k(\bar{\rho}) + 2\bar{\rho} u''_k(\bar{\rho})} \right), \quad (2.167)$$

which is suitable for the numerical search of fixed points.

Large-N

A particularly interesting limit is the large N limit, where N refers usually to the dimension of a symmetry group, e.g. the N in $O(N)$ or $SU(N)$. It allows for a systematic expansion in QFTs in $1/N$ and for many observables $N \gtrsim 3$ has been observed to be in good agreement with the limit $N \rightarrow \infty$. Additionally, analytic calculations become often possible, including an analytic solution of the flow equation for the $O(N)$ -model, c.f. [Section 2.3.4](#). Therefore, we will investigate the $O(N)$ model in the LPA and the large N limit in this section. The large N limit of [\(2.164\)](#) can be taken by rescaling the potential $U_k(\rho)$ and the invariant ρ with $N - 1$, therefore $U'(\rho)$ and $\rho U''(\rho)$ stay invariant, while the left-hand side becomes proportional to $N - 1$. With this at hand it is possible to rewrite [\(2.164\)](#) as

$$\begin{aligned} \partial_t V_k(\rho) &= \frac{\Omega_d}{(2\pi)^d} \frac{k^{d+2}}{d} \left(\frac{1}{k^2 + V'_k(\rho)} + \frac{1}{N-1} \frac{1}{k^2 + V'_k(\rho) + 2\rho V''_k(\rho)} \right) \\ &\stackrel{N \rightarrow \infty}{=} \frac{\Omega_d}{(2\pi)^d} \frac{k^{d+2}}{d} \left(\frac{1}{k^2 + V'_k(\rho)} \right). \end{aligned} \quad (2.168)$$

The radial mode has dropped out of the large N flow equation [\(2.168\)](#), only the Goldstone modes contribute in the large N limit. In order to proceed it is again advantageous to go to dimensionless coordinates, c.f. [\(2.165\)](#)

$$\partial_t u_k(\bar{\rho}) + d u_k(\bar{\rho}) + (2-d)\bar{\rho} u'_k(\bar{\rho}) = A_d \frac{1}{1 + u'_k(\bar{\rho})}, \quad (2.169)$$

where we have introduced $A_d = \frac{1}{d} \frac{\Omega_d}{(2\pi)^d}$. Taking a derivative with respect to $\bar{\rho}$ and introducing $\omega(\bar{\rho}) = u'_k(\bar{\rho})$

$$\partial_t \omega(\bar{\rho}) + 2\omega(\bar{\rho}) + (2-d)\bar{\rho} \omega'(\bar{\rho}) = -A_d \frac{\omega'(\bar{\rho})}{(1 + \omega(\bar{\rho}))^2}. \quad (2.170)$$

Introducing now additional auxiliary functions

$$\begin{aligned} a(t, \bar{\rho}, \omega) &= 1, \\ b(t, \bar{\rho}, \omega) &= (2-d)\bar{\rho} + A_d \frac{1}{(1 + \omega)^2}, \\ c(t, \bar{\rho}, \omega) &= -2\omega, \end{aligned} \quad (2.171)$$

where we have dropped the explicit x dependence of ω and it is assumed implicitly from now on. Utilising [\(2.171\)](#) we can rewrite [\(2.170\)](#) as

$$a(t, \bar{\rho}, \omega) \partial_t \omega + b(t, \bar{\rho}, \omega) \partial_{\bar{\rho}} \omega = c(t, \bar{\rho}, \omega), \quad (2.172)$$

which is a first-order quasilinear PDE. Therefore the *method of characteristics* provides a suitable tool for the solution of [\(2.172\)](#). Suppose that we know a solution $\omega(t, \bar{\rho})$, then the vector $(\partial_t \omega, \partial_{\bar{\rho}} \omega, -1)$ is a normal vector to the surface graph of $\omega = \omega(t, \bar{\rho})$. Therefore, [\(2.172\)](#) is equivalent to the requirement that the vector (a, b, c) is tangent to surface of $\omega = \omega(t, \bar{\rho})$ at every point. The characteristic curves of the PDE [\(2.172\)](#) are now the union of integral curves that make up the solution. For an illustration of this, see [Figure 2.13](#). The set of ordinary differential equations that determine the characteristics are called *Lagrange-Charpit* equations

$$\begin{aligned} \partial_s t &= a(t, \bar{\rho}, \omega), \\ \partial_s \bar{\rho} &= b(t, \bar{\rho}, \omega), \\ \partial_s \omega &= c(t, \bar{\rho}, \omega), \end{aligned} \quad (2.173)$$

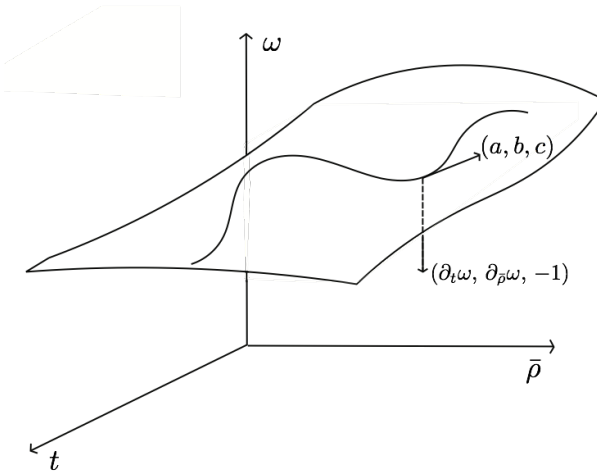


Figure 2.13.: Surface ω in the $(t, \bar{\rho})$ plane, the tangent vector (a, b, c) and the derivative vector $(\partial_t \omega, \partial_{\bar{\rho}} \omega, -1)$ as a normal vector to the surface ω .

with a geodetic parameter s and the initial conditions

$$\begin{aligned} t(s=0) &= t_\Lambda(\gamma), \\ \bar{\rho}(s=0) &= \bar{\rho}_\Lambda(\gamma), \\ \omega(s=0) &= f(\gamma), \end{aligned} \tag{2.174}$$

where γ parametrises the boundary on which the initial condition f is defined. Solving the system of equations (2.173) with initial conditions (2.174) gives us a solution $\omega(s)$ along a characteristic. In order to obtain a solution $\omega(t, \bar{\rho})$ we need to invert the relation between $(t, \bar{\rho})$ and (γ, s) , which is possible as long as

$$(a(t_\Lambda(\gamma), \bar{\rho}_\Lambda(\gamma), f(\gamma)), b(t_\Lambda(\gamma), \bar{\rho}_\Lambda(\gamma), f(\gamma))) \cdot (-\bar{\rho}'_\Lambda(\gamma), t'_\Lambda(\gamma)) \neq 0, \tag{2.175}$$

i.e. their relation is invertible. The statement (2.175) is nothing else but the requirement that the boundary is nowhere tangent to the projected characteristic curves. Turning back to our actual problem (2.169), the initial conditions are simply given by

$$\begin{aligned} t(s=0) &= 0, \\ \bar{\rho}(s=0) &= \bar{\rho}_\Lambda, \\ \omega(s=0) &= \omega_\Lambda(\bar{\rho}_\Lambda). \end{aligned} \tag{2.176}$$

We can now obtain an explicit solution of (2.173) together with the initial conditions (2.176) and $\omega_0(\bar{\rho}_0) = u'(\bar{\rho}_0)_\Lambda$,

$$\begin{aligned} t(s) &= s, \\ \omega(t) &= \omega_\Lambda \exp(-2t), \\ \bar{\rho}(t) &= \bar{\rho}_\Lambda + \int_0^t ds' \left((2-d)\bar{\rho}(s') + \frac{A}{(1+\omega_\Lambda e^{-2s'})^2} \right). \end{aligned} \tag{2.177}$$

where we have already used the first equation, $s = t$, in the latter two equations. Additionally, we have suppressed the dependence of ω_0 on $\bar{\rho}_0$ for the sake of brevity. The integral representation of $\bar{\rho}(t)$ allows a very simple access to the asymptotic regimes for $t \rightarrow 0$ (UV) and $t \rightarrow -\infty$ (IR). The integral in ?? can be performed and gives a analytic form for the implicitly equation for relation $\bar{\rho}_0(\bar{\rho})$,

$$\begin{aligned} \bar{\rho}(t) = & \bar{\rho}_\Lambda e^{(2-d)t} + \frac{A_d}{2} \frac{e^{(d-2)t}}{\omega_\Lambda} \left(\frac{e^{(d+2)t}}{e^{2t} + \omega_\Lambda} - \frac{1}{1 + \omega_\Lambda} \right. \\ & \left. - \frac{d}{(d+2)} \frac{e^{(d+2)t} {}_2F_1\left(1, \frac{d+2}{2}; \frac{d+4}{2}; -\frac{e^{2t}}{\omega_\Lambda}\right) - {}_2F_1\left(1, \frac{d+2}{2}; \frac{d+4}{2}; -\frac{1}{\omega_\Lambda}\right)}{\omega_0} \right), \end{aligned} \quad (2.178)$$

where ${}_2F_1(a, b; c; z)$ is a hypergeometric function. While the occurrence of ${}_2F_1(a, b; c; z)$ does not allow for easier access to possible solutions, it easily reduces to a set of logarithms and exponentials for a given dimension. Additionally, we have suppressed the dependence of ω_Λ on $\bar{\rho}_\Lambda$ for brevity. A similar analysis can be found in [68]. The relation $\bar{\rho}(t, \rho_\Lambda)$ can be inverted (numerically) for any given t . For given ρ and t it determines $\omega(t, \bar{\rho}) = \omega_\Lambda(\bar{\rho}_\Lambda(t, \bar{\rho}))$, the second relation in (2.177). Both forms, (2.177) and (2.178) are suitable for the study of fixed points in the $N \rightarrow \infty$ limit, see e.g. [69], for a more detailed discussion on this issue see ??.

For any further investigations, it is beneficial to look also at dimensionful quantities. Taking a derivative of (2.168) and setting $w = \partial_\rho U(\rho)$, we can immediately write down the *Lagrange-Charpit* equations

$$\begin{aligned} \partial_s t &= 1, \\ \partial_s \rho &= A_d [\Lambda e^s]^{d+2} \frac{1}{([\Lambda e^s]^2 + w)^2}, \\ \partial_s w &= 0, \end{aligned} \quad (2.179)$$

with initial conditions

$$\begin{aligned} t(s=0) &= 0, \\ \rho(s=0) &= \rho_\Lambda, \\ w(s=0) &= w_\Lambda(\rho_\Lambda). \end{aligned} \quad (2.180)$$

Solving the system (2.179) and (2.180) and utilizing directly the trivial solutions from the first and third equation in (2.179) we can write down the implicit relation for $\rho = \rho(\rho_\Lambda)$

$$\rho(t, \rho_\Lambda) = \rho_\Lambda + A_d \Lambda^{d+2} \int_0^t ds \frac{e^{(d+2)s}}{(\Lambda^2 e^{2s} + w_\Lambda(\rho_\Lambda))^2}. \quad (2.181)$$

Similar to the dimensionless case, we can carry out the integral on the right-hand side of (2.181) analytically

$$\rho(t, \rho_\Lambda) = \rho_\Lambda + A_d \Lambda^{d+2} \left[\frac{e^{(d+2)s}}{2w_\Lambda^2} \left(\frac{w_\Lambda}{e^{2s} w_\Lambda} - \frac{d}{d+2} {}_2F_1\left(1, \frac{d+2}{2}, \frac{d+4}{2}, -\frac{e^{2s}}{w_\Lambda}\right) \right) \right]_{s=0}^{s=t}, \quad (2.182)$$

where we have suppressed the dependence of w_Λ on ρ_Λ . The first quantity of interest is the minimum of the effective potential, which is determined by $w(t) = 0$ and therefore by $w_\Lambda(\rho_\Lambda(t, \rho))$. Setting $w_\Lambda = 0$ in (2.180) the integral is easily solvable and we obtain

$$\rho_{\min}(t) = \rho_{0,\min} - \Lambda^{d-2} \frac{A_d}{d-2} (1 - e^{(d-2)t}), \quad (2.183)$$

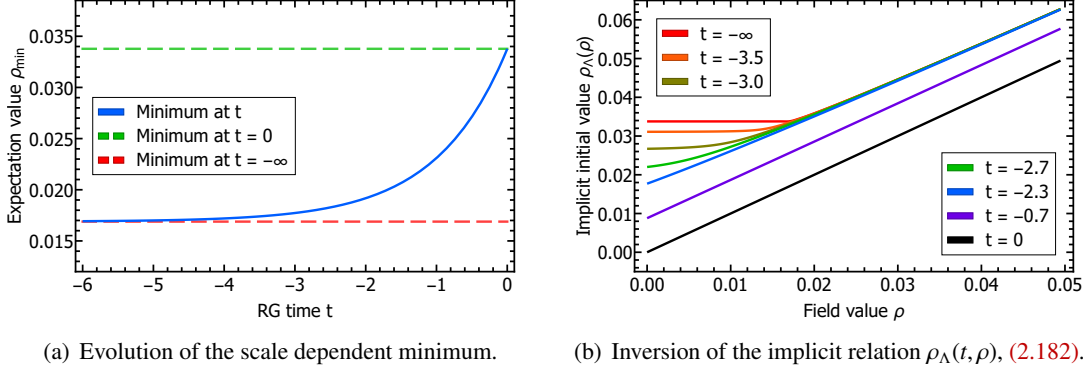


Figure 2.14.: Solution of the large N potential for $d = 3$, $\Lambda = 1$, $m_\Lambda^2 = -\frac{1}{9\pi^2}$ and $\lambda_\Lambda = 1$.

where the property $\rho_{\min}(t) \leq \rho_\Lambda$ is obvious, as already discussed in Section 2.3.4. Additionally, (2.183) seems to hint towards a peculiarity for $d = 2$. Continuous phase transitions in $d \leq 2$ are precisely the content of the Mermin-Wagner ((Mermin-Wagner-Hohenberg-Coleman) theorem [70, 71], which states the absence of phase transitions in theories with continuous symmetries. However, any connection with (2.183) should be treated with extreme care, a more detailed on this issue within the FRG can be found in [72, 73, 74, 75]. Therefore, not everything in the remainder of this section applies to $d \leq 2$. We now turn back to the inversion of (2.182), or equivalently (2.181). From (2.181) it is obvious that for $w_\Lambda(\rho_\Lambda) < 0$ there might exist a t_{crit} for which the integrand becomes singular, i.e. there exists no solution to $\rho = \rho(t < t_{\text{crit}}, \rho_\Lambda)$. Nevertheless, it is easy to see that we have $\rho(t < t_{\text{crit}}, \rho_\Lambda) = \rho_{\min}(t)$, which reproduces a convex potential. It is now easy to derive in which phase the flow will end, taking the limit $t \rightarrow -\infty$, we obtain the surprisingly simple relation, valid for all dimensions,

$$\rho_{\min}(t \rightarrow -\infty) = \rho_{\Lambda, \min} - \Lambda^{d-2} \frac{A_d}{d-2}. \quad (2.184)$$

Before we discuss its physical implications, we note that (2.184) has the peculiar property that the reduction of ρ_{\min} is independent on the initial parameters of the theory. We emphasise, however, that the initial parameters such as $\rho_{\Lambda, \min}$ carry the regularisation procedure of the theory in the terms proportional to positive powers of Λ , for the detailed discussion see Section 2.3.1. This clearly signals the subtraction as merely more than a regularisation term. Still, it carries physics (as do β -functions) which is seen in the case $d \rightarrow 0$. There, the subtraction tends towards infinity, and no initial effective potential can be found which leads to a non-vanishing minimum at $k = 0$,

$$\rho_{\min}|_{k=0, d=2} = 0. \quad (2.185)$$

Equation (2.185) is nothing but the Mermin-Wagner theorem in a nutshell: It states that no spontaneous symmetry breaking of a continuous symmetry takes place in $d = 2$ dimensions. This is reflected in the vanishing minimum in (2.185). Note also that this does not exclude the Berezinsky–Kosterlitz–Thouless phase transition.

We now turn to an explicit example, setting the initial scale to $\Lambda = 1$, going to $d = 3$ and taking a quadratic initial potential, c.f. (2.156), the initial derivative reads

$$w_\Lambda = m_\Lambda^2 + \frac{\lambda_\Lambda}{3}\rho. \quad (2.186)$$

The initial minimum is then located at $\rho_{\Lambda,\min} = -3m_\Lambda^2/\lambda_\Lambda$ and the final one at

$$\rho_{k \rightarrow 0, \min} = -3 \frac{m_\Lambda^2}{\lambda_\Lambda} - \frac{1}{(6\pi^2)}. \quad (2.187)$$

As initial parameters we chose $m_\Lambda^2 = -\frac{1}{9\pi^2}$ and $\lambda_\Lambda = 1$, resulting in

$$\rho_{\Lambda,\min} = \frac{1}{3\pi^2} \quad \text{and} \quad \rho_{k=0,\min} = \frac{1}{6\pi^2} = \frac{1}{2}\rho_{\Lambda,\min}, \quad (2.188)$$

shown in [Figure 2.14\(a\)](#). Inverting the implicit relation [\(2.182\)](#) numerically, we obtain the function $\rho_\Lambda(t, \rho)$, shown in [Figure 2.14\(b\)](#).

Exercises

This set of exercises is rather similar to the first one, but we are considering a different method, i.e. the Functional Renormalisation Group, and a slightly different theory. The Lagrangian for this theory is given by

$$\mathcal{L}[\phi] = \phi_a \frac{1}{2}(p^2 + m^2)\phi^a + \frac{\lambda}{4!}(\phi_a\phi^a)^2, \quad (2.189)$$

which is $O(N)$ -symmetric, i.e. $a \in (1, \dots, N)$. Due to spontaneous symmetry breaking the invariant $\rho = \frac{1}{2}\phi_a\phi^a$ can assume a finite expectation value, which we assume to be space-time independent throughout this set of exercises.

Exercise 4: Effective potential from the FRG

In the following we are going to calculate a differential equation for the effective potential in d space-time dimensions for a scalar theory. In order to truncate the infinite tower of equations we work in a derivative expansion, i.e. full correlation functions at vanishing momentum are given derivatives of the effective potential. This time we have to take the $O(N)$ symmetry into account, therefore we introduce the invariant $\rho = \frac{1}{2}\phi_a\phi^a$. The propagator is again given by

$$\Gamma_{\phi_i\phi_j}^{(2)}(p) = p^2 + V^{(2)}(\rho), \quad (2.190)$$

taking the substructure into account we arrive at

$$\frac{\delta}{\delta\phi_a} \frac{\delta}{\delta\phi_b} V(\rho) = \delta_{ab} V^{(1)}(\rho) + \delta_{Na} \delta_{Nb} 2\rho V^{(2)}(\rho). \quad (2.191)$$

Therefore, you can explicitly work with a single component field σ and a $(N-1)$ component field π . As a regulator we are using the Litim regulator

$$R_k(p) = (k^2 - p^2)\theta(k^2 - p^2). \quad (2.192)$$

Derive the partial differential equation for the effective potential. As an intermediate step you should find

$$\partial_t V(\rho)_k = \frac{1}{2} \int_q \left(\frac{N-1}{k^2 + V_k^{(1)}(\rho)} + \frac{1}{k^2 + V_k^{(1)}(\rho) + 2\rho V_k^{(2)}(\rho)} \right) \partial_t R_k(q). \quad (2.193)$$

As a last step, solve the integral on the right-hand side of (2.193).

Exercise 5: FRG equation for the two-point function

Solving Exercise 6 renders this exercise trivial.

Derive the FRG equation for the two-point function for the same theory as in [Exercise 4](#).

Exercise 6: FRG equations for general theories

Derive the FRG equation for the two-point function in the superfield formalism. In order to do this, recall the definitions from [Exercise 3](#). The master equation reads

$$\dot{\Gamma}_k[\Phi] = \frac{1}{2} \text{Tr} \{ G_{ab} \dot{R}^{ab} \}, \quad (2.194)$$

where the dot denote the derivative with respect to RG-time $t = \ln k/\Lambda$.

2.4. Flows for Fermi-Bose mixtures

So far we have considered a scalar ϕ^4 -theory as our example theory, here we extend our setup to generic theories with relativistic fermions and scalars. In the Standard Model this describes the matter sector with quarks q , and leptons l , coupled to the Higgs H . In the spirit of our application also to low energy QCD such a theory can model the interaction of the composite mesons, e.g. the pseudo-scalar pions $\vec{\pi}$ and scalar resonances σ with the fundamental quarks q and antiquarks \bar{q} . The mesons are composed out of quarks and anti-quarks, they are in a rough approximation $q - \bar{q}$ states. Such low energy effective models will be investigated later in [Part II](#), while the asymptotically safe Standard Model is considered in [??](#).

2.4.1. Yukawa theory

Both these situations are more elaborated version of simply adding a Dirac fermion to our scalar theory with a Yukawa interaction. The Dirac action of a massive fermion is given by

$$S_D[\psi, \bar{\psi}] = \int_x \bar{\psi}(x) (\not{d} + m_\psi) \psi(x), \quad \{\psi(x), \bar{\psi}(y)\} = 0, \quad (2.195)$$

with the Grassmann-valued fields $\psi, \bar{\psi}$, and the Euclidean Dirac operator and Clifford algebra

$$\not{d} = \gamma_\mu \partial_\mu, \quad \text{with} \quad \{\gamma_\mu, \gamma_\nu\} = 2\delta_{\mu\nu}, \quad \gamma_\mu = \gamma_\mu^\dagger, \quad \text{Tr } \gamma_\mu = 0. \quad (2.196)$$

From [\(2.196\)](#) it follows that $\gamma_\mu^2 = 1\!\!1$. For our example theory we also define γ_5 with

$$\gamma_5 = \gamma_0 \gamma_1 \gamma_2 \gamma_3, \quad \text{with} \quad \gamma_5^2 = 1\!\!1, \quad \{\gamma_5, \gamma_\mu\} = 0, \quad \text{Tr } \gamma_5 = 0, \quad (2.197)$$

where the properties of γ_5 follow from that of γ_μ in [\(2.196\)](#). Strictly speaking ψ and $\bar{\psi}$ are independent Grassmann variables in the Euclidean setup. Nonetheless, for the transformation properties in particular under chiral transformations it is useful to keep in mind the Dirac conjugation in Minkowski space-time,

$$\bar{\psi}(x) = \psi^\dagger(x) \gamma_0. \quad (2.198)$$

The coupling to an $O(2)$ scalar field $\phi = (\sigma, \pi)$ is given by the following Yukawa interaction,

$$S_h[\psi, \bar{\psi}, \phi] = \frac{h_\sigma}{\sqrt{2}} \int_x \bar{\psi}(x) [\sigma(x) + i\gamma_5 \pi(x)] \psi(x), \quad (2.199)$$

with the coupling of σ and π to the scalar and pseudo-scalar currents, $\bar{\psi}\psi$ and $\bar{\psi}\gamma_5\psi$ respectively. This signifies σ and π as scalar and pseudo-scalar fields. The Yukawa theory introduced above is completed with a kinetic term as well as an self-interaction term for the scalars, see [\(2.160\)](#),

$$S_\phi[\phi] = \frac{1}{2} \int_x \phi^a(x) [-\partial_\mu^2 + m_\phi^2] \phi^a(x) + \frac{\lambda_\phi}{2} \int_x \rho(x)^2, \quad (2.200)$$

where

$$\rho = \frac{\phi^a \phi^a}{2} = \frac{\sigma^2 + \pi^2}{2}, \quad \text{with} \quad a = 1, 2. \quad (2.201)$$

In [\(2.200\)](#) we have added a ϕ^4 term for the sake of completeness. In summary we have

$$S_Y[\psi, \bar{\psi}, \phi] = S_D[\psi, \bar{\psi}] + S_\phi[\phi] + S_h[\psi, \bar{\psi}, \phi]. \quad (2.202)$$

Note that the Yukawa theory above can also be formulated in terms of the complex scalar field $\phi = \sigma + i\pi$, reflecting the equivalence of $O(2) \simeq U(1)$.

In the absence of the fermionic mass term the theory above has a global axial $U(1)$ -symmetry under the combined transformation

$$\psi \rightarrow e^{i\alpha\gamma_5}\psi, \quad \bar{\psi} \rightarrow \bar{\psi} e^{i\alpha\gamma_5}, \quad \phi \rightarrow e^{-2i\alpha}\phi, \quad (2.203)$$

which is an axial rotation on the fermions $\psi, \bar{\psi}$ and an $O(2) \simeq U(1)$ rotation on the scalars. Note that the transformation property of $\bar{\psi}$ follows from that of ψ in Minkowski space with (2.198) and $\{\gamma_5, \gamma_\mu\} = 0$, see (2.197). The invariance of the Yukawa action (11.89) under (2.203) is easily seen with the infinitesimal transformations

$$\psi \rightarrow \psi + i\alpha\gamma_5\psi, \quad \bar{\psi} \rightarrow \bar{\psi} + i\alpha\bar{\psi}\gamma_5, \quad \sigma \rightarrow \sigma + 2\alpha\pi, \quad \pi \rightarrow \pi - 2\alpha\sigma, \quad (2.204)$$

for the fields. The infinitesimal fermionic transformations imply the infinitesimal transformation laws for the currents

$$\bar{\psi}\psi \rightarrow \bar{\psi}\psi + 2i\alpha\bar{\psi}\gamma_5\psi, \quad i\bar{\psi}\gamma_5\psi \rightarrow i\bar{\psi}\gamma_5\psi - 2\alpha\bar{\psi}\psi. \quad (2.205)$$

Note that (2.205) are the same transformation laws as for the scalar fields with the identification $\sigma \propto \bar{\psi}\psi$ and $\pi \propto i\bar{\psi}\gamma_5\psi$. Applying the global infinitesimal axial transformations (2.204), (2.205) in the Yukawa action (11.89) we are led to

$$S_Y[\psi, \bar{\psi}, \phi] \rightarrow S_Y[\psi, \bar{\psi}, \phi] + 2im_\psi \int_x \bar{\psi}(x)\gamma_5\psi(x), \quad (2.206)$$

where the transformation property of the mass term follows directly from (2.205). For proving the invariance of all the other terms in (2.206) we first notice that the scalar potential is trivially invariant as $\rho = \phi^*\phi/2$. The scalar kinetic term reads $-\int_x \phi^*\partial^2\phi$ and hence also is invariant. The variations of the two terms in the Yukawa interaction annihilate each other:

$$\sigma\bar{\psi}\psi \rightarrow \sigma\bar{\psi}\psi + 2\alpha(\pi\bar{\psi}\psi + \sigma i\bar{\psi}\gamma_5\psi), \quad \pi i\bar{\psi}\psi \rightarrow \pi i\bar{\psi}\psi - 2\alpha(\sigma i\bar{\psi}\gamma_5\psi + \pi\bar{\psi}\psi). \quad (2.207)$$

In (2.207) the first terms in the parentheses comes from the transformation of the scalar fields, while the second comes from the transformation of the currents. Finally we use that the vector current is invariant,

$$\bar{\psi}\gamma_\mu\psi \rightarrow \bar{\psi}\gamma_\mu\psi, \quad \text{and} \quad \bar{\psi}\gamma_\mu\partial_\mu\psi \rightarrow \bar{\psi}\gamma_\mu\partial_\mu\psi. \quad (2.208)$$

For (2.206) we have used that the scalar action S_ϕ is invariant under the $O(2)$ -rotations in (2.203). The Dirac term $\bar{\psi}\not{\partial}\psi$ is invariant due to the anti-commutation relations of γ_5 and γ_μ . Finally, the fermionic mass term breaks the chiral symmetry explicitly. Accordingly, it follows immediately from (2.206) for $m_\psi = 0$ the Yukawa action is invariant under axial rotations.

For $\lambda_\phi = 0$ the mass term can be absorbed in a redefinition of the field σ with

$$\sigma \rightarrow \sigma - \frac{\sqrt{2}}{h_\sigma}m_\psi. \quad (2.209)$$

Then the Yukawa action (11.89) turns into

$$S_Y[\psi, \bar{\psi}, \phi] \simeq \int_x \left\{ \bar{\psi}\not{\partial}\psi + \frac{1}{2}\phi^a \left[-\partial_\mu^2 + m_\phi^2 \right] \phi^a + \frac{h_\sigma}{\sqrt{2}}\bar{\psi}[\sigma + i\gamma_5\pi]\psi \right\} - c_\sigma \int_x \sigma, \quad (2.210)$$

with

$$c_\sigma = \frac{\sqrt{2}}{h_\sigma} m_\phi^2 m_\psi . \quad (2.211)$$

In (2.210) we have dropped a term which is independent of the fields. In (2.210) the fermionic mass term has disappeared, while the term linear in σ breaks the $O(2) \simeq U(1)$ symmetry explicitly. This makes again apparent that the scalar $O(2)$ -symmetry is nothing but the chiral symmetry of the fermions.

For $\lambda_\phi = 0$ the Yukawa action (11.89) is quadratic in the scalar field and can be solved for ϕ . Its equations of motion $\phi_0 = (\sigma_0, \pi_0)$ read

$$\sigma_0 = -\frac{h_\sigma}{\sqrt{2}} \frac{1}{-\partial^2 + m_\phi^2} \bar{\psi} \psi , \quad \pi_0 = -i \frac{h_\sigma}{\sqrt{2}} \frac{1}{-\partial^2 + m_\phi^2} \bar{\psi} \gamma_5 \psi . \quad (2.212)$$

It is easy to see with (2.205) that the EoM ϕ_0 has the transformation law (2.203) of the scalar fields as already stated above. Reinserting (2.212) in the Yukawa action gives a –non-local– four-fermi action with the axial symmetry (2.203),

$$S_{\text{NL-NJL}}[\psi, \bar{\psi}] = S_D[\psi, \bar{\psi}] - \frac{h_\sigma^2}{4} \int_x \left[(\bar{\psi} \psi) \frac{1}{-\partial^2 + m_\phi^2} (\bar{\psi} \psi) - (\bar{\psi} \gamma_5 \psi) \frac{1}{-\partial^2 + m_\phi^2} (\bar{\psi} \gamma_5 \psi) \right] . \quad (2.213)$$

In case we are interested in a low energy (effective) action we apply a derivative expansion to the effective action. In leading order this entails for (2.213)

$$S_{\text{NJL}}[\psi, \bar{\psi}] = S_D[\psi, \bar{\psi}] - \frac{\lambda_\psi}{2} \int_x \left[(\bar{\psi} \psi)^2 - (\bar{\psi} \gamma_5 \psi)^2 \right] , \quad \text{with} \quad \lambda_\psi = \frac{h_\sigma^2}{2m_\phi^2} , \quad (2.214)$$

the action of the *Nambu–Jona-Lasinio (NJL) model*. Starting with the NJL-model we also can derive the Yukawa theory in (11.89) without the kinetic term $1/2 \int_x \phi \partial^2 \phi$. This inverse transformation is the *Hubbard-Stratonovich transformation*, which is discussed in more detail in [Section 5.3](#).

2.4.2. Flow equation for Fermi-Bose mixtures

So far we have only introduced the classical action of a generic scalar-fermion model, and discussed the symmetries and other properties of our specific example. For the sake of simplicity we can reduce the theory even further to a real scalar field coupled to a Dirac fermion with $O(1) \simeq Z_2$ symmetry. It is left to quantise the theory with the flow equation. For the sake of completeness we also quote the path integral representation of the generating functional for this theory, already in the presence of regulator terms for both, scalars and fermions,

$$\mathcal{Z}_k[J, \eta, \bar{\eta}] \simeq \int [d\varphi d\psi d\bar{\psi}]_{\text{ren}} e^{-S_Y[\psi, \bar{\psi}, \varphi] - \Delta S_k[\psi, \bar{\psi}, \varphi] + \int_x [\bar{\eta}(x)\psi(x) - \bar{\psi}(x)\eta(x) + J(x)\varphi(x)]} , \quad (2.215)$$

where

$$\Delta S_k[\psi, \bar{\psi}, \varphi] = \Delta S_{\psi,k}[\psi, \bar{\psi}] + \Delta S_{\varphi,k}[\varphi] . \quad (2.216)$$

The generating functional for connected correlation function, the Schwinger functional, is given by $\mathcal{W}_k[J, \eta, \bar{\eta}] = \ln \mathcal{Z}[J, \eta, \bar{\eta}]$, and the mean fields follow as

$$\frac{\delta \mathcal{W}_k[J, \eta, \bar{\eta}]}{\delta \bar{\eta}(x)} = \langle \psi(x) \rangle , \quad \frac{\delta \mathcal{W}_k[J, \eta, \bar{\eta}]}{\delta \eta(x)} = \langle \bar{\psi}(x) \rangle , \quad \frac{\delta \mathcal{W}_k[J, \eta, \bar{\eta}]}{\delta J(x)} = \langle \varphi(x) \rangle . \quad (2.217)$$

The regulator term $\Delta S_{\phi,k}$, (2.4), for the scalars has been already discussed at length. For the distinction to the fermionic regulator function we now call the one for the scalar $R_{\phi,k}$, examples are given in (2.6) with shape functions r_ϕ as in 2.9. The fermionic one is defined similarly,

$$\Delta S_{\psi,k}[\psi, \bar{\psi}] = \int_p \bar{\psi}(-p) R_{\psi,k}(p) \psi(p), \quad \text{with} \quad R_{\psi,k} = i \not{p} r_\psi(x), \quad x = \frac{p^2}{k^2}. \quad (2.218)$$

The form of the regulator in (2.218) guarantees that the symmetries of the kinetic term are maintained by the cutoff term. In particular this applies to the axial or chiral symmetry already discussed above. In turn, a scalar cutoff term with a momentum-dependent mass function $R_{\psi,k}$ breaks chiral symmetry explicitly. Given the importance of chiral symmetry in the discussion of spontaneous chiral symmetry breaking both in QCD and also in the Standard model with the Higgs mechanism, a chiral cutoff is preferred. In order to elucidate some of the following relations and discussions we also consider explicitly the free theory with $h_\sigma = 0, \lambda_\phi = 0$. Then, the path integral in (2.215) can be solved and we arrive at

$$\mathcal{W}_k[J, \eta, \bar{\eta}] = - \int_{x,y} \bar{\eta}(x) \frac{1}{\not{\partial}[1 + r_\psi] + m_\psi} (x, y) \eta(y) + \int_{x,y} J(x) \frac{1}{-\partial^2[1 + r_\phi] + m_\phi^2} J(y). \quad (2.219)$$

The shape function $r_\psi(x)$ has to diverge for (2.218) being an infrared cutoff term. A possible choice is one of the shape functions in (2.218). A more common and natural choice are shape functions that diverge with $1/p$. We argue for this choice with considering the regularised propagator $G_\psi = \langle \psi \bar{\psi} \rangle_{\text{con}}$ of the free theory.

$$G_\psi(x, y) = \langle \psi(x) \bar{\psi}(y) \rangle_{\text{con}} = \frac{\delta^2 \mathcal{W}[J, \eta, \bar{\eta}]}{\delta \bar{\eta}(x) \delta \eta(y)} = \frac{1}{\not{\partial}[1 + r_\psi] + m_\psi}(x, y). \quad (2.220)$$

The free propagator (2.220) reads in momentum space

$$G_{\psi,k}(p) = \frac{1}{i \not{p}[1 + r_\psi(x)] + m_\psi} = \frac{-i \not{p}[1 + r_\psi(x)] + m_\psi}{p^2[1 + r_\psi(x)]^2 + m_\psi}. \quad (2.221)$$

Equation (2.221) elucidates the property of the Dirac dispersion as the 'square-root' of the scalar Klein-Gordon dispersion in the denominator. Hence, in analogy to the cutoff of the scalar theory we choose

$$[1 + r_\psi(x)]^2 = 1 + r_\phi(x) \quad \rightarrow \quad 1 + r_\psi(x) = \sqrt{1 + r_\phi(x)}, \quad \partial_t r_\psi(x) = \frac{1}{2} \frac{\partial_t r_\phi(x)}{1 + r_\phi(x)}, \quad (2.222)$$

with the scalar shape functions $r_\phi = r$ in 2.9 and $1 + r_\phi > 0$. The effective action of the theory is defined with a slight abuse of notation (no new symbols for the fermionnic mean fields)

$$\Gamma_k[\psi, \bar{\psi}, \phi] = \int_x [\bar{\eta}(x) \psi(x) - \bar{\psi}(x) \eta(x) + J(x) \phi(x)] - \mathcal{W}_k[J, \eta, \bar{\eta}] - \Delta S_k[\psi, \bar{\psi}, \phi], \quad (2.223)$$

with

$$\frac{\delta \Gamma_k[\psi, \bar{\psi}, \phi]}{\delta \bar{\psi}(x)} = -\bar{\eta}(x), \quad \frac{\delta \Gamma_k[\psi, \bar{\psi}, \phi]}{\delta \psi(x)} = -\eta(x), \quad \frac{\delta \Gamma_k[\psi, \bar{\psi}, \phi]}{\delta \phi(x)} = J(x). \quad (2.224)$$

With the relations (2.217) and (2.224) we derive straightforwardly that the propagator of the fermion is minus the inverse of the 1PI two-point function,

$$G_{\psi,k}(x, y) = \langle \psi(x) \bar{\psi}(y) \rangle_{\text{con}} = \frac{\delta^2 \mathcal{W}_k}{\delta \bar{\eta}(x) \delta \eta(y)} = \left[\frac{1}{\Gamma_k^{(2)} + R_k} \right]_{\psi \bar{\psi}}(x, y), \quad (2.225)$$

from

$$\int_z \left[\frac{\delta^2 \mathcal{W}_k}{\delta \bar{\eta}(x) \delta J(z)} \frac{\delta^2 \Gamma_k}{\delta \phi(z) \delta \psi(y)} - \frac{\delta^2 \mathcal{W}_k}{\delta \bar{\eta}(x) \delta \eta(z)} \frac{\delta^2 \Gamma_k}{\delta \bar{\psi}(z) \delta \psi(y)} - \frac{\delta^2 \mathcal{W}_k}{\delta \bar{\eta}(x) \delta \bar{\eta}(z)} \frac{\delta^2 \Gamma_k}{\delta \psi(z) \delta \psi(y)} \right] = \delta(x - y). \quad (2.226)$$

The above relation can be elucidated within the free theory. Then, only the middle term in (2.226) is left and we have

$$-\int_z \frac{\delta^2 \mathcal{W}_k}{\delta \bar{\eta}(x) \delta \eta(z)} \frac{\delta^2 \Gamma_k}{\delta \bar{\psi}(z) \delta \psi(y)} = \int_z \frac{1}{\not{d}[1 + r_\psi] + m_\psi} (x, z) (\not{d}[1 + r_\psi] + m_\psi)(z, y) = \delta(x - y). \quad (2.227)$$

The above derivation make clear that a consistent book keeping of the Grassmann properties of the n -point functions is crucially important for global consistency and in particular the relative signs of diagrams. In the following we will use the notation

$$\Gamma_{\varphi_1 \cdots \varphi_n, k}^{(n)}[\Phi] = \frac{\delta \Gamma_k[\Phi]}{\delta \varphi_n \cdots \delta \varphi_1}, \quad (2.228)$$

where φ_i are the entries in Φ , e.g. $\varphi_1 = \psi$. For the fermions this e.g. entails that

$$\Gamma_{\bar{\psi}\psi}^{(2)}(x, y) = \frac{\delta \Gamma_k[\Phi]}{\delta \psi(y) \delta \bar{\psi}(x)}. \quad (2.229)$$

The flow equation is now derived without any further reference to the path integral. The latter has been only used here for introducing some relations and notation. In analogy to the scalar case in (2.1) the infrared regularised generating functional \mathcal{Z}_k is given by

$$\mathcal{Z}_k[J, \eta, \bar{\eta}] = e^{-\Delta S_{\phi, k} \left[\frac{\delta}{\delta J} \right] - \Delta S_{\psi, k} \left[\frac{\delta}{\delta \bar{\eta}}, \frac{\delta}{\delta \eta} \right]} \mathcal{Z}[J, \eta, \bar{\eta}]. \quad (2.230)$$

Taking the t -derivative of (2.230) and using (2.225) we arrive at

$$\partial_t \Gamma_k[\psi, \bar{\psi}, \phi] = \frac{1}{2} \text{Tr } G_{\phi, k}[\psi, \bar{\psi}, \phi] \partial_t R_{\phi, k} - \text{Tr } G_{\psi, k}[\psi, \bar{\psi}, \phi] \partial_t R_{\psi, k}. \quad (2.231)$$

From its structure, (2.231) covers the flow of generic theories with bosons and fermions. The fermionic part of the flow has the relative minus sign originating in the Grassmannian nature of the fermionic fields. If (2.231) is expanded perturbatively, see Section 2.3.1, this minus sign generates the minus signs of perturbative fermionic loops. Note also that the traces for the scalar loop and the fermion loop differ by the additional sum over Dirac indices generating additional factors of 4 for diagonal matrices.

2.4.3. Condensed notation*

It is evident from the derivation in the last chapter that a uniform notation would help greatly to simplify the expressions. To that end we introduce the superfield Φ and the related symplectic metric γ with

$$(\Phi_a) = (\psi, \bar{\psi}, \phi)^T, \quad (\gamma^{ab}) = \begin{pmatrix} 0 & 1 & 0 \\ -1 & 0 & 0 \\ 0 & 0 & 1 \end{pmatrix}, \quad (2.232)$$

see also Exercise 3 and [9]. This allows us to define a dual field with

$$(\Phi^a) = \gamma^{ab} \Phi_b = (\bar{\psi}, -\psi, \phi). \quad (2.233)$$

By our convention indices are always raised from the left and lowered from the right, e.g. $\Phi^a = \gamma^{ab}\Phi_b = \Phi_b\gamma^{ab}$. This immediately implies the following identities

$$\begin{aligned}\gamma_a^b &= \gamma^{bc}\gamma_{ac} = \gamma^{cb}\gamma_{ca} = \delta_a^b \\ \gamma^a_b &= \gamma^{ac}\gamma_{cb} = \gamma^{ca}\gamma_{bc} = (-1)^{ab}\delta_b^a,\end{aligned}\quad (2.234)$$

where $(-1)^{ab}$ is -1 iff a and b are fermionic and 1 else. This notation allows us to write the cutoff term in a symmetric way,

$$\Delta S_k[\Phi] = \frac{1}{2}\Phi_a R_k^{ab}\Phi_b. \quad (2.235)$$

[Equation \(2.235\)](#) is the fully condensed notation, where the index a also sums over space-time or momenta, and the respective integrals are dropped, see also [9]. The factor 1/2 now takes into account that we doubled the fermionic cutoff term with the superfield. The superfield cutoff (R_k^{ab}) is given by the matrix

$$(R_k^{ab}) = \begin{pmatrix} 0 & -R_{\psi,k} & 0 \\ R_{\psi,k} & 0 & 0 \\ 0 & 0 & R_{\phi,k} \end{pmatrix}. \quad (2.236)$$

Substituting (2.236) in (2.235) and reinstating the momentum integral leads to the explicit representation of the cutoff term in (2.216). With the concise notation in (2.235) the generic flow equation follows straightforwardly as

$$\partial_t \Gamma_k[\Phi] = \frac{1}{2}G_{k,ab}[\Phi]\partial_t R_k^{ab}. \quad (2.237)$$

[Equation \(2.237\)](#) covers general theories with bosonic and fermionic fields, including non-Abelian gauge fields and gravity.

2.4.4. Flow for Fermi-Bose mixtures in LPA

We now evaluate the flow of our Yukawa theory in the representation (2.210) within LPA at $\psi, \bar{\psi} = 0$. Then the flow diagonalises as the two point function block-diagonalises for constant scalar fields $\phi = (\sigma, 0)$.

$$\begin{aligned}\frac{\delta^2 \Gamma_k}{\delta \bar{\psi} \delta \psi}(p) &= i \not{p} [1 + r] + \frac{h_\sigma}{\sqrt{2}}\sigma, \\ \frac{\delta^2 \Gamma_k}{\delta \phi_i \delta \phi_j}(p) &= p^2 [1 + r] + \frac{\delta^2 V(\phi)}{\delta \phi \delta \phi}.\end{aligned}\quad (2.238)$$

Note that the linear term in (2.210) drops out, i.e. the flow knows nothing about the explicit chiral symmetry breaking. This fact cannot be emphasised enough, as it entails that we simply have to solve the theory without explicit symmetry breaking and the theories with explicit symmetry breaking follows from evaluating the correlation functions $\Gamma^{(n)}$ on a different background; i.e. the EoM $\Phi_0(c_\sigma)$ with

$$\left. \frac{\delta \Gamma[\Phi]}{\delta \sigma} \right|_{\Phi=\Phi_0(c_\sigma)} = c_\sigma, \quad (2.239)$$

with c_σ defined in (2.211). We also note that the scalar part of the flow is that of the $O(2)$ -model and is given by (2.163) with $N = 2$. In the following we consider explicitly the flow (2.164) with the Litim regulator 2.9a. The fermionic flow reads for general shape functions

$$-\text{Tr } G_{\psi,k} \partial_t R_{\psi,k} = -\frac{2\Omega_d}{(2\pi)^d} k^d \int_0^\infty dx x^{d/2-1} \frac{x[1+r_\psi(x)] \partial_t r_\psi(x)}{x[1+r_\psi(x)]^2 + \frac{h_\sigma^2}{2} \frac{\sigma^2}{k^2}}, \quad (2.240)$$

with Ω_d defined in (2.71). Now we employ the fermionic regulator with the property (2.222) with the scalar shape function $r_\phi(x) = (1/x - 1)\theta(1-x)$ of the Litim regulator. This leads us to

$$r_\psi(x) = \left[\frac{1}{\sqrt{x}} - 1 \right] \theta(1-x), \quad \text{with} \quad \partial_t r_\psi(x) = \frac{1}{\sqrt{x}} \theta(1-x). \quad (2.241)$$

With (2.241) the flow (2.240) reduces to

$$-\text{Tr } G_{\psi,k} \partial_t R_{\psi,k} = -4 \frac{\Omega_d}{(2\pi)^d} \frac{k^{d+2}}{d} \frac{1}{k^2 + \frac{h_\sigma^2}{2} \sigma^2}. \quad (2.242)$$

Collecting both parts, the scalar flow with the Litim regulator, (2.164) and the fermionic one in (2.242) we arrive at the final flow equation for the effective potential $V_k(\rho)$ in our Yukawa theory in LPA,

$$\partial_t V_k(\rho) = \frac{\Omega_d}{(2\pi)^d} \frac{k^{d+2}}{d} \left(\frac{1}{k^2 + V'_k(\rho)} + \frac{1}{k^2 + V'_k(\rho) + 2\rho V''_k(\rho)} \right) - 4 \frac{\Omega_d}{(2\pi)^d} \frac{k^{d+2}}{d} \frac{1}{k^2 + h_\sigma^2 \rho}, \quad (2.243)$$

where the first part of the scalar flow comes from the pion and the second part comes from the σ field. Interestingly, up to the relative minus sign and the additional factor 4 from the Dirac trace the fermionic part of the flow (2.244) is simply the scalar flow for $N = 1$ within the ϕ^4 -approximation and $m_\phi^2 = 0$. Then $V'(\rho) + 2\rho V''(\rho) = 3\lambda_\phi$ and the above statement follows with the identification $h_\sigma^2 = 3\lambda_\phi$.

Flow of the chiral Yukawa model in LPA

With a minor modification the model introduced in the present chapter has a direct application to QCD: it is a low energy effective theory for one flavour QCD with $N_f = 1$, where N_f is the number of flavours. It contains the dynamics of quarks q, \bar{q} with $q = \psi, \bar{q} = \bar{\psi}$ and mesons σ, π , while the gluons have been integrated out. The only change to the generic model above is that the quarks q, \bar{q} live in the fundamental representation of the gauge group $SU(3)$ and hence have a colour index, q^A, \bar{q}^A with $A = 1, 2, 3$. This class of low energy effective theories is called *Quark-Meson (QM) Models*, and is frequently used for evaluating the phase structure of QCD or for hadron physics. In the flow equation (2.244) for the effective potential every operator is colour diagonal and hence this simply triggers another prefactor for the fermionic loop, while the scalar -meson- loop is unchanged. We quote the result for general gauge groups $SU(N_c)$ for the sake of completeness and defer a full discussion to ?? and Section 5.3.

$$\partial_t V_k(\rho) = \frac{\Omega_d}{(2\pi)^d} \frac{k^{d+2}}{d} \left(\frac{1}{k^2 + V'_k(\rho)} + \frac{1}{k^2 + V'_k(\rho) + 2\rho V''_k(\rho)} \right) - 4N_c \frac{\Omega_d}{(2\pi)^d} \frac{k^{d+2}}{d} \frac{1}{k^2 + h_\sigma^2 \rho}. \quad (2.244)$$

For the remainder of the chapter we drop the colour index again, and study the more generic Yukawa theory with the flow equation (2.244) in LPA. For an application of the present results to one flavour QCD one simply has to reinstate the factor $N_c = 3$ for the fermionic contributions.

Technically, (2.244) is nothing but a driven system for the effective potential, where the driving force is given by the fermionic loop. For $h_\sigma = 0$ we are back to the scalar case. The relativ signs of fermionic and bosonic flows in (2.244) allows us to discuss the structure of spontaneous symmetry breaking in a

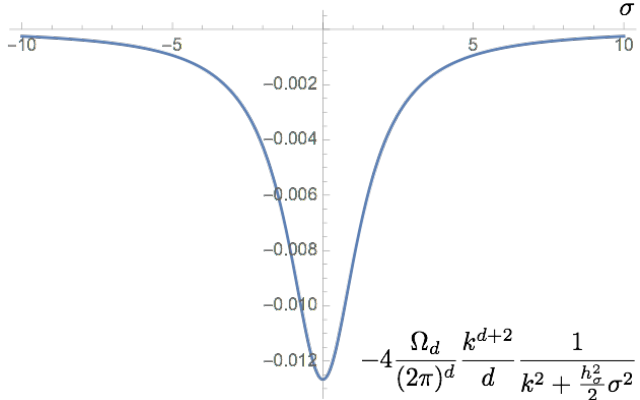


Figure 2.15.: Fermionic contribution to $\partial_t V_k$ in LPA, (2.244), in the Yukawa theory (11.89) in units of the cutoff scale k . Here, $d = 4$ and $h_\sigma = 1$.

concise way: Typically, the dynamics at large momentum scales is driven by the fermions. This holds e.g. true for QCD, where the quarks are the fundamental degrees of freedom. Their interaction with the gluons generates four fermi interactions that can be rewritten in terms of the Yukawa theory discussed here via the Hubbard Stratonovich transformation. Then, at a sufficiently large scale we are left with a small or vanishing $\lambda_{\phi,\Lambda}$, and the dynamics is driven by the quarks. The initial effective potential is then given by

$$V_\Lambda(\rho) = V_\Lambda^\phi(\rho) + V_\Lambda^\psi(\rho) = m_{\phi,\Lambda}^2 \rho + \frac{1}{2} \lambda_{\phi,\Lambda} \rho^2 + O\left(\frac{\rho}{\Lambda^2}\right), \quad (2.245)$$

where the two parts $V_\Lambda^\phi(\rho)$ and $V_\Lambda^\psi(\rho)$ compensate the Λ -dependence of the integrated bosonic and fermionic flows respectively. Note that the full initial potential is non-polynomial in most cases and only tends towards a polynomial for asymptotically large cutoff scales Λ .

We first study the fermionic flow in more detail. Its contribution to the effective potential is negative and is peaked at $\rho = 0$, see Figure 2.15. Integrating this flow down to lower scales leads to a non-convex contribution to the effective potential, its form is essentially minus the flow depicted in Figure 2.15. Indeed, the fermionic flow is easily integrated analytically as the only cutoff dependence on the right hand side of (2.240) originates in the regulator. This leads us to

$$-\int_\Lambda^{k_{\text{out}}} \frac{dk}{k} \text{Tr} G_{\psi,k} \partial_t R_{\psi,k} = -\text{Tr} \left[\ln \left(\Gamma_{\bar{\psi}\psi,k_{\text{out}}}^{(2)} + R_{\psi,k_{\text{out}}} \right) - \ln \left(\Gamma_{\bar{\psi}\psi,\Lambda}^{(2)} + R_{\psi,\Lambda} \right) \right], \quad (2.246)$$

for the notation $\Gamma_{\bar{\psi}\psi,k}^{(2)}$ see (2.228). This is simply the fermionic part of the one loop contributions to the effective action. In other words, the present LPA approximation only includes one loop fermionic contributions. Note that the integrated fermionic flow with $\bar{\psi}=0$ is regulator independent as can be seen from (2.228). The subtraction at Λ is regulator dependent, which is compensated by the initial condition, arranging for RG-consistency, see (2.35). For the Litim flow (2.242) all integrals can be performed

analytically and we arrive at

$$-\int_{\Lambda}^{k_{\text{out}}} \frac{dk}{k} \text{Tr } G_{\psi,k} \partial_t R_{\psi,k} = - \left[\frac{8}{2^d \pi^{d/2}} \frac{k^d}{d(d+2)\Gamma(\frac{d}{2})} \frac{k^2}{h_{\sigma}^2 \rho} {}_2F_1 \left(1, \frac{d+2}{2}; \frac{d+2}{2} + 1; -\frac{k^2}{h_{\sigma}^2 \rho} \right) \right]_{\Lambda}^{k_{\text{out}}}. \quad (2.247)$$

Note that the expression in the square bracket in (2.247) vanishes for $k = 0$. At $k = \Lambda$ is is dominated by Λ -dependent terms, so seemingly no information is encoded in it. Still the computation is, up to the global minus sign, the same as in the computation of the Coleman-Weinberg potential, and indeed the hypergeometric function carries the physics at hand.

To see this more clearly we restrict ourselves to $d = 4$. We also add the part $V_{\Lambda}^{(\psi)}$ of the initial effective potential V_{Λ} in (2.245), which compensates the Λ -dependence of the integrated fermionic flow. In summary the integrated flow (2.247) with k_{out} , together with $V_{\Lambda}^{(\psi)}$, has the simple form

$$V_{\text{eff}}^{(\psi)}(\rho) \simeq -\frac{1}{16\pi^2} \left[\Lambda^2 h_{\sigma}^2 \rho + (h_{\sigma}^2 \rho)^2 \left\{ \ln \frac{h_{\sigma}^2 \rho}{\Lambda^2} - \ln \left(1 + \frac{h_{\sigma}^2 \rho}{\Lambda^2} \right) \right\} \right] + V_{\Lambda}^{(\psi)}(\rho), \quad (2.248)$$

where we have dropped field independent terms. The expression in the square bracket is the flow, integrated from $k = \Lambda$ to $k = 0$. It should have the form 2.15. For $\rho \rightarrow 0$ the linear term in ρ dominates and hence with $V' \rho \rightarrow 0 < 0$ the expression is peaked at $\rho = 0$, its value being zero. For asymptotically large $h_{\sigma}^2 \rho / \Lambda^2 \gg 1$ the expression should tend towards a negative constant proportional to Λ^4 . In this regime it is more convenient to combine the logarithms to $-\ln(1 + \Lambda^2/(h_{\sigma}^2 \rho)) \propto -\Lambda^2/(h_{\sigma}^2 \rho) + O([\Lambda^2/(h_{\sigma}^2 \rho)]^2)$. Inserting this expression in the square bracket we are led to

$$-\frac{1}{16\pi^2} \left[\Lambda^2 h_{\sigma}^2 \rho + (h_{\sigma}^2 \rho)^2 \left\{ \ln \frac{h_{\sigma}^2 \rho}{\Lambda^2} - \ln \left(1 + \frac{h_{\sigma}^2 \rho}{\Lambda^2} \right) \right\} \right] \rightarrow -\frac{1}{32\pi^2} \Lambda^4 + O\left(\frac{\Lambda^2}{h_{\sigma}^2 \rho}\right). \quad (2.249)$$

In summary, the integrated flow supports chiral symmetry breaking as it generated a non-convex piece of the potential. Note however, that this term is in leading order Λ -dependent, and RG-consistency, (2.35), fixes the Λ -dependence of $V_{\Lambda}^{(\psi)}$ such that $V_{\text{eff}}(\rho)$ is Λ -independent. As mentioned below (2.245), for finite Λ the initial effective potential is necessarily non-polynomial in order to remove the term proportional to $\ln(1 + h_{\sigma}^2 \rho / \Lambda^2)$. Note also that this term vanishes for $\Lambda \rightarrow \infty$, and the only Λ -dependent terms are proportional to $\Lambda^2 \rho$ and $\rho^2 \ln h_{\sigma}^2 \rho / \Lambda^2$. This leaves us with

$$(m_{\phi,\Lambda}^{(\psi)})^2 = \frac{1}{16\pi^2} h_{\sigma}^2 \Lambda^2 + (m_{\phi}^{(\psi)})^2, \quad \lambda_{\phi,\Lambda}^{(\psi)} = -\frac{1}{16\pi^2} h_{\sigma}^2 \ln \frac{\Lambda^2}{\Lambda_{\text{QCD}}^2} + \lambda_{\phi}^{(\psi)}, \quad (2.250)$$

with finite pieces $(m_{\phi}^{(\psi)})^2$, $\lambda_{\phi}^{(\psi)}$, that carry the physics together with Λ_{QCD}^2 . The latter references scale is not independent from $\lambda_{\phi}^{(\psi)}$, as a change in the former can be absorbed in a change of the latter. Note also that only the sums $m_{\phi}^2 = (m_{\phi}^{(\psi)})^2 + (m_{\phi}^{(\phi)})^2$ and $\lambda_{\phi} = \lambda_{\phi}^{(\psi)} + \lambda_{\phi}^{(\phi)}$ enter the initial potential. Hence, we simply drop the fermionic finite pieces and use $m_{\phi}^2 = (m_{\phi}^{(\phi)})^2$, and $\lambda_{\phi} = \lambda_{\phi}^{(\phi)}$. This leads to our final result

$$V_{\text{eff}}^{(\psi)}(\rho) \simeq -\frac{1}{16\pi^2} (h_{\sigma}^2 \rho)^2 \ln \frac{h_{\sigma}^2 \rho}{\Lambda_{\text{QCD}}^2}, \quad (2.251)$$

for the fermionic part of the effective potential, where we have dropped the physics part of the initial conditions. Up to a prefactor -4 from the Dirac trace and the minus sign due to the fermionic loop, (2.251) is precisely the logarithmic part of the Coleman-Weinberg potential with the identification $h_{\sigma}^2 \rho \rightarrow \lambda \rho$ for a ϕ^4 potential $\lambda/4! \phi^2$, see e.g. lecture notes QFT II, summer term 2017, chapter 1.4, QCD lecture notes from winter term 2017-18, chapter IV F, or [76]. The Coleman-Weinberg type potential $-V_{\text{eff}}^{(\psi)}(\rho)$ from (2.251) is depicted for $h_{\sigma} = 1$ in units of Λ_{QCD} in Figure 2.16. Clearly the potential supports a

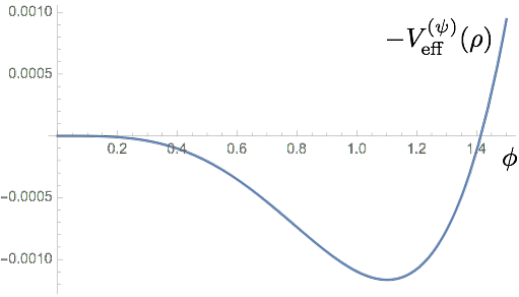


Figure 2.16.: Coleman-Weinberg type potential, $-V_{\text{eff}}^{(\psi)}(\rho)$, (2.251), for $h_\sigma = 1$ in units of Λ_{QCD} .

non-trivial minimum for ρ . It is built up in the flow and feeds into the scalar part of the flow which depends on $V'_k(\rho)$ and $V''_k(\rho)$. This part of the flow wants to restore the chiral symmetry and it is a matter of the relative size of the two parts which part wins. The relative size of the (integrated) flow is decided by the parameters in the initial effective potential $V_\Lambda(\rho)$.

This analysis can be done analytically in a complete one loop computation. Then also the scalar part can be integrated as V' and V'' in (2.244) are simply the initial V'_Λ and V''_Λ . Accordingly, we get two further contributions to the full effective action which resemble (2.251) with a relative minus sign and $h_\sigma^2 \rho \rightarrow V'(\rho)$ for the pion contribution and $h_\sigma^2 \rho \rightarrow V'(\rho) + 2\rho V''(\rho)$ for the σ -contribution. Additionally there is a finite, classical potential part of the initial effective potential V_Λ with

$$V(\rho) = m_\phi^2 \rho + \frac{\lambda_\phi}{2} \rho^2. \quad (2.252)$$

We leave it to the reader to work this out and simply quote the total result

$$V_{\text{eff}}(\rho) = V(\rho) + V_{\text{eff}}^{(\psi)}(\rho) + V_{\text{eff}}^{(\phi)}(\rho), \quad (2.253a)$$

with the scalar and fermionic flow contributions $V_{\text{eff}}^{(\phi)}$ and $V_{\text{eff}}^{(\psi)}$ respectively,

$$\begin{aligned} V_{\text{eff}}^{(\psi)}(\rho) &= -\frac{1}{16\pi^2} (h_\sigma^2 \rho)^2 \left[\ln \frac{h_\sigma^2 \rho}{\Lambda_{\text{QCD}}^2} - \frac{1}{2} \right] \\ V_{\text{eff}}^{(\phi)}(\rho) &= \frac{1}{64\pi^2} \left\{ (m_\pi^2)^2 \left[\ln \frac{m_\pi^2}{\Lambda_{\text{QCD}}^2} - \frac{1}{2} \right] + (m_\sigma^2)^2 \left[\ln \frac{m_\sigma^2}{\Lambda_{\text{QCD}}^2} - \frac{1}{2} \right] \right\}. \end{aligned} \quad (2.253b)$$

with the field-dependent mass functions $m_\pi^2(\rho)$ and $m_\sigma^2(\rho)$ defined by

$$m_\pi^2(\rho) = V'(\rho), \quad m_\sigma^2(\rho) = V'(\rho) + 2\rho V''(\rho), \quad (2.253c)$$

and the standard renormalisation conditions leading to the subtraction $-1/2$ in the square brackets. Note that this only amounts to a redefinition of the classical potential part $V(\rho)$. For a one-to-one comparison to the standard form of the Coleman-Weinberg potential additional ρ and ρ^2 contributions have to be added in order to guarantee the renormalisation conditions at hand we have not specified. In the present approach these renormalisation conditions (at $k = 0$) only determine the UV parameters $m_\psi, m_\phi^2, h_\sigma, c_\sigma$.

Finally we are interested in integrating out the quantum fluctuations non-perturbatively. This has to be done numerically. However, its consistency relies on RG-consistency of the initial conditions. For this purpose we extract the Λ -dependence of the integrated flow which can be read-off from the flow (2.244): we expand the flow at $k = \lambda$ in powers of the initial cutoff scale. This leads us to

$$\begin{aligned} \partial_t V_k(\rho)|_{k=\Lambda} &= \frac{\Omega_d}{(2\pi)^d} \frac{\Lambda^d}{d} \left(\frac{1}{1 + \frac{V'_\Lambda(\rho)}{\Lambda^2}} + \frac{1}{1 + \frac{V'_\Lambda(\rho) + 2\rho V''_\Lambda(\rho)}{\Lambda^2}} - \frac{1}{1 + \frac{h_\sigma^2 \rho}{\Lambda^2}} \right) \\ &= \frac{\Omega_d}{(2\pi)^d} \frac{1}{d} \left(\Lambda^d - \Lambda^{d-2} \left[2V'_\Lambda(\rho) + 2\rho V''_\Lambda(\rho) - h_\sigma^2 \rho \right] \right. \\ &\quad \left. + \Lambda^{d-4} \left[V'_\Lambda(\rho)^2 + \left[V'_\Lambda(\rho) + 2\rho V''_\Lambda(\rho) \right]^2 - (h_\sigma^2 \rho)^2 \right] + O(\Lambda^{d-6}) \right). \end{aligned} \quad (2.254)$$

Equation (2.254) makes the systematics apparent for general dimensions and initial effective actions. Now we restrict ourselves to the present case of a $N_f = 1$ QM model in $d = 4$ dimensions with the initial effective potential (2.245). We also drop the field-independent parts and are led to

$$\partial_t V_k(\rho)|_{k=\Lambda} \simeq -\frac{1}{32\pi^2} \left\{ \Lambda^2 \left[4\lambda_{\phi,\Lambda} \left(1 - \frac{8m_{\phi,\Lambda}^2}{\Lambda^2} \right) - h_\sigma^2 \right] \rho - \left[10\lambda_{\phi,\Lambda}^2 - h_\sigma^4 \right] \rho^2 + O\left(\frac{\rho}{\Lambda^2}\right) \right\}. \quad (2.255)$$

This leads us to the asymptotic RG equations for the UV relevant parameters $m_{\phi,\Lambda}^2, \lambda_{\phi,\Lambda}$,

$$\begin{aligned} \Lambda \partial_\Lambda m_{\phi,\Lambda}^2 &= -\frac{1}{32\pi^2} \Lambda^2 \left[4\lambda_{\phi,\Lambda} \left(1 - \frac{8m_{\phi,\Lambda}^2}{\Lambda^2} \right) - h_\sigma^2 \right], \\ \Lambda \partial_\Lambda \lambda_{\phi,\Lambda} &= \frac{1}{16\pi^2} \left[10\lambda_{\phi,\Lambda}^2 - h_\sigma^4 \right]. \end{aligned} \quad (2.256)$$

Equation (2.256) again entail that $m_{\phi,\Lambda}^2$ runs with Λ^2 and $\lambda_{\phi,\Lambda}$ runs logarithmically with Λ . Moreover, we can read off again the universal one loop β -function of the ϕ^4 -theory computed in Section 2.3.1 in (2.74). To that end we have to take into account that the scalar part of $\Lambda \partial_\Lambda \lambda_{\phi,\Lambda}$ in (2.256) is that of an $O(2)$ -theory, for $N = 1$ the factor 10 reduces to 9 as the pion would be missing. Moreover, the coupling $\lambda_\phi = \lambda/3$. Taking this into account we arrive at (2.74). Note also that the β -function in (2.256) is the universal one in the Yukawa theory with a scalar self-interaction. Note also that for asymptotically large Λ the term proportional to $m_{\phi,\Lambda}^2$ in the flow of the scalar mass is at least of two loop, as the part in $m_{\phi,\Lambda}^2$ proportional to Λ^2 only starts at one loop.

This concludes our discussion of the general properties of Fermi-Bose systems. In summary we have seen that the competing effects of scalar and fermionic contributions to the effective potential allow for and explain the rich phase structure of these theories.

3. Critical Phenomena

In the last chapters we have set up the functional renormalisation approach to QFTs. Its specific strength is the simple access to truly non-perturbative phenomena such as phase transitions and critical phenomena. This is not surprising as at their heart these are scaling phenomena. RG Methods such as the FRG are adapted to the physics of scales and hence are very amiable towards critical phenomena.

In this chapter we discuss phase transitions in generic Fermi-Bose mixtures at the example of the Yukawa model introduced in the last chapter with the action (11.89) and its flow equation (2.231). Our explicit examples here are computed in LPA, see (2.244) for the version with the Litim regulator, 2.9a for the scalar, and (2.241) for the scalar.

3.1. Phase transitions

3.1.1. Spontaneous symmetry breaking and the Goldstone theorem

In the Standard Model we have two phenomena involving spontaneous symmetry breaking. The first is the spontaneous symmetry breaking in the Higgs sector (Englert-Brout-Higgs-Guralnik-Hagen-Kibble) which provides (current) masses for the quarks and leptons as well as for the W, Z vector bosons, the gauge bosons of the weak interactions. The corresponding Goldstone boson manifest itself as the third polarisation of the massive vector bosons (Higgs-Kibble dinner).

The second phenomena is strong chiral symmetry breaking in the quark sector with a mass scale of ≈ 300 MeV. This mechanism, loosely speaking, lifts the current quark masses to constituent quark masses. For the up and down quarks the current quark mass is negligible, see Table 5.1 in Section 5.3. The corresponding Goldstone bosons, the pions $\vec{\pi}$, are composite (quark–anti-quark) states and do not appear in the QCD action.

In the following we briefly discuss similarities of and differences between these two phenomena. Before we come to the Standard Model, let us recall some basic facts about spontaneous symmetry breaking. Further details can be found in the literature. Our basic example is the $O(N)$ theory introduced in Section 2.3.4 with the action

$$S_\phi[\phi] = \frac{1}{2} \int_x (\partial_\mu \phi^a)^2 + \int_x V(\rho), \quad \text{with} \quad a = 1, \dots, N, \quad \text{and} \quad \rho = \frac{1}{2} \phi^a \phi^a, \quad (3.1)$$

and the ϕ^4 -potential

$$V(\rho) = -\mu_\phi^2 \rho + \frac{1}{2} \lambda_\phi \rho^2, \quad (3.2)$$

the generalisation of the $O(2)$ action in the example Yukawa theory studied in the last chapter. Note also that $\lambda_\phi = 3\lambda$ for the real scalar field action introduced in the very beginning in (1.1).

The following considerations only depend on the symmetries of the action, but not on the specific form (3.2). Still, the simple potential (3.2) serves as a good showcase. The action (3.1) with the potential (3.2) has an $O(N)$ -symmetry, as already stated in Section 2.3.4. It is invariant under global $O(N)$ -rotations of the field,

$$S_\phi[\Omega \phi] = S_\phi[\phi], \quad \text{where} \quad \Omega = e^{\omega^a t^a} \in O(N), \quad a = 1, \dots, \frac{N(N-1)}{2}, \quad (3.3)$$

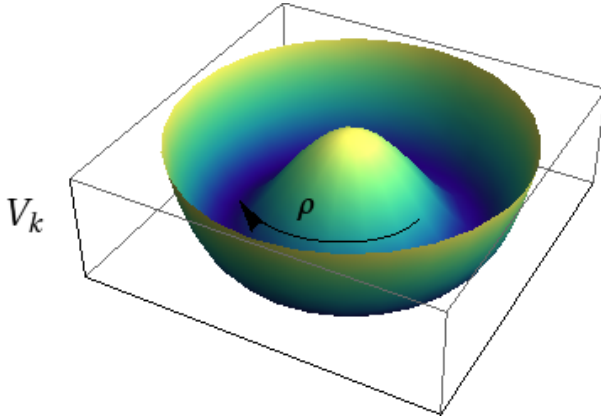


Figure 3.1.: Illustration of the Mexican hat potential for $N = 2$. The radial massive mode ρ is indicated by the arrow. The angular mode is the Goldstone mode.

where t^a are the $N(N - 1)/2$ generators of the group $O(N)$. Moreover, the potential (3.2) has a manifold of non-trivial minima, each of which breaks $O(N)$ -symmetry. This leads us to the vacuum manifold

$$V'(\rho_0) = 0, \quad \text{with} \quad \rho_0 = \frac{\mu_\phi^2}{\lambda}, \quad (3.4)$$

In Figure 3.1 the potential is depicted for the $O(2)$ -case with $N = 2$. Without loss of generality we pick a specific point on the vacuum manifold (3.4), to wit

$$\phi_0 = \begin{pmatrix} 0 \\ \vdots \\ 0 \\ \sqrt{2\rho_0} \end{pmatrix}. \quad (3.5)$$

The vacuum vector ϕ_0 in (3.5) is invariant under the subgroup (little group) $O(N - 1)$ with the generators t^a , $a = N, N + 1, \dots, N(N - 1)/2$ of $O(N)$ that acts trivially on the N th component field ϕ^N . This subgroup rotates the first $N - 1$ component fields into each other. It leaves us with $N - 1$ generators t^a , $a = 1, \dots, N - 1$ (of the quotient $O(N)/O(N - 1)$) of the $N(N - 1)/2$ generators of the group $O(N)$. In turn, a rotation of the vacuum vector within this quotient generates the full vacuum manifold. Applied to a vector $\phi^a = \delta^{Na} \sqrt{2\rho}$ with length it generates all fields,

$$\phi = e^{\frac{\theta^a}{\sqrt{2\rho_0}} t^a} \begin{pmatrix} 0 \\ \vdots \\ 0 \\ \sigma \end{pmatrix}, \quad (3.6)$$

where the denominator $1/\sqrt{2\rho_0}$ in the exponent is chosen for convenience. Commonly, the N th component field ϕ^N is expanded about the minimum $\sigma_0 = \sqrt{2\rho_0}$.

In the present lecture we choose a slightly different approach and stick to the Cartesian fields ϕ which we split into the radial mode σ and the rest, $\vec{\pi}$, i.e.

$$\phi = \begin{pmatrix} \vec{\pi} \\ \sigma \end{pmatrix}, \quad \text{with} \quad \phi_0 = \begin{pmatrix} 0 \\ \sigma \end{pmatrix}. \quad (3.7)$$

Note that in an expansion about the minimum ϕ_0 in the fields $\vec{\theta}$ and $\vec{\pi}$ agree in leading order. Using the representation (3.7) in the kinetic term in the action (3.1) we are led to

$$S_{\text{kinetic}}[\phi] = \frac{1}{2} \int_x \left[(\partial_\mu \sigma)^2 + (\partial_\mu \vec{\pi})^2 \right]. \quad (3.8)$$

The mass term of the model is given by the quadratic term of the potential in an expansion about the minimum. It reads generally

$$\frac{1}{2} \int_x m_\phi^{ab}(\phi_0) \phi^a \phi^b, \quad \text{with} \quad m_\phi^{ab}(\phi_0) = \partial_{\phi^a} \partial_{\phi^b} V(\rho_0) = \delta^{ab} V'(\rho_0) + \phi_0^a \phi_0^b V''(\rho_0). \quad (3.9)$$

Using the expansion point (3.5) leads to the mass matrix

$$m_\phi^{ab}(\phi_0) = \delta^{ab} V'(\rho_0) + 2 \delta^{Na} \delta^{Nb} \rho_0 V''(\rho_0) = \lambda_\phi \rho_0 \delta^{Na} \delta^{Nb}. \quad (3.10)$$

Equation (3.10) entails that in the symmetry-broken phase of the model we have $N - 1$ massless fields, the Goldstone fields. Note that we have not used the specific form (3.2) of the potential for this derivation. The occurrence of the massless modes in (3.10) is a specific case/manifestation of the Goldstone theorem. It entails in general that in the case of a spontaneous symmetry breaking of a continuous symmetry massless modes, the Goldstone modes, occur. Their number is related to the number of generators in the Quotient G/H , where G is the symmetry group and H is the subgroup (little group) which leaves the vacuum invariant.

3.1.2. Spontaneous symmetry breaking, quantum fluctuations and masses

The classical analysis done in Section 3.1.1 suffices to uncover the occurrence of massless modes, if spontaneous symmetry breaking occurs. However, it does not unravel the mechanism. The stability of the chosen vacuum, e.g. (3.5), necessitates, that an infinitesimal rotation on the vacuum manifold costs an infinite amount of energy. This does only happen (for continuous symmetries) in dimensions $d > 2$. In $d \leq 2$ no spontaneous symmetry breaking of a continuous symmetry occurs, which is covered by the Mermin-Wagner theorem (Mermin-Wagner-Hohenberg-Coleman). In Section 2.3.4 we have shown the LPA version the Mermin-Wagner theorem for $N \rightarrow \infty$, see (2.183) and the discussion below. In $d = 2$ dimensions theories with discrete symmetry can exhibit spontaneous symmetry breaking, e.g. the Ising model.

In the last chapter we have already seen that it is the interplay of bosonic and fermionic quantum fluctuations whether or not the effective potential, or more generally the effective action, at vanishing cutoff scale still shows non-trivial minima, to wit,

$$\left. \frac{\delta \Gamma}{\delta \phi} \right|_{\phi=\phi_{\text{EoM}}} = 0, \quad (3.11)$$

Thus, only the full analysis on the quantum level reveals the existence of spontaneous symmetry breaking. The Mermin-Wagner theorem simply entails that in lower dimensions the long range nature of the quantum fluctuations washes out the non-trivial vacua.

Let us now come back to our simple example for spontaneous symmetry breaking. Let us assume for the moment that the full effective action resembles the classical action in ???. Then the ϕ^4 -potential in (3.2) is the full quantum effective potential of the theory for $\rho \geq \rho_0$ (why is this not possible for smaller ρ ?). The full propagator of the theory is now given by

$$\langle\varphi(p)\varphi(-p)\rangle_c = \frac{1}{\Gamma^{(2)}[\phi_{\text{EoM}}]}(p, -p) = \frac{1}{p^2} \left(\delta^{ab} - \delta^{aN}\delta^{bN} \right) + \frac{1}{p^2 + \lambda_\phi \rho_0} \delta^{ab}, \quad (3.12)$$

which describes the massless propagation of the $N - 1$ Goldstone modes, and that of one massive one, the radial field σ , with mass $m_\sigma^2 = \lambda \rho_0$. This links the curvature of the effective potential to the masses of the propagating modes in the theory. Note however, that this is a Euclidean concept and finally we are interested in the pole masses of the physical excitations. They are defined via the respective (inverse) screening lengths in the spatial and temporal directions. The latter are defined by

$$\lim_{\|\vec{x}-\vec{y}\| \rightarrow \infty} \langle\phi(x)\phi(y)\rangle \sim e^{-\|\vec{x}-\vec{y}\|/\xi_{\text{spat}}}, \quad \text{and} \quad \lim_{|x_0-y_0| \rightarrow \infty} \langle\phi(x)\phi(y)\rangle \sim e^{-|x_0-y_0|/\xi_{\text{temp}}}. \quad (3.13)$$

The screening lengths $\xi_{\text{spat/temp}}$ are inversely related to the pole mass $m_{\text{pol}} = 1/\xi_{\text{temp}}$ and screening mass $m_{\text{screen}} = 1/\xi_{\text{spat}}$ respectively. In the present example with the classical dispersion p^2 these masses are identical and also agree with the curvature masses m_{curv} derived from the effective potential. This is easily seen from (3.12). The screening lengths and masses are derived from the Fourier transform of the propagator in momentum space and we have e.g. for the radial mode φ^N at $\vec{p} = 0$

$$\lim_{|x_0-y_0| \rightarrow \infty} \int \frac{dp_0}{(2\pi)} \langle\varphi^N(p_0, 0)\varphi^N(-p_0, 0)\rangle_c e^{ip_0(x_0-y_0)} \sim e^{-|x_0-y_0|\lambda_\phi\rho_0}, \quad (3.14)$$

and hence $m_{\text{pol}} = 1/\xi_{\text{temp}} = m_{\text{curv}}$. Here $\vec{p} = 0$ has only been chosen for convenience. A similar computation can be made for the spatial screening length which agrees with the temporal one. In summary this leaves us with the definition of the pole mass as the smallest value for

$$\Gamma^{(2)}(p_0 = m_{\text{pol}}, \vec{p} = 0) = 0, \quad (3.15)$$

related to the pole (or cut) that is closest to the Euclidean frequency axis. A similar definition holds for the screening mass.

In principle this allows for the extraction of the pole and screening masses from the Euclidean propagators. In practice this quickly runs in an accuracy problem if the propagator is only known numerically. Moreover, this problem is tightly related to reconstruction problems of analyticity properties from numerical data which is an ill-posed problem without any further knowledge.

As a last remark we add that the above identity between screening lengths, and pole, screening and curvature masses fails in the full quantum theory:

- the coincidence of curvature and screening/pole masses hinges on the classical dispersion proportional to p^2 , any non-trivial momentum dependence of the propagator leads to a violation.
- The coincidence of screening and pole mass hinges on the dispersion only being a function of p^2 . While this is true in the vacuum (at vanishing temperature $T = 0$ and density/chemical potential $n/\mu = 0$), finite temperature and density singles out a rest frame and the dispersion depends on \vec{p}^2 and p_0^2 separately.

Having said this, in the following we shall first use simple approximations to the full low energy effective action of QCD for extracting the physics of chiral symmetry breaking and confinement, as well as the mechanisms behind these phenomena.

3.1.3. Little reminder on the Higgs mechanism*

Now we are in the position to discuss the Higgs mechanism in the Standard Model. Again we refer to the literature for the details. Apart from its importance in the context of the asymptotically safe Standard Model, the Higgs mechanisms also serves as an example, at which we can discuss similarities and differences for strong chiral symmetry breaking. Moreover, it is the combination of both mechanisms of mass generation that leads to the observed world. The action of the Standard Model is given by

$$S_{\text{SM}}[\Phi] = \frac{1}{4} \int_x F_{\mu\nu}^a F_{\mu\nu}^a + \frac{1}{4} \int_x W_{\mu\nu}^a W_{\mu\nu}^a + \frac{1}{4} \int_x B_{\mu\nu} B_{\mu\nu} + \int_x [(D\phi)^\dagger D\phi + V_H(\phi)] + \int_x \bar{\psi} \cdot (\not{D} + m_\psi(\phi) + i\mu\gamma_0) \cdot \psi, \quad (3.16)$$

where we have introduced the gluons A_μ , the electroweak gauge bosons W, B and the Higgs, a complex scalar $S U(2)$ -doublet ϕ ,

$$\phi = \begin{pmatrix} \phi_1 \\ \phi_2 \end{pmatrix}, \quad (3.17)$$

with complex components ϕ_1, ϕ_2 . The Higgs potential V_H is a ϕ^4 -potential as (3.2) with

$$V_H(\phi) = -\mu_\phi^2 \phi^\dagger \phi + \frac{1}{2} \lambda_\phi (\phi^\dagger \phi)^2. \quad (3.18)$$

with non-trivial vacuum manifold

$$\rho_0 = \frac{\mu^2}{4\lambda} \quad \text{with} \quad \rho = \frac{1}{2} \phi^\dagger \phi. \quad (3.19)$$

In the spirit of the discussion at the end of chapter 3.1.1 we should interpret V_H as an approximation of the full effective potential of the theory. The Higgs field couples to the electroweak gauge group with the covariant derivative

$$D_\mu \phi = (\partial_\mu - ig_W W_\mu - ig_H B_\mu) \phi, \quad (3.20)$$

The mass term in (3.16) is linear in the Higgs field and vanishes for $\phi = 0$. The left-handed fermions ψ_L in the Standard Model, leptons l, \bar{l} and quarks q, \bar{q} , couple to the weak isospin (fundamental representation) with weak isospin $\pm -1/2$, while the right-handed fermions ψ_R do not couple (trivial representation) with weak isospin 0, that is for example

$$W_\mu \psi_R = 0. \quad (3.21)$$

The related covariant derivative of the fermions reads

$$D_\mu \psi = (\partial_\mu - igA_\mu - ig_W W_\mu - ig_H B_\mu) \psi. \quad (3.22)$$

The mass term $m_\psi(\phi)$ is linear in the Higgs field ϕ and hence constitutes a Yukawa interaction. It relates to the Cabibbo-Kobayashi-Maskawa-Matrix (CKM), and is not discussed in further details here. What is important in the present context, is, that a non-vanishing expectation value of the Higgs field, $\langle \phi \rangle = (0, \rho_0/\sqrt{2})$ provides mass terms for the weak gauge fields, the W, Z as well as for the (left-handed) quarks and leptons:

As in our $O(N)$ -example in the previous section we expect spontaneous symmetry breaking in the scalar Higgs sector. The current masses of the leptons and quarks are then generated by the disappearance of

the mass term for $\phi_0 \neq 0$. Since the structure of the full term is quite convoluted, we illustrate this at a simple example with one Dirac fermion ψ and a real scalar field σ . Then the Yukawa term reads in a mean field approximation

$$h\bar{\psi}\sigma\psi \xrightarrow{\text{mean field}} h\sigma_0\bar{\psi}\psi, \quad (3.23)$$

with mass $m = h\sigma_0$ which is proportional to the vacuum expectation value of the scalar field (vacuum expectation value of the Higgs) and the Yukawa coupling h .

For the masses of the gauge field we cut a long story short and simply note that in a mean field analysis as that done above for the fermion

$$(W_\mu\phi)^\dagger(W_\mu\phi) \xrightarrow{\text{mean field}} (W_\mu\phi_0)^\dagger(W_\mu\phi_0), \quad (3.24)$$

leads to mass terms for the gauge fields. Since the vacuum field ϕ_0 has vanishing upper component ϕ_1 it is a combination of the generator $t^3 = \sigma_3/2$ of the weak $SU(2)$ and the generator $1l$ of the hypercharge $U(1)$ which remains massless: the photon. This also determines the subgroup which leaves the vacuum invariant. The superficial analysis here also reveals that the quotient involves three generators and hence we have three Goldstone bosons. In summary we hence start with three gauge bosons with two physical polarisations each together with three Goldstone bosons, which adds up to nine field degrees of freedom (dof). A convenient reparameterisation (including an appropriate gauge fixing, e.g. the unitary gauge) of the Standard Model leads us to three massive vector bosons with three polarisations each, that is again nine dofs.

3.1.4. Low energy effective theory for QCD & chiral symmetry breaking

Another example even more relevant for the present work is that of strong chiral symmetry breaking. Integrating out QCD fluctuations leads to effective four-fermi couplings for the quarks that carry all the symmetries of the underlying theory that are not broken by the regulator, in particular chiral symmetry. The latter holds true for chiral regulator of the form (2.218) that are proportional to the (free) Dirac dispersion. A more detailed account within the path integral is deferred to Appendix E, most of it is repeated in the present FRG setup in Section 5.3.

In contradistinction to the more physically relevant $N_f = 2$ case treated in Appendix E we restrict ourself to $N_f = 1$, that is the $O(2)$ scalar case. From the four-quark interaction we can derive a Yukawa theory with a Hubbard-Stratonovich (HS) transformation as inversely done in Section 2.4.1.

$$\Gamma_\Lambda[q, \bar{q}, \phi] = \int_x \bar{q} \cdot (\not{d} + m_q) \cdot q + \int_x [(\partial_\mu\sigma)^2 + \partial_\mu\pi]^2 + \int_x \frac{h_\sigma}{\sqrt{2}} \bar{q} [\sigma + i\gamma_5\pi] q + \int_x V_\Lambda(\rho), \quad (3.25)$$

with $\phi = (\sigma, \pi)$ and an effective potential $V_\Lambda(\rho)$ that encodes all the quantum effects of the QCD flucutations on scale $k \geq \Lambda$. The quarks, $\psi = (q^A)$ carry colour, $A = 1, 2, 3$ and the fermionic action in (3.25) changes in comparison to (11.89) with

$$S_q[q, \bar{q}, \phi] = \int_x \bar{q}(x) (\not{d} + m_q) q(x) = \int_x \bar{q}_\xi^A(x) \left((\not{d})^{\bar{\xi}\xi} + m_q \delta^{\bar{\xi}\xi} \right) \delta_{AB} q_\xi^B(x), \quad (3.26)$$

with colour indices $A, B = 1, 2, 3$ and Dirac indices $\xi, \bar{\xi} = 1, \dots, 4$. The initial effective potential in (3.25) is given by

$$V_\Lambda(\rho) = m_{\phi,\Lambda}^2 \rho + \frac{1}{2} \lambda_{\phi,\Lambda} \rho^2, \quad (3.27)$$

where we have dropped higher terms as they are suppressed by inverse powers of the initial cutoff scale Λ . As indicated in (3.25), we want to drop the gluons below the scale Λ , which is typically of the order 1 GeV, $\Lambda \approx 1$ GeV. It is left to fix the coupling parameters

$$(m_{\phi,\Lambda}^2, \lambda_{\phi,\Lambda}, h_{\phi,\Lambda}, c_{\sigma,\Lambda}). \quad (3.28)$$

in our initial effective action Γ_Λ in (3.25). Their computation requires solving QCD for scales $k \geq \Lambda$. This is a highly non-trivial endeavour and typically an effective field theory point of view is taken: After integrating out the remaining quantum fluctuations we are led to a full low energy effective action

$$\Gamma_{\text{LEFT}}[q, \bar{q}, \phi] = \Gamma_{k=0}. \quad (3.29)$$

with the free parameters (3.28) and the effective potential $V_{\text{eff}} = V_{k=0}$. Now we can fix the couplings in the initial effective action at the scale Λ by fixing Γ_{LEFT} with suitable experimental values for observables that can be computed from (3.29). All further observables are then predictions, in particular also the phenomena in this low energy effective theory (LEFT) at finite temperature and density.

Let us start with c_σ . It will not enter the flow equation on the right hand side, its value of c_σ only determines the expectation value of the σ -field. In the present approximation σ_0 is simply the pion decay constant,

$$\sigma_0 = \langle \sigma \rangle = f_\pi, \quad f_\pi \approx 93 \text{ MeV}. \quad (3.30)$$

The latter value related to the physical f_π 's (f_π^\pm, f_π^0) measured in the experiment. Consequently c_σ could be dropped, we simply evaluate the theory on this expectation value. Accordingly, h_σ is determined by the constituent quark mass,

$$m_{q,\text{con}} = \frac{h_\sigma}{\sqrt{2}} \sigma_0 = \frac{h_\sigma}{\sqrt{2}} f_\pi \quad \rightarrow \quad h_\sigma \approx 4.56 \quad \text{with} \quad m_{\psi,\text{con}} \approx 300 \text{ MeV}. \quad (3.31)$$

Note that the constituent quark masses of the quarks depend on the model and approximation used, typical values for up and down quark masses are $m_{\psi,\text{con}} \approx 340$ MeV in full QCD. The reduced value in (3.31) for two flavour QCD is common place in the $N_f = 2$ quark-meson model, here we simply take it for the sake of definiteness for $N_f = 1$. We cannot simply measure the constituent quark mass, the related observable is the chiral condensate,

$$\langle \bar{q}(x)q(x) \rangle = - \int \frac{d^4 p}{(2\pi)^4} \text{tr} \langle q(p)\bar{q}(-p) \rangle, \quad (3.32)$$

where the trace sums over Dirac and flavour indices.

Finally we have to fix λ_ϕ and m_ϕ with the Yukawa coupling and σ -expectation value σ_0 deduced above, see also Table 3.1. Note also, that a potential further input is the value of the pion decay constant in the chiral limit,

$$f_{\pi,\chi} = f_\pi(m_\pi = 0) \approx 88 \text{ MeV}, \quad (3.33)$$

which can be determined with chiral perturbation theory, functional continuum methods or from chiral extrapolations of lattice results at different finite pion masses. This leaves us with a triple of 'observables' $(m_\pi, m_\sigma, f_{\pi,\chi})$, see Table 3.1, and a triple of EFT couplings $(m_\phi, \lambda_\phi, c_\sigma)$. Note that the inclusion of $f_{\pi,\chi}$ as an 'observable' relates to the correct chiral dynamics reflected in the curvature and four-meson interaction in the chiral limit. The pion and sigma masses are related to those found in the Particle Data Booklet (2016), [77] of the Particle Data Group (PDG). Here, the pion mass is taken between that of the charged pions π^\pm with $m_{\pi^\pm} \approx 139.57$ MeV and the neutral pion π^0 with $m_{\pi^0} \approx 134.98$ MeV, and the mass of the sigma meson is taken to be that of the $f_0(500)$, see [78], that is $m_\sigma \approx 450$ MeV, despite

Observables	Value [MeV]	EFT couplings at $k = \Lambda$	Value
f_π	93	$\sigma_0 = f_\pi$	93 MeV
m_{con}	300	$h_\sigma = \sqrt{2} \frac{m_{\text{con}}}{f_\pi}$	4.56
m_π	138	m_ϕ	$m_\phi(m_\pi, m_\sigma)$
m_σ	450	λ_ϕ	$\lambda_\phi(m_\pi, m_\sigma)$
$f_{\pi,\chi}$	88	$c_\sigma = f_\pi m_\pi^2$	$1.77 * 10^6 \text{ MeV}^3$

Table 3.1.: Low energy observables and related EFT couplings as used for the $N_f = 2$ computations. While c_σ , the σ -expectation value σ_0 and the Yukawa coupling are directly related to pion decay constant and constituent quark masses in the present approximations, the two other EFT couplings $m_{\phi,\Lambda}^2$, $\lambda_{\phi,\Lambda}$ have to be adjusted on the result for V_{eff} computed from its flow equation.

the f_0 certainly not being a simple $q\bar{q}$ state. The unclear nature of the value of m_σ is one of the biggest uncertainties for low energy EFTs. Typically, its values range from 400–550 MeV, see PDG, [77]. Seemingly, this leaves us with as many unknowns as physics input. However, c_σ can be determined from the pion mass and the pion decay constant with $m_\pi^2 = \partial_\rho V_{\text{eff}}(\rho_0)$ and $\rho_0 = \sigma_0^2/2 = f_\pi^2/2$. This follows from the EoM for σ ,

$$\partial_\sigma V_{\text{eff}}(\rho_0) = \sigma_0 m_\pi^2 = c_\sigma \quad \longrightarrow \quad c_\sigma = f_\pi m_\pi^2 \approx 1.77 * 10^6 \text{ MeV}^3. \quad (3.34)$$

We conclude that in the current approximation to the UV effective action, the pion decay constant in the chiral limit, $f_{\pi,\chi}$, is a prediction.

Here we present a crude (mean-field) estimate of its value based on the assumption of being close to the chiral limit. It is based on the expansion of the full effective potential about the unperturbed minimum in the broken phase,

$$V_{\text{eff}} = \sum_{n=2}^{\infty} \frac{\lambda_n}{n!} (\rho - \kappa)^n + c_\sigma \sigma, \quad \text{with} \quad \kappa = \frac{f_{\pi,\chi}^2}{2}, \quad \lambda_2 = \lambda_{\phi,\text{eff}}. \quad (3.35)$$

Close to the chiral limit the difference $(f_\pi - f_{\pi,\chi})/f_\pi \ll 1$ is small. In the vicinity of the unperturbed minimum κ the full effective potential can be written as

$$V_{\text{eff}} = \frac{\lambda_{\phi,\text{eff}}}{2} (\rho - \kappa)^2 + c_\sigma \sigma + O((\rho - \kappa)^2). \quad (3.36)$$

Dropping the higher terms leads us to

$$m_\pi^2 = \lambda_{\phi,\text{eff}} \frac{f_\pi^2 - f_{\pi,\chi}^2}{2}, \quad m_\sigma^2 = \lambda_{\phi,\text{eff}} \frac{3f_\pi^2 - f_{\pi,\chi}^2}{2}. \quad (3.37)$$

In this leading order, the mesonic self-coupling drops out of the relation for $f_{\pi,\chi}$ and we arrive at the estimate

$$f_{\pi,\chi} = f_\pi \sqrt{\frac{1 - 3 \frac{m_\pi^2}{m_\sigma^2}}{1 - \frac{m_\pi^2}{m_\sigma^2}}} \approx 83 \text{ MeV}, \quad \text{and} \quad \lambda_{\phi,\text{eff}} = \frac{m_\sigma^2 - m_\pi^2}{f_\pi^2} \approx 21.2. \quad (3.38)$$

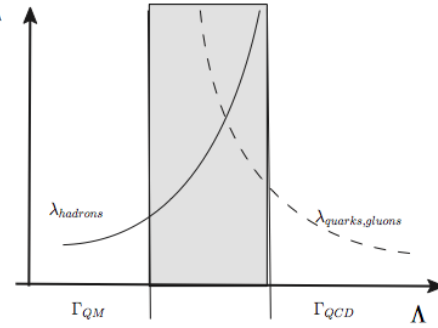


Figure 3.2.: Scale dependence of the effective four-fermi coupling. The shaded area is the regime where the effective field theory is triggered.

This is a very good agreement with the theoretical prediction of $f_{\pi,\chi} \approx 88$ MeV, in particular given the crude nature of the present estimate. Beyond the current mean field level it improves further. Still, the current EFT makes a prediction for either $f_{\pi,\chi}$ or m_σ , and the question arises which of them should be taken as a physics input: we first note that $f_{\pi,\chi} \approx 88$ MeV is under far better theoretical control than the mass of the σ -meson. Apart from the difficulties of identifying directly the σ -mesons in the EFT's at hand with a resonance in the particle spectrum, it has a large width. Hence it cannot be assumed that the curvature mass $m_{\sigma,\text{curv}}$ we use here is in good agreement with the pole mass $m_{\sigma,\text{pol}}$, see the discussion at the end of chapter 3.1.2. This is in stark contradistinction to the pion masses where the (non-trivial) identification $m_{\pi,\text{curv}} \approx m_{\pi,\text{pol}}$ holds true on the percent level. This suggests to adjust m_σ such that $f_{\pi,\chi} \approx 88$ MeV. In the mean field discussion done here this leads to $m_\sigma^2 \approx 600 - 650$ MeV. Note that with a future better determination of the curvature mass $m_{\sigma,\text{curv}}$ a semi-quantitative EFT might require higher order mesonic UV-couplings such as $\lambda_{3,\text{UV}} \neq 0$ in (3.36). This is related to the fact that the physical UV cutoff $\Lambda_{\text{UV}} \approx 1$ GeV, at which the low energy EFT is initiated, is less than one order of magnitude larger than the physical scales.

This discussion completes our EFT picture of chiral symmetry breaking in QCD. In essence it also extends to the $N_f = 2 + 1$ flavour case and beyond, then, however, a consistent determination of the low energy couplings including the correct chiral dynamics, e.g. $f_{\pi,\chi}$ is far more intricate.

3.1.5. LPA Flow for the effective potential in the quark meson model

Here we study the chiral phase transition in the $N_f = 1$ quark meson model with the UV action (3.25) within the LPA approximation. This flow has been provided in (2.244) and we quote it here,

$$\partial_t V_k(\rho) = \frac{\Omega_d}{(2\pi)^d} \frac{k^{d+2}}{d} \left(\frac{1}{k^2 + V'_k(\rho)} + \frac{1}{k^2 + V'_k(\rho) + 2\rho V''_k(\rho)} \right) - 4N_c \frac{\Omega_d}{(2\pi)^d} \frac{k^{d+2}}{d} \frac{1}{k^2 + h_\sigma^2 \rho}. \quad (3.39)$$

As a first step towards the integration of the full flow we will study the flow without feed back. In comparison to LPA this helps us to understand where fluctuation effects are important and where simple resummations may work as well.

Flow without feedback

For a first glimpse at the mechanisms at work we simply evaluate the $N_f = 1$ quark meson model for a k -independent input $\Gamma_k^{(2)} = \Gamma_\Lambda^{(2)}$ in the flow diagrams. Then, the flow can be integrated analytically and relates to the one loop result we have discussed previously. Note however that we have dropped all terms proportional to higher loop orders also in the input on the right hand side. In the present computation we simply keep the full input. Due to RG consistency it has already one loop contributions in this approximation and the integrated loop comprises a resummation.

In 2.4.4 the effective potential was solved for the Yukawa action (11.89) at one loop, the result is given in 2.253. The Dirac action (3.26) is diagonal in colour space, and the flow of the effective potential in our quark meson model is the same up to the prefactor $N_c = 3$ in front of the quark loop, leading to (2.244). In the last chapter we have explicitly done the renormalisation in order to extract the Λ -independent physics part of the initial effective potential $V_\Lambda(\rho)$ as well as of the flow.

Within applications to the FRG this is not done as already discussed in Section 3.1.4. We use the representation

$$V_{\text{eff}}(\rho) = V_\Lambda(\rho) + \Delta V_\Lambda(\rho), \quad \Delta V_\Lambda(\rho) = \int_\Lambda^0 \frac{dk}{k} \partial_t V_k(\rho). \quad (3.40)$$

with the initial effective potential (3.143). The integrated fermionic flow flow can be read of from (2.247) for general dimensions d or for $d = 4$ from (2.248). In the present QM model ist has to be multiplied by the colour factor $N_c = 3$. The pion and σ meson contribution follows similarly from (2.247), (2.248) by dividing by the Dirac trace factor 4 and the substitution rule: $h_\sigma^2 \rho \rightarrow m_\pi^2(\rho)$ and $h_\sigma^2 \rho \rightarrow m_\sigma^2(\rho)$ with 2.253c. This leads us to

$$V_{\text{eff}}(\rho) = V_\Lambda(\rho) + \Delta V_{q,\Lambda}(\rho) + \Delta V_{\phi,\Lambda}(\rho), \quad (3.41a)$$

with the meson and quark flow contributions $\Delta V_{q,\Lambda}$ and $\Delta V_{\phi,\Lambda}$ respectively,

$$\begin{aligned} \Delta V_{q,\Lambda}(\rho) &= -\frac{3}{16\pi^2} \left[\Lambda^2 h_\sigma^2 \rho - (h_\sigma^2 \rho)^2 \ln \left(1 + \frac{\Lambda^2}{h_\sigma^2 \rho} \right) \right], \\ \Delta V_{\phi,\Lambda}(\rho) &= \frac{1}{64\pi^2} \left[\Lambda^2 m_{\pi,\Lambda}^2(\rho) - (m_{\pi,\Lambda}^2(\rho))^2 \ln \left(1 + \frac{\Lambda^2}{m_{\pi,\Lambda}^2(\rho)} \right) \right. \\ &\quad \left. + \Lambda^2 m_{\sigma,\Lambda}^2(\rho) - (m_{\sigma,\Lambda}^2(\rho))^2 \ln \left(1 + \frac{\Lambda^2}{m_{\sigma,\Lambda}^2(\rho)} \right) \right]. \end{aligned} \quad (3.41b)$$

The field-dependent mass functions $m_\pi^2(\rho)$ and $m_\sigma^2(\rho)$ are defined similarly to 2.253c, but with the initial effective potential V_Λ ,

$$m_{\pi,\Lambda}^2(\rho) = V'_\Lambda(\rho) = m_{\phi,\Lambda}^2 + \lambda_{\phi,\Lambda} \rho, \quad m_{\sigma,\Lambda}^2(\rho) = m_{\phi,\Lambda}^2 + 3\lambda_{\phi,\Lambda} \rho, \quad (3.41c)$$

Now we investigate the question of spontaneous symmetry breaking in terms of the set of couplings $m_\phi^2, \lambda_\phi, h_\phi$. As mentioned before, the effect of an explicit quark mass is introduced by changing the equation of motion for σ to

$$\frac{\partial V_{\text{eff}}(\rho)}{\partial \sigma} \Big|_{\rho=\rho_0} = c_\sigma, \quad \text{where} \quad c_\sigma = \frac{\sqrt{2}}{h_\sigma} m_\phi^2 m_q, \quad (3.42)$$

see also (2.239). In summary our total set of input couplings is

$$(m_{\phi,\Lambda}^2, \lambda_{\phi,\Lambda}, h_{\phi,\Lambda}, c_{\sigma,\Lambda}). \quad (3.43)$$

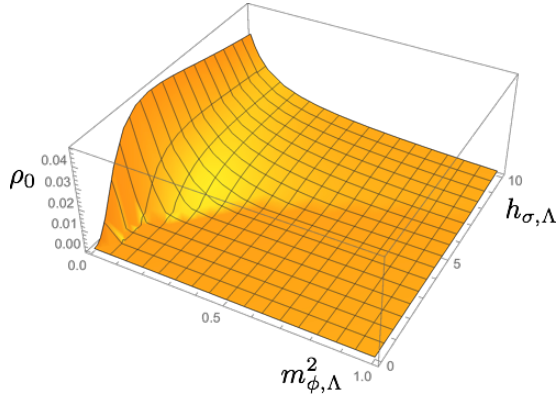


Figure 3.3.: Mean field value ρ_0 at vanishing cutoff, $k = 0$, as a function of the input couplings $m_{\phi,\Lambda}^2$ and $h_{\sigma,\Lambda}$

The fermionic mass parameter c_σ does not enter the effective potential but only the EoM for σ . Moreover, the ϕ^4 coupling in 3.41 can be absorbed in a redefinition of ρ , which leaves us with

$$\left(m_\phi^2, \frac{h_\phi}{\sqrt{\lambda_\phi}} \right). \quad (3.44)$$

In summary we simply have to discuss the minimum of the effective potential V_{eff} for $\lambda_\phi = 1$ as a function of m_ϕ^2/Λ^2 and h_σ for $m_{\phi,\Lambda}^2 \geq 0$. The latter constraint ensures that the flow gives meaningful results for $\rho \in [0, \infty]$: As the flow is not fed back, the mesonic mass functions on the right hand side of the flow have the property $m_\pi^2(0) = m_\sigma^2(0) = m_{\phi,\Lambda}^2$. Negative $m_{\phi,\Lambda}^2$ lead to singularities in the flow. These singularities are absent in the full flow due to its convexity-restoring property discussed below (2.155): This property of the full flow still holds true in LPA, but this requires feeding back the flow into the right hand side. The minimum ρ_0 is also measured in the initial cutoff scale Λ^2 .

This leads us to Figure 3.3, where we see all the expected properties.

- (i) Increasing the Yukawa coupling in the vicinity of $h_\sigma = 0$ leads to an increase of the non-trivial minimum ρ_0 . For asymptotically large Yukawa coupling $h_{\sigma,\Lambda}^2/m_{\phi,\Lambda}^2 \rightarrow \infty$ the minimum decreases again. This effect can be easily understood from the form of the integrated fermionic flow in 3.41b which is identical to that in the full LPA approximation: the negative curvature introduced at $\rho = 0$ rises quadratically with $h_{\sigma,\Lambda}^2$ to be compared with the mesonic mass term. In turn, for larger $h_{\sigma,\Lambda}^2$, $\Delta V_q(\rho)$ also approaches its flat asymptotics quicker. This leads to the fact that the potential gets steeper around $\rho = 0$, but the minimum tends towards $\rho_0 = 0$.
- (ii) Increasing $m_{\phi,\Lambda}^2$ (or $\lambda_{\phi,\Lambda}$) always decreases ρ_0 . While increasing the mesonic mass directly decreases the value of ρ_0 , increasing the mesonic self-coupling increases the symmetry restoring integrated mesonic flow ΔV_ϕ .
- (iii) The expectation value ρ_0 and the mass function $m_\sigma^2(\rho_0)$ show a characteristic scaling with the tuning parameters $h_{\sigma,\Lambda}$ or $m_{\phi,\Lambda}$ for $\rho_0 \rightarrow 0$. The ρ_0 -scaling is present in Figure 3.3, the scaling of the masses is depicted in Figure 3.4 for the physically relevant value of $h_{\sigma,\Lambda} = 4.56$, see Table 3.1. For large input mass $m_{\phi,\Lambda}^2$ chiral symmetry is restored, the quark contribution cannot generate a

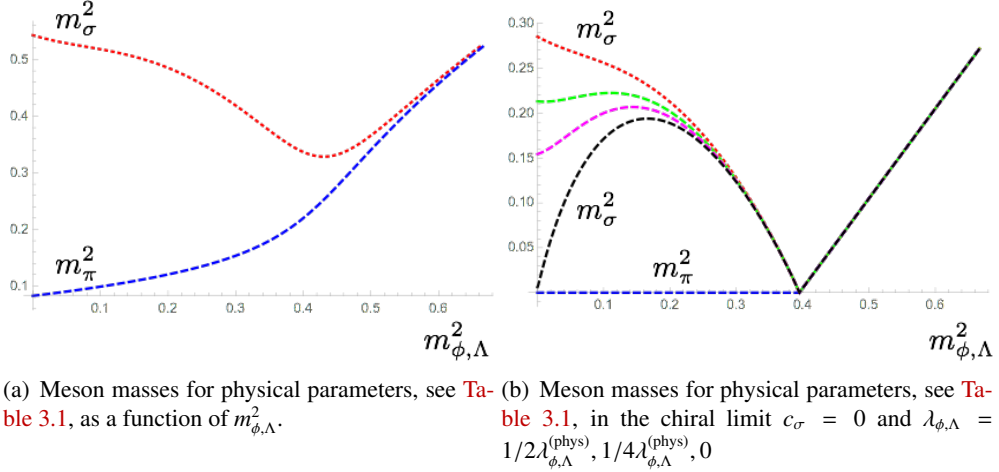


Figure 3.4.: Meson masses $m_{\sigma,\pi}^2$ in GeV as a function of $m_{\phi,\Lambda}^2$ in GeV for $\Lambda = 1$ GeV, $h_\sigma = 4.56$ and $\lambda_\phi = \lambda_{\phi,\Lambda}^{(\text{phys})} \approx 2.2$. The physical input mass is $m_{\phi,\Lambda}^2 = 0.26$ GeV 2 .

potential with non-trivial minima. Then, π and σ masses are degenerate. In turn, for small input mass $m_{\phi,\Lambda}^2$, the quark fluctuations generate a non-trivial minimum, the π is a massless Goldstone boson. As is evident from Figure 3.4, the sigma mass scales with

$$m_\sigma^2 \propto |m_{\phi,\Lambda}^2 - (m_{\phi,\Lambda}^*)^2|, \quad (3.45)$$

about the critical value for the input mass $(m_{\phi,\Lambda}^*)^2$. Such a linear scaling is the mean field scaling, which we expect in $d = 4$.

- (iv) The present LEFT is perturbatively renormalisable in contradistinction to similar four-quark LEFTs such as the NJL model. We emphasise that the perturbative non-renormalisability of the NJL model as such poses no problem for the FRG, it could be non-perturbatively renormalisable. Indeed, it is the latter property we aim for in asymptotically safe gravity.

The quark-meson model is UV unstable which can already been seen in the present perturbative approximation, see Figure 3.5. For initial cutoff scale $\Lambda \gtrsim 1$ GeV the mesonic self-coupling gets negative, indicating a physical instability in the model. This instability persists in elaborate approximations which is non-trivial evidence that the QM model as a QFT is indeed non-perturbatively unstable in the UV. The stability bound in the renormalisable quark-meson model is related to the physical UV cutoff in the NJL theory. From the FRG perspective these are identical theories via the HS transformation. Accordingly, both UV problems simply entail the physical instability of this class of models.

In summary we already see the full chiral structure of the present LEFT of QCD in the vacuum.

Full LPA Flow

No we aim for a more quantitative approach, for which we have to abandon the analyticity of perturbative results. To that end we solve the full LPA flow numerically given in (3.39). As we are more interested in

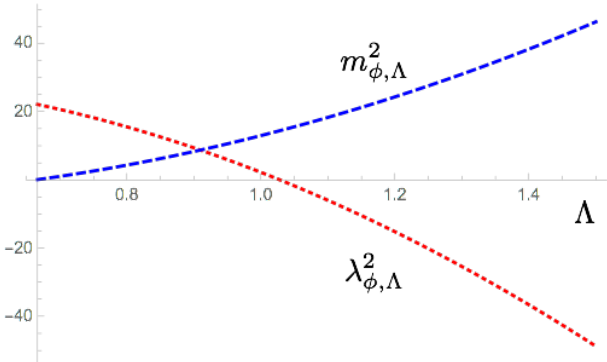


Figure 3.5.: Λ -dependence of the initial mesonic parameters $\lambda_{\phi,\Lambda}$ and $m_{\phi,\Lambda}^2$. All units are in powers of GeV.

the phase structure, we refrain from a detailed discussion here, and simply provide a comparison of the $m_{\phi,\Lambda}^2$ dependence of the meson masses, see Figure 3.6. Quantitatively the results match those in the one loop approximation. One also sees the mean field scaling at the phase transition, which is not an artefact but a property of $d = 4$.

3.2. Phase structure

In the last chapter we have seen how spontaneous symmetry breaking can occur by changing the fundamental couplings of the theory under investigation. This already covers the phenomenon of quantum phase transitions. Often one is interested in a phase structure of theories under the change of external parameters such as *temperature T*, *density n*, and external *background fields*, e.g. electric or magnetic backgrounds \vec{E} and \vec{B} , or chromo-magnetic or chromo-electric ones, $\vec{E}^a \vec{E}^a$, $\vec{B}^a \vec{B}^a$, as well as $\vec{E}^a \vec{B}^a$. The colour indices take values $a = 1, \dots, N_c^2 - 1$. The latter combination as also $\vec{E} \vec{B}$ is the topological density relevant for anomalous effects such as *anomalous chiral symmetry breaking* or *dynamical anomalous transport*.

In gravity the relevance of the background is even more important: the solution of the EoM for the metric in asymptotically safe gravity is non-trivial, leading to non-vanishing curvature invariants such as the Ricci scalar $\mathcal{R} \neq 0$. The interrelation of this non-trivial dynamical background and that of background invariance of the theory is a pivotal one in all approaches to quantum gravity and yet unsolved. For more details we refer the reader to ??.

3.2.1. Density and chemical potential

Typically, and in particular in QCD, we investigate theories within the *Grand Canonical Ensemble*, where the effective action $\Omega(T, \mu_\psi) = \Gamma[\Phi_{\text{EoM}}; T, \mu_\psi]$ is the *Grand Potential*. The (fermionic) particle number N is the derivative of the grand potential with respect to μ ,

$$N_\psi = \frac{\partial \Gamma[\Phi_{\text{EoM}}]}{\partial \mu_\psi}, \quad (3.46)$$

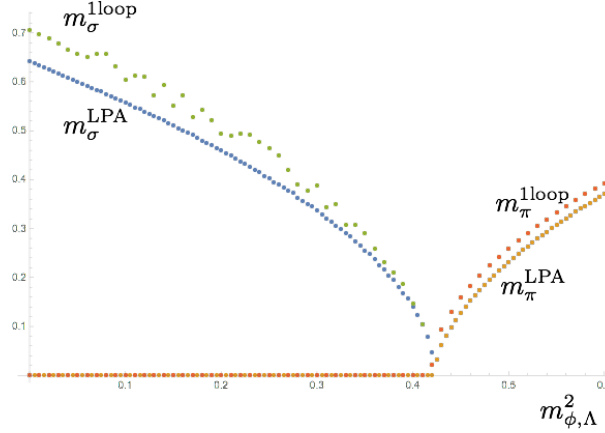


Figure 3.6.: Mesonic masses as a function of $m_{\phi,\Lambda}^2$. All units are in powers of GeV. The coupling was chosen as $\lambda_\Lambda = 10$ for the LPA and $\lambda_\Lambda = 31$ for the flow without feedback. Both calculations used a cutoff of $\Lambda = 1$ GeV.

and hence $\Gamma \propto -\mu_\psi N_\psi$. In the Standard Model we consider a chemical potential related to the particle number

$$N_\psi = \int_x n_\psi(x), \quad \text{where} \quad n_\psi(x) = \bar{\psi} \gamma_0 \psi. \quad (3.47)$$

with the fermionic density $n_\psi(x)$. This adds a chemical potential for quarks and leptons, which are the fundamental matter fields. To that end we add the respective term to the Dirac action in (5.34), to wit

$$S_D[\psi, \bar{\psi}; \mu_\psi] = \int_x \bar{\psi}(x) (\not{d} + m_\psi - \mu_\psi \gamma_0) \psi(x), \quad (3.48)$$

In frequency space this amounts to a shift of the frequency into the complex plane,

$$p_0 \rightarrow \tilde{p}_0 = p_0 + i \mu_\psi, \quad (3.49)$$

and the classical fermionic propagator reads in the presence of a chemical potential

$$G_\psi(p; \mu_\psi) = \frac{1}{i \not{p} - \gamma_0 \mu_\psi + m_\psi} = \frac{-i \not{\tilde{p}} + m_\psi}{\tilde{p}^2 + m_\psi^2}, \quad (3.50)$$

where

$$\tilde{p} = (p_0 + i \mu_\psi, \vec{p}), \quad \tilde{p}^2 = (p_0 + i \mu_\psi)^2 + \vec{p}^2, \quad \not{\tilde{p}} = \gamma_0 (p_0 + i \mu_\psi) + \vec{\gamma} \vec{p}. \quad (3.51)$$

As an example we now compute $(d^3 p n(\vec{p}^2))$, the particle number density for a spatial momentum shell at \vec{p}^2 in the classical theory. This density is obtained from the grand potential in direct analogy to the particle number (3.47). We allow for a momentum dependent chemical potential in $\Omega(T, \mu) = \Gamma[\Phi_{\text{EoM}}; t, \mu]$ by substituting the chemical potential term in (3.48) by

$$\mu_\psi \int_x \bar{\psi} \gamma_0 \psi \rightarrow \int_q \mu_\psi(q) \bar{\psi}(q) \gamma_0 \psi(q), \quad \text{with} \quad n_\psi(\vec{p}) = \frac{1}{\mathcal{V}_3} \int_{p_0} \frac{\delta \Omega(0, \mu_\psi)}{\delta \mu_\psi(p)}. \quad (3.52)$$

with the spatial volume \mathcal{V}_3 . We remark that this is not the same as allowing for a space-time dependent chemical potential $\mu_\psi(x)$ in (3.48). This leads to

$$\mu_\psi \int_x \bar{\psi} \gamma_0 \psi \rightarrow \int_q \mu_\psi(q) (\bar{\psi} \gamma_0 \psi)(q), \quad \text{where} \quad (\bar{\psi} \gamma_0 \psi)(q) = \int_s \bar{\psi}(q-s) \gamma_0 \psi(s). \quad (3.53)$$

Both definitions have their applications, in heavy ion collisions the former definition, (3.52), is more interesting due to the spatial momentum resolution of the measured particles. Note also that both agree in homogeneous situations up to a trivial volume factor.

Hence we resort to (3.52) and compute the respective momentum density by a functional derivative with respect to $\mu_\psi(p)$, evaluated at a constant μ_ψ with $\partial_\mu \mu_\psi = 0$, in momentum space this reads $\mu_\psi(p) = \mu_\psi(2\pi)^4 \delta(p)$. With this preparation we get

$$n_\psi(\vec{p}^2) = - \int_{p_0} \frac{dp_0}{2\pi} \text{tr} \gamma_0 G_\psi(p; \mu_\psi) = 4i \int_{p_0} \frac{dp_0}{2\pi} \frac{(p_0 + i\mu_\psi)}{(p_0 + i\mu_\psi)^2 + \vec{p}^2 + m^2}. \quad (3.54)$$

Equation (3.55) can be computed with the residue theorem by closing the contour in the upper half-plane. While the integral in (3.55) is finite, for closing the counter a decay behaviour of more than $1/p_0$ is required. Hence, we simply symmetrise the integral representation (3.55),

$$n(\vec{p}) = 2i \int_{p_0} \frac{dp_0}{2\pi} \left[\frac{(p_0 + i\mu_\psi)}{(p_0 + i\mu_\psi)^2 + \vec{p}^2 + m^2} - \frac{(p_0 - i\mu_\psi)}{(p_0 - i\mu_\psi)^2 + \vec{p}^2 + m^2} \right], \quad (3.55)$$

which also makes apparent that $\Omega(T, \mu_\psi)$ is a function of μ^2 . In the following we consider $\mu_\psi > 0$ for the sake of definiteness. The integrand in (3.55) has poles at

$$p_{0, \mu_\psi}^\pm = -i (\mu_\psi \pm \epsilon_p^\psi) \quad \text{and} \quad p_{0, -\mu_\psi}^\pm = i (-\mu_\psi \pm \epsilon_p^\psi), \quad (3.56)$$

for the first term in the square bracket, and the second term respectively. In (3.56) we have introduced ϵ_p^ψ for the fermionic dispersion,

$$\epsilon_p^\psi(m^2) = \sqrt{\vec{p}^2 + m^2}, \quad (3.57)$$

Accordingly, the density vanishes below the onset chemical potential $\mu_{\psi, \text{on}}$ with

$$\mu_{\psi, \text{on}}(\vec{p}) = \epsilon_p^\psi. \quad (3.58)$$

at the pole of the fermionic dispersion. For smaller chemical potentials, $\mu_\psi < \mu_{\psi, \text{on}}(\vec{p}^2)$ the integrand has two poles in each half-plane and their residues cancel. On the other hand, if the chemical potential exceed the onset chemical potential $\mu_\psi > \mu_{\psi, \text{on}}(\vec{p}^2)$, both poles of the first term in the square bracket are in the lower half plane, while both poles of the second term are in the upper one. Therefore the particle number density is given by

$$n(\vec{p}^2) = 2 \theta(\mu^2 - (\epsilon_p^\psi)^2). \quad (3.59)$$

From (3.59) to total particle number is easily inferred with a spatial momentum integral of $n(\vec{p}^2)$. This leads us to the total density

$$n(\mu) = \frac{\pi}{3} (\mu^2 - m_\psi^2)^{3/2} \theta(\mu^2 - m_\psi^2), \quad (3.60)$$

which for large $\mu \gg m_\psi^2$ rises with μ^3 . Despite its simplicity, the computation above already gives a very good insight also for fully non-perturbative computations: [Equation \(3.55\)](#) or its RG-time t derivative is still valid, the full propagator can be written as

$$G_\psi(p; T, \mu_\psi) = \frac{1}{Z_\psi} \frac{-i \left(s_\psi^{1/2} \gamma_0 \tilde{p}_0 + \vec{p} \vec{\gamma} \right) + M_\psi}{s_\psi \tilde{p}_0^2 + \vec{p}^2 + M_\psi^2}, \quad (3.61)$$

where all dressings Z_ψ , s_ψ , M_ψ are fully momentum and T, μ -dependent:

$$Z_\psi = Z_\psi(\tilde{p}; T, \mu_\psi), \quad M_\psi(\tilde{p}; T, \mu_\psi), \quad s_\psi = s_\psi(\tilde{p}; T, \mu_\psi). \quad (3.62)$$

The factor s_ψ takes into account that the spatial and temporal dressing are different as both density/chemical potential and temperature single out a rest frame. Note also that below onset the frequency dependence of the propagator dressings will be only $\tilde{p}_0 = p_0 + i\mu_\psi$, while above onset there is a genuine μ_ψ -dependence which is not covered by \tilde{p}_0 . At its heart this property has the same origin as the existence of the onset itself. It holds for all correlation functions and is called *Silver Blaze property*.

In summary, within a non-perturbative setup, the simple density formulae in [\(3.59\)](#) and [\(3.60\)](#) will change, but their structure does not. There is an onset chemical potential $\mu_{\psi, \text{on}}$ below which no density is present. This onset chemical potential signifies the position of the lowest pole or cut in the complex plane, which is encoded in the momentum dependence of the dressings. At finite temperature, thermal fluctuations ensure, that the density also has contributions below the onset. This is discussed in more detail in the next chapter.

3.2.2. Finite temperature QFT

In this chapter we provide a brief introduction to Euclidean finite temperature field theory and for bosons and fermions. We follow the introduction of the path integral in chapter 1, QFT II. Examples are given in the context of our chiral Yukawa theory.

Bosons at finite temperature

For discussing a finite temperature field theory it is convenient to consider the respective statistical field theory. Accordingly, we start with the partition function of a scalar theory at finite temperature

$$Z_T = \text{Tr } e^{-\beta \hat{H}} = \sum_n e^{-\beta E_n} \quad \text{with} \quad \beta = \frac{1}{T} \quad \text{and} \quad \hat{H}|n\rangle = E_n|n\rangle, \quad (3.63)$$

with the Hamiltonian operator of a scalar theory

$$\hat{H}[\hat{\varphi}, \hat{\pi}] = \int d^3x \left[\frac{1}{2} \hat{\pi}^2 + \frac{1}{2} (\vec{\nabla} \varphi)^2 + V(\hat{\varphi}) \right]. \quad (3.64)$$

with field operator $\hat{\varphi}$ and field momentum operator $\hat{\pi}$. In [\(3.63\)](#) we dropped the source term for the sake of brevity. [Equation \(3.63\)](#) is the standard statistical partition function at finite temperature well known from quantum mechanics. Now we rewrite this partition function in terms of a basis in field and canonical momentum space. First we note that the trace in [\(3.63\)](#) can be rewritten in terms of field eigenstates with

$$\text{Tr } e^{-\beta \hat{H}} = \int d^d\varphi \langle \varphi | e^{-\beta \hat{H}} | \varphi \rangle \quad \text{with} \quad \hat{\varphi}(\vec{x})|\phi\rangle = \varphi(\vec{x})|\phi\rangle, \quad (3.65)$$

with the eigenvalues $\varphi(\vec{x})$. Moreover, the statistical operator $e^{-\beta \hat{H}}$ can be interpreted as the evolution operator $U(0, i\beta)$ in an imaginary time from the initial state $|\varphi(t_i)\rangle$ at $t_i = 0$ to the final state $|\varphi(t_f)\rangle$ at $t_f = i\beta$ with

$$U(0, i\beta) = e^{i\hat{H}(t_f - t_i)} \quad \text{and} \quad |\varphi(t_f)\rangle = |\varphi(t_i)\rangle. \quad (3.66)$$

The identification of initial and final state is the trace condition in (3.65). Now we simply repeat all the steps for the derivation of the path integral of a scalar theory. Also adding a source term we arrive at

$$Z_T[J] = \int_{\varphi(\beta, \vec{x})=\varphi(0, \vec{x})} \int d\varphi e^{-S_T[\varphi] + \int_0^\beta d^4x J(t, \vec{x})\varphi(\vec{x})}, \quad (3.67)$$

with the periodic fields $\varphi(t + \beta, \vec{x}) = \varphi(t, \vec{x})$ and the finite temperature action $S_T[\varphi]$ with

$$S_T[\varphi] = \int_0^\beta d^4x \left[\frac{1}{2} (\partial_\mu \varphi)^2 + V(\varphi) \right], \quad \text{where} \quad \int_0^\beta d^4x = \int_0^\beta dt \int d^3x. \quad (3.68)$$

Accordingly, the path integral of a finite temperature field theory is related to a Euclidean path integral with a finite time extent in imaginary time $t \in [0, \beta]$. Note that this time does *not* describe the time evolution of the system but simply the statistical nature of the thermal partition function. The real time correlation function are obtained by a Wick rotation, for more details see finite temperature quantum field theory books such as Le Bellac or Kapusta. The correlation functions are periodic in imaginary time,

$$\langle \varphi(x_1) \cdots \varphi(t_i + \beta, \vec{x}) \cdots \varphi(x_n) \rangle = \langle \varphi(x_1) \cdots \varphi(t_i, \vec{x}) \cdots \varphi(x_n) \rangle. \quad (3.69)$$

Finally we want to repeat the computation of the effective potential in the last chapters [Section 2.4](#) at finite temperature. This is done in momentum frequency space and we would like to illustrate the differences at finite temperature at the important example of the propagator

$$G_\phi(x - y) = \langle \varphi(x)\varphi(y) \rangle - \phi(x)\phi(y), \quad (3.70)$$

with the mean fields $\phi = \langle \varphi \rangle$. The propagator in spatial momentum and frequency space is given by

$$G_\phi(\omega_n, \vec{p}) = \int_0^\beta d^4x e^{i(\omega_n t + \vec{p}\vec{x})} G_\phi(t, \vec{x}), \quad \text{where} \quad \omega_n = 2n\pi T, \quad \text{with} \quad n \in \mathbb{Z}. \quad (3.71)$$

The discrete frequencies ω_n are called *Matsubara frequencies* and originate in the finite imaginary time extent. The frequency Fourier transformation back gives

$$G_\phi(t, \vec{p}) = \sum_{n \in \mathbb{Z}} e^{-i\omega_n t} G_\phi(\omega_n, \vec{p}), \quad (3.72)$$

which has the necessary periodicity in imaginary time, $G(t + \beta, \vec{p}) = G(t, \vec{p})$, of a correlation function, see (3.69). In frequency and spatial momentum space the classical propagator looks the same as in the vacuum. We have

$$G_\phi(\omega_n, \vec{p}) = \frac{1}{\omega_n^2 + \vec{p}^2 + m^2} \quad \text{with} \quad m^2(\phi) = \partial_\phi^2 V(\phi). \quad (3.73)$$

While the Fourier transformation w.r.t. spatial momentum is also the same as at $T = 0$, that w.r.t. frequency changes. Here we discuss the Fourier transformation for $t = 0$ for the mixed representation $G_\phi(t, \vec{p})$,

$$G_\phi(t = 0, \vec{p}) = T \sum_{n \in \mathbb{Z}} \frac{1}{\omega_n^2 + \vec{p}^2 + m^2} = \frac{1}{2\epsilon_p^\phi} \coth \frac{\beta \epsilon_p^\phi}{2} = \frac{1}{2\epsilon_p^\phi} \left[1 + 2n_B(\epsilon_p^\phi) \right], \quad (3.74)$$

with the dispersion ϵ_p^ϕ and the thermal distribution function $n_B(\omega)$ given by

$$\epsilon_p^\phi(m^2) = \sqrt{\vec{p}^2 + m^2}, \quad n_B(\omega) = \frac{1}{e^{\beta\omega} - 1}. \quad (3.75)$$

The latter is the standard Bose-Einstein distribution and clearly shows the thermal nature of the Matsubara path integral.

As a warm-up of the computation for the effective potential in the Yukawa theory at finite temperature we compute that of the simple scalar theory. Its thermal part is related to the thermal pressure of the theory with potential. To that end we remind ourselves that the scalar free energy density Ω_ϕ and the pressure of the theory are given by

$$Z_T[0] = e^{-\beta\mathcal{V}\Omega_\phi}, \quad p_\phi = -\frac{\partial\mathcal{V}\Omega_\phi}{\partial\mathcal{V}} \quad \text{with} \quad \mathcal{V} = \int d^3x. \quad (3.76)$$

The one-loop contribution to the free energy density and pressure are hence given by

$$\begin{aligned} \Omega_\phi &\simeq \frac{1}{2\mathcal{V}} T \operatorname{Tr} \ln(-\partial_\mu^2 + m^2) = \frac{1}{2} T \sum_{n \in \mathbb{Z}} \int \frac{d^3p}{(2\pi)^3} \ln(\omega_n^2 + \vec{p}^2 + m^2), \\ p_\phi &\simeq -\frac{1}{2} T \sum_{n \in \mathbb{Z}} \int \frac{d^3p}{(2\pi)^3} \ln(\omega_n^2 + \vec{p}^2 + m^2), \end{aligned} \quad (3.77)$$

where we dropped the normalisations in Ω_ϕ and p_ϕ . We also remind the reader that $m^2 = m^2(\phi)$ as introduced in (3.73). Note also that the pressure is nothing but (minus) the effective potential at finite temperature. At vanishing temperature we encountered singularities in the computation of the effective potential proportional to Λ^4 , λ^2 and $\ln\Lambda$ that had to be absorbed in the bare couplings. The highest singularity proportional to Λ^4 we disregarded as the absolute value of the potential energy which cannot be measured. The expressions in (3.77) are also infinite, showing the standard divergence of zero point functions at vanishing temperature. Similarly, we could introduce a spatial momentum cutoff Λ with $p^2 \leq \Lambda^2$ and proceed as in the last chapter. In the following we shall not make this cutoff explicit for the following reason: it is one of the cornerstones, and can be proven in thermal field theory all singularities are temperature-independent. This statement can be understood heuristically as the ultraviolet singularities are short-distance singularities. At short-distance singularities the finite extent in time-direction cannot be accessed. For detailed discussions we refer to the literature, here this fact will simply come out.

For the computation we take the mass (squared) derivative of the pressure, $\partial_{m_\phi^2} p$. This removes the logarithm from the expression and leaves us with integrals and sums that can be computed by complex analysis. The mass-derivative of the pressure is related to the momentum integral of the propagator in the mixed representation $G(0, \vec{p})$ computed in (3.74),

$$\partial_{m_\phi^2} p_\phi \simeq -\frac{1}{2} \int \frac{d^3p}{(2\pi)^3} G_\phi(0, \vec{p}) = -\frac{1}{4} \int \frac{d^3p}{(2\pi)^3} \frac{1}{\epsilon_p^\phi} [1 + 2n_B(\epsilon_p^\phi)]. \quad (3.78)$$

Equation (3.78) entails that the mass-derivative of the pressure, and hence the pressure, only carries a temperature-independent singularity proportional to $1/\epsilon_p^\phi$. The term proportional to n_B vanishes in the zero temperature limit. Upon integration over m^2 the pressure is given by

$$p_\phi \simeq - \int \frac{d^3p}{(2\pi)^3} \left[\frac{1}{2} \epsilon_p^\phi + T \ln(1 - e^{-\beta\epsilon_p^\phi}) \right]. \quad (3.79)$$

The singular, temperature-independent piece pressure in (3.79) proportional to ϵ_p^ϕ is nothing but the effective potential at vanishing temperature which we have computed for a fermionic theory in the last

chapter. Its renormalisation can be performed analogously. Here we are only interested in the thermal pressure, and we subtract the pressure at vanishing temperature,

$$\begin{aligned} p_{\phi,\text{thermal}} &= p_\phi(T) - p_\phi(T = 0) \\ &= -T \int \frac{d^3 p}{(2\pi)^3} \ln \left(1 - e^{-\beta \epsilon_p^\phi} \right) = -\frac{T}{2\pi^2} \int_0^\infty dp p^2 \ln \left(1 - e^{-\beta \epsilon_p^\phi} \right). \end{aligned} \quad (3.80)$$

Equation (3.80) is manifestly finite as for large momenta $p^2 \gg m_\phi^2, T^2$ the exponential in the logarithm decays with $\exp(-p/T)$, the typical thermal decay. It is also positive as the argument in the logarithm is always smaller than one and hence the logarithm is strictly negative. With the minus sign in front of the integral this leads to a positive expression, as expected for a thermal pressure. For a given temperature (3.80) takes its maximal value for $m_\phi^2 = 0$ and decays monotonously with increasing m_ϕ^2 as the thermal part of the mass-derivative is negative, see (3.78). For $m_\phi^2 \rightarrow \infty$ the thermal pressure vanishes. Accordingly the pressure is positive for all m_ϕ^2 . For large masses $m_\phi \gg T$ the pressure decays exponentially with $\exp(-m_\phi/T)$ (up to polynomial prefactors). For vanishing masses the momentum integration can be performed easily and we arrive at

$$P_{\phi,\text{thermal}} \Big|_{m^2=0} = \frac{\pi^2 T^4}{90}. \quad (3.81)$$

The explicit result for vanishing mass is the Stefan-Boltzmann pressure of a free gas. It is the tree-level thermal pressure. Note also that (3.80) is the result for the thermal part of the (one-loop) effective potential of a bosonic theory, see (3.80).

Fermions at finite temperature

In summary we are but one step away from our goal of accessing the thermal chiral phase transition in QCD in the QM model. For that task we need to translate the results above to the -free- quark path integral. The computation of the last chapter in the vacuum carries over here, we only have to discuss the fermionic Matsubara frequencies. For that end we redo the derivation of the thermal path integral for fermions again by starting from partition function Z_T as defined in the scalar case in (3.63). Everything goes as in the scalar case except one subtlety concerning the trace. Again more details can be found in the QFT II lecture notes, chapter 2. As in the case of the bosonic field we need coherent states that allow us to define $\hat{\psi}|\psi\rangle = \psi|\psi\rangle$. For the sake of the argument we restrict ourselves to one creation and annihilation operator a, a^\dagger and Grassmann variable c . A coherent state is given by

$$|c\rangle = (1 - c a^\dagger)|0\rangle = e^{-c a^\dagger}|0\rangle \quad \text{with} \quad a|c\rangle = c a a^\dagger|0\rangle = c|0\rangle = c(1 - c a^\dagger)|0\rangle = c|c\rangle, \quad (3.82)$$

where the latter property proves the coherence property of the state. The dual state $\langle c| = |c\rangle^\dagger$ has the property

$$\langle c|a^\dagger = -\langle c|c^*. \quad (3.83)$$

In consequence, instead of periodicity of the fields in time in the scalar case coming from the trace in (3.63) we have anti-periodicity,

$$\psi(t + \beta, \vec{x}) = -\psi(t, \vec{x}), \quad (3.84)$$

that reflects the Grassmannian nature of the fermionic field. The fermionic path integral Z_ψ with the Dirac action at finite temperature and density then reads

$$Z_{\psi,T}[J] = \int_{\psi(\beta, \vec{x}) = -\psi(0, \vec{x})} d\psi d\bar{\psi} e^{-S_{D,T}[\phi] + \int_0^\beta d^4x \bar{\eta}(t, \vec{x}) \psi(\vec{x}) - \bar{\eta}(t, \vec{x}) \psi(t, \vec{x})}, \quad (3.85)$$

with the fermionic Matsubara action

$$S_{D,T}[\psi] = \int_0^\beta d^4x \bar{\psi} \cdot (\not{d} + m_\psi - \gamma_0 \mu_\psi) \cdot \psi. \quad (3.86)$$

As in the scalar case we can reveal the thermal nature of correlation functions derived from the generating functional (3.85) by looking at the Dirac propagator of the quarks in the mixed representation at vanishing time, $G_q(t, \vec{p})$. To that end we first notice that the Fourier transformation of the anti-periodic fermionic fields is reflected in a shift of the Matsubara modes by πT . We have

$$\psi(x) = T \sum_{n \in \mathbb{Z}} \int \frac{d^3 p}{(2\pi)^3} e^{-i(\omega_{n,f} t + \vec{p} \cdot \vec{x})} \psi(p_0, \vec{p}), \quad \omega_{n,f} = (2n + 1)\pi T, \quad (3.87)$$

where the additional factor $e^{i\pi T t}$ leads to the minus sign in the periodicity relation (3.84) with $e^{i\pi T(t+\beta)} = e^{i\pi} e^{i\pi T t} = -e^{i\pi T t}$. Now we perform the computation for the frequency sum of the fermionic propagator G_ψ

$$\begin{aligned} \frac{1}{4m_\psi} \text{tr } G_q(t=0, \vec{p}) &= T \sum_{n \in \mathbb{Z}} \frac{1}{(\omega_{n,f} + i\mu_\psi)^2 + \vec{p}^2 + m_\psi^2} = \frac{1}{4\epsilon_p^\psi} \left[\tanh \frac{\beta}{2} (\epsilon_p^\psi - \mu_\psi) + \tanh \frac{\beta}{2} (\epsilon_p^\psi + \mu_\psi) \right] \\ &= \frac{1}{2\epsilon_p^\psi} \left[1 - n_F(\epsilon_p^\psi - \mu_\psi) - n_F(\epsilon_p^\psi + \mu_\psi) \right], \end{aligned} \quad (3.88)$$

where the trace tr in (3.88) sums over Dirac space. The dispersion ϵ_p^ψ is given in (3.57), and the thermal distribution function $n(\omega)$ reads

$$n_F(\omega) = \frac{1}{e^{\beta\omega} + 1}, \quad (3.89)$$

the Fermi-Dirac distribution. The difference to the Bose-Einstein statistics in the scalar case originates in the anti-periodicity of the fermions related to their Grassmannian nature. For $T \rightarrow 0$ the Fermi-Dirac dispersions get sharp, $\lim_{T \rightarrow 0} n_F(\omega) \rightarrow \theta(-\omega)$ and we have for $\mu_\psi > 0$,

$$\lim_{T \rightarrow 0} \frac{1}{4m_\psi} \text{tr } G_\psi(t=0, \vec{p}) = \frac{1}{2\epsilon_p^\psi} \theta(\epsilon_p^\psi - \mu), \quad (3.90)$$

only modes with energies larger than μ propagate, the lower ones are drowned in the Fermi sea. The free energy and pressure can be derived analogously to the scalar case. The one-loop contribution to the fermionic free energy density Ω_ψ and the pressure are hence given by

$$\begin{aligned} \Omega_\psi &\simeq -\frac{T}{2\mathcal{V}} \text{Tr} \ln \left[-(\partial_\mu - \mu_\psi \delta_{\mu 0})^2 + m_\psi^2 \right] = -2T \sum_{n \in \mathbb{Z}} \int \frac{d^3 p}{(2\pi)^3} \ln \left[(\omega_{n,f} + i\mu_\psi)^2 + \vec{p}^2 + m_\psi^2 \right], \\ p_\psi &\simeq 2T \sum_{n \in \mathbb{Z}} \int \frac{d^3 p}{(2\pi)^3} \ln \left[(\omega_{n,f} + i\mu_\psi)^2 + \vec{p}^2 + m_\psi^2 \right], \end{aligned} \quad (3.91)$$

where as in the scalar case we dropped the normalisations in Ω_ψ and p_ψ . Equation (3.91) has to be compared with (3.77): the prefactor -2 in comparison to the prefactor $1/2$ in the scalar case comes from the relative minus sign and factor 2 of the fermionic loop, the symmetrisation of the frequency and spatial momentum trace and the Dirac trace: $-1 * 1/2 * 4 = -2$ instead of $1/2$ in the scalar case. For the computation of the thermal pressure we proceed similar to the scalar case with a m_ψ^2 -derivative in order

to map the pressure to (3.88). We also remove the divergent vacuum contribution which is the effective potential at vanishing temperature. The thermal part of the grand potential and the thermal fermi pressure for a single Dirac fermion are then given by

$$\Omega_{\psi,T}(\psi, \bar{\psi}) - \Omega_{\psi,T=0}(\psi, \bar{\psi}) = -\frac{1}{\pi^2} T \int_0^\infty dp p^2 \left[\ln \left(1 + e^{-\beta(\epsilon_p^\psi - \mu_\psi)} \right) + \ln \left(1 + e^{-\beta(\epsilon_p^\psi + \mu_\psi)} \right) \right] = -p_{\psi,\text{thermal}}, \quad (3.92)$$

with the fermionic dispersion (3.57). This has to be compared with (3.80) for the scalars. Both expressions for the pressure are strictly positive which is due to

$$\mp \ln \left(1 \mp e^{-\beta \epsilon_p^{\phi/\psi}} \right) \geq 0, \quad (3.93)$$

with the minus signs in the bosonic case and the plus sign in the fermionic one. The global \mp in (3.93) reflects the relative sign of fermionic and bosonic loops while the \mp reflects the Bose-Einstein vs Fermi-Dirac quantum statistics.

We close this chapter with briefly discussing the grand potential for the QM model. There, the fermionic mass $m_\psi = m_q$ in (3.92) is given by

$$m_q^2(\phi) = h_\sigma^2 \rho, \quad (3.94)$$

and the quark part of the grand potential acquires an additional factor $N_c = 3$. We pion and sigma parts of the grand potential have scalar dispersions (3.75) with the masses 2.253c. The sum of (3.80) and (3.92) with these modifications leads us to the grand potential of the QM model with $N_f = 1$ and $N_c = 3$,

$$\Omega_T(\psi, \bar{\psi}, \phi) - \Omega_{T=0}(\psi, \bar{\psi}, \phi) = \Omega_{\sigma,T} + \Omega_{\pi,T} + \Omega_{q,T} - \Omega_{\sigma,T=0} + \Omega_{\pi,T=0} + \Omega_{q,T=0} \quad (3.95a)$$

with

$$\begin{aligned} \Omega_{\sigma,T}(\phi) &= -\frac{T}{2\pi^2} \int_0^\infty dp p^2 \ln \left(1 - e^{-\beta \epsilon_p^\phi(m_\sigma^2)} \right), \\ \Omega_{\pi,T}(\phi) &= -\frac{T}{2\pi^2} \int_0^\infty dp p^2 \ln \left(1 - e^{-\beta \epsilon_p^\phi(m_\pi^2)} \right), \\ \Omega_{q,T}(\phi) &= -\frac{3}{\pi^2} T \int_0^\infty dp p^2 \left[\ln \left(1 + e^{-\beta(\epsilon_p^q(m_q^2) - \mu_\psi)} \right) + \ln \left(1 + e^{-\beta(\epsilon_p^q(m_q^2) + \mu_\psi)} \right) \right] \end{aligned} \quad (3.95b)$$

Equation (3.95) encodes all thermal and density fluctuations at one loop. As in the vacuum case for $T = 0$ we have several possibilities of how to integrate out the thermal fluctuations, e.g. either in parallel or successively. Even though being relevant for the quantitative results, it is irrelevant for the access of the mechanism of chiral symmetry restauration at large temperatures: At large temperatures the fermion exhibits a Matsubara gapping as the lowest lying Matsubara mode is πT in comparison to the vanishing one in the mesonic case. For higher temperatures more and more of the infrared fermion fluctuations are gapped. However, the fermion fluctuations triggers the spontaneous chiral symmetry breaking in the first place. Consequently at large enough temperatures chiral symmmtry breaking is melted away.

3.2.3. Flows at finite temperature and density

In the last chapters, [Section 3.2.1](#), [Section 3.2.2](#), we have briefly discussed the basics of QFT at finite temperature and density. Technically, the chemical potential simply amounts to a shift of the frequency by an imgainary part $\omega \rightarrow \omega + i\mu$, while finite temperature substitutes continuous frequencies with Matsubara frequencies,

$$\omega \rightarrow \omega_{n,\varphi_i} = 2\pi T \left(n + \frac{1}{2} \delta_{\varphi_i \psi} + i \frac{\mu_{\varphi_i}}{2\pi T} \right). \quad (3.96)$$

where φ_i are the components of the superfield Φ and $\delta_{\varphi_i \psi}$ vanishes for bosonic fields while it is unity for fermionix ones (which the exception of the auxiliary ghost fields, see [Section 5.3](#)). Consequently, all steps in the derivation of the Wetterich equation (2.27) stay the same and we are led to the general flow,

$$\partial_t \Gamma_k[\phi] = \frac{1}{2} \sum_p \text{tr} \frac{1}{\Gamma_k^{(2)}[\phi] + R_k}(p, -p) \partial_t R_k(p^2), \quad (3.97)$$

where the trace tr sums over Lorentz indices, internal indices and species of fields including relative minus signs for fermions. The only change is that the frequency integrals turns into sums over the frequencies (3.96).

Finite T flow with Frequency-independent regulators

In case the frequency dependence of the propagators and vertices is kept on the classical level, the Matsubara sums in (3.97) can be performed analytically. This leads to great technical simplifications as well as an analytic grip on the mechnisms at hand, as is already clear from the one loop analysis of the last chapter, [Section 3.2.2](#). To maintain this advantage in the FRG approach, the regulators require a trivial frequency dependence,

$$R_k(p) \rightarrow R_k(\vec{p}). \quad (3.98)$$

For the class of regulators (3.98), the only frequency dependence in (3.97) is that of the propagator. Resorting to the approximation of classical or at least analytical frequency dependences the respective Matsubara sums can be performed. Here we discuss this at the example of scalar and fermionic flows in LPA. The scalar flow is given by

$$\partial_t \Delta V_k(\rho) = \frac{1}{2} \int \frac{d^3 p}{(2\pi)^3} \partial_t R_{\phi,k}(\vec{p}) \left[T \sum_{n \in \mathbb{Z}} G_{\phi,k}(\omega_{n,\phi}, \vec{p}, \phi) \right], \quad (3.99)$$

with

$$G_{\phi,k}(\omega_{n,\phi}, \vec{p}, \phi) = \frac{1}{\omega_{n,\phi}^2 + \vec{p}^2 [1 + r_\phi(x)] + m_\phi^2(\phi)}. \quad (3.100)$$

with the spatial momentum analogue of the scalar regulator $R_{\phi,k}(p^2)$ in (2.6),

$$R_{\phi,k}(\vec{p}^2) = \vec{p}^2 r_\phi(x), \quad \text{where} \quad x = \frac{\vec{p}^2}{k^2}. \quad (3.101)$$

In (3.99) we immediately identify the sum over the propagator, (3.74), which was of pivotal importance for our one loop analysis in [Section 3.2.2](#). Using this result we arrive at

$$\partial_t \Delta V_{\phi,k}(\rho) = \int \frac{d^3 p}{(2\pi)^3} \vec{p}^2 \frac{1}{4\epsilon_{p,k}^\phi} \left[1 + 2 n_B(\epsilon_{p,k}^\phi) \right] \partial_t r_\phi(x) , \quad (3.102)$$

with the regulator-dependent dispersion

$$\epsilon_{p,k}^\phi = \sqrt{\vec{p}^2 \left[1 + r_\phi(x) \right] + m_\phi^2(\phi)} , \quad (3.103)$$

with the scalar dispersion in (3.75) and the field-dependent mass [2.253c](#) with $V \rightarrow V_k$. The first term in the square bracket in (3.102) is the vacuum flow, while the second one is the thermal contribution. It vanishes for $T \rightarrow 0$. Integrating the thermal part in (3.102) at one loop leads to the thermal grand potential, [3.95b](#).

The same reasoning can be straightforwardly applied to fermionic contributions to the flow of the effective potential in LPA,

$$\partial_t \Delta V_{\psi,k}(\rho) = - \int \frac{d^3 p}{(2\pi)^3} \text{tr} \partial_t R_{\psi,k}(\vec{p}) \left[T \sum_{n \in \mathbb{Z}} G_{\psi,k}(\omega_{n,\psi}, \vec{p}, \phi) \right] , \quad (3.104)$$

with

$$G_{\psi,k}(\omega_{n,\psi}, \vec{p}, \phi) = \frac{-i\gamma_0 \omega_{n,\psi} - i\vec{\gamma} \vec{p} \left[1 + r_\psi(x) \right] + m_\psi(\phi)}{\omega_{n,\psi}^2 + \vec{p}^2 \left[1 + r_\psi(x) \right]^2 + m_\psi^2(\phi)} , \quad (3.105)$$

with the spatial momentum analogue of the fermionic regulator (2.218),

$$R_{\psi,k}(\vec{p}) = i \vec{p} r_\psi(x) , \quad \text{with} \quad \vec{p} = \vec{\gamma} \vec{p} \quad \text{and} \quad x = \frac{\vec{p}^2}{k^2} . \quad (3.106)$$

As for the scalar case the Matsubara sum of the fermionic propagator, (3.88), was already of pivotal importance for the one loop analysis. However, in (3.105) the Matsubara sum of the propagator is multiplied with $\partial_t R_{\psi,k} = i \vec{p} \partial_t r_\psi$ instead of one. Accordingly, the result in (3.88) should be multiplied by $-2\vec{p}^2 \partial_t r_\psi$, also taking into account the factor 4 of the Dirac trace and the minus sign for the fermionic loop. In summary we are led to

$$\partial_t \Delta V_{\psi,k}(\rho) = -2 \int \frac{d^3 p}{(2\pi)^3} \frac{\vec{p}^2 \left[1 + r_\psi(x) \right]}{\epsilon_{p,k}^\psi} \left[1 - n_F(\epsilon_{p,k}^\psi - \mu_\psi) - n_F(\epsilon_{p,k}^\psi + \mu_\psi) \right] \partial_t r_\psi(x) , \quad (3.107)$$

with the regulator-dependent dispersion

$$\epsilon_{p,k}^\psi = \sqrt{\vec{p}^2 \left[1 + r_\psi(x) \right] + m_\psi^2(\phi)} , \quad (3.108)$$

with the fermionic dispersion in (3.57) and the field-dependent mass m_ψ depending on the interaction term with the scalars. For Yukawa theories and LPA it is given in (3.94).

The sum of the two flows, (3.102) and (3.107), build up the flow of the effective potential $V_k(\rho)$ in general Fermi-Bose theories. It is a very simple flow, the sacrifice for its simplicity being the reduction to the classical dispersion as well as a restriction to a spatial momentum regulator. While the former is a real restriction for the approximation, the latter is a valid choice for a class of regulators. However, this choice comes at a price, which is elaborated on in [??](#). Here we simple note that no frequency shell is singled out by frequency-independent regulators. Consequently, each cutoff step carries the full

frequency dependence. This calls for frequency-dependent approximations for the correlation functions $\Gamma_k^{(n)}$ if we aim at quantitative precision of the results. This is indeed also the outcome of an optimisation analysis. Moreover, a spatial momentum regulator spoils the Euclidean $O(4)$ invariance of the theory in the flow, a property which has to be present at $k = 0$ in the vacuum. Hence, at finite T one has to distinguish between regulator-dependent breaking of the $O(4)$ -symmetry and the physical thermal breaking. This requires the use of modified $O(4)$ -symmetry identities, to be discussed in ??.

Note also that including a general frequency-dependence spoils any advantage of the spatial momentum regulators and only complicates the task: one has now to perform the Matsubara sums numerically while the integrands only polynomially depend on the frequency. Hence, if aiming for quantitative accuracy four-dimensional $O(4)$ -symmetric regulators are the best choice. Nonetheless, the dependence on the classical dispersion can and has been upgraded to a full two-loop frequency resummation in [79]. This also allows the analytic access to the Silver blaze properties mentioned before.

Finite T flow with frequency independent Litim regulators

The flows (3.102) and (3.107) can be simplified further with the use of Litim regulators with 2.9a for scalars and (2.241) for fermions. Then for spatial momenta smaller than the cutoff scale the dispersions are flat

$$\vec{p}^2 \left[1 + r_\phi(x) \right] = k^2, \quad p^2 \left[1 + r_\psi(x) \right]^2 = k^2, \quad \vec{p}^2 \left[1 + r_\psi(x) \right] = k^2 \sqrt{x}, \quad \text{for } \vec{p}^2 \leq k^2. \quad (3.109)$$

and the t -derivatives of the shape functions r_ϕ and r_ψ are given by

$$\partial_t r_\phi(x) = \frac{2}{x} \theta(1-x), \quad \partial_t r_\psi(x) = \frac{1}{\sqrt{x}} \theta(1-x). \quad (3.110)$$

The only spatial momentum dependence left in both flows is easily integrated, to wit

$$\int \frac{d^3 p}{(2\pi)^3} \theta(1-x) = \frac{1}{3} \frac{\Omega_3}{(2\pi)^3} k^3 = \frac{1}{6\pi^2} k^3. \quad (3.111)$$

In summary, the flows of $\Delta V_{\phi,k}$ and $\Delta V_{\psi,k}$ at finite T and μ are given by

$$\partial_t \Delta V_{\phi,k}(\rho) = \frac{1}{12\pi^2} \frac{k^5}{\epsilon_k^\phi} \left[1 + 2 n_B(\epsilon_k^\phi) \right], \quad (3.112)$$

with the dispersion

$$\epsilon_k^\phi = \sqrt{k^2 + m_\phi^2(\phi)}. \quad (3.113)$$

In (3.113) the spatial momentum is simply substituted by the cutoff scale, supporting the interpretation of the cutoff scale as the running (average) momentum scale.

For the fermion we can proceed similarly and obtain

$$\partial_t \Delta V_{\psi,k}(\rho) = -\frac{1}{3\pi^2} \frac{k^5}{\epsilon_k^\psi} \left[1 - n_F(\epsilon_k^\psi - \mu_\psi) - n_F(\epsilon_k^\psi + \mu_\psi) \right], \quad (3.114)$$

with

$$\epsilon_k^\psi = \sqrt{k^2 + m_\psi^2(\phi)}. \quad (3.115)$$

The sum of the two flows (3.112) and (3.114) constitutes the flow of our chiral Yukawa theory used as our example theory for general Bose-Fermi mixtures.

3.2.4. Phase structure of the two flavour Quark Meson Model

We now use the results of the last [Section 3.2.3](#) for the QM model put forward in [Section 3.1.5](#). We also move a step closer to the physically interesting case $N_f = 2 + 1$ flavours and consider a two flavour QM model with $N_f = 2$. Furthermore we include cutoff- and ϕ -dependent wave function renormalisations $Z(\rho)$. The flavour symmetries of $N_f = 2$ flavour QCD are discussed in detail in [Appendix E](#). Here we only use that for two flavours we have the physical scalar-pseudoscalar multiplet $\phi = (\sigma, \vec{\pi})$ with the charged and neutral pions $\vec{\pi}) = (\pi^0, \pi^\pm)$. The other members of the multiplet are mass-suppressed and we simply drop them in the present analysis.

Then, the form of the respective Yukawa theory with $N_f = 2$ is similar to that of the $N_f = 1$ case, [\(3.25\)](#), in [Appendix E](#). We have in the first order of the derivative expansion,

$$\begin{aligned} \Gamma_k[\Phi] = \int_x & \left\{ Z_q(\rho) \bar{q} \left(i \not{d} + m_q - \gamma_0 \mu_q \right) q + \frac{h_\sigma(\rho)}{2} \bar{q} (\sigma + i \gamma_5 \vec{\tau} \vec{\pi}) q \right. \\ & \left. + \frac{1}{2} Z_\phi(\rho) (\partial_\mu \phi)^2 + \frac{1}{2} Z_\rho(\rho) (\partial_\mu \rho)^2 + V(\rho) \right\}, \end{aligned} \quad (3.116)$$

the two-flavour quarks $q = (u, d)$, and

$$\vec{\tau} = (\sigma_1, \sigma_2, \sigma_3), \quad \text{with} \quad \sigma_1 = \begin{pmatrix} 0 & 1 \\ 1 & 0 \end{pmatrix}, \quad \sigma_2 = \begin{pmatrix} 0 & -i \\ i & 0 \end{pmatrix}, \quad \sigma_3 = \begin{pmatrix} 1 & 0 \\ 0 & -1 \end{pmatrix}, \quad (3.117)$$

is the vector of the Pauli matrices. The mesonic $O(4)$ -field is given by

$$\phi_a = (\sigma, \vec{\pi}), \quad \rho = \frac{\sigma^2 + \vec{\pi}^2}{2}. \quad (3.118)$$

In [\(3.116\)](#) we have dropped all superscripts k , it is understood that all parameters run with the cutoff scale. Also, we have partially anticipated the running of the vertices $\Gamma_k^{(n)}$ with the appropriate powers of $Z^{(n/2)}$ as already discussed in [Section 2.3.3](#), see e.g. [2.134a](#). Finally, we have ignored the fact that the Euclidean $O(4)$ symmetry is broken by both the regulator and the temperature. This leads to different factors for the spatial momentum part and frequency part of the dispersion. This is discussed later in [Section 5.3](#).

Moreover, as explained in [Appendix E](#), the Yukawa interaction in [\(3.116\)](#) -and hence the related four quark interaction, see [\(E.14\)](#)- maximally breaks the axial $U_A(1)$. Effectively it takes into account the anomalous breaking of the axial $U_A(1)$ symmetry to be discussed later. This leaves us with the flavour symmetry group $SU(N_c) \times SU(N_f)_V \times SU(N_f)_A \times U(1)_V$ of the present $N_f = 2$ QM model. We now can take over the results for the generic scalar and fermionic flows in the last chapter, [Section 3.2.3](#), for the present Yukawa theory, after taking into account minor modifications due to the presence of wave function renormalisations: first we note that the two point functions $\Gamma_{\varphi_i \varphi_j}^{(2)}$ are proportional to the wave function renormalisations $Z_{\varphi_i}^{1/2} Z_{\varphi_j}^{1/2}$. This originates in the parameterisation used in [\(3.116\)](#) which makes apparent the RG-running of the legs of n -point functions. This suggests regulators with the respective running, see [\(2.121\)](#). Such a choice can be shown to be *RG-adapted*, see [\[9\]](#): the theory in the presence of the infrared regulator has the same RG-invariance as the full one at vanishing regulator. Apart from this formal property, it is easy to see that this choice facilitates the computations, the wave function renormalisation will drop out from the flows as already shown in [Section 2.3.3](#), and only the anomalous dimensions η_{φ_i} are present in the loops.

The flow equation for the effective potential in [\(3.116\)](#) follows from [\(3.97\)](#) as

$$\partial_t V(\rho) = \frac{3}{2} \text{Tr} G_{\pi\pi} \partial_t R_{\phi,k} + \frac{1}{2} \text{Tr} G_{\sigma\sigma} \partial_t R_{\phi,k} - \text{Tr} G_{\bar{q}q} \partial_t R_{q,k}, \quad (3.119)$$

where the factor 3 comes from the three pions with $G_{\pi_i \pi_i} = G_{\pi\pi}$ for $\phi = (\sigma, 0)$. In LPA with the spatial momentum Litim regulators the flow can be put together with [\(3.112\)](#) and [\(3.114\)](#). Here we

aim at the flow of the effective potential including cutoff-dependent but field-independent wave function renormalisations Z_σ , Z_π and Z_q . For this flow we need the propagators in the presence of the wave function renormalisations in (3.116). Their form also suggests a specific choice of regulators including the Z 's leading to their cancellation between propagator and $\partial_t R_k$ at the cost of a term proportional to the anomalous dimension, which constitutes the only new term.

To begin with we discuss first, how different wave function renormalisations $Z_\sigma \neq Z_\pi$ come about in the present $O(4)$ -symmetric theory. Consider the second derivative of (3.116) with respect to the mesonic fields at $\phi = (\sigma, \vec{\pi} = 0)$ with constant σ , leading to

$$\Gamma_{\sigma\sigma}^{(2)}(p) = [Z_\phi(\rho) + 2\rho Z_\rho(\rho)] p^2 + V'(\rho) + 2\rho V''(\rho), \quad \Gamma_{\sigma\sigma}^{(2)} = Z_\phi(\rho)p^2 + V'(\rho). \quad (3.120)$$

Equation (3.120) entails that the σ and $\vec{\pi}$ have different wave function renormalisations,

$$Z_\sigma(\rho) = Z_\phi(\rho) + 2\rho Z_\rho(\rho), \quad Z_\pi(\rho) = Z_\phi(\rho), \quad (3.121)$$

on the configurations $\phi = (\sigma, 0)$. We emphasise again that this does not break the $O(4)$ -symmetry of the theory, it simply signals an expansion point that breaks this symmetry. This fact is taken into account with bosonic regulators (3.101) is multiplied by the wave function renormalisation $Z_{\sigma/\pi} = Z_{\sigma/\pi}(\rho_0)$, evaluated at a convenient background σ_0 , e.g. the EoM σ_{EoM} , to wit

$$R_{\sigma/\pi,k}(\vec{p}^2) = Z_{\sigma/\pi} \vec{p}^2 r_\phi(x), \quad \text{with} \quad Z_{\sigma/\pi} = Z_{\sigma/\pi}(\rho_0), \quad x = \frac{\vec{p}^2}{k^2}, \quad (3.122)$$

We emphasise that the wave function renormalisations in (3.122) are necessarily ϕ -independent, they only can depend on the chose background ϕ_0 . For the quark field the situation is simpler, as we evaluate the flow at $q, \bar{q} = 0$, no direction in field space is singled out. The second q, \bar{q} -derivative of Γ_k in (3.116) is given by

$$\Gamma_{\bar{q}q}^{(2)}(p) = i Z_q(\rho) \not{p} + m_q + \frac{h_\sigma(\rho)}{2} \sigma = i Z_q(\rho) \not{p} + m_q + \frac{h_\sigma(\rho)}{2} \sigma. \quad (3.123)$$

Equation (3.123) entails that the two-point function of the quarks depends on Z_π and not on Z_σ . We now multiply the wave function renormalisation $Z_q = Z_q(\rho_0)$ in (3.106), similar to the mesonic regulators, and obtain

$$R_{q,k}(\vec{p}) = i Z_q \not{p} r_q(x), \quad \text{with} \quad Z_q = Z_q(\rho_0), \quad x = \frac{\vec{p}^2}{k^2}. \quad (3.124)$$

In (3.124) it is understood that Z_q is evaluated in the chosen background ϕ_0 . As shape functions we use the Litim regulator, as before, given by (2.241) for fermions and 2.9a for bosons. With these definitions we can easily access the regulator derivatives, made dimensionless by an appropriate power of $1/k$,

$$\frac{1}{Z_\varphi k^2} \partial_t R_\varphi(p) = x \left(\partial_t r_\varphi(x) - \eta_\varphi r_\varphi(x) \right) = \left(2 - [1-x] \eta_\varphi \right) \theta(1-x), \quad \varphi = \sigma, \pi$$

$$\frac{1}{Z_q k} \partial_t R_q(p) = i \not{p} \left(\partial_t r_q(x) - \eta_q r_q(x) \right) = i \frac{\not{p}}{\sqrt{\vec{p}^2}} \left(1 - [1 - \sqrt{x}] \eta_q \right) \theta(1-x). \quad (3.125)$$

with the anomalous dimensions η_{φ_i} , (2.115), reduced to the momentum-independent case

$$\eta_{\varphi_i} = - \frac{\partial_t Z_{\varphi_i}}{Z_{\varphi_i}}, \quad \varphi_i = \sigma, \pi, q, \quad (3.126)$$

more details can be found in Section 2.3.3. With the wave function renormalisation in the definition of the regulators, all the the propagators have global factors $1/Z_{\varphi_i}$ (or rather $1/(Z_{\varphi_i}^{1/2} Z_{\varphi_j}^{1/2})$ if including the off-diagonal propagators).

While the full first order of the derivative expansion certainly is technically accessible in the present model, it has not been considered so far. Also here we will abandon the full first order of the derivative expansion and resorted to field-independent wave function renormalisations Z_{φ_i} 's,

$$Z_{\varphi_i}(\rho) \rightarrow Z_{\varphi_i} = Z_{\varphi_i}(\rho_0). \quad (3.127)$$

This further approximation can be checked if checking the approximate field independence of the flow of the Z 's on the chosen background. This has been done in [67]. With (3.127) the equations simplify significantly. For the diagonal parts and vanishing pion and fermionic fields, $q, \bar{q} = 0, \vec{\pi} = 0$ we are led to

$$\begin{aligned} G_{\pi\pi}(p) &= \frac{1}{Z_\pi} \frac{1}{p_0^2 + \vec{p}^2 [1 + r_\phi] + \frac{1}{Z_\pi} V'(\rho)} \\ &\xrightarrow{\vec{p}^2 \leq k^2} \frac{1}{Z_\pi} \frac{1}{p_0^2 + k^2 + \frac{1}{Z_\pi} V'(\rho)}, \end{aligned}$$

for the pions and

$$\begin{aligned} G_{\sigma\sigma}(p) &= \frac{1}{Z_\sigma} \frac{1}{p_0^2 + \vec{p}^2 [1 + r_\phi] + \frac{1}{Z_\sigma} [V'(\rho) + 2\rho V''(\rho)]} \\ &\xrightarrow{\vec{p}^2 \leq k^2} \frac{1}{Z_\sigma} \frac{1}{p_0^2 + k^2 + \frac{1}{Z_\sigma} [V'(\rho) + 2\rho V''(\rho)]}, \end{aligned} \quad (3.128a)$$

for the σ . Note that for $\vec{p}^2 \leq k^2$ the propagators are independent of \vec{p}^2 , the whole \vec{p}^2 -dependence is that of the measure and that in the t -derivatives of the regulators in (3.125): there is none for the standard term, and $1 - \sqrt{\vec{p}^2/k^2}$ for the anomalous dimension. Equation (3.128) can be conveniently reparameterised with introducing renormalised fields or rather renormalisation group invariant fields,

$$\bar{\phi} = Z_\phi^{1/2} \phi, \quad \bar{\rho} = Z_\phi \rho. \quad (3.129)$$

with $Z_\phi = Z_\phi(\rho_0) = Z_\pi$. We also define $\bar{V}(\bar{\rho}) = V(\rho)$ leading to

$$\begin{aligned} \bar{m}_\pi^2(\bar{\rho}) &= \frac{1}{Z_\pi} \partial_\rho V(\bar{\rho}) = \bar{V}'(\bar{\rho}), \\ \bar{m}_\sigma^2(\bar{\rho}) &= \frac{1}{Z_\sigma} [\bar{V}'(\rho) + 2\rho \bar{V}''(\rho)] = s_\phi [\bar{V}'(\bar{\rho}) + 2\bar{\rho} \bar{V}''(\bar{\rho})], \end{aligned} \quad (3.130)$$

with the ratio s_ϕ of the wave function renormalisations of σ and π ,

$$s_\phi = \frac{Z_\pi}{Z_\sigma}. \quad (3.131)$$

The fraction s_ϕ in the σ -mass function reflects the breaking of $O(4)$ -invariance of the expansion point. Its flow is given by

$$\eta_{s_\phi} = -\frac{\partial_t s_\phi}{s_\phi} = \eta_\sigma - \eta_\pi. \quad (3.132)$$

The present choice (3.129) introduces a uniform scaling for all pion correlation functions. As the pions are the (pseudo-)Goldstone bosons of chiral symmetry breaking this is a natural choice. They have smaller masses than the σ , and moreover carry more degrees of freedom in the physical case. This also

suggests the additional approximation $\eta_{s_\phi} = 0$. However, in the vicinity of the critical point of QCD the σ gets massless as it is the critical mode. Then this further approximation has to be taken with a grain of salt. With these preparations we finally get

$$G_{\varphi\varphi}(p) = \frac{1}{Z_\varphi} \frac{1}{p_0^2 + \vec{p}^2 [1 + r_\phi] + \bar{m}_\varphi^2(\rho)}, \quad \text{with} \quad \varphi = \sigma, \pi. \quad (3.133)$$

For the quarks we have

$$\begin{aligned} G_{\bar{q}q}(p) &= \frac{1}{Z_q} \frac{-i (\gamma_0 \omega_{n,q} + \vec{p} [1 + r_q]) + M_q}{\omega_{n,q}^2 + \vec{p}^2 [1 + r_q]^2 + M_q^2} \\ &\xrightarrow{\vec{p}^2 \leq k^2} \frac{-i \left(\gamma_0 \omega_{n,q} + k \frac{\vec{p}}{\sqrt{\vec{p}^2}} \right) + M_q}{\omega_{n,q}^2 + k^2 + M_q^2}, \end{aligned} \quad (3.134)$$

with $\omega_{n,q}$ in (3.49) and

$$M_q = m_q + \frac{\bar{h}_\sigma}{2} \bar{\sigma}, \quad \text{with} \quad \bar{h}_\sigma = \frac{h_\sigma}{Z_q Z_\phi^{1/2}}. \quad (3.135)$$

In summary all wave function renormalisations only appear as global prefactors in the propagator, leading to the rescaled $\partial_t R_k$ in (3.125): the Z 's drop out of the right hand side of the flow except for the ratio s_ϕ , (3.131).

For the quark contribution to the flow of the effective potential this leads us with (3.109) and (3.110) to

$$\partial_t \Delta V_q = -\text{Tr} G_{\bar{q}q} \partial_t R_{q,k} = -4N_c N_f k^2 \int_{\vec{p}^2 \leq k^2} \frac{d^3 p}{(2\pi)^3} (1 - [1 - \sqrt{x}] \eta_q) T \sum_n \frac{1}{\omega_{n,q}^2 + k^2 + M_q^2}. \quad (3.136)$$

Up to the additional term proportional to η_q and the factor $N_f N_c$ counting degrees of freedom, this is the LPA flow (3.104). As there the spatial momentum dependence factorises and the integration can be carried out easily,

$$\int_{\vec{p}^2 \leq k^2} \frac{d^3 p}{(2\pi)^3} (1 - [1 - \sqrt{x}] \eta_q) = \frac{1}{6\pi^2} \left(1 - \frac{1}{4} \right), \quad (3.137)$$

This leads us to

$$\partial_t \Delta V_q = -\frac{N_c N_f}{3\pi^2} k^5 \left(1 - \frac{\eta_q}{4} \right) \frac{1}{\epsilon_k^q} [1 - n_F(\epsilon_k^q + \mu_q) - n_F(\epsilon_k^q - \mu_q)]. \quad (3.138)$$

The mesonic part is computed similarly. The spatial momentum dependence factorises and with (3.109) and (3.110) we have

$$\int_{\vec{p}^2 \leq k^2} \frac{d^3 p}{(2\pi)^3} (2 - [1 - x] \eta_\phi) = \frac{1}{3\pi^2} \left(1 - \frac{1}{5} \right). \quad (3.139)$$

Note that the prefactor of the η -term in (3.139) is smaller than that of the quark, which can be attributed to the quadratic versus linear dispersion. However, the (absolute value of the) anomalous dimension of

the mesons turns out to be far bigger than that of the quarks. This emphasises the importance of the η_ϕ as compared to the η_q . The mesonic flow contribution to the flow of the effective potential reads

$$\partial_t \Delta V_\phi = \frac{1}{12\pi^2} k^5 \left\{ \left(1 - \frac{1}{5}\eta_\pi\right) \frac{1}{\epsilon_k^\pi} [1 + 2n_B(\epsilon_k^\pi)] + \left(1 - \frac{1}{5}\eta_\sigma\right) \frac{1}{\epsilon_k^\sigma} [1 + 2n_B(\epsilon_k^\sigma)] \right\}. \quad (3.140)$$

Collecting all terms, the full flow equation for the effective potential reads

$$\begin{aligned} \partial_t V(\rho) = & \frac{k^5}{12\pi^2} \left\{ \sum_{\varphi=\pi,\sigma} \left(\frac{1 - \frac{1}{5}\eta_\varphi}{\epsilon_k^\varphi} [1 + 2n_B(\epsilon_k^\varphi)] \right) \right. \\ & \left. - 2N_c \frac{1 - \frac{1}{4}\eta_q}{\epsilon_k^q} [1 - n_F(\epsilon_k^q + \mu_q) - n_F(\epsilon_k^q - \mu_q)] \right\}, \end{aligned} \quad (3.141)$$

where we have set $N_f = 2$. [Equation \(3.141\)](#) has to be accompanied with the relations for the wave function renormalisations $\eta_\sigma, \eta_\pi, \eta_q$, and that for the Yukawa coupling \bar{h}_σ or $\bar{h}_\sigma(\rho)$. Often, the η 's as well as the flow of the Yukawa coupling is dropped, and the phase structure is evaluated in LPA. Given its simplicity, it gives surprisingly good results if compared with more elaborated approximations. Hence, we close this chapter with a brief qualitative discussion of the QCD phase structure on the basis of the above flow. Explicit results are shown for both LPA as well as an approximation with $\eta_{s_\phi} = 0$ and k -dependent

$$Z_\phi, Z_q, V(\rho), \bar{h}(\rho). \quad (3.142)$$

in [\[67\]](#). The model is benchmarked in the vacuum for $T, \mu_q = 0$. There the observables in [Table 3.1](#) are fixed. The initial effective action Γ_Λ with the form [\(3.116\)](#) is given by

$$\begin{aligned} \bar{V}_\Lambda(\bar{\rho}) &= \frac{\bar{\lambda}}{2} (\bar{\rho} - \bar{\kappa})^2, \\ \bar{h}_\Lambda(\bar{\rho}) &= \bar{h}, \\ Z_\phi &= Z_q = 1. \end{aligned} \quad (3.143)$$

with the values

$$\Lambda = 700 \text{ MeV}, \quad \bar{\lambda} = 71.6, \quad \bar{\kappa} = 0, \quad \bar{h} = 5.09, \quad \bar{c}_\Lambda = 2.1 \cdot 10^{-3} \text{ GeV}^3, \quad (3.144)$$

leading to the observables

$$f_\pi = 93.0 \text{ MeV}, \quad \bar{m}_\pi = 138.7 \text{ MeV}, \quad \bar{m}_\sigma = 538.2 \text{ MeV}, \quad \bar{m}_q = 298.3 \text{ MeV}. \quad (3.145)$$

This matches the values in [Table 3.1](#) except for the σ mass. Note also that the Yukawa coupling in [\(3.144\)](#) takes another values as it is a running, $\bar{\rho}$ -dependent coupling in [\[67\]](#).

The flow [\(3.141\)](#) in a given approximation with initial parameter values to match the infrared observables in [Table 3.1](#) shows chiral symmetry breaking in the vacuum. At finite temperature the quarks acquire an additional mass gap due to the lowest Matsubara frequency,

$$\omega_{n,q}^2 + k^2 + M_q^2 \geq \pi^2 T^2 + k^2 + M_q^2, \quad (3.146)$$

at vanishing chemical potential μ_q . In turn, the lowest Matsubara frequency of the meson vanished, $\omega_{0,\phi} = 0$. Hence the mesons do not acquire an additional Matsubara mass, even though they acquire thermal screening masses, the Debye masses. In summary, at finite temperature the quark fluctuations

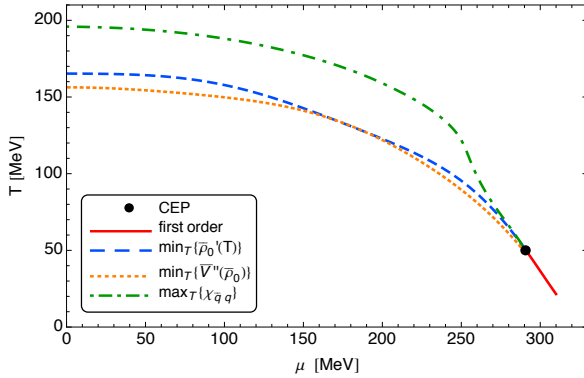


Figure 3.7.: Phase structure of QCD from the two flavour quark meson model, results from [67].

are suppressed proportional to T relative to the meson fluctuations. Consequently, spontaneous chiral symmetry breaking is melted away at sufficiently large temperature.

A similar effect holds true for finite chemical potential. This is best seen at $T = 0$, where the Dirac distribution functions in (3.141) get sharp,

$$1 - n_F(\epsilon_k^q + \mu_q) - n_F(\epsilon_k^q - \mu_q) \xrightarrow{T=0} \theta[k^2 + M_q^2 - \mu_q^2]. \quad (3.147)$$

where we have used that

$$1 - \theta(-\epsilon_k^q - \mu_q) - \theta(-\epsilon_k^q + \mu_q) = \theta[(\epsilon_k^q)^2 - \mu_q^2]. \quad (3.148)$$

In (3.147) we first of all see the Silver blaze property as well as the onset of the quark density in our model: for $\mu_q^2 < k^2 + M_q^2$ the θ -function is unity and the flow shows no μ_q -dependence. For $\mu_q^2 > M_q^2$ at $k = 0$ the quark flow has a μ_q -dependence, as only quark fluctuations with spatial momentum scales

$$k^2 \geq \mu_q^2 - M_q^2, \quad (3.149)$$

are integrated out. This leads to a finite quark density in the model. Moreover, quark fluctuations below $k^2 = \mu_q^2 - M_q^2$ drown in the Fermi sea and cannot contribute to the quark loop. Consequently, increasing μ_Q removes quark fluctuations, while the quark density in the medium rises. The latter often leads to the assumption that quarks (and baryons) get more important at larger μ . While this is certainly the fact for on-shell properties of the theory and correlation functions with non-vanishing quark number, in correlation functions with vanishing quark number the quark fluctuations are successively removed. In summary, spontaneous symmetry breaking is bound to disappear at larger chemical potential, it drowns in the Fermi sea.

These two phenomena already allow us to qualitatively draw a figure with the chiral phase structure of QCD. The chiral transition temperature $T_\chi(\mu_q)$ decreases with increasing μ and hits the μ -axis for some large μ_q . In Figure 3.7 we show the results from [67] with the running couplings (3.142). The different lines are obtained with different definitions of the crossover temperatures:

- (i) The inflection point of the chiral order parameter as a function of temperature,

$$\min_T \left\{ \frac{\partial \bar{\rho}_0}{\partial T} \right\}. \quad (3.150)$$

(ii) The minimum of the quartic meson coupling at the physical point,

$$\min_T \left\{ \frac{\partial^2 \bar{V}(\bar{\rho})}{\partial \bar{\rho}^2} \Big|_{\bar{\rho}=\bar{\rho}_0} \right\}, \quad (3.151)$$

(iii) The maximum of the chiral susceptibility,

$$\max_T \left\{ \chi_{\bar{q}q} \right\}, \quad (3.152)$$

with

$$\chi_{\bar{q}q} = \frac{\partial \langle \bar{q}q \rangle}{\partial m_q}. \quad (3.153)$$

where m_q is the current quark mass.

3.3. Fixed points

In the previous section we discussed possible strategies for the solution and the analysis of the flow equation for the 1PI effective action. Besides solving this flow equation, the topology of the renormalization group flow is another point of great interest within FRG investigations. This topology is most importantly influenced by so-called fixed points, configurations $\Gamma_k[\phi]$ which become independent of the scale k . The discussion of such configurations is rather abstract but can be reduced to configurations of couplings $\{g_j\}$ by using a specific expansion eq. (2.41) of the effective average action as discussed in detail in [Section 2.3](#). Notably, we can neglect the running of those couplings which can be eliminated with the help of field redefinitions. The latter are called redundant or inessential couplings and do not appear in physical observables. An example for a redundant coupling is the wave function renormalization.

Collecting all essential couplings in $\{g_j\}$ a renormalization group fixed point is a configuration of these couplings which does not change under a renormalization group step. A full RG step consists of three steps: the integration of the momentum shell (changing the cutoff scale), the field renormalisation and a rescaling. The first step is encoded in the Wetterich equation. The other two steps can be incorporated as described in eq. (11.25). Typically this procedure is applied within a vertex expansion but is far more general. In a vertex expansion we have schematically

$$\Gamma_k[\Phi] = \sum_{n=0}^{\infty} \Gamma_{\varphi_1 \dots \varphi_n}^{(n)} (\varphi_1 - \bar{\varphi}_1) \dots (\varphi_n - \bar{\varphi}_n), \quad \text{with} \quad \Gamma_{\varphi_1 \dots \varphi_n}^{(n)} = \left[\prod_{i=1}^n Z_{\varphi_i}^{1/2} \right] \lambda_{\varphi_1 \dots \varphi_n}^{(i)} \mathcal{T}_{\varphi_1 \dots \varphi_n}^{(i)}, \quad (3.154)$$

where the φ are the components of the super field including all fields in the theory at hand, and the product of the wave function renormalisations takes care of the field rescalings. Then, $\lambda_{\varphi_1 \dots \varphi_n}$ are the vertex couplings. The $\mathcal{T}_{\varphi_1 \dots \varphi_n}^{(i)}$ are the different tensor structures present for a given n -point function.

The couplings λ_i carry a momentum dimension, d_{λ_i} , and hence the coupling rescales under a total rescaling. Dividing λ_i by $k^{d_{\lambda_i}}$ leads to a dimensionless, scale invariant coupling (up to anomalous rescalings), to wit,

$$\hat{\lambda}_i = \frac{\lambda_i}{k^{d_{\lambda_i}}}. \quad (3.155)$$

Let us now illustrate the above definitions in our standard example, the ϕ^4 theory. Concentrating on momentum-independent couplings, that is the effective potential, we have in a vertex expansion, with $\rho = \phi^2/2$,

$$V_{\text{eff}}(\rho) = \sum_{i=1}^n \frac{\lambda_i}{n!} \rho^n, \quad (3.156)$$

with the fundamental ϕ^4 coupling $\lambda = \lambda_2$ and the mass $m^2 = \lambda_1$. The field ϕ carries the momentum dimension $d_\phi = d/2 - 1$ or $d_\rho = d - 2$. Accordingly the couplings λ_n carry the momentum dimension $d_{\lambda_n} = 4 - n(d - 2)$, their canonical momentum dimension decreases with n . The fundamental coupling, λ , has the dimension $d_\lambda = 4 - d$, while the mass has the dimension $d_{m^2} = 2$.

The scale derivative of $\hat{\lambda}_i$ governs the full cutoff running of the dimensionless couplings, it is its β -function and reads for a general theory

$$\beta_{\lambda_i} = \partial_t \hat{\lambda}_i = \left(-d_{\lambda_i} + \frac{1}{2} \sum_{j=1}^{n_i} \eta_{\varphi_j} \right) \hat{\lambda}_j + \widehat{\text{Flow}}_{\lambda_i}(\hat{\lambda}, \vec{\eta}) \quad (3.157)$$

with the anomalous dimensions $\eta_i = -k \partial_k Z_{\varphi_i} / Z_{\varphi_i}$ and

$$\widehat{\text{Flow}}_i(\{\hat{\lambda}_j\}) = \frac{1}{\prod_{i=1}^n Z_{\varphi_i}^{1/2}} \frac{1}{k^{d_{\lambda_i}}} \left[\partial_t \Gamma_{\varphi_1 \dots \varphi_n}^{(n)} \right]_{\lambda_i}, \quad (3.158)$$

is the projection of the flow on that of λ_i . The β -functions for λ_i and $\hat{\lambda}_i$ simply differ by the canonical term.

A *fixed point* in the renormalization group flow of the couplings, $\{\hat{\lambda}_j^*\}$, is defined by the vanishing of the beta functions

$$\beta_i(\vec{\lambda}^*) = k\partial_k \hat{\lambda}_i = 0, \quad \forall i. \quad (3.159)$$

Fixed points are points in theory space (the space spanned by all coupling constants) where the theory becomes scale independent. They can be either IR or UV fixed points, that is infrared or ultraviolet attractive. This depends on the flow in the vicinity of these fixed points.

The most prominent example for an UV fixed point is the Gaussian fixed point of QCD, where Gaussian means that the beta function vanishes for vanishing dimensionless couplings, $\hat{\lambda} = 0$. This fixed point signifies the asymptotic freedom of the theory and makes it valid at arbitrary high energy scales. This idea of asymptotic freedom can be generalized to the concept of asymptotic safety where the UV fixed point is situated at non-vanishing coupling constants. This scenario will be discussed in more detail in [Part III](#).

In contrast to these UV fixed points the existence of IR fixed points as well as their stability properties are important because of their relation to the phenomenon of universality, see e.g. [\[80\]](#). It is therefore important to know which theories have the same or similar fixed points in order to group them and learn more about their properties. In the following we will explain in more detail what is meant by stability properties or the similarity between fixed points. To do so we will work with dimensionless quantities throughout the rest of this section without stating it explicitly. In order to lighten the notation and since a confusion is very unlikely we will drop the hats to mark the dimensionless quantities for the rest of this section.

It is left to study the approach of the theory towards the fixed point [eq. \(3.159\)](#). To that end we introduce small perturbations around it for all couplings, and linearise the flow equations

$$\hat{\lambda}_i = \hat{\lambda}_i^* + \delta\hat{\lambda}_i, \quad \Rightarrow \quad \partial_t \hat{\lambda}_i = \underbrace{\beta_i(\vec{\lambda}^*)}_{0} + B_{ij}(\vec{\lambda}^*) \delta\hat{\lambda}_j + O(\delta\hat{\lambda}^2). \quad (3.160)$$

with the *stability matrix* B

$$B_{ij} = \frac{\partial \beta_i}{\partial \hat{\lambda}_j} \quad (3.161)$$

which describes the flow in the vicinity of the fixed point $\vec{\lambda}^*$. The stability matrix has the normalised eigenvectors \vec{e}_i with $\vec{e}_i^2 = 1$ and eigenvalues b_i ,

$$B \cdot \vec{e}_i = b_i \vec{e}_i. \quad (3.162)$$

A perturbation $\delta\hat{\lambda}$ is a linear combination of these eigenvectors with t -dependent coefficients $f_i(t)$,

$$\delta\vec{\lambda} = \sum_i f_i(t) \vec{e}_i, \quad \text{with} \quad \partial_t f_i(t) = b_i f_i(t) \quad \Rightarrow \quad f_i(t) = c_i e^{b_i t}, \quad (3.163)$$

where the vector \vec{c} is the position in coupling space at $t=0$ (if we ignore the higher order terms $O(\delta\lambda^2)$). This analysis leads us to the distinction between three different cases. Consider an eigenvector whose eigenvalue is negative. The solution of the linearized flow equation shows that its value decreases while going to larger t i.e. higher energy scales and finally approaches zero in the UV for $t \rightarrow \infty$. Since the eigenvector describes the distance from the fixed point, the corresponding direction is called UV attractive. If we lower the energy scale on the other hand the value of the eigenvector increases. Thus an UV-attractive direction is IR-repulsive. The situation obviously is opposite for positive eigenvalues. Thus

such an eigendirection is UV-repulsive and IR-attractive. The third possibility of a vanishing eigenvalue refers to a so-called marginal direction. In this case the linearization is insufficient to describe the flow and higher orders have to be considered. To summarize we distinguish between

$$\begin{aligned} b_i < 0 &\rightarrow \text{UV attractive / IR repulsive,} \\ b_i > 0 &\rightarrow \text{UV repulsive / IR attractive,} \\ b_i = 0 &\rightarrow \text{marginal.} \end{aligned} \quad (3.164)$$

These different cases can be visualized easily with some simple examples and it is again the scalar theory which allows us to do so.

As an example we consider again the ϕ^4 -theory in LPA. Then, the flow equation for the effective potential reads

$$\partial_t u_k(\bar{\rho}) = -d u_k + (d-2)\bar{\rho} u'_k + \frac{\Omega_d}{d(2\pi)^d} \frac{1}{1+u'_k + 2\bar{\rho} u''_k} \quad (3.165)$$

with the surface of the unit sphere in d dimensions, Ω_d . Furthermore, $\bar{\rho} = \phi^2/(2k^{d-2})$ and primes denote derivatives with respect to the $\bar{\rho}$. Choosing the polynomial truncation $u_k = m_k^2 \bar{\rho} + 1/2 \lambda_k \bar{\rho}^2$ the beta functions for the dimensionless mass and four-boson coupling read (we have dropped the 'hat').

$$\begin{aligned} \partial_t m_k^2 &= -2m_k^2 - A \frac{\lambda_k}{(1+m^2)^2}, \\ \partial_t \lambda_k &= (d-4)\lambda_k + B \frac{\lambda_k^2}{(1+m^2)^3} \end{aligned} \quad (3.166)$$

where the coefficients A and B evaluate to $A = 3\Omega_d/(d(2\pi)^d)$ and $B = 6A$.

Specifying to the three-dimensional case we find the Gaussian fixed point at vanishing mass and coupling as well as a non-Gaussian fixed point at $(m_*^2, \lambda_*) = (-0.08, 2.59)$. Due to the negative mass the fixed point is obviously unphysical but is suitable for our purpose of linearizing the beta function. The eigenvalues of the stability matrix evaluate to $(b_1, b_2) = (-1.84, 1.18)$. The fixed point as well as the attractive and repulsive eigendirections are depicted in the left panel of [Figure 3.8](#). A similar but more physical example is the Gross-Neveu model which was discussed in the context of the asymptotic safety scenario in [\[81\]](#). This model shows a similar structure of the beta functions. Both have a non-Gaussian fixed point with one attractive and one repulsive eigendirection.

In three dimensions the canonical dimension of the four-boson coupling is -1 . In contrast to this it becomes $+2$ in six dimensions. This is reminiscent of Newton's coupling in the theory of general relativity. Choosing the parameters A and B in [section 3.3](#) by hand to be $A = 1$ and $B = -2$ the structure of the beta functions shares some features with those of the cosmological constant and the Newton constant in the context of Quantum Einstein gravity discussed in [Part III](#). We find a non-Gaussian fixed point at $(m_*^2, \lambda_*) = (-0.33, 0.30)$ with a complex pair of critical exponents $b_{1/2} = -1 \pm 2.24 i$. This results in a spiraling approach to the fixed point as depicted in the right panel of [Figure 3.8](#). Again one can see the fixed point itself and the UV-attractive spiraling toward it due to the negative real part of the complex pair of eigenvalues.

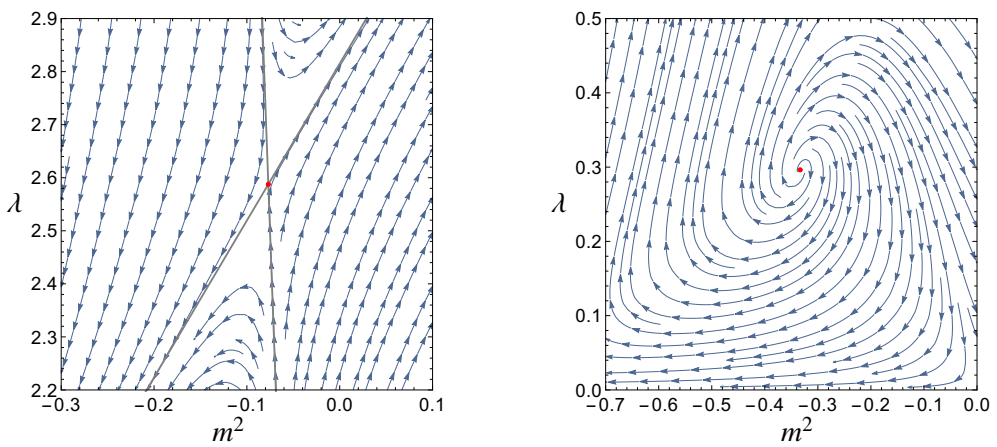


Figure 3.8.: Left panel: The RG flow close to the fixed point (red) for the beta functions section 3.3 in three dimensions.

Right panel: The RG flow close to the fixed point (red) for the beta functions section 3.3 in six dimensions with $A = 1$ and $B = -2$.

The arrows point toward UV.

Part II.

Quantum Chromodynamics from an FRG perspective

4. Introduction

The theory of strong interactions, quantum chromodynamics (QCD), has been developed on the basis of scattering experiments that showed an internal $SU(3)$ -symmetry and related charges much the same way quantumelectrodynamics (QED) shows the $U(1)$ -symmetry related to the electric charge. The corresponding gauge theory, $SU(3)$ Yang-Mills theory, is non-Abelian and hence self-interacting, i.e. the (quantized) pure gauge theory is already non-trivial, in contrast to the $U(1)$ -based QED.

5. Non-Abelian gauge theories

We start our discussion of QCD by discussing the pure gauge part or Yang-Mills part of QCD, a non-Abelian gauge theory with gauge group $SU(N_c)$ with the number of colours N_c . This discussion is also used to fix our conventions and to remind the reader of some key features of a non-Abelian gauge theory. The $SU(2)$ gauge theory has the same qualitative features as physical QCD with the $SU(3)$ gauge group, namely asymptotic freedom and confinement. As it is technically simpler we shall discuss some qualitative feature in the $SU(2)$ case. Note however, that this $SU(2)$ gauge theory should not be confused with the weak $SU(2)$ gauge theory in the Standard Model. The latter exhibits a mass gap of about 90 GeV due to the Higgs mechanism, leading to a major modification of this theory in the infrared.

As for QED, the classical action of QCD can be derived from the gauge-invariant (minimal) extension of the action of a free spin-one particle. The requirement of invariance of physics under local $SU(N_c)$ or color rotations with $\mathcal{U} \in SU(N_c)$ combined with a minimal coupling, leads us from partial to covariant derivatives

$$\partial_\mu \rightarrow D_\mu(A) = \partial_\mu - igA_\mu, \quad (5.1)$$

with $A_\mu \in su(N_c)$, the Lie algebra of $SU(N_c)$, and g is the gauge coupling. Accordingly, the gauge field is matrix valued, and hence gauge fields do not commute with each other. The latter fact leads to the pivotal qualitative difference between Abelian and non-Abelian gauge theory, the self-interaction of the gauge field. It is this property which is responsible for asymptotic freedom and in turn is also responsible for the rise of the coupling at low momenta. Note however that confinement is not simply the presence of a large coupling: the latter would still imply a Coulomb force between colour charges while confinement (in a pure gauge theory) is linked to a linear potential between colour charges. More mathematically speaking confinement can be formulated as the existence of the mass gap in pure Yang-Mills theory. This is the version of the related Millennium problem of the Clay Mathematics Institute, [82]:

Yang–Mills Existence and Mass Gap.

Prove that for any compact simple gauge group G , a non-trivial quantum Yang–Mills theory exists on \mathbb{R}^4 and has a mass gap $\Delta > 0$. Existence includes establishing axiomatic properties at least as strong as those cited in [83, 84].

More details can be obtained by the hyperlink. It is one of the open Millennium problems, and while its solution is safely beyond the scope of the present lecture course, we shall see the signatures of the mass gap directly in the present gauge fixed setting: it is reflected in the mass gap in the gluon propagator.

5.1. Basics of Yang–Mills theories

In the last chapters we have already discussed the matter sector of QCD in terms of low energy effective theories containing the Dirac action, see (5.34), (3.26). It is left to discuss the heart of QCD, the pure glue theory.

5.1.1. Classical action of Yang-Mills theory

Here we introduce the Yang-Mills action and our notation for the gauge group and gauge fields. The gauge field A_μ^a with

$$A_\mu = A_\mu^a t^a, \quad \text{with} \quad a = 1, \dots, N_c^2 - 1, \quad (5.2)$$

carries the adjoint representation of the gauge group. In (5.2) we have introduced the generators of the Lie-algebra $su(N_c)$. In the physical case $SU(3)$ the eight t^a are the Gell-Mann matrices, in $SU(2)$ the three t^a are (1/2) the Pauli matrices, $t^a = \tau^a/2$ with τ^a in (3.117).

The generators t^a satisfy the commutation relation

$$[t^a, t^b] = i f^{abc} t^c, \quad (5.3)$$

with f^{abc} being the structure constants of the Lie algebra $su(N_c)$. The normalisation is chosen as

$$\text{tr}_f(t^a t^b) = \frac{1}{2} \delta^{ab}, \quad (5.4)$$

where the trace is in the fundamental representation. In the adjoint representation the generators read $(t_{adj}^c)^{ab} = -i f^{abc}$. Inserting this representation into the general covariant derivative (5.1), it reads

$$D_\mu^{ab}(A) = \partial_\mu \delta^{ab} - g f^{abc} A_\mu^c, \quad (5.5)$$

the covariant derivative in the adjoint representation. Turning now to gauge transformations $\mathcal{U} = e^{i\omega}$, with $\omega \in su(N)$, we demand that the covariant derivative (5.1) transforms in a covariant manner

$$D_\mu(A) \rightarrow D_\mu(A^\mathcal{U}) = \mathcal{U} D_\mu(A) \mathcal{U}^\dagger. \quad (5.6)$$

We conclude immediately

$$A_\mu \rightarrow A_\mu^\mathcal{U} = \frac{i}{g} \mathcal{U} (D_\mu \mathcal{U}^\dagger) = \mathcal{U} A_\mu \mathcal{U}^\dagger + \frac{i}{g} \mathcal{U} (\partial_\mu \mathcal{U}^\dagger). \quad (5.7)$$

The field strength tensor is introduced as the curvature tensor corresponding to the covariant derivative

$$F_{\mu\nu} = \frac{i}{g} [D_\mu, D_\nu] = F_{\mu\nu}^a t^a, \quad \text{with} \quad F_{\mu\nu}^a = \partial_\mu A_\nu^a - \partial_\nu A_\mu^a + g f^{abc} A_\mu^b A_\nu^c. \quad (5.8)$$

Defined as the commutator of covariant operators, the field strength tensor $F_{\mu\nu}$ also transforms covariantly under gauge transformations

$$F_{\mu\nu}(A^\mathcal{U}) = \frac{i}{g} [D_\mu(A^\mathcal{U}), D_\nu(A^\mathcal{U})] = \mathcal{U} F_{\mu\nu}(A) \mathcal{U}^\dagger. \quad (5.9)$$

Therefore we can introduce the gauge invariant Yang-Mills action

$$S_{\text{YM}}[A] = \frac{1}{2} \int_x \text{tr} F_{\mu\nu} F_{\mu\nu} = \frac{1}{4} \int_x F_{\mu\nu}^a F_{\mu\nu}^a, \quad (5.10)$$

which is trivially gauge invariant due to the cyclic nature of the trace in (5.10). Clearly, the action (5.10) with the field strength (G.43) is a self-interacting theory with coupling constant g . It has a quadratic kinetic term and three-gluon and four-gluon vertices. This is illustrated diagrammatically in Fig. 5.1.

$S_{\text{YM}}[A] \propto$

Figure 5.1.: Diagrammatical form of the Yang-Mills action.

The full Feynman rules of QCD in the general covariant gauge are summarized in [Figure F.1](#) in [Appendix F.1](#). As in QED we can identify color-electric and color-magnetic fields as the components in the field strength tensor,

$$\begin{aligned} E_i^a &= F_{0i}^a \\ B_i^a &= \frac{1}{2} \epsilon_{ijk} F_{jk}^a. \end{aligned} \quad (5.11)$$

In contrast to QED these color-electric and magnetic fields are no observables, they change under gauge transformations. Only $\text{tr } \vec{E}^2$, $\text{tr } \vec{B}^2$, and $\text{tr } \vec{E}\vec{B}$ are observables. The latter is related to anomalous chiral symmetry breaking.

5.2. Quantization and gauge fixing

Having introduced the classical action [\(5.10\)](#) we can now turn to the issue of quantization and, closely related, gauge fixing. For now we will turn back to a path integral picture, but stress again that this is not necessary. Naïvely, the generating functional of pure YM-theory reads

$$Z[J] = \int dA \exp \left(S_{\text{YM}}[A] + \int_x J_\mu^a A_\mu^a \right). \quad (5.12)$$

However, the fundamental problem with [\(5.12\)](#) is the integration over infinite degenerate configurations due to the gauge invariance, c.f. [\(5.9\)](#). To be more precise, the equivalent gauge configurations are physically equivalent since they leave the action invariant, and are called gauge orbit $\{A^{\mathcal{U}}\}$. In terms of classical correlation functions this is reflected by the inversion problem of the two point function $S_{\text{YM}}^{(2)}(p)$, that does not exist due to the transversality of the two-point function

$$p_\mu S_{\text{YM},\mu\nu}^{(2)}(p) = p_\mu (p^2 \delta_{\mu\nu} - p_\mu p_\nu) = 0. \quad (5.13)$$

Hence, we cannot define even a classical propagator, leave aside a full propagator G_A , the latter been the pivotal ingredient for a FRG approach to gauge theories. In order to remedy this problem we remove this redundancy via a gauge fixing condition

$$\mathcal{F}[A_{\text{gf}}] = 0, \quad (5.14)$$

which corresponds to choosing one, up to potential Gribov copies, representative per gauge orbit. The occurrence of Gribov copies and their treatment will be discussed in [??](#). We will leave this issue aside

for now and assume the existence of a unique solution of the gauge fixing condition for each orbit. The gauge of chief interest for the present work is the covariant or Lorenz gauge,

$$\partial_\mu A_\mu = 0. \quad (5.15)$$

The covariant gauge has the technical advantage that it does not single out a space-time direction. This property reduces the possible tensor structure of correlation functions and hence simplifies computations. For a general gauge condition (5.14) the path integral measure dA in (5.12) can be split into an integration over physically inequivalent configurations A_{gf} and the gauge transformations \mathcal{U}

$$dA = J dA_{\text{gf}} d\mathcal{U}, \quad (5.16)$$

where J denotes the Jacobian of the transformation and $d\mathcal{U}$ is the Haar measure of the gauge group. Then, the integration over the gauge group factorises, since the action is gauge invariant, and hence it can be dropped. The computation of the coordinates transformation, including the Jacobian J in (5.16), is done using the standard Faddeev-Popov quantisation. In order to achieve this we insert a one into the path integral

$$1 = \Delta_{\mathcal{F}}[A] \int d\mathcal{U} \delta(\mathcal{F}[A^{\mathcal{U}}]) \quad \Leftrightarrow \quad \Delta_{\mathcal{F}}[A] = \left(\int d\mathcal{U} \delta(\mathcal{F}[A^{\mathcal{U}}]) \right)^{-1}. \quad (5.17)$$

We notice that $\Delta_{\mathcal{F}}[A]$ is gauge invariant due to the property $d(\mathcal{U}\mathcal{V}) = d\mathcal{U}$ with $\mathcal{V} \in SU(N_c)$ of the Haar measure: the Haar measure is invariant under multiplication with a gauge group element. In order to illustrate the effect of inserting (5.17) into path integral let us consider a general observable O , which is necessarily local and gauge invariant,

$$\langle O \rangle = \frac{\int dA O[A] e^{-S_{\text{YM}}[A]}}{\int dA e^{-S_{\text{YM}}[A]}} = \frac{\int dA d\mathcal{U} \delta(\mathcal{F}[A^{\mathcal{U}}]) \Delta_{\mathcal{F}}[A] O[A] e^{-S_{\text{YM}}[A]}}{\int dA d\mathcal{U} \delta(\mathcal{F}[A^{\mathcal{U}}]) \Delta_{\mathcal{F}}[A] e^{-S_{\text{YM}}[A]}}, \quad (5.18)$$

where all terms are gauge invariant except for the δ -distribution. Hence we can absorb the \mathcal{U} dependence via $A \rightarrow A^{\mathcal{U}^\dagger}$ and as a result the infinite integral over the Haar measure decouples in the numerator and denominator and the resulting expression is

$$\langle O \rangle = \frac{\int dA \delta(\mathcal{F}[A]) \Delta_{\mathcal{F}}[A] O[A] e^{-S_{\text{YM}}[A]}}{\int dA \delta(\mathcal{F}[A]) \Delta_{\mathcal{F}}[A] e^{-S_{\text{YM}}[A]}}. \quad (5.19)$$

In (5.19) the gauge redundancy is eliminated, and $dA_{\text{gf}} = dA \delta(\mathcal{F}[A])$. This leaves us with the computation of the Jacobian $J = \Delta_{\mathcal{F}}[A]$, which we can obtain from a suitable coordinate transformation

$$\delta(\mathcal{F}[A^{\mathcal{U}}]) = \frac{\delta(\omega - \omega_1)}{|\det \frac{\delta \mathcal{F}}{\delta \omega}|}, \quad (5.20)$$

where $\mathcal{U} = e^{i\omega}$. The algebra element $\omega_1[A]$ is defined by

$$\mathcal{F}[A_{\text{gf}} = A^{\mathcal{U}(\omega_1)}] = 0, \quad (5.21)$$

for this choice that gauge fixing condition is satisfied. We emphasise again that typically the solution of the gauge fixing condition is not unique and several Gribov copies exist. This is discuss in Appendix F.2 within a toy example. Using the definition (5.17) the resulting expression reads

$$\Delta_{\mathcal{F}}[A] = |\det \mathcal{M}_{\mathcal{F}}[A_{\text{gf}}]| \quad \text{with} \quad \mathcal{M}_{\mathcal{F}}[A] = \left. \frac{\delta \mathcal{F}}{\delta \omega} \right|_{\omega=0}. \quad (5.22)$$

The inverse Jacobian $\det \mathcal{M}_{\mathcal{F}}$ is called the Faddeev-Popov determinant and it can be computed by considering infinitesimal gauge transformations. We are left with the specification of the gauge fixing function (5.14). Here we restrict ourselves to linear gauges,

$$\mathcal{F}[A] = l_\mu A_\mu, \quad (5.23)$$

with l_μ can be a differential operator or a space-time dependent or constant vector or a combination thereof. Common choice are

$$\text{Covariant gauge : } \mathcal{F}[A] = \partial_\mu A_\mu \quad (5.24a)$$

$$\text{Coulomb gauge : } \mathcal{F}[A] = \partial_i A_i \quad (5.24b)$$

$$\text{Fock-Schwinger gauge : } \mathcal{F}[A] = x_\mu A_\mu \quad (5.24c)$$

$$\text{Axial gauge : } \mathcal{F}[A] = n_\mu A_\mu \quad (5.24d)$$

$$\text{Polyakov gauge : } \mathcal{F}[A] : A_0(x) = A_0^c(\vec{x}), \quad (5.24e)$$

where A_0^c is in the Cartan subalgebra. This gauge can be formulated in a combination of gauge fixing conditions, see e.g. [85]. The general covariant gauge 5.24a and the Fock-Schwinger gauge 5.24c have the technical advantage that they do not single out a space-time direction and therefore reduces the number of possible tensor structures of correlation functions.

In turn, Coulomb gauge 5.24b, The the axial gauge 5.24d and the Polyakov gauge 5.24e single out specific frames. For Hamiltonian formulations this singles out the Coulomb gauge as well as temporal or Weyl gauge, 5.24d with $n_\mu = \delta_{\mu 0}$, as technically convenient gauges. Note also, that most of these gauges are incomplete, residual gauge transformations are not fixed. Whether or not a gauge fixing is sufficiently complete for our purposes is decided with whether or not the propagator, $1/S_{\text{YM}}^{(2)}$ and more importantly G_A exists.

Seemingly, the Weyl gauge is also useful at finite temperature, density and external magnetic fields, where a rest frame is already singled out. However, this gauge cannot be fixed with periodic boundary conditions, the gauge fields are only periodic in $t \rightarrow t + \beta$ up to gauge transformations, the transition functions. Note that otherwise the Polyakov loop, the Wilson loop in time directions, would be trivial. Trying to make the A_0 as simple as possible while insisting on periodic fields leaves us to the Polyakov gauge.

Finally, the issue of Gribov copies is absent in the axial gauge 5.24d and Polyakov gauge 5.24e and is addressed in more detail in ??.

We are now in the position to compute the Faddeev-Popov determinant for the case of general covariant gauges 5.24a. For its computation we consider an infinitesimal gauge transformation $\mathcal{U} = 1 + i g \omega$ where we have rescaled the transformation with the strong coupling g for convenience. Such a rescaling gives global factors of powers of $1/g$ that drop out in normalised expectation values. Then, the infinitesimal variation of the linear gauge (5.23) with $l_\mu A_\mu = 0$, e.g. 5.24, follows as

$$\mathcal{F}[A^{\mathcal{U}}] = l_\mu A_\mu^{\mathcal{U}} = l_\mu A_\mu - l_\mu D_\mu \omega + O(\omega^2) \stackrel{!}{=} 0. \quad (5.25)$$

This gives us the Faddeev-Popov matrix

$$\mathcal{M}_{\mathcal{F}}[A] = -\frac{\delta l_\mu D_\mu \omega}{\delta \omega} = -l_\mu D_\mu \frac{\delta \omega}{\delta \omega} = -l_\mu D_\mu \mathbb{1}. \quad (5.26)$$

Its determinant is $\Delta_{\mathcal{F}}[A]$ in the given gauge, here we show it explicitly for the covariant gauge, 5.24a, with $l_\mu = \partial_\mu$. We assume that $-\partial^\mu D_\mu$ is a positive definite operator and we arrive at

$$\Delta_{\mathcal{F}}[A] = \det \mathcal{M}[A] = \det(-\partial_\mu D_\mu). \quad (5.27)$$

A useful observation is that determinants can be represented by a Gaussian integral. In regular space such a Gaussian integral reads

$$\int_x e^{-\frac{1}{2}x^T M x} = \frac{(2\pi)^n}{\sqrt{\det M}}. \quad (5.28)$$

We want to use this relation to replace the Faddeev-Popov determinant (5.27) in the Lagrangian. It turns out that the usual form does not give a useful action or Lagrangian. However, we can instead use two anti-commuting Grassmann fields c, \bar{c} , to wit

$$\det \mathcal{M}_{\mathcal{F}}[A] = \int dc d\bar{c} \exp \left\{ \int_{x,y} \bar{c}^a(x) \mathcal{M}_{\mathcal{F}}^{ab}(x,y) c^b(y) \right\}. \quad (5.29)$$

Finally we slightly modify the gauge by introducing a Gaussian average over the gauges

$$\delta[\mathcal{F}[A^U]] \rightarrow \int dC \delta[\mathcal{F}[A^U - C]] \exp \left\{ -\frac{1}{2\xi} \int_x C^a C^a \right\}. \quad (5.30)$$

In summary, we arrive at the gauge fixed generating functional for our Yang-Mills theory

$$Z[J_A, J_c, \bar{J}_c] = \int dA dc d\bar{c} e^{-S_A[A, c, \bar{c}] + \int_x (J_A \cdot A + \bar{J}_c \cdot c - \bar{c} \cdot J_c)}, \quad (5.31a)$$

with the gauge fixed action including a general gauge fixing term and the Faddeev-Popov ghosts c^a is

$$S_A[A, c, \bar{c}] = \frac{1}{4} \int_x F_{\mu\nu}^a F_{\mu\nu}^a + \frac{1}{2\xi} \int_x (\mathcal{F}[A]^a)^2 - \int_x \bar{c}^a \partial_\mu D_\mu^{ab} c^b, \quad (5.31b)$$

and the original gauge is achieved for $\xi = 0$.

$$S_A[A, c, \bar{c}] = \frac{1}{4} \int_x F_{\mu\nu}^a F_{\mu\nu}^a + \frac{1}{2\xi} \int_x (\partial_\mu A_\mu^a)^2 - \int_x \bar{c}^a \partial_\mu D_\mu^{ab} c^b, \quad (5.32)$$

Note that the ghost action implies a negative dispersion for the ghost, related to the determinant of the positive operator $\mathcal{M}_{\mathcal{F}} = -\partial_\mu D_\mu$. However, this is a matter of convention, we might as well use a positive dispersion, the minus sign drops out for all correlation functions which do not involve ghosts, and only those are related to scattering amplitudes. The source term with all indices reads

$$\int_x (J_A \cdot A + \bar{J}_c \cdot c - \bar{c} \cdot J_c) \equiv \int_x (J_{A,\mu}^a A_\mu^a + \bar{J}_c^a c^a - \bar{c}^a J_c^a). \quad (5.33)$$

The Feynman rules derived from 5.31b are summarized in Appendix F.1.

5.3. QCD

In Part I we have already discussed the matter part of QCD in terms of low energy effective field theories, see (5.34), (3.26). In QCD the simply change plain derivative to the covariant one in the fundamental representation and arrive at

$$S_{\text{Dirac}}[q, \bar{q}, A] = \int_x \bar{q} \left(iD^\mu + m_q + \gamma_0 \mu_q \right) q, \quad (5.34)$$

In (5.34), the fermions carry a Dirac index defining the 4-component spinor, gauge group indices in the fundamental representation of $SU(3)$, as well flavor indices, for an explicit form see (3.26). We will suppress the flavor indices as long as concentrating on QCD, as well as neglecting the doublet nature of the matter fields in the Standard Model. The Dirac operator \not{D} is diagonal in the flavor space as is the chemical potential term. The mass term depends on the current quark masses related to spontaneous symmetry breaking of the Higgs sector of the Standard Model. The up and down current quark masses are of the order $2 - 5$ MeV whereas the current quark mass of the strange quark is of the order 10^2 MeV. The other quark masses are of order $1 - 200$ GeV. In low energy QCD this has to be compared with the scale of strong chiral symmetry breaking $\Delta m \approx 300$ MeV. This mass scales are summarized in Table 5.1.

Generation	first	second	third	Charge
Mass [MeV]	1.5-4	1150-1350	170×10^3	
Quark	u	c	t	$\frac{2}{3}$
Quark	d	s	b	$-\frac{1}{3}$
Mass [MeV]	4-8	80-130	$(4.1-4.4) \times 10^3$	

Table 5.1.: Quark masses and charges. The scale of strong chiral symmetry breaking is $\Delta m \approx 300$ MeV as is Λ_{QCD} . This entails that only 2 + 1 flavours have to be considered for most applications to the phase diagram of QCD.

Evidently, for most applications of the QCD phase diagram we only have to consider the three lightest quark flavors, that is up, down and strange quark, to be dynamical. The current quark masses of up and down quarks are two order of magnitude smaller than all QCD infrared scales related to Λ_{QCD} . Hence, the up and down quarks can be considered to be massless. This leads to the important observation that the physical masses of neutrons and protons — and hence the masses of the world around us — comes about from strong chiral symmetry breaking and has nothing to do with the Higgs sector.

In turn, the mass of the strange quark is of the order of Λ_{QCD} and has to be considered heavy for application in low energy QCD. The three heavier flavors, charm, bottom and top, are essentially static they do not contribute to the QCD dynamics relevant for its phase structure even though in particular the c-quark properties and bound states are much influenced by the infrared dynamics of QCD. In summary we will consider the $N_f = 2$ and $N_f = 2 + 1$ flavor cases for the phase structure of QCD, while for LHC physics all flavors are relevant.

Again in analogy to the Yang-Mills action we describe the quantised theory using its generating functional. The full generating functional of QCD is the straightforward extension of the Yang-Mills version in 5.31a. The quark fields are Grassmann fields because of their fermionic nature, and we are led to the generating functional

$$Z[J] = \int d\Phi e^{-S_{\text{QCD}}[\Phi] + \int_x J \cdot \Phi}, \quad (5.35)$$

with the super-field Φ , and super-current J ,

$$\begin{aligned} \Phi &= (A, c, \bar{c}, \psi, \bar{\psi}), & J &= (J_A, J_c, J_{\bar{c}}, J_q, J_{\bar{q}}), \\ d\Phi &= \int dA dc d\bar{c} dq d\bar{q}, & J \cdot \Phi &= J_A \cdot A + J_c \cdot c - \bar{c} \cdot J_{\bar{c}} + J_q \cdot q - \bar{q} \cdot J_{\bar{q}}, \end{aligned} \quad (5.36)$$

where the source term with all indices reads

$$\int_x J \cdot \Phi \equiv \int_x (J_{A,\mu}^a A_\mu^a + \bar{J}_c^a c^a - \bar{c}^a J_c^a + J_{q,\eta}^{B,i} q_\eta^{B,i} - \bar{q}_{\bar{\eta}}^{B,i} J_{\bar{q},\bar{\eta}}^{B,i}), \quad (5.37)$$

with Lorentz index $\mu = 0, 1, 2, 3$, flavour index $i = 1, \dots, N_f$, adjoint and fundamental gauge group indices $a = 1, \dots, N_c^2 - 1$ and $B = 1, \dots, N_c$ respectively, and Dirac indices $\eta, \bar{\eta} = 1, \dots, 4$. The gauge-fixed action S_{QCD} in (5.35) in the Landau gauge is given by

$$S_{\text{QCD}}[\Phi] = \frac{1}{4} \int_x F_{\mu\nu}^a F_{\mu\nu}^a + \frac{1}{2\xi} \int_x (\partial_\mu A_\mu^a)^2 - \int_x \bar{c}^a \partial_\mu D_\mu^{ab} c^b + \int_x \bar{q} (iD^\mu + m_q - \gamma_0 \mu_q) q. \quad (5.38)$$

The action in (5.38) is illustrated diagrammatically as For physical observables the gauge dependence



Figure 5.2.: Diagrammatical form of the QCD action.

entering through the last two graphs in the first line, the ghost terms, is cancelled by the hidden gauge fixing dependence of the inverse gluon propagator. The Feynman rules are summarised in Appendix F.1.

5.4. Flow equations for QCD

We are now in the position to derive the flow equation for the effective action in QCD. The consequences of such an approach with a momentum cutoff in a gauge theory is then discussed in the following chapters, Section 5.7 and ??.

5.4.1. Flow equation for the effective action

To begin with, the generating functional (5.35), or more precisely the set of fields Φ , (5.36), in the gauge-fixed setting and the classical gauge-fixed action, (5.38), allows us to derive the flow equation for QCD along the same lines as done for generic theories in Part I. We define the infrared cutoff term $\Delta S_k[\Phi]$ with

$$\Delta S_k[\Phi] = \frac{1}{2} \Phi_a R_k^{ab} \Phi_b, \quad (5.39a)$$

and the regulator matrix

$$(R_k^{ab}) = \begin{pmatrix} R_A & 0 & 0 & 0 & 0 \\ 0 & 0 & -R_c & 0 & 0 \\ 0 & R_c & 0 & 0 & 0 \\ 0 & 0 & 0 & 0 & -R_q \\ 0 & 0 & 0 & R_q & 0 \end{pmatrix}. \quad (5.39b)$$

With the generic structure in momentum space

$$R_\varphi(p) = \mathcal{P}_\varphi(p) r_\varphi(x), \quad \text{with} \quad x = \frac{p^2}{k^2}, \quad x = \frac{\vec{p}^2}{k^2}. \quad (5.39c)$$

Here the φ are entries in the super field Φ with $\varphi_i = A_\mu, c, q$. The parameterisation 5.39c depends on generic dimensionless shape functions r_{φ_i} , see e.g. (2.6). The prefactors \mathcal{P}_φ carry the Lorentz, internal and the dispersion of the respective field. For its choice we first analyse the general structure of the classical two-point functions $S_{\varphi_i \varphi_j}^{(2)}(p)$ in momentum space. For the present analysis we restrict ourselves

to a general covariant gauge 5.24a, the generalisation is straightforward. We drop the δ -function of momentum conservation and get at vanishing fields and $T, \mu = 0$,

$$S_{AA,\mu\nu}^{(2),ab}(p) = \left[p^2 \delta_{\mu\nu} - \left(1 - \frac{1}{\xi} \right) p_\mu p_\nu \right] \delta^{ab}, \quad S_{\bar{c}c}^{(2),ab}(p) = p^2 \delta^{ab}, \quad S_{\bar{q}q}^{(2),AB}(p) = i \not{p} + m_q. \quad (5.40)$$

Equation (5.40) already comprises the general tensor structure of the two-point functions $\Gamma_k^{(2)}$ of QCD in a covariant gauge: for the gauge field we have transversal and longitudinal components. The respective transversal, Π^\perp , and longitudinal, Π^\parallel , projection operators read

$$\Pi_{\mu\nu}^\perp(p) = \delta_{\mu\nu} - \frac{p_\mu p_\nu}{p^2}, \quad \Pi_{\mu\nu}^\parallel(p) = \frac{p_\mu p_\nu}{p^2} = \mathbb{1} - \Pi_{\mu\nu}^\perp(p). \quad (5.41)$$

In colour space the only possible tensor at vanishing fields is δ^{ab} in the adjoint and δ^{AB} in the fundamental representation. This allows us to parameterise the full two-point functions at vanishing fields,

$$\begin{aligned} \Gamma_{AA,\mu\nu}^{(2),ab}(p) &= p^2 \left(Z_A^\perp(p) \Pi_{\mu\nu}^\perp(p) + Z_A^\parallel(p) \Pi_{\mu\nu}^\parallel(p) \right) \delta^{ab}, \\ \Gamma_{\bar{c}c}^{(2),ab}(p) &= p^2 Z_c(p) \delta^{ab}, \\ \Gamma_{\bar{q}q}^{(2),AB}(p) &= Z_q(p) (i \not{p} + M_q(p)) \delta^{AB}, \end{aligned} \quad (5.42)$$

where we have dropped the subscript k . It is understood that all quantities are k -dependent. With the classical wave function renormalisations $Z_A^\perp, Z_c, Z_q = 1$ and $Z_A^\parallel = 1/\xi$. Within a gauge invariant regularisation scheme only the transversal wave function renormalisation Z_A^\perp receives quantum corrections and the Slavnov-Taylor Identities (STIs) guarantee $Z_A^\parallel = 1/\xi$. Within the present FRG framework the regularisation breaks gauge invariance, and the *modified* STIs (mSTIs) guarantee $Z_A^\parallel \rightarrow 1/\xi$ only in the limit $k \rightarrow 0$. This is discussed below in Section 5.7.

With (5.42) a generic choice for the dispersions for the regulators in 5.39c is

$$\begin{aligned} \mathcal{P}_{A,\mu\nu}^{ab}(p) &= p^2 \left[\bar{Z}_A^\perp(p) \Pi_{\mu\nu}^\perp(p) + \bar{Z}_A^\parallel(p) \Pi_{\mu\nu}^\parallel(p) \right] \delta^{ab}, \\ \mathcal{P}_c^{ab}(p) &= \bar{Z}_c(p) p^2 \delta^{ab}, \\ \mathcal{P}_q^{AB}(p) &= \bar{Z}_q(p) \not{p} \delta^{AB}. \end{aligned} \quad (5.43)$$

The prefactors $\bar{Z}_\varphi(p)$ are typically chosen such, that they leads to RG-adapted regulators as well as facilitating the numerical computation. For dispersions with a finite mass gap a common choice is

$$\bar{Z}_\varphi(p) = Z_\varphi(p) - \frac{(p^2 Z_\varphi)(p \rightarrow 0)}{p^2}, \quad (5.44)$$

where we have assumed a bosonic classical dispersion $p^2 + m_\varphi^2$. The scale dependent effective action $\Gamma_k[\Phi]$ is now defined similarly to the general Fermi-Bose mixtures in (2.223) as the modified Legendre transform of the Schwinger functional $\mathcal{W}[J] = \ln Z[J]$ with (5.35), and the cutoff term 5.39a,

$$\Gamma_k[\Phi] = \int_x J \cdot \Phi - \mathcal{W}[J] - \Delta S_k[\Phi]. \quad (5.45)$$

This concludes our FRG setup in QCD. Using the infrared cutoff function 5.39a we derive straightforwardly the Wetterich equation for QCD,

$$\partial_t \Gamma[\Phi] = \frac{1}{2} \text{Tr} G_k[\Phi] \partial_t R_k = \frac{1}{2} \text{Tr} G_{AA}[\Phi] \partial_t R_A - \text{Tr} G_{\bar{c}c} \partial_t R_c - \text{Tr} G_{\bar{q}q} \partial_t R_q, \quad (5.46)$$

$$\partial_t \Gamma_k[\Phi] = \frac{1}{2} \left(\text{orange loop} - \text{dotted loop} - \text{solid loop} + \frac{1}{2} \text{dashed loop} \right)$$

Figure 5.3.: Functional Renormalisation group equation for QCD with dynamical hadronisation, see [Section 6.2](#). The first two loops, gluon and ghost loop, comprise the pure glue system. The third -quark- loop comprises the matter fluctuations. The first three loops have to be present if a full infrared regularisation of the system is required. The last loop is a hadronic one, which can be introduced by means of dynamical hadronisation. It is not present in [\(5.46\)](#), and may be dropped.

its diagrammatic form depicted in [Figure 5.3](#).

As in the other examples studied before we now have to initialise the theory at a large momentum scale $\Lambda/\Lambda_{\text{QCD}} \gg 1$ deep in the perturbative regime. Thanks to asymptotic freedom this provides us with an excellent grip on the initial effective action

$$\Gamma_\Lambda[\Phi] = S_{\text{UV}}[\Phi], \quad (5.47)$$

where S_{UV} comprises all UV-relevant terms. This certainly includes all terms in the classical action [\(5.38\)](#). However, we shall see that these terms scale differently to each other beyond one loop. Moreover (broken) gauge symmetry leads to a mass term in the UV action Γ_Λ ,

$$S_{\text{UV}} \propto \frac{1}{2} m_{A,\Lambda}^2 \int_x A_\mu^a A_\mu^a, \quad \text{with} \quad m_{A,\Lambda}^2 \propto \Lambda^2. \quad (5.48)$$

We emphasise that [\(5.48\)](#) does not imply that we have a massive gauge theory. The physical theory is defined at $k = 0$, where we have

$$m_{A,k=0}^{\parallel 2} = [p^2 Z_A^\parallel(p)]_{p^2=0} = 0, \quad (5.49)$$

the longitudinal mass vanishes as necessary in QCD. The fate of the transversal mass parameter, $m_{A,k=0}^{\perp 2}$, is directly related to the *physical* mass gap in QCD discussed in the beginning of [Chapter 5](#), and hence to confinement. We shall see that

$$m_{A,k=0}^{\parallel 2} = [p^2 Z_A^\perp(p)]_{p^2=0} > 0, \quad (5.50)$$

the transversal gluon propagator has a mass gap. The property [\(5.50\)](#) has profound consequences, for example it is a necessary condition for confinement at low temperatures [\[86, 87, 88\]](#). Its generation in Yang-Mills theory and in QCD is not fully settled yet: while we have come far in the past two decades in terms of both, conceptual and technical/numerical advances, it is fair to say that a fully satisfactory consistent computation of the mass gap has not been achieved yet.

5.4.2. Flow equation for correlation functions

Vertex expansion in QCD

The flow equation for the effective action for QCD cannot be solved. In QCD we resort to a systematic vertex expansion, [Section 2.3.3](#), in quantitative approximations this vertex expansion is enhanced by full

effective potentials of multi-quark interactions at low energies in the form of mesonic potentials. For this vertex expansion we introduce a general parameterisation of the n -point functions $\Gamma_k^{(n)}$ with an expansion in a complete set of tensor structures $\mathcal{T}_{\varphi_1 \dots \varphi_n}^{(i)}$ with $i = 1, \dots, i_{\max}$,

$$\Gamma_{\varphi_1 \dots \varphi_n}^{(i)} = \sum_i \lambda_{\varphi_1 \dots \varphi_n}^{(i)} \mathcal{T}_{\varphi_1 \dots \varphi_n}^{(i)}, \quad (5.51)$$

The coefficients or *dressing functions* $\lambda_{\varphi_1 \dots \varphi_n}^{(i)}$ comprise the dynamics of the theory. More specifically, the $\lambda_{\varphi_1 \dots \varphi_2}^{(i)}$ carry the dispersion and masses of the theory, the respective tensor structures of the two-point functions in QCD are

$$\mathcal{T}_{AA}^{(1)} = p^2 \Pi_{\mu\nu}^\perp(p) \delta^{ab}, \quad \mathcal{T}_{\bar{c}c}^{(1)} = p^2 \delta_{\mu\nu} \delta^{ab}, \quad \mathcal{T}_{\bar{q}q}^{(1)} = \not{p} \mathbb{1}, \quad \mathcal{T}_{\bar{q}q}^{(2)} = \mathbb{1}. \quad (5.52)$$

Equation (5.52) is a complete basis of the tensor structures of the two-point function $\Gamma^{(2)}$ in QCD: The dressing functions $\lambda_{\varphi_1 \varphi_2}$ are

$$Z_A(p) = \lambda_{AA}^{(1)}(p), \quad Z_c(p) = \lambda_{\bar{c}c}^{(1)}(p), \quad Z_q(p) = \lambda_{\bar{q}q}^{(1)}(p), \quad M_q(p) = \frac{\lambda_{\bar{q}q}^{(2)}(p)}{\lambda_{\bar{q}q}^{(1)}(p)}, \quad (5.53)$$

the wave function renormalisations Z_φ of all fields and the quark mass function M_q . The classical tensor structures of the three- and four-point vertices, the primitively divergent vertices in QCD, allowing for definitions of the strong running coupling

$$\alpha_s = \frac{g^2}{4\pi}. \quad (5.54)$$

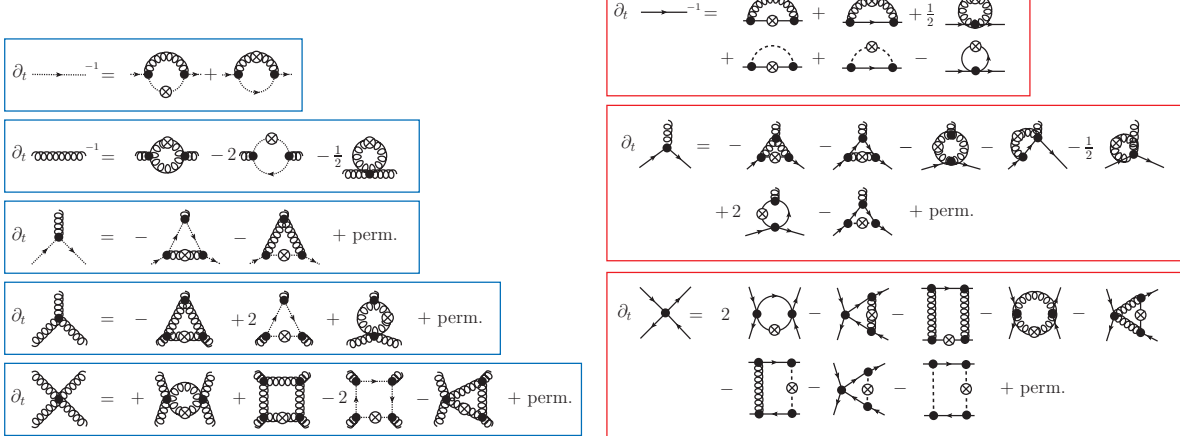
We access the vertices at the symmetric point \bar{p} , and consider the three combinations in the pure glue sector

$$\begin{aligned} \alpha_{\bar{c}cA} &= \frac{1}{4\pi} \frac{\left[\lambda_{\bar{c}cA}^{(1)}(\bar{p}) \right]^2}{Z_A(\bar{p}) Z_c^2(\bar{p})}, \\ \alpha_{A^3} &= \frac{1}{4\pi} \frac{\left[\lambda_{A^3}^{(1)}(\bar{p}) \right]^2}{Z_A^3(\bar{p})}, \\ \alpha_{A^4} &= \frac{1}{4\pi} \frac{\lambda_{A^4}^{(1)}(\bar{p})}{Z_A^2(\bar{p})}, \end{aligned} \quad (5.55)$$

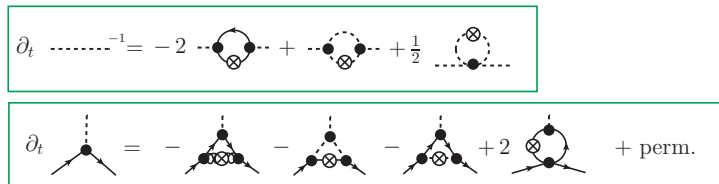
and the α_s from the quark-gluon vertex,

$$\alpha_{\bar{q}qA} = \frac{1}{4\pi} \frac{\left[\lambda_{\bar{q}qA}^{(1)}(\bar{p}) \right]^2}{Z_A(\bar{p}) Z_q^2(\bar{p})}, \quad (5.56)$$

As the strong coupling is marginal in four dimensions, these running couplings are two-loop universal: their RG- β -functions agree up to two-loop. Note that this universality neither entails universality of $\partial_t \alpha_{s,i}$ beyond one loop with $i = \bar{c}cA, A^3, A^4, \bar{q}qA$, nor does it imply the same momentum-dependence beyond one loop. This is important if it comes to quantitative approximations and will be discussed later.



(a) Flow of pure glue correlations, matter loops and some diagrams with higher order vertices are dropped (b) Flow of matter-glue correlations, some diagrams with higher order vertices are dropped



(c) Flow of hadronic correlations, some diagrams with higher order vertices are dropped

Figure 5.4.: Flows for two-, three-, and four-point functions in QCD including dynamical hadronisation.
In Figure 5.4(a) we dropped the closed matter loops.

Flow equation for two-, three-, and four point functions

We now discuss the flow equations for correlation functions $\Gamma_k^{(n)}$ with $n = 2, 3, 4$, the primitively divergent correlation functions in QCD. This is the minimal set of correlation functions to be considered for a minimally self-consistent solution in QCD: These correlation functions are present in the flow of the propagators, and hence are important for the discussion of the mass gap mentioned above. Here we concentrate on pure Yang-Mills theory as an illustrative, yet already important example.

The flows for the QCD correlation functions are derived by taking field derivatives at vanishing fields. The flows of the two-, three-, and four-point functions is depicted in [Figure 5.4](#). The flow equations in [Figure 5.4](#) are exact up to the omission of some diagrams with higher order vertices dropped for the sake of simplicity. For example, in the flow for the gluon propagator, the ghost tadpole is missing. We have also dropped the closed matter loops in flow of the pure glue correlations in [Figure 5.4\(a\)](#). Accordingly, as it stands, [Figure 5.4\(a\)](#) describes the pure Yang-Mills flow, which is discussed below. Also, for the considerations in the present chapter the flow of the hadronic correlations is dropped. It is only present if rewriting channels of multi-quark interactions in terms of the exchange of a dynamical degree of freedom as described in [Section 2.4.1](#)

We now proceed with the discussion of a solution of the above equations at the example of pure Yang-

Mills theory. Hence we restrict ourselves to [Figure 5.4\(a\)](#), where the matter contributions have been dropped anyway. In the following we concentrate on the flow equations for gluon and ghost propagators on the basis of given vertices. This is a common simple approximation used in functional methods. Typically, the vertices are either taken to be classical or as solutions to the (m)STIs, see [Section 5.7](#). Here we pick up a vertex suggestion which encodes already the running of the coupling as well as that of the legs of a given vertex. It has been already discussed in [Section 2.3.3](#) in the context of the vertex expansion scheme, see [\(2.114\)](#). For example, for the ghost-gluon vertex in Yang-Mill theory it reads

$$\Gamma_{\bar{c}cA}^{(3)}(q, p) = Z_A^{1/2}(p + q) Z_c^{1/2}(p) Z_c^{1/2}(q) S_{\bar{c}Ac}^{(3)}(p, q; g_{\bar{c}Ac}), \quad (5.57)$$

with

$$S_{\bar{c}cA,\mu}^{(3),abc}(q, p) = i g_{\bar{c}Ac} q_\mu f^{abc}. \quad (5.58)$$

In [\(5.57\)](#) and [\(5.58\)](#), p is the ghost and q is the anti-ghost momentum, according to the notation [\(2.228\)](#) used in the current lecture notes for $\Gamma_{\varphi_1 \dots \varphi_n}^{(n)}(p_1, \dots, p_n)$. For the classical vertex see also [Appendix F.1](#), [Figure F.1](#). The approximation [\(5.58\)](#) entails

$$\lambda_{\bar{c}cA}^{(1)}(q, p) = \sqrt{4\pi\alpha_{\bar{c}cA}} Z_A^{1/2}(p + q) Z_c^{1/2}(p) Z_c^{1/2}(q), \quad (5.59)$$

with the classical tensor structure

$$\mathcal{T}_{\bar{c}cA}^{(1)}(q, p) = \frac{1}{g} S_{\perp, \bar{c}cA}^{abc}(q, p). \quad (5.60)$$

A complete set of tensor structures contains one further tensor and is dropped here. The ghost-gluon vertex in [\(5.57\)](#) is accompanied by the purely gluonic three-gluon and four-gluon vertices,

$$\begin{aligned} \Gamma_{A^3}(p_1, p_2) &= \prod_{i=1}^3 Z_A^{1/2}(p_i) S_{A^3}^{(3)}(p_1, p_2; g_{A^3}), \\ \Gamma_{A^4}(p_1, p_2, p_3) &= \prod_{i=1}^4 Z_A^{1/2}(p_i) S_{A^4}^{(4)}(p_1, p_2, p_3; g_{A^4}), \end{aligned} \quad (5.61)$$

where $p_3 = -(p_1 + p_2)$ for $\Gamma_{A^3}^{(3)}$ and $p_4 = -(p_1 + p_2 + p_3)$ for $\Gamma_{A^4}^{(4)}$. The classical vertices are provided in [Appendix F.1](#), [Figure F.1](#). It is left to choose the running couplings $\alpha_{s,i}$ in [\(5.55\)](#). In the present qualitative analysis we identify all couplings with

$$\alpha_{s,i} = \bar{\alpha}_s, \quad \text{with} \quad i = (\bar{c}cA, A^3, A^4). \quad (5.62)$$

This concludes the setup for the present computations. It is left to provide a definition for $\bar{\alpha}_s$. One option is given by identifying $\bar{\alpha}_s$ with one of the $\alpha_{s,i}$, a simple choice being the ghost-gluon coupling, as it has the least demanding flow equation. Here we follow a slightly different road, that indeed allows us to compute a running coupling from the propagators or rather the wave function renormalisations of the ghost and the gluon. This possibility is unique to the Landau gauge.

5.5. Functional Renormalisation for QCD in the Landau gauge

Hence we now further restrict our gauge and resort to the Landau gauge, $\xi = 0$. This flow has several interesting properties that facilitate formal considerations as well as numerical computations. These properties originate in the fact, that for the Landau gauge, the splitting into the longitudinal, redundant,

gauge fixing degrees of freedom, the gauge fibre) and the transversal, dynamical, 'gauge invariant' degrees of freedom, the base base, is orthogonal. This is already reflected in the transversality of the gluon propagator G_A and the cutted gluon propagator $G_A \partial_t R_A G_A$,

$$l_\mu G_{A,\mu\nu}^{ab}(l) = 0, \quad l_\mu [G_A \partial_t R_A G_A]_{\mu\nu}^{ab}(l) = 0, \quad (5.63)$$

no propagation takes place in the longitudinal subspace. This property leads to a separation of flows for transversal and longitudinal correlation functions. While the latter one depend on both, transversal and longitudinal correlation functions, the former set is closed.

5.5.1. Closed functional relations for purely transversal correlation functions

To see this let us first consider completely transversal flows. These correlation functions are defined by contracting all gluonic vertices with the transversal projection operators Π^\perp ,

$$\Gamma_{\perp, A^m \varphi^{n-m}, \mu_1 \dots \mu_m}^{(n)}(p_1, \dots, p_m, p_{m+1}, \dots, p_n) := \prod_{i=1}^m \Pi_{\mu\nu}^\perp(p_i) \Gamma_{A^m \varphi^{n-m}, \mu_1 \dots \mu_m}^{(n)}(p_1, \dots, p_m, p_{m+1}, \dots, p_n), \quad (5.64)$$

with $0 \leq m \leq n$, and the remaining $n - m$ fields are not gluons, $\varphi_j \neq A_\mu$ for $j = 1, \dots, n - m$ for $m < n$. Longitudinal correlation functions are then defined as the complement of the set $\{\Gamma^{(n),\perp}\}$ defined in (5.64). This property reads

$$p_1 \mu_1 \Gamma_{\parallel, A^m \varphi^{n-m}, \mu_1 \dots \mu_m}^{(n)}(p_1, \dots, p_m, p_{m+1}, \dots, p_n) = 0, \quad \text{for } m \geq 1, \quad (5.65)$$

for some permutation of the A_{μ_i} . Now we concentrate on the flow of the transversal correlation functions, that carry the dynamics. We find

$$\partial_t \Gamma_\perp^{(n)} = \text{Flow}_\perp^{(n)}[\{\Gamma_\perp^{(m \leq m+2)}\}, R_k], \quad (5.66)$$

where $\text{Flow}^{(n),\perp}$ stands for the transversally projected diagrams on the right hand side of the flow, following from the definition (5.64). This entails that gluonic legs of vertices in the diagrams are all contracted with transversal projection operators. For the external ones this is evident due to the explicit contraction with Π^\perp , the internal legs are contracted with the gluon propagators in the loops, which are transversal, see (5.63). Explicitly we have

$$G_{A,\mu\nu}^{ab}(l) = \Pi_{\mu\rho}^\perp(l) G_{A,\rho\sigma}^{ab}(l) \Pi_{\sigma\nu}^\perp(l), \quad (5.67)$$

and similarly for $G_A \partial_t R_A G_A$. This proves (5.66). The set of equation can be again formulated very concisely in terms of a master flow equation, only valid for $\xi = 0$,

$$\partial_t \Gamma[\Phi^\perp] = \frac{1}{2} \text{Tr} G_k[\Phi^\perp] \partial_t R_k, \quad \text{with} \quad \Phi^\perp = (\Pi_{\mu\nu}^\perp A_\nu, c, \bar{c}, q, \bar{q}). \quad (5.68)$$

We remark that $\Gamma^{(2)}[\Phi^\perp] = (\delta^2 / \delta \Phi^2 \Gamma_k)[\Phi = \Phi^\perp]$, i.e. it includes the gauge fixing term. Alternatively, (5.68) can be achieved with a purely transversal regulator. Such a choice regularises the theory fully, as there is no propagation in the longitudinal direction in the first place.

Equation (5.68) makes explicit, that the flow of transversal correlation functions is closed. Note that this implies a huge reduction of the set of flow equations for correlation functions required for the dynamics of the system. Also technically this is a very important simplification.

A direct consequence of (5.67) is the fact, that the flow of longitudinal correlation functions (5.65) requires the knowledge of the transversal correlation functions: The flow of all longitudinal correlation functions -even the completely longitudinal ones- depend on vertices with at least one transversal leg. This leads to a chain of dependences finally ending in one on purely transversal vertices. Note that this does not entail that the flow of a specific longitudinal correlation functions depends explicitly on fully transversal correlation functions, but the solution of the flows of the involved vertices eventually requires also fully transversal vertices. This can be summarized as

$$\{\partial_t \Gamma_{\parallel}^{(n)}\} = \{\text{Flow}_{\parallel}^{(n)}\}[\{\Gamma_k^{(m)}\}, R_k], \quad (5.69)$$

the right hand side requires the knowledge of all correlation functions. From the structure of the proofs, or rather sketches of proofs, it is evident, that these properties extend to general functional relations in terms of loops, and in particular also to DSEs and n PI hierarchies. We write in general, [89] for QCD and [62] for gravity,

$$\begin{aligned} \Gamma_{\perp}^{(n)} &= \text{FunRel}_{\perp}^{(n)}[\{\Gamma_{\perp}^{(m)}\}], \\ \Gamma_{\parallel}^{(n)} &= \text{FunRel}_{\parallel}^{(n)}[\{\Gamma^{(m)}\}]. \end{aligned} \quad (5.70)$$

From the flow relations (5.66), (5.69) the generic relation (5.70) follows from an integration over the cutoff scale. Equation (5.70) is intriguing as it reduces the computational effort to solving the transversal, dynamical set of equations. The symmetry relation in a gauge fixed theory is encoded in STIs which also fall into the class of functional relations (5.70) for longitudinal correlation functions. Consequences of the latter fact are discussed in Section 5.7.

5.5.2. Non-renormalisation theorem for the ghost-gluon vertex

Now we continue with another interesting property of the Landau gauge, the non-renormalisation theorem for the ghost-gluon vertex [90]. It originates in the same orthogonal splitting in transversal and longitudinal correlations as discussed above. Here we briefly discuss its kinematical origin, more details can be found in the literature. We first note that the transversal part of the ghost-gluon vertex has only one tensor structure,

$$\Gamma_{\perp, \bar{c}cA}^{abc}(q, p) = \lambda_{\perp, \bar{c}cA}(q, p) \mathcal{T}_{\perp, \bar{c}cA}(q, p), \quad (5.71)$$

with the general parameterisation (5.51). For the classical vertex we have $\lambda_{\perp, \bar{c}cA}(q, p) = g$. It is simple to prove that $\mathcal{T}_{\perp, \bar{c}cA}$ is the only transversal tensor structure in (5.71): all tensor structures are proportional to the momenta q_μ and p_μ with the only possible gauge group tensor structure f^{abc} . However, due to transversality we can add $-(p_\mu + q_\mu)$ to the latter, converting it to $-q_\mu$.

For the non-renormalisation theorem it is sufficient to discuss the flow of the ghost-gluon vertex

$$\partial_t \Gamma_{\bar{c}cA}^{(3)}(q, p), \quad (5.72)$$

with ghost momentum p and antighost momentum q . It is depicted in Figure 5.4(a). As discussed in Section 2.3.1, the necessity of an ultraviolet renormalisation is in one to one correspondence to an asymptotic cutoff dependence with positive powers of k or a constant behaviour. In turn, a decay behaviour with $k \rightarrow \infty$ implies the absence of an RG running. We first inspect the explicit two diagrams in Figure 5.4(a) in the flow of the ghost-gluon vertex. These are the only diagrams present on the one-loop level. The missing diagrams in Figure 5.4(a) with $\Gamma^{(4)}$ and $\Gamma^{(5)}$ are absent at one loop and are discussed later. Note however, that the question of non-renormalisation is already decided with the first two diagrams.

We notice that both diagrams are already linear in the anti-ghost momentum q , if the ghost-gluon vertex $\Gamma_{\bar{c}cA}^{(3)}$ has this property. Since the classical ghost gluon vertex (5.58) is linear in the anti-ghost momentum, and hence the flow also carries this property (if restricting ourselves to the diagrams depicted in Figure 5.4(a)). This leaves us with a potentially logarithmically divergent diagram as the integrand has the momentum dimension -4 , and hence the momentum integral is dimensionless with dimension 0. Accordingly, for large cutoff scales the loop tends towards a constant.

Now we concentrate on the vertex with the external ghost line in both diagrams. It is attached to a ghost propagator and a gluon propagator (not an external gluon line). With (5.71) this leaves us with the momentum structure

$$\Gamma_{\bar{c}cA,\rho}(l-p, p) G_{A,\rho\sigma}^{ab}(l) G_c(l-p) \propto (l-p)_\rho G_{A,\rho\sigma}^{ab}(l) G_c(l-p) = -p_\rho G_{A,\rho\sigma}^{ab}(l) G_c(l-p). \quad (5.73)$$

where l is the loop momentum. Equation (5.73) leads to a further linear momentum dependence on an external momentum. Consequently, the remaining integral carries the momentum dimension -1 . In summary we conclude

$$\lim_{k \rightarrow \infty} \partial_t \Gamma_{\bar{c}cA}^{(3)}(q, p) \propto \frac{1}{k}. \quad (5.74)$$

Equation (5.74) is the non-renormalisation theorem of the ghost-gluon vertex in terms of its flow. The kinematic structure of its proof carries over directly to the higher order diagrams, as it is only based on two properties:

- (i) ghost-gluon vertices are at least linear in the anti-ghost momenta,
- (ii) the transversality of the gluon propagator.

Now we come back to the task of conveniently choosing $\bar{\alpha}_s$ in (5.62). The non-renormalisation of the ghost-gluon coupling entails that the vertex has no RG-running. Accordingly, the RG-running of the coupling $\alpha_{s,\bar{c}cA}$ in (5.55) is already comprised in the product of gluon and ghost wave function renormalisations, $Z_A Z_c^2$. This suggests the definition of the following *propagator coupling*, [?],

$$\bar{\alpha}_s(\bar{p}) = \frac{1}{4\pi} \frac{g^2}{Z_A(\bar{p}) Z_c^2(\bar{p})}, \quad (5.75)$$

with the initial coupling $g = g_\Lambda$ up to global normalisations. It differs from the ghost-gluon vertex coupling by $\lambda_{\bar{c}cA}(\bar{p})$. As the latter has no RG-running, its momentum-dependence can only kick in at two-loop level. Indeed it can be shown to be mild and we shall drop it for the following consideration. A further simplification is achieved by using the property of the flow diagrams, that they are peaked at loop momenta $q^2 \approx k^2$, and use

$$\bar{\alpha}_s = \bar{\alpha}_s(\bar{p}^2 = k^2). \quad (5.76)$$

Evidently, the flow equations simplify enormously with the Vertex Ansätze above. We are left with simple one loop diagrams with running couplings and $\eta_A(q^2), \eta_c(q^2)$ with loop momenta q .

5.6. Yang-Mills correlation functions in the Landau gauge

5.6.1. Yang-Mills propagators in the Landau gauge

In this chapter we derive the flow equations for the Yang-Mills propagators, the gluon and ghost propagators. The propagators are primarily important for the approach and also carry eminent physics information. They also allow us, to discuss the setup of approximations in QCD. Also, the general projection procedure for extracting the flows of the coefficients of specific tensor structure correlation functions is introduced at this example. Most of the technical details are deferred to [Appendix F.3](#).

Truncation and projection operators

We start by specifying the content of our truncation, which contains a full basis for the propagators as well as the classical tensor structures of the primitively divergent vertices:

$$\begin{aligned}
\mathcal{T}_{\bar{c}c}^{(1)} &= p^2 \delta^{ab}, \\
\mathcal{T}_{AA}^{(1)} &= p^2 \Pi_{\mu\nu}^\perp(p) \delta^{ab}, \\
\mathcal{T}_{AA}^{(2)} &= p^2 \Pi_{\mu\nu}^\parallel(p) \delta^{ab}, \\
\mathcal{T}_{\bar{c}cA}^{(1)} &= i f^{abc} p_\mu, \\
\mathcal{T}_{AAA}^{(1)} &= i f^{abc} [(p_2 - p_3)_\mu \delta_{\nu\rho} + (p_3 - p_1)_\nu \delta_{\rho\mu} + (p_1 - p_2)_\rho \delta_{\mu\nu}], \\
\mathcal{T}_{AAAA}^{(1)} &= f^{ade} f^{bce} [\delta_{\mu\nu} \delta_{\rho\sigma} - \delta_{\mu\rho} \delta_{\nu\sigma}] + f^{ace} f^{bde} [\delta_{\mu\nu} \delta_{\rho\sigma} - \delta_{\mu\sigma} \delta_{\nu\rho}] \\
&\quad + f^{abe} f^{cde} [\delta_{\mu\rho} \delta_{\nu\sigma} - \delta_{\mu\sigma} \delta_{\nu\rho}]. \tag{5.77}
\end{aligned}$$

The indices are in canonical order and associated to the external legs in the same, usual canonical order. In order to project onto the tensor structures of the two-point functions $\mathcal{T}_{\bar{c}c}^{(1)}$ and $\mathcal{T}_{AA}^{(1)}$ we require their projection operators in addition. The second tensor structure for the gluon is quoted for the sake of completeness. In the Landau gauge it drops out completely. In general one can differentiate between two different cases, the tensor structures taken into account for an operator account for a basis, which renders the their associated projection operators unique. If the tensor structures taken into account do not account form a basis, one loses the uniqueness of the projection operators, making them effectively a part of the truncation. For the case at hand, we have the tensor structures form a basis for the two-point functions as well as for the ghost-gluon vertex, but not for the three-gluon and four-gluon vertex. Summarizing, a projection operator has the following property

$$\mathcal{P}_{\varphi_{i_1} \dots \varphi_{i_N}}^{(j)} \Gamma^{\varphi_{i_1} \dots \varphi_{i_N}} = \lambda_{\varphi_{i_1} \dots \varphi_{i_N}}^{(j)}, \tag{5.78}$$

i.e. it projects onto the scalar dressing function associated to a given tensor structure. Since we will only derive the flow for the two-point functions in this section, we only require the projection operators for the case we have a basis in (5.77) and do not need to discuss any errors arising due to the ambiguity in choosing a projection operator. The required projection operators are easily derived, since they have to be proportional to their own tensor structure and the normalization is fixed by a simple trace, resulting in

$$\begin{aligned}
\mathcal{P}_{\bar{c}c}^{(1)} &= \frac{1}{d_A} \frac{1}{p^2} \mathcal{T}_{\bar{c}c}^{(1)} \\
\mathcal{P}_{AA}^{(1)} &= \frac{1}{d_A} \frac{1}{d-1} \frac{1}{p^2} \mathcal{T}_{AA}^{(1)}, \tag{5.79}
\end{aligned}$$

where $d_A = N_c^2 - 1$ is the dimension of the adjoint representation, i.e. the "number" of gluons and d is the space-time dimension, i.e. $d - 1$ is the number of transversal modes.

Parameterisation and regulators

To each tensor structure in (5.77) we associate a scalar dressing function $\lambda_{\varphi_i\dots}$, as introduced previously. Additionally, we recall the parametrisation for the scalar dressing functions of the two-point functions, see (5.52)

$$\begin{aligned}\lambda_{\bar{c}c}^{(1)} &= Z_c(p), \\ \lambda_{AA}^{(1)} &= Z_A(p) \left[1 + \frac{m_A^2}{p^2} \right].\end{aligned}\tag{5.80}$$

where we have used (5.52) with one slight modification: in (5.80) we have introduced a mass parameter for the gluon, accounting for the relevant running of the gluon mass term, c.f. the discussion in Section 5.4.1, at the end of this chapter and in Section 5.7. This ensures that we can choose $Z_A(p) > 0$ even for negative mass parameters $m_{A,k}^2 < 0$. In this case we have to choose

$$\lambda_{AA}^{(1)}(p^2 = m_A^2) = 0.\tag{5.81}$$

Then the zero of $\lambda_{AA}^{(1)}$ is reflected in the parameterisation, as is its sign: $\text{sign} \lambda_{AA}^{(1)}(p) = \text{sign}(p^2 + m_A^2)$, which leaves us with a positive $Z_A(p)$ and a finite $\eta_A(p)$. Note that for strictly positive $\lambda_{AA}^{(1)}(p)$ we choose

$$Z_A(0)m_A^2 = \lambda_{AA}^{(1)}(p^2 0).\tag{5.82}$$

With positive Z_φ we can introduce the usual parametrisation of the regulators

$$\begin{aligned}R_c(p) &= Z_c(p) p^2 r_c(x), \\ R_A(p) &= Z_A(p) p^2 r_A(x),\end{aligned}\tag{5.83}$$

where $x = p^2/k^2$, for the regulator matrix in field space see 5.39b. In order to proceed we still need propagators, i.e. the inverted two-point functions. For this we note that Π^\perp projects on an orthogonal subspace, together with the diagonal structure in colour space, and therefore it is trivial to check that the propagators after introducing the regulator are given by

$$\begin{aligned}G_{\bar{c}c}(p) &= \frac{\mathcal{T}_{\bar{c}c}^{(1)}}{p^2} \frac{1}{Z_c(p)} \frac{1}{p^2 [1 + r_c(x)]}, \\ G_{AA}(p) &= \frac{\mathcal{T}_{AA}^{(1)}}{p^2} \frac{1}{Z_A(p)} \frac{1}{p^2 [1 + r_A(x)] + m_A^2},\end{aligned}\tag{5.84}$$

where the occurrence of only $\mathcal{T}_{AA}^{(1)}$ only holds in the Landau gauge. Utilising the properties of the projection operator $\Pi_{\mu\sigma}^\perp(p) \Pi_{\sigma\nu}^\perp(p) = \Pi_{\mu\nu}^\perp(p)$ it is beneficial to calculate the $(G \partial_t R G)(q)$ terms before calculating any diagrams

$$\begin{aligned}(G \partial_t R_k G)_{\bar{c}c}(q) &= (G_{\bar{c}c} \partial_t R_c G_{\bar{c}c})(q) = \delta^{ab} \frac{1}{Z_c(q)} \frac{1}{q^2} \frac{\partial_t r_c(x) - \eta_c(q) r_c(x)}{[1 + r_c(x)]^2}, \\ (G \partial_t R_k G)_{AA}(q) &= (G_{AA} \partial_t R_A G_{AA})(q) = \delta^{ab} \Pi_{\mu\nu}^\perp(q) \frac{q^2}{Z_A(q)} \frac{\partial_t r_A(x) - \eta_A(q) r_A(x)}{(q^2 [1 + r_A(x)] + m_A^2)^2}.\end{aligned}\tag{5.85}$$

Note that with the current choice of the regulators, (5.83), both, the propagators as well as the cutted propagators are proportional to the classical propagators.

We remark that while the above is the most uniform and hence formally attractive procedure, it comes to a high numerical price: at each flow step the zero of the two point function has to be determined. Of course this is possible but not convenient. Thus, in practical applications the mass function m_A^2 is absorbed in the Z_A with $\lambda_{AA}^{(1)}(p) = Z_A(p) p^2$. Then the flow of $Z_A(p)$ carries the full dynamics including the flow of the mass gap. In turn, this implies that in general the regulator cannot be chosen to be proportional to $Z_A(p)$ as the latter may be negative. We choose

$$R_A(p) = \bar{Z}_A(p) p^2 r_A(x), \quad (5.86)$$

where $\bar{Z}_A(p) > 0$ is related but not identical to $Z_A(p)$. The technical details are provided in [Appendix F.4](#).

5.6.2. Solution and interpretation

The computation is deferred to [Appendix F.3](#), where all steps are done explicitly. We are now in the position to solve flow equations for the ghost- and gluon propagators in the Landau gauge. We provide results with classical vertices with running couplings (5.76) as well as with the vertex construction discussed in [Section 5.4.2](#) and [Section 5.4.2](#). Inserting all ingredients in the flow, we are led to

$$\begin{aligned} \eta_c(p) = - \int_q 4\pi \bar{\alpha}_s \frac{p^2 q^2 - (p \cdot q)^2}{p^2 q^2 (p + q)^2} \\ \times \frac{1}{[1 + r_c(x)] \left[1 + r_A(x_{p+q}) + \frac{\bar{m}_A^2}{x_{p+q}} \right]} \left[\frac{[\partial_t - \eta_c(q)] r_c(x)}{1 + r_c(x)} + \frac{[\partial_t - \eta_A(p + q)] r_A(x_{p+q})}{1 + r_A(x_{p+q}) + \frac{\bar{m}_A^2}{x_{p+q}}} \right], \end{aligned} \quad (5.87)$$

where

$$\bar{m}_A^2 = \frac{m_A^2}{k^2}, \quad \text{and} \quad x = \frac{q^2}{k^2}, \quad x_{p+q} = \frac{(p + q)^2}{k^2}. \quad (5.88)$$

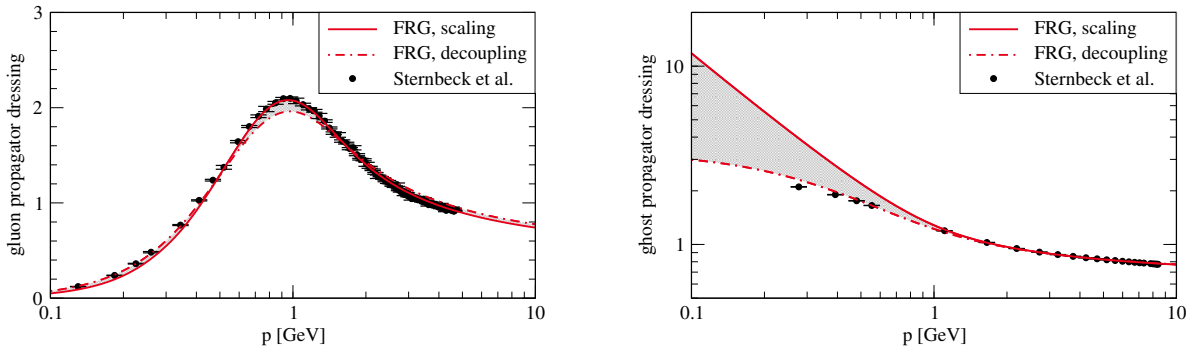
The strong running coupling $\bar{\alpha}_s(p, q)$ depends on the chosen approximation. [Equation \(5.87\)](#) is the generic form of flows with RG-adapted regulators. The first factor of the integrand in the first line is the standard one-loop integrand. This already entails that we simply can take over the results, or check our results, for the tensor contractions and integrands from one loop perturbation theory. The second factor in the first line is nothing but a definition of a running 'coupling', as its RG-scaling is governed by the β -function. Within the approximation (5.59) we have

$$\frac{\lambda_{\perp, \bar{c}cA}^2(q, p)}{Z_c(p) Z_c(q) Z_A(p + q)} = 4\pi \bar{\alpha}_s, \quad (5.89)$$

while for a constant ghost-gluon vertex the Z 's survive. In either case the remaining integral has a simple structure, but has to be solved numerically.

The above analysis nicely shows the uniformity of the flow and the separation of the dynamical part from the regularisation and the one loop contraction. With the parameterisation used in the numerical computations: $m_A^2 = 0$ and the choice of regulators in ?? we are led to

$$\begin{aligned} \eta_c(p) = - \int_q 4\pi \bar{\alpha}_s \frac{p^2 q^2 - (p \cdot q)^2}{p^2 q^2 (p + q)^2} \frac{\bar{Z}_A(p + q)}{[1 + r_c(x)] [Z_A(p + q) + \bar{Z}_A(p + q) r_A(x_{p+q})]} \\ \times \left[\frac{[\partial_t - \eta_c(q)] r_c(x)}{1 + r_c(x)} + \frac{[\partial_t - \bar{\eta}_A(p + q)] r_A(x_{p+q})}{Z_A(p + q) + \bar{Z}_A(p + q) r_A(x_{p+q})} \right], \end{aligned} \quad (5.90)$$



(a) Gluon dressing $1/Z_A(p)$ from [54] in comparison to [91]. (b) Ghost dressing $1/Z_c(p)$ from [54] in comparison to [91].

Figure 5.5.: Gluon dressing $1/Z_A$ (left) and ghost dressing $1/Z_c$ (right) from [54] in comparison to the lattice results from [91].

In the flow equation for the gluon propagator the same procedure can be applied and we arrive at

$$\eta_A = -\frac{1}{Z_A(p^2) p^2} \mathcal{P}_{AA}^{(1)} [\mathcal{D}_{AA}^{(1)} + \mathcal{D}_{AA}^{(2)} + \mathcal{D}_{AA}^{(3)}] \quad (5.91)$$

with

$$\frac{\lambda_{\bar{c}cA}(q, -(p+q)) \lambda_{\bar{c}cA}(p+q, -q)}{Z_A(p) Z_c(q) Z_c(p+q)} = \frac{\lambda_{AAAA}(p, -p, -q)}{Z_A(p) Z_A(q)} = 4\pi \bar{\alpha}_s. \quad (5.92)$$

Equation (5.87) and (5.91) can be solved numerically, the results in the currently most advanced and quantitative approximation, [54], are depicted in Figure 5.5. While the gluon propagator shows a mass gap reflected in the vanishing dressing $1/Z_A(p)$ for $p^2 \rightarrow 0$, the ghost propagator shows an infrared enhancement.

Mass gap in Yang-Mills theory and the gluon mass gap

Before we discuss these properties in the light of the underlying gauge symmetry in the next chapter, we want to provide some physics implications of these properties.

Seemingly, Yang-Mills theory is gapless with the existence of an infrared enhanced ghost propagator. However, keep in mind that the ghost is an auxiliary field, no observable is constructed with the explicit occurrence of the ghost field. Observables are constructed from gauge invariant, *local*, operators $\mathcal{O}[A_\mu]$. An example is

$$\mathcal{O}[A_\mu] = \text{tr } F_{\mu\nu}^2(x_1) \text{tr } F_{\mu\nu}^2(x_2). \quad (5.93)$$

Its expectation value is the correlation between the action densities at the positions x_1 and x_2 , and is part of the two-point correlation of the energy-momentum tensor. With (1.19) the expectation value is given by

$$\langle \mathcal{O}[A_\mu] \rangle = \mathcal{O} \left[G_{A\varphi_i} \frac{\delta}{\delta \varphi_i} + A_\mu \right] \Big|_{\Phi=0}, \quad (5.94)$$

where $\Phi = (A_\mu, c, \bar{c}) = 0$ is the solution to the equation of motion. Clearly, general observables have a diagrammatic description, where the propagators connected to the positions x_1, \dots, x_n , are only the gluonic ones. Hence the infrared enhancement of the ghosts is not seen in observables (for non-singular vertices). In turn, for non-singular vertices the physical correlation length ξ_O of observables is related to the mass gap in the gluon propagator. In the present example this is

$$\lim_{|x_1-x_2|} \left| \left\langle \text{tr} F_{\mu\nu}^2(x_1) \text{tr} F_{\mu\nu}^2(x_2) \right\rangle - \left\langle \text{tr} F_{\mu\nu}^2(x_1) \right\rangle \left\langle \text{tr} F_{\mu\nu}^2(x_2) \right\rangle \right| \propto e^{-|x_1-x_2|/\xi_O}. \quad (5.95)$$

This already indicates that the mass gap in the Landau gauge gluon propagator is related to the physical mass gap in QCD.

Quality of the approximation

In [Figure 5.6](#), taken from [54], we show the scaling solution for the propagators in different truncations. A more extensive discussion is found in [54]. In all cases, the full momentum dependence of the propagators is taken into account whereas different approximations are used for the vertices:

- (i) Including only RG-scale-dependent constant vertex dressing functions is the minimal approximation that can produce a scaling solution with a physical gluon mass gap, and is the one discussed in detail above. The dot-dashed (magenta) line in [Figure 5.6](#) corresponds to an approximation with constant vertex dressing functions evaluated at the symmetric configuration with momentum $O(250 \text{ MeV})$. Hence the vertices are only RG-scale-dependent vertices.
- (ii) For the dashed blue results the dressing functions for the transversally projected classical tensor structures have been approximated with a single momentum variable $\bar{p}^2 \equiv \frac{1}{n} \sum_{i=1}^n p_i^2$. Reducing the momentum dependence to a single variable requires the definition of a momentum configuration to evaluate the flow. Here, we use the symmetric point configuration, defined by $p_i \cdot p_i = p^2$ and $p_i \cdot p_j = -1/(n-1)$ for $i \neq j$, where $n = 3$ (4) for the three(four)-gluon vertex.
- (iii) Finally, the solid red line corresponds to our best truncation. This takes into account the full momentum dependence of the classical tensors structures of the three-point functions as well as the four-gluon vertex in a symmetric point approximation. Additionally, all (three-dimensional) momentum configurations of the four-gluon vertex that are needed in the tadpole diagram of the gluon propagator equation have been calculated and coupled back in this diagram.

Finally, the reliability of our approximation can be assessed by comparing the two simpler truncations to the result obtained in our best truncation scheme. We observe that our results apparently converge towards the lattice result, as we improve the momentum approximation for the vertices.

Initial conditions, relevant parameters and gauge invariance

As described in the first part of the lecture notes, the effective action at a large cutoff scale contains all UV-relevant terms in the action, that are not forbidden by symmetry. This includes all terms present in the classical action. In terms of vertices this is specified by the tensor structures (5.77). For a gauge invariant regularisation such as dimensional regularisation we would infer

$$Z_{A,\Lambda} = Z_{c,\Lambda} = 1, \quad m_{A,\Lambda}^2 = 0, \quad Z_{A,\Lambda}^\parallel = \frac{1}{\xi} \quad \text{and} \quad \lambda_{\bar{c}cA} = \lambda_{A^3} = \lambda_{A^4} = g. \quad (5.96)$$

[Equation \(5.96\)](#) leaves us with one relevant parameter, the strong coupling g , or $\alpha_s = g^2/(4\pi)$. The present momentum regularisation breaks gauge invariance, the standard Slavnov-Taylor identities (STI) get modified with terms proportional to the regulator R_k , leading to *modified* STIs (mSTIs). Consequently

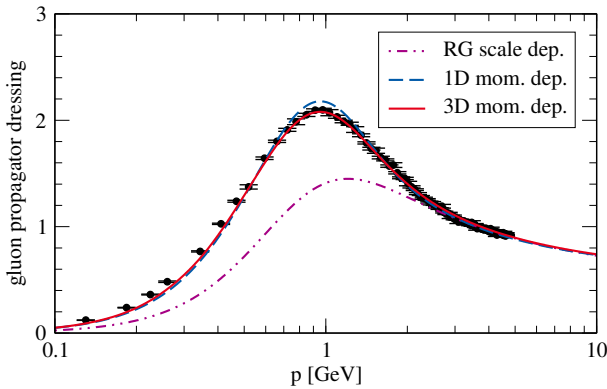


Figure 5.6.: Gluon propagator dressings obtained with different momentum approximations, see [Section 5.6.2](#) for details.

the different vertex dressing are only related to each other but not identical. Moreover, the gluon wave function renormalisation cannot be unity, instead we have (5.80) with

$$m_{A,k}^2 = (m_{A,k}^\parallel)^2 \propto k^2 \neq 0, \quad k \rightarrow \infty. \quad (5.97)$$

where m_A^2 has been introduced in (5.80) as the transversal mass, $m_A^2 = (m_A^\perp)^2$. [Equation \(5.97\)](#) seems to introduce a mass in Yang-Mills theory. However, gauge invariance at $k = 0$ enforces, that the longitudinal two-point function is trivial, $\Gamma_{A,\parallel}^{(2)} = S_{A,\parallel}^{(2)}$. This implies

$$(m_{A,k=0}^\parallel)^2 = 0. \quad (5.98)$$

[Equation \(5.98\)](#) fixed a unique $m_{A,\Lambda}^2$ ($(m_{A,k=0}^\parallel)^2 = 0$). In summary, there is one relevant parameter, g_Λ . Note however, that (5.98) leaves us with a quadratic fine-tuning problem due to (5.97). Moreover, the alert reader certainly noticed that this also induces the necessity of computing longitudinal correlation functions, as (5.98) is a constraint on the longitudinal mass. This brings back the whole longitudinal tower via the back door. Even worse so, both towers have to be solved with the same quadratic precision, otherwise the transversal mass parameter, $m_{A,k=0}^2$ contains large errors.

Finally we remark that

$$m_{A,k=0}^2 \neq (m_{A,k=0}^\parallel)^2 = 0, \quad (5.99)$$

requires *singular* vertices, for a precise definition of *singular* in this context, and a detailed discussion see [54]. These singularities cannot be generated from the flow, except in terms of a spontaneous symmetry breaking. So far, no such mechanism has been found, though interesting and promising mechanisms have been put forward.

Instead, for [Figure 5.5](#) and [Figure 5.6](#) we have relied on a specific solution which has infrared scaling properties, the *scaling* solution. This infrared scaling is uniquely reached for a specific $m_{A,\Lambda}^2$, and hence only requires the resolution of the quadratic fine-tuning solution. It can be also shown, that all the other allowed mass parameters lie in a small vicinity of this scaling solution, see [Figure 5.7](#) from [54]. We emphasise that while in this case we have a -finite- mass gap, this should not be confused with the propagator of a massive physical state. In order to avoid this confusion, we shall refer to it as the

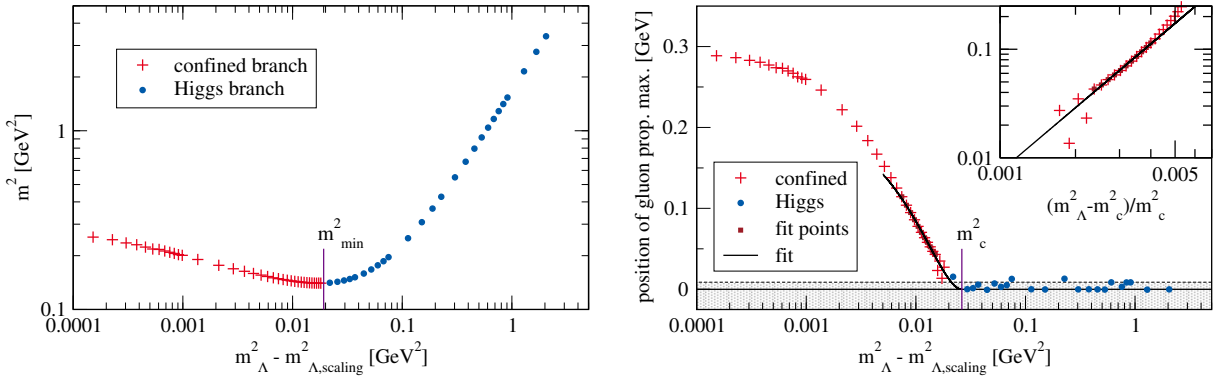


Figure 5.7.: Left: Gluon mass gap as a function of the gluon mass parameter $m_\Lambda^2 - m_{\Lambda,\text{scaling}}^2$, where $m_{\Lambda,\text{scaling}}^2$ denotes the gluon mass parameter that yields the scaling solution. Right: Momentum value at which the gluon propagator assumes its maximum, as a function of the gluon mass parameter $m_\Lambda^2 - m_{\Lambda,\text{scaling}}^2$. The inlay exposes the power law behaviour of the gluon propagator maximum in the vicinity of the transition region. Both plots were obtained from our numerically less-demanding 1D approximation. We have repeated this analysis in the transition regime from Higgs-type to confinement branch also with the best approximation and find the same behaviour. The shaded area marks momentum scales that are not numerically resolved in the present work. The points in this region rely on a generic extrapolation. The figure is taken from [54].

decoupling solution, even though it is also common referred to as the *massive* solution. The existence of this family of solutions relates to the Gribov problem of global gauge fixing, which remains unsolved at present. The related intricacies and the modified Slavnov-Taylor identities in the presence of the regularisation is described in the next chapter.

5.7. Quantum gauge symmetry & modified Slavnov-Taylor identities

Up to now we have simply studied the solution of the propagator flow equations. In the discussion of this solution we have seen, that the STIs in the presence of the regulator are of eminent importance for the existence of the mass gap in the gluon propagator, and hence directly important for confinement. Consequently we now discuss the manifestation of gauge invariance in the present gauge fixed approach. We discuss both, the STI that is treated to standard gauge transformations on the fields, as well the BRST (C.Becchi, A.Rouet, R.Stora [92] and I.V.Tyutin [93]) transformations, that allow us to write the symmetry transformations in form of an exact derivative. The latter property leads to a purely algebraic form of the symmetry identity.

5.7.1. Gauge transformations and Slavnov-Taylor identities

Here we restrict ourselves to gauge fixed Yang-Mills theory, as introduced in Section 5.2. The inclusion of charged matter fields is straightforward and all important identities are stated in the end, ???. Gauge transformations with $\mathcal{U} = e^{i\omega}$ for gluon and ghost fields read

$$\begin{aligned} A_\mu^U &= \frac{i}{g} U \left(D_\mu U^\dagger \right) = A_\mu + [D_\mu, \omega] + O(\omega^2) \\ c^U &= U c U^\dagger = c - i g [c, \omega] + O(\omega^2) \\ \bar{c}^U &= U \bar{c} U^\dagger = \bar{c} - i g [\bar{c}, \omega] + O(\omega^2), \end{aligned} \quad (5.100)$$

where ghost and anti-ghost have been set to transform as tensors under gauge transformations. The generator of the gauge transformations in (5.100) can be written as

$$\delta_{\text{gauge}}^a = -D_\mu^{ab} \frac{\delta}{\delta A_\mu^b} - ig f^{abc} \left(c_c \frac{\delta}{\delta c_b} + \bar{c}_c \frac{\delta}{\delta \bar{c}_b} \right). \quad (5.101)$$

One readily sees that $\int_x \omega^a(x) \delta_{\text{gauge}}^a(x) \Phi(y)$ generates the terms linear in ω in (5.100). Note that (5.100) or (5.101) is not an invariance of the gauge fixed action: while the Yang-Mills action is gauge invariant, neither the gauge fixing term nor the ghost action is. Still, the operator δ_{gauge} has the form of the operator in the generalised Dyson-Schwinger equation (1.40) discussed in Section 1.3. The total derivative operator inserted there is $\delta/\delta\varphi(x)\Psi[\varphi] = \delta_{\text{gauge}}^a$. This is seen explicitly within the representation

$$\delta_{\text{gauge}}^a = -\frac{\delta}{\delta A_\mu^b} D_\mu^{ab} + ig \left(\frac{\delta}{\delta c_b} f^{abc} c_c + \frac{\delta}{\delta \bar{c}_b} \bar{c}_c \right), \quad (5.102)$$

where the derivatives act on everything to the right and we have used that $f^{abb} = 0$. Consequently we have

$$\frac{1}{Z[J]} \int dA dc d\bar{c} \delta_{\text{gauge}}^a \left[e^{-S_A[A,c,\bar{c}]} + \int_x (J_A \cdot A + \bar{J}_c \cdot c - \bar{c} \cdot J_c) \right] = \left\langle \int J \cdot \delta_{\text{gauge}}^a \Phi - \delta_{\text{gauge}}^a (S_{\text{gf}} + S_{\text{gh}}) \right\rangle = 0, \quad (5.103)$$

with $J = (J_A, J_c, \bar{J}_c)$. Equation (5.103) entails that δ_{gauge}^a carries a projection of the shift invariance of the theory represented by the Dyson-Schwinger equations. Note that this does not entail that it carries a symmetry of the underlying classical theory, in particular we have

$$\delta_{\text{gauge}}^a e^{-S_A[A,c,\bar{c}]} = \delta_{\text{gauge}}^a (S_{\text{gf}} + S_{\text{gh}}) \neq 0. \quad (5.104)$$

Equation (5.104) leads to the non-trivial expectation values in (5.103), while the transformation of the source terms simply carry the transformations of the fields. That δ_{gauge}^a indeed carries the gauge invariance of the theory, is seen within a restriction to gauge invariant observables $\langle O[A] \rangle$ with $O[A^U] = O[A^U]$. Then we have

$$-\frac{\delta}{\delta A_\mu^b} D_\mu^{ab} \left[O[A] \int dc d\bar{c} e^{-S_A[A,c,\bar{c}]} \right] = 0. \quad (5.105)$$

In (5.105) we have used that in the absense of sources for the ghost and anti-ghost we can integrate out c, \bar{c} , thus undoing the introduction of unity with the Faddeev-Popov trick.

Carrying out explicitly the δ_{gauge}^a variations in (5.103) of leads us to

$$(\bar{D}_\mu^{ab} J_\mu^b - ig f^{abc} (\bar{\eta}^b \langle c^c \rangle - \langle \bar{c}^c \rangle \eta^b)) (x) = \left\langle \frac{1}{\xi} D_\mu^{ab}(x) \partial_\mu \partial_\nu A_\nu^b(x) - \frac{g}{2} f^{abc} \partial_\mu [\bar{c}^b D_\mu^{cd} c^d] \right\rangle. \quad (5.106)$$

Slavnov-Taylor Identity (STI)

In summary, δ_{gauge}^a indeed carries the underlying gauge symmetry in terms of a projected (on the gauge fibre) DSEs. These projected DSEs, (5.103), are the *Slavnov-Taylor identities* (STIs), see (5.106).

While such a representation of gauge symmetry encodes all information, it is not a symmetry of the gauge fixed theory. It is the latter fact that will lead to loop terms in the STIs, see the right hand side of (5.106). In other words, the symmetry transformation looses its algebraic nature on the quantum level. An invariance of the gauge fixed action requires also the transformation of the gauge fixing itself. This is achieved by the BRST transformations discussed in the next chapter.

5.7.2. BRST symmetry

In the present chapter we briefly discuss BRST symmetry for the current setup. For a more detailed account we refer to the literature. For an understanding of the BRST transformations it is useful to start with the remark at the end of the last chapter: while the gauge transformation of the gauge field leaves the Yang-Mills action invariant, for an algebraic representation of gauge symmetry on the gauge fixed action with the extended field space we have to find a transformation of the ghost and anti-ghost that generate a respective transformation of the gauge fixing term. This transformation has to generate gauge transformations on the gauge field, this leaves us with the freedom of choosing ω . We also see that the Fadeev-Popov operator acts to the right with the covariant derivative, the ghost carries the adjoint representation. Accordingly, we have to find a transformation of the anti-ghost which leads to an invariance. As gauge field and ghost transform under gauge transformations, the anti-ghost transformation has to 'gauge-transform' the gauge fixing condition. In more geometrical terms this rotates the frame according to the rotation of the fields A_μ, c .

This combined transformation of the fields $\Phi = (A_\mu, c, \bar{c})$ is the BRST symmetry. The infinitesimal BRST transformations δ_{BRST} reads

$$\delta_{\text{BRST}}\Phi = \delta\lambda \mathfrak{s}\Phi, \quad (5.107)$$

with the BRST generator \mathfrak{s} acts on Φ and an infinitesimal Grassmann parameter $\delta\lambda$. The BRST operator \mathfrak{s} has the action

$$\begin{aligned} \mathfrak{s} A_\mu^a &= D_\mu^{ab} c^b, \\ \mathfrak{s} c^a &= -\frac{g}{2} f^{abc} c^b c^c, \\ \mathfrak{s} \bar{c}^a &= \frac{1}{\xi} \mathcal{F}^a[A], \end{aligned} \quad (5.108)$$

and is Grassmannian. Accordingly, the Grassmannian $\delta\lambda$ ensures, that the BRST variations $\delta_{\text{BRST}}\Phi_i$ are Grassmannian for $\Phi_i = c, \bar{c}$ and commute with c, \bar{c} for $\Phi_i = A_\mu$. As discussed in the beginning of this chapter, the BRST transformations $\mathfrak{s}\Phi_i$ of gauge field and ghost are simply gauge transformations with the Grassmannian algebra element $\omega \sim c$. The BRST transformation of the anti-ghost is the shift of the gauge fixing condition that arranges for the invariance of the gauge fixed action 5.31b: while the Yang-Mills action and $D_\mu c$ are invariant under the combined BRST transformations of gauge field and ghost, the gauge transformation of the gauge fixing term due to $A_\mu \rightarrow A_\mu + \delta_{\text{BRST}}A_\mu$ is compensated by the BRST transformation of the anti-ghost. This is demonstrated explicitly in ???. In order to keep equations readable we will employ a superfield notation in addition and collect all fields in a vector Φ , c.f. [Section 2.3.1](#) or [Exercise 3](#). With this at hand the BRST variation can be written as

$$\mathfrak{s} = \int_x (\mathfrak{s}\Phi_i) \frac{\delta}{\delta\Phi_i} \quad (5.109)$$

and the invariance of the classical action reduces to

$$\mathfrak{s}S[\Phi] = 0. \quad (5.110)$$

As for the standard gauge transformation, the BRST operator \mathfrak{s} in (5.109) can be written in terms of a total derivative

$$\mathfrak{s} = \int_x \frac{\delta}{\delta\Phi_i} (\mathfrak{s}\Phi_i), \quad (5.111)$$

where we have again used that $f^{abb} = 0$. Moreover, $(\mathfrak{s}\Phi_i)$ commutes with $\delta/\delta\Phi_i$ as the BRST transformations of the ghost and anti-ghosts are not Grassmannian. This leads us directly to the projected DSE

$$\frac{1}{Z[J_\Phi]} \int dA dc d\bar{c} \mathfrak{s} \left[e^{-S_A[A,c,\bar{c}]+\int_x (J_A \cdot A + J_c \cdot c - \bar{c} \cdot J_{\bar{c}})} \right] = 0, \quad (5.112)$$

In contradistinction to the projected DSE (5.103) for gauge transformations, the projected DSE (5.112) carries a symmetry of the underlying gauge-fixed action, see (5.110). This leads straightforwardly to

$$\int_x \langle J_A \cdot \mathfrak{s}A - J_c \cdot \mathfrak{s}c - J_{\bar{c}} \cdot \mathfrak{s}\bar{c} \rangle = 0, \quad (5.113)$$

the STI in terms of BRST transformations. In (5.113) we have used that

$$\mathfrak{s} J_A A = J_A \mathfrak{s}A, \quad \mathfrak{s} J_c c = -J_c \mathfrak{s}c, \quad \mathfrak{s} \bar{c} J_{\bar{c}} = J_{\bar{c}} \mathfrak{s}\bar{c}, \quad \text{and} \quad J \cdot \Phi = J_A A + J_c c - \bar{c} J_{\bar{c}}. \quad (5.114)$$

Equation (5.113) makes apparent that the BRST transformations are symmetry transformations: the equation only encodes the transformation of the source terms, and hence simply carries the classical, algebraic, BRST symmetry of Yang-Mills theory in the extended field space. Note however, that the BRST variations of the fields are quadratic in the fields. This entails in particular, that $\langle \mathfrak{s}A_\mu \rangle$ and $\langle \mathfrak{s}c \rangle$ involve non-trivial two-point functions, in contradistinction to the expectation values of the gauge variations of the fields.

Gauge fixing fermion, Nakanishi-Laudrup field and anti-field formalism

The latter fact seems to imply that we loose the algebraic nature of the symmetry on the quantum level. A way out of the seeming non-algebraic nature of the STI (5.113) is the introduction of source terms for the BRST variations of the fields in the generating functional: $Z[J] \rightarrow Z[J, Q]$ with additional source term

$$\int_x Q \cdot \mathfrak{s}\Phi = \int_x (Q_A \mathfrak{s}A + Q_c \mathfrak{s}c + Q_{\bar{c}} \mathfrak{s}\bar{c}). \quad (5.115)$$

Then, the non-trivial expectation values $\langle \mathfrak{s}\Phi \rangle$ in (5.113) can be represented in terms of derivatives w.r.t. the BRST sources Q_i with $i = A_\mu, c, \bar{c}$, rendering the STI algebraic again. However, the source term for the anti-ghost is not BRST invariant, $\mathfrak{s}^2 \bar{c} = \frac{1}{\xi} \mathfrak{s}\mathcal{F}[A] \neq 0$, and triggers further non-trivial contributions to (5.113), leading to

$$\int_x \left\langle J_A \cdot \mathfrak{s}A - J_c \cdot \mathfrak{s}c - J_{\bar{c}} \cdot \mathfrak{s}\bar{c} - \frac{1}{\xi} (\partial_\mu Q_c) \mathfrak{s}A_\mu \right\rangle = 0. \quad (5.116)$$

In (5.116) we have restricted ourselves to a covariant gauge and have performed a partial integration, leading to the minus sign in the last term. This results in the wished-for algebraic STI, using

$$\langle \mathfrak{s}\Phi_i \rangle = \frac{1}{Z[J, Q]} \frac{\delta Z[J, Q]}{\delta Q_i}. \quad (5.117)$$

The form of the STI in (5.116) makes even more apparent, that the invariance under a BRST transformation of gauge field and ghost requires a respective transformation of the gauge fixing condition.

The most elegant resolution for this fact is the introduction of a field for the BRST variation of the anti-ghost \bar{c} , or rather the gauge fixing. This is the Nakanishi-Laudrup field B^a with

$$S_{\text{gf}}[A, B] = \int_x \left(B^a \partial_\mu A_\mu^a - \frac{\xi}{2} B^a B^a \right), \quad (5.118)$$

which reduces to the standard gauge fixing term $S_{\text{gf}}[A]$ on-shell, that is on the EoM for B ,

$$S_{\text{gf}}[A] = S_{\text{gf}}[A, B_{\text{EoM}}] \quad \text{with} \quad B_{\text{EoM}}^a = \frac{1}{\xi} \partial_\mu A_\mu^a. \quad (5.119)$$

If we now use this formulation off-shell, the anti-ghost BRST transformation (5.108) is given by $\mathfrak{s}\bar{c} = B^a$. The BRST transformations in this further extended field space reads,

$$\begin{aligned} \mathfrak{s}A_\mu^a &= D_\mu^{ab} c^b, \\ \mathfrak{s}c^a &= -\frac{g}{2} f^{abc} c^b c^c, \\ \mathfrak{s}\bar{c}^a &= B^a, \\ \mathfrak{s}B^a &= 0. \end{aligned} \quad (5.120)$$

The BRST generator s with (5.120) is now nilpotent,

$$\mathfrak{s}^2 = 0. \quad (5.121)$$

Then, the gauge fixed action in Yang-Mills theory reads

$$S_A[\Phi] = S_{\text{YM}}[A] + \int_x \mathfrak{s}\psi[\Phi], \quad (5.122)$$

with the *gauge-fixing fermion*, see e.g. [94],

$$\psi[\Phi] = \bar{c}^a \partial_\mu A_\mu^a - \frac{\xi}{2} \bar{c}^a B^a, \quad (5.123)$$

with $\int_x \mathfrak{s}\psi[\Phi] = S_{\text{gf}}[A, B] + S_{\text{gh}}[A, c, \bar{c}]$. to show this identity one has to take into account that

$$\mathfrak{s}\bar{c}^a \partial_\mu A_\mu^a = (\mathfrak{s}\bar{c}^a) \partial_\mu A_\mu^a - \bar{c}^a \partial_\mu (\mathfrak{s}A_\mu^a). \quad (5.124)$$

The superfield Φ now also includes the Nakanishi-Laudrup field,

$$\Phi = (A_\mu, c, \bar{c}, B). \quad (5.125)$$

Equation (5.122) is manifestly BRST invariant: the Yang-Mills action is gauge invariant and $\mathfrak{s}^2\psi$ is invariant as \mathfrak{s} is nilpotent. In summary we have

$$\mathfrak{s}S_A[\Phi] = 0. \quad (5.126)$$

We emphasise again, that $S_A[A, c, \bar{c}, B]$ reduces to the standard gauge fixed action on the EoM for B , see (5.118): $S_A[A, c, \bar{c}] = S_A[A, c, \bar{c}, B_{\text{EoM}}]$. Within this formulation the last term in (5.116) is missing, and the anti-ghost term is trivial.

5.7.3. Slavnov-Taylor Identities for the Effective Action

Compliance with (5.106) or (5.113) guarantees the gauge invariance of observables. However in computation approaches one usually works with the quantum effective action $\Gamma[\Phi]$. Recalling the basic relation between the effective action and the sources

$$J_A = \frac{\delta\Gamma}{\delta A}, \quad J_c = -\frac{\delta\Gamma}{\delta c}, \quad J_{\bar{c}} = -\frac{\delta\Gamma}{\delta \bar{c}}. \quad (5.127)$$

STI for gauge transformations

Now we substitute the relations (5.127) into (5.106). We also use that the field dependence on the right hand side is, linear: $\langle \delta_{\text{gauge}} \hat{\Phi} \rangle = \delta_{\text{gauge}} \Phi$ with $\Phi = \langle \hat{\Phi} \rangle$. This leads us to

$$\mathcal{W}[\Phi] = 0, \quad \text{with} \quad \mathcal{W}[\Phi] = \delta_{\text{gauge}}^a \Gamma[\Phi] - \left\langle \delta_{\text{gauge}}^a (S_{\text{gf}} + S_{\text{gh}}) \right\rangle, \quad (5.128)$$

encoding the condition for gauge invariant observables in terms of the quantum effective action $\Gamma[\Phi]$. The right hand side of (5.128) can be written in terms of loop diagrams. As in the DSE this leads to one and two loop diagrams in classical and full vertices and full propagators.

STI for BRST transformations

A more concise representation of the underlying gauge invariance is achieved with the BRST formulation discussed in Section 5.7.2. With the Nakanishi-Laudrup field B and sources Q_i with $i = A_\mu, c, \bar{c}$ for the BRST variations $\mathfrak{s}\Phi$ the generating functional reads,

$$Z[J, Q] = \int \mathcal{D}\Phi e^{-S[A, c, \bar{c}, B] + J \cdot A + J_c \cdot c - \bar{c} J_{\bar{c}} + Q_A \mathfrak{s}A + Q_c \mathfrak{s}c + Q_{\bar{c}} \mathfrak{s}\bar{c}}, \quad (5.129)$$

with $J = (J_A, \eta, \bar{\eta})$ and $Q = (Q_A, Q_c, Q_{\bar{c}})$. Note that the BRST source term $\int_x Q_{\bar{c}} \mathfrak{s}\bar{c}$ corresponds to a source term for B , since $\mathfrak{s}\bar{c} = B$. As the BRST source terms only involve $\mathfrak{s}\Phi$, they are invariant under BRST transformations, $\mathfrak{s} \int_x Q \cdot \mathfrak{s}\Phi = 0$. Accordingly, the STI (5.113) does not change, and reads in terms of the generating functional $Z[J, Q]$,

$$\int_x \left(\frac{\delta Z}{\delta Q_A} \cdot J_A - \frac{\delta Z}{\delta Q_c} \cdot J_c - \frac{\delta Z}{\delta Q_{\bar{c}}} \cdot J_{\bar{c}} \right) = 0. \quad (5.130)$$

In (5.130) we have brought all currents to the right. This is possible as either the current J_i or the BRST-transformation $\mathfrak{s}\Phi_i$ is Grassmannian, but not both. The effective action is the Legendre transform of $Z[J_\Phi, Q_\Phi]$ with respect to the current J_Φ , while Q_Φ is a spectator,

$$\Gamma[\Phi, Q_\Phi] = \int J_\Phi \cdot \Phi - \ln Z[J_\Phi, Q_\Phi], \quad \text{with} \quad \frac{\delta\Gamma[\Phi, Q_\Phi]}{\delta Q_i} = -\frac{1}{Z[J_\Phi, Q_\Phi]} \frac{\delta Z[J_\Phi, Q_\Phi]}{\delta Q_i}, \quad (5.131)$$

with $i = A_\mu, c, \bar{c}, B$. Collecting everything, we are led to the *Quantum Master Equation*,

$$\frac{\delta\Gamma}{\delta Q_\Phi} \cdot \frac{\delta\Gamma}{\delta\Phi} = 0, \quad (5.132)$$

Quantum Master Equation (QME)

where the left hand side of (5.132) reads more explicitly

$$\frac{\delta\Gamma}{\delta Q_\Phi} \cdot \frac{\delta\Gamma}{\delta\Phi} = \int_x \left(\frac{\delta\Gamma}{\delta Q_{A,\mu}^a(x)} \frac{\delta\Gamma}{\delta A_\mu^a(x)} + \frac{\delta\Gamma}{\delta Q_c^a(x)} \frac{\delta\Gamma}{\delta c^a(x)} + \frac{\delta\Gamma}{\delta Q_{\bar{c}}^a(x)} \frac{\delta\Gamma}{\delta \bar{c}^a(x)} \right). \quad (5.133)$$

As a simple example we consider the classical action, $\Gamma = S$ in (5.132). After a straightforward calculation one arrives at $\mathfrak{s}S[\phi] = 0$, i.e. the BRST invariance of the classical action.

We can use (5.132) to define a generator of quantum BRST transformations

$$\mathfrak{s}_\Gamma = \frac{\delta\Gamma}{\delta Q_A^a} \cdot \frac{\delta}{\delta A} + \frac{\delta\Gamma}{\delta Q_c} \cdot \frac{\delta}{\delta c} + \frac{\delta\Gamma}{\delta Q_{\bar{c}}} \cdot \frac{\delta}{\delta \bar{c}}, \quad (5.134)$$

which we can use to rewrite (5.132) as

$$\mathfrak{s}_\Gamma \Gamma = 0. \quad (5.135)$$

Finally, the anti-ghost field appears only linearly in the generating function Z . Utilising the DSE with an anti-ghost derivative, we arrive at

$$\langle \partial_\mu D_\mu c \rangle - \eta = 0 \quad \Leftrightarrow \quad \partial_\mu \frac{\delta\Gamma}{\delta Q_{A,\mu}} + \frac{\delta\Gamma}{\delta \bar{c}} = 0, \quad (5.136)$$

Integrating out the B-Field and using (5.136), we arrive at

$$\frac{\delta\Gamma}{\delta Q_A} \cdot \frac{\delta\Gamma}{\delta A} + \frac{\delta\Gamma}{\delta Q_c} \cdot \frac{\delta\Gamma}{\delta c} - \int_x \left\{ \frac{1}{\xi} (\partial_\nu A_\nu^a) \partial_\mu \frac{\delta\Gamma}{\delta Q_{A,\mu}^a} \right\} = 0. \quad (5.137)$$

see (5.116). In (5.137) it is evident that the variation of the anti-ghost simply amounts to a gauge transformation of the gauge fixing term, as it was introduced in the first place.

5.7.4. Modified Slavnov-Taylor identities

The STIs discussed in the last chapter get modified by the gauge or BRST variation of the cutoff term, leading to *modified Slavnov-Taylor identities* (mSTIs). These mSTIs reduce to the standard ones for $R_k = 0$.

We start with a brief discussion of the mSTI in terms of δ_{gauge} . Adding the additional term to the classical action simply changes the expression on the right hand side of (5.106), (5.128). Moreover, due to the modification of the Legendre transform in the definition of the scale-dependent effective action $\Gamma_k[\Phi, Q]$ in (2.22), the currents are given by (2.23). Here we already allow for the general case with BRST sources. In the present case we have

$$J_A(x) = \frac{\delta(\Gamma_k + \Delta S_k)}{\delta A(x)}, \quad J_c = -\frac{\delta(\Gamma_k + \Delta S_k)}{\delta c}, \quad J_{\bar{c}} = -\frac{\delta(\Gamma_k + \Delta S_k)}{\delta \bar{c}}. \quad (5.138)$$

Note also that the BRST charges are spectators in the Legendre transform, and hence we have

$$\mathfrak{s}\Phi = \frac{\delta\Gamma_k[J, Q]}{\delta Q} = -\frac{\delta Z_k[J, Q]}{\delta Q}, \quad (5.139)$$

as the cutoff term does not depend on Q .

mSTI for gauge transformations

We first restrict ourselves to the case $Q = 0$ with $\Gamma[\Phi] = \Gamma[\Phi, Q = 0]$, and consider gauge transformations. Then, (5.128) translates into

$$\mathcal{W}_k[\Phi] = 0, \quad (5.140)$$

with $\Phi = (A_\mu, c, \bar{c})$ and

$$\mathcal{W}_k[\Phi] = \delta_{\text{gauge}}^a \Gamma_k[\Phi] - \left\langle \delta_{\text{gauge}}^a (S_{\text{gf}} + S_{\text{gh}}) \right\rangle - \left(\left\langle \delta_{\text{gauge}}^a \Delta S_k \right\rangle - \delta_{\text{gauge}}^a \Delta S_k \right), \quad (5.141)$$

where the last term in the definition of the Slavnov-Taylor operator \mathcal{W}_k comes from the modification of the Legendre transform in the definition of $\Gamma_k[\Phi]$. This modification of the STI can be written in terms of a one loop term similar to the flow equation itself. Evidently, it is proportional to the regulator and vanishes for $R_k = 0$, leaving us with the standard STI (5.128).

mSTI for BRST transformations

In the STI on the basis of BRST variations, (5.132), we have to take into account the missing BRST invariance of the cutoff term in the STI for the generating functional. This leads us to

$$\int_x \left(\frac{\delta Z}{\delta Q_A} \cdot J_A - \frac{\delta Z}{\delta Q_c} \cdot J_c - \frac{\delta Z}{\delta Q_{\bar{c}}} \cdot J_{\bar{c}} \right) = \langle \mathfrak{s} \Delta S_k[\Phi] \rangle, \quad (5.142)$$

with $\Phi = (A_\mu, c, \bar{c}, B)$. Inserting (5.138) for the currents, and (5.139) for the BRST variations, we arrive at

$$\frac{\delta \Gamma_k}{\delta Q_\Phi} \cdot \frac{\delta(\Gamma_k + \Delta S_k)}{\delta \Phi} = -\langle \mathfrak{s} \Delta S_k \rangle \quad \rightarrow \quad \frac{\delta \Gamma_k}{\delta Q_\Phi} \cdot \frac{\delta \Gamma_k}{\delta \Phi} = -\langle \mathfrak{s} \Delta S_k \rangle - \frac{\delta \Gamma_k}{\delta Q_\Phi} \cdot \frac{\delta \Delta S_k}{\delta \Phi} \quad (5.143)$$

The right hand side of (5.143) is computed in Appendix F.4.1, and gives a term similar to the loop in the flow equation, see (F.32). We also drop the subscript k again, it is implicitly understood, and quote

$$-\langle \mathfrak{s} \Delta S_k \rangle + \mathfrak{s} \Delta S_k = R^{ij} G_{jl} \frac{\delta^2 \Gamma_k[\Phi, Q]}{\delta \Phi_l \delta Q^i}, \quad (5.144)$$

where G is the regularized propagator. The derivation of (5.144) can be found in Appendix F.4.1. With this at hand, we arrive at the modified Slavnov-Taylor Identity

$$\frac{\delta \Gamma}{\delta Q_\Phi} \cdot \frac{\delta \Gamma}{\delta \Phi} = R^{ij} G_{jl} \frac{\delta^2 \Gamma_k[\Phi, Q]}{\delta \Phi_l \delta Q^i}. \quad (5.145)$$

modified Slavnov-Taylor Identity (mSTI)

5.7.5. modified STI at work

Here we discuss a crucially important example for the consequences of the mSTIs, the gluon mass term. First we recall, that the standard STI entails that the quantum corrections of the gluon two point function, $\Gamma_{AA}^{(2)}$ are purely transversal. To that end we take a ghost and gluon derivative of the master equation at vanishing regulator, $\mathcal{R}_k = 0$, and at the equations of motion at vanishing BRST sources, with $Q_\Phi = 0$ given by $\Phi_0 = (0, B_{\text{EoM}} = 1/\xi \partial_\mu A_\mu)$, see (5.118).

$$\frac{\delta^2}{\delta A_\mu(x) \delta c(y)} \left[\frac{\delta \Gamma}{\delta Q_\Phi} \cdot \frac{\delta \Gamma}{\delta \Phi} \right]_{\Phi=0, Q=0} = \left[\frac{\delta}{\delta c(y)} \frac{\delta \Gamma}{\delta Q_{A,\nu}} \right] \cdot \left[\frac{\delta}{\delta A_\mu(x)} \frac{\delta \Gamma}{\delta A_\nu} \right] + \left[\frac{\delta}{\delta A_\mu(x)} \frac{\delta \Gamma}{\delta Q_{\bar{c}}} \right] \cdot \left[\frac{\delta}{\delta c(y)} \frac{\delta \Gamma}{\delta \bar{c}} \right] \Big|_{\Phi=0, Q=0} = 0. \quad (5.146)$$

No we use the anti-ghost equation (5.136) and arrive at

$$\left[\frac{\delta}{\delta c(y)} \frac{\delta \Gamma}{\delta Q_{A,\nu}} \right] \cdot \left[\Gamma_{AA,\nu\mu}^{(2)} - \partial_\mu \frac{\delta}{\delta A_\mu(x)} \frac{1}{\xi} \partial_\nu A_\nu \right] \Big|_{\Phi=0, Q=0} = 0, \quad (5.147)$$

where we have also used that $\delta \Gamma / \delta Q_{\bar{c}} = B_{\text{EoM}} = 1/\xi \partial_\mu A_\mu$.

The c -derivative of the BRST-variation of the gauge field at vanishing fields and BRST sources is proportional to p_ν in momentum space. No other Lorentz vector is present. Then, the STI in momentum space follows as

$$p_\nu \Gamma_{\nu\mu}^{(2)} = \frac{1}{\xi} p^2 p_\mu = p_\nu S_{\text{gf},\nu\mu}^{(2)}. \quad (5.148)$$

We immediately conclude from (5.148) that the longitudinal wave function renormalisation

$$Z_A^\parallel(p) = \lambda_{AA}^{(2)}(p), \quad (5.149)$$

with the longitudinal tensor structure $\mathcal{T}_{AA}^{(2)}$ defined in (5.77) is trivial within a gauge invariant regularisation and reads

$$Z_A^\parallel = \frac{1}{\xi}. \quad (5.150)$$

Now we proceed to the modified STI. There we get loop contributions from the right hand side from (5.145). Including a regulator matrix $\mathcal{R}_k = S^{(2)} r(y)$ with $r_a(y) = r_c(y) = r(y)$ and $y = p^2/k^2$, we obtain at one loop level

$$(m^\parallel)^2 = \alpha_s \frac{N_c}{4\pi} k^{d-2} \int dy y^{\frac{d}{2}-2} \frac{r(g)}{(1+r(g))^2} \left(\frac{11}{2} - d - \frac{5}{d} + \xi \left(1 - \frac{1}{d} \right) + \left(\frac{7}{2} - \frac{6}{d} \right) \frac{y \partial_y r}{1+r(y)} \right) \gtrless 0. \quad (5.151)$$

6. Chiral symmetry breaking in QCD

In the last chapters we have discussed the computation of correlation functions in pure Yang-Mills theory. By now the results for Yang-Mills correlation functions are on a quantitative level. In [Chapter 3](#) we also have discussed low energy effective theories of QCD. It is left to show, how to connect the UV sector of QCD with dynamical quarks and gluons with the IR sector with dynamical hadrons.

In [Appendix E](#) it is discussed, how this comes about qualitatively: loop diagrams in QCD generate four-fermi interactions which allows us to define low energy NJL-type theories or quark-meson theories. In the present chapter we show how this idea can be made quantitative within the FRG approach.

6.1. Apparent convergence

The emergence of dynamical low energy degrees of freedom that take over the dynamics of the fundamental microscopic degrees of freedom has a very concise formulation within the FRG approach.

6.1.1. Success & failure

Moreover, in the first part of the lecture course we have discussed apparent convergence of systematic approximation schemes and in particular of the vertex expansion as used in QCD, see [Section 2.3.3](#): this approximation scheme typically shows a very rapid convergence, and our Yang-Mills results confirm this for the glue sector in QCD. This rapid convergence is based on two pillars,

- (i) Phase space suppression: diagrams with higher order vertices, that originate from quantum effects and are not present in the classical action, typically come with large suppression factors due to the angular integrations.
- (ii) Finite couplings: the total suppression of diagrams is proportional to the phase space suppression multiplied by the coupling or vertex strengths of the vertices involved. In turn, the phase space suppression can be undone by large or even diverging couplings.

Heuristically both the occurrence of apparent convergence and its potential failure in the vertex expansion can be explained as follows. Higher order vertices involve the scattering of multiple particles or fields, in QCD these are ghosts, gluons and quarks. In the absence of large correlation and scattering lengths these scatterings are of rather point-like nature. Consequently multi-scatterings are suppressed as they are less probable: for a scattering of n fields these fields have to meet at a small space-time area. This is what is behind the phase space suppression.

This small probability can only be overcome by two effects:

- (i) large density of the fields involved
- (ii) resonant interactions

6.1.2. Resonant interactions and large densities in QCD

Both phenomena are important in QCD. The first effect, (i), is present if increasing, for example, the baryon or quark density, or the isospin density, the small probability of multi-scattering of quarks is

overcome. Far from non-equilibrium situations, as e.g. present in the early stages of a heavy-ion collision, the gluons are overoccupied which also overcomes the phase space suppression.

The second effect, (ii), is already present in vacuum QCD: at low energies hadrons are forming, which manifests itself in resonant interaction channels in multi-fermion vertices, see [Chapter 3](#) and [Appendix E](#). For mesons this simply amounts to considering resonant channels with the same quantum numbers as the mesons. For baryons the formation is expected to happen predominantly in steps, first a diquark is forming via a resonant diquark channel in the four-quark interaction, and then the diquark scatters with a quark into a baryon via a resonant quark-diquark interaction. While present, the baryon channel in the twelve quark scattering vertex is supposedly subdominant. Indeed, this picture is confirmed in explicit computations with Bethe-Salpether equations (BSE), utilising DSE input, see [\[6\]](#).

This leaves us with a consistent, but rather difficult task in Minkowski space, to take all the hadron resonances into account successively. In turn, in Euclidean space the scale ordering is very helpful: the Euclidean momentum scale of chiral symmetry breaking and of hadronisation is of the order of a couple of 100 MeV. For the cutoff scale this is $k_{\text{had}} \approx 500$ MeV. At this scale hadrons are forming. While the pions, and to some extend also the σ , are still dynamical off-shell below this scale, the off-shell dynamics of the other hadronic resonances is suppressed. In summary, it is expected that the pseudoscalar pion channel, and the scalar σ channel in the four-quark interaction are resonant, but the others do not play a rôle. This is indeed confirmed in the explicit computation.

6.1.3. Off-shell fluctuations and on-shell expansions

We close this discussion with an important remark that is often overlooked: the suppression of the higher hadronic resonance takes place in the diagrams in the flow equations, it is *off-shell*. It does not entail at all, that these resonances do not play an important rôle on-shell. This subtlety explains for example, that important thermodynamical observables such as the pressure or the scale anomaly, related to the free energy $\Gamma[\Phi_{\text{EoM}}]$, can be computed in a relatively straightforward manner within the FRG approach from the knowledge of the gluon, ghost and quark two-point function. In turn, within a hadron resonance gas approach, this requires taking into account hundreds of resonances. Loosely speaking, the latter approach expands the off-shell loops in the flow equation for the effective action in terms of asymptotic hadronic states. Such an expansion has a bad convergence. In turn, the off-shell expansion converges rapidly due to the suppression factors $m_{\text{had}}^2/k_{\text{had}}^2 \ll 1$ for the off-shell effects of higher hadronic resonances.

6.2. Dynamical hadronisation

With the discussion in the previous chapter we now concentrate on the introduction of dynamical effective degrees of freedom for the scalar and pseudo-scalar channels of the general four-quark scattering vertex $\Gamma_{qq\bar{q}\bar{q}}^{(4)}$. In low energy effective theories this is done with the Hubbard-Stratonovitch transformation discussed in detail in [Section 2.4](#), [Chapter 3](#), [Appendix E](#).

6.2.1. Flows with composite operators

In the FRG approach this transformation has a natural analogue which goes beyond the classical identification of a composite field. It has been introduced as *rebozonisation* in [\[95\]](#). There the original Hubbard-Stratonovitch (HS) transformation of the scalar and pseudo-scalar bilinear fermionic operators into the scalar and psuedo scalar mesonic σ and $\vec{\pi}$ fields have been discussed. This transformation has been introduced in a scale-dependent way, allowing for a vanishing flow of the four-quark coupling λ_q of the scalar–pseudo-scalar channel, for the definitions see [Appendix E](#),

$$\partial_t \lambda_q = 0, \quad (6.1)$$

A first application to chiral symmetry breaking QCD can be found in [96], see also [97]. The setup in [95, 96] as well as in [98, 99] can be understood as a scale-dependent version of the HS-transformation and draws a lot from this analogy. Note however, that it goes qualitatively beyond the HS transformation as it removes the respective channel of the four-quark interaction on the level of the full quantum effective action.

In the present lecture notes we use the more general approach put forward in [9]. In this form it has been applied to QCD in [53, 52, 55]. This approach relies on the introduction of sources for the composite operators, that are then defined only implicitly via their flow. This allows for the introduction of generic composite operators beyond quadratic or bilinear ones as used in [95, 96]. For this general case it has been applied in [72, 75].

Due to its universal applicability to general bound state/resonance and condensation phenomena it is now called *Dynamical Condensation*, and more specifically *Dynamical Hadronisation* in QCD.

The starting point of this approach is the generating functional for QCD, $\mathcal{Z}[J_\varphi]$, see (5.35). Here, φ is the superfield of the fundamental degrees of freedom of QCD,

$$\hat{\varphi} = (\hat{A}_\mu, \hat{c}, \hat{\bar{c}}, \hat{q}, \hat{\bar{q}}), \quad \text{with} \quad \varphi = \langle \hat{\varphi} \rangle, \quad (6.2)$$

possibly also containing the Nakanishi-Laudrup field, and J_φ are the respective currents. For the present analysis we drop the Nakanishi-Laudrup field as well as the BRST sources. As the present analysis involves some intricacies and requires a careful distinction between the mean field and the fluctuation field, we for once distinguished the two fields in (6.2): mean field is φ , it is the expectation value of the fluctuation field/field operator $\hat{\varphi}$, which is integrated over.

We now add a source term for the cutoff-dependent composite field $\hat{\phi}[\varphi]$, related to the scalar and pseudo-scalar fermionic bilinears. The respective superfield (mean field) is

$$\Phi = (A_\mu, c, \bar{c}, q, \bar{q}, \phi), \quad \text{with} \quad \phi = \langle \hat{\phi} \rangle. \quad (6.3)$$

In the presence of a source term $\int J_\phi \hat{\phi}$ for the composite field the generating functional (5.35) turns into

$$\mathcal{Z}[J] = \int [d\hat{\varphi}] e^{-S_{QCD}[\hat{\varphi}] - \Delta S_k[\hat{\varphi}, \hat{\phi}] + \int_x (J_\varphi \cdot \hat{\varphi} + J_\phi \hat{\phi})}, \quad (6.4)$$

with

$$J = (J_\varphi, J_\phi), \quad J_\varphi = (J_A, J_c, J_{\bar{c}}, J_q, J_{\bar{q}}). \quad (6.5)$$

The cutoff term $\Delta S_k[\varphi, \hat{\phi}]$ also contains a cutoff term for the composite field,

$$\Delta S_k[\hat{\Phi}] = \frac{1}{2} \Phi_i R_k^{ij} \Phi_j. \quad (6.6)$$

The effective action is now defined with the modified Legendre transform with respect to all currents, J . From its form it reads the same as in 5.45,

$$\Gamma_k[\Phi] = \int_x J \cdot \Phi - \mathcal{W}_k[J] + \Delta S_k[\Phi], \quad \text{with} \quad \Delta S_k[\Phi] = \frac{1}{2} \Phi_i R^{ij} \Phi_j. \quad (6.7)$$

The effective action $\Gamma_{QCD}[\Phi] = \Gamma_{k=0}[\Phi]$ defined in (6.7) is the action of first principle QCD in the following sense: the latter action, $\Gamma_{QCD}[\varphi] = \Gamma_{k=0}[\varphi]$, is obtained from (6.7) on the EoM for ϕ ,

$$\Gamma_{QCD}[\varphi] := \Gamma_{QCD}[\varphi, \phi_{EoM}[\varphi]], \quad \text{with} \quad \left. \frac{\delta \Gamma_{QCD}[\Phi]}{\delta \phi} \right|_{\phi=\phi_{EoM}[\varphi]} = 0 \quad (6.8)$$

On the equations of motion we have $J_\phi = 0$ and the generating functional $\mathcal{Z}[J]$ reduces to $\mathcal{Z}[J_\varphi]$. We also emphasise that the correlation functions of quarks and gluons in QCD are obtained by taking the respective field derivatives of the hadronised effective action after the EoM of ϕ is used: $\phi_{\text{EoM}}[\varphi]$ depends on the fundamental fields φ and is hit by the φ -derivatives.

Now we briefly discuss the Legendre transform (6.7) in the presence of a composite operator, more details can be found in [9]. In order to have an explicit, simple but also relevant example we choose $\hat{\phi}(x) = \hat{\bar{q}}(x)\hat{q}(x)$. Then the Legendre transform in (6.7) involves the diagonal part of the scalar quark two-point function. Indeed, we have introduced the chiral condensate $\langle \hat{\bar{q}}(x)\hat{q}(x) \rangle$ as a field, as

$$\phi(x) = \frac{\delta W[J]}{\delta J_\phi(x)} = \langle \hat{\phi}(x) \rangle = \langle \hat{\bar{q}}(x)\hat{q}(x) \rangle_{\text{con}} + \bar{q}(x)q(x), \quad (6.9)$$

with $\langle \hat{\bar{q}}(x)\hat{q}(x) \rangle_{\text{con}} = \text{tr } G_{\bar{q}q}$, where the trace tr sums over Dirac, group and flavour indices. Note that the mean field term $\bar{q}(x)q(x)$ in (6.9) is already determined, and can be subtracted in the source term in (6.7) with

$$\int_x J_\phi(x)\phi(x) \rightarrow \int_x J_\phi(x)[(\phi(x) + \bar{q}(x)q(x))], \quad (6.10)$$

which is a two-point particle irreducible (2PPI) formulation. The latter is reminiscent to a 2PI formulation. There, however, a current is introduced for the full two-point function, in the present example $\bar{q}(x)q(y)$. Another important example for a 2PPI formulation is a composite field for $\bar{q}(x)\gamma_0 q(x)$, with $\phi(x) = n(x)$, the density. This leads to density functional theory.

While (6.10) can be used in the present formulation, and allows for a more standard interpretation of the composite field, it also complicates the flow equations due to the implicit dependences. Therefore we refrain from introducing the mean field term in the current and stick to (6.7). Moreover, we do not aim for an explicit definition of the operator $\hat{\phi}$, but rather of the expectation value of its t -derivative $\langle \partial_t \hat{\phi} \rangle$. This is possible as the flow equation can be shown to only depend on the latter, and does not require the explicit definition of $\hat{\phi}$.

This fact can be seen by taking a t -derivative of the effective action with $\partial_t \Gamma[\Phi] = \partial_t W[J]$, where both derivatives are taken at fixed argument of the respective functional. This leads us to

$$\partial_t \Gamma[\Phi] = \frac{1}{2} \langle \hat{\Phi}_i (\partial_t R_k^{ij}) \hat{\Phi}_j \rangle + \langle \hat{\phi} R_\phi \partial_t \hat{\phi} \rangle - \int_x J_\phi \langle \partial_t \hat{\phi} \rangle - \frac{1}{2} \Phi_i (\partial_t R_k^{ij}) \Phi_j. \quad (6.11)$$

The first term on the right hand side of (6.11) is the standard flow term $1/2 \text{Tr } G_k \cdot \partial_t R_k$, while the other two terms originate in the potential t -dependence of the composite operator $\hat{\phi}$. The last term is already proportional to $\langle \partial_t \hat{\phi} \rangle$, while the second one is a non-trivial correlation function. There we resort to the standard procedure and pull out the field $\hat{\phi}$ in terms of a j -derivative with (1.12), to wit

$$\langle \hat{\phi} R_\phi \partial_t \hat{\phi} \rangle = \left(G_{\phi \Phi_i} \frac{\delta}{\delta \Phi_i} + \phi \right) R_\phi \langle \partial_t \hat{\phi} \rangle. \quad (6.12)$$

This leads us to the flow equation in the presence of a generic composite operator in terms of the mean of its t -derivative,

$$\partial_t \Gamma[\Phi] + \int_x \langle \partial_t \hat{\phi} \rangle \frac{\delta \Gamma[\Phi]}{\delta \phi} = \frac{1}{2} G_{ij} \partial_t R_k^{ij} + G_{\phi \Phi_i} \frac{\delta}{\delta \Phi_i} R_\phi \langle \partial_t \hat{\phi} \rangle + \left(\phi R_\phi - \int_x \frac{\delta \Delta S_k[\Phi]}{\delta \phi} \right) \langle \partial_t \hat{\phi} \rangle. \quad (6.13)$$

In (6.13) we have used that

$$J_\phi = \frac{\delta(\Gamma[\Phi] + \Delta S_k[\Phi])}{\delta \phi}. \quad (6.14)$$

The term in parenthesis in (6.13) vanishes and we are left with the standard flow and two additional terms proportional to $\langle \partial_t \hat{\phi} \rangle [\Phi]$. We simply have to choose this function in terms of the mean superfield Φ in order to get a closed equation. This does not require the definition of the operator $\hat{\phi}$ or $\partial_t \hat{\phi}$, however it requires that the choice for $\langle \partial_t \hat{\phi} \rangle [\Phi]$ is consistent with being an expectation value. In an abuse of notation we shall write

$$\partial_t \phi_k [\Phi] := \langle \partial_t \hat{\phi} \rangle [\Phi]. \quad (6.15)$$

We emphasise again that $\partial_t \phi_k [\Phi]$ is at our disposal and has but nothing to do with the t -derivative of ϕ which vanishes identically: $\partial_t \phi \equiv 0$. This leads us to our final flow equation in the presence of composite operators,

$$\left(\partial_t + \partial_t \phi [\Phi] \frac{\delta}{\delta \phi} \right) \Gamma [\Phi] = \frac{1}{2} \text{Tr} \frac{1}{\Gamma^{(2)} [\Phi] + R_k} \partial_t R_k + \text{Tr} \left[\frac{1}{\Gamma^{(2)} [\Phi] + R_k} \right]_{\phi \Phi_i} \frac{\delta \partial_t \phi [\Phi]}{\delta \Phi_i} \partial_t R_\phi. \quad (6.16)$$

Flow Equation with Dynamical Hadronisation

Equation (6.16) allows us to remove the scalar and pseudo-scalar momentum channels of the four-quark interaction. To that end we choose the function $\partial_t \phi_k [\Phi]$ with an overlap with $\bar{q}(x) q(x)$ and $\bar{q}(x) \gamma_5 \vec{\tau} q(x)$: its square ϕ^2 should have an overlap with the scalar and pseudoscalar four-quark channels. We define

$$\partial_t \phi_k = \partial_t A_k \begin{pmatrix} \bar{q} q \\ i \bar{q} \gamma_5 \vec{\tau} q \end{pmatrix} + \partial_t B_k \phi = \partial_t A_k \bar{q} \tau q + \partial_t B_k \phi, \quad (6.17)$$

with $\vec{\tau} = (\sigma_1, \sigma_2, \sigma_3)$, see (3.117) and $\tau = (1\!\!1, i \gamma_5 \vec{\tau})$. Note that (6.17) entails that the operator $\partial_t \hat{\phi}$ is highly non-trivial: it cannot depend on the mean fields, but its expectation value contains a simple product of the latter. In a given approximation in the vertex expansion this can be arranged for in an expansion in powers of field operators. Note also, that (6.17) can be easily integrated, its solution being

$$\phi_k = A_k \bar{q} \tau q + B_k \phi, \quad (6.18)$$

Both, (6.17) and (6.18) do not fix $\hat{\phi}$ or $\partial_t \hat{\phi}$. Indeed $\hat{\phi} \neq \phi_k$ and similarly for $\partial_t \hat{\phi}$: the operators cannot depend on the mean fields as this would spoil the Legendre transform, or rather the relations between derivatives of \mathcal{W} and Γ .

Practically, in the vertex expansion used in QCD we do not have to resolve this issue, and simply use (6.17). In a given order of the vertex expansion with a maximal power of fields, N_{\max} this leads to the following condition: we expand the operator $\partial_t \hat{\phi}$ in correlation functions,

$$\partial_t \hat{\phi} = \sum_n c^{i_1 \dots i_n} \hat{\Phi}_{i_1} \dots \hat{\Phi}_{i_n}, \quad (6.19)$$

Equation (6.19) has the expectation value

$$\partial_t \phi [\Phi] = \sum_n \frac{1}{n!} d^{i_1 \dots i_n} \Phi_{i_1} \dots \Phi_{i_n}. \quad (6.20)$$

with the $c^{i_1 \dots i_n}$ -dependent expansion coefficients

$$d^{i_1 \dots i_m} = \sum_n c^{i_1 \dots i_n} \left[\prod_{j=1}^m \frac{\delta}{\delta \Phi_{i_j}} \langle \hat{\Phi}_{i_1} \dots \hat{\Phi}_{i_n} \rangle [\Phi] \right]_{\Phi=0}. \quad (6.21)$$

where we have assumed an expansion about $\Phi = 0$ for the sake of simplicity. Then, (6.17) in the given order N_{\max} of the vertex expansion requires

$$d^i = \delta^{\beta \phi} \partial_t B_k, \quad d^{ij} = (\delta^{\beta \bar{q}} \delta^{jq} - \delta^{\beta q} \delta^{j\bar{q}}) \partial_t A_k, \quad d^{i_1 \dots i_n} = 0 \quad \text{for } n \geq 3. \quad (6.22)$$

The condition (6.22) can always be satisfied, but of course we cannot guarantee the convergence of the expansion. We consider the latter a rather academic problem.

6.2.2. BRST Master equation with composite fields

The approach of dynamical hadronisation or more generally dynamical condensation is based on the simple introduction of additional sources for composite operators. In our physically relevant example we discussed scalar and pseudoscalar mesonic fields. Even in this case we could also have considered diquark channels of the four-quark interaction. There, the respective quark bilinear is $q(x)\mathcal{T}_{\text{diquark}}q(x)$ with a diquark tensor structure $\mathcal{T}_{\text{diquark}}$, for the complete basis of four-quark interactions for $N_f = 2$ see [Appendix E](#). The related four-quark interaction is schematically written by

$$\text{tr } q(x)\mathcal{T}_{\text{diquark}}q(x)\bar{q}(x)\gamma_0\mathcal{T}_{\text{diquark}}^\dagger\gamma_0\bar{q}(x). \quad (6.23)$$

The diquark operator carries colour and hence is not directly related to an asymptotic state. However, off-shell diquark fluctuations are potentially relevant at large densities, see e.g. [\[100, 19\]](#). If including this channel via dynamical hadronisation, hence adding a source term, the master equation [\(5.143\)](#) changes accordingly. We rely on the formulation with the Nakanishi-Laudrup field with an exact BRST operator \mathfrak{s} with $\mathfrak{s}^2 = 0$. We simply add a BRST source term [\(5.115\)](#) further sources for the BRST variation of the composite fields ϕ_i ,

$$\int_x Q \cdot \mathfrak{s}\Phi = \int_x (Q_A \mathfrak{s}A + Q_c \mathfrak{s}c + Q_{\bar{c}} \mathfrak{s}\bar{c} + Q_{\phi_i} \mathfrak{s}\hat{\phi}_i), \quad (6.24)$$

where we have allowed for several composite fields $\hat{\phi}_i$ with $i = 1, \dots, n$. Now we use that the path integral representation of the generating functional $\mathcal{Z}[J, Q]$ has not changed, only the currents are now given by [\(6.5\)](#) and [\(6.24\)](#). Hence the modified BRST master equation looks the same as without the composite operators, and is given by [\(5.143\)](#).

Seemingly we still have a problem as the dynamical hadronisation procedure introduced here relies on an implicit definition of the operator $\hat{\phi}$. Only the expectation value of its flow is required, see [\(6.17\)](#) for our mesonic example. However, this is enough to deduce the BRST transformations on mean field level, and hence classically. For our mesonic example we infer from the explicit mean field solution ?? $\phi_{\text{classical}} \propto \bar{q}\tau q$ and hence

$$\mathfrak{s}\phi_{\text{classical}} = 0, \quad (6.25)$$

and hence it drops out completely: its flow is proportional to the Q_ϕ -derivative of $\Gamma^{(2)}$ which vanishes,

$$\partial_t \frac{\delta \Gamma}{\delta Q_\phi} = -\frac{1}{2} \text{Tr } G_k \partial_t \frac{\delta \Gamma^{(2)}}{\delta Q_\phi} G_k \partial_t R_k. \quad (6.26)$$

We start with a vanishing Q_ϕ -derivative of $\Gamma[\Phi, Q]$, and as its flow is proportional to a Q_ϕ -derivative, no dependence is generated.

In the generic flow the deduction of $\phi_{\text{classical}}$ may be more difficult. Then we can infer the Q_ϕ -derivative from the the expectation value $\langle \hat{\phi} \rangle$. A BRST transformation of the integration fields $\hat{\phi}$ is a simple reparameterisation. As the action and the BRST sources are BRST invariant, we are led to

$$\langle \mathfrak{s}\hat{\phi} \rangle + \langle \hat{\phi} \int_x J \cdot \mathfrak{s}\Phi \rangle - \langle \hat{\phi} (\mathfrak{s}\Phi_i) R_k^{ij} \Phi_j \rangle = 0. \quad (6.27)$$

In terms of the effective action and its derivative this reads

$$\frac{\delta \Gamma}{\delta Q_\phi} + \frac{\delta \Gamma}{\delta \Phi_i} \left(G_{\phi\Phi_j} \frac{\delta}{\delta \Phi_j} + \phi \right) \left[\frac{\delta \Gamma}{\delta Q_{\Phi_i}} - R^{ij} G_{jl} \frac{\delta^2 \Gamma_k[\Phi, Q]}{\delta \Phi_l \delta Q^i} \right] = 0. \quad (6.28)$$

which can be resolved (iteratively) for the RBST-variation w.r.t. Q_ϕ . In particular, we can extract $\mathfrak{s}\phi_{\text{classical}}$.

6.2.3. Dynamical hadronisation at work

In this chapter we sketch the application of the above framework of dynamical hadronisation. We have introduced it in order to control resonant channels of four-quark interactions. Let us now discuss the flow of the four-quark coupling λ_q in a minimal approximation with

$$\Gamma_{\text{QCD}}[\Phi] = \Gamma_{\text{QCD}}[\varphi] + \int_x \left\{ -\frac{1}{2}\phi \partial^2 \phi + V_k(\rho) + \frac{h_\sigma}{2} \bar{q} (\sigma + i\gamma_5 \vec{\tau} \vec{\pi}) q - \frac{\lambda_q}{4} \int_x [(\bar{q} q)^2 - (\bar{q} i\gamma_5 \vec{\tau} q)^2] \right\}, \quad (6.29)$$

where $\Gamma_{\text{QCD}}[\varphi]$ comprises all terms that do not depend on the composite field ϕ . Let us now consider the flow equation of the scalar channel of the four-quark interaction in the symmetric regime with the expansion point $\Phi = 0$. We take the forth quark–anti-quark derivative in the scalar channel at vanishing fields and consider the left hand side of (6.16) and vanishing momentum.

$$\begin{aligned} \frac{\delta^2}{\delta(\bar{q}q)^2} \left[\partial_t \Gamma + \int_x \partial_t \phi \frac{\delta \Gamma}{\delta \phi} \right]_{\Phi=0} &= \partial_t \Gamma_{(\bar{q}q)(\bar{q}q)}^{(4)}[0] + 2\partial_t A_k \Gamma_{(\bar{q}q)\phi}^{(3)}[0] \\ &= \frac{1}{2} \partial_t \lambda_q + \partial_t A_k h_\sigma. \end{aligned} \quad (6.30)$$

The right hand side of the flow equation is given by a sum of flow diagrams, $\text{Flow}_{(\bar{q}q)(\bar{q}q)}^{(4)}$, depicted in ???. We demand a vanishing flow for λ_q and arrive at

$$\partial_t A_k = -\frac{1}{h_k} \text{Flow}_{(\bar{q}q)(\bar{q}q)}^{(4)} \quad \leftrightarrow \quad \partial_t \lambda_q = 0. \quad (6.31)$$

Equation (6.31) determines the free coefficient $\partial_t A_k$. Note that it is an implicit equation as the right hand side also depends on $\partial_t A_k$ via the last term in the flow (6.16). Typically, this term is dropped in applications.

7. QCD at finite temperature

7.1. Confinement

In Chapter 6 we have discussed the emergence of strong chiral symmetry breaking in QCD which is ultimately related to the growth of the strong coupling $\alpha_s(p^2)$ towards the infrared, $p^2 \rightarrow 0$. This growth triggers a growth in the four-quark interaction that develops a resonance at the chiral symmetry breaking (momentum) scale. It is also the simplicity of this mechanism or better its representation in terms of correlation functions that allowed us to derive a relatively simple low energy effective theory that incorporates strong chiral symmetry breaking in QCD.

In Section 3.2 this setup was used to explore strong chiral symmetry breaking at finite temperature. Thermal fluctuations decrease the strong coupling $\alpha_s(p^2)$ and finally melt-down chiral symmetry breaking. This is monitored in a simple way by the temperature-dependence of the chiral order parameter, the expectation value of the scalar sigma field, $\sigma_0 \propto \langle \bar{\psi}\psi \rangle$.

We hope for a similarly simple picture for the phenomenon of confinement in the formulation of QCD in terms of correlation functions. Indeed we shall see that while the mechanism and dynamics of confinement is rather intricate in comparison, we have simple signatures of confinement in terms of its order parameter, the potential of which can be derived from low order correlation functions of quarks and gluons. It also allows us to extend the low energy EFTs introduced and used in the last chapters to also incorporate confinement. This set-up then enables us to study the confinement-deconfinement phase transition at finite temperature as well as the full phase structure at finite temperature and density. Before we start, a word of caution is required: this fascinating area has been the subject of intense studies over the past decades and has many facets ranging from mathematical physics -and in particular topological considerations- to phenomenological applications and the relation of the confinement dynamics to hadronic properties of QCD. Here we only can scratch the surface and shall take a practical approach: the lecture aims at being self-contained for the computations discussed, other equally interesting subjects are mentioned but not detailed. A fully comprehensive study is way beyond the scope of the current lecture course.

To begin with we discuss the question of the symmetry behind confinement and the related order parameter. For having a clean setting we restrict ourselves to pure Yang-Mills theory with static quark sources. Then confinement is the phenomenon that a quark–anti-quark pair experiences a linear potential when pulled apart. The expectation value of such a state $\langle O_{q\bar{q}}(\vec{x}, \vec{y}) \rangle$ with a static quark q at the position \vec{x} and a static anti-quark \bar{q} at the position \vec{y} is related to its free energy $F_{q\bar{q}}$,

$$\langle O_{q\bar{q}}(\vec{x}, \vec{y}) \rangle \propto e^{-F_{q\bar{q}}(r)}, \quad r = \|\vec{x} - \vec{y}\|. \quad (7.1)$$

In (7.1) we have used translation invariance present in an infinite volume, and hence the free energy only depends on the distance r between the quark and the anti-quark. For small distances the strong coupling $\alpha_s(p \propto 1/r \rightarrow \infty) \rightarrow 0$ gets small and perturbation theory is applicable. Therefore we expect a Coulomb-type potential with a $1/r$ dependence for $r \rightarrow \infty$. At large distances $r \rightarrow \infty$ the strong coupling grows large and perturbation theory is not applicable anymore. In this regime confinement predicts a linear dependence of the free energy/potential on r . This leads us to

$$\lim_{r \Lambda_{\text{QCD}} \rightarrow 0} F_{q\bar{q}}(r) \propto \frac{1}{r} \quad \text{and} \quad \lim_{r \Lambda_{\text{QCD}} \rightarrow \infty} F_{q\bar{q}}(r) \propto \sigma r, \quad (7.2)$$

where $\sigma \propto (420) \text{ MeV}^2$ in pure Yang-Mills theory is the string tension. As remarked before there are no scales in pure Yang-Mills theory except the dynamical scale Λ_{QCD} , so the explicit value above is up to our disposal, and we should rather determine a ratio of scales such as $\sqrt{\sigma}/\Lambda_{\text{QCD}}$. Typically the string tension is used to gauge other observables such as the critical temperature of the confinement-deconfinement phase transition at finite temperature. We will come back to this point later.

7.1.1. Order parameters for confinement

The computation of the expectation value in (7.1) enables us at vanishing temperature to monitor the r -dependence of the free energy of a $q\bar{q}$ -pair. It also provides us with an order parameter for confinement: to that end we consider the limit $r \rightarrow \infty$. If confinement is present the free energy tends towards infinity in this limit and the expectation value $\langle O_{q\bar{q}} \rangle$ vanishes. In turn, if we still had a Coulomb-type potential for large distances we get a finite value for $\langle O_{q\bar{q}} \rangle$. This is what we expect for large temperature. As we have seen in the discussion of chiral symmetry breaking at finite temperature, increasing temperatures effectively increases the energy scale of the system. This heuristic argument is discussed in more details later. In summary we expect

$$\lim_{r \rightarrow \infty} \langle O_{q\bar{q}} \rangle = \begin{cases} 0, & T < T_{\text{conf}} \\ > 0, & T > T_{\text{conf}} \end{cases}. \quad (7.3)$$

Accordingly, we have a clear signature for the confining phase as well as the deconfining phase. The above discussion also makes clear why we restricted ourselves first to pure Yang-Mills theory with static quarks: in the presence of dynamical quarks quark–anti-quark pairs can be created if the potential $V_{q\bar{q}}$ between quark and anti-quark is large enough. These additional q, \bar{q} can bind with the original pair into new $q\bar{q}$ pairs. This leads to a shielding of color force between the original pair and the effective potential levels at a finite value for $r \rightarrow \infty$.

The operator $O_{q\bar{q}}$ is discussed in detail in [Appendix F.5](#) and [Appendix F.6](#). Here we simply summarise that the expectation value of a quark–anti-quark pair at the respective positions \vec{x} and \vec{y} is given by

$$\langle \bar{q}(y) \mathcal{W}_{C_{y,x}}[A] q(x) \rangle, \quad (7.4)$$

with the Wilson line

$$\mathcal{W}_{C_{x,y}}[A] = \mathcal{P} e^{-i g \int_{C_{x,y}} A_\mu(z) dz_\mu}, \quad (7.5)$$

where \mathcal{P} is the path ordering operator. For more details see [Appendix F.5](#), and in particular the discussion below (F.38), leading to (F.45).

A static quark–anti-quark pair is generated in QCD in the infinite quark mass limit. Then the quark–anti-quark pair is generated at the initial time t_0 and is annihilated at the final time t_1 . Moreover, the quark is simply sitting at the position \vec{x} , and the anti-quark is sitting at the position \vec{y} , keeping the distance $L = \|\vec{x} - \vec{y}\|$ for all times. The respective closed worldline C is shown in [Figure 7.1](#).

Accordingly, for this worldline the operator in (7.4) is proportional to the traced closed Wilson line, the Wilson loop. We are led to

$$W[L, T] = \langle \text{tr}_f \mathcal{W}_C \rangle, \quad \mathcal{W}_C = \mathcal{P} e^{-i g \oint_C A_\mu(z) dz_\mu}. \quad (7.6)$$

In the limit, where the time T tends towards infinity, the correlation function (7.6) is proportional to the exponential of the interaction energy $E(L)$ of this state (times T). All other contributions vanish exponentially fast with $(E_i - E(L))T > 0$, where E_i is the energy of the related state. We have

$$\lim_{T \rightarrow \infty} W[L, T] = F(L) E^{-E(L)T}, \quad (7.7)$$

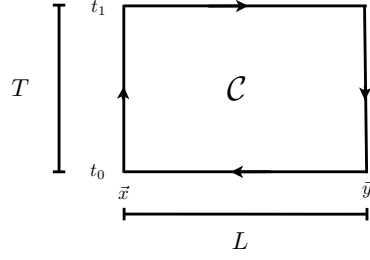


Figure 7.1.: $\bar{q}(y)q(x)$ pair.

which relates to the exponential of the free energy of a static quark–anti-quark state. The prefactor $F(L)$ relates to the overlap of the Wilson loop with the ground state. In the confining phase the Wegner-Wilson loop is given by $W[T, L] \simeq e^{-F_{\bar{q}q}[T, L]}$ with $F_{\bar{q}q}[T, L]$ having a linear dependence on both L and T . The linear dependence in L we have discussed before. The linear dependence in T simply follows from the fact that in our Euclidean formulation the time direction is not different from the spatial ones. Hence we conclude

$$\lim_{L, T \rightarrow \infty} W[T, L] \simeq e^{-\sigma LT}, \quad (7.8)$$

with the string tension σ . [Equation \(7.8\)](#) is the area law that signals confinement as does the linear potential. It is left to discuss the symmetry behind the confinement-deconfinement phase transition. This will be discussed in chapter [7.2](#).

In [Appendix F.6](#) the Wilson loop is computed in QED at one loop as an illustrative example. As expected, we arrive at the Coulomb potential, [\(F.51\)](#),

$$V_{e^+e^-}(L) = -\frac{e^2}{4\pi} \frac{1}{L}. \quad (7.9)$$

Note also that the L -dependence in [\(7.9\)](#) already follows from dimensional arguments without any further computation.

Adapting, within a bold step, the above analysis in QCD within a Gaussian approximation (no self-interaction of the gluons), we are led to the same result, up to a colour factor $\text{tr}_f t^a t^a = N_c C_F = (N_c^2 - 1)/2$. This is to be expected in perturbation theory, which is what the Gaussian approximation relies on.

In turn, relying on this approximation also in the non-perturbative confining sector of QCD or Yang-Mills theory, the static potential has the behaviour $V_{q\bar{q}} \sim L$, it is linear in the distance between quark and anti-quark. This requires a gluon propagator

$$\lim_{p \rightarrow 0} \langle A_\mu(p) A_\nu(-p) \rangle \propto \frac{1}{(p^2)^2}, \quad (7.10)$$

which is the limit of what is allowed in a covariant local quantum field theory. [Equation \(7.10\)](#) suggests gluon dominance (over the ghost) in the infrared. Indeed, such propagators have been computed in the Landau gauge in the Mandelstam approximation (no ghosts). However, it turns out that in the Landau gauge the gluon propagators are not infrared enhanced as [\(7.10\)](#) but infrared suppressed. Moreover, any n -loop contribution (even in full propagators and vertices) to the Wilson loop expectation value does not show the required linear behaviour, it only comes about by a full resummation of all diagrams. Nonetheless these considerations show that gauge fixing should be rather seen as offering the possibility to device an appropriate parameterisation of the theory rather than a liability. For example, it can be shown that in Coulomb gauge the Gaussian approximation is working at least qualitatively.

7.2. Confinement-deconfinement phase transition at finite temperature

The dynamics of confinement and the confinement-deconfinement phase transition is the second cornerstone of the low energy QCD phenomenology we have to unravel. Here we aim at a treatment of this phenomenon within the continuum formulation of QCD similar to that of the chiral phase structure in [Section 3.2](#). We mainly concentrate on the effective potential of the order parameter, the Polyakov loop. This observable is derived directly from the Wilson loop discussed before.

7.2.1. Polyakov loop and Polyakov loop potential

Order parameter for the confinement-deconfinement phase transition

We consider a rectangular Wilson loop, [Figure 7.1](#), within the static situation also used in the previous chapters [7.1.1](#). At finite temperature T the time is limited to $t \in [0, \beta]$ with $\beta = 1/T$, see chapter [3.2.2](#). Moreover, the gauge fields are periodic in time up to gauge transformations, i.e.

$$A_\mu(t + \beta, \vec{x}) = \frac{i}{g} T(t, \vec{x}) (D_\mu T^\dagger(t, \vec{x})) , \quad (7.11)$$

with $T(t, \vec{x}) \in S U(N)$ are the *transition functions*. It follows from [\(7.11\)](#) that under gauge transformations they transform as

$$T^U(t, \vec{x}) = U(t + \beta, \vec{x}) T(t, \vec{x}) U^\dagger(t, \vec{x}) , \quad (7.12)$$

they parallel transport gauge transformations from t to $t + \beta$. The transformation property [\(7.11\)](#) ensures the periodicity of gauge invariant quantities. It is indeed possible to restrict ourselves to strictly periodic fields, $t \equiv 1\|$, even though this limits the possible gauge choice. For the time being we restrict ourselves to the periodic case and discuss the general case at the end. The state we want to construct is the one, where we describe a static quark–anti-quark pair for all times. To that end we take a path that extends in time direction from $t = 0$ to β . Then the spatial paths at fixed time $t = 0$ and $t = \beta$ have to be identified (up to the orientation) due to the periodicity on the lattice, as well as the fact that we have restricted ourselves to periodic gauge fields. We conclude that the path $C[L, \beta]$ splits into two loops winding around the time direction at the points \vec{x} and \vec{y} with $L = |\vec{x} - \vec{y}|$. The Wilson loop expectation value is then given by

$$\frac{1}{N_c^2} W[L, \beta] = \langle W_{C[L, \beta]}[A] \rangle = \langle L[A_0](\vec{x}) L^\dagger[A_0](\vec{y}) \rangle , \quad (7.13)$$

where $L[A_0]$ is the Polyakov loop variable with

$$L = \frac{1}{N_c} \text{tr}_f P(\beta, \vec{x}) , \quad \text{with} \quad P(t, \vec{x}) = \mathcal{P} e^{-i g \int_0^t A_0(\tau, \vec{x}) d\tau} . \quad (7.14)$$

The normalisation of the Polyakov loop is such that it is unity for a vanishing gauge field, $L[0] = 1$. It lives in the fundamental representation as it is related to a creation operator of a quark. It is gauge invariant under periodic gauge transformations that keep the strict periodicity of the gauge field we have required. In general we have

$$L[A^U] = \frac{1}{N_c} \text{tr}_f [U^\dagger(\beta, \vec{x}) U(0, \vec{x})] P(\beta, \vec{x}) , \quad (7.15)$$

where we have used the cyclicity of the trace. The combination $[U^\dagger(\beta, \vec{x}) U(0, \vec{x})]$ is unity for periodic gauge transformations, which is the case we have restricted ourselves to when deriving [\(7.13\)](#) from the

gauge invariant Wilson loop. In the general case the two spatial parts of the path at $t = 0, \beta$ only cancel up to the transition functions. Working through the derivation we get

$$L = \frac{1}{N_c} \text{tr}_f T(0, \vec{x}) P(\beta, \vec{x}), \quad (7.16)$$

which is also gauge invariant under non-periodic gauge transformations. Here we only consider $T \equiv \mathbb{1}$ but (7.16) has to be used for example in the temporal axial gauge $A_0 \equiv 0$. Evidently, in this gauge (7.14) simply is one. However, in order to achieve this gauge non-periodic gauge transformations (in time) have to be used. Then, the whole physics information of the Polyakov loop is stored in the transition function T instead of the gauge field. While this is not a convenient choice in continuum formulations it is a common choice on the lattice. There is obtained by taking trivial temporal link variables $U_0 = \mathbb{1}$ for all but the last link from $t = \beta - a$ to β .

We now come back to our main line of arguments, and restrict ourselves to the fully periodic case. The Wilson loop in (7.13) is an order parameter for confinement: in the confining phase it tends towards zero for large distances, $L \rightarrow \infty$, due to the area law,

$$\lim_{L \rightarrow \infty} W[L, \beta] \simeq \lim_{L \rightarrow \infty} e^{-\sigma \beta L} = 0. \quad (7.17)$$

In turn, in the deconfined regime of the theory the quark–anti-quark potential $V_{q\bar{q}}$ is Coulomb-like, $V_{q\bar{q}} \propto 1/|\vec{x} - \vec{y}|$ and the Wilson loop follows a perimeter law, leading to

$$\lim_{L \rightarrow \infty} W[L, \beta] > 0. \quad (7.18)$$

In conclusion the Wilson loop expectation value or Polyakov loop two-point correlation function for $L \rightarrow \infty$ serves as an order parameter for confinement at finite temperature. Moreover, in this limit we can use the clustering decomposition property of a *local* quantum field theory,

$$\lim_{|\vec{x} - \vec{y}| \rightarrow \infty} \langle A(\vec{x})B(\vec{y}) \rangle - \langle A(\vec{x}) \rangle \langle B(\vec{y}) \rangle = 0. \quad (7.19)$$

for local operators A and B . Hence we conclude that

$$\lim_{L \rightarrow \infty} W[L, \beta] = \langle L[A_0](\vec{x}) \rangle \langle L^\dagger[A_0](\vec{y}) \rangle, \quad (7.20)$$

it only depends on the temporal component of the gauge field. The Polyakov loop expectation value $\langle L[A_0] \rangle$ does not depend on the spacial variable due to translation invariance. Thus also the Polyakov loop expectation value itself serves as an order parameter for confinement,

$$\langle L[A_0] \rangle = \begin{cases} 0 & \text{confining phase} \\ \neq 0 & \text{deconfining phase} \end{cases} \quad (7.21)$$

Center-Symmetry and the confinement-deconfinement phase transition

So far we have argued on a heuristic level which led us to (7.21) as an order parameter, without even discussing the symmetry behind the pattern in (7.21): we are searching for a symmetry that is preserved by the Yang-Mills action but does not keep $\langle L[A_0] \rangle$ invariant. This is the center symmetry of the gauge group. The center elements are those elements that commute with all other elements in the gauge group. In $SU(N)$ these are the N th roots of unity in the groups. For the cases used here, the example group $SU(2)$ and the physical group $SU(3)$, the centers \mathcal{Z} are

$$\mathcal{Z}_{SU(2)} = \{\mathbb{1}, -\mathbb{1}\} \simeq Z_2, \quad \mathcal{Z}_{SU(3)} = \{\mathbb{1}, \mathbb{1}e^{\frac{2}{3}\pi i}, \mathbb{1}e^{\frac{4}{3}\pi i}\} \simeq Z_3. \quad (7.22)$$

where the identities $\mathbb{1}$ in $SU(2)$ and $SU(3)$ are $\mathbb{1}_{2 \times 2}$ and $\mathbb{1}_{3 \times 3}$ respectively. The non-trivial center elements in (7.22) are related to combinations of generators in the algebra. This relation is not unique as the eigenvalues of the combination of algebra elements is only determined up to $2\pi n$ with $n \in \mathbb{Z}$. For example, one representation is

$$SU(2) : -\mathbb{1} = e^{\pi i \sigma_3}, \quad SU(3) : \mathbb{1} e^{\frac{2}{3}\pi i} = e^{2\pi i \frac{1}{\sqrt{3}}\lambda_8}, \quad \mathbb{1} e^{\frac{4}{3}\pi i} = e^{2\pi i \frac{2}{\sqrt{3}}\lambda_8}. \quad (7.23)$$

with the Pauli matrices in (E.8) and the Gell-Mann matrices

$$\begin{aligned} \lambda_1 &= \begin{pmatrix} 0 & 1 & 0 \\ 1 & 0 & 0 \\ 0 & 0 & 0 \end{pmatrix}, & \lambda_2 &= \begin{pmatrix} 0 & -i & 0 \\ i & 0 & 0 \\ 0 & 0 & 0 \end{pmatrix}, & \lambda_3 &= \begin{pmatrix} 1 & 0 & 0 \\ 0 & -1 & 0 \\ 0 & 0 & 0 \end{pmatrix}, & \lambda_4 &= \begin{pmatrix} 0 & 0 & 1 \\ 0 & 0 & 0 \\ 1 & 0 & 0 \end{pmatrix}, \\ \lambda_5 &= \begin{pmatrix} 0 & 0 & -i \\ 0 & 0 & 0 \\ i & 0 & 0 \end{pmatrix}, & \lambda_6 &= \begin{pmatrix} 0 & 0 & 0 \\ 0 & 0 & 1 \\ 0 & 1 & 0 \end{pmatrix}, & \lambda_7 &= \begin{pmatrix} 0 & 0 & 0 \\ 0 & 0 & -i \\ 0 & i & 0 \end{pmatrix}, & \lambda_8 &= \frac{1}{\sqrt{3}} \begin{pmatrix} 1 & 0 & 0 \\ 0 & 1 & 0 \\ 0 & 0 & -2 \end{pmatrix}, \end{aligned} \quad (7.24)$$

in the fundamental representation of $SU(3)$. The generators of the $SU(3)$ algebra are $t_{\text{fund}}^a = \lambda^a/2$. In the adjoint representation the generators of the algebra are given by the structure constants, see (5.5). The $SU(3)$ structure constants are given by

$$\begin{aligned} SU(2) : \quad f^{abc} &= \epsilon^{abc}, \\ SU(3) : \quad f^{123} &= 1, \quad f^{147} = f^{246} = f^{257} = f^{345} = \frac{1}{2}, \quad f^{156} = f^{367} = \frac{1}{2}, \quad f^{458} = f^{678} = \frac{1}{2}. \end{aligned} \quad (7.25)$$

Hence, in the adjoint representation these elements are all represented by $\mathbb{1}$,

$$Z_{\text{ad}} = \mathbb{1}_{\text{ad}}, \quad \text{for } Z \in \mathcal{Z}. \quad (7.26)$$

In the adjoint representation every center element is mapped to the identity, $z = \mathbb{1}_{\text{ad}}, \forall z \in \mathcal{Z}$. Hence we have

$$\mathcal{Z}_{\text{ad}} = \{\mathbb{1}_{\text{ad}}\}. \quad (7.27)$$

As the gauge fields and the ghosts live in the adjoint representation, the gauge-fixed Yang-Mills action is trivially invariant under center transformations. In turn, the Polyakov loop $L[A_0]$ is the trace of the Polyakov line $P(\beta, \vec{x})$ in the *fundamental* representation, see (7.14). It transforms with

$$P(\beta, \vec{x}) \rightarrow z P(\beta, \vec{x}), \quad \text{with } z \in \mathcal{Z}. \quad (7.28)$$

We conclude that in the center-symmetric phase of the theory the Polyakov loop expectation value (7.21) has to vanish while in the center-broken phase it is finite.

The center symmetry can be made even more explicit if evaluating the traced Polyakov loop for constant fields. Then we can assume the fields to lay in the Cartan subalgebra, as we can always rotate the field into the Cartan subalgebra with constant gauge transformations. We expand the Cartan-valued field A_0 in the fundamental representation in the color eigenfunctions and eigenvalues of A_0 . In the present context it always occurs in combination with temperature and coupling in Matsubara sums with $2\pi Tn + gA_0 = 2\pi T(n + \beta g/(2\pi)A_0)$, and we define the dimensionless algebra-valued field

$$\hat{\varphi} = \frac{\beta g}{2\pi} A_0, \quad L(\hat{\varphi}) = L[A_0] = \text{tr } e^{-2\pi i \hat{\varphi}}. \quad (7.29)$$

The eigenvalue equation of the field $\hat{\varphi}$ in the fundamental representation is given by

$$\hat{\varphi}^f |\varphi_n^f\rangle = \nu_n^f |\varphi_n^f\rangle, \quad n \in 1, \dots, N_c, \quad (7.30)$$

where the superscript f indicates the fundamental representation. The eigenvalues for $SU(2)$ and $SU(3)$ are given by

$$SU(2) : \nu_n^f \in \left(\pm \frac{\varphi}{2} \right), \quad SU(3) : \nu_n^f \in \left(\pm \frac{\varphi_3 + \frac{1}{\sqrt{3}}\varphi_8}{2}, -\frac{1}{\sqrt{3}}\varphi_8 \right). \quad (7.31)$$

Using (7.30) and (7.31) in the Polyakov loop in $SU(2)$ we arrive at

$$\hat{\varphi} = \varphi_3 \frac{\sigma^3}{2} \xrightarrow{\varphi=\varphi_3} L(\varphi) = \cos \pi \varphi, \quad (7.32)$$

For $SU(3)$ we have

$$\hat{\varphi} = \frac{2\pi}{\beta g} \left(\varphi_3 \frac{\lambda^3}{2} + \varphi_8 \frac{\lambda^8}{2} \right) \longrightarrow L(\varphi_3, \varphi_8) = \frac{1}{3} \left(e^{\frac{2\pi i \varphi_8}{\sqrt{3}}} + 2 \cos(\pi \varphi_3) e^{-\frac{2\pi i \varphi_8}{\sqrt{3}}} \right), \quad (7.33)$$

with $\lambda^{3,8}$ given in (7.24). As the Polyakov loop potential (for vanishing chemical potential) has minima at $\varphi_3 = 0$ we can work with the Polyakov loop variable at $\varphi_8 = 0$,

$$L(\varphi) = \frac{1}{3} (1 + 2 \cos \pi \varphi), \quad (7.34)$$

with $L(\varphi) = L(\varphi_3 = \varphi, 0)$. Then, confinement is signaled by the (mean) gauge field configurations

$$\varphi = \frac{1}{2} \quad \text{for } SU(2), \quad \text{and} \quad \varphi = \frac{2}{3} \quad \text{for } SU(3). \quad (7.35)$$

Having identified the symmetry we can invoke universality to predict the scaling of the order parameter in the vicinity of the phase transition:

For $SU(2)$ we are in the Ising universality class, the symmetry group being Z_2 . If $SU(2)$ -Yang-Mills exhibits a second order phase transition (and it does), it should have Ising scaling. This is indeed seen. For $SU(3)$ the symmetry group is Z_3 and we expect a first order phase transition which is also seen. Our explicit computations later will not incorporate the full fluctuation analysis so detecting Ising scaling is out of reach here. However, we are able to see the second and first order nature of the respective phase transitions. This closes our very rough symmetry discussion.

We also would like to get an intuitive understanding for the Polyakov loop expectation value. We have argued for the Wilson loop expectation value, that it is related to the expectation value of a static quark-anti-quark pair,

$$W[L, \beta] \simeq \langle \bar{q}(\vec{x}) \mathcal{P} e^{-i g \int_{C_{\vec{x}, \vec{y}}} A_\mu dz_\mu} q(\vec{y}) \rangle, \quad (7.36)$$

where the path-ordered phase ensures gauge invariance. Using -naively- the clustering decomposition property (or short declustering) for $|\vec{x} - \vec{y}| \rightarrow \infty$, we can decompose the expectation value in (7.36) in the product of the expectation value of a quark state and an anti-quark state. Naturally the latter have to vanish as the creation of a single quark or anti-quark requires an infinite energy. However, be aware of the fact that the quark and anti-quark states do not belong to the Hilbert space of QCD and hence we cannot apply declustering that easily.

Still, the Polyakov loop expectation value is related to the heuristic situation described above. To see this more clearly let us consider a static quark. This situation can be achieved by taking the infinite quark mass limit, $m_q \rightarrow \infty$. The Dirac equation

$$(\not{D} + m_\psi) \psi = 0, \quad (7.37)$$

then reduces to a space-independent equation as the quark cannot move, $\vec{\partial}_x \psi = 0$. Hence, the Dirac equation (7.37) reads in the static limit

$$(\gamma_0 D_0 + m_\psi) \psi = 0. \quad (7.38)$$

A solution to this equation is given by

$$\psi(x) = P^\dagger(t, \vec{x}) \psi_0(x), \quad \text{with} \quad (\gamma_0 \partial_0 + m_\psi) \psi_0 = 0. \quad (7.39)$$

where ψ_0 solves the free Dirac equation, and $P(t, \vec{x})$ is the untraced Polyakov loop (7.14). For proving (7.39) we use that $(D_0 P^\dagger(t, \vec{x})) = 0$ following from (F.43). Hence, in a -vague- sense we can identify the expectation value of the trace Polyakov loop L , (7.14), with the interaction part of a static quark.

Order parameter potential in functional approaches

As in the case of chiral symmetry breaking we would like to compute the effective potential of the order parameter, $V_{\text{Pol}}(L)$. It turns out to be a formidable task both on the lattice and in the continuum. Note however, that the computation of the expectation value itself is simple on the lattice.

The order parameter as introduced above, expectation value of the Polyakov loop $\langle L \rangle$, is given by the EoM of the Polyakov loop potential,

$$\frac{\partial V_{\text{Pol}}(L)}{\partial L} \Big|_{L=L_{\text{EoM}}} = 0, \quad (7.40)$$

restricting ourselves to constant L . In functional approaches neither the expectation value of L nor its potential are easily accessible. These approaches are typically formulated in terms of the gauge field A_μ , and $L[A_0]$ is a complicated function of the temporal gauge field A_0 . In terms of a field expansion (related to the vertex expansion) the computation of $\langle L[A_0] \rangle$ requires the computation of a series of correlation functions in any order of A_0 . Moreover, the Polyakov loop potential is only implicitly defined as

$$V_{\text{Pol}}(L) = \frac{1}{\beta V_3} \Gamma[A_0(L)], \quad \text{with} \quad L(A_0) = \langle \hat{L} \rangle(A_0), \quad (7.41)$$

where \hat{L} is the traced Polyakov loop operator, and L is its expectation value. In (7.41) we have restricted ourselves to constant L and A_0 , while the spatial gauge field and the ghost, anti-ghost vanish, $A_i = 0$, $c = \bar{c} = 0$.

The solution of the implicit relation $A_0(L)$ requires the computation of the expectation value of the Polyakov loop $L(A_0)$ for general backgrounds A_0 . This very non-trivial task is complicated further by the fact that while L is gauge invariant, A_0 is not. Nonetheless, (7.41) already suggests a resolution of all these intricacies: instead of computing $V_{\text{Pol}}(L)$ as a function of L , we simply compute it as a function of A_0 , and employ A_0^{EoM} as an order parameter. We define in a slight abuse of notation

$$V_{\text{Pol}}(A_0) = V_{\text{Pol}}(L) = \frac{1}{\beta V_3} \Gamma[A_0], \quad (7.42)$$

with the EoM

$$\frac{\partial V_{\text{Pol}}(A_0)}{\partial A_0} \Big|_{A_0=A_0^{\text{EoM}}} = 0. \quad (7.43)$$

Evidently A_0^{EoM} is also an order parameter. However, it also is a gauge variant quantity, and its use as an order parameter is not appealing. This asks for the definition of a gauge invariant effective action and hence a gauge invariant effective potential $V_{\text{Pol}}(A_0)$ with $V_{\text{Pol}}(A_0^U) =_{\text{Pol}} (A_0)$. This is discussed in the next chapter.

7.2.2. Background field formalism

With in the background field approach a gauge invariant effective action can be defined. For a covariant gauge fixing this approach is based on an upgrade of our covariant gauge fixing to the *background gauge*: To that end we split our gauge field in a background \bar{A} and a fluctuation a , to wit

$$A_\mu = \bar{A}_\mu + a_\mu. \quad (7.44)$$

While the background \bar{A} is kept fixed, a carries all the quantum fluctuations. In the path integral the integration over A then turns into one over a . So far nothing has been changed. Now we modify our gauge fixing,

$$\partial_\mu A_\mu = 0 \rightarrow \bar{D}_\mu a = 0, \quad \text{with} \quad \bar{D}_\mu = D_\mu(\bar{A}). \quad (7.45)$$

For $\bar{A} = 0$ we regain the orginial covariant gauge fixing. For the background gauge fixing the gauge fixed classical action with ghost term reads

$$S_A[\bar{A}, a, c, \bar{c}] = S_A[A] + \frac{1}{2\xi} \int_x (\bar{D}_\mu^{ab} a_\mu^b)^2 + \bar{c}^a \bar{D}_\mu^{ad} D_\mu^{db} c^b. \quad (7.46)$$

In the presence of the background field and with the gauge fixing (7.45) we have an additional -auxiliary-gauge symmetry: the gauge-fixed action is invariant under *background gauge transformations*

$$\begin{aligned} \bar{A}_\mu^U &= \frac{i}{g} U (\bar{D}_\mu U^\dagger), \\ a^U &= U a_\mu U^\dagger c^U = U c U^\dagger, \quad \bar{c}^U = \bar{c} U^\dagger. \end{aligned} \quad (7.47a)$$

With 7.47 the background field transforms as a gauge field under gauge transformations, while the Yang-Mills fluctuation field transforms as a tensor,

$$\Phi = (A_\mu, c, \bar{c}), \quad \text{with} \quad \Phi^U = U \Phi U^\dagger. \quad (7.47b)$$

Importantly, the full gauge field A_μ also transforms as a gauge field,

$$A^U = \frac{i}{g} U (D_\mu U^\dagger). \quad (7.47c)$$

Evidently, invariance under 7.47 holds true for the Yang-Mills action, it is left to show this for the gauge fixing and ghost term. The gauge fixing condition (7.45) transforms as a tensor under 7.47: $\bar{D}_\mu a \rightarrow U \bar{D}_\mu a U^\dagger$ and hence $\text{tr}(\bar{D}_\mu a)^2$ is invariant under 7.47. The Faddeev-Popov operator \mathcal{M} in the background gauge is given by

$$\mathcal{M} = -\bar{D}_\mu D_\mu \rightarrow U \bar{D}_\mu D_\mu U^\dagger. \quad (7.48)$$

It also transforms as a tensor and hence the ghost term is gauge invariant under 7.47. However, the background gauge symmetry is an auxiliary symmetry. The physical gauge transformations are those of the fluctuation field at fixed background \bar{A} , the *quantum gauge transformations*

$$\bar{A}_\mu^U = \bar{A}_\mu, \quad a^U = U (D_\mu U^\dagger) \quad \longrightarrow \quad A^U = \frac{i}{g} U (D_\mu U^\dagger). \quad (7.49)$$

Again this can be understood by choosing the standard covariant gauge with a vanishing background. Then, (7.49) is the only gauge transformation left, while 7.47 leads to a non-vanishing background and hence changes the gauge fixing. The neat feature of the background field formalism is that it can be shown

that both transformations are indeed related via *background independence* of the quantum equations of motion. Therefore background gauge invariance under the transformations 7.47 carries physical gauge invariance, more details can be found in Appendix F.7

Still, the introduction of the background seems to complicate matters but it indeed facilitates computations and gives a more direct access to physics. Here we explore both properties. First we note that the introduction of \bar{A} leads to an effective action that depends on two fields,

$$\Gamma[A] \rightarrow \Gamma[\bar{A}, a]. \quad (7.50)$$

Switching of the mean value of the fluctuation field, $a = 0$ leads to a (background) gauge invariant action

$$\Gamma[A] = \Gamma[A, a = 0]. \quad (7.51)$$

It can be shown, see Appendix F.7, that solutions of the EoM for $\Gamma[\bar{A}, a]$ for a implies one for \bar{A} . Moreover, they can be mapped to

$$\frac{\delta\Gamma[A]}{\delta A} = 0. \quad (7.52)$$

see (F.59).

In summary this leaves us with the task to compute $\Gamma[A]$ which carries the information about the Polyakov loop potential $V_{\text{pol}}[A_0]$. The respective EoM A_0^{EoM} serves as an order parameter for confinement.

7.2.3. Polyakov loop potential in functional approaches

Summarising the discussion of the last chapters, we have been led to an order parameter potential

$$V_{\text{pol}}[A_0] = \frac{1}{\beta V_3} \Gamma[A_0], \quad (7.53)$$

for constant background fields A_0 . The potential (7.53) is center-symmetric and its minima A_0^{EoM} are either center-symmetric or break center symmetry. Hence they serve as order parameters. The potential Equation (7.53) is easily computed non-perturbatively within the FRG approach, and it gives access to the confinement-deconfinement phase transition. Moreover, correlation functions have to be computed on the EoM, and hence we also need A_0^{EoM} for the computation of correlation functions.

Before computing the potential and its minima $A_0^{\text{EoM}} = \langle \bar{A}_0 \rangle$ we discuss the relation to the expectation value of the Polyakov loop. For that purpose we consider the algebra element of the Polyakov loop, $\hat{\varphi}$, which transforms as a tensor under gauge transformations,

$$\hat{\varphi}^U(\vec{x}) = U(0, \vec{x}) \hat{\varphi}(\vec{x}) U^\dagger(0, \vec{x}). \quad (7.54)$$

Equation (7.54) entails that the eigenvalues of $\hat{\varphi}$ are gauge invariant as they do not change under a unitary rotation of $\hat{\varphi}$. Moreover, evidently they are order parameters for confinement. In short we write

$$\varphi = \langle \hat{\varphi} \rangle. \quad (7.55)$$

Now we use that the Polyakov loop potential is gauge invariant. Hence, we may consider the Polyakov gauge for the background field,

$$\bar{A}_0^{\text{Polyakov}}(x) = \bar{A}_0^c(\vec{x}). \quad (7.56)$$

Then we have a direct relation between $\hat{\varphi}$ and the background field,

$$\bar{A}_0^{\text{Polyakov}} = \hat{\varphi}, \quad (7.57)$$

and due to the equivalence of EoMs of a_0 and \bar{A}_0 we have,

$$\bar{A}_0^{\text{EoM}} = \varphi[\bar{A}_0^{\text{EoM}}], \quad (7.58)$$

This finally relates the two order parameters. We emphasise that this relation is not necessary for the order parameter property of \bar{A}_0^{EoM} .

The Polyakov loop potential $V_{\text{pol}}[A_0]$ is now computed non-perturbatively within the FRG approach. Perturbative computations of the Polyakov loop potential at one- and two-loop have been performed 30 years ago, starting with the seminal one loop computations in [101] and [102] in 1980 (published 81). Perturbation theory is an expansion about vanishing fields, and hence an expansion about $L = 1$. The resulting -analytic- potential has a minimum at $A_0 = 0$ with $L = 1$. This is discussed below in more detail. For the sake of comparison with the FRG computation we present the details of the standard perturbative one-loop computation in [Appendix F.8](#).

We proceed with the non-perturbative computation of the Polyakov loop potential in a way that still keeps the analogy to the one loop computation in [Appendix F.8](#). Even though this is an approximation, both the numerical result as well as the conceptual structure are also present in the full computation. To that end we rewrite the flow equation for the effective action in terms of a total derivative w.r.t. the RG-time t and an RG improvement term,

$$\partial_t \Gamma[\bar{A}, \Phi] = \frac{1}{2} \text{Tr} \partial_t \ln (\Gamma^{(2)}[\bar{A}, \Phi] + R_k) - \frac{1}{2} \text{Tr} G_k[\Phi] \partial_t \Gamma^{(2)}[\Phi], \quad (7.59)$$

The second term on the right hand side of (7.59) is a RG improvement term which we drop in the following. This is justified approximation as long as $|\partial_t \Gamma^{(2)}[\Phi]/k^2| \ll 2$, the full anomalous dimension is not exceeding $|\partial_t R_k| \lesssim 2$.

Now we proceed with the explicit computation of the effective potential at one loop. For the Polyakov loop potential the only mean field of interest is the temporal component of the gauge field, and the other fields are put to zero. We will perform this computation first on the one-loop level with the classical ghost and gluon propagators. Finally we will introduce the fully non-perturbative propagators to this one-loop computation. This re-sums infinitely many diagrams and carries the essential non-perturbative computation. The explicit results are in semi-quantitative agreement with the full results obtained with functional renormalisation group methods and also show a good agreement with the lattice results.

Before using the full non-perturbative machinery we start with the somewhat simpler perturbative analysis of an SU(2) symmetric example. The classical two point functions for constant A_0 backgrounds are given by

$$S_{AA,\mu\nu}^{(2)}[A_0] = -D^2 \delta_{\mu\nu} + \left(1 - \frac{1}{\xi}\right) D_\mu D_\nu, \quad S_{\bar{c}\bar{c}}^{(2)}[A_0] = -D^2, \quad (7.60)$$

and we use regulators $R_k = S^{(2)}[\bar{A}_0] r(x)$, where either $S^{(2)}$ is evaluated at D_0, \vec{q} and $x = -\bar{D}^2/k^2$ or $S^{(2)}$ is evaluated at $(0, \vec{q})$ and $x = \vec{q}^2/k^2$. The flow splits into a transversal and longitudinal gluon part and a ghost part. In d -dimensional perturbation theory the flow of the potential reads

$$\partial_t V_{\text{pert}}[A_0] = \frac{1}{2} T \sum_{n \in \mathbf{Z}} \int d^3 q \text{tr} \frac{\partial_t R_k}{\vec{q}^2 + (2\pi n T + g A_0)^2 + R_k} ((d-1) + 1 - 2), \quad (7.61)$$

where $(d-1)$, 1 and -2 are the prefactors of the transversal, longitudinal and ghost loop after the Lorentz contractions. Note that the result is independent of the gauge fixing parameter. In (7.61) we have not specified the regulator R_k as the result does not depend on it. For convenience we can either choose a regulator that only depends on the spatial momenta, $R_k = R_k(\vec{q}^2)$, or we take one which depends on all momenta, $R_k = R_k((2\pi n T + g A_0)^2 + \vec{q}^2)$. In the latter case the dependence on the background field is important as otherwise background gauge invariance is broken.

The perturbative computation is simplified for regulators $R_k(\vec{q}^2)$. Then we are left with a Matsubara sum of the classical propagator with a mass k^2 . Moreover we can expand pull out the temperature factor $2\pi T$, and write the gauge field $\varphi = \beta g A_0/(2\pi)$ in terms of the eigenvalues ν_i of φ . Note that the ν_i are the eigenvalues of the field φ in the adjoint representation, and not the ν_i^f in (7.30) in the fundamental representation. This leaves us to

$$\begin{aligned} T \sum_{n \in \mathbf{Z}} \text{tr} \frac{2k^2}{k^2 + (2\pi T)^2(n + \varphi)^2} &= \sum_{i=1}^{N_c^2-1} T \sum_{n \in \mathbf{Z}} \frac{2k^2}{k^2 + (2\pi T)^2(n + \nu_i)^2} \\ &= \frac{k}{4} \sum_i^{N_c^2-1} \left[\coth \left(\frac{\beta k}{2} + i\pi\nu_i \right) + \coth \left(\frac{\beta k}{2} - i\pi\nu_i \right) \right]. \end{aligned} \quad (7.62)$$

The spatial momentum integral with $\vec{q}^2 \leq k^2$ is trivial and gives a factor proportional to k^3 . The remaining t -integral can be computed with the techniques discussed in Appendix F.8 leading to the Weiss potential [101, 102],

$$\beta^4 V_{\text{pol}}(A_0) = \frac{\pi^2}{12} \left[4 \left(\tilde{\varphi} - \frac{1}{2} \right)^2 - 1 \right]^2 - \frac{\pi^4}{45} (N_c^2 - 1). \quad (7.63)$$

see also (F.76).

Now we proceed to the non-perturbative computation with the finite temperature gluon propagators, see Figure 7.2, Figure 7.3. First we discuss the flow (7.59) without the RG improvement term. Then the Polyakov loop potential for constant temporal gauge fields is given by

$$V_{\text{pol}}(A_0) = \frac{1}{2} \text{Tr} \ln G_A^{-1}(A_0) - \text{Tr} G_c^{-1}(A_0) - \mathcal{N}, \quad (7.64)$$

where the color traces in (7.64) are in the adjoint representation and CN is the normalisation of the potential which we leave open for now.

From Fig. E we know that the gluon propagator exhibits a mass gap for low momenta. In turn, for large momenta it runs logarithmically. This behaviour is also present at finite temperature, see Fig. 7.3. There we plot the momentum dependence of the dressing of the chromo-magnetic gluon propagator for different temperatures. Both, results from functional methods and from gauge-fixed lattice simulations are shown. The dressing is defined as

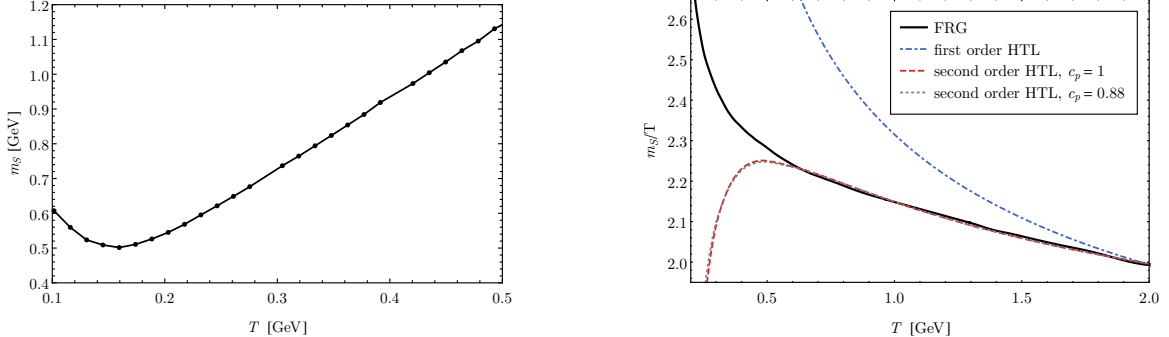
$$\frac{1}{Z_A^M(\vec{p}^2)} = \frac{1}{2} \vec{p}^2 \langle A_i(0, \vec{p}) A_i(0, -\vec{p}) \rangle, \quad (7.65)$$

it is the dressing of the gluon propagator perpendicular to the heat bath. In Fig. 7.2 we plot the temperature-dependent mass (screening mass) of chromo-electric gluon propagator, the gluon propagator parallel to the heat bath,

$$\frac{1}{Z_A^E(\vec{p}^2)} = \vec{p}^2 \langle A_0(0, \vec{p}) A_0(0, -\vec{p}) \rangle. \quad (7.66)$$

Note that the simple relations (7.65), (7.66) are only valid for $p_0 = 0$. For $p_0 \neq 0$ one has to use the thermal projection operators, see e.g. [56]. At large temperatures we expect them to tend towards their perturbative values. This is indeed happening, however, we need higher order thermal perturbation theory. The one-loop Debye mass is given by

$$m_D^0 = \sqrt{\frac{N}{3}} g_T T + O(g_T^2 T), \quad (7.67)$$



(a) Screening mass m_s in units of GeV at low temperatures. In the limit $T \rightarrow 0$ the screening mass smoothly tends towards its finite $T = 0$ value, see back curve in Fig. 7.3.

(b) Dimensionless Debye screening m_s/T mass at high temperatures in comparison with leading order perturbation theory (7.67) and the Arnold-Yaffe prescription (7.68) for accommodating beyond leading order effects [103].

Figure 7.2.: Debye screening mass m_s , plot taken from [56], for more details see there.

and is also displayed in Fig. 7.2. For the comparison, the temperature-dependent coupling is fully non-perturbative and has been also taken from [56] for internal consistency, for more details see there. In [103] higher order effects have been taken into account, leading to

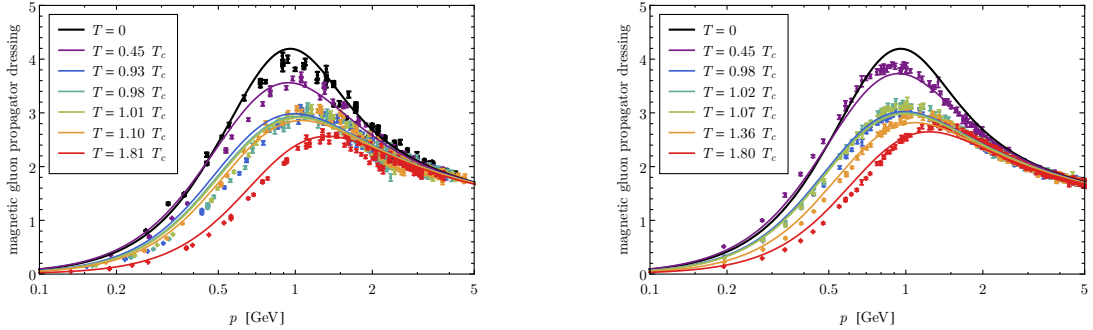
$$m_D = m_D^0 + \left(c_D + \frac{N}{4\pi} \ln \left(\frac{m_D^0}{g_T^2 T} \right) \right) g_T^2 T + O(g_T^3 T). \quad (7.68)$$

Equation (7.68) already leads to a very good agreement with the full result above 600 MeV. At low temperatures, the mass settles at its $T = 0$ value, indicated by the $1/T$ behaviour of m_d/T in Fig. 7.2(b), and the perturbative prescriptions fail even with the full non-perturbative coupling. The Debye mass itself for low temperatures is depicted in Fig. 7.2(a), from which it is evident that a temperature-independent (or decaying) additional part $\Delta m_D(T = 0) \approx 380$ MeV to m_D^0 would lead to agreement up to ≈ 150 MeV. In conclusion a good semi-quantitative approximation to the thermal propagator (in particular the chromomagnetic one) is the perturbative propagator with a temperature-dependent mass term. It goes beyond the scope of the present lecture notes to present a full computation, here we simply investigate the qualitative effect of such a mass gap, first done in [86], for a full, comprehensive analysis see [107]. We revisit (F.67) for simple massive propagators

$$G_A \propto \frac{1}{(2\pi T)^2 (n + \varphi)^2 + \vec{p}^2 + m_T^2}, \quad (7.69)$$

even dropping the perturbative running. While the latter is important for the correct scaling (fixing Λ_{QCD} and hence for the correct T_c) it is not important for the confining property. With the propagator (7.69) we are led to

$$\begin{aligned} V_{\text{mode}}(\varphi, m) &= \frac{T}{4\pi^2} \sum_{\pm} \sum_{n=1}^{\infty} \frac{1}{n} (e^{\pm 2\pi i n \varphi} - 1) \int_0^{\infty} dp p^2 e^{-(\beta \sqrt{p^2 + m^2})n} \\ &= \frac{T^4}{4\pi^2} \sum_{\pm} \sum_{n=1}^{\infty} \frac{1}{n} (e^{\pm 2\pi i n \varphi} - 1) \int_0^{\infty} d\bar{p} \bar{p}^2 e^{-(\sqrt{\bar{p}^2 + \beta^2 m^2})n}. \end{aligned} \quad (7.70)$$



(a) Magnetic gluon dressing in $SU(2)$ from [56] in comparison with $SU(2)$ lattice results from [104, 105]. (b) Magnetic gluon dressing in $SU(2)$ from [56] in comparison with $SU(3)$ lattice results from [106].

Figure 7.3.: Magnetic gluon propagator dressing (7.65).

The momentum integration in (7.71) cannot be performed analytically. However, in the zero temperature limit the terms in the sum decays with $e^{(-\beta m)n}$ up to polynomials. This is seen easily for the absolute value of the mode potential,

$$\begin{aligned}
 |V_{\text{mode}}(\varphi, m)| &\leq \frac{T^4}{4\pi^2} \sum_{n=1}^{\infty} \frac{1}{n} \int_0^{\infty} d\bar{p} \bar{p}^2 e^{-\left(\sqrt{\bar{p}^2 + \beta^2 m^2}\right)n} \\
 &\leq \frac{T^4}{4\pi^2} \sum_{n=1}^{\infty} \frac{1}{n} \left[\int_0^{\beta m} d\bar{p} \bar{p}^2 e^{-(\beta m)n} + \int_0^{\beta m} d\bar{p} \bar{p}^2 e^{-\bar{p}n} \right] \\
 &\xrightarrow{\beta m \rightarrow \infty} T^4 \text{Pol}(\beta m) e^{-\beta m}, \tag{7.71}
 \end{aligned}$$

with a polynomial $\text{Pol}(\beta m)$. In summary the mode potential decays exponentially for gapped propagators. This entails that for sufficiently small temperatures the contributions of the chromo-electro and the two chromo-magnetic modes decay exponentially. The longitudinal gauge mode stays trivial and gives the contribution $2V_{\text{mode}}(\varphi)$. Now we use that the ghost propagator keeps its $1/(-D^2)$ behaviour it already has perturbatively. In a covariant gauge this is already suggested from the ghost-gluon vertex which is linear in the anti-ghost momentum. Hence, all loop corrections to the inverse ghost propagator are proportional to p^2 from the onset. If no additional singularity is created from the propagators in the loops it stays this way. Since the gluon propagator is gapped this is only possible with a global non-trivial scaling.

Let us now study the case of a trivial ghost propagator and a gapped gluon propagator. In this case we

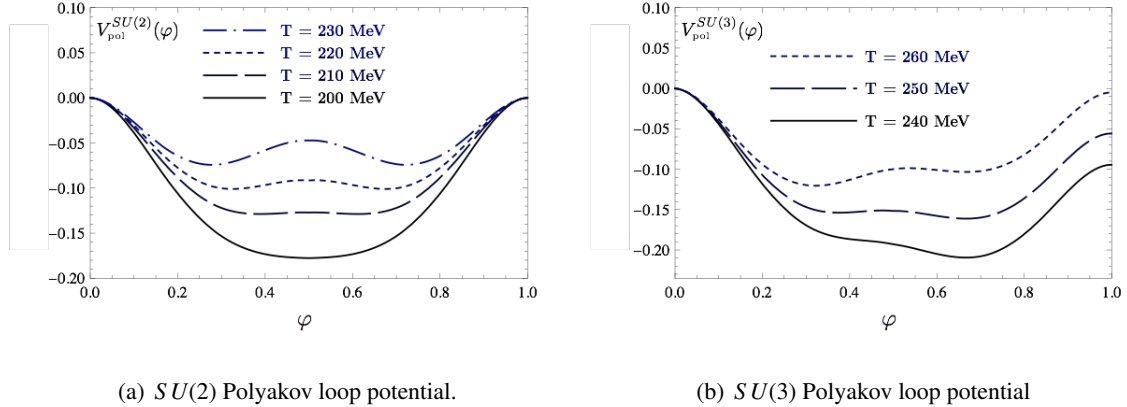


Figure 7.4.: $SU(2)$ and $SU(3)$ Polyakov loop potential taken from [107] for different temperatures across the phase transition. The potentials exhibits the second and first order of the $SU(2)$ and $SU(3)$ transitions respectively. The full $SU(3)$ potential is shown in Figure 7.6.

conclude that

$$\begin{aligned} \lim_{T \rightarrow 0} V_{\text{Pol}}(A_0) &\simeq \frac{1}{2} \lim_{T \rightarrow 0} \text{Tr} \ln G_A^{-1}(A_0) - \lim_{T \rightarrow 0} \text{Tr} G_c^{-1}(A_0) \\ &\simeq \frac{1}{2} \text{Tr} \ln (-D_\rho^2)(A_0) - \text{Tr} \ln (-D_\rho^2)(A_0) \end{aligned} \quad (7.72)$$

$$= -\frac{1}{2} \text{Tr} \ln (-D_\rho^2)(A_0) = \sum_i V_{\text{mode}}(\varphi_i). \quad (7.73)$$

With the mode potential (F.64), see Fig. F.6 this gives confinement. The present qualitative study can be extended to a fully non-perturbative one with the help of functional methods, leading to the $SU(2)$ and $SU(3)$ potentials depicted in Fig. 7.4 taken from [107]. The respective Polyakov loop expectation values $L[\langle A_0 \rangle]$ are shown in Fig. 7.5.

The above considerations also hold in full Yang-Mills theory without approximations. This allows us to formulate a confinement criterion in Yang-Mills theory with (7.64), (F.69) and (7.71):

Confinement criterion.

'In covariant gauges the gluon propagator has to be gapped relative to the ghost at low temperatures'

put forward in [86]. Note that we have been led to this criterion in the one-loop resummed approximation with (7.64). However, it can be proven in Yang-Mills theory without approximations on the basis of the functional renormalisation group, [86, 107], as well as Dyson-Schwinger equations and the two-particle irreducible (2PI) formalism [107]. It also extend beyond the covariant gauges, e.g. to the Coulomb gauge. In QCD with dynamical QCD -as expected- the quark contributions spoil the applicability of the

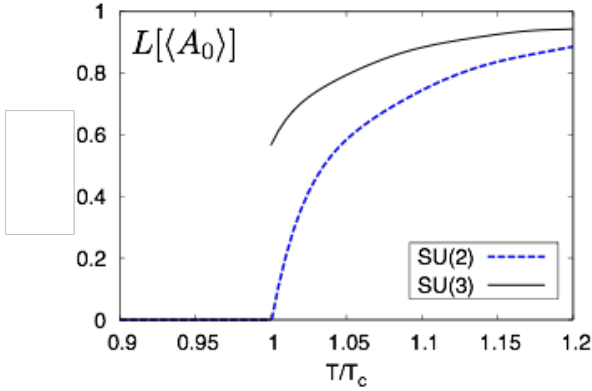


Figure 7.5.: Polyakov loop expectation values $L[\langle A_0 \rangle]$ for $SU(2)$ and $SU(3)$ taken from [86].

confinement criterion as they introduce center-breaking terms to the potential, for a detailed discussion see [107].

We close this chapter with some remarks on the order parameter we introduced. We started with the Polyakov loop variable $\langle L[A_0] \rangle$, but computed the Polyakov loop potential $V_{\text{pol}}[A_0]$ with the order parameter $\langle A_0 \rangle$ or $L[\langle A_0 \rangle]$. As both are order parameters for the same symmetry, this is not relevant for us. Still, one can investigate their relation: evidently they are not the same but only agree in a Gaussian approximation,

$$\langle L[A_0] \rangle \neq L[\langle A_0 \rangle], \quad (7.74)$$

Dropping for the moment the necessary renormalisation of $\langle A_0 \rangle$, they satisfy the Jensen inequality,

$$\langle L[A_0] \rangle \leq L[\langle A_0 \rangle], \quad (7.75)$$

see [86]. We conclude that if $L[\langle A_0 \rangle] = 0$, so is $\langle L[A_0] \rangle$. In turn, one can show that $L[\langle A_0 \rangle]$ vanishes if $\langle L[A_0] \rangle$ does, see [87]. While $L[\langle A_0 \rangle]$ has so far only been computed with functional methods, we have a solid results for $\langle L[A_0] \rangle$ from the lattice, both in Yang-Mills theory and in QCD. More recently, $\langle L[A_0] \rangle$ has been also computed with the FRG on the basis of $L[\langle A_0 \rangle]$ in quantitative agreement with the lattice results [108], see ???. This computation relies on the flow equation for composite operators O derived in [9],

$$\partial_t O[\Phi] = -\frac{1}{2} \text{Tr} (G_k \partial_t R_k G_k)_{ij} \frac{\delta^2}{\delta \Phi_i \delta \Phi_j} O[\Phi]. \quad (7.76)$$

Equation (7.76) holds for general expectation values $\langle O[\hat{\Phi}] \rangle$ including their disconnected parts. For example it holds for the full two-point function $\langle \hat{\Phi}_i \hat{\Phi}_j \rangle = G_{ij} + \Phi_i \Phi_j$, but not for the connected part. It also holds true for operators that depend on currents, for example also $\delta \Gamma / \delta \Phi$. Note that this does not include Γ itself. For expectation values there is a very elegant and simple derivation, see [109]: we introduce a current J_O for the operator O under investigation. Then the effective action also depends on this current, $\Gamma = \Gamma[\Phi, J_\Phi]$, and example being the currents for the BRST transformations. The flow of $\langle O[\hat{\Phi}] \rangle$ is then simply obtained by a J_O -derivative (at $J_O = 0$), leading to (7.76).

Seemingly, the relation between $\langle L[A_0] \rangle$ and $L[\langle A_0 \rangle]$ is rather non-trivial. However, it has been shown in [108] that most of the difference between $\langle L[A_0] \rangle$ and $L[\langle A_0 \rangle]$ comes from a temperature dependent normalisation of the former. In any case there is a relation

$$\langle L[A_0] \rangle(\varphi) \quad (7.77)$$

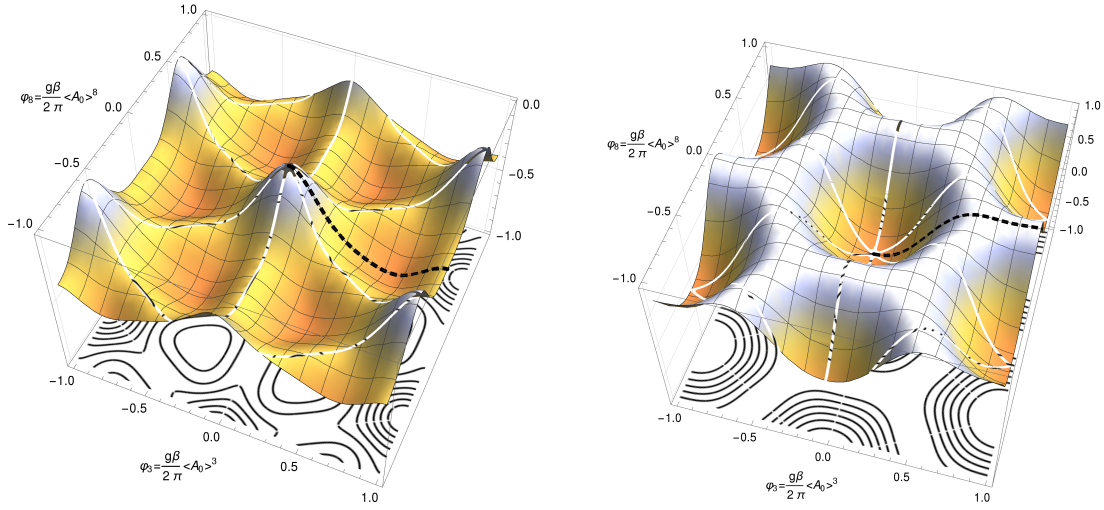


Figure 7.6.: The infrared glue potential, $V(\varphi_3, \varphi_8)$, is shown in the confined phase (left, $T = 236$ MeV) and in the deconfined phase (right, $T = 384$ MeV). We restrict ourselves to the line $\varphi_8 = 0$ and $\varphi_3 \geq 0$ (indicated by the black, dashed line), where one of the equivalent minima is always found, and where $L[\langle A_0 \rangle]$ is real and positive semi-definite.

that maps $\varphi = \beta g/(2\pi)\langle A_0 \rangle$ to the Polyakov loop expectation value in a given background, as discussed before. In principle this allows to determine $V_{\text{pol}}[L]$ from $V_{\text{pol}}[A_0]$. This would be interesting for Polyakov loop assisted low energy effective models.

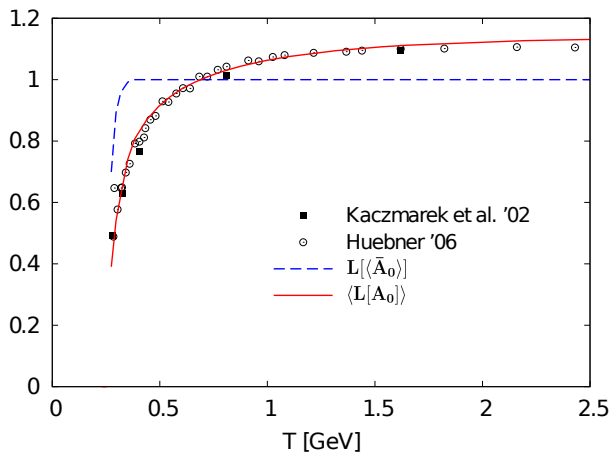


Figure 7.7.: Expectation value of $\langle L[A_0] \rangle$ versus $L[\langle \bar{A}_0 \rangle]$ from [108]. Both observables are order parameters for the confinement-deconfinement phase transition. Moreover, $L[\langle \bar{A}_0 \rangle] = 1$ entails $\langle \bar{A}_0 \rangle = 0$.

8. A glimpse at the phase structure of QCD

In this final chapter we briefly summarise the present state of the art of functional RG applications to the phase structure of QCD. Given the amount of additional challenges at finite temperature and density.

The FRG works up to no has been done at finite temperature and density, that lives up to the quantitatively satisfactory level such as the vacuum QCD applications [52, 56], and for finite temperature Yang-Mills [56]. This applies as well to DSE applications. Moreover, as discussed in the beginning, lattice simulations face a severe sign problem for densities $\mu_B/T \gtrsim 2 - 3$. In summary no quantitatively reliable simulation for densities and temperatures with $\mu_B/T \gtrsim 2 - 3$ is available. For the quest of the critical end point (CEP) this lack of quantitative precision entails that even qualitative statements about its location have to be taken with a grain of salt. In turn, the existence of the CEP in the temperature and density regime with $\mu_B/T \lesssim 2 - 3$ is very unlikely. This has first been suggested on the basis of results from functional methods, see e.g. [110, 111], for more details see [112, 113] and the recent DSE review [7], and since then has been corroborated by more recent lattice results, see e.g. [?, ?].

In [53, 114] it has been shown that at vanishing temperature and density some of the quantitative results of [52, 56] can already be obtained in an approximation to the effective action, that only includes cutoff dependent vertex functions and propagators instead of dealing with the full momentum dependence of the correlation functions. This holds true apart from the highly non-trivial momentum dependence of the gluon propagator, which encodes confinement. Therefore, in [53, 114] vacuum QCD correlation functions have been computed on the basis of quantitative vacuum Yang-Mills results.

Consequently this suggests an approximation written as an expansion about quantitative vacuum QCD and finite temperature Yang-Mills results. To begin with, we expand the flow about the $T, \mu = 0$ results,

$$\partial_t \Gamma_{T,\mu}[\Phi] = \partial_t \Gamma_{0,0}[\Phi] + \partial_t \Delta\Gamma_{T,\mu}[\Phi], \quad \text{with} \quad \Delta\Gamma_{T,\mu}[\Phi] = \Gamma_{T,\mu}[\Phi] - \Gamma_{0,0}[\Phi]. \quad (8.1)$$

This allows us to write solve the flow for $\Delta\Gamma_{T,\mu}[\Phi]$ on the basis of the vacuum results,

$$\partial_t \Delta\Gamma_{T,\mu}[\Phi] = \partial_t \Gamma_{0,0}[\Phi] + \left[\text{Tr } G_k[\Phi] \partial_t R_k|_{T,\mu} - \text{Tr } G_k[\Phi] \partial_t R_k|_{T,\mu=0} \right]. \quad (8.2)$$

The flow of the finite T, μ correlation functions is obtained from (8.2) by taking the respective field derivatives. For $\partial_t \Gamma_{0,0}^{(n)}$ the quantitative vacuum results are used. Then, the flows $\partial_t \Delta\Gamma_{T,\mu}^{(n)}$ can be solved within a k -dependent approximation for the vertex and propagator dressings with this input. Here we adopt the following truncation for the Euclidean scale-dependent effective action Γ_k for $N_f = 2$ and $N_f = 2 + 1$,

$$\begin{aligned} \Gamma_k = \int_x & \left\{ \frac{1}{4} F_{\mu\nu}^a F_{\mu\nu}^a + Z_{c,k} (\partial_\mu \bar{c}^a) D_\mu^{ab} c^b + \frac{1}{2\xi} (\partial_\mu A_\mu^a)^2 + Z_{q,k} \bar{q} (\gamma_\mu D_\mu) q \right. \\ & \left. - \lambda_{q,k} [\bar{q} \tau^0 q]^2 - (\bar{q} \gamma_5 \vec{\tau} q)^2 \right] + h_k \bar{q} (\tau^0 \sigma + i \gamma_5 \vec{\tau} \cdot \vec{\pi}) q + \frac{1}{2} Z_{\phi,k} (\partial_\mu \phi)^2 + V_k(\rho) - c \sigma \right\}, \end{aligned} \quad (8.3)$$

with $\int_x = \int_0^{1/T} dx_0 \int d^3x$ and $\tau = (\tau^0, \vec{\tau}) = (\mathbb{1}, \vec{\sigma})$. In (11.75) we only consider the four-quark interactions and mesonic composite fields for the scalar–pseudo-scalar multiplet. This approximation is based on the observation that at $T, \mu = 0$ both terms produce negligible contributions for cutoff scales $k \gtrsim 500$ MeV above the onset of chiral symmetry breaking, [52, 56]. For cutoff scales in the vicinity of the onset of chiral symmetry breaking and below, $k \lesssim 500$ MeV the other two-flavour channels and even more so the

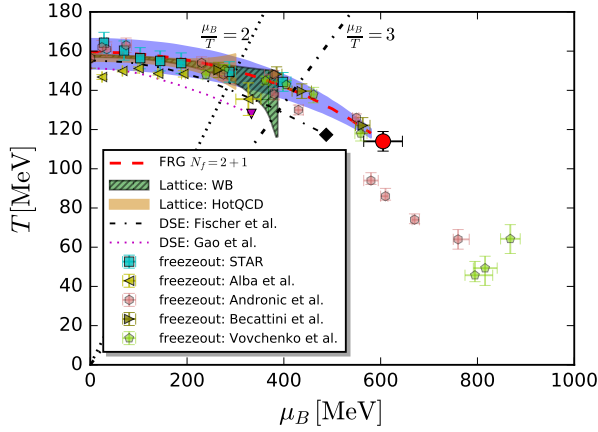


Figure 8.1.: Phase diagram in the plane of the temperature and the baryon chemical potential. The blue band denote the continuous crossover for the $N_f = 2$ and $2+1$ flavor QCD, respectively; and the red star and circle is the CEP. Taken from [116].

s -quark channels are not dynamical anymore due to their large mass scales. Indeed, sizable contributions are only triggered by the pion channel. This is in line and supports chiral perturbation theory.

We emphasise that at large densities/chemical potential we expect offshell contributions from diquark or density channels, while the irrelevance of offshell s -quark channels still is a good approximation. Still the importance of the additional $N_f = 2$ flavour channels has been investigated thoroughly in effective theories in [100, 115], leading to a semi-quantitative agreement of both approximations up to large densities after an appropriate rescaling. Accordingly the two theories differ by the Dirac term in the effective action, and hence by the respective additional s -quark loops. This is important for purely gluonic correlation functions and amounts to a relative change in the physics scale Λ_{QCD} as well as the respective β -functions. This is very similar to respective DSE computations, a difference being the backreaction in the purely gluonic diagrams which is taken into account in the present work.

In the action (11.75) the mesonic field $\phi = (\sigma, \vec{\pi})$ is in the $O(4)$ -representation with $\rho = \phi^2/2$; Z 's are the wave function renormalizations for respective fields with subscript k denoting the dependence of renormalization group (RG) scale. The covariant derivative in the fundamental and adjoint representations of $SU(N_c)$ reads

$$D_\mu = \partial_\mu - iZ_{A,k}^{1/2} \bar{g}_k A_\mu^a t^a, \\ D_\mu^{ab} = \partial_\mu \delta^{ab} - Z_{A,k}^{1/2} \bar{g}_k f^{abc} A_\mu^c, \quad (8.4)$$

respectively, where $\bar{g}_k = \sqrt{4\pi\bar{a}_{s,k}}$ is the RG-invariant strong coupling which is specified in ???. f^{abc} is the structure constant for the $SU(N_c)$ group, whose Lie algebra is $[t^a, t^b] = if^{abc} t^c$ with the normalization $\text{Tr} t^a t^b = \frac{1}{2}\delta^{ab}$ for the generators.

The first four terms on the r.h.s. of Equation (11.75) constitute the classical QCD action. The gluonic field strength tensor reads

$$F_{\mu\nu}^a = Z_{A,k}^{1/2} (\partial_\mu A_\nu^a - \partial_\nu A_\mu^a + Z_{A,k}^{1/2} \bar{g}_k f^{abc} A_\mu^b A_\nu^c), \quad (8.5)$$

and the Landau gauge $\xi = 0$ is chosen in this work; c^a and q denote the ghost and quark fields respectively. The results are summarised in Figure 8.1.

Part III.

Quantum Gravity from an FRG perspective

9. Introduction

The four known fundamental forces in physics, the electro-magnetic, weak, strong and gravitational force describe the world around us. While the first three ones are described by gauge theories with the gauge groups $U(1) \times SU(2)$ and $SU(3)$ for the electro-weak and strong forces respectively, the gravitational force derives from the equivalence principle.

Curiously the gravitational force differs from the others strongly. First of all the gravitational force is very weak. It is 39 orders of magnitude weaker than the electric force and still 26 orders of magnitude weaker than the weak force which is, as the name already says, very weak. Another difference is that the best description of gravity, given by General Relativity (GR), is based on a completely different concept, the curved spacetime. The most important distinction is the fact that all other three forces can be quantised in a perturbative setting, and are summarised within the Standard Model of Particle Physics. However, GR is perturbatively non-renormalisable. This we will discuss at the end of this section after shortly recapitulating the basics of classical GR.

9.1. Classical general relativity

Comparing the gravitational force to the other forces of nature one realises that the gravitational one is special. The speciality is hidden in the universality of the gravitational interaction and can be described by the

Einstein Equivalence Principle: *In small enough regions of spacetime the laws of physics reduce to those of Special Relativity. Thus, locally it is impossible to detect a gravitational field.*

In other words a physicist in a box (without observing the outside world) cannot distinguish between the existence of a gravitational field and uniform acceleration. Due to the special rôle of gravity we have to give up the concept of global inertial frames and restrict ourselves to local inertial frames. Therefore the theory we are looking for has to be independent of the chosen coordinates. In a mathematical language we have to find a theory that is diffeomorphism invariant. All this leads us to the concept of curved spacetime, which can be described by a differentiable manifold.

Within the concept of curved spacetime the gravitational interaction is described with the curvature of the manifold and thus the gravitational degrees of freedom are given by the metric field $g_{\mu\nu}(x)$. The metric admits a unique Riemannian and torsion free connection, the Levi-Civita connection Γ . Its components are the Christoffel symbol,

$$\Gamma^\sigma{}_{\mu\nu} = \frac{1}{2} g^{\sigma\rho} (\partial_\mu g_{\nu\rho} + \partial_\nu g_{\rho\mu} - \partial_\rho g_{\mu\nu}) . \quad (9.1)$$

The parallel transport of scalars, vectors and second rank tensors are given by

$$\nabla_\rho \phi = \partial_\rho \phi, \quad \nabla_\rho A_\mu = \partial_\rho A_\mu - \Gamma^\sigma{}_{\mu\rho} A_\sigma, \quad \nabla_\rho T_{\mu\nu} = \partial_\rho T_{\mu\nu} - \Gamma^\lambda{}_{\rho\mu} T_{\lambda\nu} - \Gamma^\Lambda{}_{\rho\nu} T_{\mu\lambda}, \quad (9.2)$$

and the generalisation to higher tensors is straightforward. The two most important properties of Γ are

$$\begin{aligned} \text{torsion freeness:} & \quad \Gamma^\sigma{}_{\mu\nu} - \Gamma^\sigma{}_{\nu\mu} = 0, \\ \text{metric compatibility:} & \quad \nabla_\rho g_{\mu\nu} = \partial_\rho g_{\mu\nu} - \Gamma^\lambda{}_{\rho\mu} g_{\lambda\nu} - \Gamma^\Lambda{}_{\rho\nu} g_{\mu\lambda} = 0, \end{aligned} \quad (9.3)$$

with the covariant derivative ∇ . This connection vanishes for flat spacetimes and can be used to analyse the motion of a test particle in a curved spacetime. Thus it is one of the main objects used to characterise curvature. Such a test particle is described by the action

$$S_{\text{testparticle}} = \frac{1}{2} \int ds^2 = \frac{1}{2} \int g_{\mu\nu}(x) \frac{dx^\mu}{d\tau} \frac{dx^\nu}{d\tau} d\tau. \quad (9.4)$$

Without the influence of any other force a test particle moves on curves satisfying the Euler-Lagrange equations of this action. This tells us nothing but the fact that the test particle chooses the shortest path between two points. Note that on a curved manifold the shortest path not necessarily is a straight line. An example for illustration would be the shortest path between two point on the surface of the earth. The aforementioned Euler-Lagrange equations read

$$\frac{d^2 x^\mu}{d\tau^2} + \Gamma^\mu_{\rho\sigma} \frac{dx^\rho}{d\tau} \frac{dx^\sigma}{d\tau} = 0. \quad (9.5)$$

It is also called the geodesic equation and the solutions $x_\mu(\tau)$, parametrised by τ , are called geodesic curves. These are the shortest paths in a curved spacetime with a metric $g_{\mu\nu}$ and corresponding connections $\Gamma^\mu_{\rho\sigma}$.

Another object used to describe the curvature of a given manifold is the Riemann tensor or curvature tensor. It is a $(1, 3)$ -tensor and given by a combination of the Christoffel symbols

$$R^\rho_{\sigma\mu\nu} = \partial_\mu \Gamma^\rho_{\nu\sigma} - \partial_\nu \Gamma^\rho_{\mu\sigma} + \Gamma^\rho_{\mu\lambda} \Gamma^\lambda_{\nu\sigma} - \Gamma^\rho_{\nu\lambda} \Gamma^\lambda_{\mu\sigma}. \quad (9.6)$$

This tensor satisfies several symmetries. Very useful identities are the so-called Bianchi identities. The most important relations for the Riemann tensor are

skew symmetry:	$R_{\mu\nu\rho\sigma} = -R_{\nu\mu\rho\sigma} = -R_{\mu\nu\sigma\rho},$
interchange symmetry:	$R_{\mu\nu\rho\sigma} = R_{\rho\sigma\mu\nu},$
first Bianchi identity:	$R_{\mu[\nu\rho\sigma]} = R_{\mu\nu\rho\sigma} + R_{\mu\sigma\nu\rho} + R_{\mu\rho\sigma\nu} = 0,$
second Bianchi identity:	$\nabla_{[\lambda} R_{\rho\sigma]\mu\nu} = \nabla_\lambda R_{\rho\sigma\mu\nu} + \nabla_\sigma R_{\lambda\rho\mu\nu} + \nabla_\rho R_{\sigma\lambda\mu\nu} = 0.$

(9.7)

Here the square brackets in the indices indicate an anti symmetrisation. Further useful objects are the contractions of the Riemann tensor. The first is the so-called Ricci tensor $R_{\mu\nu}$, which is a $(0, 2)$ -tensor. The contraction of this Ricci tensor is called the Ricci scalar R . Using these two we can define a further tensor $G_{\mu\nu}$ which is called the Einstein tensor. These three new objects are defined as

$$R_{\mu\nu} = R^\lambda_{\mu\lambda\nu}, \quad R = R^\mu_{\mu}, \quad G_{\mu\nu} = R_{\mu\nu} - \frac{1}{2}R g_{\mu\nu}. \quad (9.8)$$

The symmetry relations for the Riemann tensor reduce to the fact that the Ricci tensor is symmetric within its two indices. Furthermore using the second Bianchi identity (9.7) one can show that the Einstein tensor satisfies $\nabla^\mu G_{\mu\nu} = 0$.

There are many more curvature invariants. Some we will use later, such as the Weyl tensor

$$C_{\mu\nu\rho\sigma} = R_{\mu\nu\rho\sigma} + \frac{1}{d-2} (R_{\mu\sigma} g_{\nu\rho} - R_{\mu\rho} g_{\nu\sigma} + R_{\nu\rho} g_{\mu\sigma} - R_{\nu\sigma} g_{\mu\rho}) + \frac{R}{(d-1)(d-2)} (g_{\mu\rho} g_{\nu\sigma} + g_{\mu\sigma} g_{\nu\rho}), \quad (9.9)$$

where d is the spacetime dimension. In two and three spacetime dimensions the Weyl tensor vanishes identically. In $d \geq 4$ the Weyl tensor is generally non-vanishing. The square of the Weyl tensor is related to the other curvature invariants by

$$C_{\mu\nu\rho\sigma}^2 = \frac{2}{(d-1)(d-2)} R^2 - \frac{4}{d-2} R_{\mu\nu}^2 + R_{\mu\nu\rho\sigma}^2, \quad (9.10)$$

which will be important later for determining a basis for the higher-order curvature operators.

With the Riemann tensor and the derived curvatures, Ricci tensor, Ricci scalar and Einstein tensor we can derive a geometrical theory of gravity. In analogy to standard field theories we aim for a 'minimally' coupled theory of gravity that describes classical relativity and leads to a $1/r$ gravitational potential in the non-relativistic limit. These conditions are satisfied for the *Einstein-Hilbert action*

$$S_{\text{EH}}[g_{\mu\nu}] = \frac{1}{16\pi G} \int d^d x \sqrt{-\det g_{\mu\nu}} (R - 2\Lambda) . \quad (9.11)$$

The usual measure $d^d x$ of the spacetime integral has to be combined with $\sqrt{-\det g_{\mu\nu}}$ to give a diffeomorphism invariant measure. Diffeomorphism transformations are generated by the Lie derivative \mathcal{L}_ω with

$$\mathcal{L}_\omega \phi = \omega^\mu \partial^\mu \phi = \omega^\mu \nabla^\mu \phi . \quad (9.12)$$

More generally it holds, that the Lie derivative can be represented in terms of covariant derivatives w.r.t. torsion free connections, but is metric-independent. For example, for vectors and rank-two tensors we have

$$\begin{aligned} \mathcal{L}_\omega A_\mu &= \omega^\rho \partial_\rho A_\mu + A_\rho \partial_\mu \omega^\rho = \omega^\rho \nabla_\rho A_\mu + A_\rho \nabla_\mu \omega^\rho , \\ \mathcal{L}_\omega T_{\mu\nu} &= \omega^\rho \partial_\rho T_{\mu\nu} + T_{\rho\nu} \partial_\mu \omega^\rho + T_{\mu\rho} \partial_\nu \omega^\rho = \omega^\rho \nabla_\rho T_{\mu\nu} + T_{\rho\nu} \nabla_\mu \omega^\rho + T_{\mu\rho} \nabla_\nu \omega^\rho , \end{aligned} \quad (9.13)$$

It is in most cases more convenient to use the form with covariant derivatives, which allows to use metric compatibility. In particular this entails for $T_{\mu\nu} = g_{\mu\nu}$ that

$$\mathcal{L}_\omega g_{\mu\nu} = g_{\rho\nu} \nabla_\mu \omega^\rho + g_{\mu\rho} \nabla_\nu \omega^\rho , \quad (9.14)$$

the first term on the right-hand side of the Lie derivative of a general rank-two tensor in (9.13) is missing. Note also that while (9.14) seemingly depends on all powers of $g_{\mu\nu}$ due to the presence of covariant derivatives, it is in fact linear in $g_{\mu\nu}$ as it can be expressed in terms of partial derivatives, see (9.13).

In summary, the Einstein-Hilbert action is invariant under diffeomorphism transformations

$$g_{\mu\nu} \rightarrow g_{\mu\nu} + \mathcal{L}_\omega g_{\mu\nu} , \quad (9.15)$$

with an infinitesimal diffeomorphism parameter ω_μ : the Ricci scalar R as well as $\sqrt{-\det g_{\mu\nu}}$ are diffeomorphism invariant, and hence the Einstein-Hilbert action (9.11) is. The Ricci scalar encodes Newton's gravitational law in the non-relativistic limit, the $1/r$ dependence is reflected in the p^2 dependence of the (inverse) graviton propagator $S_{gg}^{(2)}[g = \eta]$. Here η is the flat Minkowski metric, $\text{diag}(-1, 1, 1, 1)$, and we adopted the notation from (1.11) for n -th field derivatives for quantum gravity. The equations of motion derived from the Einstein-Hilbert action are the Einstein equations in the absence of matter,

$$G_{\mu\nu} + \Lambda g_{\mu\nu} = 0 \quad \Rightarrow \quad R_{\mu\nu} = \Lambda g_{\mu\nu} . \quad (9.16)$$

The second equation results from the first one by taking the trace and reinserting the result for four dimensions. These famous vacuum field equations have several well known solutions. One is the flat Minkowski space $g_{\mu\nu} = \eta_{\mu\nu} \Rightarrow R = 0$. Another very famous solution for vanishing cosmological constant is the Schwarzschild solution. It describes the spacetime outside a massive point particle and can be used to investigate the gravitational field around objects like the sun or non-rotating black holes. The so-called deSitter solution is used e.g. in cosmological models. It is maximally symmetric, which means

$R_{\mu\nu\rho\sigma} \sim (g_{\mu\rho}g_{\nu\sigma} - g_{\mu\sigma}g_{\nu\rho})$, and it has $R > 0$. The corresponding line element reads

$$\begin{aligned} ds^2 &= -dt^2 + \alpha^2 \cosh^2(t/\alpha) \left[d\chi^2 + \sin^2 \chi (d\theta^2 + \sin^2 \theta d\phi^2) \right], \\ x &= \alpha \cosh(t/\alpha) \sin \chi \cos \theta, \\ y &= \alpha \cosh(t/\alpha) \sin \chi \sin \theta \cos \phi, \\ z &= \alpha \cosh(t/\alpha) \sin \chi \sin \theta \sin \phi. \end{aligned} \quad (9.17)$$

There is as well a so called anti-deSitter solution similar to the deSitter one. It is as well maximally symmetric but it has $R < 0$.

Now we add matter to the pure gravity action (9.11). The simplest case is a minimally coupled scalar field ϕ within a potential V . The corresponding action is given by

$$S_{\text{matter}}[g_{\mu\nu}, \phi] = -\frac{1}{2} \int d^d x \sqrt{-\det g_{\mu\nu}} (g^{\mu\nu} \nabla_\mu \phi \nabla_\nu \phi - V(\phi)). \quad (9.18)$$

Here the kinetic term consists of covariant derivatives ∇_μ in order to be diffeomorphism invariant. For the scalar field the covariant derivative reduces to the partial derivative. The potential $V(\phi)$ should be invariant under diffeomorphisms as well. This is just a simple example for a matter Lagrangian. It could of course also contain fermionic fields, gauge fields or non-minimal couplings such as e.g. $R\phi\phi$.

The energy-momentum tensor corresponding to the minimally coupled scalar field in (9.18) is given by

$$T_{\mu\nu} = \frac{-2}{\sqrt{-\det g_{\mu\nu}}} \frac{\delta S_{\text{matter}}}{\delta g^{\mu\nu}} = \nabla_\mu \phi \nabla_\nu \phi - \frac{1}{2} g_{\mu\nu} g^{\rho\sigma} \nabla_\rho \phi \nabla_\sigma \phi - g_{\mu\nu} V(\phi). \quad (9.19)$$

The energy-momentum tensor for a fluid in equilibrium is important for cosmological applications and is diagonal $T^{\mu\nu} = \text{diag}(\rho, p, p, p)$. Its elements are the density ρ and the hydrostatic pressure p . There are a number of energy conditions that have to be satisfied by $T_{\mu\nu}$ and can be found e.g. in [117]. For brevity we will not comment on them here.

The equation of motion can be derived by asking for $\sqrt{-\det g} \frac{\delta S}{\delta g^{\mu\nu}} = 0$, with the combined action $S = S_{\text{EH}} + S_{\text{matter}}$ from (9.11) and (9.18), and reads

$$\frac{1}{8\pi G} \left[R_{\mu\nu} - \frac{1}{2} (R - 2\Lambda) g_{\mu\nu} \right] = T_{\mu\nu}. \quad (9.20)$$

These are also called Einstein's field equations and we wrote them in a way that the matter contributions are on the right-hand side and the gravitational ones on the left-hand side. These equations can be interpreted in several ways. One way is to say that the matter (right-hand side) tells spacetime how to curve (left-hand side). Another way would be to say that the curvature of spacetime (left-hand side) tells the matter (right-hand side) how to move. This coupling between the two ingredients makes the solution very hard. Usually one sticks to numerical methods.

9.2. Failure of Perturbative Quantisation

GR is a very successful theory for length scales larger than the Planck scale \sqrt{G} . For smaller length scales quantum gravity may play an important role. For the inclusion of quantum gravity effects we first consider Euclidean perturbation theory based on the Wick rotated Einstein-Hilbert action

$$S_{\text{EH}}[g_{\mu\nu}] = \frac{1}{16\pi G} \int d^d x \sqrt{g} (2\Lambda - R), \quad (9.21)$$

where from now on we use the standard abbreviation

$$\sqrt{g} := \sqrt{\det g_{\mu\nu}}. \quad (9.22)$$

The very naive path integral quantisation gives us the generating functional

$$\int [dg_{\mu\nu}]_{\text{ren}} e^{-S_{\text{EH}}} . \quad (9.23)$$

The definition (9.23) faces multiple problems, the most severe ones go beyond that encountered in non-Abelian gauge theories. In the latter theories gauge symmetry led to redundancies in the path integral measure that were eliminated via gauge fixing. In quantum gravity redundancies in the path integral measure occur due to diffeomorphism invariance. This intricacy is amended by the standard gauge fixing procedure, as introduced below.

The more serious problems with (9.23) come from the lack of positivity of S_{EH} and the missing perturbative renormalisability of the theory. In summary, both the existence as well as the unitarity of the theory are at stake.

Standard perturbation theory is based on a coupling expansion or rather amplitude expansion of the theory at hand about the free, quadratic theory. The Einstein-Hilbert action can be expanded up to arbitrary powers in the metric field, as done e.g. in [118] up to forth order. More generally such an expansion is done about a given background $\bar{g}_{\mu\nu}$ with

$$g_{\mu\nu} = \bar{g}_{\mu\nu} + \sqrt{G} h_{\mu\nu} , \quad (9.24)$$

with the metric fluctuation $h_{\mu\nu} = 1/\sqrt{G}(g_{\mu\nu} - \bar{g}_{\mu\nu})$. Evidently, the fluctuation field $h_{\mu\nu}$ is a difference of metrics and hence not a metric itself. The normalisation with \sqrt{G} gives us a standard kinetic term for $h_{\mu\nu}$ with no dependence on the Newton coupling G , though an unusual normalisation with $1/(32\pi)$. For the *linear split* in (9.24) the path integral can be performed in terms of fluctuation field $h_{\mu\nu}$ and reads naively

$$Z[J^{\mu\nu}; \bar{g}_{\mu\nu}] \propto \int [dh_{\mu\nu}]_{\text{ren}} e^{-S_{\text{EH}}[\bar{g}_{\mu\nu} + \sqrt{G} h_{\mu\nu}] + \int d^d x \sqrt{\bar{g}} J^{\mu\nu} h_{\mu\nu}} . \quad (9.25)$$

We emphasise that despite being an Euclidean theory lowering and rising indices has to be considered with care as it introduces dependences on the dynamical field $g_{\mu\nu}$. In (9.25) we integrate over $h_{\mu\nu}$, and the generating functional is a function of the current $J^{\mu\nu}$. The n -th current-derivatives give the correlation functions of the fluctuation field $h_{\mu\nu}$, and the source term depends on the determinant of the background metric, $\int d^d x \sqrt{\bar{g}}$. If we had used the determinant of the full metric $\det g_{\mu\nu}$, $J^{\mu\nu}$ -derivatives would not generate n -point functions of the fluctuation field. This intricacy is already the first hint at an important property and problem in quantum gravity, that of the *background independence* of its formulation.

The linear split in (9.24) has an equivalent but simpler analogue in a non-Abelian gauge theory based on the action

$$S_{\text{YM}}[A] = \frac{1}{4g_s^2} \int_x F_{\mu\nu}^a F_{\mu\nu}^a , \quad \text{with} \quad F_{\mu\nu} = \partial_\mu A_\nu - \partial_\nu A_\mu + f^{abc} A_\mu^b A_\nu^c , \quad (9.26)$$

where in comparison to (5.10) we have absorbed the coupling in the definition of A_μ ; the respective covariant derivative is $D_\mu = \partial_\mu - iA_\mu$. Then an expansion

$$A_\mu = \bar{A}_\mu + g_s a_\mu , \quad (9.27)$$

gives us the standard kinetic term of the fluctuation field a_μ with no dependence on the strong coupling g_s and a standard kinetic operator with

$$S_{\text{YM}}^{(2)}[\bar{A}] = -\bar{\mathcal{D}}_T + \bar{D}_\mu \bar{D}_\nu , \quad \text{with} \quad \mathcal{D}_T = D_\rho^2 \delta_{\mu\nu} + 2i F_{\mu\nu} . \quad (9.28)$$

where D_ρ^2 is the Laplace operator of a spin-zero field and \mathcal{D}_T is the spin-one Laplacian in the gauge theory. Equation (9.28) reduces to the standard transversal dispersion for vanishing background field $\bar{A} = 0$ with the transversal and longitudinal projection operators given in (5.41).

For non-vanishing background such an orthogonal splitting is still possible, the respective orthogonal projection operators are the covariant generalisations of (5.41),

$$\Pi_{\mu\nu}^\perp(D) = \delta_{\mu\nu} - \frac{D_\mu D_\nu}{D^2}, \quad \Pi_{\mu\nu}^\parallel(p) = \frac{D_\mu D_\nu}{D^2} = \delta_{\mu\nu} - \Pi_{\mu\nu}^\perp(D), \quad (9.29)$$

with $\Pi^\perp(D)^2 = \Pi^\perp(D)$, $\Pi^\parallel(D)^2 = \Pi^\parallel(D)$, $\Pi^\perp(D)\Pi^\parallel(D) = 0$ and $\Pi^\perp(D) + \Pi^\parallel(D) = \mathbb{I}$. Within this setup we discuss the transversality of the classical two-point function in a given background. For non-vanishing background we get

$$\bar{D}_\mu S_{\text{YM},\mu\nu}^{(2)}[\bar{A}] = [\bar{D}_\mu, \bar{F}_{\mu\nu}]. \quad (9.30)$$

The right-hand side of (9.30) simply is the equation of motion for Yang-Mills theory. Accordingly the kinetic term is transversal and hence cannot be inverted, only if the background field \bar{A}_μ is a solution of the EoM. Still, a gauge fixing is required for an evaluation of the quantised theory as the path integral carries an infinite redundancy.

The same holds true for GR. Due to diffeomorphism invariance the two-point function $S_{\text{EH}}^{(2)}$ is not invertible for $\bar{g}_{\mu\nu}$ that solve the Einstein equations. The gravity analogue of (9.28) is lengthy and its explicit form is deferred to the Appendix G.2, see also [?]. Analogously to the split of non-Abelian gauge fields in transversal and longitudinal modes, the gravitational fluctuation field $h_{\mu\nu}$ can be written in terms of traceless transversal tensor modes, vector modes and scalar modes. This is the *York-decomposition*, for more details see the discussion in Appendix G.2.1 around (G.11). This decomposition reads

$$h_{\mu\nu} = h_{\mu\nu}^{\text{TT}} + 2\bar{\nabla}_{(\mu}\xi_{\nu)} + \left(\bar{\nabla}_\mu \bar{\nabla}_\nu - \frac{\bar{g}_{\mu\nu}}{d} \bar{\nabla}^2 \right) \sigma + \frac{1}{d} \bar{g}_{\mu\nu} h, \quad (9.31)$$

and the projection is done in terms of the background metric and covariant derivative. For a flat background this is done explicitly in Appendix G.2.2. In (9.31), the full fluctuation field $h_{\mu\nu}$ is decomposed in a *transverse traceless* tensor mode $h_{\mu\nu}^{\text{TT}}$, a vector mode ξ_μ , a scalar mode σ and the trace mode $h = \bar{g}^{\mu\nu} h_{\mu\nu}$. Note again that the decomposition is done with respect to the background metric $\bar{g}_{\mu\nu}$.

We still have to perform the gauge fixing, which is done similarly to QCD in a covariant gauge. To be more explicit, We consider linear gauge fixing conditions for the fluctuating graviton field h with

$$F_\mu[\bar{g}, h] = L_\mu^{\rho\sigma}[\bar{g}]h_{\rho\sigma} = 0. \quad (9.32)$$

The gauge fixing (9.32) is implemented with a standard gauge fixing term

$$S_{\text{gf}}[\bar{g}, h] = \frac{1}{2\alpha} \int d^d x \sqrt{\bar{g}} \bar{g}^{\mu\nu} F_\mu F_\nu, \quad (9.33)$$

with the gauge-fixing parameter α . The most common choices for α are the Landau–DeWitt gauge $\alpha = 0$ and the Feynman–’t Hooft gauge $\alpha = 1$. The Feynman–’t Hooft gauge $\alpha = 1$ often simplifies perturbative computations, as it results in a rather simple form of the graviton propagator. However, as in the FRG approach to QCD, the gauge fixing parameter α is scale-dependent and the Feynman–’t Hooft gauge at one scale, e.g. the initial scale $k = \Lambda$, is not maintained in the flow. In turn, the Landau–DeWitt gauge $\alpha = 0$ has the advantage that it maximally disentangles gauge and non-gauge modes, as well as being a -trivial- fixed point of the RG flow [119].

The gauge condition F_μ depends on g and \bar{g} and has to be chosen such that the gauge-fixing action (9.33) is invariant under background gauge transformations 10.2b. In the following, we use de-Donder-type gauge fixings of the form

$$F_\mu[\bar{g}, h] = \bar{\nabla}^\alpha h_{\alpha\mu} - \frac{1+\beta}{4} \bar{\nabla}_\mu \bar{g}^{\alpha\beta} h_{\alpha\beta}, \quad (9.34)$$

where β is a second gauge parameter and it is often taken to be $\beta = 1$ for the sake of simplicity. Note that often the latter term in (9.34) is written as $\bar{g}^{\alpha\beta}\bar{\nabla}_\mu h_{\alpha\beta}$. This is an equivalent formulation due to metric compatibility, see (9.3).

Following the Faddeev-Popov procedure of the gauge fixing, see section 5.2 of Part II, we are led to a Faddeev-Popov determinant or ghost action. The Faddeev-Popov operator $M[\bar{g}, h]$ for (9.34) is the diffeomorphism variation with (9.14) of the gauge-fixing condition and reads

$$M_{\mu\nu}[\bar{g}, h] = \bar{\nabla}^\rho \left(g_{\mu\nu} \nabla_\rho + g_{\rho\nu} \nabla_\mu \right) - \frac{1+\beta}{2} \bar{g}^{\sigma\rho} \bar{\nabla}_\mu g_{\nu\sigma} \nabla_\rho . \quad (9.35)$$

Here the covariant derivatives with respect to g and \bar{g} are ∇_μ and $\bar{\nabla}_\mu$, respectively. Following further the lines of section 5.2 of Part II we exponentiate this determinant. The Faddeev-Popov trick leads to the ghost action

$$S_{\text{gh}}[\bar{g}, h, c, \bar{c}] = \int d^d x \sqrt{\bar{g}} \bar{c}^\mu M_{\mu\nu} c^\nu . \quad (9.36)$$

The ghost action has vertices to all powers of the background metric $\bar{g}_{\mu\nu}$ but it is linear in the fluctuation field $h_{\mu\nu}$. In summary the complete gauge-fixed Einstein-Hilbert action reads

$$S_{\text{grav}}[\bar{g}, \Phi] = S_{\text{EH}}[g] + S_{\text{gf}}[\bar{g}, h] + S_{\text{gh}}[\bar{g}, \Phi] , \quad (9.37)$$

Here we have introduced the pure gravity multifield

$$\Phi = (h_{\mu\nu}, c_\mu, \bar{c}_\mu) . \quad (9.38)$$

This leads us to the path integral of gauge-fixed quantum gravity

$$Z[J; \bar{g}] = \int [d\Phi]_{\text{ren}} e^{-S_{\text{grav}}[\bar{g}_{\mu\nu}, \Phi] + \int d^4 x \sqrt{\bar{g}} J \cdot \Phi} . \quad (9.39)$$

with S_{grav} given in (9.37). From (9.39) we obtain the Feynman rules for the graviton propagator and the three- and four-graviton vertex as shown in Figure 9.1. They are proportional to $1/p^2$, $\sqrt{G}p^2$ and Gp^2 respectively due to a rescaling of the metric field with \sqrt{G} . These rules already appear in a purely gravitational theory. If we add a matter part, e.g. (9.18), to the Einstein-Hilbert action (9.11) further Feynman rules arise. Generally these might look like those of Figure 9.2. The curly lines are gravitons and the full lines correspond to matter fields, which might be scalars, fermions or gauge fields.

Below we present a full power counting analysis of Einstein-Hilbert gravity. To begin with, we discuss the canonical momentum dimensions of the couplings of the theory, G and Λ . This analysis already indicates that perturbative renormalisability is at stake. We find

$$\begin{aligned} [\sqrt{g}] &= 0 , & [G] &= [d^d x \sqrt{g} R] = 2 - d , & [g_{\mu\nu}] &= 0 , \\ [R] &= 2 , & [\Lambda] &= 2 , & [h_{\mu\nu}] &= 1 . \end{aligned} \quad (9.40)$$

Thus for $d = 4$ the gravitational coupling has a negative mass dimension, already indicating the probable failure of perturbation theory. The critical dimension of gravity is $d = 2$ with $[G]_{d=2} = 0$. This serves as a starting point for an ϵ -expansion of $d = 4$ gravity about $d = 2$ with $d = 2 + \epsilon$.

Let us now discuss the divergences of perturbative quantum gravity. Analogous to the standard perturbative analysis in a quantum field theory, see e.g. [120], we consider a general graph γ with E external lines and L loops. Furthermore it can contain I internal propagators as well as v_3 three- and v_4 four-graviton vertices. An example of such a graph with $I = 11, E = 3, v_3 = 7, v_4 = 1$ and $L = 4$ is depicted in Figure 9.3. Counting the powers of momenta in a general graph shows us that it diverges like $\Lambda^{\delta(\gamma)}$, where

Λ is a UV cutoff for the momentum integrals and the index of the graph $\delta(\gamma)$ reads

$$\delta(\gamma) = dL - 2(I - \sum_{n=3}^{\infty} v_n). \quad (9.41)$$

This counting of powers of momenta in the graph works as follows. For any loop we get a d dimensional momentum integral and thus a p^d , where d is the number of spacetime dimensions. For any propagator we get a p^{-2} and any n -graviton vertex gives us a p^2 , see Figure 9.1. The relation (9.41) can be simplified by replacing the number of internal propagators by the number of external lines. For any graph we get

$$E + 2I = \sum_{n=3}^{\infty} n v_n. \quad (9.42)$$

Furthermore the number of loops is expressed by

$$L = I + 1 - \sum_{n=3}^{\infty} v_n. \quad (9.43)$$

The proof of this relation can be done iteratively. Inserting (9.42) and (9.43) into (9.41) gives us the index of the graph independent of the number of loops but depending on the external lines. The result reads

$$\delta(\gamma) = d - \frac{d-2}{2}E + \sum_{n=3}^{\infty} v_n \delta(v_n), \quad (9.44)$$

with of the n -graviton vertices $\delta(v_n)$, which is given by

$$\delta(v_n) = \frac{1}{2}(n-2)(d-2), \quad (9.45)$$

This index is the negative of the canonical dimension of the coupling constant and thus, due to (9.40), for gravity $\delta(V_n) > 0$ holds for $n > 2$.

Now consider the grade of divergence $\Lambda^{\delta(\gamma)}$ for graphs with a fixed number of external lines. For simplicity we take two external lines, which corresponds to the vacuum polarisation. To 1-loop order these

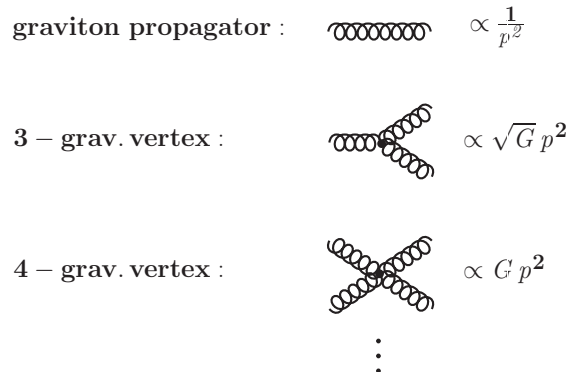


Figure 9.1.: Feynman rules for graviton propagator, three-graviton vertex and four-graviton vertex.

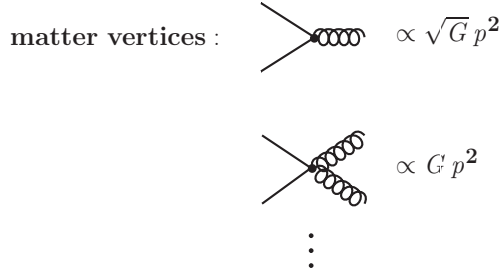


Figure 9.2.: Feynman rules for gravitons coupled to matter.

graphs are shown in [Figure 9.4](#). 't Hooft and Veltman showed that the counter terms for these graphs vanish on-shell. These counter terms usually are introduced to cancel the divergences by redefinition of the coupling constants. Thus the 1-loop divergences in gravity can be cured by a renormalisation of the fields [\[121\]](#). Unfortunately this does not hold to higher orders. If we go beyond 1-loop the divergences $\Lambda^{\delta(\gamma)}$ are getting worse, which can be seen in [\(9.44\)](#). Going to higher-loop order, while keeping the number of external legs fixed, means including more vertices v_n , which leads to an increasing $\delta(\gamma)$ due to the positive $\delta(v_n)$. Thus going to higher-loop order produces new divergences and therefore this is a hint that infinitely many counter terms are needed to absorb these divergences.

At two loop, the Goroff-Sagnotti counter term is generated [\[122, 123, 124\]](#). It is given by

$$S_{\text{GS}} = \frac{1}{\varepsilon} \frac{209}{2880} \frac{1}{(4\pi)^4} \int d^4x \sqrt{g} C_{\mu\nu}{}^{\kappa\lambda} C_{\kappa\lambda}{}^{\rho\sigma} C_{\rho\sigma}{}^{\mu\nu}, \quad (9.46)$$

where $C_{\mu\nu\rho\sigma}$ is the Weyl tensor, see [\(9.9\)](#). This is the first counter term that does not vanish on-shell. It is commonly interpreted, though not proven, as the onset of counter terms that cannot be reabsorbed by a redefinition of fields. In summary, this shows that Einstein-Hilbert gravity is most likely perturbatively non-renormalisable due to the negative mass dimension of the Newton coupling.



Figure 9.3.: An exemplary graph with three external gravitons and four loops.

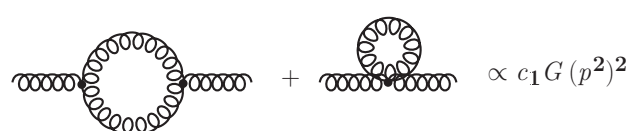
$$\text{Diagram A} + \text{Diagram B} \propto c_1 G (p^2)^2$$


Figure 9.4.: Vacuum polarisation to 1-loop order.

10. RG approach to quantum gravity

In the last chapter we have seen that the perturbative renormalisation of Einstein-Hilbert gravity fails. This does not entail that Einstein-Hilbert quantum gravity does not exist, but cannot be expanded about vanishing Newton coupling, the Gaußian, free, theory. Such an expansion works in QCD due to *asymptotic freedom*. Assuming for the moment the existence of quantum gravity based on the Einstein-Hilbert action, we can study its phase structure and in particular its fixed points, see [Section 3.3](#). In terms of a fixed point analysis the failure of perturbative renormalisability simply reflects that the Gaußian fixed point is repulsive. Indeed, we shall see that this is the case.

Therefore, in the absence of an UV attractive Gaußian fixed point we search for a non-Gaußian interacting attractive fixed point. Then the theory is attracted to this fixed point for asymptotically large momentum scales, and is well-defined. If such a fixed point exists, the theory is called *asymptotically safe*. This concept generalises that of asymptotic freedom and was introduced by S. Weinberg in 1979 to quantum gravity [125]. Evidently, this encompasses and generalises asymptotic freedom, which is a -trivial- subcase.

In particular this general scenario requires a finite number of UV attractive directions, spanning the *critical surface* at this fixed point. The reason is that a coupling constant of the fundamental theory corresponds to a UV attractive direction can have any value in the IR and thus has to be fixed by experiment. Consequently, an infinite-dimensional critical surface amounts to infinitely many parameters in the theory, potentially spoiling the predictive power. In turn, the IR value of a coupling constant corresponding to a UV repulsive direction on the other hand only depends on the UV relevant couplings, and hence is a prediction.

Such asymptotic safety scenarios have been investigated in a variety of models ranging from four-fermion models [126, 127, 128, 129] and Yukawa systems [130, 131, 132], over extra-dimensional gauge theories [133] to non-linear sigma models [134, 135, 136, 137]. Further examples can be found in [81, 138, 139, 140]. In the present lecture notes, we concentrate on the asymptotic safety scenario for quantum gravity.

10.1. Flow equations for quantum gravity

In [Chapter 9](#) we have set-up the gauge-fixed approach to quantum gravity. While it cannot be treated in perturbation theory about the Gaußian fixed point, this serves as the starting point for the FRG formulation of quantum gravity: we assume that we can expand the full effective action Γ_k of quantum gravity about the gauge-fixed action $S_{\text{grav}}[\bar{g}, \Phi]$ in [\(9.37\)](#). We add a cutoff term $\Delta S_k[\bar{g}, \Phi]$ to the classical action in the path integral [\(9.39\)](#) and arrive at

$$Z_k[J; \bar{g}] = \int \int [d\Phi]_{\text{ren}} e^{-S_{\text{grav}}[\bar{g}, \Phi] - \Delta S_k[\bar{g}_{\mu\nu}, \Phi] + \int d^d x \sqrt{\bar{g}} J \cdot \Phi}. \quad (10.1)$$

Before we specify the cutoff term, we discuss the remnant of diffeomorphism symmetry present in the path integral.

The presence of the background metric, as for the background gauge field in QCD, allows us to define an auxiliary diffeomorphism transformation: the diffeomorphism transformation of the full metric, $g_{\mu\nu} \mapsto g_{\mu\nu} + \mathcal{L}_\omega g_{\mu\nu}$ in [\(9.14\)](#) can be decomposed in two different ways. The first one is the original diffeomorphism transformation of the dynamical metric field

$$h_{\mu\nu} \mapsto h_{\mu\nu} + \mathcal{L}_\omega (\bar{g}_{\mu\nu} + h_{\mu\nu}), \quad \bar{g}_{\mu\nu} \mapsto \bar{g}_{\mu\nu}, \quad (10.2a)$$

the *quantum* diffeomorphism transformation. The second, auxiliary, transformation is

$$h_{\mu\nu} \mapsto h_{\mu\nu} + \mathcal{L}_\omega h_{\mu\nu}, \quad \bar{g}_{\mu\nu} \mapsto \bar{g}_{\mu\nu} + \mathcal{L}_\omega \bar{g}_{\mu\nu}, \quad (10.2b)$$

the *background* diffeomorphism transformation. While the former symmetry, 10.2a, is gauge-fixed, and broken by the cutoff term, the latter auxiliary one, 10.2b, is present in the gauge-fixed action (9.37)

In order to also preserve this symmetry in the presence of the cutoff term, we choose *background-covariant* cutoff functions.

It is left to specify the cutoff term $\Delta S_k[\bar{g}, \Phi]$. This is done similarly to QCD, see in particular Section 5.4.1. The cutoff term is quadratic in the fluctuation super field Φ and reads

$$\Delta S_k[\Phi] = \frac{1}{2} \Phi_a R_k^{ab} \Phi_b, \quad (10.3a)$$

and the regulator matrix

$$(R_k^{ab}) = \begin{pmatrix} R_h & 0 & 0 \\ 0 & 0 & -R_c \\ 0 & R_c & 0 \end{pmatrix}. \quad (10.3b)$$

With the generic structure in momentum space

$$R_\varphi(p) = \mathcal{P}_\varphi(\nabla_{\bar{g}}) r_\varphi(x), \quad \text{with} \quad x = \frac{\Delta_{\bar{g}}}{k^2}, \quad \text{and} \quad \varphi_i = h_{\mu\nu}, c_\mu. \quad (10.3c)$$

The parameterisation 10.3c depends on generic dimensionless shape functions r_{φ_i} , see e.g. (2.6). The prefactors \mathcal{P}_φ carry the Lorentz, internal and the dispersion of the respective field. As in other theories we typically choose \mathcal{P}_φ being proportional to (part of the) classical two-point functions $S_{\varphi_i \varphi_j}^{(2)}(p)$.

The choice 10.3a is not invariant under quantum diffeomorphism transformations 10.2a, but respects the background diffeomorphism transformations 10.2b. More explicitly it reads

$$\Delta S_k = \frac{1}{2} \int d^d x \sqrt{\bar{g}} h_{\mu\nu} R_h [\Delta_{\bar{g}}]^{\mu\nu\rho\sigma} h_{\rho\sigma} + \int d^d x \sqrt{\bar{g}} \bar{c}_\mu R_c [\Delta_{\bar{g}}]^{\mu\nu} c_\nu, \quad (10.4)$$

where the regulators are proportional to $S_{\text{grav}}^{(2)}[\bar{g}]$. The first part acts as a cutoff term for the gravitational modes and the second part is the cutoff for the ghost modes. With these definitions we are finally led to the Wetterich equation for quantum gravity,

$$\partial_t \Gamma_k[\bar{g}, \Phi] = \frac{1}{2} \text{Tr } G_{hh}[\Phi] \partial_t R_h - \text{Tr } G_{c\bar{c}}[\Phi] \partial_t R_c. \quad (10.5)$$

with

$$G_{hh}[\Phi] = \left[\frac{1}{\Gamma^{(2)}[\bar{g}, \Phi] + R_k} \right]_{hh}, \quad G_{c\bar{c}}[\Phi] = \left[\frac{1}{\Gamma^{(2)}[\bar{g}, \Phi] + R_k} \right]_{c\bar{c}}. \quad (10.6)$$

The RG time t is again the logarithm of the scale k and the minus sign in front of the ghost part arises due to the Grassmannian nature of the ghost fields. Note that we now have a dependence on \bar{g} as well as on h . This spurious dependence on two fields will be eliminated later on by setting $h_{\mu\nu} = 0$ at $k = 0$.

10.2. Background independence in quantum gravity

Most applications of the FRG to quantum gravity to date do not resolve the difference between background and fluctuation field and employ the background field approximation. There only one metric $g_{\mu\nu} = \bar{g}_{\mu\nu} + h_{\mu\nu}$ is used in the effective action. However, the non-trivial interplay of the metric fluctuations with the background plays a decisive rôle for background independence of the theory. These non-trivial relations are governed by non-trivial split-Ward or Nielsen identities (NIs), see e.g. [141, 142, 143, 9, 144, 145, 146, 147, 148, 149, 150, 151] for formal progress and applications in scalar theories, gauge theories and gravity. Accordingly, the background field approximation violates the NIs, which leads to the seemingly contradictory situation that it is at odds with background independence even though it only features one metric. In the past decade quite some progress has been made in overcoming the background field approximation, see [143, 9, 152, 153, 154, 144, 58, 155, 59, 156, 29, 60, 61, 157, 147, 145, 148, 149, 158, 62, 159, 160, 151, 161, 141, 142, 146, 150].

10.2.1. Approaches to fluctuation and background correlation functions

All these works should be seen in the context of gaining background independence and physical diffeomorphism invariance in asymptotically safe gravity. Here we briefly summarise the state of the art within the different approaches.

(1) One approach utilises the fact that the NIs relate background metric correlations to fluctuation ones. This leaves us with a system of one type of correlations and it is possible to solve the system of flow equations for fluctuation correlation functions either directly or implicitly. This strategy has been set up and pursued in [141, 142, 143, 9, 144, 145, 146, 147, 148, 149, 150, 151] for generic theories within the background field approach. At present, applications in gravity still utilise the background field approximation beyond either the first order, or the second order in the fluctuation field [144]. Such a closure of the flow equation with the background field approximation is mandatory and all approaches aim at introducing this approximation on a high order of the fluctuation field. Note in this context that it is only the second and higher order n -point functions of the fluctuation field that drive the flow.

(2a) A second approach utilises the fact that the dynamics of the system is carried by the correlation functions of the fluctuation field. This is also reflected by the fact that the system of flow equations for the fluctuation correlations is closed. Consequently one may solve these flows for a specific background metric that facilitates the computation, e.g. the flat background. Then, background correlations are computed within an expansion or extension about the flat background in order to access the physical background that solves the quantum EoM. This strategy has been set up and pursued in [58, 155, 59, 29, 60, 61, 158, 62, 159, 160, 161] for gravity, also guided by successful applications in non-Abelian gauge theories, see e.g. [86, 162, 163, 88, 164]. At present, fluctuation correlations up to the four-point function have been included [62], as well as a full fluctuation effective potential [161]. First results in a Taylor expansion of the background about a flat one have been presented in [159].

(2b) A third approach avoids the latter step of extending the results to physical backgrounds by computing instantly the flow equations for the fluctuation correlation functions for general backgrounds. This has been investigated in [152, 153, 154, 156]. As in the other approaches, the background field approximation has been used for higher correlation functions. At present, this holds for all correlation functions beyond the one-point function of the fluctuation field.

10.3. General framework

10.3.1. FRG and Nielsen identities for gravity

In order to compute correlation functions in quantum gravity we utilise the FRG approach to gravity [165]. In this approach the functional integral involves a momentum dependent mass function R_k , which acts as an infrared regulator suppressing momenta $p^2 \lesssim k^2$ relative to the cutoff scale k . This leads to a scale-dependent effective action $\Gamma_k[\bar{g}, \phi]$, which includes contributions from high momentum fluctuations. Here the dynamical metric $g_{\mu\nu} = \bar{g}_{\mu\nu} + \sqrt{Z_h G_N} h_{\mu\nu}$ is expanded around a non-dynamical background metric \bar{g} with the fluctuations h . The fluctuation field is rescaled with Newton's coupling such that it has the standard mass-dimension one of a bosonic field. In this chapter we utilise a linear metric split and we restrict \bar{g} to spherical backgrounds.

An important issue in quantum gravity is the background independence of physical observables. They are expectation values of diffeomorphism invariant operators, and hence do not depend on the gauge fixing. Examples for such observables are correlations of the curvature scalar. Another relevant example is the free energy of the theory, $-\log Z[\bar{g}, J = 0]$, with $\delta Z[\bar{g}, J = 0]/\delta \bar{g} = 0$. These observables cannot depend on the choice of the background metric, which only enters via the gauge fixing. The latter fact is encoded in the NI for the effective action: The difference between background derivatives and fluctuation derivatives is proportional to derivatives of the gauge fixing sector,

$$\text{NI} = \frac{\delta \Gamma}{\delta \bar{g}_{\mu\nu}} - \frac{\delta \Gamma}{\delta h_{\mu\nu}} - \left\langle \left[\frac{\delta}{\delta \bar{g}_{\mu\nu}} - \frac{\delta}{\delta \hat{h}_{\mu\nu}} \right] (S_{\text{gf}} + S_{\text{gh}}) \right\rangle = 0, \quad (10.7)$$

where S_{gf} is the gauge fixing term and S_{gh} is the corresponding ghost term, and $h_{\mu\nu} = \langle \hat{h}_{\mu\nu} \rangle$. Note that (10.7) is nothing but the Dyson-Schwinger equation for the difference of derivatives w.r.t. \bar{g} and h . For the fully diffeomorphism-invariant Vilkovisky-deWitt or geometrical effective action the relation (10.7) is even more concise: the split is not linear and we have $g = \bar{g} + f(\bar{g}, h)$, where $f(\bar{g}, h) = \sqrt{G_N} h + O(h^2)$ depends on the Vilkovisky connection. The NI then reads

$$\text{NI}_{\text{geo}} = \frac{\delta \Gamma_{\text{geo}}}{\delta \bar{g}_{\mu\nu}} - C(\bar{g}, h) \frac{\delta \Gamma_{\text{geo}}}{\delta h_{\mu\nu}} = 0, \quad (10.8)$$

where $C(\bar{g}, h)$ is the expectation value of the (covariant) derivative of $h(\bar{g}, g)$, for a discussion in the present FRG setting see [143, 9, 144, 145].

The NIs, (10.7) and (10.8), entail that in both cases the effective action is not a function of $g = \bar{g} + h$ or $g = \bar{g} + f(\bar{g}, h)$ respectively. This property holds for general splits, and prevents the simple expansion of the effective action in terms of diffeomorphism invariants. Apart from this disappointing consequence of the NIs, it also entails good news: the effective action only depends on one field as background and fluctuation derivatives are connected.

An important property that follows from background independence is the fact that a solution of the background equation of motion (EoM)

$$\frac{\delta \Gamma[\bar{g}, h]}{\delta \bar{g}_{\mu\nu}} \Big|_{\bar{g}=\bar{g}_{\text{geom}}, h=0} = 0, \quad (10.9)$$

is also one of the quantum EoM,

$$\frac{\delta \Gamma[\bar{g}, h]}{\delta h_{\mu\nu}} \Big|_{\bar{g}=\bar{g}_{\text{geom}}, h=0} = 0. \quad (10.10)$$

see e.g. [164] for a discussion of this in Yang-Mills theories. In (10.9) and (10.10) we have already taken the standard choice $h = 0$ but the statement hold for general combinations $\bar{g}_{\text{EoM}}(h)$ that solves either of the equations. The concise form (10.8) for the geometrical effective action makes it apparent that a solution of either EoM, (10.9) or (10.10), also entails a solution of the other one. Note that at $h = 0$ we have $C(\bar{g}, 0) = 1$.

Even though less apparent, the same holds true for the effective action in the linear split: to that end we solve the quantum EoM (10.10) as an equation for $\bar{g}_{\text{geom}}(h)$. As the current J in the generating functional simply is $J = \delta\Gamma/\delta h$, the quantum EoM implies the vanishing of J and the effective action is given by $\Gamma[\bar{g}_{\text{geom}}(0), 0] = -\log Z[\bar{g}, J = 0]$, the free energy. However, we have already discussed that $\log Z[\bar{g}, 0]$ is background-independent and it follows that (10.9) holds.

The above properties and relations are a cornerstone of the background formalism as they encode background independence of observables. The NIIs also link background diffeomorphism invariance to the Slavnov-Taylor identities (STIs) that hold for diffeomorphism transformations of the fluctuation field: the quantum deformation of classical diffeomorphism symmetry is either encoded in the expectation value of the gauge fixing sector or in the expectation value $C(\bar{g}, h)$.

At finite k , the regulator term introduces a genuine dependence on the background field. Then $\log Z_k[\bar{g}, 0]$ is not background independent. Consequently the STIs turns into modified STIs (mSTIs) and the NIIs turn into modified NIIs (mNIIs). For the linear split, the mNI reads

$$\text{mNI} = \text{NI} - \frac{1}{2} \text{Tr} \left[\frac{1}{\sqrt{\bar{g}}} \frac{\delta \sqrt{\bar{g}} R_k[\bar{g}]}{\delta \bar{g}_{\mu\nu}} G_k \right] = 0, \quad (10.11)$$

see [141, 142] for details, and [64, 65] for applications to quantum gravity. Importantly the right-hand side of (10.11) signals the loss of background independence. It is proportional to the regulator and vanishes for $k \rightarrow 0$ where background independence is restored. A similar violation of background independence linear in the regulator is present in the geometrical approach, see [143, 9, 144, 145].

In summary this leaves us with non-equivalent solutions to the EoMs in the presence of the regulator: a solution of the quantum EoM (10.10) does not solve the background EoM (10.9). However, typically the asymptotically safe UV regime of quantum gravity is accessed in the limit $k \rightarrow \infty$ as this already encodes the important scaling information in this regime. In the present paper we also follow this strategy and hence we have to deal with different solutions of background and quantum EoMs, if they exist at all. Note that the right-hand side of the mNI is simply the expectation value of the background derivative of the regulator term. Accordingly it is the background EoM that is deformed directly by the presence of the regulator while the quantum EoM feels its influence only indirectly. Therefore it is suggestive to estimate the physical UV-limit of the EoM in the limit $k \rightarrow 0$ by the quantum EoM in the limit $k \rightarrow \infty$. Studies in asymptotically safe quantum gravity have focused so far on finding solutions to (10.9). For instance in [166] they didn't find a solution to (10.9) in a polynomial expansion with the background field approximation. Other approaches with the background field approximation found a solution with the exponential parameterisation [167, 168] and within the geometrical approach [169, 170]. In this work we are for the first time able to disentangle (10.9) and (10.10) in a quantum gravity setting and look for separate solutions to the EoMs.

We disentangle the background and fluctuation field by expanding the scale dependent effective action around a background according to

$$\Gamma_k[\bar{g}, h] = \sum_{n=0}^{\infty} \frac{1}{n!} \Gamma_k^{(0,n)}[\bar{g}, h=0] h^n. \quad (10.12)$$

The flow equations that govern the scale-dependence of the vertex functions are obtained by n field derivatives of the flow equation for the effective action (10.5). They are depicted in a diagrammatic language in Figure 10.2 for cases $n = 2$ and $n = 3$. These flow equations are familiar from computations on a flat background [58, 59, 29, 62], here however all propagators and vertices depend non-trivially on the background.

From here on we drop the index k to improve readability, the scale dependence of the couplings, correlation functions and wave function renormalisations is implicitly understood.

$$\begin{aligned}\partial_t \Gamma_k^{(2)} &= -\frac{1}{2} \text{Diagram A} + \text{Diagram B} - 2 \text{Diagram C} \\ \partial_t \Gamma_k^{(3)} &= -\frac{1}{2} \text{Diagram D} + 3 \text{Diagram E} - 3 \text{Diagram F} + 6 \text{Diagram G}\end{aligned}$$

Figure 10.1.: Displayed are the diagrammatic representations of the flows of the graviton two- and three-point functions. Double and dashed lines represent dressed graviton and ghost propagators respectively, while filled circles denote dressed vertices. Crossed circles stand for regulator insertions. All quantities are explicit background curvature dependent and carry further background curvature dependence via the spectral value of the respective vertex/propagator.

10.3.2. Background independence in non-perturbative expansion schemes

It is important to discuss the relations of the approaches described in section 10.2 in particular for future developments and the full resolution of *physical* background independence. This chapter extends a similar discussion from [62] in the context of modified STIs for diffeomorphism transformations to NIIs. Despite its importance one may skip this chapter for a first reading as its results are not necessary for the derivations and computations presented in this work.

We have technically very different options to access physical background independence of quantum gravity. Seemingly they have different advantages and disadvantages. For example, approach (1) via the NIIs has the charm of directly implementing background independence. In turn, the results of (2b) may apparently not satisfy the NIIs.

For resolving this issue it is instructive to discuss approach (2a). There the fluctuation correlation functions are computed for a specific background. Results for general backgrounds have then to be obtained with an expansion/extension of the results for the specific background. This could be done via the NIIs in which case background independence is guaranteed. This procedure for guaranteeing STIs and NIIs has been discussed in detail in [89] in the context of non-Abelian gauge theories, and in [62] for gravity. We briefly repeat and extend the structural argument presented there: First we notice that the functional equations for all correlation functions can be cast in the form

$$\Gamma^{(n,m)}[\bar{g}, h] = \text{FRG}_{n,m}[\{\Gamma^{(i \leq n, 2 \leq j \leq m+2)}[\bar{g}, h]\}, \bar{g}]. \quad (10.13)$$

Eq. (10.13) follows from integrating the functional renormalisation group equations for $\Gamma^{(n,m)}$, which have precisely the same structure for all theories: the flows of $\Gamma^{(n,m)}$ are given by one-loop diagrams with full propagators and full vertices. The latter are given in terms of the correlation functions $\{\Gamma^{(i \leq n, 2 \leq j \leq m+2)}\}$, see e.g. [9, 89]. This also entails that the lowest fluctuation correlation function that contributes to the diagrams is the two-point function, i.e. the propagator.

In gravity (10.13) follows straightforwardly from ?? by integrating the flow equation and taking \bar{g} - and h -derivatives. As a side remark we note that the order of derivatives on the right-hand side is different within other functional approaches. For example, for Dyson-Schwinger equations (DSE) the right-hand side $\text{DSE}_{n,m}$ for the $\Gamma^{(n,m)}$ depends on $\{\Gamma^{(i \leq n, j \leq m+r-2)}\}$ and contain up to $r-2$ -loop diagrams. Here r is the highest order of the field in the classical action, see e.g. [9]. In typical examples of renormalisable theories we have $r=3, 4$, but in gravity we have $r=\infty$. This singles out the flow equation for gravity as the only functional approach that only connects a finite order of correlation functions in each equation. The coupling of the whole tower of equations then comes from the highest order correlation functions on the right-hand side. In turn, each DSE already contains all orders on the right-hand side of (10.13), that is $2 \leq j$ without upper bound. Similar statements as for the DSE hold for 2PI or n PI hierarchies.

Importantly, for all functional approaches the right-hand side of (10.13) goes only up to the same order of background metric derivatives, $i \leq n$. This allows us to view (10.13) as functional relations for the

highest order background metric correlation functions that have as an input $\{\Gamma^{(n-1,m)}\}$. Moreover, the NI relates a derivative w.r.t. \bar{g} to one w.r.t. h . For emphasising the similarities to the functional relations (10.13) we rewrite the NI. For simplicity we use the linear split NI, (10.7) and (10.11),

$$\Gamma^{(n,m)}[\bar{g}, h] = \Gamma^{(n-1,m+1)}[\bar{g}, h] + \mathcal{N}_{n,m}[G, \{\Gamma^{(i \leq n-1, j \leq m+1)}[\bar{g}, h]\}, \bar{g}], \quad (10.14)$$

where \mathcal{N} stands for the expectation value in (10.7), and additionally for the regulator loop in (10.11), and we have singled out the propagator G for elucidating the orders of the correlation functions on both sides. Importantly, (10.14) makes the fact apparent that for the NI, (10.7) and (10.11), the order of background derivatives is at most $n - 1$. Note also that (10.14) is nothing but the difference of the Dyson-Schwinger equation for h and \bar{g} derivatives. In this difference the terms with the higher vertices with $j \geq m + 2$ drop out.

In summary this leaves us with two towers of functional relations. While the first one, (10.13) describes the full set of correlation functions, the second one, (10.14) can be used to iteratively solve the tower of mixed fluctuation-background correlations on the basis of the fluctuating correlation functions $\{\Gamma^{(0,m)}\}$. In both cases we can solve the system for the higher-order correlations of the background on the basis of the lower order correlations. If we use (10.14) with an iteration starting with the results from the flow equation for $\{\Gamma^{(0,m)}[\bar{g}_{\text{sp}}, h]\}$ for a specific background \bar{g}_{sp} , this closure of the system automatically satisfies the NI. Accordingly, *any* set of fluctuation correlation functions $\{\Gamma^{(0,m)}[\bar{g}_{\text{sp}}, h]\}$ can be iteratively extended to a full set of fluctuation-background correlation functions in an iterative procedure. Note that this procedure can be also applied to the case (2b).

While this seems to indicate that satisfying the symmetry identities is not relevant (it can be done for all inputs), it points at a more intricate structure already known from non-Abelian gauge theories. To that end let us assume we have derived a global unique solution of all correlation functions within this iterative procedure starting from the fluctuations correlation functions. If no approximation is involved, this solution automatically would satisfy the full set of functional relations for $\{\Gamma^{(n,m)}\}$ that can be derived from the flow equation. However, in the presence of approximations these additional functional relations represent infinite many additional constraints on the iterative solution. These constraints are bound to fail in generic non-perturbative approximation schemes as any functional relation triggers specific resummations in given approximations. It is a priori not clear which of the functional relations are more important. Note also that typically the iterative solutions of the symmetry identities are bound to violate the locality constraints of local quantum field theories that are tightly connected to the unitarity of the theory. In conclusion it is fair to say that only a combination of all approaches is likely to provide a final resolution of *physical* background independence and diffeomorphism invariance in combination with unitarity.

10.4. Einstein-Hilbert Truncation

Now we discuss methods approximately solve the flow equation (10.5). In general we have to take into account all terms that are invariant under the imposed symmetry, which is the diffeomorphism invariance. The easiest truncation for the quantum gravity system is the Einstein-Hilbert truncation taking into account the scalar curvature R and the cosmological constant term. Higher-order truncations deal with higher-derivative terms like R^2 , R^3 as well as $R_{\mu\nu}R^{\mu\nu}$, etc.. Furthermore one can couple matter to the gravitational theory. We will come back to this point in chapter 11.

In 1996 M. Reuter investigated the flow equation for quantum gravity in the Einstein-Hilbert truncation [165]. This truncations is rather simple but still keeps the most important features of better truncations. Thus we discuss this example in more detail. Explicitly the Einstein-Hilbert truncation reads

$$\Gamma_k = 2\kappa^2 Z_k \int d^d x \sqrt{g} [-R + 2\Lambda_k] + S_{\text{gf}} + S_{\text{gh}}, \quad (10.15)$$

with

$$\kappa^2 = (32\pi G)^{-1}, \quad G_k = G Z_k^{-1}. \quad (10.16)$$

Here the scale dependence of the Newton coupling G_k is encoded in the wave-function renormalisation Z_k and G is the bare Newton coupling.

We first look at the left-hand side of (10.5). The derivative with respect to the RG time t acts on the Newton coupling G_k and the cosmological constant Λ_k or, equivalently, on Z_k and Λ_k . Applying this to (10.15) yields

$$\begin{aligned} \partial_t \Gamma_k^{\text{grav}} &= 2\kappa^2 \int d^d x \sqrt{g} [-(\partial_t Z_k) R + 2(\partial_t Z_k \Lambda_k)] \\ &= 2Z_k \kappa^2 \int d^d x \sqrt{g} [\eta_g R + 2(k^2 \partial_t \lambda_k + 2\Lambda_k - \eta_g \Lambda_k)], \end{aligned} \quad (10.17)$$

where we have introduced the anomalous dimension $\eta_g = -(\partial_t Z_k)/Z_k = -\partial_t \ln Z_k$ as well as the dimensionless renormalised cosmological constant $\lambda_k = \Lambda_k k^{-2}$. We have one term proportional to $\sqrt{g}R$ and one proportional to \sqrt{g} . The same terms we will find on the right-hand side of (10.5) together with higher-order terms. The comparison of left- and right-hand side yields expressions for the anomalous dimension η_g and the beta function for the cosmological constant $\beta_\lambda = \partial_t \lambda_k$. The beta function for the dimensionless renormalised Newton coupling, $g_k = G_k k^{d-2} = G k^{d-2}/Z_k$, follows directly from the anomalous dimension

$$\beta_g = \partial_t g_k = (d-2+\eta_g) g_k. \quad (10.18)$$

The $d-2$ results from the t derivative acting on k^{d-2} . It is the negative of the canonical dimension of the Newton constant and thus this term is called the dimensional running.

Now we turn to the right-hand side of (10.5). We first compute the graviton propagator $G_h = (\Gamma^{(2h)} + R_k)^{-1}$ from the Einstein-Hilbert truncation (10.15). The Einstein-Hilbert ansatz for the graviton two-point function $\Gamma^{(2h)}$ is obtained by two functional derivatives of (10.15) with respect to the fluctuation field $h_{\mu\nu}$. It has four open indices and depends explicitly on the gauge parameters α and β as well as on background curvature invariants \bar{R} , $\bar{R}_{\mu\nu}$, $\bar{R}_{\mu\nu\rho\sigma}$ constructed from the background metric $\bar{g}_{\mu\nu}$. We can exploit the freedom of choosing the background metric to correspond to a maximally symmetric space

$$\bar{R}_{\mu\nu} = \frac{1}{d} \bar{g}_{\mu\nu} \bar{R}, \quad \bar{R}_{\mu\nu\rho\sigma} = \frac{1}{d(d-1)} (\bar{g}_{\mu\rho} \bar{g}_{\nu\sigma} - \bar{g}_{\mu\sigma} \bar{g}_{\nu\rho}) \bar{R}. \quad (10.19)$$

An explicit result for the graviton two-point function is displayed in Appendix G.2.

The inversion of the two-point function on general curved backgrounds is non-trivial. We use the maximally symmetric space (10.19) as well as a suitable tensor basis. The tensor basis is for example the transverse-traceless York decomposition [171] or the Stelle decomposition []. The decompositions consist of a separation of the trace and the longitudinal parts of the metric fluctuation $h_{\mu\nu}$,

$$h_{\mu\nu} = h_{\mu\nu}^{\text{TT}} + h_{\mu\nu}^{\text{L}} + \frac{1}{d} \bar{g}_{\mu\nu} h. \quad (10.20)$$

Here h is the trace $h = \bar{g}^{\mu\nu} h_{\mu\nu}$ and $h_{\mu\nu}^{\text{TT}}$ is transverse $\bar{\nabla}^\mu h_{\mu\nu}^{\text{TT}} = 0$ and traceless $\bar{g}^{\mu\nu} h_{\mu\nu}^{\text{TT}} = 0$. The longitudinal part is decomposed further by introducing a transverse vector field ξ and a corresponding scalar σ . The final result for the fluctuation of the metric reads

$$h_{\mu\nu} = h_{\mu\nu}^{\text{TT}} + \bar{\nabla}_\mu \xi_\nu + \bar{\nabla}_\nu \xi_\mu + \left(\bar{\nabla}_\mu \bar{\nabla}_\nu - \frac{1}{d} \bar{g}_{\mu\nu} \bar{\Delta} \right) \sigma + \frac{1}{d} \bar{g}_{\mu\nu} h. \quad (10.21)$$

We have split the unconstrained spin-2 field $h_{\mu\nu}$ into constrained fields of spin-2 $h_{\mu\nu}^{\text{TT}}$, spin-1 ξ and spin-0 σ and h . This split simplifies the inversion of $\Gamma_k^{(2)} + R_k$. In case of a flat background $\bar{g}_{\mu\nu} = \delta_{\mu\nu}$ the projection operators are rather simple and so is the inversion. Details can be found in [Appendix G.2](#).

In the following we restrict ourselves to the deDonder-type gauge $\alpha = 0, \beta = 1$. Then the propagator is diagonal with only transverse-traceless and trace mode entries. The entries are given by, see [Appendix G.2, \(G.17\)](#),

$$G_{h^{\text{TT}} h^{\text{TT}}} = \frac{32\pi}{k^2 Z_h} \frac{1}{p^2 (1 + r_k(p^2)) + \mu + \frac{2}{3}r}, \quad G_{h^{\text{Tr}} h^{\text{Tr}}} = \frac{32\pi}{k^2 Z_h} \frac{-\frac{8}{3}}{p^2 (1 + r_k(p^2)) + \frac{2}{3}\mu}. \quad (10.22)$$

Within the York decomposition the Einstein Hilber truncation of the flow equation reads

$$\partial_t \Gamma_k[\bar{g}, \Phi] = \frac{1}{2} \text{Tr} G_{h^{\text{TT}} h^{\text{TT}}} \partial_t R_{h^{\text{TT}}} + \frac{1}{2} \text{Tr} G_{h^{\text{Tr}} h^{\text{Tr}}} \partial_t R_{h^{\text{Tr}}} \quad (10.23)$$

After inverting $\Gamma_k^{(2)} + R_k$ we have to consider the traces on the right-hand side of [\(10.5\)](#). These can be evaluated with heat-kernel techniques as explained in [\[165\]](#) and [Appendix G.1](#). As a result we get a term proportional to $\sqrt{g}R$ and one to \sqrt{g} . We also get higher-order terms, which we neglect for the moment. The comparison with the left-hand side [\(10.17\)](#) yields the beta functions for the Newton coupling and the cosmological constant as discussed above.

For simplicity, we first discuss the heat-kernel expansion only for the graviton approximation, i.e., in the approximation where only the transverse-traceless spin-2 mode is contributing. In many cases this is a sufficient approximation that contains the most important physical features.

The propagator of the transverse-traceless spin-2 mode is given by

$$G_{h^{\text{TT}}} = \left. \frac{1}{\Gamma^{(2)} + R_k} \right|_{h^{\text{TT}}} = \frac{32\pi}{Z_k} \frac{1}{\Delta(1 + r_k(\Delta)) - 2\Lambda_k + C\bar{R}}, \quad (10.24)$$

with

$$C = \frac{d(d-3)+4}{d(d-1)} \xrightarrow{d \rightarrow 4} \frac{2}{3}. \quad (10.25)$$

In [\(10.24\)](#) we have specified the regulator to be

$$R_k = \left. \Gamma^{(2)} \right|_{\lambda_k=\bar{R}=0} \cdot r_k \left(\frac{\Delta}{k^2} \right), \quad (10.26)$$

with a shape function r_k that can be, for example, a Litim-type cutoff

$$r_k(x) = \left(\frac{1}{x} - 1 \right) \Theta(1-x). \quad (10.27)$$

We have to take the trace

$$\begin{aligned} \text{Tr} G_{h^{\text{TT}}} \partial_t R_k &= \text{Tr} \frac{\Delta(\partial_t r_k(\Delta) - \eta_g r_k(\Delta))}{\Delta(1 + r_k(\Delta)) - 2\Lambda_k + C\bar{R}} \\ &= \text{Tr} \frac{\Delta(-2\frac{\Delta}{k^2} r'_k(\Delta) - \eta_g r_k(\Delta))}{\Delta(1 + r_k(\Delta)) - 2\Lambda_k} - C\bar{R} \text{Tr} \frac{\Delta(-2\frac{\Delta}{k^2} r'_k(\Delta) - \eta_g r_k(\Delta))}{(\Delta(1 + r_k(\Delta)) - 2\Lambda_k)^2} \end{aligned} \quad (10.28)$$

With the heat-kernel formulas from [Appendix G.1](#) we obtain for example for the first term

$$\begin{aligned} \text{Tr} \frac{\Delta(-2\frac{\Delta}{k^2}r'_k(\Delta) - \eta_g r_k(\Delta))}{\Delta(1 + r_k(\Delta)) - 2\Lambda_k} &= \frac{1}{(4\pi)^{\frac{d}{2}}} \left(B_0(\Delta) Q_2 \left[\frac{\Delta(-2\frac{\Delta}{k^2}r'_k(\Delta) - \eta_g r_k(\Delta))}{\Delta(1 + r_k(\Delta)) - 2\Lambda_k} \right] \right. \\ &\quad \left. + B_2(\Delta) Q_1 \left[\frac{\Delta(-2\frac{\Delta}{k^2}r'_k(\Delta) - \eta_g r_k(\Delta))}{\Delta(1 + r_k(\Delta)) - 2\Lambda_k} \right] \right) \\ &= \frac{1}{(4\pi)^{\frac{d}{2}}} \int d^4x \sqrt{g} \left[5\Phi_2^1(-2\Lambda_k) - \frac{5}{6}\bar{R}\Phi_1^1(-2\Lambda_k) \right] \end{aligned} \quad (10.29)$$

where the Φ_m^n are the threshold functions

$$\Phi_n^p(\omega) = \frac{1}{\Gamma(n)} \int_0^\infty dz z^{n-1} \frac{z(-2zr_k(z) - \eta_g r_k(z))}{(z(1 + r_k(z)) + \omega)^p} = \frac{1}{\Gamma(n)} \frac{1}{(1 + \omega)^p} \left(\frac{2}{n} - \frac{\eta_g}{n(n+1)} \right). \quad (10.30)$$

In the last line we have evaluated the threshold functions for the Litim-type cutoff [\(10.27\)](#). A similar expression holds for the second term in [\(10.28\)](#).

After the comparison of the left-hand and right-hand side we obtain the flow equations

$$\begin{aligned} \partial_t g_k &= (2 + \eta_g)g_k, \\ \eta_g &= -\frac{5}{6\pi}g_k \left(2\frac{1 - \frac{1}{6}\eta_g}{(1 - 2\lambda_k)^2} + \frac{1 - \frac{1}{4}\eta_g}{1 - 2\lambda_k} \right), \\ \partial_t \lambda_k &= -4\lambda_k + \frac{\lambda_k}{g_k} \partial_t g_k + \frac{5}{4\pi}g_k \frac{1 - \frac{1}{6}\eta_g}{1 - 2\lambda_k}. \end{aligned} \quad (10.31)$$

Already in this simple truncation we find a non-Gaußian fixed point at the values

$$(g_k^*, \lambda_k^*) = (0.86, 0.18). \quad (10.32)$$

The critical exponents, which are the negative eigenvalues of the stability matrix, of the fixed point are given by

$$\theta_{1,2} = 2.9 \pm 2.6i. \quad (10.33)$$

Now we consider the full equations that include the other graviton and the ghost modes. Their inclusion is straightforward and follows the same route as that for the transverse traceless part considering the full graviton propagator [G.14](#) with some choice for the regulator, e.g. [\(G.15\)](#) or [\(G.16\)](#). Here we simply cite the result for $\alpha = 0$ and $\beta = 1$, see e.g. [\[62\]](#),

$$\begin{aligned} \partial_t g &= 2g - g^2 f_{R^1}(\lambda; \eta_h, \eta_c), \\ \partial_t \lambda &= -4\lambda + \lambda \frac{\partial_t g}{g} + g f_{R^0}(\lambda; \eta_h, \eta_c), \end{aligned} \quad (10.34)$$

where the functions f_{R^0} and f_{R^1} read

$$\begin{aligned} f_{R^0}(\lambda; \eta_h, \eta_c) &= \frac{1}{24\pi} \left(\frac{(10 - 8\lambda)(6 - \eta_h)}{1 - 2\lambda} - 8(6 - \eta_c) \right), \\ f_{R^1}(\lambda; \eta_h, \eta_c) &= \frac{1}{24\pi} \left(\frac{93 + 204\lambda_2 - 300\lambda^2 - \eta_h(17 + 36\lambda - 60\lambda^2)}{3(1 - 2\lambda)^2} + 10(5 - \eta_c) \right). \end{aligned} \quad (10.35)$$

10.5. Correlation functions of the fluctuation field

10.5.1. Covariant expansion

The effective action $\Gamma_k[\bar{g}, \Phi]$ depends on the background metric $\bar{g}_{\mu\nu}$ and the fluctuation superfield $\Phi = (h_{\mu\nu}, c_\mu, \bar{c}_\mu)$, see ??, separately. The functional flow equation ?? is accompanied by the functional mSTIs & mNIs for the effective action that monitor the breaking of quantum diffeomorphism invariance, see ?? in ???. In order to solve ??, we employ a vertex expansion around a given background $\bar{g}_{\mu\nu}$, to wit

$$\Gamma_k[\bar{g}, \phi] = \sum_{n=0}^{\infty} \sum_{|n_\phi|=n} \frac{1}{n_\phi!} \Gamma_k^{(\phi_{i_1} \dots \phi_{i_n})} [\bar{g}, 0] \phi_{i_1} \dots \phi_{i_n}, \quad (10.36)$$

Here we have introduced the short-hand notation

$$\Gamma_k^{(\phi_{i_1} \dots \phi_{i_n})} [\bar{g}, 0] = \left. \frac{\delta^n \Gamma_k [\bar{g}, \phi]}{\delta \phi_{i_1} \dots \delta \phi_{i_n}} \right|_{\phi=0}, \quad (10.37)$$

which specifies one entry of the general fluctuation n -point function $\Gamma_k^{(n)} = \Gamma_k^{(0,n)}$, see also ???. Also we have introduced the tuple $n_\phi = (n_h, n_c, \dots)$ that contains the number of graviton legs n_h , ghost legs n_c in the respective n -point function. In the later chapters this tuple will also contain the number of matter legs. In (10.36) the super-indices i_j occurring twice imply a sum over discrete indices and an integral over continuous variables. In this chapter, we include the full flow of the vertex functions up to the graviton three-point function, while in the next chapter we will also include the graviton four-point function. As discussed in ??, the expansion coefficients $\Gamma_k^{(n)}$ satisfy mSTIs as well as mNIs with $\Gamma_k^{(n,m)}$ being defined in ???. For the sake of simplicity we now restrict ourselves to the gauge fixing used in this dissertation, ?? with $\alpha = 0$. Then the fluctuation graviton propagator is transverse: it is annihilated by the gauge fixing condition.

An important feature of the functional RG equations is that for $\alpha = 0$ the flow equations for the transverse vertices $\Gamma_{k,T}^{(n)}$ are closed: the external legs of the vertices in the flow are transverse due to the transverse projection of the flow, the internal legs are transverse as they are contracted with the transverse propagator. Schematically this reads

$$\partial_t \Gamma_{k,T}^{(n)} = \text{Flow}_T^{(n)}[\{\Gamma_{k,T}^{(m)}\}]. \quad (10.38)$$

In other words, the system of transverse fluctuation correlation functions is closed and determines the dynamics of the system. On the other hand, the mSTIs are non-trivial relations for the longitudinal parts of vertices in terms of transverse vertices and longitudinal ones. This leads us to the schematic relation

$$\Gamma_{k,L}^{(n)} = \text{mSTI}^{(n)}[\{\Gamma_{k,T}^{(m)}\}, \{\Gamma_{k,L}^{(m)}\}], \quad (10.39)$$

see [89] for non-Abelian gauge theories. In consequence, the mSTIs provide no direct information about the transverse correlation functions without further constraint. In the perturbative regime this additional constraint is given by the uniformity of the vertices, for a detailed discussion in non-Abelian gauge theories see [54].

Accordingly, our task reduces to the evaluation of the coupled set of flow equations for the transverse vertices $\Gamma_{k,T}^{(n)}$. Each transverse vertex can be parameterised by a set of diffeomorphism-invariant expressions. Restricting ourselves to local invariants and second order in the curvature we are left with

$$R, \quad R^2, \quad R_{\mu\nu}^2. \quad (10.40)$$

The square of the Weyl tensor C^2 is eliminated via the Gauß-Bonnet term, which is a topological invariant. Higher-derivative terms, such as

$$R^{\mu\nu} f_{\mu\nu\rho\sigma} (\nabla) R^{\rho\sigma} \quad \text{with} \quad f(0) = 0, \quad (10.41)$$

$$\begin{aligned}
\partial_t \Gamma_k &= \frac{1}{2} \text{(blue loop)} - \text{(red loop)} \\
\partial_t \Gamma_k^{(h)} &= -\frac{1}{2} \text{(blue loop)} + \text{(blue loop)} + \text{(red loop)} \\
\partial_t \Gamma_k^{(2h)} &= -\frac{1}{2} \text{(blue loop)} + \text{(blue loop)} - 2 \text{(blue line)} \text{(red loop)} \\
\partial_t \Gamma_k^{(c\bar{c})} &= \dots \text{(red loop)} + \text{(red loop)} \dots \\
\partial_t \Gamma_k^{(3h)} &= -\frac{1}{2} \text{(blue loop)} + 3 \text{(blue line)} \text{(blue loop)} - 3 \text{(blue line)} \text{(blue loop)} + 6 \text{(blue line)} \text{(red loop)} \\
\partial_t \Gamma_k^{(4h)} &= -\frac{1}{2} \text{(blue loop)} + 3 \text{(blue line)} \text{(blue loop)} + 4 \text{(blue line)} \text{(blue loop)} - 6 \text{(blue line)} \text{(blue loop)} \\
&\quad - 12 \text{(blue line)} \text{(blue loop)} + 12 \text{(blue line)} \text{(blue loop)} - 24 \text{(blue line)} \text{(red loop)}
\end{aligned}$$

Figure 10.2.: Diagrammatic representation of the flow of the vertex functions up to the graviton four-point function. The flow of any n -point function depends on the $(n+1)$ - and $(n+2)$ -point functions. Double and dotted lines represent graviton and ghost propagators, respectively. All vertices are dressed and denoted by filled circles. Crossed circles stand for regulator insertions. Symmetrisation with respect to interchange of external momenta p_i is understood.

are also taken into account. Without the constraint $f(0) = 0$, equation (10.41) also includes R^2 and $R_{\mu\nu}^2$, more details on this basis can be found in [section 10.6](#). Note that also non-diffeomorphism-invariant terms are generated by the flow. In the next chapter we will discuss all invariants which are included in the parameterisation of our vertices, see [subsection 10.6.3](#).

For the background vertices $\Gamma_k^{(n,0)}$ we use the following: the NIs become trivial in the IR as we approach classical gravity. Moreover, for one of the two IR fixed points this implies that the derivative with respect to a background field is the same as a derivative with respect to a fluctuation field. This allows us to impose the trivial NIs in the IR, and all couplings are related. Then, the couplings at $k > 0$ follow from the flow equation. However, for the fluctuation couplings this amounts to solving a fine-tuning problem in the UV.

10.6. Flows of correlation functions

In this section we discuss the technical details of the covariant expansion scheme used in this dissertation, including the approximations used and their legitimisation.

10.6.1. Covariant tensors and uniformity

The flows of the n -point correlation functions are generated from the FRG equation ?? by taking n -th order fluctuation field derivatives in a background \bar{g} . In [Figure 10.2](#) we display the all flow equations up the four-point function in a diagrammatic language. In order to solve the flow equation, we employ a vertex ansatz [58, 172] including the flow of all relevant vertices up to the graviton three-point function in this chapter and up to the graviton four-point function in the next chapter. This vertex ansatz disentangles

the couplings of background and fluctuation fields by introducing individual couplings Λ_n and G_n for each n -point function. These individual couplings are introduced at the level of the n -point correlators and replace the cosmological constant Λ and Newton's coupling G_N of the classical Einstein-Hilbert action after performing the respective field derivatives. In summary, for the flat background $\bar{g}_{\mu\nu} = \delta_{\mu\nu}$ our vertex ansatz reads

$$\Gamma_k^{(\phi_1 \dots \phi_n)}(\mathbf{p}) = \left(\prod_{i=1}^n Z_{\phi_i}^{\frac{1}{2}}(p_i^2) \right) G_n^{\frac{n}{2}-1}(\mathbf{p}) \mathcal{T}^{(\phi_1 \dots \phi_n)}(\mathbf{p}; \Lambda_n), \quad (10.42)$$

where

$$\mathcal{T}^{(\phi_1 \dots \phi_n)}(\mathbf{p}; \Lambda_n) = G_N S_{\text{EH}}^{(\phi_1 \dots \phi_n)}(\mathbf{p}; \Lambda \rightarrow \Lambda_n), \quad (10.43)$$

denote the tensor structures extracted from the classical gauge-fixed Einstein-Hilbert action ???. The only flowing parameter in these tensors $\mathcal{T}^{(\phi_1 \dots \phi_n)}$ is Λ_n , while $G_n(\mathbf{p})$ carries the global scale- and momentum dependence of the vertex. In the above equations, $\mathbf{p} = (p_{\phi_1}, \dots, p_{\phi_n})$ denotes the momenta of the external fields ϕ_i of the vertex.

Apart from their flow equations, the n -point functions in (10.42) also satisfy standard RG-equations, see e.g. [9]. These RG-equations entail the reparameterisation invariance of the theory under a complete rescaling of all scales including k . With the parameterisation given in (10.42), this RG-running is completely carried by the wave function renormalisations $Z_{\phi_i}(p_i^2)$ of the fields ϕ_i , see e.g. [172, 59]. Consequently, the G_n and Λ_n are RG-invariant, and hence are more directly related to observables such as S -matrix elements. This parameterisation of the vertices also ensures that the wave function renormalisations never appear directly in the flow equations, but only via the anomalous dimensions

$$\eta_{\phi_i}(p_i^2) = -\partial_t \ln Z_{\phi_i}(p_i^2). \quad (10.44)$$

$G_n(\mathbf{p})$ is the gravitational coupling of the n -point function, while Λ_n denotes the momentum-independent part of the correlation function. In particular, Λ_2 is related to the graviton mass parameter $M^2 = -2\Lambda_2$. Finally, all the parameters Z_{ϕ_i} , G_n , and Λ_n are scale-dependent, but we have dropped the subscript k in order to improve readability.

In principle, all tensor structures, including non-diffeomorphism-invariant ones, are generated by the flow, but for our vertex functions we choose to concentrate on the classical Einstein-Hilbert tensor structures in the presence of a non-vanishing cosmological constant. Despite the restriction to these tensor structures, the n -point functions have an overlap with higher curvature invariants via the momentum dependence of the gravitational couplings. For example, the complete set of invariants that span the graviton wave function renormalisation is given by

$$R, \quad R^{\mu\nu} f_{\mu\nu\rho\sigma}^{(2)}(\nabla) R^{\rho\sigma}, \quad (10.45)$$

where the superscript of f indicates that it is a covariant tensor contributing to the two-point correlation function. Note also that we now drop the restriction on f present in (10.41). Then, this invariant naturally includes R^2 and $R_{\mu\nu}^2$ as the lowest order local terms. If we also allow for general momentum-dependencies, the corresponding covariant functions f are given by given by

$$f_{R^2, \mu\nu\rho\sigma}^{(2)} = \delta_{\mu\nu}\delta_{\rho\sigma} P_{R^2}^{(2)}(-\nabla^2), \quad f_{R_{\mu\nu}^2, \mu\nu\rho\sigma}^{(2)} = \frac{1}{2} (\delta_{\mu\rho}\delta_{\nu\sigma} + \delta_{\mu\sigma}\delta_{\nu\rho}) P_{R_{\mu\nu}^2}^{(2)}(-\nabla^2). \quad (10.46)$$

The lowest order local terms, R^2 and $R_{\mu\nu}^2$, are given by $P_{R^2}^{(2)} = 1$ and $P_{R_{\mu\nu}^2}^{(2)} = 1$, respectively. Note that (10.46) also allows for non-local terms in the IR, i.e. anomaly-driven terms with $P_{R^2}^{(2)} = 1/\nabla^2$, see e.g. [173]. In turn, higher curvature invariants do not belong to the set of the graviton wave function renormalisation since they are at least cubic in the graviton fluctuation field.

We resort to a uniform graviton propagator in order to limit the already large computer-algebraic effort involved. The uniform wave function renormalisation is then set to be that of the combinatorially dominant tensor structure, the transverse-traceless graviton wave function renormalisation, thereby estimating the wave function renormalisations of the other modes by the transverse-traceless one. Such uniform approximations have been very successfully used in thermal field theory. There, usually the tensor structures transverse to the heat-bath are used as the uniform tensor structure, for a detailed discussion see e.g. [174] and references therein. This approximation is typically supported by combinatorial dominance of this tensor structure in the flow diagrams. Indeed, as already indicated above, the transverse-traceless mode gives the combinatorially largest contribution to the flow of the vertices computed here. Note that such an approximation would get further support if the R tensor structures dominate the flows, which indeed happens in the present computation. Within this approximation the R^2 tensor structures drop out on the left-hand side of the graviton flow, since R is already quadratic in the transverse-traceless graviton fluctuation field: in other words, the tensors defined by $f_{R^2}^{(2)}$ in (10.46) have no overlap with the transverse-traceless graviton.

The set of invariants that span the gravitational coupling $G_3(\mathbf{p})$ is given by

$$R, \quad R^{\mu\nu} f_{\mu\nu\rho\sigma}^{(3)}(\nabla) R^{\rho\sigma}, \quad R^{\mu\nu} R^{\rho\sigma} f_{\mu\nu\rho\sigma\omega\zeta}^{(3)}(\nabla) R^{\omega\zeta}. \quad (10.47)$$

Again, the invariants R^2 and R^3 can be excluded from this set due to their order in transverse-traceless graviton fluctuation fields. In consequence, $G_4(\mathbf{p})$ is the only coupling in our setup that has overlap with R^2 contributions and higher terms in $f_{R^2}^{(4)}$.

Furthermore, in subsection 10.6.3 we will show that the by far dominant contribution to $G_3(\mathbf{p})$ in the momentum range $0 \leq p^2 \leq k^2$ stems from the invariant R . All higher momentum dependencies of the graviton three-point function are covered by the momentum dependence of the graviton wave function renormalisation. This was already observed in [29]. As already briefly mentioned above, it gives further support to the current uniform approximation: the assumption of uniformity allows us to restrict ourselves to computing the Einstein-Hilbert tensor structure for the transverse-traceless graviton as the combinatorially dominating tensor structure. The striking momentum-independence of the actual numerical flows supports a momentum-independent approximation of G_3 . In terms of ?? it implies that the dominant tensor structure for the transverse-traceless mode is given by $f_R^{(3)}$ with $P_R^{(3)} = 1$. The $R_{\mu\nu}^2$ tensor structure vanishes approximately, see ??.

In contrast to the situation for the two- and three point function, the R^2 invariant overlaps with our transverse-traceless projection for the graviton four-point function. Indeed, its flow receives significant contributions from the invariant R^2 . It follows that for the graviton four-point function R is not the only dominant invariant in the momentum range from $p = 0$ to $p = k$, as we show in ???. In consequence we either have to disentangle contributions from R and R^2 tensor structures in terms of an additional tensor structure or we resolve the momentum dependence of $G_4(\mathbf{p})$. In the present work we follow the latter procedure, see ?? for details.

10.6.2. Projection onto n -point functions

The flow equations for the couplings Λ_n and G_n are obtained by the following projection onto the flow of the graviton n -point functions $\partial_t \Gamma_k^{(n)}$. We use the classical Einstein-Hilbert tensor structures $\mathcal{T}^{(n)}(\mathbf{p}; \Lambda_n)$ (cf. (10.43)) as a basis for our projection operators. Furthermore, we project onto the spin-two transverse-traceless part of the flow, which is numerically dominant. Moreover, classical transverse-traceless graviton propagator is gauge independent and carries the only propagating degrees of freedom. This transverse-traceless projection operator is then applied to all external graviton legs. The flow of the couplings Λ_n is then extracted with the help of the momentum-independent part of said tensor structures, namely $\Pi_{\Lambda_n} = \mathcal{T}^{(n)}(0; \Lambda_n)/\Lambda_n$. For the couplings G_n we use $\Pi_{G_n} = \mathcal{T}^{(n)}(\mathbf{p}; 0)/p^2$. Dividing by Λ_n and p^2 ensures that the projection operators are dimensionless and scale-independent.

In principle, the flow of any n -point function depends on all external momenta $p_i, i \in \{1, \dots, n\}$, where e.g. p_n can be eliminated due to momentum conservation. For the two-point function, the momentum configuration is trivial, and only one momentum squared, p^2 , needs to be taken into account. In contrast, this dependence becomes increasingly complex for the higher n -point functions: The three-point function depends on three parameters (two momenta squared and one angle), the four-point function already depends on six parameters, and so on. To simplify the computations, we use a maximally symmetric $(n - 1)$ -simplex configuration for all n -point-functions, thereby reducing the momentum dependence to a single parameter. In the context of Yang-Mills theories, this approximation has been shown to be in good agreement with lattice computations on the level of the flow of the propagator [54]. Notably, in the symmetric momentum configuration all external momenta have the same absolute value p , and the same angles between each other. The scalar product of any two momenta in this momentum configuration then reads

$$p_i \cdot p_j = \frac{n\delta_{ij} - 1}{n - 1} p^2, \quad (10.48)$$

where δ_{ij} denotes the Kronecker delta. Note that such a symmetric momentum configuration only exists up to the $(d + 1)$ -point function, where d is the dimension of spacetime.

In the following, the expressions $\text{Flow}^{(n)}$ stand for the dimensionless right-hand sides of the flow equations divided by appropriate powers of the wave function renormalisations. More explicitly, we define

$$\text{Flow}_i^{(n)}(p^2) = \frac{\partial_t \Gamma_i^{(n)}(p^2)}{Z_\phi^{\frac{n}{2}}(p^2) k^{2-n}}, \quad (10.49)$$

where the index i represents the projection on some tensor structure. We use the transverse-traceless projection operator Π_{TT} , the projection operators Π_{G_n} and Π_{Λ_n} mentioned earlier for the graviton n -point functions, as well as the transverse projection operator Π_T for the ghost propagator. Note that the objects $\text{Flow}_i^{(n)}$ do not contain any explicit factors of the wave function renormalisations Z_ϕ . Instead, their running appears via the anomalous dimensions η_ϕ .

Last but not least, we choose to model the regulator functions R^{ϕ_i} on the corresponding two-point functions at vanishing mass, i.e.

$$R^{\phi_i}(p_i^2) = \Gamma^{(\phi_i \phi_i)}(p_i^2) \Big|_{m_{\phi_i}=0} r_{\phi_i}(p_i^2/k^2). \quad (10.50)$$

Here, $r_{\phi_i}(p_i^2/k^2)$ denotes the regulator shape function. For all fields we choose the Litim-type flat regulator [175, 15, 176, 177], to wit

$$r(x) = (x^{-1} - 1) \Theta(1 - x). \quad (10.51)$$

This choice allows for analytic flow equations for all couplings that are evaluated at vanishing external momenta. Furthermore, we introduce the dimensionless couplings

$$\mu = M^2 k^{-2}, \quad \lambda_n = \Lambda_n k^{-2}, \quad g_n = G_n k^2. \quad (10.52)$$

At the UV and IR fixed points, the flow of these dimensionless couplings vanishes.

10.6.3. Momentum dependence of the graviton n -point functions

We now investigate the momentum dependence of the flow of the graviton n -point functions as defined in equation (10.49). We restrict ourselves to the momentum range $0 \leq p^2 \leq k^2$ as well as to the transverse-traceless part of the graviton n -point functions.

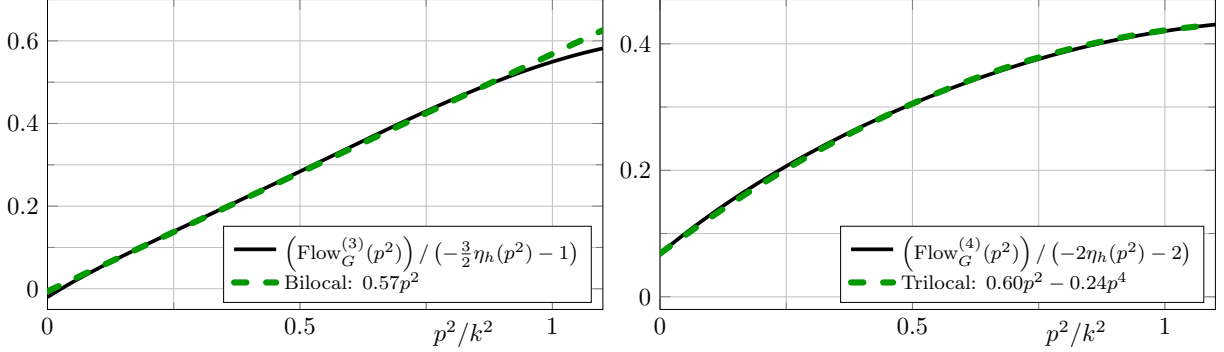


Figure 10.3.: Momentum dependence of the flow of the graviton three-point function (left) and the graviton four-point function (right) divided by $(-\frac{n}{2}\eta_h(p^2) - n + 2)$ as defined in (10.53). The flows are evaluated at $(\mu, \lambda_3, \lambda_4, g_3, g_4) = (-0.4, 0.1, -0.1, 0.7, 0.5)$ and $\lambda_6 = \lambda_5 = \lambda_3$ as well as $g_6 = g_5 = g_4$. The flows have such a simple polynomial structure as long as all couplings λ_n remain small, i.e. $|\lambda_n| \lesssim 1$. Importantly, the inclusion of a p^4 term in the left panel offers no significant improvement. Note that the constant parts of the functions are irrelevant for the beta functions since they are extracted from a different tensor projection. For $p^2 > k^2$ the momentum dependence of the flows is not polynomial anymore.

The first non-trivial result is that the flows of the graviton three- and four-point functions projected on the tensor structure of the gravitational coupling and divided by $(-\frac{n}{2}\eta_h(p^2) - n + 2)$ are well described by a polynomial in p^2 , provided that the couplings λ_n are small

$$\frac{\text{Flow}_G^{(3)}(p^2)}{-\frac{3}{2}\eta_h(p^2) - 1} \approx a_0 + a_1 p^2, \quad \frac{\text{Flow}_G^{(4)}(p^2)}{-2\eta_h(p^2) - 2} \approx b_0 + b_1 p^2 + b_2 p^4, \quad (10.53)$$

with some constants a_i and b_i that depend on the evaluation point in theory space. This momentum dependence is displayed in Figure 10.3. We emphasise that these equations only hold in the momentum range $0 \leq p^2 \leq k^2$, if the flow is generated by Einstein-Hilbert vertices, and if the constant parts of the vertices are small, i.e. $|\lambda_n| \lesssim 1$. If the condition of small λ_n is violated, then the flow as in (10.53) is non-polynomial. We did not compute the flow generated by an action including higher curvature terms, however, we suspect that the flow will still be polynomial but possibly of a higher degree.

It is important to note that the graviton three- and four-point functions have a different highest power in p^2 . This is a second non-trivial result for the following reasons: as already mentioned before, the coupling $g_3(p^2)$ has an overlap with R and $R_{\mu\nu}^2$, and higher derivative terms in $f_{R_{\mu\nu}^2}^{(3)}$, but not with any R^2 tensor structures in $f_{R^2}^{(3)}$, cf. (10.46). For example, the generation of $R_{\mu\nu}^2$ with $P_{R_{\mu\nu}^2}^{(3)} = 1$ would manifest itself in a p^4 -contribution to the flow of the graviton three-point function. Eq.(10.53) and Figure 10.3 show that such a p^4 -contribution as well as higher ones are approximately vanishing. This demonstrates in particular that the generation of $R_{\mu\nu}^2$ is non-trivially suppressed. In other words,

$$f_{R_{\mu\nu}^2}^{(3)} \approx 0, \quad (10.54)$$

where the superscript indicates the three-graviton vertex.

On the other hand, the projection on $g_4(p^2)$ overlaps with R , $R_{\mu\nu}^2$, R^2 tensor structures, and the related higher derivatives terms in $f_{R_{\mu\nu}^2}^{(4)}$ and $f_{R^2}^{(4)}$. It also overlaps with curvature invariants to the third power with covariant tensors such as $f_{R_{\mu\nu}^3}^{(4)}$ and similar ones. Note that it has no overlap with $f_{R^3}^{(4)}$.

Similarly to possible p^4 -contributions for the three-graviton vertex, p^6 -contributions and even higher powers in p^2 could be generated but are non-trivially suppressed. The p^4 -contribution to the flow, which

is described in (10.53) and displayed in Figure 10.3, could stem from either R^2 or $R_{\mu\nu}^2$ tensor structures. Now we use (10.54). It entails that the graviton three-point vertex does not generate the diffeomorphism invariant term $R_{\mu\nu}^2$, although it has an overlap with it. This excludes $R_{\mu\nu}^2$ as a relevant UV direction, which would otherwise be generated in all vertices. This statement only holds if we exclude non-trivial cancellations of which we have not seen any signature. Accordingly we set

$$f_{R_{\mu\nu}^2}^{(4)} \approx 0, \quad (10.55)$$

and conclude that this p^4 -contribution or at least its UV-relevant part stems solely from R^2 . It may be used to determine $f_{R^2}^{(4)}$.

In summary, the above statements about the momentum-dependencies are highly non-trivial and show that R^2 -contributions are generated while $R_{\mu\nu}^2$ and other higher derivative terms are strongly suppressed. These non-trivial findings also allow us to determine the most efficient way to project precisely onto the couplings of different invariants. This is discussed in subsection 10.6.6.

We close this section with a brief discussion of the effect of higher derivative terms on perturbative renormalisability and the potential generation of massive ghost states. As already discussed in [178] in a perturbative setup, it is precisely the $R_{\mu\nu}^2$ term that makes the theory perturbatively renormalisable. However, in this setup it gives rise to negative norm states. On the other hand, the R^2 term neither ensures perturbative renormalisability, nor does it generate negative norm states. This is linked to the fact that the R^2 term does not contribute to the transverse-traceless part of the graviton propagator. Consequently, the non-trivial suppression of $R_{\mu\nu}^2$ tensor structures might be interpreted as a hint that we do not suffer from massive ghost states. However, a fully conclusive investigation requires the access to the pole structure of the graviton propagator, and hence a Wick rotation. Progress in the direction of real-time flows in general theories and gravity has been made e.g. in [179, 180, 181, 182, 183, 184, 185, 186, 187].

10.6.4. Higher-order vertices and the background effective action

The results in the last section immediately lead to the question about the importance of the higher-order covariant tensor structures like e.g. f_{R^n} that have no overlap with the graviton n -point functions computed in this chapter. These are potentially relevant for the flows of G_5 and G_6 . These tensors have been dropped here, thus closing our vertex expansion. However, we may utilise previous results obtained within the background field approximation for estimating their importance: first we note that R^2 gives rise to a new relevant direction, as we will show in subsection 10.7.1. This has also been observed for the background field approximation [188, 189, 190, 191, 192]. There it has also been shown that the critical dimensions of the R^n -terms approximately follow their canonical counting [192]. Furthermore, our results so far have sustained the qualitative reliability of the background field approximation for all but the most relevant couplings. Indeed, it is the background field-dependence of the regulator that dominates the deviation of the background approximation from the full analysis for the low order vertices, and in particular the mass parameter μ of the graviton. This field-dependence is less relevant for the higher order terms. Thus, we may qualitatively trust the background field approximation for higher curvature terms. This means that they are of sub-leading importance and can be dropped accordingly.

Finally, the above findings together with those from the literature suggest that an Einstein-Hilbert action is generating a diffeomorphism-invariant R^2 term but not an $R_{\mu\nu}^2$ term in the diffeomorphism-invariant background effective action $\Gamma_k[g] = \Gamma_k[g, \phi = 0]$. Moreover, no higher-derivative terms are generated if a non-trivial wave function renormalisation $Z_h(p^2)$ and graviton mass parameter $\mu = -2\lambda_2$ are taken into account. Note that this only applies for an expansion with $p^2 < k^2$. This is a very interesting finding as it provides strong non-trivial support for the semi-quantitative reliability of the background approximation in terms of an expansion in R for spectral values smaller than k^2 subject to a resolution of the fluctuating graviton propagator: μ and Z_h have to be determined from the flows of the fluctuation fields or in terms of the mNIs.

10.6.5. Flow equations for the couplings

We obtain the flow equations for the couplings the n -point function, that are contracted with the projection operators as described in subsection 10.6.2. The flow equations for the couplings up to graviton three-point function remain unchanged compared to the last chapter and the procedure how we obtain them is described in ??.

We have to emphasise again that the momentum dependence of the flow for $g_3(p^2)$ is trivial, see Figure 10.3. This allows for an easy extraction of the momentum dependence and as in the last chapter we use a bilocal projection between $p = 0$ and $p = k$. From this we obtain an equation for $g_3(k^2)$. In contrast, the flow of the graviton four-point function exhibits a p^4 contribution, implying a non-trivial $g_4(p^2)$. This makes the extraction of the momentum dependence more tricky. Still we obtain the flow equation for $g_4(k^2)$ from a bilocal momentum projection at $p^2 = 0$ and $p^2 = k^2$, but this uses a further approximation that relies on the fact that the coupling λ_4 remains small. We refer to this equation as a bilocal equation. It is explicitly displayed in App. G.8, see equation (G.33). Within our setup this equation gives the best approximation of the vertex flows since it feeds back the most important momentum information into the flow. This further entails that the coupling $g_4(k^2)$ includes information about the invariants R and R^2 . In the next section we also show a trilocal momentum projection that disentangles the contribution from R and R^2 , but consequently feeds less information about the vertex flow back.

The flow equation for λ_4 is obtained from the momentum independent part of the graviton four-point function and is explicitly displayed in App. G.8

10.6.6. Disentangling R and R^2 tensor structures

In this section we present projection operators that disentangle contributions from R and R^2 tensor structures to the flows of the couplings $g_n(p^2)$. In the present setup this only allows us to switch off the R^2 coupling and thus to check the importance of the R^2 coupling.

For the disentanglement, we have to pay attention to two things: First of all, a local momentum projection at $p^2 = 0$ is very sensitive to small fluctuations and in consequence not very precise with regard to the whole momentum range $0 \leq p^2 \leq k^2$. This is explicitly shown in App. G.7. Hence, we have to rely on non-local momentum projections. Here the highest polynomial power of p^2 , as indicated in (10.53), dictates the simplest way of projecting on the p^2 -coefficient. The graviton three-point function is at most quadratic in the external momentum, and consequently it is enough to use a bilocal projection at $p^2 = 0$ and $p^2 = k^2$. The resulting equation (G.34) can be found in App. G.8.

The graviton four-point function, on the other hand, has p^4 as its highest momentum power, i.e. it is of the form

$$f(p^2) = b_0 + b_1 p^2 + b_2 p^4, \quad (10.56)$$

see also (10.53). Thus a bilocal momentum projection would not extract the p^2 coefficient b_1 alone. Instead, we use a trilocal momentum projection at $p^2 = 0$, $p^2 = k^2/2$, and $p^2 = k^2$ in order to solve the above equation for b_1 . Consequently we solve a system of linear equations and obtain

$$b_1 = -3f(0) + 4f(k^2/2) - f(k^2). \quad (10.57)$$

The resulting flow equation (G.35) is again presented in App. G.8.

For even higher order momentum contributions we would have to use even more points of evaluation. These momentum projections together with the observation of (10.53) guarantee that we project precisely on the p^2 coefficient in the whole momentum range $0 \leq p^2 \leq k^2$.

A natural upgrade of the current approximations amounts to the introduction of a second tensor structure that is orthogonal to the Einstein-Hilbert one in terms of these projections. Within our uniformity assumption this is considered to be sub-leading, and the momentum-dependence of $g_4(p^2)$ takes care of

the contribution of the R^2 tensor structure $f_{R^2}^{(4)}$. While the orthogonal projection on the respective flow is simple, its back-feeding demands a two tensor structure approximation of the three- and four-graviton vertex in the flow, the implementation of which is deferred to future work.

Here, we only perform a further check of the relevance of the R^2 tensor structure. This sustains the fact that the inclusion of the four-graviton vertex with its contribution of the R^2 tensor structure leads to an additional UV-relevant direction. To that end we generalise our ansatz for the graviton four-point function such that we can extract a flow equation for both the Einstein-Hilbert tensor structure as well as for the R^2 tensor structure. As already mentioned above, we cannot feed the generated coupling back into the flows, since they are given by vertices with Einstein-Hilbert tensor structures. Instead we compute the fixed point value that arises only from the Einstein-Hilbert tensor structures.

As the ansatz for the transverse-traceless graviton four-point function we choose

$$\Gamma_k^{(4)}(p^2) = Z_h^2(p^2) G_4 \left(C_{\Lambda_4}^{G_4} \Lambda_4 + C_{p^2}^{G_4} p^2 + C_{\Omega_4}^{G_4} \Omega_4 p^4 \right), \quad (10.58)$$

which is precisely the vertex that emerges from the sum of Einstein-Hilbert tensor structure and R^2 tensor structure. The related generating diffeomorphism-invariant action for this four-graviton vertex is

$$S = S_{\text{EH}} + \frac{1}{16\pi G_N} \int d^4x \sqrt{g} \Omega R^2, \quad (10.59)$$

where S_{EH} is defined as in ???. The flow of Ω_4 is then obtained by the trilocal momentum projection described below (10.56). For b_2 we obtain

$$b_2 = 2f(0) - 4f(k^2/2) + 2f(k^2). \quad (10.60)$$

The explicit form of the resulting flow equation (G.36) for the dimensionless coupling $\omega_4 = \Omega_4 k^2$ is given in App. G.8. Note that in the present approximation, the flows do not depend on the coupling ω_4 since it does not feed back into the vertices.

10.6.7. Computational details

The computations of correlation functions described in this section involve contractions of very large tensor structures. To give a rough estimate: the classical Einstein-Hilbert three-point vertex alone consists of around 200 terms, and the classical graviton propagator of 7 terms. For the box diagram of the flow of the graviton four-point function, displayed in Figure 10.2, this results in a total number of approximately $200^4 \cdot 7^4 \approx 4 \cdot 10^{12}$ terms, if no intermediate simplifications are applied.

These contractions are computed with the help of the symbolic manipulation systems *FORM* [193, 194] and *Mathematica*. For individual tasks, we employ specialised *Mathematica* packages. In particular, we use *xPert* [195] for the generation of vertex functions, *DoFun* [196] to obtain symbolic flow equations, and the *FormTracer* [197] to create optimised *FORM* scripts to trace diagrams.

10.7. Asymptotic safety

In this section, we discuss the UV fixed point structure of our system. We first present our best result, which includes the tensor structures as presented in subsection 10.6.1 and in particular in (10.45) and (10.47). The underlying UV-relevant diffeomorphism invariants turn out to be Λ , R , and R^2 . The R^2 coupling is included via the momentum dependence of the gravitational coupling $g_4(p^2)$, see subsection 10.6.3. As a main result we find an attractive UV fixed point with three attractive directions. The third attractive direction is related to the inclusion of the R^2 coupling.

We further analyse the stability of this UV fixed point with respect to the identification of the higher couplings. We also analyse the previous truncation from ?? and compare the stability of both truncations.

Here we find that the improvement of the truncation increases the stability of the system. In particular, we find a rather large area in the theory space of higher couplings where the UV fixed point exists with three attractive directions throughout.

Lastly, we discuss the importance of the R^2 coupling. In subsection 10.6.6 we have constructed projection operators that disentangle the contributions from R and R^2 tensor structures. This allows us to switch off the R^2 coupling and compare the stability of the reduced system to that of the full system. We find that the reduced system is significantly less stable, and that the area in the theory space of higher couplings where the fixed point exists is rather small. This highlights the importance of the R^2 coupling.

10.7.1. UV fixed point

In this section we display the UV fixed point structure of our full system. This means that we feed back the generated R^2 coupling via the momentum dependence of the gravitational coupling $g_4(p^2)$, as discussed in subsection 10.6.3. Fixed points are by definition points where the flows of the dimensionless couplings vanish. In consequence, we look for the roots of the equations (G.29), (G.32), (G.34), and (G.33). We use the identification scheme $g_6 = g_5 = g_4$ and $\lambda_6 = \lambda_5 = \lambda_3$. We find a UV fixed point at the values

$$(\mu^*, \lambda_3^*, \lambda_4^*, g_3^*, g_4^*) = (-0.45, 0.12, 0.028, 0.83, 0.57) . \quad (10.61)$$

The fixed point values are similar to those of the previous truncation in the last chapter, see ???. The biggest change concerns the graviton mass parameter, which is now less negative and thus further away from its pole. Moreover, it is remarkable that the new couplings λ_4 and g_4 are close to their lower counterparts λ_3 and g_3 , but not at precisely the same values. Since we use the difference between these couplings to parameterise the breaking of diffeomorphism invariance, this is more or less what we expected. This issue is further discussed in the next section.

We do not have access to the full stability matrix of the UV fixed point due to the unknown flow equations of the higher couplings. For this reason, we discuss two different approximations of the stability matrix. The main difference between these two approximations concerns the order of taking the derivatives and identifying the higher couplings, which is explained in more detail in App. G.4. We argue that in a well converged approximation scheme the most relevant critical exponents should not depend on the approximation of the stability matrix. Thus, we can use the two different approximations to judge the quality of the current level of truncation. We define the critical exponents as minus the eigenvalues of the stability matrix. We call the critical exponents of the first approximation $\bar{\theta}_i$, and the ones of the second approximation $\tilde{\theta}_i$. The critical exponents using the first approximation are given by

$$\bar{\theta}_i = (4.7, 2.0 \pm 3.1i, -2.9, -8.0) , \quad (10.62)$$

while the critical exponents using the second approximation are

$$\tilde{\theta}_i = (5.0, 0.37 \pm 2.4i, -5.6, -7.9) . \quad (10.63)$$

Hence this fixed point has three attractive directions in both approximations of the stability matrix. The third attractive direction compared to the system of the graviton three-point function, cf. ??, is related to the fact that the graviton four-point function has an overlap with R^2 , which we feed back via the momentum dependence of the gravitational coupling $g_4(p^2)$. The R^2 coupling has also been relevant in earlier computations with the background field approximation [188, 189, 190, 191, 192]. In addition, note that the most attractive eigenvalue is almost identical in both approximations of the stability matrix. This is a positive sign towards convergence since it is expected that the lowest eigenvalue is the first that converges, cf. App. G.4.

Furthermore, the anomalous dimensions at the UV fixed point read

$$(\eta_h^*(0), \eta_h^*(k^2), \eta_c^*(0), \eta_c^*(k^2)) = (0.56, 0.079, -1.28, -1.53), \quad (10.64)$$

where we have chosen to display the anomalous dimensions at the momenta that feed back into the flow. All anomalous dimensions stay well below the reliability bound $\eta_{\phi_i}(p^2) < 2$, which we will introduce later in ??.

10.7.2. Stability

In the following we investigate the UV fixed point from the previous section by varying the identification of the higher couplings. Again we look for the roots of the equations (G.29), (G.32), (G.34), and (G.33). These equations however still depend on the higher couplings g_5 , g_6 , λ_5 , and λ_6 . We have to identify these couplings with the lower ones or set them to constants in order to close the flow equations.

It is a natural choice to simply set these higher couplings equal to lower ones, e.g. $g_6 = g_5 = g_3$ and $\lambda_6 = \lambda_5 = \lambda_3$, as done in the previous section. The couplings would fulfil this relation exactly in a fully diffeomorphism invariant setup. However, such a diffeomorphism invariant setup is not at hand. In fact, we can parameterise the breaking of diffeomorphism invariance via these couplings, e.g. by writing $g_n = g_3 + \Delta_{g_n}$. Here we have designated g_3 as a reference coupling since it is the lowest genuine gravitational coupling. For this reason, it is also the most converged gravitational coupling within this vertex expansion, thus justifying this choice. In general we expect Δ_{g_n} to be small and in consequence we vary the identification of the higher couplings only in this part of the theory space of higher couplings. The quantity Δ_{g_4} is indeed small at the UV fixed point presented in the last section, see (10.61). More precisely, it takes the value $|\Delta_{g_4}/g_3| \approx 0.3$ at this UV fixed point.

In this analysis we choose to identify

$$g_5 = \alpha_1 g_3, \quad g_6 = \alpha_2 g_3, \quad (10.65)$$

and $\lambda_6 = \lambda_5 = \lambda_3$ for simplicity, and investigate the existence of the UV fixed point as a function of the parameters α_1 and α_2 . In Figure 10.4 the area where an attractive UV fixed point exists is displayed in blue. In the left panel, this is done for the previous truncation (μ, λ_3, g_3) , see ??, and in the right panel for the current truncation $(\mu, \lambda_3, \lambda_4, g_3, g_4)$. At the border of the blue area the UV fixed point either vanishes into the complex plane or loses its attractiveness. Remarkably, both areas are rather large, suggesting that the existence of the UV fixed point is quite stable. Even more conveniently, the area increases with the improved truncation, suggesting that the system is heading towards a converging limit. Note that the number of attractive directions of the UV fixed point is constant throughout the blue areas, namely two in the left panel and three in the right panel.

We further analyse the fixed point values that occur within the blue area in the right panel of Figure 10.4. Interestingly, the fixed point values are rather stable throughout the whole area where the UV fixed point exists. More precisely, they stay within the following intervals:

$$\begin{aligned} \mu^* &\in [-0.72, -0.19], & \lambda_3^* &\in [-0.018, 0.29], & \lambda_4^* &\in [-1.2, 0.12], \\ g_3^* &\in [0.22, 1.4], & g_4^* &\in [0.11, 0.97]. \end{aligned} \quad (10.66)$$

Hence, in particular the fixed point value of λ_3 is already confined to a very small interval, and also a very small number. The latter is important since some of our approximations rely on the fact that the λ_n are small, see subsection 10.6.3. The fact that λ_4^* is varying more strongly than λ_3^* is not surprising since we expect λ_3 to be better converged, being a lower coupling. The fixed point values of g_3 and g_4 seem to try to compensate the change induced by the identification. Thus, g_3^* and g_4^* become larger towards the identification $g_6 = g_5 = 0$ and smaller towards $g_6 = g_5 = 2g_3$. The shape of the area in the left panel in particular suggests the relation $g_4^* < g_3^*$, which is fulfilled by the improved truncation almost throughout

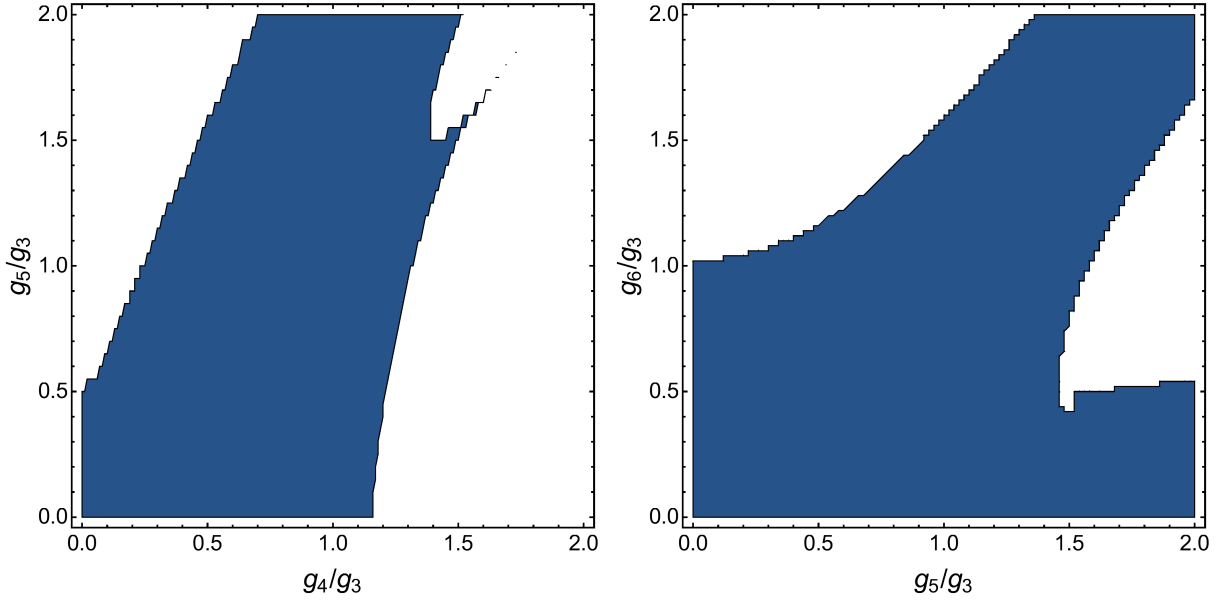


Figure 10.4.: Plots of the existence of an attractive non-trivial UV fixed point (blue) dependent on the higher couplings. Left: The system (μ, λ_3, g_3) , see also ??, dependent on the higher couplings g_4 and g_5 . Right: The system $(\mu, \lambda_3, \lambda_4, g_3, g_4)$ dependent on the higher couplings g_5 and g_6 . The higher couplings $\lambda_{n>n_{\max}}$ are always identified with λ_3 . The blue area marks the region where an attractive UV fixed point was found. At the border of this area the fixed point either vanishes into the complex plane or loses its attractiveness. In both systems the area where the fixed point exists is rather large and contains the identification $g_{n>n_{\max}} = g_3$. Conveniently, the area increases for the better truncation, indicating that the system becomes more stable with an improvement of the truncation. The number of attractive directions is uniformly two in the left panel and three in the right panel.

the whole area where the fixed point exists. This is indeed a non-trivial prediction that has been fulfilled by our approximation scheme.

A further study of the dependence of the UV fixed point properties on the choice of identification is given in App. G.6.

10.7.3. Importance of the R^2 tensor structure

In the previous subsection we have fed back the R^2 contributions to the flow via the momentum-dependent gravitational coupling $g_4(p^2)$. In order to check the quality of our approximation and to investigate the influence of the R^2 tensor structure on the fixed point structure of the system, we switch off the R^2 contribution in this section. We do the latter by projecting onto the p^2 part of the flow via a trilocal momentum projection scheme, cf. subsection 10.6.3 and subsection 10.6.6. This is both an examination of the influence of R^2 on the results presented in the previous subsections, as well as a proof of concept for disentangling the tensor structures of different invariants. Our analysis in this subsection suggests that leaving out the contribution of R^2 leads to significantly less stable results.

In Figure 10.5 we display the result for the same analysis as in the previous section, but with the trilocal equation (G.35) for g_4 instead. We find two fixed points with rather similar fixed point values. However, we are only interested in identifying the area in the theory space of the higher couplings where at least one UV fixed point exists. Thus, we unify both areas and obtain the blue area displayed in Figure 10.5. This area forms a rather narrow band whose total area is significantly smaller than for the momentum dependent gravitational coupling $g_4(p^2)$, cf. Figure 10.4. The identification $g_6 = g_5 = g_3$ also does not

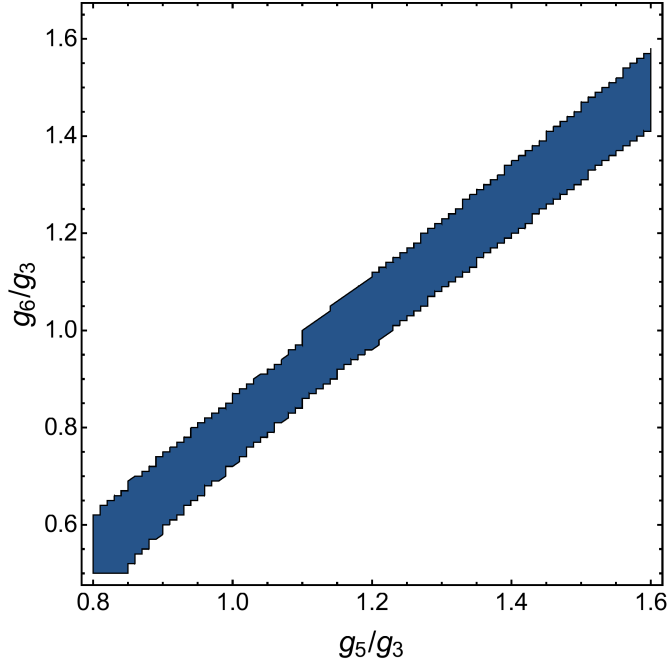


Figure 10.5.: Plot of the existence of an attractive non-trivial UV fixed point (blue) dependent on the higher couplings g_5 and g_6 . Here, the trilocal equation for the gravitational coupling g_4 was used, which allows us to switch off the R^2 coupling. We found two different fixed points with rather similar fixed point values. Each fixed point has its own area of existence in the theory space of the higher couplings. The blue area marks the unified area of both fixed points. Nevertheless, the area is significantly smaller than the areas displayed in [Figure 10.4](#). This reflects the importance of the R^2 coupling.

lie within these regions, but just outside of them. Since we switched off the R^2 contribution, a less stable fixed point structure was to be expected, and consequently these results highlight the importance of the R^2 coupling.

10.8. IR behaviour

In this section, we discuss the IR behaviour of the present theory of quantum gravity. We only consider trajectories that lie within the UV critical hypersurface, i.e. trajectories that are UV finite, and which end at the UV fixed point presented in [\(10.61\)](#) for $k \rightarrow \infty$. In this section we use the analytic flow equations given in App. [G.9](#) for simplicity, and set the anomalous dimensions to zero, i.e. $\eta_\phi = 0$. This approximation gives qualitatively similar results, as discussed in App. [G.7](#).

In the IR, it is particularly interesting to examine the background couplings \bar{g} and $\bar{\lambda}$. In the limit $k \rightarrow 0$ the regulator vanishes by construction and the diffeomorphism invariance of the background couplings is restored. Hence they become observables of the theory. The flow equations for the background couplings are displayed in App. [G.5](#).

In general we look for trajectories that correspond to classical general relativity in the IR. This implies that the quantum contributions to the background couplings vanish and in consequence that they scale classically according to their mass dimension. The classical scaling is described by

$$\bar{g}, g_3, g_4 \sim k^2, \quad \bar{\lambda}, \mu, \lambda_3, \lambda_4 \sim k^{-2}. \quad (10.67)$$

We use the classical scaling in the flow from the UV fixed point to the IR in order to set the scale k in

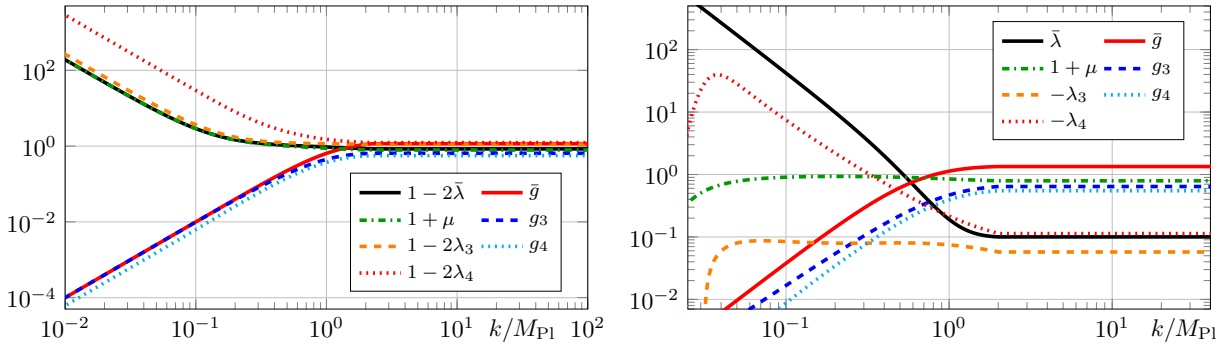


Figure 10.6.: Examples of UV finite trajectories from the UV fixed point (10.61) towards the IR. In the left panel all couplings scale classically below the Planck scale and reach their UV fixed point values shortly above the Planck scale. In the right panel some couplings show non-classical behaviour even below the Planck scale, which is triggered by the graviton mass parameter μ flowing towards the pole of the graviton propagator at $\mu = -1$. However, in this case the numerics break down at $k \approx 0.02M_{\text{Pl}}$ due to competing orders of the factor $(1 + \mu)$ close to the singularity at $\mu = -1$. The trajectories in both panels correspond to theories that behave like classical general relativity in the IR. Note that some couplings are plotted shifted or with a minus sign in order to keep them positive over the whole range.

units of the Planck mass M_{Pl} . We need to find a large enough regime where $\bar{g} \sim k^{-2}$. This entails that Newton's coupling is a constant in this regime and sets the scale k via $G_N = M_{\text{Pl}}^{-2} = \bar{g}k^{-2}$.

In Figure 10.6, two exemplary trajectories are displayed. In the left panel all couplings scale classically below the Planck scale and reach their UV fixed point values shortly above the Planck scale. All quantum contributions are suppressed simply by the fact that $\mu \rightarrow \infty$. In the right panel on the other hand some couplings exhibit a non-classical behaviour even below the Planck scale, which is triggered by the graviton mass parameter μ flowing towards the pole of the graviton propagator at $\mu = -1$. This entails that the dimensionful graviton mass parameter $M^2 = \mu k^2$ is vanishing in the IR. This IR behaviour is analogous to the one observed in [59], and recently also [186]. Remarkably, not only μ is behaving non-classically but also λ_3 , even though it is not restricted by any pole. However, in this scenario the numerics break down at $k \approx 0.02M_{\text{Pl}}$ due to competing orders of the factor $(1 + \mu)$ close to the singularity at $\mu = -1$.

In the left panel we have tuned the background couplings \bar{g} and $\bar{\lambda}$ so that they are equal to the lowest corresponding fluctuation coupling in the IR, i.e. $\bar{g} = g_3$ and $\bar{\lambda} = \lambda_2 = -\mu/2$ for $k \ll M_{\text{Pl}}$. This is equivalent to solving a trivial version of the Nielsen identities (NIs). Since all quantum contributions are suppressed by the graviton mass parameter going to infinity in the IR, $\mu \rightarrow \infty$, the NI in ?? reduces to

$$\frac{\delta\Gamma[\bar{g}, h]}{\delta\bar{g}_{\mu\nu}} = \frac{\delta\Gamma[\bar{g}, h]}{\delta h_{\mu\nu}} \quad \text{for} \quad \mu \rightarrow \infty \quad \& \quad k \rightarrow 0. \quad (10.68)$$

In consequence, we should see that all couplings coincide in this limit, $\bar{g} = g_n$ and $\bar{\lambda} = \lambda_n$. This is not the case in the left panel of Figure 10.6 since we have only fine tuned the background couplings, and thus we have two further degrees of freedom that could be used for fine-tuning, stemming from the three dimensional UV critical hypersurface.

In summary, we find different types of trajectories that correspond to classical general relativity in the IR. The main difference lies in the behaviour of the graviton mass parameter μ , which flows to infinity in one case and to minus one in the other case. Both scenarios are equivalent to general relativity in the end, in particular since only the background couplings become observables in the limit $k \rightarrow 0$.

System	μ^*	λ_3^*	λ_4^*	g_3^*	g_4^*	$\bar{\theta}_i$	$\tilde{\theta}_i$	
μ, g_3, λ_3	-0.57	0.095		0.62		$1.3 \pm 4.1i$ 7.3 -3.5	-12 -7.4	
μ, g_3, λ_3, g_4	-0.53	0.086		0.74 0.67		$2.1 \pm 3.8i$ $0.75 \pm 1.5i$	-3.6 -11 -7.8 $\pm 3.5i$	
$\mu, g_3, \lambda_3, \lambda_4$	-0.58	0.17	0.032	0.48		4.1 6.2	$0.35 \pm 2.6i$ 1.8 -3.4	-8.3 -8.8
$\mu, g_3, \lambda_3, g_4, \lambda_4$	-0.45	0.12	0.028	0.83 0.57		4.7 5.0	$2.0 \pm 3.1i$ $0.37 \pm 2.4i$	-2.9 -8.0 -5.6 -7.9

Table 10.1.: Properties of the non-trivial UV fixed point for different orders of the vertex expansion scheme, computed for momentum dependent anomalous dimensions $\eta_{\phi_i}(p^2)$ and bilocally projected Newton's couplings $g_n(k^2)$. The critical exponents $\bar{\theta}_i$ and $\tilde{\theta}_i$ stem from two different approximation of the stability matrix as discussed in App. G.4. The fixed points are computed with the identifications $g_6 = g_5 = g_{\max}$ and $\lambda_6 = \lambda_5 = \lambda_3$. We observe that the fixed point values are only varying mildly between the different orders of the vertex expansion. Notably, if we compare the critical exponents of the two approximations of the stability matrix, we observe that the difference becomes smaller with an increasing order of the vertex expansion. This is precisely what one would expect of a systematic approximation scheme that is approaching a converging limit.

10.9. Towards apparent convergence

In this section we discuss and summarise the findings of this chapter concerning apparent convergence. On the one hand, the order of our vertex expansion is not yet high enough to fully judge whether the system approaches a converging limit. Nevertheless, we have collected several promising first hints that we want to present in the following.

We have introduced two different approximations to the stability matrix, as presented in App. G.4. We have argued that in a well converged approximation scheme the most relevant critical exponents should not depend on the approximation of the stability matrix. In Table 10.1 we display the UV fixed point properties for different orders of the vertex expansion. The first system is without the graviton four-point function and exactly the same as in ???. Then we look at systems where we add either only an equation for $g_4(k^2)$ (cf. (G.33)), or only an equation for λ_4 (cf. (G.32)). Lastly, we display our best truncation including all couplings up to the graviton four-point function, see subsection 10.7.1. We observe that the fixed point values of the couplings vary only mildly with an improving truncation, although there is no clear pattern to those variations. The most important piece of information is the difference between the critical exponents from the two different approximations of the stability matrix. While the difference is rather large in the truncation of the graviton three-point function, it is becoming smaller with each improvement of the truncation. At the level of the graviton four-point function, the critical exponents show only a small difference. This is precisely what we expect, and thus we interpret this as a sign that the system is approaching a converging limit.

Another important piece of information comes from the stability of the UV fixed point under different closures of the flow equation. In a well converged expansion scheme, the properties of the UV fixed point should be completely insensitive to the details of the closure of the flow equation. We have performed this analysis in subsection 10.7.2. We observed that the area in which the UV fixed point exists in the theory space of higher couplings is indeed increasing with the improvement of the truncation. Furthermore, we saw that the UV fixed point values are confined to small intervals. We again interpret this as a sign that

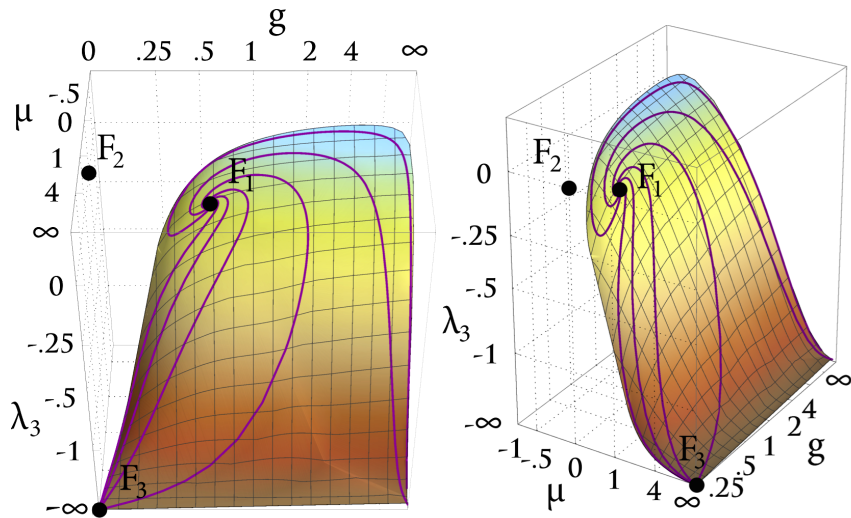


Figure 10.7.: Phase diagram for the couplings g , λ_3 and μ in two different views. The phase diagram was calculated using the analytic equations ???. The system exhibits a non-trivial UV fixed point, F_1 , with two attractive and one repulsive direction. The Gaussian fixed point and a non-trivial IR fixed point are denoted as F_2 and F_3 , respectively. The set of trajectories that approach F_1 constitutes two-dimensional UV critical hypersurface represented in gradient colours.

the system is approaching a converging limit.

In summary, we have already seen several signatures of apparent convergence although we are only at the level of the graviton four-point function within the present systematic expansion scheme. This suggests that we are on a promising path and that the present setup will eventually lead to a converging limit.

11. Gravity and matter

11.1. Gravity-matter systems

We start from the gauge-fixed Einstein-Hilbert action with minimally coupled scalars and fermions as well as gauge-fixed gauge theory with N_v gauge fields. The classical Euclidean action reads

$$\begin{aligned} S = & \frac{1}{16\pi G_N} \int d^4x \sqrt{g} (2\Lambda - R) + S_{\text{gf+gh,gravity}} \\ & + \frac{1}{2} \sum_{i=1}^{N_s} \int d^4x \sqrt{g} g^{\mu\nu} \partial_\mu \varphi^i \partial_\nu \varphi^i + \sum_{j=1}^{N_f} \int d^4x \sqrt{g} \bar{\psi}^j \not{\nabla} \psi^j \\ & + \frac{1}{2} \int d^4x \sqrt{g} g^{\mu\nu} g^{\rho\sigma} \text{tr} F_{\mu\rho} F_{\nu\sigma} + S_{\text{gf+gh,gauge}}, \end{aligned} \quad (11.1)$$

where $F_{\mu\nu}$ is the field-strength tensor of the gauge field A_μ . The gravity gauge fixing is of the linear de-Donder type in the Landau gauge limit. We also use the Landau gauge in the Yang-Mills sector. For the covariant Dirac operator $\not{\nabla}$ we use the spin-base invariant formulation [198, 199, 200]. Under the impact of quantum gravity, Abelian and non-Abelian gauge theories can approach a free fixed point [201, 202, 203, 204, 205, 160], such that the corresponding gauge couplings vanish, and the non-Abelian ghost sector decouples. Hence for our computation only the total number of gauge fields, N_v , is relevant. We focus on $N_s = N_v = 2N_f = 1$.

Expanding the metric about a flat background

$$g_{\mu\nu} = \delta_{\mu\nu} + \sqrt{G_N} h_{\mu\nu}, \quad (11.2)$$

schematically leads to interactions of the form

$$\begin{aligned} \Gamma \sim & \int d^4x (\sqrt{G_{N,h}} h(\partial h)(\partial h) + \sqrt{G_{N,c}} h(\partial \bar{c})(\partial c) \\ & + \sqrt{G_{N,\varphi}} h(\partial \varphi)(\partial \varphi) + \sqrt{G_{N,\psi}} h \bar{\psi} \gamma \partial \psi \\ & + \sqrt{G_{N,A}} h(\partial A)(\partial A)) + \dots, \end{aligned} \quad (11.3)$$

where we replaced G_N by avatars of the Newton coupling $G_{N,i}$ corresponding to the interactions, $i \in \{h, c, \varphi, \psi, A\}$. In addition to the Newton couplings, the expansion of the cosmological constant term results in a two-graviton coupling μ and a three-graviton coupling λ_3 [59, 29].

More generally we write

$$\begin{aligned} \Gamma_k[\bar{g}, \phi] = & \sum_{n=0}^{\infty} \frac{1}{n!} \Gamma_k^{(\phi_1 \dots \phi_n)}[\bar{g}, 0] \phi_1 \dots \phi_n \\ = & \Gamma_k[\bar{g}, 0] + \Gamma_k^{(h)}[\bar{g}, 0] h + \frac{1}{2} \Gamma_k^{(2h)}[\bar{g}, 0] h^2 \\ & + \frac{1}{3!} \Gamma_k^{(3h)}[\bar{g}, 0] h^3 + \frac{1}{2} \Gamma_k^{(\bar{c}c)}[\bar{g}, 0] \bar{c} c \\ & + \frac{1}{2} \Gamma_k^{(\bar{\psi}\psi)}[\bar{g}, 0] \bar{\psi} \psi + \frac{1}{2} \Gamma_k^{(\varphi\varphi)}[\bar{g}, 0] \varphi^2 + \dots. \end{aligned} \quad (11.4)$$

This vertex expansion of the scale dependent effective action was introduced in [58, 59, 29] in the context of pure quantum gravity. In other related works, anomalous dimensions were computed with vertex expansions on a flat background and were used in combination with the background-field approach [206, 155, 207]. Together with [29], however, the present work is the first minimally self-consistent analysis of such vertex flows in quantum gravity.

We also want to briefly compare the present expansion scheme with the standard heat kernel expansion in the background field approximation. In this approximation it is assumed that the scale dependent effective action is a functional of only one single metric field $g = \bar{g} + h$. Note that this approximation has the seeming benefit of a diffeomorphism invariant expansion scheme and a closed, diffeomorphism invariant effective action. However, the background field approximation does not satisfy the non-trivial Slavnov-Taylor identities for the dynamical metric h as well as the Nielsen identity, that link \bar{g} -dependences and h -dependences, see in particular [143, 9, 203, 144, 208, 209, 145]. Hence, while based on a diffeomorphism-invariant effective action, the background field approximation is at odds with diffeomorphism invariance for this very reason. Note that this also implies that background independence is at stake. The potential severeness of the related problems has been illustrated early on at the simpler example of a non-Abelian gauge theory in [141]. These problems can either be resolved in the present approach within a flat background expansion, the geometrical effective action approach, see [210, 143, 9, 144], or in the bi-metric approach, see [152, 154]. Results within these approaches also allow for a systematic check of the reliability of the background field approximation. Note also that the full resolution of the background independence within the bi-metric approach requires the computation of h -correlation function functions of the order two and higher as it is only these correlation functions that enter the flow equation on the right hand side. So far, this has not been undertaken.

The heat kernel computation expands the solution in powers of the Ricci scalar R , to wit

$$\dot{\Gamma}_k[g] = c_0 \int d^4x \sqrt{g} + c_1 \int d^4x \sqrt{g} R + O(R^2). \quad (11.5)$$

The coefficients $c_0 = c_0(\dot{\bar{g}}, \dot{\lambda})$ and $c_1 = c_1(\dot{\bar{g}}, \dot{\lambda})$ are related to flow of the background couplings. By computing the flow for the graviton two-point function for this hypothetical situation according to

$$\mathcal{F} \circ \dot{\Gamma}_k^{(2h)}[\bar{g}] \Big|_{\bar{g}=\delta} = c_0 \mathcal{T}^{(2h)}(0) + c_1 \mathcal{T}^{(2h)}(\mathbf{p}), \quad (11.6)$$

where \mathcal{F} denotes the Fourier transform, we observe that the coefficients c_0 and c_1 are obtained analogously from the momentum independent and momentum dependent parts of the graviton two-point function, respectively. The tensor structures \mathcal{T} are defined later in (11.9). In consequence, we extract exactly the same information from the flow within the flat vertex expansion that is obtained in the heat kernel approach. In case of higher order operators, we are even able to distinguish between the flows of e.g. R^2 and $R_{\mu\nu}R^{\mu\nu}$. Considering the realistic situation that the flow is not a functional of only one single metric but of a background and a fluctuating field, the vertex expansion further conveniently disentangles the flows of their corresponding couplings. In summary the present approach retains the results of standard heat kernel computation although it is evaluated on a flat background but has significant advantages in the non-single metric of quantum gravity.

In order to obtain running couplings from the flow of the n -point functions we employ a vertex dressing according to

$$\Gamma_k^{(\phi_1 \dots \phi_n)} = \sqrt{\prod_{i=1}^n Z_{\phi_i}(p_i^2)} G_n^{\frac{n}{2}-1} \mathcal{T}^{(\phi_1 \dots \phi_n)}, \quad (11.7)$$

where Z_{ϕ_i} denote the wavefunction renormalisations of the respective fields in ϕ which are functions of the field momenta p_i^2 . $\mathcal{T}^{(\phi_1 \dots \phi_n)}$ is the tensor structure of the respective vertex and shall be defined

The figure consists of four parts, each showing a three-point vertex with its dressing formula.
 - Top-left: A vertex with three external lines labeled \$p_{h_1}\$, \$p_{h_2}\$, and \$p_{h_3}\$. The formula is \$= \sqrt{Z_h(p_{h_1}^2)Z_h(p_{h_2}^2)Z_h(p_{h_3}^2)}G_3^{1/2}\mathcal{T}^{(3h)}(\mathbf{p};\Lambda_3)\$.
 - Top-right: A vertex with three external lines labeled \$p_h\$, \$p_{\bar{c}}\$, and \$p_c\$. The formula is \$= \sqrt{Z_h(p_h^2)Z_c(p_{\bar{c}}^2)Z_c(p_c^2)}G_3^{1/2}\mathcal{T}^{(h\bar{c}c)}(\mathbf{p})\$.
 - Bottom-left: A vertex with three external lines labeled \$p_h\$, \$p_{\varphi_2}\$, and \$p_{\varphi_1}\$. The formula is \$= \sqrt{Z_h(p_h^2)Z_\varphi(p_{\varphi_1}^2)Z_\varphi(p_{\varphi_2}^2)}G_3^{1/2}\mathcal{T}^{(h\bar{\varphi}\varphi)}(\mathbf{p})\$.
 - Bottom-right: A vertex with three external lines labeled \$p_h\$, \$p_\psi\$, and \$p_\psi\$. The formula is \$= \sqrt{Z_h(p_h^2)Z_\psi(p_\psi^2)Z_\psi(p_\psi^2)}G_3^{1/2}\mathcal{T}^{(h\bar{\psi}\psi)}(\mathbf{p})\$.

Figure 11.1.: Vertex dressing of all three-point vertices used in this work. The vertex dressing consist of the respective wave function renormalisations, couplings and tensor structures. The first line in the figure depicts all pure gravity three-point vertices while the second line shows the ones with gravity-matter-interactions.

in (11.9). In general, we assign to any n -vertex an individual, momentum dependent Newton's constant $G_n(\mathbf{p})$, with $\mathbf{p} = (p_1, \dots, p_n)$. In this work, however, we approximate all G_n as one, momentum-independent coupling, $G_n(\mathbf{p}) \equiv G_3 =: G$. Note, that Z_ϕ and G are scale dependent, although we drop the subscript k here and in the following for notational convenience. In Figure 11.1 the vertex dressing of all involved the three-point vertices are given according to (11.7). Generalisations to higher order vertices can be inferred from (11.7). Note, that (11.7) suggests an expansion in rescaled fields $\bar{\phi}$ and rescaled vertices $\bar{\Gamma}^{(\phi_1\dots\phi_n)}$ with

$$\phi = \frac{\bar{\phi}}{\sqrt{Z_\phi}}, \quad \bar{\Gamma}^{(\phi_1\dots\phi_n)} = \frac{\Gamma^{(\phi_1\dots\phi_n)}}{\sqrt{\prod_{i=1}^n Z_{\phi_i}(p_i^2)}} \simeq G_n^{\frac{n}{2}-1}, \quad (11.8)$$

see also [172, 9, 59]. Such a rescaling absorbs the RG-running of the vertices in the fields, and hence is an expansion in RG-invariant, but cutoff-dependent, quantities, for more details on this aspect see [172, 9, 59]. The underlying structure is elucidated by the kinetic term $\bar{\Gamma}^{(\phi_1\phi_2)}$: it has the classical form without wave function renormalisation, and hence does not scale under RG-transformations. This discussion highlights the rôle of the couplings G_n as RG-invariant running couplings.

The tensor structures \mathcal{T} are given by variations of the classical action S with respect to the fluctuation fields. More precisely, the latter read

$$\mathcal{T}^{(\phi_1\dots\phi_n)}(\mathbf{p};\Lambda_n) = S^{(\phi_1\dots\phi_n)}(\mathbf{p};\Lambda \rightarrow \Lambda_n, G_N \rightarrow 1). \quad (11.9)$$

In (11.9) the classical action S is given by the Einstein-Hilbert action added by covariant fermion and scalar kinetic terms according to

$$S = S_{\text{EH}} + \int d^4x \sqrt{g} \bar{\psi}_i \not{\partial} \psi_i + \frac{1}{2} \int d^4x \sqrt{g} g_{\mu\nu} \partial^\mu \varphi_i \partial^\nu \varphi_i, \quad (11.10)$$

where we used the conventional slash-notation for the contraction of the spin-covariant derivative ∇^μ with gamma matrices. The covariant kinetic terms for the matter fields in (11.10) lead to minimal coupling between gravity and matter in the present truncation. For the formulation of fermions in curved spacetime we use the spin-base invariance formalism introduced in [198, 199, 200]. This allows to circumvent possible ambiguities arising in the vielbein formalism and relies on spacetime dependent γ -matrices and the spin-connection Γ^μ . As a result, $\not{\partial}$ reads

$$\not{\partial} = g_{\mu\nu} \gamma(x)^\mu \nabla^\nu = g_{\mu\nu} \gamma(x)^\mu (\partial^\nu + \Gamma(x)^\nu), \quad (11.11)$$

if it acts on a spinor as in (11.10). In the following, we drop the explicit spacetime dependence of the latter quantities for a more convenient notation. The gauge-fixed Einstein-Hilbert action S_{EH} in (11.10)

reads

$$S_{\text{EH}} = \frac{1}{16\pi G_N} \int d^4x \sqrt{g} (2\Lambda - R) + S_{\text{gf}} + S_{\text{gh}}, \quad (11.12)$$

where Λ denotes the classical cosmological constant and R is the curvature scalar. The terms S_{gf} and S_{gh} are the gauge fixing and the Faddeev-Popov-ghost action, respectively. Both latter contributions are determined by the gauge condition F_μ . The gauge fixing action reads

$$S_{\text{gf}} = \frac{1}{32\pi\alpha} \int d^4x \sqrt{\bar{g}} \bar{g}^{\mu\nu} F_\mu F_\nu. \quad (11.13)$$

In this work, we apply a De-Donder-type linear gauge given by

$$F_\mu = \bar{\nabla}^\nu h_{\mu\nu} - \frac{1+\beta}{4} \bar{\nabla}_\mu h^\nu_\nu, \quad (11.14)$$

with $\beta = 1$. Furthermore, we apply the Landau-limit of vanishing gauge parameter, $\alpha \rightarrow 0$. The Faddeev-Popov operator corresponding to (11.14) is of the form

$$\mathcal{M}_{\mu\nu} = \bar{\nabla}^\rho (g_{\mu\nu} \nabla_\rho + g_{\rho\nu} \nabla_\mu) - \bar{\nabla}_\mu \nabla_\nu. \quad (11.15)$$

The Landau-limit $\alpha \rightarrow 0$ is particularly convenient since it provides a sharp implementation of the gauge fixing. This assures furthermore, that the corresponding gauge-fixing parameter is at a fixed point of the renormalisation group flow [211].

The vertex flows discussed here carry additional spacetime and momentum indices. In order to obtain scalar flow equations for the couplings the appropriate projection of the flows is a crucial part of the present truncation and goes along the same lines as in [29]. It can be summed up in a three step procedure:

- (i) We decompose $\mathcal{T}^{(n_h)}$, where n_h is the number of variations with respect to h , into its momentum dependent and momentum independent part according to

$$\mathcal{T}^{(n_h)}(\mathbf{p}; \Lambda_{n_h}) = \mathcal{T}^{(n_h)}(\mathbf{p}; 0) + \Lambda_{n_h} \mathcal{T}^{(n_h)}(0; 1). \quad (11.16)$$

In (11.16), the first term on the right-hand side is quadratic in the external graviton momenta \mathbf{p} for the current truncation. The second term is momentum independent.

- (ii) From (11.16) we take the dimensionless tensors $\mathcal{T}^{(n_h)}(\mathbf{p}; 0)/\mathbf{p}^2$ and $\mathcal{T}^{(n_h)}(0; 1)$ and separately multiply all spacetime-index pairs of both tensors with transverse-traceless projection operators Π_{TT} . This leaves us with the two tensors $\mathcal{T}_{\text{TT}}^{(n_h)}(\mathbf{p}; 0)/\mathbf{p}^2$ and $\mathcal{T}_{\text{TT}}^{(n_h)}(0; 1)$, each of them carries $2n_h$ spacetime indices.
- (iii) We contract the left and the right hand side of the vertex flow with these two tensors, in order to obtain Lorentz-scalar expressions. Hereby, the tensors $\mathcal{T}_{\text{TT}}^{(n_h)}(\mathbf{p}; 0)/\mathbf{p}^2$ and $\mathcal{T}_{\text{TT}}^{(n_h)}(0; 1)$ are used to project the tensorial flow onto the scalar flows of G_{n_h} and Λ_{n_h} , respectively.

The projection operators are detailed in Appendix ???. In addition to the spacetime indices, the vertex flows carry spinor, flavour and colour indices. These however, can be trivially traced out after multiplying appropriately with γ and \not{p} -matrices.

After having traced out all discrete indices the resulting flow still depends on the external field momenta \mathbf{p} . This dependence is dealt with by choosing a specific kinematic configuration. Since all vertices obey momentum conservation this choice is only relevant for n -point vertices with $n \geq 3$. In this work, the flow of the graviton three-point function is the highest order vertex flow and thus it is the only flow that

needs a fixed kinematic configuration. For the latter, we choose the maximally symmetric configuration, to wit

$$|p_1| = |p_2| =: p, \quad \vartheta = 2\pi/3, \quad (11.17)$$

where ϑ is the angle between p_1 and p_2 . Note, that p_3 was eliminated using momentum conservation. This way, both sides of the flow equations for all vertices only depend on the scalar momentum parameter p . Note, that due to the vertex construction (11.7) and the choice of regulators R_k^ϕ to be specified below there are no single wavefunction renormalisations Z_{ϕ_i} in the flow. Instead, the latter always enter in terms of the corresponding anomalous dimensions η_{ϕ_i} defined by

$$\eta_{\phi_i}(p^2) := -\partial_t \ln Z_{\phi_i}(p^2). \quad (11.18)$$

Consequently, the flow of a generic ϕ^n -vertex reads schematically

$$\text{Flow}^{(\phi^n)} = \int_q (\dot{r}_{\phi_i}(q^2) - \eta_{\phi_i}(q^2)r_{\phi_i}(q^2)) F_i^{(\phi^n)}(p, q, \dots), \quad (11.19)$$

where we have defined $\text{Flow}^{(\phi^n)}$ as

$$\text{Flow}^{(\phi^n)}(p^2) := \frac{\dot{\Gamma}^{(\phi_1 \dots \phi_n)}(p^2)}{\prod_{i=1}^n \sqrt{Z_{\phi_i}(p^2)}}. \quad (11.20)$$

In (11.19), r_{ϕ_i} denotes the regulator shape function corresponding to the field ϕ_i and the functions $F_i^{(\phi^n)}$ encode the contributions of the field ϕ_i to the flow of the ϕ^n -vertex. The functions F_i depend on the external and loop momenta, p and q , respectively, as well as on the couplings G and Λ_n . The remaining p -dependence in (11.19) is projected out differently, depending on the quantity to be extracted. The momentum projection will be discussed below.

Summarising the present truncation, we consider the renormalisation group flow for the n -point correlation functions in a system of minimally-coupled gravity and matter. To this end, we employ a vertex expansion of the scale dependent effective action about a flat metric background to derive flow equations for the n -point correlators up to order three. The RG-invariant vertex dressing (11.7) allows to derive independently the flows of the momentum-independent couplings G , Λ_2 and Λ_3 as well as the momentum-dependent anomalous dimensions $\eta_h(p^2)$, $\eta_c(p^2)$, $\eta_\psi(p^2)$ and $\eta_\varphi(p^2)$. The couplings G and Λ_3 are computed from the transverse-traceless part of the graviton three-point function in the symmetric momentum configuration. Diffeomorphism invariant background couplings are computed from the solution of the dynamical couplings. Altogether, the present truncation yields the flow of the scale dependent parameters,

$$\{\bar{G}, \bar{\Lambda}, G, \Lambda_2, \Lambda_3, \eta_h(p^2), \eta_c(p^2), \eta_\psi(p^2), \eta_\varphi(p^2)\}. \quad (11.21)$$

11.2. Yang-Mills–gravity system with the FRG

In the present work, we quantise the Yang-Mills–gravity system within the functional renormalisation group (FRG) approach. The general idea is to integrate-out quantum fluctuations of a given theory successively, typically in terms of momentum or energy shells, $p^2 \sim k^2$. This procedure introduces a scale dependence of the correlation functions, which is most conveniently formulated in terms of the scale-dependent effective action Γ_k , the free energy of the theory. Its scale-dependence is governed by the flow equation for the effective action, the Wetterich equation [21], see also [25, 26],

$$\partial_t \Gamma_k[\bar{g}; \phi] = \frac{1}{2} \text{Tr} \left[\frac{1}{\Gamma_k^{(0,2)}[\bar{g}; \phi] + R_k} \partial_t R_k \right], \quad (11.22)$$

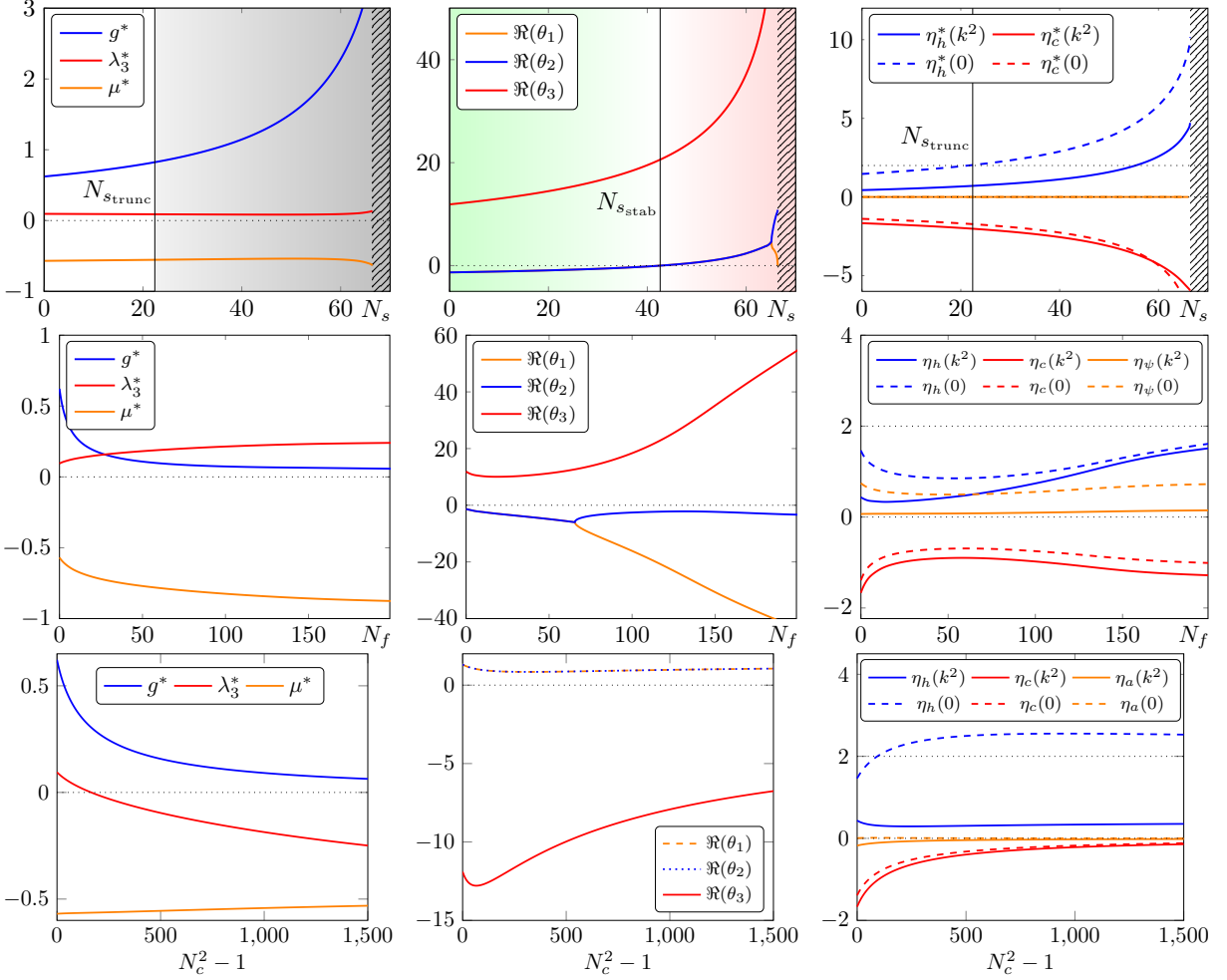


Figure 11.2.: Fixed point values, critical exponents and anomalous dimensions as a function of N_s , N_f and N_c

where the trace sums over species of fields, space-time, Lorentz, spinor, and gauge group indices, and includes a minus sign for Grassmann valued fields. For the explicit computation, we employ the flat regulator [175, 15], see App. G.11.1. From here on, we drop the index k for notational convenience. The scale dependence of couplings, wave function renormalisations, or the effective action is implicitly understood.

The computation utilises the systematic vertex expansion scheme as presented in [58, 59, 29, 60, 158, 62] for pure gravity as well as matter-gravity systems: the scale dependent effective action that contains the graviton-gluon interactions is expanded in powers of the fluctuation super field ϕ defined in (G.40),

$$\Gamma[\bar{g}, \bar{A}; \phi] = \sum_n \frac{1}{n!} \Gamma_{\mathbf{a}_1 \dots \mathbf{a}_n}^{(\phi_1 \dots \phi_n)} [\bar{g}, \bar{A}, 0] \phi_{\mathbf{a}_1} \dots \phi_{\mathbf{a}_n}. \quad (11.23)$$

In (11.23), we resort to de-Witt's condensed notation. The bold indices sum over species of fields, space-time, Lorentz, spinor, and gauge group indices. The auxiliary background field is general. Here, we choose it as $\bar{\phi} = (\bar{A} = 0, \bar{g} = \text{id})$ for computational simplicity. In this work, we truncate such that we obtain a closed system of flow equations for the gluon two- and the graviton two- and three-point functions, $\partial_t \Gamma^{(aa)}$, $\partial_t \Gamma^{(hh)}$, and $\partial_t \Gamma^{(hhh)}$. The corresponding flow equations are derived from (11.22) by functional differentiation.

The pure gravity part of the effective action Γ_{grav} in (11.23) is constructed exactly as presented in [58,

[59, 29, 60, 158, 62]. This construction is extended to the Yang-Mills part. Moreover, for the flow equations under consideration here, only terms with at most two gluons contribute. In summary, our approximation is based solely on the classical tensor structures S_{cl} that are derived from (G.41). The correlation functions follow as,

$$\Gamma_{\mathbf{a}_1 \dots \mathbf{a}_n}^{(\phi_1 \dots \phi_n)} = \left(\prod_{i=1}^n Z_{\phi_i}^{\frac{1}{2}} \right) S_{\text{cl}, \mathbf{a}_1 \dots \mathbf{a}_n}^{(\phi_1 \dots \phi_n)} (\mathbf{p}; g_{\phi_1 \dots \phi_n}, \lambda_{\phi_1 \dots \phi_n}), \quad (11.24)$$

where the Z_{ϕ_i} are the wave function renormalisations of the corresponding fields and $\mathbf{p} = (p_1, \dots, p_n)$. The $g_{\phi_1 \dots \phi_n}, \lambda_{\phi_1 \dots \phi_n}$ are the couplings in the classical tensor structures that may differ for each vertex. In the present approximation, these couplings are extracted from the momentum dependence at the symmetric point, and hence, carry part of the non-trivial momentum dependence of the vertices. The projection procedure is detailed later. We further exemplify the couplings at the example of the pure graviton and the gauge-graviton vertices. Each graviton n -point function, $\Gamma^{(h_1 \dots h_n)}$, depends on the dimensionless parameters

$$g_n \equiv g_{h^n} = G_n k^2, \quad \lambda_n \equiv \lambda_{h^n} = \Lambda_n / k^2, \quad (11.25a)$$

and a mixed gauge-graviton $(n+2)$ -point function on

$$g_{A^2 h^n} = G_{A^2 h^n} k^2, \quad g_{A^2 h^n} = G_{A^2 h^n} k^2. \quad (11.25b)$$

In particular the parameters λ_n should not be confused with the cosmological constant, for more details see, e.g., [62]. In the present approximation we identify all gravity couplings

$$g_{A^m h^n} = g_3 =: g, \quad \lambda_{n>2} = \lambda_3, \quad \lambda_2 = -\frac{1}{2}\mu, \quad (11.26)$$

the general case without this identification is discussed in section 11.6. Note that the identification in (11.26) introduces (maximal) diffeomorphism invariance to the effective action: in order to elucidate this statement, we discuss the full effective action for constant vertices. With $g = \bar{g} + \sqrt{G}Z_h^{1/2}h$ and $A = \bar{A} + Z_a^{1/2}a$ and (11.26), the current approximation can schematically be written as a sum of the classical action and a mass-type term for the fluctuation graviton,

$$\begin{aligned} \Gamma[\bar{g}, \bar{A}; \phi] &= S_{\text{cl}}[g, A]|_{G=G_3, \Lambda=\Lambda_3} + \Delta\Gamma[\bar{g}] \\ &\quad + \frac{k^4}{2} Z_h(\mu + 2\lambda_3) h_{\mathbf{a}} \mathcal{T}_{\mathbf{ab}} h_{\mathbf{b}}, \end{aligned} \quad (11.27)$$

where $\mathcal{T}_{\mathbf{ab}} = S_{\text{EH ab}}^{(hh)}(p^2 = 0; g = 1, \lambda = 1)$ is the tensor structure of the second derivative of the cosmological constant term. The λ_3 term cancels with the corresponding contribution in the first line, and thus, μ is the coupling of this tensor structure. This is the minimal approximation that is susceptible to the non-trivial symmetry identities, both the modified STIs and the Nielsen identities present in gauge-fixed quantum gravity. This information requires the non-trivial running of wave function renormalisations $Z_{\bar{g}}, Z_{\bar{A}}, Z_h, Z_c, Z_a$, that of the graviton mass parameter μ , as well as the dynamical gravity interactions g and λ_3 . Note that at a (UV) fixed point the flows of the couplings μ, g , and λ_3 vanish while the anomalous dimensions do not vanish.

The last identification in (11.26) reflects the fact that $-2\lambda_2$ is the dimensionless mass parameter of the graviton. Note however that μ is not a physical mass of the graviton in the sense of massive gravity: in the classical regime of gravity, it is identical to the cosmological constant, $\bar{\lambda} = -\frac{1}{2}\mu$. Higher order operators in particular g_{a^n} may couple back in an indirect fashion, see, e.g., [204]. In summary, this leads us to an

expansion of the mixed fluctuation terms (with both, powers of a and powers of h) of the effective action (11.23)

$$\begin{aligned} \Gamma[\bar{g}, \bar{A}; \phi] \Big|_{\text{mixed}} &= \Gamma_{\mathbf{a}_1 \mathbf{a}_2}^{(ah)} a_{\mathbf{a}_1} h_{\mathbf{a}_2} + \frac{1}{2} \Gamma_{\mathbf{a}_1 \mathbf{a}_2 \mathbf{a}_3}^{(ahh)} a_{\mathbf{a}_1} h_{\mathbf{a}_2} h_{\mathbf{a}_3} \\ &+ \frac{1}{2} \Gamma_{\mathbf{a}_1 \mathbf{a}_2 \mathbf{a}_3}^{(aah)} a_{\mathbf{a}_1} a_{\mathbf{a}_2} h_{\mathbf{a}_3} + \frac{1}{4} \Gamma_{\mathbf{a}_1 \mathbf{a}_2 \mathbf{a}_3 \mathbf{a}_4}^{(aahh)} a_{\mathbf{a}_1} a_{\mathbf{a}_2} h_{\mathbf{a}_3} h_{\mathbf{a}_4} \\ &+ \frac{1}{12} \Gamma_{\mathbf{a}_1 \mathbf{a}_2 \mathbf{a}_3 \mathbf{a}_4 \mathbf{a}_5}^{(aahhh)} a_{\mathbf{a}_1} a_{\mathbf{a}_2} h_{\mathbf{a}_3} h_{\mathbf{a}_4} h_{\mathbf{a}_5} + O(a^3 h, ah^3). \end{aligned} \quad (11.28)$$

As we consider also correlation functions of the background gluon, we need the expansion of the fluctuation vertices in (11.28) in the background field, i.e.,

$$\Gamma_{\mathbf{a}_1 \mathbf{h}_2}^{(ah)} [\bar{A}] = \Gamma_{\mathbf{a}_1 \mathbf{h}_2}^{(ah)} [0] + \Gamma_{\mathbf{b}_1 \mathbf{a}_1 \mathbf{h}_2}^{(\bar{A}ah)} [0] \bar{A}_{\mathbf{b}_1} + O(\bar{A}^2), \quad (11.29)$$

in an expansion about vanishing background gauge field. In the following, we consider trivial metric and gluon backgrounds $\bar{g} = \mathbb{I}$ and $\bar{A} = 0$. In this background, the terms of the order $O(a^3 h, ah^3)$ do not enter the flow equations of the gluon and graviton propagators nor that of the graviton three-point function. This is the reason why they have not been displayed explicitly in (11.28). Note that with this background choice, the terms linear in a in the second line in (11.28) vanish.

In this trivial background, we can use standard Fourier representations for our correlation functions. In momentum space, the above correlation functions are given as follows: the gluon two-point function reads

$$\Gamma_{\mu\nu}^{(aa)}(p_1, p_2) = Z_a^{\frac{1}{2}}(p_1^2) Z_a^{\frac{1}{2}}(p_2^2) \left. \frac{\delta^2 S_A}{\delta a^\mu(p_1) \delta a^\nu(p_2)} \right|_{\phi=0}. \quad (11.30)$$

The graviton two-point function is parameterised according to the prescription presented in [58, 59, 29, 60, 158, 62],

$$\Gamma_{\mu\nu\alpha\beta}^{(hh)}(p_1, p_2) = Z_h^{\frac{1}{2}}(p_1^2) Z_h^{\frac{1}{2}}(p_2^2) \left. \frac{G_2 \delta^2 S_{\text{EH}}(G_2, \Lambda_2)}{\delta h^{\mu\nu}(p_1) \delta h^{\alpha\beta}(p_2)} \right|_{\phi=0}, \quad (11.31)$$

where $-2\Lambda_2 = \mu k^2$ as introduced in (11.26). Note that the right-hand side of (11.31) does not depend on G_2 . The two-gluon–one-graviton vertex is given by

$$\begin{aligned} \Gamma_{\mu\nu\alpha\beta}^{(aah)}(p_1, p_2, p_3) &= Z_a^{\frac{1}{2}}(p_1^2) Z_a^{\frac{1}{2}}(p_2^2) Z_h^{\frac{1}{2}}(p_3^2) \\ &\times \left. \frac{G_3^{\frac{1}{2}} \delta^3 S_A}{\delta a^\mu(p_1) \delta a^\nu(p_2) \delta h^{\alpha\beta}(p_3)} \right|_{\phi=0}, \end{aligned} \quad (11.32)$$

with scale- and momentum-dependent wave function renormalizations Z_a for the gluon and Z_h for the graviton and a scale-dependent gravitational coupling G_3 . The other n -point functions have a completely analogous construction, which is not displayed here.

In addition to the fluctuation vertices, we also need mixed vertices involving two background gluons and the fluctuation fields as in (11.29), $\Gamma^{A^2 h^n}$ and $\Gamma^{A^2 a^n}$ with $n = 1, 2$. They are parameterised as in (11.30) - (11.32) with $Z_a \rightarrow Z_A$. We also would like to emphasise two structures that facilitate the present computations:

- (1) As we consider the flow equations for the gluon two-point function, and the graviton two- and three-point functions, only the terms quadratic in a_μ in (11.28) contribute to the graviton-gluon interactions in the flow equations. The non-Abelian parts in the F^2 term do not contribute since they are of order three and higher. Hence, modulo trivial colour factors δ^{ab} , the vertices defined above are identical for $SU(N)$ and $U(1)$ gauge theories.

$$\text{Flow}_h^{(aa)} = -\frac{1}{2} \left(\text{Diagram 1} + \text{Diagram 2} + \text{Diagram 3} \right)$$

Figure 11.3.: Diagrammatic depiction of graviton contributions to the flow of the gluon propagator. Wiggle and double lines represent gluon and graviton propagators, respectively.

- (2) In principle, the derivatives in $F^{\mu\nu}$ are covariant derivatives with respect to the Levi-Civita connection. However, since $F^{\mu\nu}$ is asymmetric, and the Christoffel-symbols symmetric in the paired index, the latter cancel out, and the covariant derivatives can be replaced by partial derivatives.

In the end, we are interested in the gravitational corrections to the Yang-Mills beta function, and the Yang-Mills contributions to the running in the gravity sector. The beta functions of the latter have been discussed in great detail in [58, 59, 29, 158, 62]. In the Yang-Mills sector, we make use of the fact that the wave function renormalisation Z_A of the background gluon is related to the background (minimal) coupling by

$$Z_{\alpha_s} = Z_A^{-1}, \quad (11.33)$$

which is derived from background gauge invariance of the theory. The latter can be related to quantum gauge invariance with Nielsen identities, see [212, 141, 143, 9, 144] in the present framework. This also relates the background minimal coupling to the dynamical minimal coupling of the fluctuation field. Note that this relation is modified in the presence of the regulator, in particular, for momenta $p^2 < k^2$. There the interpretation of the background minimal coupling requires some care. The running of the background coupling is then determined by

$$\partial_t \alpha_s = \beta_{\alpha_s} = \eta_A \alpha_s, \quad (11.34)$$

with the gluon anomalous dimension

$$\eta_A := -\frac{\partial_t Z_A}{Z_A}. \quad (11.35)$$

Note that in general all these relations carry a momentum dependence as $Z_A(p^2)$ carries a momentum dependence. This will become important in the next section for the physics interpretation of the results.

11.3. Graviton contributions to Yang-Mills

In this section we compute the gravitational corrections to the running of the gauge coupling. The key question is if graviton-gluon interactions destroy or preserve the property of asymptotic freedom in the Yang-Mills sector. The running of the gauge coupling can be calculated from the background gluon wave function renormalisation. Its flow equation is derived from (11.22) with two functional derivatives w.r.t. \bar{A} . Schematically it reads

$$\partial_t \Gamma^{(\bar{A}\bar{A})}(p) = \text{Flow}_A^{(\bar{A}\bar{A})}(p) + \text{Flow}_h^{(\bar{A}\bar{A})}(p), \quad (11.36)$$

where the first term contains only gluon fluctuations and the second term is induced by graviton-gluon interactions. The diagrammatic form of the second term is displayed in Figure 11.3. This split is reflected in a corresponding split of the anomalous dimension

$$\eta_A(p^2) = \eta_{A,A}(p^2) + \eta_{A,h}(p^2). \quad (11.37)$$

$$\left\langle \text{---} \text{---} \text{---} \right\rangle_{\Omega_p} = \frac{1}{2} \left\langle \text{---} \text{---} \text{---} \text{---} \right\rangle_{\Omega_p}$$

Figure 11.4.: Kinematic identity for the one- and two-graviton–two-gluon scattering vertices for $r_a = 0$ and $\Gamma_A^{(2)} \simeq S_A^{(2)}$, taken from [203, 216].

Note that in the present approximation we have $\eta_{A,h} = \eta_{a,h}$. This originates in the fact that the fluctuation graviton only couples to gauge invariant operators.

Asymptotic freedom is signalled by a negative sign of the gluon anomalous dimension as the beta function for the coupling is proportional to η_A . We know that the pure gluon contributions $\eta_{A,A}$ are negative. Hence, the question whether asymptotic freedom is preserved in the Yang-Mills–gravity system boils down to the sign of the gravity contributions $\eta_{A,h}$, and we arrive at

$$\eta_{A,h} \leq 0 \iff \text{asymptotic freedom}. \quad (11.38)$$

The anomalous dimension in (11.38) depends on cutoff and momentum scales. For small momentum scales $p^2/k^2 \rightarrow 0$ the regulator induces a breaking of quantum-gauge and quantum-diffeomorphism invariance: the respective STIs of the fluctuation field correlation functions are modified. This necessitates also a careful investigation of the background observables, which only carry physics due to the relation of background gauge- and diffeomorphism invariance.

Note that asymptotic freedom as defined in (11.38) only applies to the minimal coupling. Higher order fluctuation couplings are not necessarily vanishing. Indeed, it has been shown that the asymptotically safe fixed points of general matter and gauge fields coupled to gravity can not be fully asymptotically free in the matter and gauge field sector, see [213, 61, 214, 204, 215]. In the present work, this leads to a^4 vertices from higher-order invariants such as $(\text{tr } F^2)^2$ and $\text{tr } F^4$ with fixed point values proportional to $g_a^2/(1 + \mu)^3$ with $g_a = g$ in our approximation. Moreover, these vertices generate a tadpole diagram that contribute to the gluon propagator. Apart from shifting the Gaussian fixed point of higher order operators in the Yang-Mills sector to an interacting one, see [204] for the $U(1)$ case, it also deforms the gluon contribution to the Yang-Mills beta function. Its qualitative properties will be discussed later, as it is important for the large N_c behaviour of the fixed point. However, a full inclusion is deferred to future work.

11.3.1. Background observables

The discussion of physics content of background observables and its relation to gauge- and diffeomorphism invariance has been initiated for the Yang-Mills–gravity system in [203, 216]. There it has been shown that $\eta_{a,h} = 0$ vanishes for

$$\frac{r_a}{1 + r_a} \frac{1}{1 + r_h} = 0, \quad (11.39)$$

due to a non-trivial kinematic identity. This identity relates angular averages of one- and two-graviton–two-gluon scattering vertices in the absence of a gluon regulator r_a , see Figure 11.4. In other words, for a combination of regulators that satisfy (11.39) the quantum-gauge and quantum-diffeomorphism symmetry violating effects of the regulators do not effect the kinematic identity that holds in the absence of the regulator.

This structure requires some care in the interpretation of the running of background observables for $k \rightarrow \infty$: while the physics properties of the dynamical fluctuation fields should not depend on the choice of the regulators, background observables do not necessarily display physics in this limit. By now we

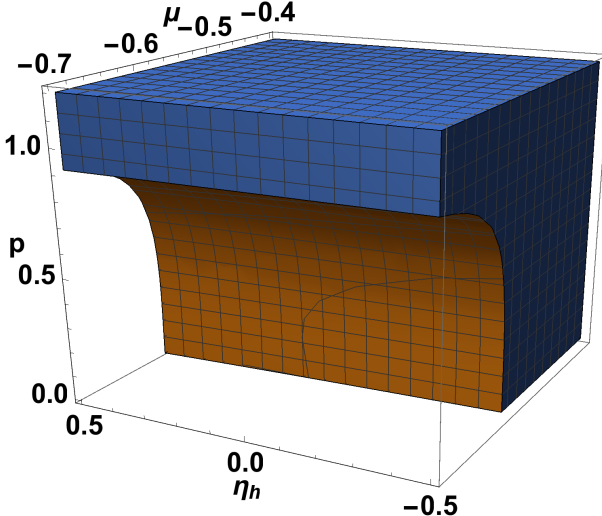


Figure 11.5.: Sign of the graviton contributions to the gluon anomalous dimension $\eta_{a,h}$ as a function of η_h , μ , and p . The coloured region indicates $\text{sgn } \eta_{a,h} < 0$. At $p = k$ the whole displayed region supports asymptotic freedom.

know of many examples for the latter deficiency ranging from the beta function of Yang-Mills theory, see [141], to the behaviour of the background couplings in pure gravity, [58, 59, 29, 158, 62] and matter-gravity systems [60, 214]. Moreover, we have already argued that the relation between the dynamical and the background minimal coupling only holds without modifications for sufficiently large momenta.

In summary, this implies the following for the interpretation of background observables: we either choose pairs of regulators that satisfy (11.39) or we evaluate background observables for momentum configurations that are not dominantly affected by the breaking of quantum-gauge and quantum-diffeomorphism invariance. Here, we will pursue the latter option that gives us more freedom in the choice of regulators. For the computation of the graviton contribution to the running of the Yang-Mills background coupling, this implies that we have to evaluate the flow of the two-point function for sufficiently large external momenta,

$$p^2 \gtrsim k^2. \quad (11.40)$$

For these momenta, the three-point function diagrams effectively satisfy (11.39), and the anomalous dimension $\eta_{a,h}(p^2)$ carries the information about the graviton contribution of the beta function of the background coupling.

11.3.2. Gravity supports asymptotic freedom

The results of the discussion on background observables in the previous subsection 11.3.1 allow us to access the question of asymptotic freedom of the minimal Yang-Mills coupling. With the construction of the effective action (11.28), we obtain a flow equation for $\partial_t \Gamma^{(aa)}$, which is projected with the transverse projection operator

$$P_T^{\mu\nu}(p) = \delta^{\mu\nu} - \frac{p^\mu p^\nu}{p^2}. \quad (11.41)$$

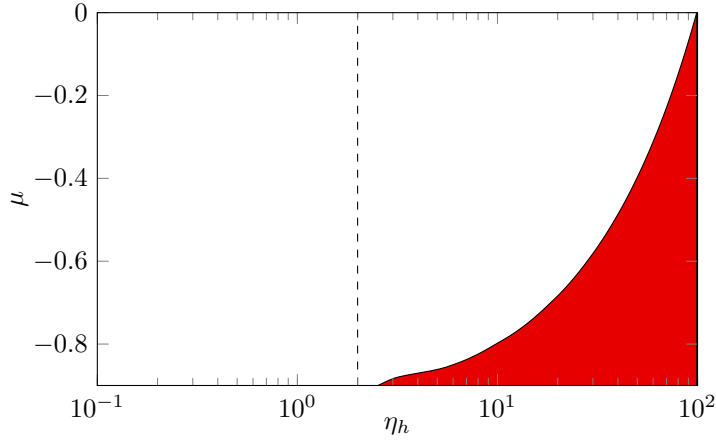


Figure 11.6.: Sign of the graviton contributions to the gluon anomalous dimension $\eta_{a,h}(k^2)$ as a function of η_h and μ . The red region indicates $\text{sgn } \eta_{a,h}(k^2) > 0$ and the loss of asymptotic freedom. The dashed line marks $\eta_h = 2$.

The graviton-induced contributions to the resulting flow equation take the form

$$\begin{aligned} P_T^{\mu\nu}(p) \partial_t \Gamma_{\mu\nu}^{(aa)}(p) &= \text{Flow}_h^{(aa)}(p^2) = \\ Z_a(p^2) g \int_q &\left((\dot{r}(q^2) - \eta_a(q^2)r(q^2)) f_a(q, p, \mu) \right. \\ &\left. + (\dot{r}(q^2) - \eta_h(q^2)r(q^2)) f_h(q, p, \mu) \right), \end{aligned} \quad (11.42)$$

where the terms on the right-hand side originate from diagrams with a regulator insertion in the gluon and graviton propagator, respectively. The left-hand side is simply given by

$$P_T^{\mu\nu} \partial_t \Gamma_{\mu\nu}^{(aa)}(p) = p^2 \partial_t Z_a(p^2). \quad (11.43)$$

Dividing by $Z_a(p^2)$, one obtains an inhomogeneous Fredholm integral equation of the second kind for the gluon anomalous dimension,

$$\eta_a(p^2) = f(p^2) + g \int \frac{d^4 q}{(2\pi)^4} K(p, q, \mu, \eta_h) \eta_a(q^2). \quad (11.44)$$

This integral equation can be solved using the resolvent formalism by means of a Liouville-Neumann series. In this work we approximate the full momentum dependence by evaluating the anomalous dimension in the integrand in (11.44) at $q^2 = k^2$. This is justified since the integrand is peaked at $q \approx k$ due to the regulator. With this approximation, (11.44) can be evaluated numerically for all momenta. This approximation was already used in [60] and lead to results in good qualitative agreement with the full momentum dependence. Details of the full solution are discussed in App. G.11.3. With the approximation to (11.44), we investigate the sign of the graviton contributions to the gluon propagator. These contributions are functions of the gravity couplings, which in turn depend on the truncation. It is therefore interesting to evaluate $\eta_{a,h}$ with a parametric dependence on the gravity couplings, in order to obtain general conditions under which asymptotic freedom is guaranteed.

The gluon anomalous dimension is of the form $\eta_a(p^2, g, \mu, \eta_h)$. In order to avoid the unphysical regulator dependence potentially induced by the violation of the kinematical identity (11.39) we choose the momentum $p^2 = k^2$ in order to satisfy (11.40). In summary, this provides us with a minimal coupling α_s ,

$$\partial_t \alpha_s = \beta_{\alpha_s} = \eta_a(k^2) \alpha_s. \quad (11.45)$$

$$\text{Flow}_a^{(2h)} = -\frac{1}{2} \text{Diagram A} + \text{Diagram B}$$

Figure 11.7.: Diagrammatic depiction of the gluon contributions to the flow of the graviton propagator. Wiggly and double lines represent gluon and graviton propagators, respectively.

As a main result in the present section, we conclude that

$$\beta_{\alpha_s} \leq 0 \quad \text{for } \mu > -1 \quad \text{and} \quad \eta_h(k^2) \leq 2. \quad (11.46)$$

The restriction to $\eta_h \leq 2$ is also the bound on the anomalous dimension advocated in [60]. To be more precise, $\eta_h > 2$ only changes the sign of the Yang-Mills beta function in the limit $\mu \rightarrow -1$. For other values of μ , very large values of η_h are necessary in order to destroy asymptotic freedom, e.g. for $\mu = -0.4$ the bound is $\eta_h \approx 50$. The precise bound is displayed in Figure 11.6, where the red region indicates $\beta_{\alpha_s} > 0$.

Despite the necessary restriction to momenta $p^2 \gtrsim k^2$ for its relation to the physical background coupling, we have also evaluated $\eta_{a,h}$ for more general momentum configurations and a range of gravity parameters μ and η_h : in Figure 11.5, the sign of the graviton-induced part of the gluon anomalous dimension $\eta_{a,h}$ is plotted in the momentum range $0 \leq p^2 \leq k^2$. For small momenta, $\eta_{a,h}$ changes sign for $\mu \rightarrow -1$. Again it can be shown that this does not happen for regulators with (11.39).

In order to understand the patterns behind Figure 11.5 and Figure 11.6 it is illuminating to examine $\eta_{a,h}(p^2 = 0)$ for flat regulators (G.60) with a p^2 derivative. It reads

$$\eta_{a,h} = -\frac{g}{8\pi} \left(\frac{8 - \eta_a}{1 + \mu} - \frac{4 - \eta_h}{(1 + \mu)^2} \right). \quad (11.47)$$

The first term on the right-hand side stems from $\partial_t R_{k,a}$ and is positive for $\eta_a < 8$. The second stems from $\partial_t R_{h,k}$. It is non-vanishing for $\eta_h = 0$ and hence already contributes at one-loop order. Its very presence reflects the breaking of the non-trivial kinematical identity depicted in Figure 11.4 as it is proportional to it. The interpretation of $\eta_{a,h}$ as the graviton-induced running of the Yang-Mills background coupling crucially hinges on physical quantum gauge invariance: it is important to realise that only with the relation between the auxiliary background gauge invariance and quantum gauge invariance the latter carries physics. In turn, in the momentum regime where the kinematical identity is violated, physical gauge invariance is not guaranteed, and background gauge invariance reduces to an auxiliary symmetry with no physical content. Accordingly, one either has to evaluate $\eta_{a,h}(p^2)$ for sufficiently large momenta $p^2 \gtrsim k^2$ or utilises regulators that keep the kinematical identity Figure 11.4 at least approximately for all momenta.

In summary, Figure 11.5 and Figure 11.6 entail that $\text{sgn}(\eta_{a,h}) < 0$ holds for physically relevant momenta and values of the gravity couplings. Thus asymptotic freedom is preserved. We have argued that (11.45) provides the correct definition for the beta function of the minimal coupling of Yang-Mills theory with $\text{sgn}(\beta_{\alpha_s}) \leq 0$. Hence we conclude that an ultraviolet fixed point in the spirit of the asymptotic safety scenario is compatible with asymptotic freedom of the minimal coupling in Yang-Mills theories. In App. G.11.4, we utilise different approximations to the gluon anomalous dimension, and we discuss in detail the regimes where it changes the sign in the parameter space of the gravity couplings.

11.4. Yang-Mills contributions to gravity

This section is concerned with the impact of gluon fluctuations on the gravity sector. The fully coupled system is analysed subsequently in section 11.5.

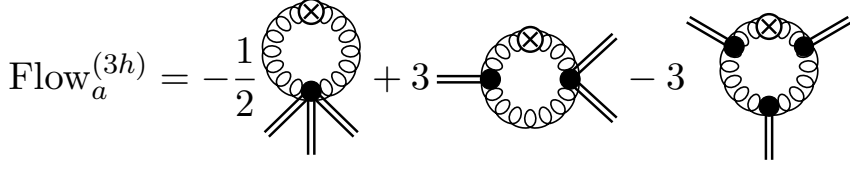


Figure 11.8.: Diagrammatic depiction of the gluon contributions to the flow of the graviton three-point function. Wiggly and double lines represent gluon and graviton propagators, respectively.

11.4.1. General structure

For the question of asymptotic safety, we have to investigate the gluon contributions to the graviton propagator as well as to the graviton three-point function. This allows us to compute the corrections to the running of the gravity couplings (μ, g, λ_3) due to gluon fluctuations.

The gluon corrections to the graviton two- and three-point function split analogously to the graviton corrections to Yang-Mills theory in the preceding section, since for any graviton n -point function the structure is given by

$$\text{Flow}^{(nh)} = \text{Flow}_h^{(nh)} + \text{Flow}_a^{(nh)}, \quad (11.48)$$

with graviton and gluon contributions denoted by $\text{Flow}_h^{(nh)}$ and $\text{Flow}_a^{(nh)}$, respectively. For example, the gluon contributions to the flow of the graviton two- and three-point function are depicted in [Figure 11.7](#) and [Figure 11.8](#). Accordingly, the beta function for Newton's coupling including gluon corrections has the structure

$$\begin{aligned} \partial_t g &= (2 + 3\eta_h) g \\ &+ g^2 (A_h(\mu, \lambda_3) + \eta_h B_h(\mu, \lambda_3) + C_a + \eta_a D_a), \end{aligned} \quad (11.49)$$

where we have used the identifications [\(11.26\)](#). In [\(11.49\)](#), A_h and B_h originate from graviton loops and they depend on μ and λ_3 , while C_a and D_a are generated by gluon loops and are just numbers. Similarly the beta function for λ_3 has the structure

$$\begin{aligned} \partial_t \lambda_3 &= \left(-1 + \frac{2}{3}\eta_h + \frac{\partial_t g}{2g} \right) \lambda_3 \\ &+ g (E_h(\mu, \lambda_3) + \eta_h F_h(\mu, \lambda_3) + G_a + \eta_a H_a). \end{aligned} \quad (11.50)$$

Throughout this chapter we display the anomalous dimensions η_h, η_a as momentum independent. Note, however, that they are momentum dependent and we approximate their momentum dependence by evaluating them at $p = k$ if they appear in an integral, see [\[60\]](#) for details.

Moreover, the Yang-Mills contributions to the graviton propagator enter the above beta function [\(11.49\)](#) via the graviton anomalous dimension η_h and the graviton mass parameter μ . These equations have the general form

$$\begin{aligned} \eta_h &= g (I_h(\mu, \lambda_3) + \eta_h J_h(\mu, \lambda_3) + K_a + \eta_a L_a), \\ \partial_t \mu &= (\eta_h - 2)\mu \\ &+ g (M_h(\mu, \lambda_3) + N_h(\mu, \lambda_3)\eta_h + O_a + \eta_a P_a), \end{aligned} \quad (11.51)$$

where again all pure gravity contributions are labelled with an index h and the one generated by gluons with an index a . Note again that all the Yang-Mills contributions do not depend on μ and λ_3 , as the corresponding diagrams do not involve graviton propagators and pure graviton vertices, see [Figure 11.7](#) and [Figure 11.8](#). In particular, this implies that these terms have no $1/(1 + \mu)$ singularity in the limit $\mu \rightarrow -1$. Furthermore, all these diagrams contain a closed gluon loop, and hence, all the factors in the above equations with an index a are proportional to $N_c^2 - 1$.

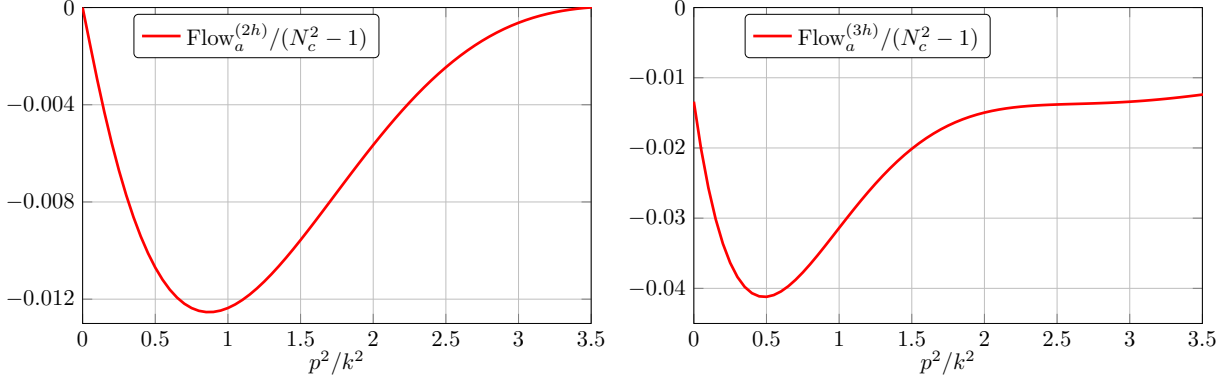


Figure 11.9.: The momentum dependence of $\text{Flow}_a^{(2h)}/(N_c^2 - 1)$ (left) and $\text{Flow}_a^{(3h)}/(N_c^2 - 1)$ (right) for $g = 1$ and $\eta_a = 0$ on the right-hand side of the flow.

11.4.2. Contributions to the graviton propagator

The gluon contribution to the graviton propagator has been studied in a derivative expansion around $p^2 = 0$ in [216] where it was shown that this projection is insufficient due to the non-trivial momentum dependence of the flow. The latter is characterized by a dip at $p^2 \approx k^2$. It has been shown in [58] that this structure is also present in the full flow, i.e. including the graviton contributions and that projections at momentum scales close to the cutoff are necessary, see also [29, 62]. We have rederived the momentum dependence of $\text{Flow}_a^{(2h)}(p^2)$, see Figure 11.9.

For the projection at $p^2 = 0$ and flat regulators (G.60), we rederive the result of [216] and obtain for the momentum-independent part

$$\text{Flow}_a^{(2h)}(p^2 = 0) = gZ_h(N_c^2 - 1) \frac{1}{60\pi} \eta_a. \quad (11.52)$$

Surprisingly, this contribution is proportional to η_a . This happens due to a cancellation between both diagrams displayed in Figure 11.7. Note that this cancellation only occurs for the flat regulator. For other regulators the contribution can be either positive or negative. This is discussed in App. G.11.2 and will play a crucial rôle in the later analysis.

For the computation of the graviton anomalous dimension, we resort to a finite difference projection, which is of the general form

$$\frac{\text{Flow}_a^{(2h)}(p_1^2) - \text{Flow}_a^{(2h)}(p_2^2)}{p_1^2 - p_2^2} = gZ_h(N_c^2 - 1)(\alpha + \beta \eta_a), \quad (11.53)$$

where α and β depend only on p_1 and p_2 . This is rooted in the fact that there are only internal gluon propagators and graviton-gluon vertices, and these do not depend on λ_3 and μ as discussed in the last section. For $p_2 = 0$ and $p_1 \rightarrow p_2$, i.e. a p^2 -derivative at $p^2 = 0$, we obtain

$$\alpha = \beta = -\frac{1}{12\pi} \approx -0.027. \quad (11.54)$$

For a finite difference with $p_1^2 = k^2$ and $p_2 = 0$, we obtain

$$\alpha \approx -0.012, \quad \beta \approx -0.0033. \quad (11.55)$$

(11.54) and (11.55) display the gluon contribution to $-\eta_h$; thus, the gluon contribution to η_h is positive independent of the momentum projection scheme. Note however that (11.54) and (11.55) display a qualitatively different behaviour, and (11.55) is the correct choice due to the momentum dependence of the flow. This has already been observed in the pure gravity computations in [58, 59, 29, 62] and emphasises the importance of the momentum-dependence. In this work we use a finite difference between $p_1^2 = p^2$ and $p_2^2 = -\mu k^2$ for the equation of $\eta_h(p^2)$, see [59, 60] for details.

11.4.3. Contributions to the three-point function

The contributions to the graviton three-point function enter the beta function of the Newton's coupling g (11.49) via C_a and D_a and the beta function of λ_3 (11.50) via G_a and H_a . The diagrammatic representation of these contributions is shown in Figure 11.8. Here, the contribution to $\partial_t g$ is the momentum dependent part and the contribution to $\partial_t \lambda_3$ in the momentum independent part to the graviton three-point function. For the projection on the couplings g and λ_3 , we use precisely the same projection operators as in [29]. These are different projection operators for g and λ_3 , and we mark this with an index G and Λ in the following.

We have seen in the previous sections, that the momentum dependence of the flow plays a crucial rôle, and key properties may be spoiled if non-trivial momentum dependence is not taken into account properly. Therefore, we resolve the momentum dependence of the contributions $\text{Flow}_{G,a}^{(3h)}(p^2)$, which is shown in the right panel of Figure 11.9. Interestingly, the contribution is peaked at $p^2 = \frac{1}{2}k^2$ and is not well described by p^2 in the region $0 \leq p^2 \leq k^2$. Because of this non-trivial structure, the contribution to $\partial_t g$ depends on the momenta where it is evaluated. For general momenta p_1^2 and p_2^2 , we obtain

$$\frac{\text{Flow}_{G,a}^{(3h)}(p_1^2) - \text{Flow}_{G,a}^{(3h)}(p_2^2)}{p_1^2 - p_2^2} = g^{\frac{3}{2}} Z_h^{\frac{3}{2}} (N_c^2 - 1) (\gamma + \delta \eta_a), \quad (11.56)$$

where γ and δ again only depend on p_1^2 and p_2^2 . Evaluated as derivatives, i.e., $p_2^2 = 0$ and $p_1^2 \rightarrow 0$, we arrive at

$$\gamma = -\frac{7}{30\pi} \approx -0.074, \quad \delta = -\frac{1}{570\pi} \approx -0.00056. \quad (11.57)$$

With $p_1^2 = k^2$ and $p_2^2 = 0$, they are given by

$$\gamma \approx -0.018, \quad \delta \approx -0.0014. \quad (11.58)$$

As in the case of the gluon propagator, the sign of the derivative definition agrees with the bi-local one but they differ strongly in their magnitude. In the present work, we use (11.58). The contribution to λ_3 is always evaluated at vanishing momentum. We obtain

$$\text{Flow}_{\Lambda,a}^{(3h)}(p^2 = 0) = g^{\frac{3}{2}} Z_h^{\frac{3}{2}} (N_c^2 - 1) \frac{3 - \eta_a}{60\pi}. \quad (11.59)$$

11.4.4. Mixed graviton-gluon coupling

So far, we have only considered pure gluon and pure graviton correlation functions in the coupled Yang-Mills–gravity system. Indeed, the results that will be presented in section 11.5 are based on precisely these correlation functions, and other couplings are identified according to (11.26). In section 11.6, we will then discuss the stability of the results under extensions of the truncation. In particular, we will have a look at the inclusion of a flow equation for the graviton–two-gluon coupling g_a .

The flow equation for g_a is derived analogously to the g_3 coupling from three-graviton vertex: we build the projection operator from the classical tensor structure $S^{(haa)}$ with a transverse traceless graviton and two transverse gluons. This projection operator is contracted with both sides of the flow equation for this specific vertex. The equation is further evaluated at the momentum symmetric point [29]. The resulting p^2 part gives the flow equation for g_a . We obtain an analytic flow equation for g_a by a p^2 derivative at $p^2 = 0$. The resulting flow equation is given in App. G.11.9.

For the computations in section 11.6, we use the preferred method of finite differences. In particular, we choose the evaluation points $p^2 = k^2$ and $p^2 = 0$. With this method, we do not obtain analytic flows but we take more non-trivial momentum dependences into account [29, 62]. The computation is simplified by the fact that the present flow is actually vanishing at $p^2 = 0$. Consequently, the finite difference equals to an evaluation at $p^2 = k^2$, and the momentum derivative gives the same result as a $1/p^2$ division.

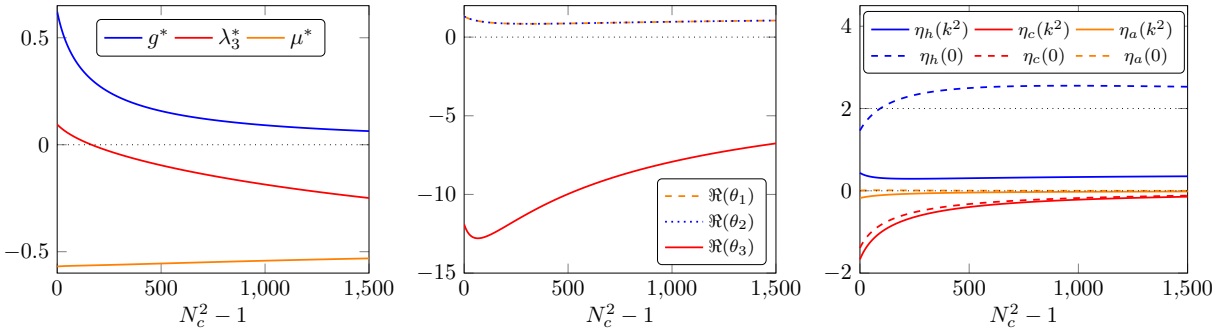


Figure 11.10.: Properties of the UV fixed point as a function of $N_c^2 - 1$ in the uniform approximation with one Newton's coupling. Displayed are the fixed point values (left panel), the critical exponents (central panel), and the anomalous dimensions (right panel).

11.4.5. Momentum locality

We close this section with a remark on the momentum locality introduced in [29] as a necessary condition for well-defined RG flows. It was shown to be related to diffeomorphism invariance of the theory. It entails that flows should not change the leading order of the large momentum behaviour of correlation functions.

The asymptotics of the diagrams for the graviton two-point function, ordered as displayed in Figure 11.7, are

$$\begin{aligned} \text{Diag}_1^{(2h)}(p^2 \rightarrow \infty) &= -g \frac{8 - \eta_a}{12\pi}, \\ \text{Diag}_2^{(2h)}(p^2 \rightarrow \infty) &= g \frac{8 - \eta_a}{12\pi}, \end{aligned} \quad (11.60)$$

while the asymptotics for the graviton three-point function, again ordered as displayed in Figure 11.8, are

$$\begin{aligned} \text{Diag}_1^{(3h)}(p^2 \rightarrow \infty) &= -g^{3/2} \frac{8 - \eta_a}{19\pi}, \\ \text{Diag}_2^{(3h)}(p^2 \rightarrow \infty) &= g^{3/2} \frac{4(8 - \eta_a)}{19\pi}, \\ \text{Diag}_3^{(3h)}(p^2 \rightarrow \infty) &= -g^{3/2} \frac{3(8 - \eta_a)}{19\pi}. \end{aligned} \quad (11.61)$$

Consequently we again have a highly non-trivial cancellation between different diagrams, which leads to the property of momentum locality. In summary, we assert

$$\lim_{p^2/k^2 \rightarrow \infty} \frac{\partial_t \Gamma^{(2h,3h)}(p^2)}{\Gamma^{(2h,3h)}(p^2)} = 0, \quad (11.62)$$

at the symmetric point in the transverse traceless mode. Hence, the full flows of the graviton two- and three-point functions including Yang-Mills corrections are momentum local.

11.5. Asymptotic safety of Yang-Mills–gravity

In this section, we provide a full analysis of the ultraviolet fixed point of the coupled Yang-Mills–gravity system. It is characterised by the non-trivial fixed point of Newton's coupling g , the coupling of the momentum-independent part of the graviton three-point function λ_3 , and the graviton mass parameter μ while the minimal gauge coupling vanishes, $\alpha_s = 0$.

11.5.1. Finite N_c

The fully coupled fixed point shows some remarkable features. The fixed point values are displayed in the left panel of [Figure 11.10](#). The fixed point value of the graviton mass parameter remains almost a constant as a function of N_c . The Newton's coupling is approaching zero, while λ_3^* becomes slowly smaller and crosses zero at $N_c^2 \approx 166$. This behaviour can be understood from the equations: the leading contribution from Yang-Mills to $\partial_\mu\mu$ cancels out, and only a term proportional to η_a remains, see [\(11.52\)](#). The latter is small at the fixed point, and hence, the effect on $\partial_\mu\mu$ is strongly suppressed. The fall off of g^* and λ_3^* is explained by the respective contribution in the flow equations, see [\(11.58\)](#) and [\(11.59\)](#).

The critical exponents of the fixed point, which are given by minus the eigenvalues of the stability matrix, are displayed in the central panel of [Figure 11.10](#). They remain stable over the whole investigated range. Two critical exponents form a complex conjugated pair. The real part of this pair is positive and thus corresponds to two UV attractive directions. The third critical exponent is real and negative and corresponds to a UV repulsive direction. The eigenvector belonging to the latter exponent points approximately in the direction of λ_3 , which is in accordance with pure gravity results [\[29\]](#).

In the right panel of [Figure 11.10](#), we show the anomalous dimensions at the fixed point, evaluated at $p^2 = 0$ and $p^2 = k^2$. The ghost and gluon anomalous dimensions tend towards zero for increasing N_c . Most importantly, $\eta_a(k^2)$ is always negative, which is a necessary condition for asymptotic freedom in the Yang-Mills sector. The graviton anomalous dimension does not tend towards zero. At $p^2 = k^2$, it is getting smaller with an increasing N_c despite the positive gluon contribution [\(11.55\)](#). The reason is that the anomalous dimension is also proportional to g^* , which is decreasing, and this effect dominates over the gluon contribution. At $p^2 = 0$, on the other hand, the gluon contribution is also positive but larger in value, see [\(11.54\)](#), and consequently, dominates over the decrease in g^* . $\eta_h(0)$ is increasing, crosses the value 2 and starts to decrease again for large N_c . As mentioned in [\(G.58\)](#), $\eta < 2$ is a bound on regulators that are proportional to the respective wave function renormalisation. In our case, $\eta_h(0)$ exceeds the value 2 just slightly and remains far from the strict bound, which is $\eta_h < 4$, see [\[60\]](#) for details.

The fixed point values of the background couplings are displayed in [Figure 11.11](#). The equations for the pure gravity part are identical to the ones in [\[62\]](#) and the gluon part is identical to the one in [\[217\]](#). In this setting, the background couplings behave very similar to the dynamical ones. The background Newton's coupling goes to zero with $1/N_c^2$ while the background cosmological constant goes to a constant for large N_c . Interestingly, the background coupling approach their asymptotic behaviour faster than the dynamical ones.

11.5.2. Large N_c scaling

In the limit $N_c \rightarrow \infty$, the couplings approach the fixed point values

$$\begin{aligned} g^* &\rightarrow \frac{89}{N_c^2} + \frac{8.0 \cdot 10^4}{N_c^4}, & \mu^* &\rightarrow -0.45 - \frac{3.3 \cdot 10^2}{N_c^2}, \\ \lambda_3^* &\rightarrow -0.71 + \frac{2.4 \cdot 10^3}{N_c^2}. \end{aligned} \tag{11.63}$$

As expected, the 't Hooft coupling $g^* N_c^2$ is going to a constant in the large N_c limit. This behaviour is also displayed in [Figure 11.12](#) for finite N_c . Remarkably, μ^* and λ_3^* remain finite. In the λ_3 equation, this originates from a balancing of the gluon contribution with the canonical term. In the μ equation, on the other hand, all contributions go to zero in leading order and the fixed point value of μ follows from the

second order contributions. The asymptotic anomalous dimensions follow as

$$\begin{aligned}\eta_h(0) &\rightarrow 2 + \frac{2.7 \cdot 10^3}{N_c^2}, & \eta_h(k^2) &\rightarrow 0.36 + \frac{2.9 \cdot 10^2}{N_c^2}, \\ \eta_c(0) &\rightarrow -\frac{1.3 \cdot 10^2}{N_c^2}, & \eta_c(k^2) &\rightarrow -\frac{1.5 \cdot 10^2}{N_c^2}, \\ \eta_a(0) &\rightarrow -\frac{8.7}{N_c^2}, & \eta_a(k^2) &\rightarrow -\frac{22}{N_c^2},\end{aligned}\tag{11.64}$$

which satisfy the bounds $\eta_i \leq 2$ necessary for the consistency of the regulators that are proportional to Z_h, Z_c, Z_a . Note that only the graviton anomalous dimension is non-vanishing in this limit. Importantly, the gluon anomalous dimension approaches zero from the negative direction, which means that it supports asymptotic freedom in the Yang-Mills sector. The asymptotic value $\eta_h(0) = 2$ follows directly from the demand that all contributions in the μ equation have to go to zero in leading order, as discussed in the last paragraph. The critical exponents are given by

$$\begin{aligned}\theta_{1,2} &\rightarrow 1.2 \pm 2.1i + \frac{(1.1 \mp 5.6i) \cdot 10^3}{N_c^2}, \\ \theta_3 &\rightarrow -2.3 - \frac{14 \cdot 10^3}{N_c^2}.\end{aligned}\tag{11.65}$$

The fixed point has two attractive and one repulsive direction for all colours. Remarkably, the values of the critical exponents remain of order one. The background couplings approach the values

$$\bar{g}^* \rightarrow \frac{9.4}{N_c^2} - \frac{1.3 \cdot 10^2}{N_c^4}, \quad \bar{\lambda}^* \rightarrow 0.38 - \frac{1.4}{N_c^2}.\tag{11.66}$$

Again, the background 't Hooft coupling $\bar{g}^* N_c^2$ remains finite in the large N_c limit, which is also displayed in [Figure 11.12](#).

In summary, we have found a stable UV fixed point with two attractive directions. The fixed point values, the critical exponents and the anomalous dimensions are of order one. In [Figure 11.10](#) we display this behaviour up to $N_c^2 = 1500$, and in this section, we have augmented this with a solution for $N_c \rightarrow \infty$. Consequently, we conclude that the system is asymptotically safe in the gravity sector and asymptotically free in the Yang-Mills sector for all N_c .

11.5.3. Decoupling of gravity-induced gluon self-interactions

It has been advocated in [\[213\]](#) that interacting matter-gravity systems necessarily contain self-interacting matter fixed points. This has been investigated in scalar, fermionic and Yukawa systems in, e.g., [\[61, 214, 215\]](#).

Recently, also a Yang-Mills–gravity system with an Abelian $U(1)$ gauge group has been investigated [\[204\]](#). It was found that the coupling of the fourth power of the field strength, F^4 , takes a finite fixed point value, while the minimal coupling that enters the covariant derivative can be asymptotically free. As already mentioned before in [section 11.3](#), the same happens in Yang-Mills–gravity systems. In particular, we are led to

$$w_2^* (\text{tr} F_{\mu\nu}^2)^2 + v_4^* \text{tr} F_{\mu\nu}^4,\tag{11.67}$$

with $w_2^* \neq 0$ and $v_4^* \neq 0$ without non-trivial cancellations. A quantitative computations of these fixed point couplings is deferred to future work. Here, we simply discuss their qualitative behaviour: even if

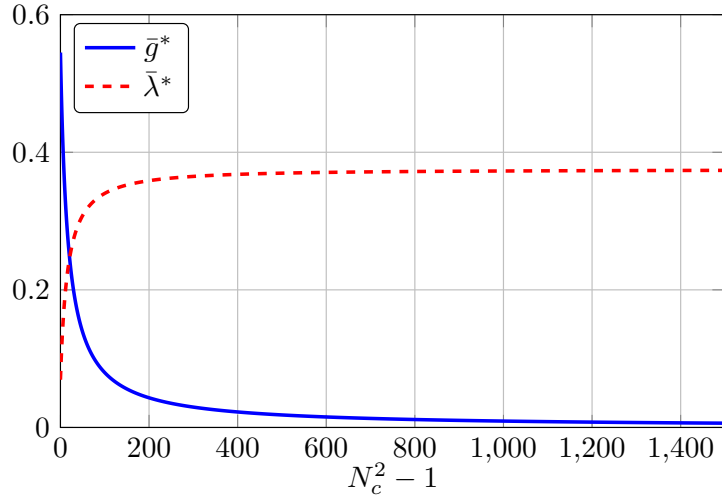


Figure 11.11.: Displayed are the background couplings \bar{g}^* and $\bar{\lambda}^*$ as a function of $N_c^2 - 1$ evaluated at the UV fixed point displayed in [Figure 11.10](#). The coupling \bar{g}^* is going to zero with $\frac{1}{N_c^2}$ and $\bar{\lambda}^*$ goes to the constant 0.38, see [\(11.65\)](#).

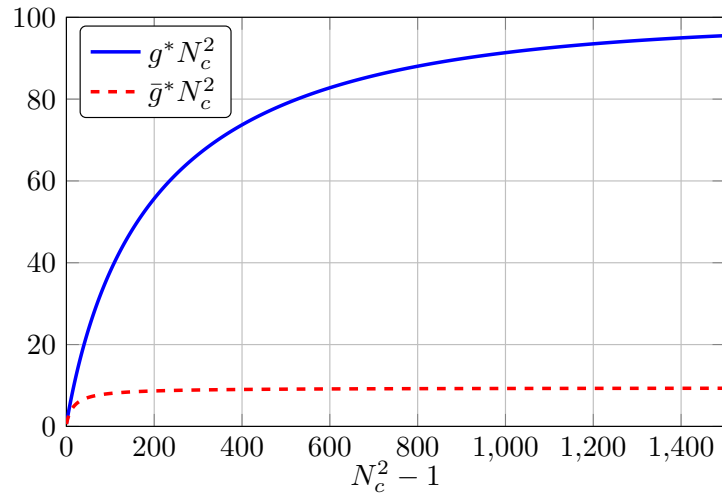


Figure 11.12.: Displayed are the fixed point 't Hooft couplings $g^* N_c^2$ and $\bar{g}^* N_c^2$ as a function of $N_c^2 - 1$. The couplings approach the asymptotic values $g^* N_c^2 \rightarrow 89$ and $\bar{g}^* N_c^2 \rightarrow 9.4$, see [\(11.63\)](#) and [\(11.65\)](#).

not present in the theory, the couplings w_2 and v_4 are generated by diagrams with the exchange of two gravitons, see [Figure 11.13](#). In leading order, these diagrams are proportional to

$$\frac{g^2}{(1+\mu)^3} \propto \frac{1}{N_c^4} \rightarrow 0, \quad (11.68)$$

and vanish in the large N_c scaling of [\(11.63\)](#). It is simple to show that the further diagrams in the fixed point equations of w_2, v_2 proportional to w_2, v_2 decay even faster when using [\(11.68\)](#) for the diagrams. Finally, we get additional gluon tadpole contributions proportional to ω_2^*, v_4^* for the running of the Yang-Mills beta function. In leading order these contributions are proportional to N_c^2 due to a closed gluon loop. Together with the fixed point scaling of ω_2^*, v_4^* in [\(11.68\)](#) this leads to a $1/N_c^2$ decay of these contributions. They have the same large N_c scaling as the pure gravity contributions but also share the

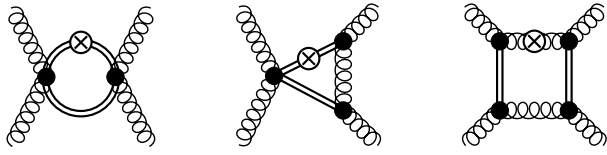


Figure 11.13.: Diagrammatic depiction of the graviton induced higher-order gluon interactions. Wiggly and double lines represent gluon and graviton propagators, respectively.

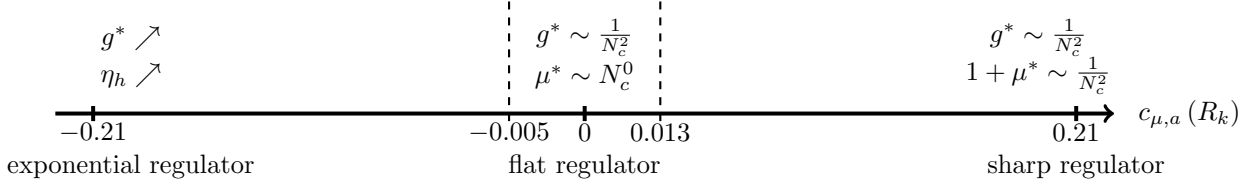


Figure 11.14.: Schematic picture of the dynamical scale readjustment mechanisms as a function of the coefficient $c_{\mu,a}(R_k)$.

same negative sign supporting asymptotic freedom, see [204] for a study in $U(1)$ theories.

We close this chapter with a qualitative discussion of the stability for the interacting fixed point: as ω_2, v_2 do not couple into the pure gravity subsystem, the stability matrix is skew symmetric, and the eigenvalues are computed in the respective sub-systems. Both, the gravity as well as the ω_2, v_4 sub-systems are stable in the limit $g \rightarrow 0$.

This concludes our analysis of the large N_c behaviour of quantum gravity with the flat regulator and the identification (11.26). As expected, Newton's coupling g shows the $1/N_c^2$ behaviour discussed in section G.10.

11.6. UV dominance of gravity

11.6.1. Dynamical scale fixing

In section 11.5, we used the identifications of all Newton's couplings (11.26). In the present chapter, we discuss the general case without this identification. We provide a comprehensive summary of results and the underlying structure, more details can be found in App. G.11.8. While we have argued in section G.10 that the present Yang-Mills–gravity system, as well as all free-matter–gravity systems are asymptotically safe, the interesting question is how and if at all in the present approximation this is dynamically observed.

Within the iterative procedure in section G.10, we arrived at a fixed point action that is identical to that of the pure gravity sector with fixed point values for g_n^* , λ_n^* , and μ^* . We also have $g_a = g_3$ due to the expansion of the metric $g_{\mu\nu} = \bar{g}_{\mu\nu} + \sqrt{g_3} k^2 h_{\mu\nu}$ with $k = k_h$. Note also that in such a two-scale setting with k_h and k_a , the latter rather is to be identified with k_a^{UV} and not with k_a^{IR} . As the effect of the latter has been absorbed in a renormalisation of Newton's coupling prior to the integrating out of graviton fluctuations (or rather their suppression with $k_h \rightarrow \infty$), this sets the graviton cutoff scale $k_h = k$ as the largest scale in the system. This leads to (G.59) that effectively induces

$$k^2 \simeq N_c^2 k_a^2, \quad (11.69)$$

in the large N_c limit. Note that with a rescaling of our unique cutoff scale in section 11.5 with N_c^2 we already arrive at the N_c -independent fixed-point values (11.63). The large values come from dropping the N_c -independent prefactor in the ratio G/G_{eff} . The latter fact signals the unphysical nature of fixed

point values, which within this two-scale setting also extends to the product $g^* \lambda^*$, typically used in the literature as a potentially rescaling-invariant observable.

Despite (G.59) being a natural relative scale setting, without any approximation the full system of flow equations with $k_h = k_a$ should adjust itself dynamically to this situation with $g_a^* \sim g_c^* \sim g^*$ and with $g^* \propto 1/N_c^2$ in the large N_c limit. In the present approximation this can happen via two mechanisms that both elevate the graviton fluctuations to the same N_c strength as the gluon fluctuations: the graviton propagator acquires a N_c scaling

$$k^2 G_h(p^2 = 0) = \frac{1}{Z_h} \frac{1}{1 + \mu} \propto N_c^2, \quad (11.70)$$

after an appropriate rescaling of the couplings, for more details see App. G.11.8. We proceed by discussing the two dynamical options that the system has to generate the N_c scaling in (11.70):

- (1) Evidently, (11.70) can be achieved via

$$\mu^* \propto -1 + c_+/N_c^2, \quad (11.71)$$

with a positive constant c_+ . Note that (11.71) is not present in the fixed point results in section 11.5. Accordingly, adding the fixed-point equation for g_a has to trigger this running. Below we shall investigate this possibility in more detail.

- (2) The N_c scaling can also be stored in $1/Z_h$. As we have chosen regulators that are proportional to Z_h , this leads to an effective elimination of Z_h from the system; its only remnant is the anomalous dimension η_h in the cutoff derivative. Since $1/Z_h \propto (k^2)^{\eta_h/2-1}$, the anomalous dimension η_h has to grow large and positive in order to effectively describe the N_c scaling in (11.70),

$$\eta_h \rightarrow \infty. \quad (11.72)$$

In the present setting with $R_{h,k} \propto Z_h$, this option cannot be investigated as (11.72) violates the bound

$$R_{h,k} \propto Z_h \quad \Rightarrow \quad \eta_h < 2, \quad (11.73)$$

for the regulator. For $\eta_h > 2$, the regulators of type (11.73) cannot be shown to suppress UV degrees of freedom anymore in the limit $k \rightarrow \infty$ as $\lim_{k \rightarrow \infty} R_k(p^2) \rightarrow 0$ for $\eta_h > 2$. This bound was introduced and discussed in [60] within the scalar-gravity system, where η_h grows beyond this bound for the number of scalars N_s getting large. It was stated there that the stability of the scalar-gravity system could not be investigated conclusively since the regulator cannot be trusted anymore. In the light of the present results and discussion, we know that the free-matter system is asymptotically safe. Then, the growing η_h signals that the system wants to accommodate (11.70) with a growing $1/Z_h$.

We emphasise that the physics of both options, (1) and (2), is captured by (11.70) and is identical. Which part of the scaling of the propagator is captured by μ and which one by Z_h is determined by the projection procedure. Note that the latter is also approximation dependent.

In summary the coupled Yang-Mills–gravity system approaches the large N_c limit via (11.70). Whether or not this is seen in the current approximation with the cutoff choice (11.73) is a technical issue. If the approximation admits option (1) then the fixed point can be approached, if (2) or a mixture of (1) and (2) is taken then the fixed point cannot be seen due to the regulator bound in our setup. We emphasise again that this does not entail the non-existence of the fixed point, which is guaranteed by the analysis of section G.10. The analysis here evaluates the capability of the approximation to capture this fixed point.

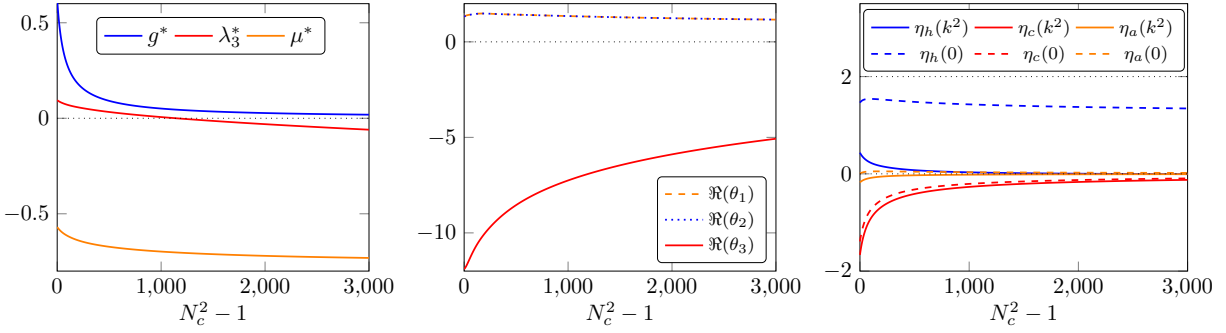


Figure 11.15.: Properties of the UV fixed point as a function of $N_c^2 - 1$ in the uniform approximation with one Newton's coupling and with $c_{\mu,a} = \frac{1}{24\pi} \approx 0.0133$. Displayed are the fixed point values (left panel), the critical exponents (central panel), and the anomalous dimensions (right panel).

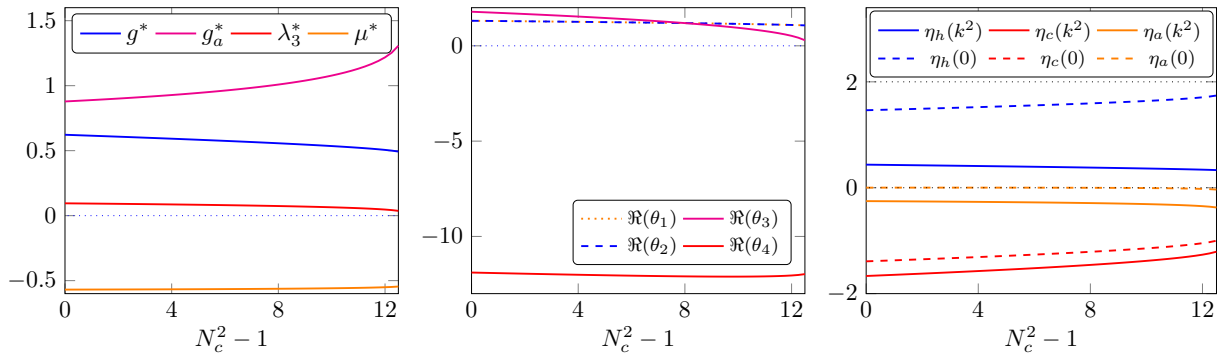


Figure 11.16.: Properties of the UV fixed point as a function of $N_c^2 - 1$ in the approximation with two Newton's couplings and with the flat regulator, $c_{\mu,a} = 0$. Displayed are the fixed point values (left panel), the critical exponents (central panel), and the anomalous dimensions (right panel).

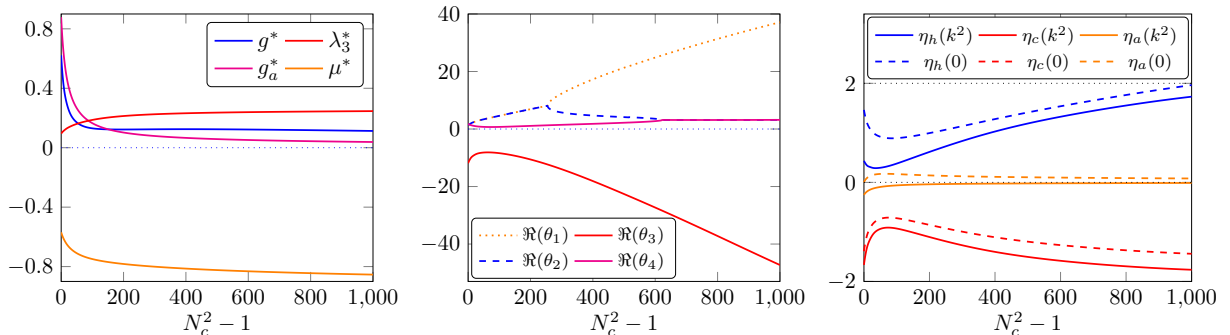


Figure 11.17.: Properties of the UV fixed point as a function of $N_c^2 - 1$ in the approximation with two Newton's couplings and with $c_{\mu,a} = \frac{1}{4\pi} \approx 0.08$. Displayed are the fixed point values (left panel), the critical exponents (central panel), and the anomalous dimensions (right panel).

The understanding of this structure and guaranteeing this capability of the approximation is of chief importance when evaluating the stability of more complex matter-gravity systems with genuine matter self-interaction: no conclusion concerning the stability of these systems can be drawn if the capability problem for the free-matter–gravity systems is not resolved. Moreover, even if the fixed points exist, their physics may be qualitatively biased by this problem.

11.6.2. Results in the extended approximation

In the following analysis, we concentrate on the g_a fixed point equation and keep $g_c = g$. Before we extend the approximation to this case, let us reevaluate the results with $g_a = g$ in the light of the last subsection 11.6.1. There it has been deduced that a consistent N_c scaling requires $g^* \propto 1/N_c^2$ and either (11.71) or (11.72), or both. Figure 11.10 shows the consistent large N_c scaling for Newton's coupling but neither (11.71) nor (11.72). This comes as a surprise as the system is asymptotically safe and the large N_c limit in the approximation $g = g_a$ is seemingly stable. To investigate this stability, we examine the regulator dependence of the coefficients of the flow equations. To that end, we notice that the coefficients in the μ equation (and the g_3, g_a equations) are of crucial importance for the stability of the system. The coefficient $c_{\mu,a} = -1/(60\pi)\eta_a$ of the Yang-Mills contribution to the graviton mass parameter is proportional to the gluon anomalous dimension η_a : the leading coefficient vanishes, see G.87 and (G.93). Indeed, choosing other regulators, the leading order term is non-vanishing with

$$-0.2 \lesssim c_{\mu,a}(R_k) \lesssim 0.2, \quad (11.74)$$

see App. G.11.2. Typically, it supersedes the η_a -dependent term, and the flat regulator appears to be a very special choice. If $c_{\mu,a} \gtrsim 0.013$, we indeed find a solution, which is consistent with (11.71), see Figure 11.15 for $c_{\mu,a} = \frac{1}{24\pi} \approx 0.0133$. In turn, for $c_{\mu,a} \lesssim -0.005$, we find solutions with growing η_h , hence in the class (11.72). Accordingly, this solution is not trustworthy with η_h beyond the bound (11.73). Its failure simply is one of the approximation (within this choice of regulator) rather than that of asymptotic safety.

In summary this leads us to a classification of the regulators according to the large N_c limit: they either induce the dynamical readjustment of the scales via (11.71) or via (11.72) or they fall in between such as the flat cutoff. Within the current approximation it is required that the readjustment happens via (11.71). Now we are in the position to discuss the general case with $g_a \neq g$. An optimal scenario would be that the inclusion of the g_a equation already stabilises the system such that it enforces the dynamical readjustment via (11.71) for all regulators proportional to Z_h . However, as we shall see, the general scheme from the uniform approximation persists with this upgrade of the approximation.

No apparent N_c scaling for μ and η_h

In the uniform approximation with one Newton's coupling (11.26), this scenario was taken with regulators with $-0.005 \lesssim c_{\mu,a} \lesssim 0.013$. A typical regulator in this class is the flat regulator used in the present work. This scenario does not enhance the graviton propagator and hence, does not fulfil (11.70). The stability of the results in the large N_c limit in the uniform approximation must thus rather be considered a mere coincidence. Indeed in the extended truncation with $g \neq g_a$, the enhancement of the graviton propagator is not triggered by the included g_a equation, and consequently, the flat regulator does not have a stable large N_c limit anymore. The fixed point values, critical exponents, and the anomalous dimensions in this approximation are shown in Figure 11.16. The fixed point values show a marginal N_c dependence up to the point where the fixed point vanishes into the complex plane at $N_c^2 \approx 13.5$, which is signalled by one of the critical exponents going towards zero. The vanishing critical exponent can be associated with g_a . Typically, this is interpreted as a sign for the failure of asymptotic safety. Here it is evident that the truncation cannot accommodate the dynamical readjustment of the scales that takes place in the full system. This could also signal an over-complete system: g and g_a are related by diffeomorphism invariance. In any case, the failure of the approximation can either lead to the divergence of the couplings [related to (11.72)], or in complex parts of the fixed point values. For the flat regulator, the latter scenario is taken.

Scenario with $1 + \mu \propto 1/N_c^2$

This scenario requires regulators with $c_+ < c_{\mu,a} < c_{\max}$. A typical regulator in this class is the sharp regulator, see (G.62) and Figure 11.14. Here, we do not present a full analysis of this case but only

change the coefficient $c_{\mu,a}$ accordingly. This is justified in terms of linear small perturbations of the system: $c_{\mu,a}$ is the only leading order coefficient in the system that exhibits a qualitative change when changing the regulator away from the flat regulator. Note however, that this change ceases to be small for large N_c as $c_{\mu,a}$ is multiplied by N_c^2 . If accompanied by a respective change of the relative cutoff scales k_h/k_a , this factor could be compensated. Then, however, we are directly in the stable regulator choice with (G.59). Here, we are more interested in the dynamical stabilisation and we refrain from the rescaling. The system exhibits the $1/N_c^2$ scaling in the Newton's couplings, g^* and g_a^* , as well as the mass parameter μ^* , see Figure 11.17 for $c_{\mu,a} \approx 0.08$. However, with this choice, the critical exponents of the fixed point become rather large. We determined the constant $c_+ \approx 0.07$.

Scenario with η_h growing large

This scenario requires regulators with $-c_{\min} < c_{\mu,a} < -c_-$. A typical regulator in this class is the exponential regulator, see (G.61) and Figure 11.14. For this class of regulators, both couplings grow large, and we have the scenario with (11.72) bound to fail to provide fixed point solutions beyond a maximal N_c due to the failure of the approximation scheme.

11.6.3. Resumé: Signatures of asymptotic safety of Yang-Mills–gravity systems

In summary, with the choice of the regulator, we can dial the different scenarios that all entail the same physics: the dynamical readjustment of the respective scales in the gauge and gravity subsystems and the asymptotic safety of the combined system. The two different scenarios are described in section 11.6.2 and section 11.6.2. Both scenarios entail the same physics mechanism: the enhancement of the graviton propagator, see (11.70). This triggers the dominance of gravity in the ultraviolet, which is clearly visible in the consecutive integrating out of degrees of freedom discussed in section G.10. The crucial property for the validity of this structure is the asymptotic freedom of the Yang-Mills system, and hence, the existence of the gauge system in a given background. This property is trivially present in systems with free matter coupled to gravity, and hence the present analysis extends to these cases.

This leaves us with the question of how to reevaluate the existing results on matter-gravity system in the light of the present findings. We first notice that the helpful peculiarity of the Yang-Mills–gravity system that allowed us to easily access all the different scenarios, is the possibility to choose the sign of $c_{\mu,a}$ with the choice of the regulator. Clearly, the gauge contribution to the running of the graviton mass parameter plays a pivotal rôle for how the enhancement of the graviton propagator in (11.70) is technically achieved. In the other matter-gravity system this parameter has a definite sign, which is why one sees a specific scenario for typical regulators. Collecting all the results and restricting ourselves to truncations that resolve the difference between fluctuation and background fields, [60], we find the following:

- (1) Fermion-gravity systems: they fall into the class section 11.6.2, and the asymptotic safety of the system can be accessed in the approximation. The required large flavour N_f pattern with (11.71) is visible in the results.
- (2) Scalar-gravity systems: they fall into the class section 11.6.2, and for large enough number of scalars N_s , the fixed point seemingly disappears due to the fixed point coupling g^* and anomalous dimension η_h growing too large.
- (3) Vector-gravity/Yang-Mills–gravity systems: this system has been discussed here, and it falls into all classes, section 11.6.2, section 11.6.2 and section 11.6.2. This also includes the $U(1)$ system.
- (4) Self-interacting gauge-matter–gravity systems: these systems only fall into the pattern described in section 11.6.2, section 11.6.2, and section 11.6.2 if the gauge-matter system is itself ultraviolet

stable. For example, one flavour QED exhibits a UV-Landau pole and is stabilised by gravity, which makes the combined system asymptotically safe, for a comprehensive analysis see [204, 218]. Adding more flavours potentially destabilises the system; however, such an analysis has to avoid the interpretation of the seeming failure of asymptotic safety described here. One possibility to take this into account is the scale adjustment (G.59). This discussion also carries over to general gauge-matter-gravity systems including the Standard Model and its extensions.

In summary, this explains the results obtained in gravitationally interacting gauge-matter-gravity systems, which are the basis of general gauge-matter-gravity system. While it suggests the use of relative cutoff scales such as (G.59), it still leaves us with the task of devising approximations that are capable of capturing the dynamical readjustment of scales that happens in gravitationally interacting gauge-matter-gravity systems. In particular, the marginal operator $R^2 \ln(1 + R/k_a^{\text{IR}^2})$, cf. (G.56), has to be included as discussed in subsection G.10.2.

Besides this task, the present analysis also requires a careful reanalysis of phenomenological bounds on ultraviolet fixed point couplings. It is well-known that the values of the latter are subject to rescalings and only dimensionless products of couplings such as $g^* \lambda^*$ possibly have a direct physical interpretation. We have argued here that the dynamically adjusted or explicitly adjusted relative cutoff scales ask for a reassessment also of these dimensionless products.

11.7. Effective universality

In the absence of a cosmological constant, General Relativity with matter is parameterized by one single coupling, the Newton coupling G_N . It governs both, the gravitational self-interaction as well as the gravity-matter interactions. In the presence of quantum fluctuations the single classical Newton coupling is promoted to potentially different running couplings, related to the interaction vertices of gravitons with each other, with their Faddeev-Popov ghosts and with matter. The scale-dependence of these avatars of the Newton coupling is encoded in their β -functions. This structure is familiar from gauge theories such as QED or QCD. For marginal, i.e., dimensionless couplings the corresponding avatars exhibit two-loop universality due to gauge symmetry. Hence in the perturbative regime all vertices can be described by a single gauge coupling. The Newton coupling is not marginal. Therefore universality of the distinct β -functions is not automatic. Nevertheless, the underlying symmetry manifests itself in relations between the various Newton couplings, the Slavnov-Taylor identities (STIs). These can lead to significant differences between the various avatars in a non-perturbative regime of the theory. An example is given by Landau gauge Yang-Mills theory in the infrared. There the three-gluon coupling even becomes negative while the other couplings remain positive, see e.g. [54, 219, 220, 221, 222].

It is a key result of this work that the β -functions of the different avatars of the Newton coupling agree semi-quantitatively in the asymptotically safe UV regime in gravity-matter systems. This result is summarized in Figure 11.18, showing that a region of effective universality exists in the space of couplings. The location of the fixed point falls into this region. We interpret the non-trivial emergence of effective universality as a manifestation of the near-perturbative nature of asymptotically safe gravity. This supports a rather appealing scenario: the residual interactions in the UV are just strong enough to induce asymptotic safety, while allowing for near-canonical scaling of higher-order operators. The near-canonical scaling is indeed observed, see e.g. [192, 223] as is the existence of the fixed point in perturbative studies [224]. Additionally, the asymptotically safe Standard Model [225, 202, 226, 205, 227, 228] favors a perturbative nature of the fixed point.

We start from the gauge-fixed Einstein-Hilbert action with minimally coupled scalars and fermions as

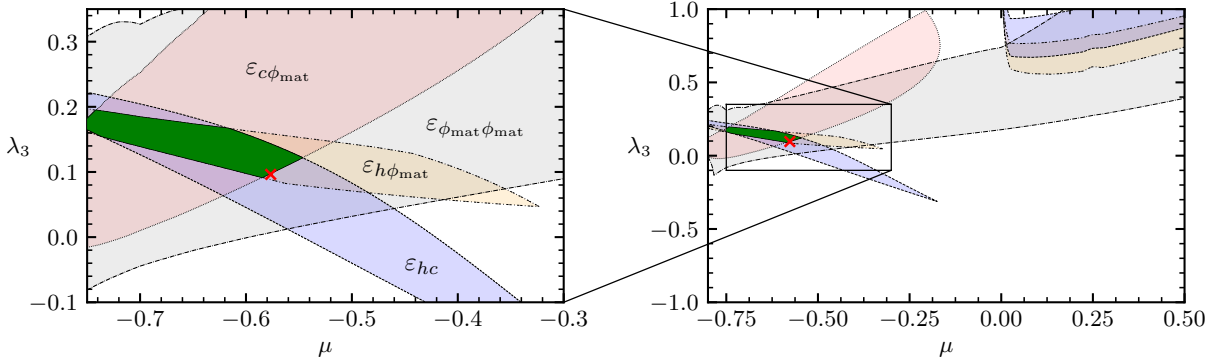


Figure 11.18.: Regions in the μ - λ_3 -plane at $G = 0.58$ where different sectors of the gravity-matter system are effectively universal ($\phi_{\text{mat}} = (\varphi, \psi, A)$). Green region: effective universality in all avatars of the Newton coupling. Red cross: UV fixed point.

well as gauge-fixed gauge theory with N_v gauge fields. The classical Euclidean action reads

$$\begin{aligned} S = & \frac{1}{16\pi G_N} \int d^4x \sqrt{g} (2\Lambda - R) + S_{\text{gf+gh,gravity}} \\ & + \frac{1}{2} \sum_{i=1}^{N_s} \int d^4x \sqrt{g} g^{\mu\nu} \partial_\mu \varphi^i \partial_\nu \varphi^i + \sum_{j=1}^{N_f} \int d^4x \sqrt{g} \bar{\psi}^j \nabla \psi^j \\ & + \frac{1}{2} \int d^4x \sqrt{g} g^{\mu\nu} g^{\rho\sigma} \text{tr} F_{\mu\rho} F_{\nu\sigma} + S_{\text{gf+gh,gauge}}, \end{aligned} \quad (11.75)$$

where $F_{\mu\nu}$ is the field-strength tensor of the gauge field A_μ . The gravity gauge fixing is of the linear de-Donder type in the Landau gauge limit. We also use the Landau gauge in the Yang-Mills sector. For the covariant Dirac operator ∇ we use the spin-base invariant formulation [198, 199, 200]. Under the impact of quantum gravity, Abelian and non-Abelian gauge theories can approach a free fixed point [201, 202, 203, 204, 205, 160], such that the corresponding gauge couplings vanish, and the non-Abelian ghost sector decouples. Hence for our computation only the total number of gauge fields, N_v , is relevant. We focus on $N_s = N_v = 2N_f = 1$.

Expanding the metric about a flat background

$$g_{\mu\nu} = \delta_{\mu\nu} + \sqrt{G_N} h_{\mu\nu}, \quad (11.76)$$

schematically leads to interactions of the form

$$\begin{aligned} \Gamma \sim & \int d^4x (\sqrt{G_{N,h}} h(\partial h)(\partial h) + \sqrt{G_{N,c}} h(\partial \bar{c})(\partial c) \\ & + \sqrt{G_{N,\varphi}} h(\partial \varphi)(\partial \varphi) + \sqrt{G_{N,\psi}} h \bar{\psi} \gamma \partial \psi \\ & + \sqrt{G_{N,A}} h(\partial A)(\partial A)) + \dots, \end{aligned} \quad (11.77)$$

where we replaced G_N by avatars of the Newton coupling $G_{N,i}$ corresponding to the interactions, $i \in \{h, c, \varphi, \psi, A\}$. In addition to the Newton couplings, the expansion of the cosmological constant term results in a two-graviton coupling μ and a three-graviton coupling λ_3 [59, 29].

11.7.1. Beta functions

We compute the β -functions with the functional renormalization group (FRG), for general reviews see [229, 9, 230, 231, 10, 232]. For gravity it was pioneered in the seminal paper of [165], for reviews see

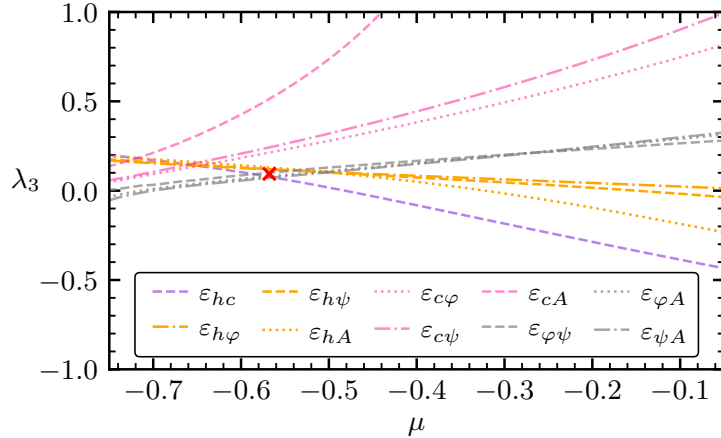


Figure 11.19.: Lines with $\varepsilon_{ij} = 0$ in the μ - λ_3 -plane at $G = G_h^*$. The red star marks the UV fixed point, see (11.82).

[233, 234, 235, 236, 237, 238]. Here we follow the setup in [58, 59, 29, 60, 239, 240, 160, 64, 241]. The involved algebra is handled using the symbolic manipulation system FORM [193, 194] and the FormTracer [197] as well as the Mathematica package xAct [242, ?, ?, ?]. We provide a Mathematica notebook containing the final β -functions in numerical form [?].

We work with dimensionless running couplings, e.g., $G_i = G_{N,i} k^2$ for all avatars of the Newton coupling. It is already instructive to examine a simplified form of the β -functions for the different avatars of the Newton coupling,

$$\beta_{G_i} = 2G - a_i G^2 + O(G^3), \quad (11.78)$$

where all avatars of the Newton coupling are identified, $G_i = G$. The coefficients a_i of the quadratic terms read

$$(a_h, a_c, a_\varphi, a_\psi, a_A) = (3.7, 3.8, 2.9, 2.9, 2.6), \quad (11.79)$$

when evaluated at $\mu = -0.58$ and $\lambda_3 = 0.096$. These are precisely the fixed-point values that we will present later, see (11.82). Already in the present simple approximation, the coefficients differ by no more than 32%. For quantitative studies, we use a measure for the relative deviation of the β -functions introduced in [64],

$$\varepsilon_{ij}(G, \mu, \lambda_3) = \left| \frac{\Delta\beta_{G_i} - \Delta\beta_{G_j}}{\Delta\beta_{G_i} + \Delta\beta_{G_j}} \right|_{G_i=G_j=G}, \quad (11.80)$$

where $i, j \in \{h, c, \varphi, \psi, A\}$. $\Delta\beta_{G_i}$ is the anomalous part of the β -function β_{G_i} obtained by subtracting the canonical running,

$$\Delta\beta_{G_i} = \beta_{G_i} - 2G_i. \quad (11.81)$$

In the case of effective universality ε_{ij} is close to zero. Larger values of ε_{ij} signal a stronger deviation from effective universality. This measure can be applied pairwise to the 10 distinct pairs of β -functions. Due to a rather mild G dependence around the fixed point with $G_h^* = 0.58$, cf. (11.82), we focus the discussion on the μ - λ_3 -plane at G_h^* .

A first nontrivial result concerns the existence of distinct lines where the individual components of ε_{ij} vanish in the μ - λ_3 -plane, cf. Figure 11.19. These lines cross pairwise in a bounded region. Moreover, the different crossing points lie near each other. This is crucial and highly nontrivial, as the distinct $\varepsilon_{ij} = 0$

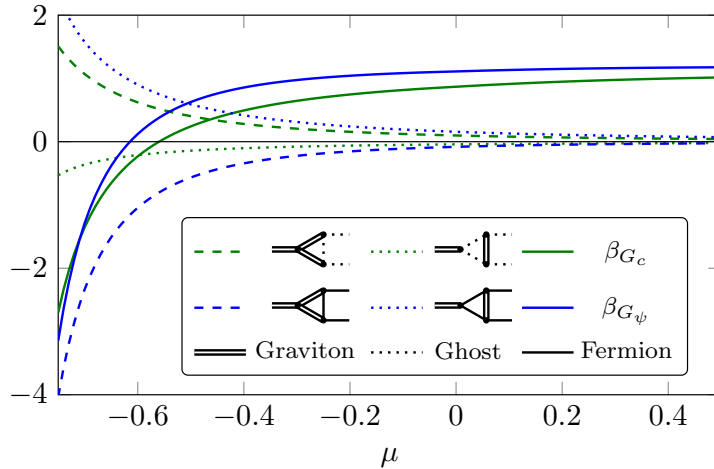


Figure 11.20.: Nontrivial cancellations between different diagrams. We show the μ dependence at $G = G_h^*$ and $\lambda_3 = \lambda_3^*$ of β_{G_c} and β_{G_ψ} , and of two contributing diagrams.

lines have quite different slopes. Therefore, there is a priori no reason to intersect pairwise in a relatively small region in the μ - λ_3 -plane. As we tentatively correlate the emergence of effective universality, i.e., an agreement of the β -functions, with a near-perturbative nature of the system, the vicinity of the $\varepsilon_{ij} = 0$ lines is a preferred region for the couplings.

In the gravity-matter system investigated in this work the interacting Reuter fixed point lies at

$$(G_h^*, G_c^*, G_\varphi^*, G_\psi^*, G_A^*, \mu^*, \lambda_3^*) \quad (11.82) \\ = (0.58, 0.55, 0.74, 0.74, 0.84, -0.58, 0.096).$$

The values of the different vertex couplings are related by the STIs but they are not necessarily identical. This potential difference is ignored in the ensuing qualitative discussion where we assume full universality for the sake of simplicity.

The flow in the vicinity of the fixed point is governed by the critical exponents at linearized order of the β -functions. The STIs entail that only two of our couplings are independent. They are related to the classical Newton coupling and the cosmological constant. This renders only a subset of critical exponents physical. In our setting, the critical exponents turn out to be quantitatively similar, and close to the values obtained by setting $G_i = G$ before calculating the stability matrix by taking derivatives of the β -function. This constitutes another strong indication for effective universality, and provides an estimate of $\text{Re } \theta \approx 1.3 - 1.7$ for the physical critical exponent of the Newton coupling.

Crucially, our result requires nontrivial cancellations between the diagrams that contribute to the distinct β -functions. It is therefore not an automatic consequence of our choice of truncation that is inspired by classical diffeomorphism invariance. As a specific example we highlight β_{G_c} and β_{G_ψ} in Figure 11.20. There we find an overall similarity of the β -functions while individual diagrams do not agree. Such cancellations appear unlikely to be generated by chance and we interpret them as a hint that the existence of the $\varepsilon_{ij} = 0$ lines and a fixed point in their vicinity is indeed a nontrivial result.

11.7.2. Sources of deviations from effective universality

For a stringent assessment of the deviation of the fixed point from $\varepsilon_{ij} = 0$, we have to evaluate its possible origins. In the present work we explore the Einstein-Hilbert truncation with minimally coupled matter. Yet, at an asymptotically safe fixed point, higher-curvature couplings [243, 192, 244, 63, 245], nonminimal gravity-matter couplings [240, 241] and matter-self interactions [246, 204, 215] are also present. Accordingly, our fixed-point values as well as the location of the $\varepsilon_{ij} = 0$ lines are subject to

a systematic error $\delta\epsilon$. A comparison of the fixed point to the $\epsilon_{ij} = 0$ lines is only meaningful within $\delta\epsilon$. A rough estimate for the systematic error – strictly speaking an estimate for a lower bound on it – can be obtained by comparing changes in fixed-point values under extensions of the truncation. Specifically, we compare a state-of-the-art study [62] with a previous work in the same scheme [60] to obtain differences in fixed-point values $\delta G_h, \delta\mu, \delta\lambda_3$. The relative variation of fixed-point values is similar in other extensions of truncations, see, e.g., [240, 159]. The average $\delta\epsilon$ of the $\delta\epsilon_{ij}$ is given by

$$\delta\epsilon = \frac{1}{10} \sum_{\substack{i,j \\ j < i}} \left[\left| \frac{\partial\epsilon_{ij}}{\partial G} \delta G_h \right| + \left| \frac{\partial\epsilon_{ij}}{\partial\mu} \delta\mu \right| + \left| \frac{\partial\epsilon_{ij}}{\partial\lambda_3} \delta\lambda_3 \right| \right]_{\substack{G=G^* \\ \mu=\mu^* \\ \lambda_3=\lambda_3^*}}, \quad (11.83)$$

resulting in $\delta\epsilon \approx 0.2$. As a key result, we stress that $\epsilon_{ij} \approx 0.2$ is compatible with effective universality within this estimate of the error $\delta\epsilon$, cf. contours in [Figure 11.19](#). Accordingly, at the UV fixed point, the avatars of the Newton coupling are compatible with effective universality.

The presence of higher-order operators results in a second source of deviations of a more involved nature: It is rooted in the challenge of projecting correlation functions onto specific operators and the related couplings, e.g., the avatars of the Newton coupling. For instance, at the level of the graviton three-point function, the terms contributing to our result for β_{G_h} include $\sqrt{g}R$ and $\sqrt{g}R_{\mu\nu}R^{\mu\nu}$, both expanded to third order in h . In the present gauge-fixed and regularized setting, one faces the additional challenge to account for nondiffeomorphic operators.

The higher-order contributions in the three-graviton and the graviton-matter vertices are *not* related to each other, as they are linked to distinct classically diffeomorphism invariant operators such as, e.g., $\sqrt{g}R_{\mu\nu}R^{\mu\nu}$ vs $\sqrt{g}R^{\mu\nu}\partial_\mu\varphi\partial_\nu\varphi$. From the observed small value of the ϵ_{ij} , we conclude that such higher-order operators, which could spoil effective universality completely, have a subleading impact.

Let us elucidate this point with an explicit example: Assume for the moment, that our evaluation of β_{G_h} would lead to $2G + \Delta\beta_{G_h} + \delta\beta_{\text{Ric}}$. Here, $\delta\beta_{\text{Ric}}$ is an additional part of similar magnitude as $\Delta\beta_{G_h}$, that originates from the running of the $\sqrt{g}R_{\mu\nu}R^{\mu\nu}$ coupling and contributes to β_{G_h} due to our (non-diagonal) projection procedure. Even assuming perfect agreement between all actual β_{G_i} , our result for ϵ_{hi} would be greater than 0.3. The observation that all ϵ_{ij} satisfy $\epsilon_{ij} \lesssim 0.2$ can tentatively be interpreted as a hint for the subleading nature of higher-curvature couplings. Accordingly, our projection prescription isolates the various Newton couplings without a large ‘contamination’ from higher-order terms. At the same time, this suggests that the ‘backreaction’ of these specific higher-order terms, once included in a truncation, should be small, as indeed observed in several approximations, e.g., [192, 223].

11.7.3. Modified Slavnov-Taylor identities

In a gauge-fixed setting, the fluctuation couplings are related by nontrivial Slavnov-Taylor identities (STIs). In the flow-equation setup, the regulator function is quadratic in the fluctuation fields and further breaks the diffeomorphism invariance. This turns the STIs into modified STIs (mSTIs) that now contain explicit regulator contributions, see e.g. [247, 165, 9, 143, 152, 144]. The mSTIs imply that couplings that derive from the same classical structure differ at the quantum level. Thus, $\epsilon_{ij} = 0$ is not to be expected in a quantum setting, even in the absence of the systematic effects discussed above. Since the mSTIs arise as a consequence of quantum effects, the perturbative limit with vanishing couplings features trivial mSTIs. In the nonperturbative regime of gauge theories, the mSTIs become nontrivial with QCD being an excellent example, see e.g. [54, 55]. If we ascribed the full difference in the fixed-point values of the different avatars of the Newton coupling to nontrivial mSTIs then $\epsilon_{ij} \approx 0.2$ would translate into a factor of roughly 0.7 between the fixed-point values. Taking our cue from QCD, where different avatars of the gauge coupling even feature distinct signs in the nonperturbative regime and thus much larger relative differences, we tentatively conclude that our results imply a near-perturbative nature of the asymptotically safe fixed point. More specifically, the analogue of mSTIs in QCD, see

[55], suggests a grouping of fixed-point values into the pair $\{G_h, G_c\}$ and the triple $\{G_\varphi, G_\psi, G_A\}$, with a nontrivial contribution from the mSTI differentiating between the former and the latter. This grouping is indeed apparent in the fixed-point values in (11.82). In contrast, the ‘matter-like’ behavior of $\varepsilon_{c\phi_{\text{mat}}}$ and ε_{hc} away from the fixed point, cf. Figure 11.18, is a direct consequence of the diagrammatic structure underlying the β -functions.

11.7.4. Implications

We observe that the fixed point yields $\varepsilon_{ij} \approx 0.2$, which is compatible with zero within our estimate for the systematic error. This entails a compatibility of the fixed point with effective universality within our present setup. The result has several important implications.

Firstly, it strongly suggests that the zero of the β -functions observed above is actually a true fixed point, in contrast to a truncation artefact. For the latter, there is no reason why delicate cancellations as observed above should occur. Their presence strongly hints at the impact of a symmetry principle. We view the delicate cancellations that occur in all pairs of β -functions as strong evidence for the physical nature of the asymptotically safe Reuter fixed point.

Secondly, we contrast the observed fixed-point structure with that of a system where $h_{\mu\nu}$ is a spin-2 field living on a fixed background. Then $h_{\mu\nu}$ would *not* be part of the dynamic spacetime geometry. If it was just another ‘matter’ field protected by shift symmetry, it would feature derivative couplings like those that we have examined here. Yet, the absence of a symmetry principle relating the distinct G ’s would make a semi-quantitative agreement of the fixed-point values rather unlikely. The presence of this dynamical symmetry linked to the underlying dynamical diffeomorphism invariance of quantum gravity is corroborated further by the previously observed momentum locality of specific propagator and vertex flows, [29, 62]. This property entails that the leading momentum dependence of different diagrams cancel non-trivially at large momenta. Our result could thus be interpreted as highlighting the geometric origin of $h_{\mu\nu}$ with its corresponding spacetime diffeomorphism symmetry and background independence.

Thirdly, we contrast the relative deviation of fixed-point values of different avatars of the Newton coupling with significantly larger deviations in nonperturbative QFTs. The relation between different avatars of the gauge coupling is carried by mSTIs, which allow large deviations of these classically equal avatars in a nonperturbative regime governed by large quantum fluctuations. The significantly smaller differences between the different Newton couplings can accordingly be interpreted as a consequence of a near-perturbative regime, where mSTIs simplify and a more ‘classical’ notion of diffeomorphism symmetry is realized.

11.8. Asymptotically safe Standard Model

The discovery of a relatively light Higgs leads to the intriguing possibility that the Standard Model can be extended up to the Planck scale, where its ultraviolet instability is cured by asymptotic safety induced by quantum gravity. In turn, the existence of the AS fixed point restricts the potential infrared completions of the asymptotically safe Standard Model: the finite number of UV relevant parameters are fixed by the respective number of infrared measurements. Then, all other measurements have to agree with the predictions of the asymptotically safe theory.

Moreover, such a setting could possibly explain part of the mass hierarchies present in the Standard model. Here we discuss such a possibility at the example of the mass of the top quark, following [228]. The top quark is substantially heavier than all the other quarks, with a pole mass of $M_t \approx 173$ GeV [248] significantly larger than the pole mass of the second-heaviest quark, the bottom at $M_b \approx 4.9$ GeV [77]. In the Standard Model, neither the two values nor their difference can be derived. The masses are determined by the Yukawa couplings y_t, y_b to the Higgs, once it acquires a vacuum expectation value.

The action of the Standard Model decomposes in the pure gauge part of QCD and the electroweak interactions with

$$S_{\text{SM,gauge}} = \frac{1}{4} \int_x \text{tr} F_{\mu\nu}^2 = \frac{1}{2} \int_x \left(\frac{1}{2} B_{\mu\nu}^2 + \text{tr} W_{\mu\nu}^2 + \text{tr} G_{\mu\nu}^2 \right), \quad (11.84)$$

where $F_{\mu\nu}$ is the field strength of the $U(1) \times SU(2) \times SU(3)$ gauge group of the Standard model, which decays in the $U(1)$ Hypercharge fieldstrength $B_{\mu\nu}$ with coupling g' , the weak $SU(2)$ fieldstrength $W_{\mu\nu}$ with coupling g_w , and the strong $SU(3)$ fieldstrength $G_{\mu\nu}$ with coupling g_s .

These gauge fields are coupled via Dirac terms to the fermionic matter fields ψ of the theory, the leptons l and quarks q . We have

$$S_{\text{SM,Dirac}} = i \int_x \psi \not{D} \psi, \quad \text{with} \quad \not{D} = \not{D}_{\text{QCD}} - i \gamma_\mu (g' Y_W B_\mu - i g_w W_\mu), \quad (11.85)$$

with the hypercharge $U(1)$ gauge field B_μ and the weak $SU(2)$ gauge field W_μ with $W_\mu = W_\mu^a \tau^a$ and $\tau = (\sigma^1, \sigma^2, \sigma^3)$. The electric charge Q is related to the hypercharge and the weak isospin with

$$Q = T_3 + Y_W, \quad (11.86)$$

implying for the right handed fermions $Q = Y_W$. The Higgs is a strong $SU(3)$ scalar, and the Higgs sector of the Standard Model reads schematically

$$S_{\text{SM,Higgs}} = \int_x \left\{ (D_\mu \phi)^\dagger (D_\mu \phi) + \mu^2 (\phi^\dagger \phi) + \lambda (\phi^\dagger \phi)^2 \right\} + S_{\text{SM,Yukawa}}, \quad \text{with} \quad \phi = \frac{1}{\sqrt{2}} \begin{pmatrix} \phi^+ \\ \phi^0 \end{pmatrix}, \quad (11.87)$$

with the (eletric) charged Higgs field ϕ^+ and the neutral one, ϕ^0 . Note also that

$$D_\mu \phi = (\partial_\mu - i g' Y_W B_\mu - i g_w W_\mu) \phi, \quad (11.88)$$

with $G_\mu \phi = 0$. The Yukawa term is given -very- schematically by

$$S_{\text{Yukawa}} = \int_x (\bar{\psi}_i C_{ij} \phi \psi_j + \text{h.c.}), \quad (11.89)$$

with the matrix of the Yukawa couplings C . The heavy quark part of the Yukawa sector reads

$$S_{\text{Yukawa}} = \int_x (y_t \bar{Q} \phi^c t_R - y_b \bar{Q} \phi b_R - y_\tau \bar{L} \phi \tau_R + \text{h.c.}), \quad (11.90)$$

with

$$\bar{Q} = (t_L, L), \quad L = (\nu_\tau, \tau)_L, \quad \phi = \frac{1}{\sqrt{2}} \begin{pmatrix} \phi^+ \\ v + H \end{pmatrix}, \quad (11.91)$$

with the expectation value $v \approx 246 \text{ GeV}$ of the Higgs field, [249]. The low-energy values of y_t, y_b are free parameters in the Standard Model, fixed by comparing to experiment. We propose a mechanism that could generate the mass difference dynamically and uniquely determine the values of both masses from first principles. The mechanism follows from microscopic physics in the ultraviolet (UV), where an interplay of quantum gravity and gauge boson dynamics generates asymptotic safety [125, 165], i.e., an interacting Renormalization Group (RG) fixed point at transplanckian scales. This fixed point prevents

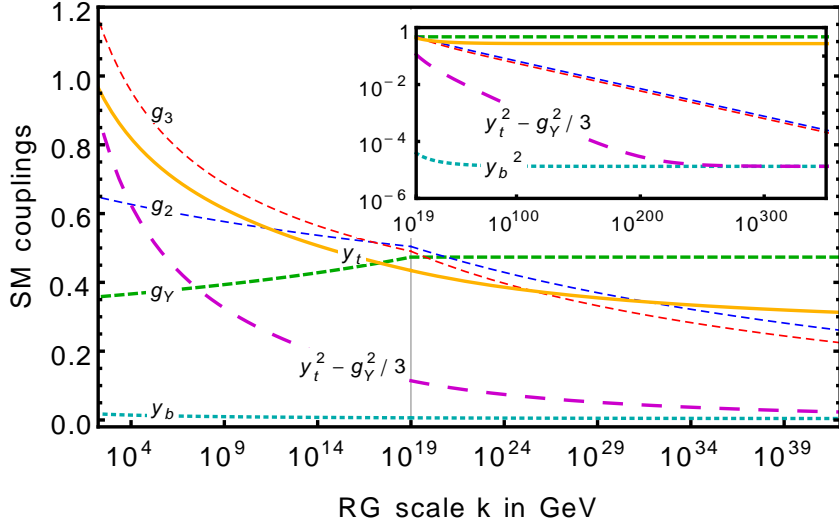


Figure 11.21.: RG trajectory of Standard-Model couplings for $f_g = 9.7 \times 10^{-3}$ and $f_y = 1.188 \times 10^{-4}$, reaching $g(k_{\text{IR}}) = 0.358$, $y_t(k_{\text{IR}}) = 0.965$, and $y_b(k_{\text{IR}}) = 0.018$ at $k_{\text{IR}} = 173 \text{ GeV}$. We also plot $y_t^2 - g_y^2/3$ (pink, wide-dashed), which approaches y_{b*}^2 (dotted) in the far UV, cf. Eq. (11.96).

Landau-pole type behaviour in the running couplings, rendering the Standard Model UV-complete. The fixed point determines the values of y_t and y_b in the UV. This mechanism combines the fixed-point scenarios explored in [226, 205], see also [202], where the top pole mass and Abelian gauge coupling are retrodicted separately. Due to the two quarks' unequal electric charges, y_t and y_b assume uniquely determined, different values at $M_{\text{Planck}} = 10^{19} \text{ GeV}$, cf. Fig. 11.21. This results in a retrodiction of unequal top and bottom masses at the electroweak scale. The viability of this mechanism hinges on the quantum numbers of the top and bottom quark: in our approximation, significant deviations from the measured charge ratio are incompatible with the observed masses.

We now explain the mechanism, by following the RG flow from the UV fixed point through the transplanckian regime down to the electroweak scale.

11.8.1. Ultraviolet fixed point

There are strong indications for an asymptotically safe regime in quantum gravity, where the running gravitational couplings reach a scale-invariant regime that UV-completes the theory [165, 250, 251, 252, 191, 243, 253, 185, 192, 207, 156, 60, 244, 254, 62, 170, 159, 63, 255]. Quantum-gravity fluctuations impact the scale dependence of running matter couplings [256, 257, 201, 202, 203, 205, 204, 160, 225, 258, 259, 215, 214, 260, 226]. For the gauge couplings of the Standard Model, g_3 for SU(3), g_2 for SU(2) and g_Y for the Abelian hypercharge, the one-loop beta functions and coefficients read [261, 262, 263]

$$\begin{aligned} \beta_{g_i} &= k \partial_k g_i(k) = b_{0,i} g_i^3 / (16\pi^2) - f_g g_i, \\ b_{0,3} &= -7, \quad b_{0,2} = -\frac{19}{6}, \quad b_{0,Y} = \frac{19 + 36(Y_b^2 + 2Y_Q^2 + Y_t^2)}{6}. \end{aligned} \quad (11.92)$$

$Y_{t,b,Q}$ are the hypercharges of the right-handed top and bottom quark and the left-handed SU(2) quark doublet, respectively. f_g encodes the quantum-gravity contribution that acts like an anomalous dimension for the gauge couplings, and we assume that additional terms are subleading. These additional contributions are proportional to the product of g_i and quantum-gravity-induced higher-order couplings. The fixed-point values of the latter are of the same order as f_g , see the discussion in [214, 204, 215]. They

enter the β_{g_i} through a loop diagram, leading to a suppression by $\frac{1}{16\pi^2}$ in comparison to the direct contribution in Eq. (11.92), see [215]. We work with the one-loop beta functions to explain the mechanism, explicitly checking that two-loop effects only lead to quantitative changes. We focus on $f_g \geq 0$, as found in truncations of the functional RG flow [21, 26] under the impact of asymptotically safe quantum gravity [201, 202, 203, 205, 204, 160], see [233, 235, 236, 238] for reviews. In the asymptotically safe regime beyond the Planck scale, $f_g = \text{const.}$ holds as a consequence of gravitational fixed-point scaling. For the non-Abelian gauge couplings, this reinforces the asymptotically free fixed point at $g_{3*} = 0 = g_{2*}$. For the Abelian gauge coupling, the positive one-loop coefficient, generated by screening quantum fluctuations of charged matter, and the antiscreening gravity contribution cancel at an interacting fixed point [202, 205, 264],

$$\beta_{g_Y}\Big|_{g_Y=g_{Y*}} = 0, \quad g_{Y*}^2 = \frac{16\pi^2}{b_{0,Y}} f_g. \quad (11.93)$$

Quantum-gravity contributions to the running of the Yukawas supplement the one-loop beta functions [265]

$$\begin{aligned} \beta_{y_{t(b)}} &= \frac{y_{t(b)}}{16\pi^2} \left(\frac{3y_{b(t)}^2}{2} + \frac{9y_{t(b)}^2}{2} - \frac{9}{4}g_2^2 - 8g_3^2 \right) \\ &\quad - f_y y_{t(b)} - \frac{3y_{t(b)}}{16\pi^2} (Y_Q^2 + Y_{t(b)}^2) g_Y^2. \end{aligned} \quad (11.94)$$

For the quantum-gravity contribution, $f_y = \text{const}$ holds in the asymptotically safe transplanckian regime [258, 259, 215, 214, 260, 226] generating an interacting fixed point at $y_{t,b,*} \neq 0$ through the interplay with Abelian fluctuations: At the fixed point at $g_{2*} = 0 = g_{3*}$ and g_{Y*} in Eq. (11.93), we obtain

$$y_{t/b*}^2 = \frac{8}{3}\pi^2 \left(f_y + \frac{3f_g(2Y_Q^2 + 3Y_{t/b}^2 - Y_{b/t}^2)}{2b_{0,Y}} \right). \quad (11.95)$$

Specifying to Standard-Model charges $Y_t = 2/3$, $Y_b = -1/3$, and $Y_Q = 1/6$, yields a fixed-point equation that is the key relation of our scenario

$$y_{t*}^2 - y_{b*}^2 = \frac{1}{3}g_{Y*}^2. \quad (11.96)$$

This relation enforces $y_{t*} \neq y_{b*}$ in the far UV because $g_{Y*} \neq 0$. The difference in fixed-point values, $y_{t(b)*}$, has an intuitive physical interpretation: The interacting fixed point for the Yukawas is generated through a balance of quantum fluctuations of matter with gauge and gravity fluctuations. The two fixed-point values $y_{t(b)*}$ must be unequal since Abelian gauge boson fluctuations couple more strongly to the top than to the bottom quark, as the top has a larger hypercharge, i.e., $Y_t^2 > Y_b^2$. To compensate the combined impact of gravity and gauge boson fluctuations and generate a fixed point, the top Yukawa coupling must be larger, $y_{t*} > y_{b*}$.

The beta functions in Eqs. (11.92) and (11.94) admit further fixed-point solutions, e.g., $g_{Y*} = 0$, $y_{b*} = 0$, $y_{t*} > 0$ explored in [226], cf. light-green shaded region in Fig. 11.22. Here, we focus on the most predictive fixed-point solution, cf. Eqs. (11.93) and (11.95), leading to retrodictions of the top mass M_t , the bottom mass M_b and the Abelian hypercharge coupling g_Y at the electroweak scale.

11.8.2. RG flow at transplanckian scales

Starting from Eq. (11.96), the couplings deviate from their fixed-point values during the RG flow towards the infrared (IR). For real fixed-point values, Eq. (11.96) implies $y_{t*} > y_{b*}$, and the RG flow conserves

this inequality: The ratio $y_t(k)/y_b(k)$ cannot become smaller than 1 if $y_{t*}/y_{b*} > 1$ in the UV. The flow of the ratio is given by

$$\beta_{\frac{y_t}{y_b}} = \frac{1}{16\pi^2} \frac{y_t}{y_b} (3(y_t^2 - y_b^2) - g_Y^2). \quad (11.97)$$

For $y_t(k)/y_b(k) \rightarrow 1$ from above, the beta function becomes negative due to the contribution of the Abelian gauge coupling. Hence, the ratio $y_t(k)/y_b(k)$ is driven away from 1 towards larger values. Once created by the fixed-point structure, the relation $y_t(k) - y_b(k) > 0$ is thus preserved down to the IR, cf. Fig. 11.21.

Specifically, the trajectories in Fig. 11.21 arise as follows. Since $f_g = \text{const.}$ in the transplanckian regime, $g_Y(k > M_{\text{Planck}}) = g_{Y*}$ holds. This results from the competition of the two distinct contributions in Eq. (11.92): The screening matter contribution, encoded in $b_{0,Y}g_Y^3 > 0$ drives any small deviation $g_Y(k) = g_{Y*} + \delta$ with $\delta > 0$ back to $\delta = 0$ under the RG flow to the IR. Conversely, the antiscreening gravity contribution, encoded in $-f_g g_Y < 0$, drives any small deviation $g_Y(k) = g_{Y*} - \delta$ with $\delta > 0$ back to $\delta = 0$. In other words, the fixed point is IR attractive, cf. thick dashed green line in Fig. 11.21.

This is in contrast to the behavior of the non-Abelian gauge couplings, where the gravity contribution triggers a power-law running in the transplanckian regime. Since both, the gravity-contribution and the matter contribution to the beta functions $\beta_{g_{2,3}}$ are antiscreening, the free fixed-point is IR repulsive. Hence, deviations from it are allowed in the transplanckian regime and $g_{2,3}$ grow under the RG flow to the IR, until they reach the experimentally determined values at IR scales.

This dynamics for the gauge couplings leads to a more intricate behavior of the Yukawas: although the fixed point in Eq. (11.95) is IR attractive, the Yukawas run as soon as $g_{2,3}$ deviate from zero significantly, cf. Fig. 11.21. Their running is determined by a critical trajectory $y_{t(b)}(k) = y_{t(b)}(g_2(k), g_3(k))$ on which they exhibit a slight growth towards the IR. The non-Abelian gauge contribution to the flow of the Yukawas is negative. This counteracts the screening effect of matter fluctuations. Thus, tiny deviations $y_t(k) = y_{t*} + \delta$ with $\delta > 0$ are no longer driven back exactly to y_{t*} for $g_{2,3}(k) > 0$. The critical trajectory is IR attractive, i.e., starting from their fixed-point values, the Yukawa couplings are fixed uniquely at M_{Planck} .

11.8.3. RG flow between the Planck and the electroweak scale

At the Planck scale, quantum-gravity effects switch off dynamically as f_g, f_y are proportional to the Newton coupling measured in units of k . In asymptotic safety, it is constant at transplanckian scales, but falls off as k^{-2} below M_{Planck} , making quantum-gravity effects negligible there, cf. [250, 251]. To model this behavior, we implement a sharp transition to $f_g = 0 = f_y$ for $k \leq M_{\text{Planck}}$. Below M_{Planck} , we follow the one-loop running in the Standard Model, attracted by a partial IR fixed-point [266, 267, 268]. At the electroweak scale, where the Higgs acquires a vacuum expectation value, the two Yukawas determine the top and bottom mass. The inequality $y_t(k) > y_b(k)$, generated by the properties of the transplanckian regime, is preserved under the Standard-Model flow, as Eq. (11.97) still holds. The difference in fixed-point values between y_t and y_b thus generates a mass difference between M_t and M_b .

So far, we have explained how a mass difference between the two quarks could result from their unequal quantum numbers as a consequence of an asymptotically safe fixed point. We now test the quantitative viability of this mechanism in our approximation by using approximately observationally viable values. To accommodate $g_Y(k_{\text{IR}} = 173 \text{ GeV}) = 0.358$ in accordance with observations, $f_g = 9.7 \times 10^{-3}$ is required. Together with the values $g_2(k_{\text{IR}}) = 0.64779$ and $g_3(k_{\text{IR}}) = 1.1666$ see, e.g., [269] this also fixes the running of the non-Abelian gauge couplings at all scales. Then, $f_y = 1.188 \cdot 10^{-4}$ is required to obtain $y_b(k = 4.2 \text{ GeV}) = 0.024$. This translates into a bottom pole mass [77] of $M_b = 4.9 \text{ GeV}$. Given this input, the mechanism presented here generates $y_t(k = 168 \text{ GeV}) = 0.967$ corresponding to a top pole mass [77] of $M_t = 178 \text{ GeV}$. All three retrodicted quantities, M_t, M_b and g_Y , come out rather close to their observed values with the input of two free parameters, f_y and f_g . The above values f_y, f_g lie in

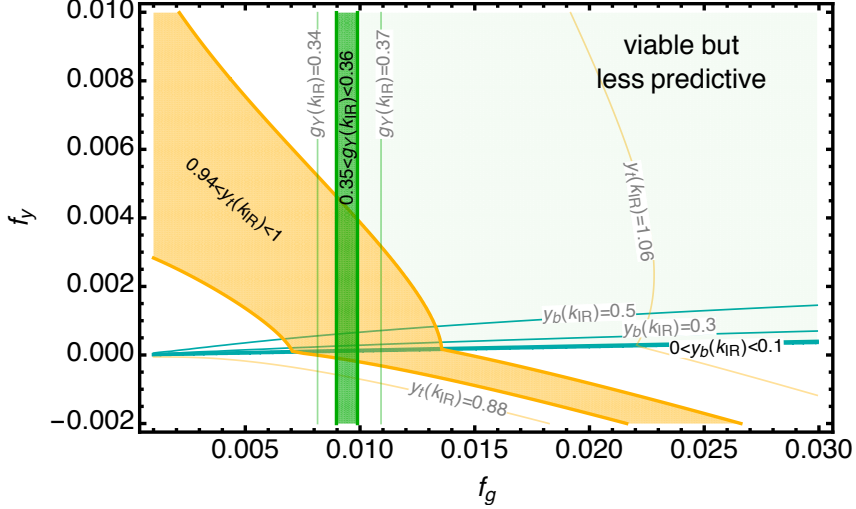


Figure 11.22.: IR values of retrodicted couplings $g_Y(k_{\text{IR}})$, $y_t(k_{\text{IR}})$ and $y_b(k_{\text{IR}})$ at $k_{\text{IR}} = 173$ GeV as a function of the two independent quantum-gravity contributions f_g and f_y .

the vicinity of fixed-point values obtained in an approximation for quantum gravity minimally coupled to matter fields of the Standard Model [207]. A quantitatively precise calculation of f_y, f_g is subject to future studies. These studies must include higher-order curvature operators as in [260, 215] and non-minimal matter-curvature couplings as in [253, 259, 240] to determine the gravitational fixed-point values which directly set f_g and f_y .

As the UV fixed point is generated from a balance of the leading quantum-gravity contribution with the one-loop matter contribution and lies at small Standard-Model couplings, its existence is expected to be stable under the extension to higher-loop orders in the Standard-Model sector. Including two-loop terms in the Standard-Model running [270, 271, 272, 273, 274, 275], $f_g = 9.8 \times 10^{-3}$ yields $g_Y(k_{\text{IR}}) = 0.358$ and $f_y = 1.1266 \times 10^{-4}$ gives a bottom pole-mass of $M_b = 4.9$ GeV. This retrodicts a top pole-mass of $M_t = 182$ GeV.

Analyzing an extended setting going beyond the third generation could provide a future test of the present model. Extending our study to the quarks of the second generation requires to account for the CKM mixing matrix. Inspecting the beta-functions for the strange and charm Yukawa under the simplifying assumption of a diagonal mixing matrix at y_{t*}, y_{b*} and g_{Y*} yields a fixed point at vanishing Yukawas for charm and strange which is IR-attractive in the strange and thus retrodicts $M_s/M_t \simeq 0$. Testing whether the tiny ratio $M_s/M_t \approx 5 \cdot 10^{-4}$ is compatible with our setting requires to go beyond the above simplifying assumptions in more complete studies but should provide a critical future test of the present proposal. In the charm, this fixed point is IR repulsive, rendering the charm asymptotically free. Therefore M_c/M_t is not retrodicted. Specifically, $M_c/M_t \approx 7 \cdot 10^{-3}$ can be accommodated in our setting.

11.8.4. Exploring the gravitational parameter space

We now explore f_g and f_y away from the specific values used above. This exploits the link between electroweak and Planck-scale physics in order to constrain the microscopic gravitational parameter space by the requirement to match IR observables, in the spirit of [215].

In our approximation, the low-energy value of g_Y only depends on f_g . Hence, lines of constant f_g in Fig. 11.22 correspond to lines of fixed $g_Y(k_{\text{IR}} = 173\text{GeV})$. In contrast, $y_{t/b}(k_{\text{IR}})$ depend on f_y as well as on f_g through the gauge contributions in Eq. (11.94). Thus, lines of constant $y_{t/b}(k_{\text{IR}})$ are not simply lines of constant f_y .

Fig. 11.22 visualizes that the existence of an intersection area of the three approximately observationally

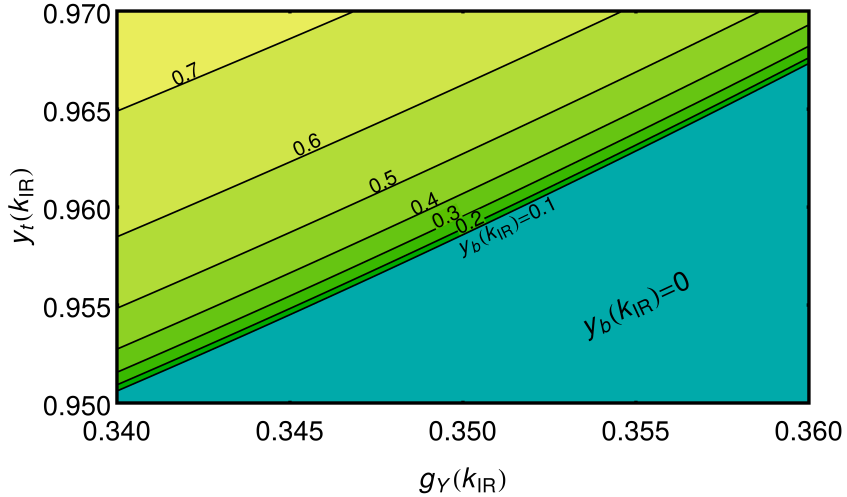


Figure 11.23.: Bottom Yukawa coupling $y_b(k_{\text{IR}})$ at $k_{\text{IR}} = 173$ GeV as a function of the IR values of $g_Y(k_{\text{IR}})$ and $y_t(k_{\text{IR}})$.

viable contours defined by $0 < y_b(k_{\text{IR}}) < 0.1$, $0.94 < y_t(k_{\text{IR}}) < 1$ and $0.35 < g_Y(k_{\text{IR}}) < 0.36$ is a nontrivial result. An intersection does not occur for arbitrary combinations of values. For instance, $g_Y(k_{\text{IR}}) > 0.4$ and $0.94 < y_t(k_{\text{IR}}) < 1$ are incompatible with a non-zero bottom mass in our approximation. Thus, in our approximation, values close to the observed ones appear to be singled out by asymptotic safety. The fixed-point in Eq. (11.96) shows that y_{b*}^2 depends on the difference of the squares of y_{t*} and g_{Y*} . Accordingly, small variations of these two numbers away from $y_{t*}^2 = g_{Y*}^2/3$ result in a fast growth of the value of $y_b(k_{\text{IR}})$. Due to the different U(1) hypercharges of top and bottom, the line $M_b = M_t$ cannot be reached, and a difference $M_t - M_b > 0$ always persists. On the other hand, a very large difference, $M_t - M_b \simeq M_t$ requires a choice of the gravity parameters in a relatively small region of the gravitational parameter space, such that the system sits close to the phase-transition line to vanishing bottom mass. In our approximation, this region translates into close-to Standard-Model values for $g_Y(k_{\text{IR}})$ and M_t , cf. Fig. 11.23.

In summary, we have uncovered a non-trivial UV fixed point for the Standard Model couplings $g_{Y*} \neq 0$ and $y_{t(b)*} \neq 0$ induced by asymptotically safe gravity, that generically results in a mass difference between the top and bottom quark, i.e., $M_t > M_b$. This fixed point retrodicts $(g_Y(k_{\text{IR}}), M_t, M_b)$, in terms of two gravitational parameters (f_g, f_y) . In our study the retrodiction is in approximate agreement with the observed IR values, cf. Fig. 11.22.

11.8.5. Three observations

1) *Universality of gravity contributions:* A key assumption of our study is the independence of the quantum-gravity contributions from internal symmetries: gravity is the only known force that couples universally to all matter fields such that f_g is independent of the gauge group. A significant violation of this universality leads to a quantitative failure of the above scenario. Specifically, let the gravitational contribution to the running of the non-Abelian gauge couplings be given by $f_g \rightarrow f_{g,nA}$ in Eq. (11.92). The rate at which $g_{2,3}$ grow above the Planck scale is thereby increased (lowered) for $f_{g,nA} > (<)f_g$. This affects how fast the Yukawa couplings increase in the transplanckian regime. Only $f_{g,nA} \approx f_g$ results in an observationally viable range for $y_t(k_{\text{IR}})$, cf. Fig. 11.24. Thus, the independence of the gravitational contribution from the gauge group is suggested by the observed values of $y_b(k_{\text{IR}})$, $y_t(k_{\text{IR}})$ and $g_Y(k_{\text{IR}})$.

2) *Setting the scale:* A second central assumption underlying our study is that the scale at which the gravitational contributions switch off is the Planck scale. We test whether another, presently unknown

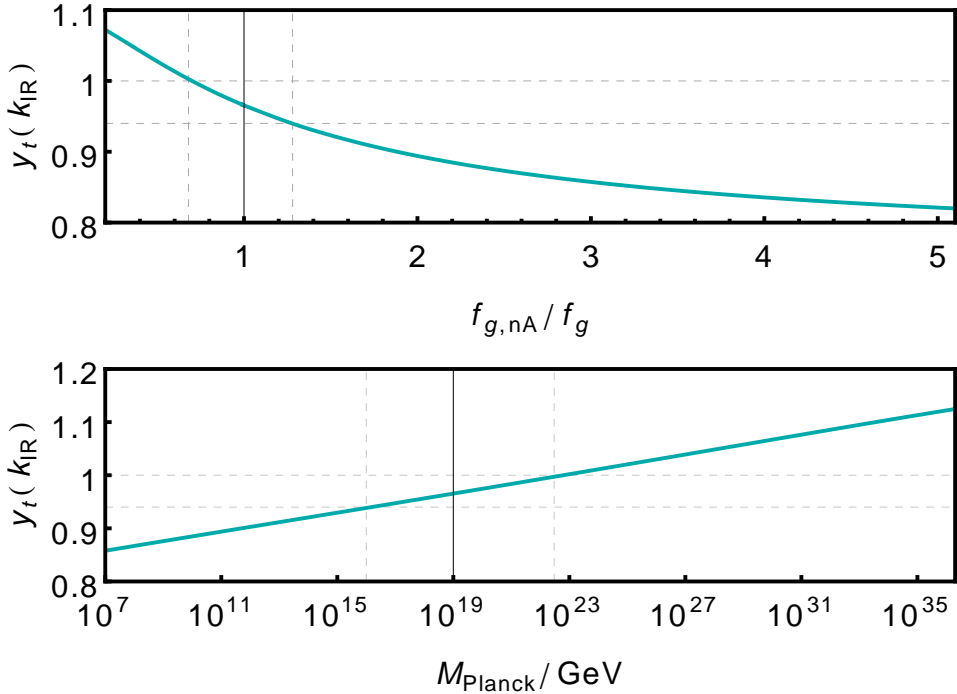


Figure 11.24.: Top-Yukawa coupling $y_t(k_{\text{IR}})$ at $k_{\text{IR}} = 173$ GeV as a function of a non-universal gravity contribution $f_{g,\text{nA}}/f_g$ (upper panel) and of a modified Planck scale M_{Planck} (lower panel) for fixed $g_Y(k_{\text{IR}}) = 0.358$ and $M_b = 4.9$ GeV.

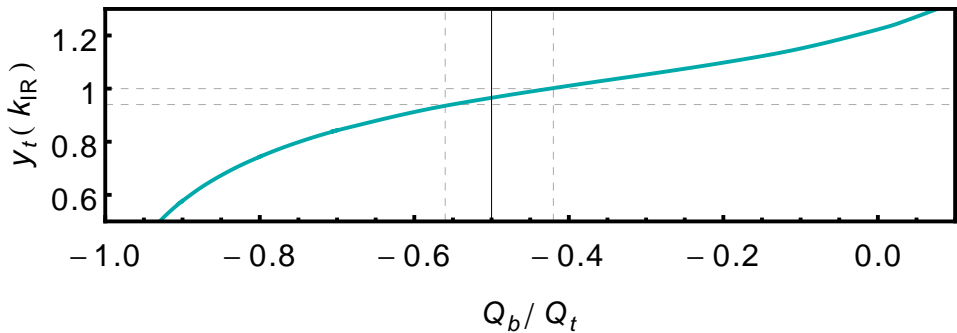


Figure 11.25.: Top-Yukawa coupling $y_t(k_{\text{IR}})$ at $k_{\text{IR}} = 173$ GeV as a function of the charge ratio Q_b/Q_t for fixed $g_Y(k_{\text{IR}}) = 0.358$ and $M_b = 4.9$ GeV.

universally coupled interaction could underlie the proposed mechanism. Its scale would of course not be tied to the Planck scale. Varying the scale significantly away from 10^{19} GeV results in a mismatch of M_b/M_t with the observed values, cf. upper panel in Fig. 11.24. Given the electroweak scale, which is an input of our calculation, the Planck mass can thus be estimated by demanding that the model realizes a mass ratio in the vicinity of the observed ratio of M_b/M_t in our approximation.

3) Selecting electric charges for top and bottom: The top-bottom mass-difference is rooted in distinct fixed-point values in Eq. (11.96). Varying the quantum numbers of the top and bottom from their values in the Standard Model results in a modified running of g_Y , y_t and y_b and an altered fixed-point relation

$$y_{b*}^2 = y_{t*}^2 - (Q_t^2 - Q_b^2)g_{Y*}^2. \quad (11.98)$$

Here, we keep the top and bottom in a doublet of the SU(2). The hypercharges of the doublet Y_Q and singlets $Y_{b/t}$ are linked to the electric charges by $Y_t = Q_t$, $Y_b = Q_b = Q_t - 1$, $Y_Q = Q_t - \frac{1}{2}$, where the

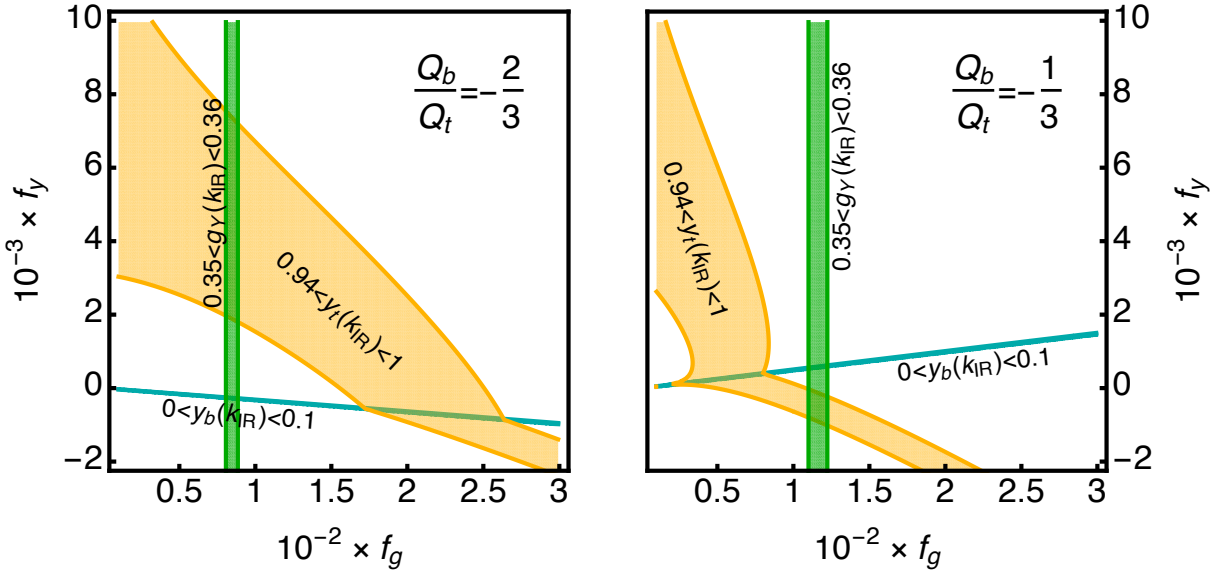


Figure 11.26.: IR-values of the retrodicted couplings $g_Y(k_{IR})$, $y_t(k_{IR})$ and $y_b(k_{IR})$ at $k_{IR} = 173$ GeV as a function of the two quantum gravity contributions f_g and f_y at modified charge ratio, $Q_b/Q_t = -2/3$ (left-hand panel); $Q_b/Q_t = -1/3$ (right-hand panel).

last equality ensures equal electric charges for the right- and left-handed quarks. It turns out that for $Q_b/Q_t < -1/2$, $M_t/M_b \rightarrow 0$, whereas for $Q_b/Q_t > -1/2$, $M_t/M_b \rightarrow 1$, cf. Fig. 11.25. The reason lies in the dynamics of the green, cyan and yellow contours in Fig. 11.26: An increase in Q_b/Q_t triggers a growth in f_g , since $b_{0,Y}$ increases with Q_b/Q_t . Thus, the green contour moves to the right as a function of Q_b/Q_t . Simultaneously, the cyan and yellow contours move towards each other as $y_{b*} \rightarrow y_{t*}$ for $Q_b/Q_t \rightarrow 1$. Accordingly, the three contours single out a value of Q_b/Q_t at which they intersect in one location in the f_g , f_y plane. This value agrees with the Standard Model value $Q_b/Q_t = -1/2$.

12. Asymptotically safe back holes and cosmology

The truncation can as well be supplemented by boundary terms. These have been considered in [276]. The authors added a Gibbons-Hawking term

$$\Gamma_k^\partial = -\frac{1}{16\pi G_k^\partial} \int_{\partial\mathcal{M}} d^{d-1}x \sqrt{H} (2K - 2\Lambda_k^\partial) \quad (12.1)$$

to the Einstein-Hilbert truncation. Here H is the boundary metric and K is the trace of the extrinsic curvature. G_k^∂ and Λ_k^∂ denote the boundary Newton constant and the boundary cosmological constant respectively. It was shown that the ratio of G_k and G_k^∂ is not preserved by RG running.

The applicability of the Asymptotic Safety scenario to theories with extra dimensions was shown in [277] by calculating the fixed points in dimensions larger than four. An even more general setting was considered in [278]. There two-dimensional surfaces, embedded in D -dimensional space, are investigated. Here the limit $D \rightarrow 0$ corresponds to two-dimensional gravity.

The conformally reduced version of the Einstein-Hilbert truncation was investigated first in [279]. There the authors considered a metric $g_{\mu\nu}$ of the form

$$g_{\mu\nu} = \phi^2 \hat{g}_{\mu\nu}. \quad (12.2)$$

The scalar function $\phi(x)$ is the conformal factor and $\hat{g}_{\mu\nu}$ is a non-dynamical reference metric. Separating the conformal factor into a background χ and the expectation value of the fluctuation f the conformally reduced Einstein-Hilbert truncation reads

$$\Gamma_k = -\frac{3}{4\pi G_k} \int d^d x \sqrt{-\hat{g}} \left[-\frac{1}{2}(\chi + f)\hat{\square}(\chi + f) + \frac{1}{12}\hat{R}(\chi + f)^2 - \frac{1}{6}\Lambda_k(\chi + f)^4 \right]. \quad (12.3)$$

Here \hat{R} and $\hat{\square}$ are the scalar curvature and Laplace operator of the reference metric. It was shown that this reduced system has a fixed point similar to the full Einstein-Hilbert truncation. This reduced ansatz was developed further in [280] by replacing the quartic term proportional to the cosmological constant by an arbitrary running potential. In [281] these investigations have been broadened by the inclusion of an R^2 term and the conformal anomaly term. The conformally reduced Einstein-Hilbert truncation has been compared in detail to the standard Einstein-Hilbert truncation and a minisuperspace approximation in [282]. Here the minisuperspace truncation is (12.3) with space independent conformal factor and the authors find a limit cycle shielding the UV fixed point. Note that a limit cycle was seen in [283] as well. The Weyl invariance of asymptotically safe Quantum Gravity has been considered in [284]. It was shown that the RG flow can preserve the invariance if a dilaton is coupled to it. These results have been developed further in [285] by inclusion of conformally coupled matter fields.

In [184] a different type of renormalisation group equation was considered. The results for the so called proper time flow equation confirms the known results of the ERGE. Another approach was put forward in [143]. This gauge invariant flow equation is based on the Vilkovisky-de-Witt geometrical formalism

[286, 287] and was used in [144] to investigate among others the proposed IR fixed point in Quantum Einstein Gravity at $(g_*, \lambda_*) = (0, 1/2)$. This point was investigated as well in [288, 58]. **I guess you would like to have a bit more here ...?** Yet another derivation of the flow equation was considered in [289]. In this work the functional integral over phase space instead of configuration space was considered for the derivation. The same authors proposed in [290] the consideration of a flow equation for the effective Hamiltonian action. Both approaches might be applied to gravitational theories in the future and hopefully provide new insights.

Other descriptions of gravity have been investigated as well. Switching from the metric as the fundamental degree of freedom to the vielbeins e^a_μ by setting

$$g_{\mu\nu} = \eta_{ab} e^a_\mu e^b_\nu \quad (12.4)$$

and introducing the spin connection ω^{ab}_μ leads us to a classically equivalent formulation provided by the Hilbert-Palatini action. Adding a term which does not contribute to the equations of motion with the so called Immirzi parameter γ in front leads us to the Holst action. This was used as a truncation ansatz in [291] and reads

$$\Gamma_k^{\text{Holst}} = -\frac{1}{16\pi G_k} \int d^4x e \left[e_a^\mu e_b^\nu \left(F^{ab}_{\mu\nu} - \frac{1}{2\gamma_k} \epsilon^{ab}_{cd} F^{cd}_{\mu\nu} \right) - 2\Lambda_k \right]. \quad (12.5)$$

For brevity we do not specify $F^{ab}_{\mu\nu}$. The authors have been able to construct an asymptotically safe scenario. Furthermore, a perturbative investigation of this first-order formalism can be found in [292]. A setup between the aforementioned and the metric formalism was considered in [293]. In this work the authors use the Einstein-Hilbert truncation with the metric replaced by the vielbeins and without considering the spin connection as an independent field variable.

Instead of the metric or the vielbeins as the fundamental fields one can consider a decomposition of the metric with a foliated structure of spacetime

$$g_{\mu\nu} = \begin{pmatrix} \epsilon N^2 + N_i N^i & N_j \\ N_i & \sigma_{ij} \end{pmatrix}. \quad (12.6)$$

Here the fundamental degrees of freedom are the lapse function N , the shift vector N^i and the spatial metric σ_{ij} . This decomposition was used in [185, 294] e.g. to investigate the Lorentzian signature $\epsilon = -1$.

Another important issue we did not mention so far is the fact that in our calculation we encounter two metrics. Within the background field approach we introduced the background field ???. A physical viable theory has to be independent of the background and thus a separated treatment of the two metrics is necessary. This has been put forward in [152] and was developed further in [153, 154]. The so called bimetric truncation in [154] considers both metrics as dynamical quantities and reads

$$\Gamma_k = -\frac{1}{16\pi G_k} \int d^d x \sqrt{-g} [R - 2\Lambda_k] - \frac{1}{16\pi G_k^B} \int d^d x \sqrt{-\bar{g}} [\bar{R} - 2\Lambda_k^B] - \frac{M_k}{8\pi G_k} \int d^d x \sqrt{-g} \left(\frac{\sqrt{g}}{\sqrt{\bar{g}}} \right)^n \quad (12.7)$$

with the corresponding gauge fixing and ghost term. The quantities labeled with a bar or a B correspond to background quantities and are not fixed any more. The third term is special for the bimetric consideration and was motivated in [153]. Again the Asymptotic Safety scenario was confirmed.

Some general considerations as e.g. in [295] about the bare action or the separation into the so called diamagnetic and paramagnetic contributions to the flow equations [296] shed some further light on the underlying processes and should be mentioned here as well.

Besides these formal considerations, necessary to convince ourselves that gravity is indeed asymptotically safe, it is of course interesting to see what phenomenological consequences arise out of this scenario. Black Holes for example are known to evaporate due to Hawking radiation. The semiclassical treatment shows that the mass of the Black Hole decreases and the temperature increases. Nevertheless close to the Planck temperature the semiclassical approach is likely to break down and a quantum-gravitational treatment is necessary. In [297] the authors take quantum fluctuations into account by inserting a k -dependent Newton constant into the Schwarzschild metric

$$ds^2 = -f(r, k)dt^2 + \frac{dr^2}{f(r, k)} + r^2d\Omega^2, \quad f(r, k) = 1 - \frac{2G(r, k)M}{r}. \quad (12.8)$$

Here r and t are the Schwarzschild radial and time coordinate, M is the mass and $d\Omega^2 = d\theta^2 + \sin^2\theta d\phi^2$ is the line element of the two dimensional sphere. The k -dependent Newton constant is transformed into a r -dependent one. This is done with the identification of the RG scale k with a physical scale by assuming

$$k(r) = \frac{\xi}{d(r)} \quad (12.9)$$

with a constant ξ and a distance function $d(r)$ specified in [297]. This RG improvement leads to the observation that quantum corrections are irrelevant for large masses and thus the semiclassical treatment is trustworthy. Furthermore it is shown that the Hawking radiation stops when the Black Hole reaches a critical lowest mass. Thus a remnant stays as the final state of the evaporation process. Effects of higher derivative terms within the truncation have been considered in [298] and the authors of [299] investigated rotating Black Holes by using the RG-improved Kerr metric. The work [297] was developed further in [300] by considering the evaporation process dynamically and using the Vaidya metric and in [301] a collapsing ball of dust was investigated. There the authors argue that the singularity can be avoided. A very recent investigation of the thermodynamic properties of Black Holes can be found in [302].

However the Black Holes have been just a first playground to investigate phenomenological consequences of the Asymptotic Safety scenario. In [303, 304, 305] the scattering cross section for RG-improved Black Holes was discussed for models with large extra dimensions. This is relevant for Black Hole production scenarios at the Large Hadron Collider. The different collaborations find different results since they are not using the same identification for the RG scale k . This points at the most important issue for RG improvement, the identification of scales. This identification has to be done with as much physical input as possible since the final result is sensitive to the choice. In [306] the author discusses the RG improvement very generally and argues that the identification of scales should be done in the action and not in the equations of motion or the solutions thereof.

The effect of asymptotically safe gravity on further collider signals have been investigated as well. In [307, 308] graviton-mediated Drell-Yan processes have been investigated while large or warped extra dimensions have been assumed. This work was extended in [309]. These processes, where a quark-antiquark pair annihilates to a virtual graviton which goes to a lepton pair are usually suppressed by the Planck scale. However, in higher dimensional models the Planck scale can be lowered to the TeV range and thus these processes become relevant. Instead of Drell-Yan processes, in [310] photon-photon scattering was considered. The influence of asymptotically safe gravity on the Standard Model of particle physics was considered as well to make predictions for the Higgs-boson mass [225, 311]. The results are indeed compatible with the LHC measurements [312].

The fractal properties of spacetime have been investigated for asymptotically safe gravity since they can be compared to other approaches to quantum gravity like Causal Dynamical Triangulations. In [313] it is argued that the spectral dimension of spacetime (the dimension seen by a random walker) is two at the non-Gaussian fixed point. This is a result of the fixed point itself and is independent of the used truncation. Furthermore it is argued that the spectral dimension becomes four in the IR. These investigations have been extended to all scales in [314] and are reconsidered in [315] within a R^2 truncation.

One very popular area we did not mention so far, the cosmology. The first work about asymptotically safe cosmology was [316]. There the authors considered the Robertson-Walker metric

$$ds^2 = -dt^2 + a(t)^2 \left[\frac{dr^2}{1 - Kr^2} + r^2 (d\theta^2 + \sin^2 \theta d\phi^2) \right]. \quad (12.10)$$

Note that here t is not the RG time, but the real time. The dynamics of the scale factor $a(t)$ is determined by inserting the Robertson-Walker metric into Einstein's field equation with scale dependent Newton constant and cosmological constant

$$R_{\mu\nu} - \frac{1}{2}g_{\mu\nu}R = -\Lambda_k g_{\mu\nu} + 8\pi G_k T_{\mu\nu}. \quad (12.11)$$

As a scale identification the authors used $k(t) = \frac{\xi}{t}$. Furthermore they used a homogeneous and isotropic energy-momentum tensor

$$T_\mu^\nu = \text{diag}(-\rho, p, p, p). \quad (12.12)$$

Within this setting it was argued that asymptotically safe cosmology might be free of the horizon and flatness problem of standard cosmology. This work was extended in [317] and the influence of a proposed IR fixed point was investigated in [318, 319].

At the very beginning mainly the effects which appear close to fixed points have been investigated [251]. Later on complete trajectories have been considered which describe our universe [320]. Such a trajectory has to satisfy some constraints. Most importantly a long classical regime is required. It is shown that renormalisation group effects occur not only at small distance scales but also at scales larger than those of the classical regime. Especially the effects on galaxy rotation curves are considered in [321, 322]. These effects might explain the observational data of spiral galaxies without introducing dark matter.

Of course also inflationary scenarios have been investigated. In [323, 324] the authors show how power law inflation might appear due to the RG running of the cosmological constant without introducing an inflaton field. It stops automatically when the RG running has reduced. Nearly exponential expansion was found in [325, 326]. The evolution of cosmological perturbations within such an inflationary scenario was considered in [327] and an extension to $f(R)$ theories was considered in [328]. Here the scale k was considered proportional to the Hubble rate $H(t) = \frac{\partial_t a(t)}{a(t)}$. Starting with the Einstein-Hilbert action and assuming a scale identification $k^2 \propto R$ leads to an effective $f(R)$ type gravity. This was investigated in [329]. A scalar-tensor theory can be reformulated within the $f(R)$ framework as well [330]. Finally, the renormalisation group improved version of a scalar field inflationary scenario was considered in [331] and the inclusion of running matter coupling have been derived as well [332].

Summarising, one can say that lots of evidence has been gathered, that gravity is asymptotically safe. Furthermore, new insight into the technical details as well as to the underlying physics was gained. Finally, phenomenological applications showed that the Asymptotic Safety scenario opens might give alternative explanations to effects like galaxy rotation curves and inflation. Although this sound very promising a lot of work is lying in front of us. Examples for open issues are the debated IR behaviour close to the pole of diverging anomalous dimension or the correct way of implementing the RG improvement.

12.1. Quantum Improved Schwarzschild-(A)dS and Kerr-(A)dS Space-times

The consistent quantisation of gravity is an open challenge to date. One of the candidates is the asymptotic safety (AS) scenario for quantum gravity [125], its attraction being the possible quantum-field theoretical ultraviolet completion of the Standard Model with gravity. If realised, it is the minimal UV closure of high energy physics including gravity within a purely field-theoretical set-up.

One of the prominent and characteristic properties of asymptotically safe gravity is its ultraviolet scaling regime for momentum scales k larger than the Planck scale M_{pl} . In the AS set-up, the latter is defined as the scale beyond which quantum gravity corrections dominate the physics and agrees well with the classical Planck scale. In this regime, the Newton's coupling G and cosmological constant Λ , as well as all further couplings of terms, e.g. of the higher curvature invariants R^n , run according to their canonical scaling. For the Newton's coupling and cosmological constant in particular, this entails $G(k) \propto 1/k^2$ and $\Lambda(k) \propto k^2$ respectively, instead of the classical constant behaviour. Consequently, the physics at these scales looks rather different to that of general relativity.

Black holes offer one of the few possibilities where such deviations from classical general relativity may be observed as they feature large curvatures. Asymptotically safe quantum black holes have been amongst the first applications of asymptotically safe gravity after its first explicit realisation within the functional renormalisation group [165]. Within such a renormalisation group setting, the Newton's coupling and cosmological constant are naturally elevated to couplings running with the momentum (RG) scale k . Then, classical solutions of the Einstein field equations are quantum improved by replacing Newton's and the cosmological constant by functions depending on a respective length scale. The k -dependent RG-runnings, equipped with an identification between momentum and length scales, serve as an ansatz for these functions. The earliest works investigated the Schwarzschild space-time [333, 297] followed by studies of the Kerr space-time [299] and Schwarzschild-(A)dS geometries [334]. Black holes in higher dimensions have been studied in [305]. All works, summarised in [335], match the classical results of general relativity in the low energy limit, but show significant changes for the number of horizons, test particle trajectories, the Hawking temperature, and the entropy around the Planckian regime. There is evidence for a cold, extremal Planck-sized remnant, which is a smallest black hole with zero temperature, a possibly promising answer to the endpoint of black hole evaporation. By studying dynamical, non-vacuum solutions such as the Vaidya space-time, the processes of black hole formation [336] and evaporation [300] can be addressed directly, leading to the same conclusions as above. The quantum effects render the central curvature singularity at $r = 0$ less divergent, some scenarios lead to a complete resolution. A detailed study on the implications for the laws of black hole thermodynamics was performed in [302]. Most of the above results for a quantum improved space-time were obtained by using a cut-off identification based on a classical space-time. This was addressed in [321] and [337], where a consistent framework with an underlying quantum space-time was introduced.

In this work, we present a new scale identification based on the quantum improved classical Kretschmann scalar. This approach takes the running of the couplings into account which removes unphysical features in the resulting geometries. For the first time in this quantum gravity set-up, the Kerr-(A)dS geometry, as the most general vacuum black hole solution including a cosmological constant, is studied in great detail. As a special case ($a = 0$), the results for Schwarzschild-(A)dS are presented separately. The ordinary Schwarzschild and Kerr solutions are also contained by setting the cosmological constant to zero.

This work is structured as follows: we start with a brief review of the AS scenario of quantum gravity in section 12.2, and discuss the studied geometries in section 12.3. The novel scale identification is discussed in section 12.4. Results on horizons and the GR-limit are presented in section 12.5, the global structure in section 12.6, test particle trajectories in subsection 12.6.3, the curvature singularity in section 12.7, and Hawking temperatures and the black hole evaporation process in section 12.8. Some technical details are deferred to the appendices which contain in particular a discussion of proper distance matchings, see appendix G.12.3.

12.2. Asymptotic Safe Quantum Gravity

By now asymptotically safe quantum gravity has been studied in an impressive wealth and depth of approximations including higher derivative terms, the full $f(R)$ potential as well as the inclusion of matter, see e.g. [338, 234, 235, 237, 236, 238] and references therein. The specific shape of the running of $G(k)$

and $\Lambda(k)$ depends on the regularisation scheme or regulator which also defines part of the scale identification. Moreover, despite the advances in the approximation schemes used in recent computations, the systematic error estimates are still relatively large. However, while these details do not affect the results of this work qualitatively, all runnings have to meet the following general constraints:

1. The existence of a UV fixed point, that is, the dimensionless couplings g and λ become constant in the UV-limit:

$$(g, \lambda) \xrightarrow{k \rightarrow \infty} (g_*, \lambda_*) . \quad (12.13)$$

2. The effective theory should recover the classical theory of general relativity in the IR-limit, i.e. G and Λ approach Newton's constant G_0 and a cosmological constant Λ_0 respectively, reducing the effective action to the Einstein-Hilbert action:

$$G, \Lambda \xrightarrow{k \rightarrow 0} G_0, \Lambda_0 \Leftrightarrow g \sim k^2 \text{ and } \lambda \sim k^{-2} . \quad (12.14)$$

The running of $g(k)$ and $\lambda(k)$ is typically obtained numerically. In the following, we approximate them by analytical expressions, which show the same features and are compatible with the above constraints in the UV and IR. For instance, a comparison with the results of the systematic vertex expansion up to the fourth order in [62] is provided in [Figure 12.18](#) in the appendix. The following scale runnings are used,

$$\begin{aligned} g(k) &= \frac{G_0 g_* k^2}{g_* + G_0 k^2} & \Leftrightarrow G(k) &= \frac{G_0 g_*}{g_* + G_0 k^2} , \\ \lambda(k) &= \frac{\Lambda_0}{k^2} + \lambda_* & \Leftrightarrow \Lambda(k) &= \Lambda_0 + \lambda_* k^2 . \end{aligned} \quad (12.15)$$

The functional dependence of $g(k)$ was already used in [297] and $\lambda(k)$ agrees with the expression used in [335] without the logarithmic term. G_0 and Λ_0 are the IR-values of the gravitational and cosmological coupling, whereas g_* and λ_* are the fixed point values of the dimensionless couplings. In the following analysis, we choose the numerical values at the fixed point to be the ones for the background couplings obtained in appendix B of [62], together with their identification scheme in (34):

$$g_* = 1.4 , \quad \lambda_* = 0.1 . \quad (12.16)$$

The dependence of Newton's coupling G and cosmological constant $\Lambda(k)$ on the running scale k reflects the non-trivial dependence of the full effective action at vanishing cutoff scale on the Laplacian Δ , as well as the existence of higher order terms. As in earlier works, we use the following strategy to take into account these terms: we use solutions to the Einstein field equations and assume that quantum gravity effects can be modeled by momentum-dependent G and Λ , equipped with a relation to convert the momentum into a length scale. The now r -dependent G and Λ are inserted back into the classical solution, yielding a quantum improved space-time. This procedure is the analogue of the Uehling's correction in QED, see [339] and [297] for more details. In the context of asymptotically save gravity, it has been shown in [334], that a quantum improved metric in the above sense can be a solution to the field equations derived from the quantum improved Einstein-Hilbert action in the UV-limit, at least in the spherically symmetric case. Furthermore, the quantum improved metric, together with its observables, approach the results obtained from general relativity in the IR, and thus show the correct low energy limit.

In the following we need the couplings $G(r)$ and $\Lambda(r)$ as functions of radius r rather than momentum scale k . Thus, we have to establish a relation $k(r)$ in order to arrive at $G(k(r))$, $\Lambda(k(r))$. A commonly used ansatz for $k(r)$ is

$$k(r) = \frac{\xi}{D(r)} , \quad (12.17)$$

with constant ξ and a r -dependent function D with momentum dimension minus one (length), encoding the physical scales. Our choice $\xi = 1/\sqrt{\lambda_*}$ is further motivated in appendix G.12.1.

12.3. Investigated Geometries

In this work, we study geometries based on solutions of the Einstein equations with cosmological constant, but vanishing stress-energy tensor. Depending on the sign of the cosmological constant, the space-time is called asymptotically de Sitter (dS), flat, or anti-de Sitter (AdS). As the stress-energy tensor is zero, the black hole is allowed to have a mass and angular momentum, but no charge. Thus, we study the Schwarzschild-(A)dS space-time of a non-rotating black hole and the Kerr-(A)dS space-time for a rotating black hole.

The Kerr-(A)dS geometry is the most general vacuum black hole solution, which includes a cosmological constant. Hence the Schwarzschild-(A)dS as well as the Schwarzschild and Kerr solutions in flat space can be obtained from Kerr-(A)dS by either setting the rotations parameter a or the cosmological coupling Λ to zero. In our analysis, we discuss the quantum improved Schwarzschild-(A)dS and Kerr-(A)dS solution, but the results can be easily extended to asymptotically flat space-times. Below we briefly summarise some basic properties of these geometries.

12.3.1. Schwarzschild-(A)dS

The Schwarzschild-(A)dS solution is a two-parameter family of solutions of the non-vacuum Einstein equations, labeled by (M, Λ) . It is explicitly given by

$$\begin{aligned} ds^2 &= -f(r)dt^2 + f^{-1}(r)dr^2 + r^2d\Omega^2, \\ f(r) &:= 1 - \frac{2MG}{r} - \frac{\Lambda}{3}r^2, \end{aligned} \tag{12.18}$$

with $t \in (-\infty, \infty)$, $r \in (0, \infty)$, Newton's constant G , the cosmological constant Λ and $d\Omega^2$ the metric on S^2 . This solution is spherically symmetric and displays a curvature singularity at $r = 0$ if $M \neq 0$. For $\Lambda = 0$, it reduces to the Schwarzschild solution in flat space and for $M = 0$ but $\Lambda \neq 0$, one obtains the metric describing AdS or dS, depending on the sign of Λ . Therefore, this metric interpolates between a Schwarzschild solution on small scales and an (A)dS solution on large scales. Horizons are solutions to $f(r) = 0$.

12.3.2. Kerr-(A)dS

The Kerr-(A)dS solutions form a three parameter family, labelled by (M, J, Λ) . Unlike in the flat case, M and J cannot be interpreted as mass and angular momentum of the black hole anymore, however, for convenience we still refer to them as mass and angular momentum in the text below. The metric is given by [340],

$$\begin{aligned} ds^2 &= -\frac{\Delta_r}{\rho^2 \Xi^2} \left(dt - a \sin^2 \theta d\phi \right)^2 + \frac{\rho^2}{\Delta_r} dr^2 + \frac{\rho^2}{\Delta_\theta} d\theta^2 \\ &\quad + \frac{\Delta_\theta \sin^2 \theta}{\Xi^2 \rho^2} \left(adt - (r^2 + a^2)d\phi \right)^2, \end{aligned} \tag{12.19}$$

with

$$\begin{aligned}
a &:= \frac{J}{M} , \\
\rho^2 &:= r^2 + a^2 \cos^2 \theta , \\
\Delta_r &:= (r^2 + a^2)(1 - \frac{\Lambda}{3} r^2) - 2GMr , \\
\Delta_\theta &:= 1 + \frac{\Lambda}{3} a^2 \cos^2 \theta , \\
\Xi &:= 1 + \frac{\Lambda}{3} a^2 .
\end{aligned} \tag{12.20}$$

The parameter a is referred to as rotation parameter and is restricted by

$$\frac{1}{3}\Lambda a^2 > -1 , \tag{12.21}$$

in order to preserve the Lorentzian signature of the metric. The coordinate ranges are $t \in (-\infty, \infty)$, $r \in (0, \infty)$, $\theta \in [0, \pi]$ and $\phi \in [0, 2\pi]$. It can be shown that this solution reduces to a Kerr black hole in the limit of small r , whereas for large r it gives back the metric of (A)dS. In the case of $a = 0$, one recovers the Schwarzschild-(A)dS metric of a non-rotating black hole (12.18). For $\Lambda = 0$, the metric reduces to the one of a Kerr black hole in flat space. For $M = 0$ and $a = 0$, we recover (A)dS. For $M \neq 0$, there is a curvature singularity at $r = 0$ in the equatorial plane $\theta = \frac{\pi}{2}$. Horizons correspond to solutions of $\Delta_r = 0$.

12.4. Scale Identification

In pure gravity systems, i.e. systems with vanishing stress-energy tensor, there is no unique way to fix the scale identification. In fact, it turns out that physical features of the space-time such as the number of horizons, Hawking temperatures and the strength of the curvature singularity actually do depend on the particular choice of $k(r)$. Motivated by dimensional analysis, one simple way to identify the momentum scale of the FRG set-up with a length scale is an inverse proportionality. However, this ansatz is completely insensitive to typical scales of the underlying space-time. Therefore, different scale setting procedures have been brought forward, for instance on the level of the field equations, e.g. [334]. A more feasible approach to account for space-time features is to use proper distance integrals. As such, they give rise to diffeomorphism invariant quantities. Proper distance integrals based on classical space-times were suggested in [297]. Later, it was pointed out in [321, 337], that this procedure can be upgraded to a consistent setting by computing the proper distance already in the quantum improved geometry.

Here, we investigate this approach for Schwarzschild-(A)dS and Kerr-(A)dS space-times. However, using two different integration contours for the computation of the proper distance in the upgraded scheme yields ill-defined quantities. In case of a radial integration path, we find diverging surface gravities for all horizons. This results in divergent Hawking temperatures, independent of the black hole parameters. In case of a path prescribed by the timelike geodesic of an infalling observer, we find an identically vanishing eigentime. The analysis and results for the proper distances are given in appendix G.12.3.

In light of these results, a different identification scheme is required. Such a scheme has to be based on other diffeomorphism invariant quantities, for example on curvature scalars. In cosmological contexts, the Ricci scalar R has been used [329, 341]. However, the classical Ricci scalar cannot be used, since it vanishes identically for vacuum solutions of the Einstein field equations. Thus, in the following analysis,

we will base our scale identification on the Kretschmann scalar $K = R_{\alpha\beta\gamma\delta}R^{\alpha\beta\gamma\delta}$, a diffeomorphism invariant quantity of momentum dimension four. This motivates the scale identification

$$D_K(r) = \frac{1}{\chi(K - K_\infty)^{1/4}}, \quad (12.22)$$

with a constant χ , chosen to be $\chi = \left(\frac{1}{8}\right)^{1/4}$ in the following calculations, and $K_\infty = K(r = \infty) = 8/3\Lambda_0^2$, using (12.23). We subtract the Kretschmann scalar at $r \rightarrow \infty$, otherwise $D(r)$ would approach a constant in the IR and therefore G and Λ would fail to display the correct IR-limit G_0 and Λ_0 respectively, cf. (12.15). For simplicity, we base the matching on the classical Kretschmann scalar in the equatorial plane ($\theta = \pi/2$). For both, Kerr-(A)dS and Schwarzschild-(A)dS we arrive at

$$K = \frac{8}{3}\Lambda^2 + \frac{48M^2}{r^6}G^2. \quad (12.23)$$

The quantum improved version of the classical Kretschmann scalar (12.23), referred to as K_{qu} , provides a consistent framework accounting for typical scales of the underlying (quantum) geometry. Of course it would be desirable to use the true Kretschmann scalar, computed directly from the quantum improved metric. This is left for future work. On a technical level, the RG-improved version turns (12.22) into a functional equation for $D_K(r)$. In order for this equation to have a positive, real solution, χ must be constrained to $\chi < (3/8)^{1/4}$, such that the expression under the root in the UV-expression in Table G.5 remains positive. In appendix G.12.1, we discuss the impact of χ on the results. Also, the quantum improved version of classical Kretschmann scalar (12.23) approaches the classical version for $r \rightarrow \infty$, but this does not hold for D_K , given by (12.22), because $K_{\text{qu}} \rightarrow K_\infty$ is faster than $K_{\text{cl}} \rightarrow K_\infty$. The curvature near the singularity, the construction of the Penrose diagrams, and the UV-limits for each proper distance are discussed in appendix G.12.5.

12.5. Lapse Function and Number of Horizons

With the running couplings G and Λ from the previous section, physical properties of the quantum improved space-times can be deduced. Central tools are the lapse functions $f(r)$ and $\Delta(r)$, whose roots determine the location of horizons in the space-time. These zeros are shown to be Killing horizons in appendix G.12.2, implying that they can be assigned a constant surface gravity, which turns out to be proportional to the first derivative of the lapse function evaluated at the horizon. This can be used to address thermodynamical processes such as the endpoint of black hole evaporation via Hawking radiation. Another interesting question is that of the similarity of the quantum improved geometry to the classical geometry in general relativity, serving as a metric ansatz for the quantum improvement.

In this section, we will discuss the lapse functions $f(r)$ and $\Delta(r)$ for the Kretschmann matching by determining the number of horizons and comparing them with the lapse functions of general relativity. We first start with asymptotically AdS space-times, i.e. $\Lambda_0 < 0$, and comment on the results for $\Lambda_0 > 0$ subsequently. The results for all other matchings can be found in appendix G.12.3.

12.5.1. Schwarzschild-AdS

Classically, i.e. for constant G & $\Lambda_0 < 0$, the lapse function $f(r)$ shows just one zero corresponding to the event horizon of the black hole, whereas the quantum improved Schwarzschild geometry shows up to two horizons, if a consistent matching is adopted, Figure 12.1. Starting at very large masses, well above the Planck mass, we find two horizons, generated by a minimum of the lapse function. Comparing with the classical lapse function in Figure 12.2 shows that the outer horizon of the quantum improved space-time coincides with the event horizon of the classical black hole. The larger the mass, the better

the agreement and the more the inner horizon moves towards zero. Hence, increasing the mass makes the black holes more classical. Decreasing the mass causes the minimum to shrink and the horizons to move towards each other. There exists a critical mass M_c around two Planck masses, $M_c \approx 2M_{\text{Pl}}$, when the minimum is also a zero of the lapse function. Then, both horizons merge and $f(r)$ has a double root. We will see later, that this geometry is similar to a classical, extreme Reissner-Nordström black hole in AdS. For masses below the critical mass, the minimum is above zero and no horizons are present.

The results for matchings computed in space-times with running couplings agree with the matchings based on space-times with constant couplings on the position of the outer horizon, but differ significantly for smaller radii. These differences emerge because in the latter case, the matching is based on a classical geometry, whereas we actually study a quantum geometry with running couplings. Varying the amplitude for negative Λ_0 does not affect the qualitative results, but changes the scale.

12.5.2. Kerr-AdS

A classical, non-extremal Kerr-AdS space-time has two horizons: a Cauchy horizon inside the black hole event horizon. In contrast to the Schwarzschild case discussed above, the quantum improvement of this space-time does not allow for more horizons than in the classical geometry. Since the proper distances vanish identically in the consistent scenarios, we show only the results for the Kretschmann matching in [Figure 12.3](#) and the dependence on the rotation parameter for fixed mass in [Figure 12.4](#). The results for the linear matching can be found in appendix [G.12.3](#). In general, the consistent quantum improved version displays the same behaviour as the classical solution. However, the inner horizon in the quantum improved space-time is located at larger radii than the classical Cauchy horizon, [Figure 12.5](#).

12.5.3. Asymptotically de Sitter spaces

If we take the space-time to be asymptotically de Sitter, we find the possibility to get up to three horizons. The additional horizon is generated by the positive cosmological constant in the IR and appears in the classical regime at large radii. The typical shapes of $f(r)$ and $\Delta_r(r)$ are displayed in [Figure 12.6 & Figure 12.7](#) for the Kretschmann matching, the dependence on the amplitude of Λ_0 is shown in [Figure 12.8 & Figure 12.9](#). Varying m controls the position of the two inner horizons via the formation of a minimum, whereas Λ_0 governs the location of the outer horizon. Thereby, the interplay of the amplitudes of m and Λ_0 dictates the number of horizons. Although we cannot provide an analytical condition involving m and Λ_0 for the space-time exhibiting three horizons, it is suggestive to see it as the generalised version of the condition for a classical Kerr-dS space-time to have three horizons. This also implies that both quantum improved space-times have two distinct extremal cases: both inner horizons merge at a mass $m = M_*$ yielding an extremal black hole inside the cosmological horizon. Or both outer horizons merge at $m = M^*$, forming the largest Schwarzschild/Kerr-dS black hole possible, analogous to the Nariai space-time.

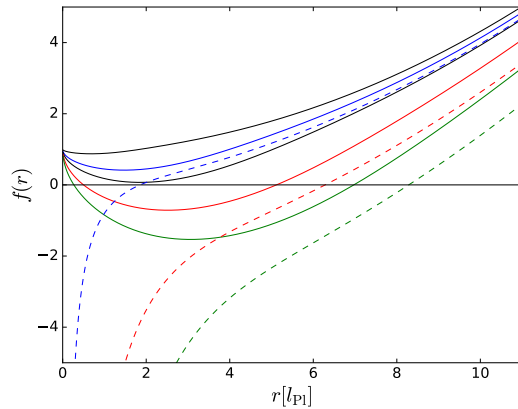


Figure 12.1.: $f(r)$ from (12.18) based on the Kretschmann scalar matching for increasing mass from top to bottom. Results based on the quantum improved Kretschmann scalar are given by solid curves, whereas results based on the classical Kretschmann scalar are dashed. The parameters are $\Lambda_0 = -0.1$ and $M = 0.1, 1, 2, 5, 9M_{\text{Pl}}$. Curves of the same mass have the same colour.

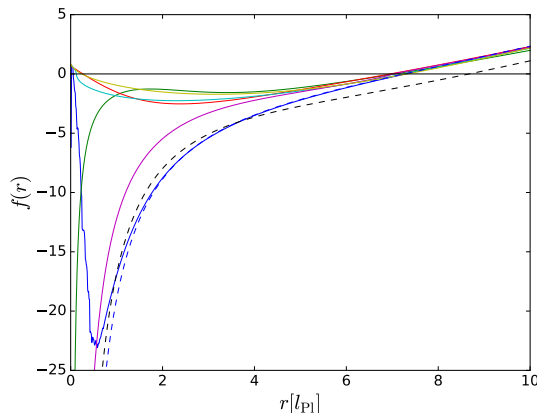


Figure 12.2.: Comparison of $f(r)$ for all matchings with the classical result from general relativity for $M = 10M_{\text{Pl}}$ and $\Lambda_0 = -0.1$. Matching based on the quantum geodesic in dark blue, classical geodesic in dark green, quantum radial path in light blue, classical radial path in purple, quantum Kretschmann scalar in light green, classical Kretschmann scalar in dashed black, linear matching in red and the result from general relativity in dashed dark blue. All matchings, apart from the classical Kretschmann setting, agree with the classical position of the outer black hole horizon.

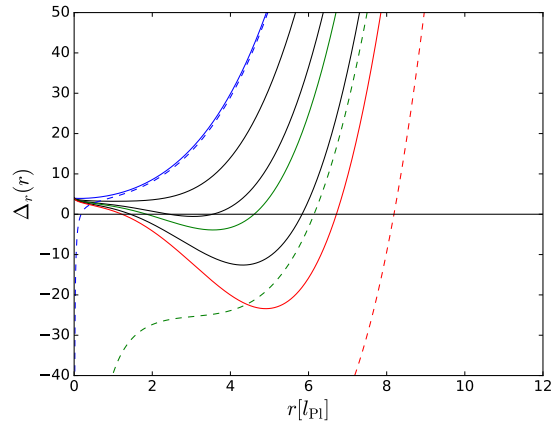


Figure 12.3.: $\Delta_r(r)$ from (12.20) based on the Kretschmann scalar matching for increasing mass from top to bottom. Results based on the quantum improved Kretschmann scalar are given by solid curves, whereas results based on the classical Kretschmann scalar are dashed. With parameters $\Lambda_0 = -0.1$, $a = 2$ and $M = 0.1, 2, 4, 5, 7, 9M_{\text{Pl}}$. Curves of the same mass have the same colour.

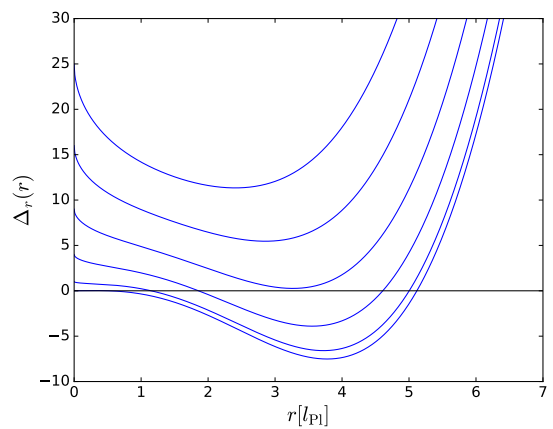


Figure 12.4.: $\Delta_r(r)$ based on the quantum Kretschmann scalar matching for fixed mass $M = 5M_{\text{Pl}}$ and $\Lambda_0 = -0.1$, but increasing $a = 0, 1, 2, 3, 4, 5$ from bottom to top.

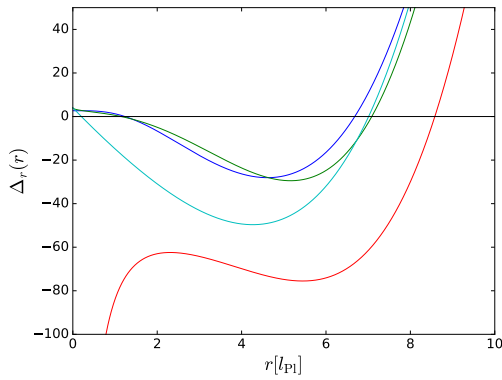


Figure 12.5.: Comparison of $\Delta_r(r)$ for the linear matching in dark blue, the classical Kretschmann setting in red, the quantum Kretschmann setting in green and the classical result from general relativity in light blue, with $M = 10M_{\text{Pl}}$, $a = 2$ and $\Lambda_0 = -0.1$. Apart from the classical Kretschmann setting, all other matchings agree with the classical position of the outer horizon.

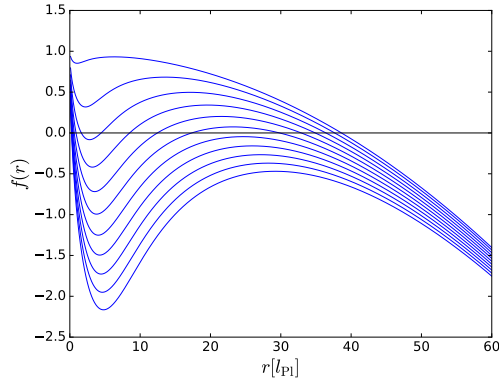


Figure 12.6.: $f(r)$ for asymptotic dS with $\Lambda_0 = 0.001$ for increasing mass $M = 0.1, 1, 2, 3, 4, 5, 6, 7, 8, 9, 10M_{\text{Pl}}$ from top to bottom.

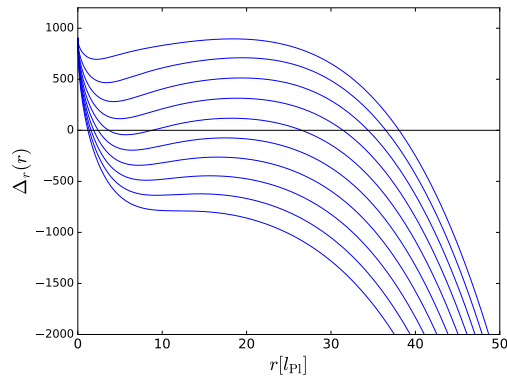


Figure 12.7.: $\Delta_r(r)$ for asymptotic dS with $\Lambda_0 = 0.001$ and $a = 30$ for increasing mass $M = 1, 3, 5, 7, 9, 11, 13, 15, 17, 19M_{\text{Pl}}$ from top to bottom.

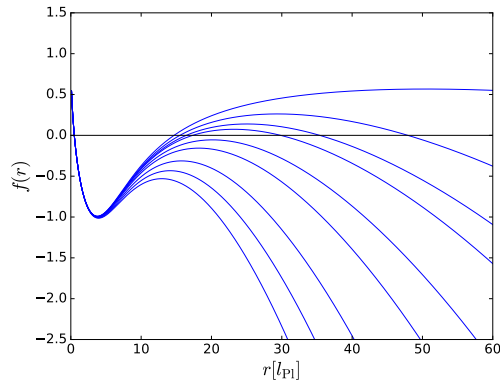


Figure 12.8.: $f(r)$ for asymptotic dS for increasing $\Lambda_0 = 0.0001, 0.0005, 0.0008, 0.001, 0.0015, 0.002, 0.003, 0.004, 0.005$ from top to bottom and fixed mass $M = 5M_{\text{Pl}}$.

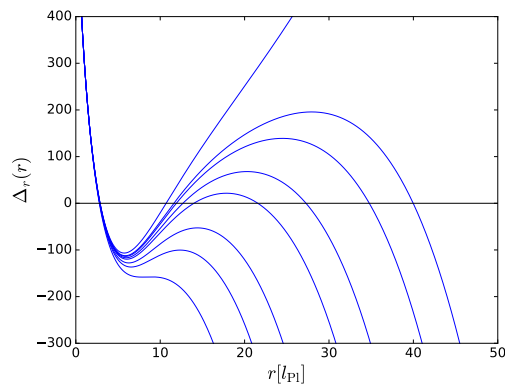


Figure 12.9.: $\Delta_r(r)$ for asymptotic dS for increasing $\Lambda_0 = 0.0001, 0.0005, 0.0006, 0.0007, 0.0009, 0.0015, 0.002, 0.003$ from top to bottom. Fixed mass $M = 5M_{\text{Pl}}$ and $a = 30$.

12.6. Global Structure, Penrose Diagrams and Particle Trajectories

In contrast to the classical Schwarzschild-(A)dS and Kerr-(A)dS geometries of general relativity, the quantum improved counterparts can exhibit a different number of horizons and hence may show a different global structure, depicted in terms of Penrose diagrams. It turns out that both geometries, i.e. one based on the Schwarzschild and the other on the Kerr metric, have the same Penrose diagram. The resulting diagram is equivalent to the classical Reissner-Nordström or Kerr geometry. Hence, the quantum improvements of the metric lead to a unified global structure for quantum improved black hole space-times based on solutions of the Einstein field equations. Yet, as it is shown in section [subsection 12.6.3](#) below, particles move differently in each geometry.

We start by determining whether the singularity is time-like, space-like or null. To that end we compute the norm of the normal vector of a hypersurface of constant r in the limit $r \rightarrow 0$. The norm turns out to be the rr -element of the inverse metric g^{rr} , yielding

$$g_{\text{Sch}}^{rr} \stackrel{r \rightarrow 0}{=} 1 \quad \& \quad g_{\text{Kerr}}^{rr} \stackrel{r \rightarrow 0}{\rightarrow} \frac{1}{\cos^2 \theta}. \quad (12.24)$$

Hence, the singularity is time-like in both cases, irrespective of whether the space-time is asymptotically AdS or dS. As it is shown in appendix [G.12.2](#), zeros of f and Δ_r correspond to Killing horizons. The succession of sign changes of the lapse function dictates how the hypersurfaces of constant r change from time-like over null to space-like.

12.6.1. Asymptotically anti-de Sitter space-times

The lapse function of Schwarzschild-AdS and the Kerr-AdS space-time share the same qualitative features, resulting in the same Penrose diagram. The formal construction of the maximally extended space-time works the same as for the classical Kerr space-time, for instance see [342, 340], but now with an asymptotic AdS-patch. For a mass larger than the critical mass M_c , the lapse function has two distinct roots, so the space-time exhibits two horizons, [Figure 12.10](#). When $m = M_c$, both roots coincide and we find an extremal black hole with just one horizon. For even lower masses, that is $m < M_c$, no horizon is present, but the singularity still exists, cf. [section 12.7](#), leaving a space-time with a naked singularity. Later, via a heuristic argument, we will argue that this unphysical space-time cannot be formed by gravitational collapse.

12.6.2. Asymptotically de Sitter space-times

The results for the Schwarzschild- and Kerr-dS geometries agree with each other. The space-time exhibits two distinguished masses, $M_* < M^*$, at which two of the possible three horizons merge. Starting with $M_* < m < M^*$, the space-time has three distinct horizons, two of them are associated with the black hole and one with the positive cosmological constant on large scales, [Figure 12.11](#). This case is equivalent to the classical Kerr-dS geometry. For $m = M^*$, the outer black hole horizon and the cosmological horizon merge. This leaves an extremal space-time containing a maximally sized black hole, [Figure 12.12](#), similar to the Nariai space-time. For even larger masses, there is just one horizon left, [Figure 12.13](#). On the other end, the de Sitter space-time contains an extremal black hole if $m = M_*$. For $m < M_*$, we have a de Sitter geometry containing singularity, which is naked for observers within the cosmological horizon. The construction of the maximally extended space-time is analogous to the one for the classical Kerr-dS case, described for instance in [340].

12.6.3. Particle Trajectories

In order to investigate whether particles propagate differently in the quantum space-times as compared to general relativity, we study their trajectories. Although most new effects in quantum improved space-

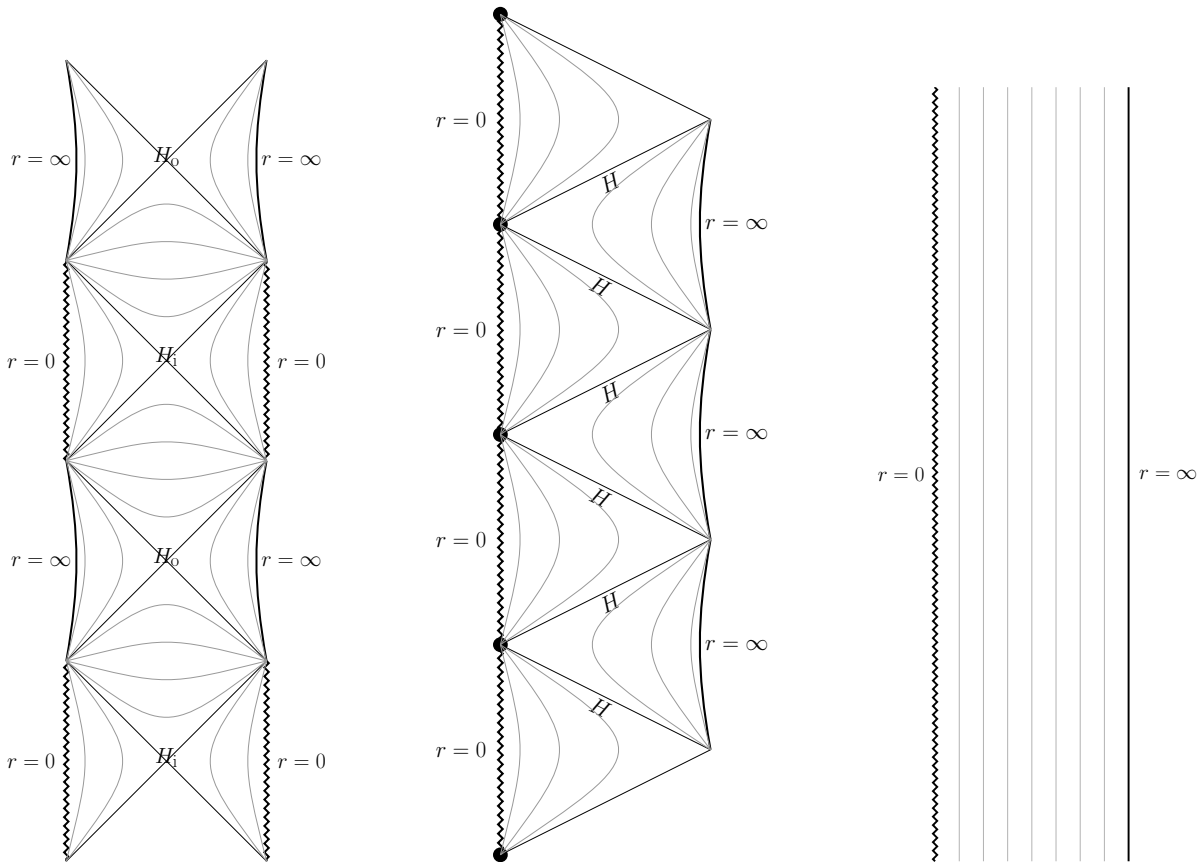


Figure 12.10.: Penrose diagrams for quantum improved Schwarzschild- and Kerr-AdS space-times. hypersurfaces $r = \text{const.}$ are drawn in grey, each diagram can be further extended in vertical direction. To the left the Penrose diagram for the non-extremal black hole with outer horizon H_o and inner horizon H_i , the timelike singularity ($r = 0$) and conformal infinity ($r = \infty$). In the middle the diagram for the extremal geometry with just one horizon H . The black dots are not part of the singularity. To the right, the diagram for AdS with a naked singularity at $r = 0$.

times happen around the Planck scale, there are possibly deviations from classical trajectories already on length scales well above. Our set-up in the following is a test mass with zero angular momentum L along its (timelike) geodesic in a non-extremal geometry, neglecting all backreactions. Furthermore, we are allowed to restrict the motion to the equatorial plane, see [343] for more details. In order to classify orbits into categories, for instance orbits terminating at the central curvature singularity or bound ones, it suffices to study only the change of the radial coordinate.

Schwarzschild

In the quantum improved Schwarzschild geometry, the equation for the radial motion of a test mass, starting with zero angular momentum L at some distance r with energy E , reads according to (G.124)

$$\dot{r}^2 = E^2 - f(r) , \quad (12.25)$$

where \dot{r} denotes the change of the radial coordinate along the geodesic parametrised by the eigentime. This equation is only dependent on r and can be thought of as an energy equation per unit mass for the total energy E of the test particle in an effective, one-dimensional potential $f(r)$. As was already found

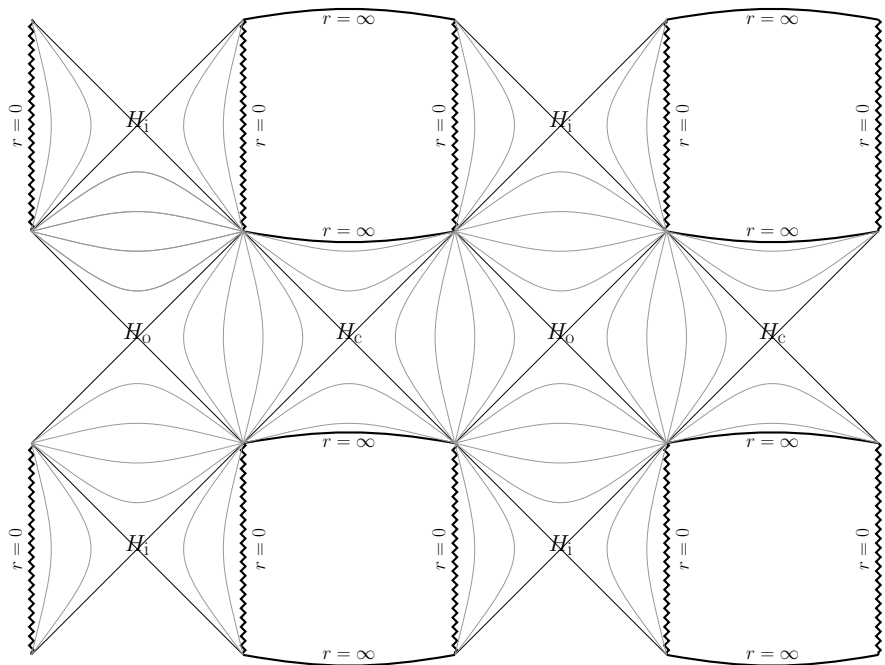


Figure 12.11.: Penrose diagram for quantum improved Schwarzschild- and Kerr-dS geometry with the three horizons of a non-extremal black hole configuration. Starting at the timelike singularity at $r = 0$, we first cross the inner horizon H_i and then the outer horizon H_o before crossing the cosmological horizon H_c and reaching conformal infinity $r = \infty$. This diagram can be further extended into all directions. Again, $r = \text{const.}$ hypersurfaces are depicted by grey curves.

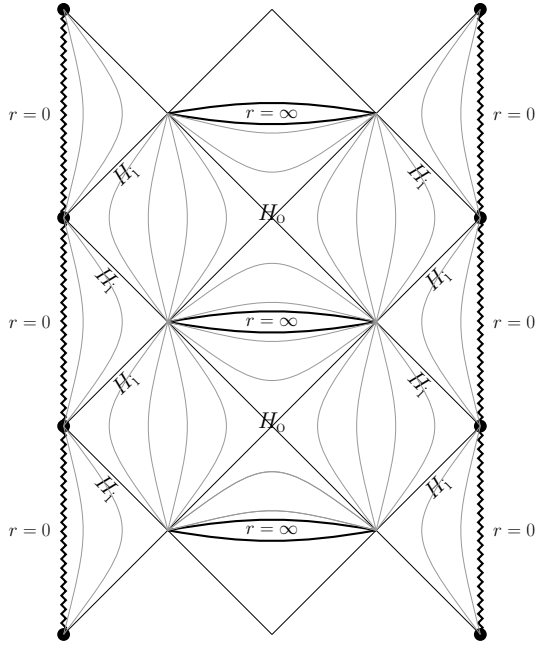


Figure 12.12.: Penrose diagram for quantum improved Schwarzschild- and Kerr-dS geometry with the two horizons of an extremal black hole configuration. Starting at the curvature singularity at $r = 0$, we first cross the inner horizon H_i and then the outer one H_o , before arriving at conformal infinity $r = \infty$. This diagram can be further extended to the top and bottom as well. The black dots are not part of the singularity. The displayed pattern of the $r = \text{const.}$ hypersurfaces is the one for $m = M^*$. For $m = M_*$, the hypersurfaces between the horizons become spacelike.

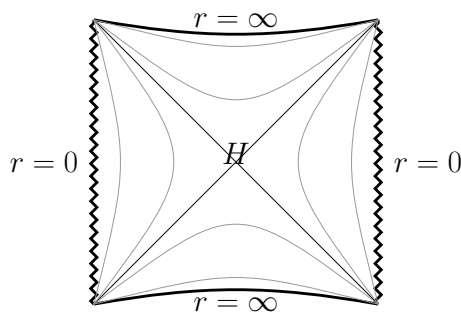


Figure 12.13.: Penrose diagram for the quantum improved Schwarzschild- and Kerr-AdS configuration showing only one horizon H , always shielding the singularity at $r = 0$ from an observer near conformal infinity $r = \infty$.

in [297] for the asymptotically flat case, possible trajectories are the same as in the classical Reissner-Nordström scenario, thereby differing significantly from a classical Schwarzschild set-up. The only difference to the asymptotically flat case arises at large scales, where the effective potential $f(r) \rightarrow \pm\infty$, depending on whether the space-time is asymptotically de Sitter or anti-de Sitter. Recalling the shape of $f(r)$, e.g. [Figure 12.1](#), we note that the effective potential is repulsive close to the singularity. In an asymptotically AdS geometry and for a test mass with energy E , the following options are possible, all being bound orbits in radial direction:

1. If E equals the minimum of the lapse function f_{\min} , then the particle is on a circular, stable orbit in the region between the horizons. The radius is determined by the distance where the repulsive singularity balances the repulsive negative asymptotical cosmological constant.
2. For $f_{\min} < E < 0$, the particle is on a bound orbit, remaining in the region between both horizons.
3. If $0 < E < 1$, the orbit will again be bound, but now the particle periodically crosses horizons. For instance, first starting in the region outside of the outer horizon, the trajectory will first cross the outer horizon, then the inner one. Because it cannot overcome the repulsive barrier of the singularity, it is bounced back and the radius is increasing again. By crossing another horizon, it will end up in an identical patch of the extended space-time. This motion continues indefinitely and the particle will travel through infinitely many universes. We will comment on the physicality of this scenario at the end of this section.
4. If $E > 1$, the energy of the particle can overcome the potential barrier and manages to approach the singularity at $r = 0$ with non-zero kinetic energy. But in contrast to the classical Schwarzschild-AdS scenario, the particle again follows a path through infinitely many identical universes, reaching the singularity in each of them.

For the case of a non-extremal black hole with asymptotic de Sitter patch, we note that the maximum f_{\max} is always smaller than one. Therefore, we find scenarios one and two from above, but also some differences:

5. The case $0 < E < f_{\max}$ admits a bound orbit, equivalent to scenario three with the outer turning point of the particle being located between the cosmological and the outer black hole horizon, as well as an unbound one beyond the cosmological horizon.
6. For $E = f_{\max}$, the particle is at rest at the distance, where the attracting force of the black hole balances the attraction generated by the positive cosmological constant on large scales. This is an unstable equilibrium, since small perturbations cause the particle either to move inwards in a similar way to five, or to escape to infinity.
7. In contrast to all above cases, the orbit is unbound in radial direction for $E > f_{\max}$, and the particle can escape to infinity. Depending on whether or not $E \geq 1$, it can reach the singularity at $r = 0$.

Kerr

The equation for the change of the radial coordinate along the geodesic of a test particle with energy E and zero angular momentum L in the equatorial plane of the Kerr geometry reads (cf. (G.130)),

$$\dot{r}^2 = R(r) := \frac{E^2 \Xi^2 [(r^2 + a^2)^2 - a^2 \Delta_r] - r^2 \Delta_r}{r^4}, \quad (12.26)$$

where we introduced the function $R(r)$ for convenience. For a fixed geometry (G_0, Λ_0, M, a) , the energy E of the particle determines the allowed orbits. In the following, we continue closely along the more detailed analysis of the classical Kerr-(A)dS geometry carried out in [343]. Since the above equation is quadratic in \dot{r} , geodesics always have to satisfy $R(r) \geq 0$. A simple root of $R(r)$ corresponds to a turning point, where the particle comes to rest. A circular orbit of constant $r = r_0$ requires both \dot{r} and \ddot{r} to vanish at r_0 , translating via equation (12.26) into the condition of $R(r)$ having an extremum as well as a zero at r_0 . Depending on whether this extremum is a maximum or minimum, the circular orbit will be stable or unstable. Hence, $R(r)$ having at least a double zero at r_0 is a sufficient condition for a circular orbit.

The function $R(r)$ for Kerr-AdS is displayed in Figure 12.14. At large radii, the repulsiveness of the effective AdS space-time prevents particles from escaping to infinity. There exists a special energy E_0 , above which observers inevitably fall into the singularity along a terminating orbit. For $E = E_0$, three types of orbits are possible. $R(r)$ exhibits a double zero at r_0 , allowing for an unstable, circular orbit. For radii larger than r_0 , we find a bound orbit, crossing both horizons. Particles starting at $r < r_0$ are accelerated along terminating trajectories and will end up in the singularity. However, if $E < E_0$, the double root splits and we find the possibility of having bound orbits as well as terminating ones at radii below the inner horizon. For the smallest energies, $E \rightarrow 0$, the particle moves from horizon to horizon. The only difference for Kerr-dS compared to the AdS case, is that particles can always escape to infinity, see Figure 12.15.

The trajectories have been calculated for an idealised, pointlike observer, neglecting any backreaction on the geometry. However, the location of the inner horizon is typically at about the Planck scale, where backreaction effects should be taken into account. The quantum improved Schwarzschild case turns out to be similar to the classical Reissner-Nordström space-time, for which it was shown that there is a blueshift instability at the inner (Cauchy) horizon. Additionally, it was shown in [344], that perturbations of initial data cause the Cauchy horizon to be replaced by a null singularity. Due to the similarities between the quantum improved Schwarzschild and the classical Reissner-Nordström space-time, it is tempting to speculate that the classical findings might also hold for the quantum case. Hence, one has to take the above results with care, especially the many world trajectories. Summarising, there are differences between the classical and the quantum improved geometry, but they only become relevant at very small length scales, where the results have to be taken with a grain of salt.

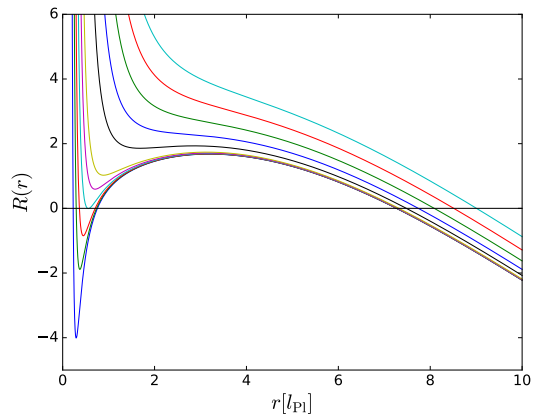


Figure 12.14.: $R(r)$ from (12.26) for Kerr-AdS with $G_0 = 1, \Lambda_0 = -0.1, M = 10M_{\text{Pl}}, a = 1$ and increasing particle energy E from bottom to top.

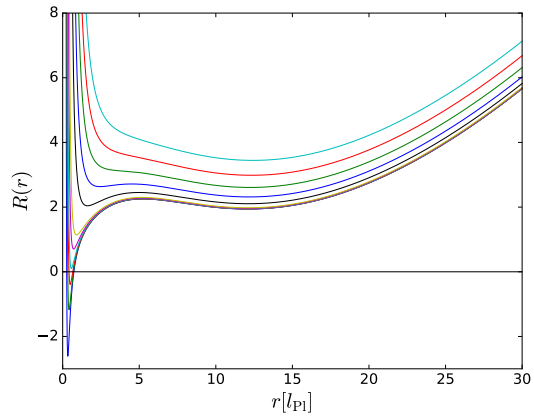


Figure 12.15.: $R(r)$ from (12.26) for Kerr-dS with $G_0 = 1, \Lambda_0 = 0.01, M = 10M_{\text{Pl}}, a = 1$ and increasing particle energy E from bottom to top.

12.7. Curvature Singularity & Effective Energy-momentum Tensor

Since quantum gravity effects become important in high curvature regimes, it is expected that they alter the nature of the curvature singularity at $r = 0$. Previous results from asymptotic safe quantum gravity [335, 305, 334] and other quantum gravity scenarios, e.g. [345], predict a substantial weakening of the singularity or even its disappearance. A weakening of the singularity manifests itself for instance in changes of the Kretschmann scalar. We compute the Ricci scalar R as well as the Kretschmann scalar K of the quantum improved geometries in the UV fixed point regime, and compare the findings with the classical result of general relativity. Table 12.1 lists the highest degree of divergence of the Ricci and Kretschmann scalar for both investigated geometries for all discussed matchings. Upon comparison with the classical result of general relativity, the consistent quantum scenarios display a weakening of the singularity but not a complete resolution.

In the quantum improved space-times, the Ricci scalar is diverging too, because we have changed the geometry which is not a vacuum solution of the Einstein field equations anymore. In fact, it is a geometry with an effective energy-momentum tensor [330], induced by the running couplings. Using the classical field equations, this effective energy-momentum tensor $T_{\mu\nu}^{\text{eff}}$ can be computed by calculating the Einstein tensor $G_{\mu\nu}$ from the quantum improved metric,

$$G_{\mu\nu} + \Lambda_0 g_{\mu\nu} =: 8\pi G_0 T_{\mu\nu}^{\text{eff}} . \quad (12.27)$$

Note that $T_{\mu\nu}^{\text{eff}}$ is covariantly conserved, assuming a metric connection, $\nabla^\mu g_{\mu\nu} = 0$, because the Einstein tensor satisfies the Bianchi identity $\nabla^\mu G_{\mu\nu} = 0$ by construction. However, physical interpretations of this effective energy-momentum tensor in terms of matter have to be drawn with great care. For instance, it turns out that the T_{rr}^{eff} is diverging at horizons, $f(r) = 0$, because $G_{rr} = \frac{f^{-1} + rf'}{fr^2}$ and $g_{rr} = 1/f(r)$. Additionally, it has been shown in [299], that $T_{\mu\nu}^{\text{eff}}$ in the quantum improved flat Kerr geometry violates the weak, the null, the strong and the dominant energy condition. We expect similar results in the present case, including the cosmological constant. These observations suggest that quantum gravity contributions to the energy-momentum tensor are of a fundamentally different nature than the ones of conventional matter and should not be interpreted as matter. In fact, the running couplings should be taken into account already on the action level, resulting in different field equations. This is done for example in Quantum Einstein Gravity (QEG) [235], based on the quantum improved Einstein Hilbert action

$$S = \int d^4x \sqrt{-g} \left[\frac{R - 2\Lambda(r)}{16\pi G(r)} \right] . \quad (12.28)$$

The resulting new field equations [251], based on the runnings (12.15), read the same as (12.27) with

$$8\pi G_0 T_{\mu\nu}^{\text{eff}} = -\lambda_* k^2(r) g_{\mu\nu} + G(r)(\nabla_\mu \nabla_\nu - g_{\mu\nu} \square) \frac{1}{G(r)} . \quad (12.29)$$

It has been shown in [346], that the covariant conservation of the effective energy-momentum tensor in QEG is equivalent to the following relation between the running couplings,

$$R \nabla_\mu \left(\frac{1}{G(r)} \right) - 2\nabla_\mu \left(\frac{\Lambda(r)}{G(r)} \right) = 0 . \quad (12.30)$$

This relation is not satisfied by our quantum improved Schwarzschild-(A)dS and Kerr-(A)dS metrics, meaning that they are not solutions to the new field equations (12.27) with (12.30), derived in the Einstein-Hilbert truncation of a potentially more complicated fundamental action.

	classical	cl. Kretschmann	qu. Kretschmann	linear	cl. radial path	qu. radial path	cl. geodesic	qu. geodesic
R_{Sch}	$4\Lambda_0$	$\sim \text{const}$	$\sim r^{-3/2}$	$\sim r^{-2}$	$\sim \text{const}$	$\sim r^{-2}$	$\sim \text{const}$	$\sim r^{-3/2}$
K_{Sch}	$\sim r^{-6}$	$\sim r^{-6}$	$\sim r^{-3}$	$\sim r^{-4}$	$\sim r^{-6}$	$\sim r^{-4}$	$\sim r^{-6}$	$\sim r^{-3}$
R_{Kerr}	$4\Lambda_0$	$\sim r^{-3}$	$\sim r^{-2}$	$\sim r^{-4}$	$\sim r^{-4}$	—	$\sim r^{-4}$	—
K_{Kerr}	$\sim r^{-6}$	$\sim r^{-6}$	$\sim r^{-4}$	$\sim r^{-8}$	$\sim r^{-8}$	—	$\sim r^{-8}$	—

Table 12.1.: Ricci scalar R and Kretschmann scalar K for Schwarzschild- and Kerr-AdS for different matchings compared to the classical result.

12.8. Horizon Temperatures and Black Hole Evaporation

In this section, we first establish the fact, that surface gravities in space-times based on the quantum improved version of the radial path proper distance are divergent, before discussing the Hawking temperatures in the Kretschmann scenario. Finally, we will discuss implications on the black hole evaporation process.

The Hawking temperature of a black hole in flat space received by an observer at infinity is given by $T_H = \frac{\kappa}{2\pi}$ [347], with surface gravity κ of the event horizon. For an observer at finite distance r in the static region outside the black hole, the above expression is modified by a redshift factor,

$$T_H = \frac{\kappa}{2\pi} \frac{1}{\sqrt{g(K, K)}} , \quad (12.31)$$

where $g(K, K)$ is the norm of the static Killing vector K . In more general terms, a surface gravity can be assigned to any Killing horizon of a space-time. Gibbons and Hawking showed in [340], that cosmological horizons also emit radiation which can be detected by an observer in the static space-time region. In general, emission is a consequence of the observer not being able to access the space-time hidden behind the horizon(s), thereby being fundamentally unable to measure the quantum state of the complete universe (see [340] for a more detailed discussion). The notion of a horizon temperature only appears to be meaningful for observers in a static space-time region, since only such observers detect radiation of this temperature. Taking Reissner-Norström as example, this is only the case for the region outside the black hole. In between the horizons, the space-time is not static anymore and inside the inner horizon, the space-time is static again, but connected to the singularity. This would require to impose boundary conditions at the singularity, being far from obvious. Hence in the following, we only refer to a horizon having a temperature, if the horizon is the boundary of a static region, not connected to the singularity. In appendix G.12.2, horizons in the quantum improved space-time are shown to be Killing horizons, thus a surface gravity can be assigned to each of them.

Technically, the surface gravity κ of a Killing horizon can be computed by taking the covariant derivative of the norm of the Killing vector, or alternatively via a periodicity in Euclidean time introduced in [348]. In any case, we find

$$\kappa_{\text{Sch}} = \frac{1}{2} |f'(r_0)| \quad \& \quad \kappa_{\text{Kerr}} = \frac{1}{2} \frac{|\Delta'_r(r_0)|}{(r_0^2 + a^2)} , \quad (12.32)$$

r_0 being the radial coordinate of the horizon. Since horizons are zeros of $f(r)$ and $\Delta_r(r)$ respectively, (G.112) implies that the derivative of the proper distance $D'(r)$ diverges at the horizons for the quantum version of the radial path. As addressed in appendix G.12.4 in detail, this does not necessarily mean that

the proper distance itself is diverging at a horizon, unless the horizon is extremal. But computing the surface gravity explicitly via (12.32) generates the following terms, proportional to $D'(r)$, and therefore diverging at the horizons,

$$f'(r) \sim \frac{2}{3r^2} \left(-\frac{6G_0^2 g_* \lambda_* M r D(r)}{(g_* \lambda_* D^2(r) + G_0)^2} + \frac{r^4}{D^3(r)} \right) D'(r),$$

$$\Delta'(r) \sim \left(\frac{2r^2 (a^2 + r^2)}{3D^3(r)} - \frac{4G_0^2 g_* \lambda_* M r D(r)}{(g_* \lambda_* D^2(r) + G_0)^2} \right) D'(r). \quad (12.33)$$

The terms in the brackets are in general non-vanishing at the horizons. In particular, this holds also for arbitrary large masses in the classical regime, where it is known that the surface gravity and Hawking temperature stays finite. This is the main reason why we consider the scale identification based on the quantum radial path as unphysical. In contrast, along with the proper distance based on a geodesic, the construction based on the Kretschmann scalar shows no divergent behaviour at the horizons and therefore leads to finite Hawking temperatures.

Next, we discuss the mass dependence of the surface gravities, focusing on the quantum Kretschmann scenario from now on. It suffices to look at the slope of the lapse function at each horizon, since it is proportional to the surface gravity. The results for Schwarzschild-AdS and Schwarzschild-dS can be found in [Figure 12.16](#) and [Figure 12.17](#), the plots for the Kerr cases are qualitatively the same. The whole evolution, appearance and disappearance of horizons is driven by the formation of a minimum of the lapse function. The quantum improved Schwarzschild-AdS space-time exhibits no horizon up to the critical mass $M_c \approx 1.2M_{Pl}$. At $M = M_{crit}$, the minimum of the lapse function is at zero, hence the slope is zero and so are the surface gravities. For growing mass, the slope becomes steeper because the minimum expands, thus the surface gravities grow in amplitude. In contrast, κ_{cl} in general relativity diverges for $M \rightarrow 0$. However, the surface gravity of the outer horizon matches the classical one for sufficiently large masses. The Schwarzschild-dS scenario can have up to three horizons and two special masses, $M_* \approx 2M_{Pl}$ and $M^* \approx 5.8M_{Pl}$, at which two of the three horizons merge. Starting in the $M < M_*$ regime, there is no black hole, but only the cosmological horizon. The case $M = M_*$ corresponds to the case $M = M_c$ from above. For $M_* < M < M^*$, there are three horizons and the back hole gets bigger for increasing mass, until $M = M^*$, when the black hole has reached its maximal size and its outer horizons merges with the cosmological horizon to an extremal horizon with zero temperature.

In AdS space-times, an observer in the static region could only measure a temperature coming from the black holes' event horizon, whereas in dS space-times, the observer would measure a mixture of two thermal spectra at different temperatures, one coming from the back hole and one from the cosmological horizon. In the static region outside the black hole, one valid choice for the Killing vector in (12.31) is $K = \partial/\partial t$, yielding $g(K, K) = g_{tt}$. In the Schwarzschild geometries, this implies that an observer located at a horizon would measure an infinite temperature, in accordance with general relativity. In Schwarzschild-AdS, the temperature drops to zero for an infinitely distant observer, as g_{tt} diverges.

In the dS-scenario, there exists a distance between the horizons, at which the observed temperature becomes minimal, s because f has a maximum. In the Kerr geometries, $\partial/\partial t$ is timelike only outside the ergoregion. A static Killing vector field for the entire region outside the black hole can be obtained by linearly combining the two Killing vectors of a Kerr space-time, see appendix [G.12.2](#). Since all above observations equally apply for classical as well as quantum improved space-times, the is no qualitative difference for an observer measuring horizon temperatures in a classical or a quantum space-time, except in the Planckian regime.

As final point, we would like to address the black hole evaporation process. A standard mechanism to form black holes is gravitational collapse. If the mass of a collapsing object is larger than the Tolman-Oppenheimer-Volkoff mass around $2M_\odot$, no other force can counterbalance gravity and the object collapses to form a black hole. Assuming that a macroscopic Schwarzschild or Kerr black hole has formed

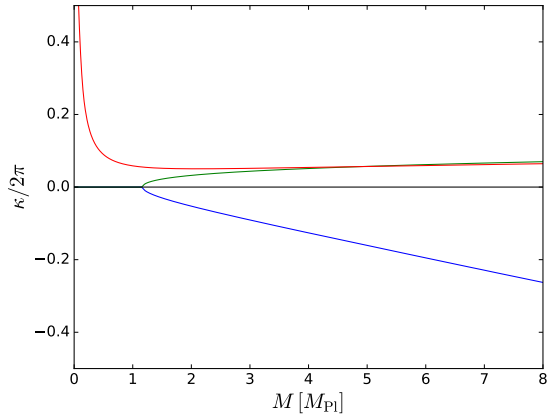


Figure 12.16.: $f'(r)$ as function of the mass M for the quantum improved Schwarzschild-AdS geometry for $\Lambda_0 = -0.1$. Inner horizon in blue, outer horizon in green. The outer horizon agrees with the temperature of the event horizon in general relativity in red for large masses. Taking absolute values yields the surface gravities.

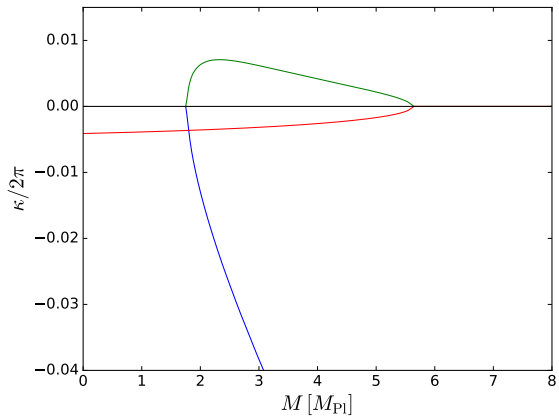


Figure 12.17.: $f'(r)$ as function of the mass M for the quantum improved Schwarzschild-dS geometry for $\Lambda_0 = 0.001$. The cosmological horizon in red, the inner black hole horizon in blue and the outer black hole horizon in green. Taking absolute values yields the surface gravities.

via this process, well above the critical mass, it will emit Hawking radiation and thereby lose energy. This causes the black hole to shrink steadily, as its mass is decreasing. This process continues, until the critical mass M_{crit} is reached. The temperature then becomes zero and therefore the radiation stops. Hence, the naked singularity case with $M < M_{\text{crit}}$ can never be reached via this process and we end up with a zero temperature, Planck-sized, extremal black hole, often referred to as remnant. This remnant serves as shield, guaranteeing that the cosmic censorship conjecture remains satisfied. However, in [349] it was shown that extremal black hole configurations with zero temperature suffer from an instability at the extremal horizon. Remnant endpoints were also found in other studies within asymptotic safety [300, 305] and beyond [350]. Based on a classical expression for the proper distance it has been shown in [334, 335] that the Schwarzschild-AdS black hole evaporates completely. A more suitable set-up to discuss the evaporation process is given by the dynamical Vaidya space-time, used in [300]. There, a Planck-sized, cold remnant as endpoint has been found.

12.9. Summary

In this work, the quantum improved Kerr-(A)dS black hole was studied for the first time within a self-consistent scale identification procedure. The latter is based on the Kretschmann scalar. The Kerr-(A)dS geometry also includes the Schwarzschild-(A)dS, as well as ordinary Schwarzschild and Kerr space-times as special cases, by setting either the rotation parameter a or the cosmological constant Λ_0 to zero.

Both quantum improved geometries show the same global structure in terms of a timelike curvature singularity at $r = 0$ and the same number of horizons. Furthermore, it has also been shown that the outer black hole horizon corresponds to the classical black hole event horizon. The timelike character of the singularity at $r = 0$ in principle allows particles to avoid the singularity. The quantum corrections to the classical metric render the singularity less divergent, but none of the studied scenarios was able to resolve it completely. However, this singularity will always be dressed by a horizon, such that there is no violation of the cosmic censorship conjecture.

The horizons being Killing horizons admit a temperature, causing the black hole to evaporate. In the Planckian regime, however, the heat capacity of a tiny black hole stays positive, $\frac{\partial T}{\partial M} > 0$, in contrast to the classical case. Thus, the evaporation process comes to an end when the Hawking temperature of the black hole is zero, leaving an extremal, cold, Planck-sized remnant, serving as cosmic censor. This is a thermodynamically stable endpoint, because any additional mass absorbed by the black hole will radiate away until the temperature is again zero. It would be interesting to see what implications for the black hole information paradox can be drawn from the generic existence of such remnants.

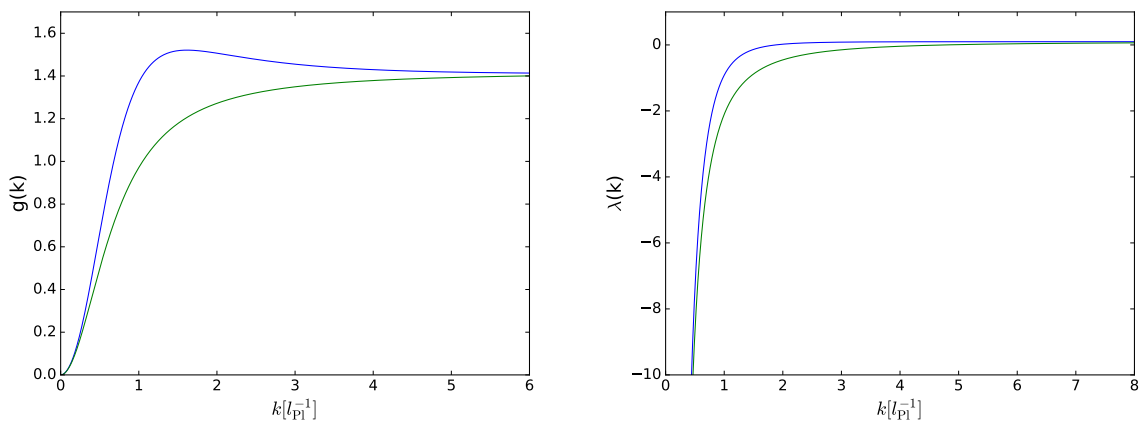


Figure 12.18.: Running of the dimensionless couplings g and λ as a function of momentum scale k for the analytical expressions from (12.15) in green and from a fourth order vertex expansion based on [62] in blue. Both approach their UV fixed point values, $g_* = 1.4$ & $\lambda_* = 0.1$, for $k \rightarrow \infty$.

Part IV.

Appendix

A. Fourier Conventions

This appendix summarises our Fourier conventions. We denote bosonic fields with ϕ and fermionic fields with ψ and $\bar{\psi}$. However the conventions are used for other fields as well, i.e. for the bosonic vector fields A_μ , the bosonic tensor fields $h_{\mu\nu}$ in gravity, and the fermionic ghost and anti-ghost fields c, \bar{c} (QCD) and c_μ, \bar{c}_μ (gravity). The Fourier transformation reads

$$\begin{aligned} \phi(x) &= \int \frac{d^d p}{(2\pi)^d} \phi(p) e^{i p_\mu x_\mu}, & \psi(x) &= \int \frac{d^d p}{(2\pi)^d} \psi(p) e^{i p_\mu x_\mu}, & \bar{\psi}(x) &= \int \frac{d^d p}{(2\pi)^d} \bar{\psi}(p) e^{-i p_\mu x_\mu}, \\ \phi(p) &= \int d^d x \phi(x) e^{-i p_\mu x_\mu}, & \psi(p) &= \int d^d x \psi(x) e^{-i p_\mu x_\mu}, & \bar{\psi}(p) &= \int d^d x \bar{\psi}(x) e^{i p_\mu x_\mu}. \end{aligned} \quad (\text{A.1})$$

with the orthogonality relations

$$\int d^d x e^{-i p_\mu x_\mu} = (2\pi)^d \delta(p), \quad \int \frac{d^d p}{(2\pi)^d} e^{i p_\mu x_\mu} = \delta(x), \quad (\text{A.2})$$

At finite temperature the time direction is compactified with $x_0 \in [0, \beta]$ with $\beta = 1/T$, see e.g. [Section 3.2.2](#). Then the discrete version of the above Fourier convention has to be used, and frequencies are only the discrete Matsubara modes

$$\omega_n^b = 2\pi T n, \quad \omega_n^f = 2\pi T \left(n + \frac{1}{2}\right), \quad \text{with } n \in \mathbb{Z}. \quad (\text{A.3})$$

ω_n^b for fields with Bose-Einstein statistics, and ω_n^f for fields with Fermi-Dirac statistics. Note in this context that the fermionic ghost and anti-ghost, c, \bar{c} have Matsubara modes ω_n^b . As the relation for the spacial directions do not change we only consider the transformation in time and frequency.

$$\begin{aligned} \phi(x) &= T \sum_{n=-\infty}^{\infty} \phi_n(\vec{x}) e^{i \omega_n^b x_0}, & \psi(x) &= T \sum_{n=-\infty}^{\infty} \psi_n e^{i \omega_n^f x_0}, & \bar{\psi}(x) &= T \sum_{n=-\infty}^{\infty} \bar{\psi}_n e^{-i \omega_n^f x_0}, \\ \phi_n(\vec{x}) &= \int_0^\beta dx \phi(x) e^{-i \omega_n^b x_0}, & \psi_n(\vec{x}) &= \int_0^\beta dx \psi(x) e^{-i \omega_n^f x_0}, & \bar{\psi}_n(\vec{x}) &= \int_0^\beta dx \bar{\psi}(x) e^{i \omega_n^f x_0}. \end{aligned}$$

with the orthogonality relations

$$\int_0^\beta dx_0 e^{i \omega_n^b x_0} = \beta \delta_{n,0}, \quad T \sum_{n=-\infty}^{\infty} e^{i \omega_n^b x_0} = \sum_{n=-\infty}^{\infty} \delta(x_0 + n\beta).$$

B. Saddle point expansion of the effective action

For the saddle point expansion we expand [eq. \(1.24\)](#) the classical action $S[\phi + \varphi']$ around $\varphi = 0$ to obtain

$$e^{-\Gamma[\phi]} = \int [d\varphi']_{\text{ren}} \exp \left\{ -S[\phi] + \int_x \left(\frac{\delta(\Gamma[\phi] - S[\phi])}{\delta\phi} \right) \varphi' - \frac{1}{2} \int_{x_1, x_2} S^{(2)}[\phi](x_1, x_2) \varphi'(x_1) \varphi'(x_2) + O(\varphi'^3) \right\}, \quad (\text{B.1})$$

where $S^{(2)}[\phi](x_1, x_2)$ is the second derivative of $S[\phi]$ w.r.t. the mean field ϕ . The first term in the exponent is independent of the quantum field φ and can be pulled in front of the path integral. The second term which is linear in the fluctuation field φ' is proportional to $\Gamma - S$ which only contains contributions that are at least one loop. Only its square and higher powers survive the integration of the fluctuation field as $\langle \varphi' \rangle = 0$. Hence it is at least of two-loop order and is dropped in the present one loop analysis. Restricting ourselves to the lowest -quadratic- order in the saddle point expansion we are left with a Gaussian integral leading to the well-known one loop result,

$$\Gamma^{\text{1-loop}}[\phi] = S[\phi] + \frac{1}{2} \text{Tr} \ln S^{(2)}[\phi], \quad (\text{B.2})$$

to be compared with [\(1.38\)](#) derived from the DSE [\(1.28\)](#).

C. Calculation of Matsubara sums

We review the calculation of series frequently encountered in the Matsubara formalism. As an example consider the flow equation for the effective potential in a scalar theory at temperature T

$$\partial_t V_k(\rho) = \frac{T}{2} \sum_q G(q_0, \vec{q}) \partial_t R_k(q_0, \vec{q}), \quad (\text{C.1})$$

with $q_0 = 2\pi nT$ and the notation \oint denotes both integration and summation

$$\sum_q = \sum_{n=-\infty}^{\infty} \int_{\vec{q}}. \quad (\text{C.2})$$

For the beginning we will restrict ourselves to bosonic Matsubara sum, the generalization to fermions is obvious and will be stated at the end. Technically, it is easier to start with the summation in (C.1) and therefore we consider problems of the form

$$\mathcal{M}_{\text{bos}} = T \sum_{n=-\infty}^{\infty} f(2n\pi T), \quad (\text{C.3})$$

where the generic function f is assumed to be sufficiently well behaved, analytic on the real axis and decays sufficiently fast at infinity, this is usually the case for integrands encountered in flow equations. Recalling the residue theorem

$$\oint_{\gamma} dz g(z) = 2\pi i \sum_{k=1}^N \text{ind}_{\gamma}(a_k) \text{res}(g, a_k), \quad (\text{C.4})$$

where a_k are the poles of $g(z)$ contained in the closed path γ , $\text{ind}_{\gamma}(a)$ is the winding number of γ with respect to a and $\text{Res}(g, a)$ is the residue of g at a . Utilizing the requirement of analyticity on the real axis, the sum in (C.3) can be rewritten to an integral by means of the residue theorem (C.4), by introducing an additional function that has poles at $q_0 = 2\pi nT$

$$\mathcal{M}_{\text{bos}} = \frac{i}{2} \oint_{\gamma} dz f(z) [1 + 2n_B(i z)], \quad (\text{C.5})$$

where the path γ encloses the real axis without enclosing any additional non-analyticities of $f(z)$ in positive direction and n_B . In (C.5) we have used that the poles of n_B are located at the Matsubara modes $2n\pi T$ and contribute with a residue of $iT/2$. It would have been sufficient to use $i n_B(i z)$ as factor to achieve this, but we are using $i/2 [1 + 2n_B(i z)]$ because it makes successive calculations often more convenient. Turning back to (C.5) we can cut the contour γ open at $\pm\infty$ and close them individually at infinity by means of Jordan's lemma in the complex plane. As a result we can express the Matsubara sum in (C.3) as

$$\mathcal{M}_{\text{bos}} = T \sum_{n=-\infty}^{\infty} f(2n\pi T) = \frac{1}{2i} \sum_{k=1}^N \text{res}(f, z_k) [1 + 2n_B(i z_k)], \quad (\text{C.6})$$

where the z_k are the poles of $f(z)$ and the additional minus sign comes from the winding number when closing the paths at infinity.

Turning to fermions, it turns out that it only necessary to replace the thermal kernel in (C.5)

$$\mathcal{M}_{\text{fer}} = T \sum_{n=-\infty}^{\infty} f((2n+1)\pi T) = \frac{1}{2i} \sum_{k=1}^N \text{res}(f, z_k) [1 - 2n_F(i z_k)] . \quad (\text{C.7})$$

D. Grassmann variables: Reminder

Fermionic fields are described by Grassmann variables which are anticommuting numbers. Thus for two Grassmann variables c_1 and c_2 the anticommutator vanishes

$$\{c_1, c_2\} = 0. \quad (\text{D.1})$$

It follows directly that $c_1^2 = c_2^2 = 0$ and thus any function of Grassmann variables is given by an expansion

$$f(c) = f(0) + \frac{df}{dc}(0)c. \quad (\text{D.2})$$

The integration is defined by

$$\int dc 1 = 0, \quad \int dc c = 1 \quad \Rightarrow \quad \int dc f(c) = \frac{d}{dc} f(0). \quad (\text{D.3})$$

The formulation can be extended straight forward to complex Grassmann variables by introducing

$$c = \frac{1}{\sqrt{2}} (c_1 + i c_2), \quad \bar{c} = \frac{1}{\sqrt{2}} (c_1 - i c_2) \quad (\text{D.4})$$

with real Grassmann variables c_1 and c_2 . It follows immediately that $\bar{c}c = -c\bar{c}$.

Now let us use N -dimensional vectors of complex Grassmann variables, c_i and c_j . It is easily shown that for a unitary transformation $c'_i = U_{ij}c_j$ the product of complex Grassmann variables transforms as $\prod_i c'_i = (\det U) \prod_i c_i$. Hence, the integral $\prod_i \int d\bar{c}_i dc_i$ is invariant under such unitary transformations. This allows us to evaluate a Gaussian integral which involves a Hermitian matrix M_{ij} with eigenvalues denoted by m_i ,

$$\begin{aligned} \prod_{n=1}^N \int d\bar{c}_n dc_n \exp\left(-\sum_{i,j} \bar{c}_i M_{ij} c_j\right) &= \prod_{n=1}^N \int d\bar{c}_n dc_n \exp\left(-\sum_i \bar{c}_i m_i c_i\right) \\ &= \prod_{n=1}^N \int d\bar{c}_n dc_n \left(1 - \sum_i \bar{c}_i m_i c_i\right) \\ &= \det M. \end{aligned} \quad (\text{D.5})$$

In the first line we have used a unitary transformation to diagonalise M . In the second line we have used eq. (D.2) and eq. (D.3). Notice that for non-Grassmannian variables the Gaussian integral would be proportional to the square root of the inverse determinant.

E. Low energy effective theories of QCD

The Higgs mechanism in the electroweak sector of the Standard Model leads to (current) quark masses for the up and down quark of a couple of MeVs, $(m_{u/d})_{\text{cur}} \approx 2\text{-}5$ MeV, see Table 5.1. However, the masses of the nucleons, the protons and neutrons, is about 1 GeV (proton (uud) ≈ 938 MeV, neutron (udd) ≈ 940 MeV), that is two orders of magnitude bigger. In other words, the three constituent quarks in the nucleons must have an effective mass of about $(m_{u/d})_{\text{con}} \approx 300\text{-}400$ MeV, the constituent quark masses. We already infer from this that there should be a further mechanism to generate this mass scale.

In low energy QCD with its mass scale $\Lambda_{\text{QCD}} \approx 200 - 300$ MeV the electroweak sector of the Standard Model decouples as do the heavier quarks. We are left with two light (up and down) and one heavy quark (charm), Table 5.1. Within fully quantitative computations of the QCD dynamics at low energies the strange quark with its current mass of about 1.2 GeV is also added. Still, its dynamics is very much suppressed at momentum scales of Λ_{QCD} . For the present structural analysis we first resort to two flavour QCD ($N_f = 2$) with the Euclidean action

$$S_{\text{QCD}}[\Phi] = \frac{1}{4} \int_x F_{\mu\nu}^a F_{\mu\nu}^a + \int_x \bar{q} \cdot (\not{D} + m_q - \mu \gamma_0) \cdot q, \quad (\text{E.1})$$

where the quark q is a Dirac spinor with two flavours and $\Phi = (A_\mu, c, \bar{c}, q, \bar{q})$ is the two-flavour super field. The action in (E.1) is illustrated diagrammatically as The physics of the matter sector at low energies and temperatures, and not too large densities is well-described by quark-hadron models, the most prominent of which is the Nambu-Jona-Lasino model. From the perturbative point of view these models are seeded in the four-fermi coupling already being generated from the propagators and couplings depicted in Fig. E.1 at tree level. The related tree level diagram is depicted in Fig. E.2. Its s -channel has the structure

$$g^2 (\bar{q} \gamma_\mu t^a q)(p) \Pi_{\mu\nu}(p) \frac{1}{p^2} (\bar{q} \gamma_\mu t^a q)(p), \quad (\text{E.2})$$

describing the scattering of quarks. In (E.2) the t^a are generators of the color gauge group and the fermions are summed over the two flavours. Accordingly, (E.2) generates a four-fermi interaction with a non-trivial momentum structure in the effective action of QCD.

The full momentum- and tensor structure is complicated even for the present simplified $N_f = 2$ case. As in the four-fermi theory (Fermi theory) for weak interactions we resort to an approximation with point-like interactions (no momentum dependence). Then (E.2) can be rewritten in terms of an effective *local* (point-like) four-fermi interaction. Such a rewriting in terms of local four-fermi interactions holds for energies that are sufficiently low and do not resolve the large momentum structure of the scattering in (E.2). Moreover, the coupling is dimensionful and has the canonical momentum dimension -2 (related to the $1/p^2$ term in (E.2)). In the Fermi theory of weak interactions this is the electroweak scale. In the present case it has to be related to the QCD mass gap proportional to Λ_{QCD} .

We postpone the detailed analysis of this scale, and first concentrate on the tensor structure of (E.2). This is constrained by the symmetries of the theory, for a full discussion of the symmetry pattern we refer to the literature, e.g. [351, 232] and literature therein. Since the current masses of the light quarks are nearly vanishing we first work in the chiral limit. Then, any interaction that is generated by the dynamics of QCD carries chiral symmetry: the related four-fermi interaction is chirally invariant, that is

Figure E.1.: Diagrammatical form of the QCD action.

the invariance under the chiral transformations

$$q \rightarrow e^{i\frac{1\pm\gamma_5}{2}\alpha} q \quad \rightarrow \quad \bar{q} \rightarrow \bar{q} e^{i\frac{1\pm\gamma_5}{2}\alpha} \quad \text{with} \quad \gamma_5 = \gamma_0\gamma_1\gamma_2\gamma_3, \quad \text{and} \quad \{\gamma_5, \gamma_\mu\} = 0, \quad (\text{E.3})$$

which holds separately for each vector current $q\gamma_\mu t^a q$. Furthermore, in the chiral limit QCD is invariant under flavour rotations $SU(N_f)$. For example, for $N_f = 2$ with up (u) and down (d) quarks and the flavour isospin group with $SU(2)$, the transformation reads

$$q = \begin{pmatrix} u \\ d \end{pmatrix} \rightarrow V \begin{pmatrix} u \\ d \end{pmatrix}, \quad \text{with} \quad V = e^{i\theta^a \tau^a} \in SU(2), \quad (\text{E.4})$$

with $a = 1, 2, 3$. For the 2+1 flavour case also considered here the respective symmetry is $SU(3)_F$. Chiral symmetry entails that the flavour rotations are a symmetry for the left- and right-handed quarks separately and the combined symmetry is $SU(2)_L \times SU(2)_R$ with symmetry transformations $V_{L/R} = e^{i\frac{1\pm\gamma_5}{2}\theta^a t^a}$. Including also the chiral $U(1)$ rotations leads us to the full symmetry group

$$G_{\text{sym}} = SU(N_c) \times SU(N_f)_V \times SU(N_f)_A \times U(1)_V \times U(1)_A, \quad (\text{E.5})$$

where we have also taken into account the gauge group $SU(N_c)$. If we approximate (E.2) by a point-like four-fermi interaction, one has to expand the tensor $\gamma_\mu \otimes \gamma_\nu$ multiplied by gauge group and flavour tensors. Then, the most general symmetric Ansatz is a combination of the tensor structures

$$\begin{aligned} (V - A) &= (\bar{q}\gamma^\mu q)^2 + (\bar{q}\gamma^\mu\gamma^5 q)^2 \\ (V + A) &= (\bar{q}\gamma^\mu q)^2 - (\bar{q}\gamma^\mu\gamma^5 q)^2 \\ (S - P) &= (\bar{q}^f q^g)^2 - (\bar{q}^f\gamma^5 q^g)^2 \\ (V - A)^{\text{adj}} &= (\bar{q}\gamma^\mu t^a q)^2 + (\bar{q}\gamma^\mu\gamma^5 t^a q)^2, \end{aligned} \quad (\text{E.6})$$

where f, g are flavour indices and $(\bar{q}^f q^g)^2 \equiv \bar{q}^f q^g \bar{q}^g q^f$. While each separate term in the tensors in (E.6) is invariant under gauge transformation, and under the flavour vector transformations, axial rotations in $SU(N_f)_A \times U(1)_A$ rotate the terms on the right hand side in (E.6) into each other. For a related full analysis we refer to the literature. However, below we shall exemplify these computations at the relevant example of the scalar–pseudo-scalar channel

The chiral invariants (E.6) can be rewritten using the Fierz transformations which relates different four-fermi terms on the basis of the Grassmann natures of the fermions. These transformations are explained and detailed in the literature, see e.g. [351, 232]. Here we just concentrate on the scalar–pseudo-scalar channels in physical two-flavour QCD with $N_c = 3$ and $N_f = 2$. These channels are related to the scalar σ -meson and the pseudo-scalar pions $\vec{\pi}$. The $(S - P)$ -channel is given by

$$(S - P) = \frac{1}{2} [(\bar{q}q)^2 + (\bar{q}\vec{\pi}q)^2 - (\bar{q}\gamma^5 q)^2 - (\bar{q}\gamma^5\vec{\pi}q)^2], \quad (\text{E.7})$$

$$\lambda_\psi = \text{Diagram} \propto \text{Sum of Diagrams} + \text{Sum of Diagrams} + \text{Sum of Diagrams}$$

Figure E.2.: One loop diagrams for the four-fermi coupling λ_q in QCD.

where $\vec{\tau} = (\sigma_1, \sigma_2, \sigma_3)$ with Pauli matrices

$$\sigma_1 = \begin{pmatrix} 0 & 1 \\ 1 & 0 \end{pmatrix}, \quad \sigma_2 = \begin{pmatrix} 0 & -i \\ i & 0 \end{pmatrix}, \quad \sigma_3 = \begin{pmatrix} 1 & 0 \\ 0 & -1 \end{pmatrix}, \quad (\text{E.8})$$

The representation (E.7) simplifies the identification of the scalar mode $\bar{q}q$ related to the scalar σ -meson, and the pseudo-scalar modes $i\bar{q}\gamma_5\vec{\tau}q$ related to the pseudo-scalar (axial-scalar) pions $\vec{\pi}$.

We shall use the representation (E.7) in the following investigations of the chiral properties of low energy QCD. Hence we discuss its symmetry properties in more detail, and show explicitly its invariance under G_{sym} . To begin with, the invariance of $(S - P)$ under gauge and flavour $U_V(1)$ transformation is apparent. The flavour $S U(2)_V$ transformations $q \rightarrow e^{i\theta^a\tau^a}q$ trivially leaves $\bar{q}q$ and $\bar{q}\gamma_5 q$ invariant. For the vector and pseudo-vector bilinears we concentrate on infinitesimal transformations $e^{i\theta^a\tau^a} = 1 + i\theta^a\tau^a + O(\theta^2)$. Then the second term in (E.7) transforms as

$$(\bar{q}\vec{\tau}q)^2 \longrightarrow (\bar{q}\vec{\tau}q)^2 + 2i\theta^a(\bar{q}\vec{\tau}q)(\bar{q}[\vec{\tau}, \tau^a]q) = (\bar{q}\vec{\tau}q)^2 - 2\theta^a\epsilon^{bac}(\bar{q}\tau^b q)(\bar{q}\tau^c q) = (\bar{q}\vec{\tau}q)^2. \quad (\text{E.9})$$

The invariance of the last term in (E.7) under $S U(2)_V$ transformations follows analogously. Finally, axial transformations relate the first two terms to the last two terms. We exemplify this property with the axial $U_A(1)$ rotations $q \rightarrow e^{i\gamma_5\alpha}q$, where we consider infinitesimal transformations with $e^{i\gamma_5\alpha} = 1 + i\gamma_5\alpha + O(\alpha^2)$. Concentrating on the scalar and pseudo-scalar terms we have

$$(\bar{q}q)^2 - (\bar{q}\gamma^5 q)^2 \longrightarrow (\bar{q}q)^2 - (\bar{q}\gamma^5 q)^2 + 4i\alpha[(\bar{q}q)(\bar{q}\gamma_5 q) - (\bar{q}\gamma^5 q)(\bar{q}q)] = (\bar{q}q)^2 - (\bar{q}\gamma^5 q)^2, \quad (\text{E.10})$$

The invariance for the full expression in (E.7) follows analogously. It is left to study $S U(2)_A$ transformations. Now we show that (E.7) also carries the $S U(2)_A$ -invariance. To that end we consider infinitesimal $S U(2)_A$ transformations $e^{i\gamma_5\theta^a\tau^a} = 1 + i\gamma_5\theta^a\tau^a + O(\theta^2)$ of the combination $(\bar{q}q)^2 - (\bar{q}\gamma^5\vec{\tau}q)^2$, and use the Lie algebra identity

$$\tau^a\tau^b = \delta^{ab} + i\epsilon^{abc}\tau^c, \quad \rightarrow \quad \{\tau^a, \tau^b\} = 2\delta^{ab}. \quad (\text{E.11})$$

Then we are led to

$$(\bar{q}q)^2 - (\bar{q}\gamma^5\vec{\tau}q)^2 \longrightarrow (\bar{q}q)^2 - (\bar{q}\gamma^5\vec{\tau}q)^2 + 2i\theta^a[(\bar{q}q)(\bar{q}\gamma_5\tau^a q) - (\bar{q}\gamma^5\tau^b q)(\bar{q}\{\tau^a, \tau^b\}q)] = (\bar{q}q)^2 - (\bar{q}\gamma^5 q)^2. \quad (\text{E.12})$$

The invariance of the combination $(\bar{q}\gamma_5 q)^2 - (\bar{q}\vec{\tau}q)^2$ is shown along the same lines. Consequently (E.7) is invariant under $S U(2)_A$ transformation and hence under the full symmetry group G_{sym} .

In QCD, we have experimental evidence for the breaking of the axial $U_A(1)$ -symmetry, i.e. the pseudo-scalar η' -meson (in $N_f = 2$ the η) is anomalously heavy. This mass-difference can be nicely explained

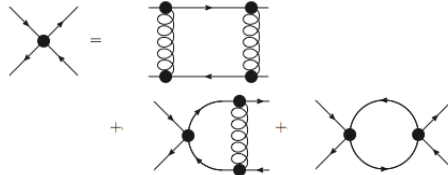


Figure E.3.: One loop diagrams for the four-fermi coupling λ_q from the action (E.18).

by the anomalous breaking of axial $U_A(1)$ symmetry. Consequently, giving up axial $U_A(1)$ -symmetry we have to consider more four-fermi interactions as in (E.6) (altogether 10 invariants for $N_f = 2$), in particular

$$\frac{1}{2} \left[(\bar{q}q)^2 - (\bar{q}\vec{\tau}q)^2 + (\bar{q}\gamma^5 q)^2 - (\bar{q}\gamma^5 \vec{\tau}q)^2 \right]. \quad (\text{E.13})$$

It is the relative minus signs in the scalar and pseudo-scalar terms in comparison to (E.7) that leads to the breaking of $U_A(1)$ -symmetry. This is easily seen by re-doing the infinitesimal analysis (E.10) in (E.13). It also follows easily that the other symmetries still hold, in particular the $SU(2)_V \times SU(2)_A$ invariance follows as (E.13) contains the same $SU(2)_V \times SU(2)_A$ -invariant combinations of four-quark terms as (E.7). Hence we conclude that the combination (E.13) only breaks $U_A(1)$ -symmetry, and adding up the two channels (E.7) and (E.13) leads to the $U_A(1)$ -breaking combination

$$\frac{1}{2} \left[(\bar{q}q)^2 - (\bar{q}\gamma^5 \vec{\tau}q)^2 \right]. \quad (\text{E.14})$$

Equation (E.14) is invariant under the remaining symmetries $SU(N_c) \times SU(N_f)_V \times SU(N_f)_A \times U(1)_V$. This concludes our brief discussion of the global symmetries of QCD in the chiral limit.

In summary the following picture emerges: assume we perform a chain of scattering experiments of QCD/Standard Model starting at the electroweak scale ≈ 90 GeV towards the strong QCD scale Λ_{QCD} . At each scale we can describe the quantum equations of motion and scattering experiments by a suitably chosen effective action $\Gamma[\phi]$.

On the level of the path integral for QCD this is described by the Wilsonian idea of integrating out momentum modes above some momentum scale k ,

$$Z_k[J] = \int [d\Phi]_{p^2 \geq k^2} e^{-S_{\text{QCD}}[\Phi] + \int_x J \cdot \Phi} \quad \Rightarrow \quad \text{Effective Action } \Gamma_k[\Phi], \quad (\text{E.15})$$

with the super current J . The path integral measure in (E.15) only contains an integration over fields Φ_k that are non-vanishing for $p^2 \geq k^2$: $\Phi_k(p^2 < k^2) \equiv 0$. After Legendre transformation this leads us to an effective action $\Gamma_k[\Phi]$ that only contains the quantum effects of scales larger than the running (RG) scale k and serves as a classical action for the quantum effects with momentum scales $p^2 < k^2$. This effective action also carries the symmetries of the fundamental QCD action, as long as these symmetries are not (anomalously) broken by quantum effects.

We know already from the perturbative renormalisation programme that this amounts to adjusting the (running) coupling in the (classical) action with the sliding (experimental) momentum scale. In such a Wilsonian setting this is very apparent. The running of the coupling comes from the loop diagrams that are evaluated at the momentum scale k . On top of this momentum adjustment of the fundamental

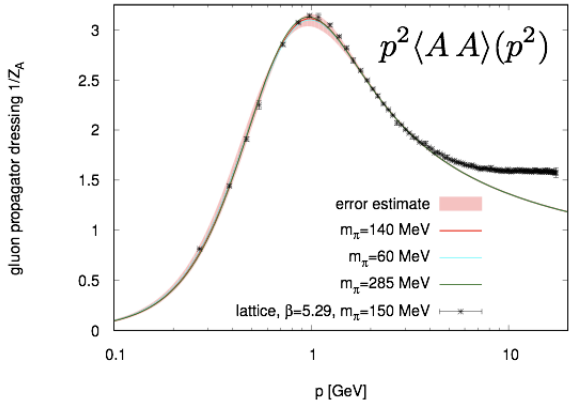


Figure E.4.: Gluon propagator for $N_f = 2$ from the lattice and from non-perturbative diagrammatic methods, taken from [55].

parameters of the theory one also creates additional terms in the -effective- action. The one of importance for us is the four-fermi terms argued for above. It is created at one-loop with the box diagrams depicted in [Figure E.2](#). This leads us finally to the following four-fermi interaction in the effective action,

$$\Gamma_{\text{4-fermi}}[\phi]|_{\text{1-loop}} = -\frac{\lambda_q}{4} \int [(\bar{q}q)^2 - (\bar{q}\gamma^5 \vec{\tau} q)^2] + \dots \quad \text{with} \quad \lambda_q \propto \alpha_s^2, \quad (\text{E.16})$$

where it is understood that the coupling λ_q carries the running momentum or RG scale k introduced above. Together with the kinetic term of the quarks this is the classical action of the Nambu–Jona-Lasinio type model. [Equation \(E.16\)](#) holds for massless quarks and two flavours, $N_f = 2$. The two terms in [\(E.16\)](#) carry the same quantum number as the scalar and axial-scalar excitations in low energy QCD, the sigma-meson σ and pion $\vec{\pi}$ respectively. The one loop diagrams generating the four-fermi coupling λ_q are depicted in [Fig. E.2](#). In line with the picture outlined above the four-fermi coupling λ_q at a given momentum scale $p^2 = k^2$ should be computed with the loop momenta q in the box diagrams in [Figure E.2](#) being bigger than k . Then the related diagram is peaked at this scale and we conclude by dimensional analysis that

$$\lambda_{q,k} \simeq \alpha_{s,k}^2 \frac{1}{k^2}. \quad (\text{E.17})$$

Note that this coupling feeds back into the loop expansion of other correlations functions such as the quark propagator and quark-gluon vertices. However, in comparison to other (one-loop) diagrams it is suppressed by additional orders of the strong coupling α_s . In turn, in the low momentum regime where α_s grows strong it gives potentially relevant contributions. Indeed, taking as a starting point for a loop analysis the sum of the QCD action [\(E.1\)](#) and the four-fermi term [\(E.16\)](#)

$$\Gamma[\phi] \simeq S_{\text{QCD}}[\phi] + \Gamma_{\text{4-fermi}}[\phi], \quad (\text{E.18})$$

we get also self-interaction terms of the four-fermi coupling proportional to λ_q^2 as well as terms proportional to $\alpha_s \lambda_q$. This is depicted in [Figure E.3](#).

The glue sector of QCD is expected to have a mass gap already present in the purely gluonic theory, related to the confinement property of Yang-Mills theory. Then this has to manifest itself in a decoupling of the gluonic contribution to the four-fermi coupling in [Figure E.3](#). In the Landau gauge this mechanism is easily visible due to the mass gap in the gluon propagators, see Fig. E for lattice results and results from non-perturbative diagrammatic methods.

Note that the gluon propagator is gauge dependent, and the careful statement is that the Landau gauge facilitates the access to the related physics. One should not confuse this with a massive gluon, as the gluon is no physical particle and shows positivity violation. Moreover, the gluonic sector is certainly relevant for the confining physics and hence the decoupling discussed above only takes place in the matter sector for the specific question under investigation, the mechanism of strong chiral symmetry breaking.

F. Quantisation & gauge fixing

F.1. Feynman rules for QCD in the covariant gauge

In this Appendix we depict the Feynman rules for QCD in the general covariant gauge.

$$\begin{array}{c} a \\ \text{---} \\ p_\mu \end{array} \quad \begin{array}{c} b \\ \text{---} \\ k_\nu \end{array} = \delta^{ab} \delta^{(4)}(p+k) \left(\delta_{\mu\nu} - (1-\xi) \frac{p_\mu p_\nu}{p^2} \right) \frac{1}{p^2}$$

$$\begin{array}{c} a \\ \text{---} \\ p \end{array} \quad \begin{array}{c} b \\ \text{---} \\ k \end{array} = -\delta^{ab} \delta^{(4)}(p+k) \frac{1}{p^2}$$

$$\begin{array}{c} \rightarrow \\ p \end{array} \quad \begin{array}{c} \rightarrow \\ k \end{array} = \delta^{(4)}(p+k) \frac{1}{i \not{p} + m}$$

$$\begin{array}{c} a \\ \text{---} \\ c \end{array} \quad \begin{array}{c} \downarrow \\ \text{---} \\ b \end{array} \quad \begin{array}{c} k_{1,\mu} \\ \text{---} \\ k_{3,\rho} \end{array} \quad \begin{array}{c} k_{2,\nu} \\ \text{---} \\ d \end{array} = i g f^{abc} (2\pi)^4 \delta^{(4)}(k_1 + k_2 + k_3) \left[(k_2 - k_1)_\rho \delta_{\mu\nu} + (k_1 - k_3)_\nu \delta_{\mu\rho} + (k_3 - k_2)_\mu \delta_{\nu\rho} \right]$$

$$\begin{array}{c} a \\ \text{---} \\ c \end{array} \quad \begin{array}{c} b \\ \text{---} \\ d \end{array} \quad \begin{array}{c} k_{1,\mu} \\ \text{---} \\ k_{4,\sigma} \end{array} \quad \begin{array}{c} k_{2,\nu} \\ \text{---} \\ k_{3,\rho} \end{array} = g^2 (2\pi)^4 \delta^{(4)} \left(\sum_{i=1}^4 k_i \right) \left[f^{iab} f^{icd} (\delta_{\mu\rho} \delta_{\nu\sigma} - \delta_{\mu\sigma} \delta_{\nu\rho}) + f^{iac} f^{ibd} (\delta_{\mu\nu} \delta_{\rho\sigma} - \delta_{\mu\sigma} \delta_{\nu\rho}) + f^{iad} f^{ibc} (\delta_{\mu\nu} \delta_{\rho\sigma} - \delta_{\mu\rho} \delta_{\nu\sigma}) \right]$$

$$\begin{array}{c} a \\ \text{---} \\ b \end{array} \quad \begin{array}{c} \downarrow \\ q \end{array} \quad \begin{array}{c} \text{---} \\ c \end{array} \quad \begin{array}{c} k_\mu \\ \text{---} \\ p \end{array} = -i g f^{abc} p_\mu (2\pi)^4 \delta^{(4)}(p-q-k)$$

$$\begin{array}{c} a \\ \text{---} \\ q \end{array} \quad \begin{array}{c} \text{---} \\ p \end{array} = -i g \gamma_\mu T^a (2\pi)^4 \delta^{(4)}(p-q-k)$$

Figure F.1.: Feynman rules.

F.2. Faddeev-Popov quantisation & Gribov copies within a toy model

F.2.1. Faddeev-Popov quantisation

In order to get a more intuitive feeling for the Faddeev–Popov procedure, we contrast the quantization within a gauge theory with the according procedure within a classical 0+2 dimensional toy model. Discussing the toy model, we follow [352], where it was firstly introduced. Within the toy model, the gauge field A_μ finds its analogue within the two spacial coordinates x_1 and x_2 . The path integral over the field configurations is accordingly translated into the integral over two dimensional space. While we care for the gauge symmetry and its consequences in the gauge theory, the toy model offers rotational symmetry as its counterpart. When we distinguish gauge invariant and gauge dependent degrees of freedom in the gauge theory, analogously we have to address the polar coordinates (r, φ) in the toy model. In the following table, we proceed in contrasting the computation of the Faddeev-Popov determinant and the generating functional / partition function for the gauge theory / toy model.

General Gauge Theory	0+2 dim Theory
An overview over analogue quantities	
A_μ	(x, y)
$\int dA$	$\int d^2x$
gauge invariance	rotational invariance
Generating functional / partition function and gauge transformation / rotation	
$Z = \int dA \exp(-S[A])$	$Z = \int d^2x e^{-S(r)}$
$\downarrow \mathcal{U} = e^{ig\omega}$	\downarrow
$A^\omega = \mathcal{U} A_\mu \mathcal{U}^\dagger + \frac{i}{g} \mathcal{U} \partial_\mu \mathcal{U}^\dagger$	$x_1^\theta = x_1 \cos(\theta) + x_2 \sin(\theta)$

$$\begin{aligned} Z &= \int dA \exp(-S[A]) & Z &= \int d^2x e^{-S(r)} \\ \downarrow \mathcal{U} &= e^{ig\omega} & \downarrow & \\ A^\omega &= \mathcal{U} A_\mu \mathcal{U}^\dagger + \frac{i}{g} \mathcal{U} \partial_\mu \mathcal{U}^\dagger & x_1^\theta &= x_1 \cos(\theta) + x_2 \sin(\theta) \end{aligned}$$

The Faddeev–Popov ‘1‘ reads

$$1 = \int dg \delta[\mathcal{F}[A^\omega]] \Delta_{\mathcal{F}}[A]$$

$$1 = \int_0^{2\pi} d\theta \delta(x_1^\theta) \Delta_{\mathcal{F}}(\vec{x})$$

with

with

$$\begin{aligned} \Delta_{\mathcal{F}}[A] &= \left(\int dg \delta[\mathcal{F}[A]] \right)^{-1} \\ &= \sum_{\omega_0} |\det \frac{\delta \mathcal{F}}{\delta \omega}|_{A=A^\omega} \end{aligned}$$

$$\begin{aligned} \Delta_{\mathcal{F}}(\vec{x}) &= \left(\int_0^{2\pi} d\theta \delta(x_1^\theta) \right)^{-1} \\ &= \left(\int d\theta \frac{\delta(\theta - \arctan(x_1/x_2))}{| -x_1 \sin(\theta) + x_2 \cos(\theta)|} \right. \\ &\quad \left. + \frac{\delta(\theta + \arctan(x_2/x_1 + \pi))}{| -x_1 \sin(\theta) + x_2 \cos(\theta)|} \right)^{-1} \\ &= \frac{r(\vec{x})}{2} \end{aligned}$$

We insert the Faddeev–Popov determinant into the generating functional / partition function and get

$$\begin{aligned}
Z &= \int dA e^{-S[A]} \\
&= \int dA dg \delta[\mathcal{F}[A^g] \Delta_{\mathcal{F}}[A]] e^{S[A]} \\
&= \int dA \delta[\mathcal{F}[A]] \Delta_{\mathcal{F}[A]} e^{-S[A]} \left[\int dg \right] \\
&= \int dA_{gf} \Delta_{\mathcal{F}}[A_{gf}] e^{-S[A_{gf}]} \left[\int dg \right] \\
Z &= \int d^2x e^{-S(r)} \\
&= \int d^2x \int d\theta \delta(x_1^\theta) \frac{r}{2} e^{-S(r)} [2\pi] \\
&= \int_0^\infty d^2x x_2 e^{-S(\sqrt{x_2^2})} [2\pi] \quad (\text{F.1})
\end{aligned}$$

with $x_2 = r(\vec{x} = (0, x_2)^T)$

F.2.2. Gribov Ambiguity within a toy model

Let us consider a two dimensional system with vanishing angular momentum and illustrate therewith the meaning of the Gribov ambiguity following [353] and [352]. The constraint of vanishing angular momentum can be put down in form of

$$\begin{aligned}
L &= x_1 p_2 - x_2 p_1 \\
&= 0. \quad (\text{F.2})
\end{aligned}$$

At this point, we can either choose to switch into description via polar coordinates, thus having the rotational (“gauge”) invariant coordinate r and the rotational “gauge” variant coordinate φ . As expected, the Lagrangian would only depend on the rotation invariant degree of freedom. Or, if we did not choose new, problem-suited coordinates, we could start the “gauge” fixing procedure. To this end, we would first of all impose our gauge fixing condition, namely demand

$$\mathcal{F}(q) = x_2 = 0. \quad (\text{F.3})$$

This gauge fixing would reduce our configuration space to the x_1 axis, see also [Figure F.2](#), leaving us with two equivalent Gribov copies, as each gauge orbit picks x_1 and $-x_1$ both describing physically the same situation. The Gribov Horizon (GH) can be found at the point $x_1 = x_2 = 0$. Thus the ambiguity can be overcome by further restriction to the positive values of x_1 , which simultaneously defines a fundamental modular region (FMR).

F.3. Flow equations for Yang-Mills propagators

Contributing diagrams

The relevant diagrams are depicted in [Figure 5.4\(a\)](#), the diagrams are labelled as $\mathcal{D}_{\varphi_1 \dots \varphi_N}^{(j)}$ and it denotes the j -th diagram in [Figure 5.4\(a\)](#) associated to the correlation function labelled by $\varphi_1 \dots \varphi_N$. In order to shorten the notation we have introduced the auxiliary variables $x_q = q^2/k^2$ and $x_{p+q} = (p+q)^2/k^2$.

Diagram 1: $\mathcal{D}_{\bar{c}c}^{(1)}$:

The expression to compute reads

$$\mathcal{P}_{\bar{c}c}^{(1)} \mathcal{D}_{\bar{c}c}^{(1)} = \mathcal{P}_{\bar{c}c}^{(1)} \left\{ \left[\Gamma_{\bar{c}cA}^{(3)}(p, q) \right]_\mu^{acd} \left[(G \partial_t R_k G)_{\bar{c}c}(-q) \right]^{ce} \left[\Gamma_{\bar{c}cA}^{(3)}(-q, -p) \right]_\nu^{ebf} \left[G_{AA}(p+q) \right]_{\mu\nu}^{df} \right\}. \quad (\text{F.4})$$

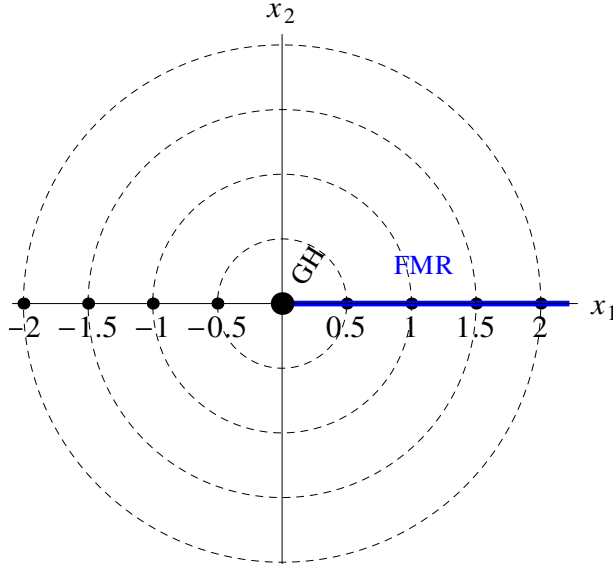


Figure F.2.: An illustration of a particle in two dimensions with vanishing angular momentum. Dashed lines indicate equivalent configurations. Imposing the gauge fixing (F.3) reduces the configuration space to the x_1 axis, still containing two Gribov copies of each physical configuration. The Gribov Horizon (GH) separates the halfspaces containing the copies. Further restriction to positive values of x_1 defines the fundamental modular region (FMR) only containing the minimal set of (physical) configurations.

Colour trace

The relevant colour trace is

$$\delta^{ab} f^{acd} \delta^{ce} f^{ebf} \delta^{df} = -C_2(A) d_A, \quad (\text{F.5})$$

where $C_2(A)$ is the quadratic Casimir of the adjoint representation, in $SU(N_c)$ we have $C_2(A) = N_c$.

Lorentz trace

The relevant Lorentz trace is

$$p_\mu(-q)_\nu \Pi_{\mu\nu}^\perp(p+q) = \frac{p^2 q^2 - (p \cdot q)^2}{(p+q)^2}. \quad (\text{F.6})$$

Result

Putting everything together, we obtain

$$\begin{aligned} \mathcal{P}_{\bar{c}c}^{(1)} \mathcal{D}_{\bar{c}c}^{(1)} &= C_2(A) \int_q \left\{ \frac{\lambda_{\bar{c}cA}(p, q) \lambda_{\bar{c}cA}(-q, -p)}{Z_A(p+q) Z_c(q)} \frac{p^2 q^2 - (p \cdot q)^2}{(p+q)^2} \right. \\ &\quad \left. \frac{\partial_t r_c(x_q) - \eta_c(q) r_c(x_q)}{q^2 [1 + r_c(x_q)]^2} \frac{1}{(p+q)^2 [1 + r_A(x_{p+q})] + m_{AA}^2} \right\}. \end{aligned} \quad (\text{F.7})$$

Diagram 2: $\mathcal{D}_{\bar{c}c}^{(2)}$:

The expression to compute reads

$$\mathcal{P}_{\bar{c}c}^{(1)} \mathcal{D}_{\bar{c}c}^{(2)} = \mathcal{P}_{\bar{c}c}^{(1)} \left\{ \left[\Gamma_{\bar{c}cA}^{(3)}(p, -(p+q)) \right]_{\mu}^{acd} \left[(G \partial_t R_k G)_{AA}(-q) \right]_{\mu\nu}^{df} \left[\Gamma_{\bar{c}cA}^{(3)}(p+q, -p) \right]_{\nu}^{ebf} \left[G_{\bar{c}c}(p+q) \right]_{\sigma}^{ce} \right\}. \quad (\text{F.8})$$

Colour trace

The relevant colour trace is

$$\delta^{ab} f^{acd} \delta^{ce} f^{ebf} \delta^{df} = -C_2(A) d_A, \quad (\text{F.9})$$

Lorentz trace

The relevant Lorentz trace is

$$p_{\mu} (p+q)_{\nu} \Pi_{\mu\nu}^{\perp}(q) = p^2 - \frac{(p \cdot q)^2}{q^2}. \quad (\text{F.10})$$

Result

Putting everything together, we obtain

$$\begin{aligned} \mathcal{P}_{\bar{c}c}^{(1)} \mathcal{D}_{\bar{c}c}^{(2)} &= C_2(A) \int_q \left\{ \frac{\lambda_{\bar{c}cA}(p, -(p+q)) \lambda_{\bar{c}cA}(p+q, -p)}{Z_A(q) Z_c(p+q)} \frac{p^2 q^2 - (p \cdot q)^2}{(p+q)^2} \right. \\ &\quad \left. \frac{\partial_t r_A(x_q) - \eta_A(q) r_A(x_q)}{\left(q^2 [1 + r_A(x_q)] + m_A^2 \right)^2 [1 + r_c(x_{p+q})]} \right\}. \end{aligned} \quad (\text{F.11})$$

Diagram 3: $\mathcal{D}_{AA}^{(1)}$:

The expression to compute reads

$$\mathcal{P}_{AA}^{(1)} \mathcal{D}_{AA}^{(1)} = \mathcal{P}_{AA}^{(1)} \left\{ \left[\Gamma_{AAA}^{(3)}(p, q) \right]_{\mu\rho\sigma}^{acd} \left[(G \partial_t R_k G)_{AA}(-q) \right]_{\rho\kappa}^{ce} \left[\Gamma_{AAA}^{(3)}(-q, -p) \right]_{\kappa\nu\lambda}^{ebf} \left[G_{AA}(p+q) \right]_{\sigma\lambda}^{df} \right\}. \quad (\text{F.12})$$

Colour trace

The relevant colour trace is

$$\delta^{ab} f^{acd} \delta^{ce} f^{ebf} \delta^{df} = -C_2(A) d_A, \quad (\text{F.13})$$

Lorentz trace

The relevant Lorentz trace is

$$\begin{aligned} &\Pi_{\mu\nu}^{\perp}(p) \Pi_{\rho\kappa}^{\perp}(q) \Pi_{\sigma\lambda}^{\perp}(p+q) \\ &\left[(2q+p)_{\mu} \delta_{\rho\sigma} - (2p+q)_{\rho} \delta_{\sigma\mu} + (p-q)_{\sigma} \delta_{\mu\rho} \right] \\ &\left[-(2p+q)_{\kappa} \delta_{\lambda\nu} + (2q+p)_{\nu} \delta_{\kappa\lambda} + (p-q)_{\lambda} \delta_{\kappa\nu} \right] \\ &= 4 \frac{p^2 q^2 - (p \cdot q)^2}{p^2 q^2 (p+q)^2} \left((d-1)(p+q)^2 + (p \cdot q)^2 + p^2 \left((2d-2)(p \cdot q) + (3d-4)q^2 \right) \right). \end{aligned} \quad (\text{F.14})$$

Result

Putting everything together, we obtain

$$\begin{aligned} \mathcal{P}_{AA}^{(1)} \mathcal{D}_{AA}^{(1)} &= C_2(A) \int_q \left\{ \frac{\lambda_{AAA}(p, q) \lambda_{AAA}(-q - p)}{Z_A(q) Z_{AA}(p + q)} \right. \\ &\quad \frac{4}{d-1} \frac{p^2 q^2 - (p \cdot q)^2}{p^2(p+q)^2} \left((d-1)(p+q)^2 + (p \cdot q)^2 + p^2 \left((2d-2)(p \cdot q) + (3d-4)q^2 \right) \right) \\ &\quad \left. \frac{\partial_t r_A(x_q) - \eta_A(q) r_A(x_q)}{\left(q^2 [1 + r_A(x_q)] + m_A^2 \right)^2} \frac{1}{(p+q)^2 [1 + r_A(x_{p+q})] + m_A^2} \right\}. \end{aligned} \quad (\text{F.15})$$

Diagram 4: $\mathcal{D}_{AA}^{(2)}$:

The expression to compute reads

$$\mathcal{P}_{AA}^{(1)} \mathcal{D}_{AA}^{(2)} = -\mathcal{P}_{AA}^{(1)} \left\{ \left[\Gamma_{\bar{c}cA}^{(3)}(q, -(p+q)) \right]_\mu^{cda} \left[(G \partial_t R_k G)_{\bar{c}c}(-q) \right]^{cf} \left[\Gamma_{\bar{c}cA}^{(3)}(p+q, -q) \right]_\nu^{efb} \left[G_{\bar{c}c}(p+q) \right]^{de} \right\}. \quad (\text{F.16})$$

Colour trace

The relevant colour trace is

$$\delta^{ab} f^{cda} \delta^{cf} f^{efb} \delta^{de} = -C_2(A) d_A, \quad (\text{F.17})$$

Lorentz trace

The relevant Lorentz trace is

$$q_\mu (p+q)_\nu \Pi_{\mu\nu}^\perp(p) = q^2 - \frac{(p \cdot q)^2}{p^2}. \quad (\text{F.18})$$

Result

Putting everything together, we obtain

$$\begin{aligned} \mathcal{P}_{AA}^{(1)} \mathcal{D}_{AA}^{(2)} &= -\frac{C_2(A)}{d-1} \int_q \left\{ \frac{\lambda_{\bar{c}cA}(q, -(p+q)) \lambda_{\bar{c}cA}(p+q, -q)}{Z_c(q) Z_{cA}(p+q)} \frac{1}{(p+q)^2} \left(1 - \frac{(p \cdot q)^2}{p^2 q^2} \right) \right. \\ &\quad \left. \frac{\partial_t r_c(x_q) - \eta_c(q) r_c(x_q)}{\left[1 + r_c(x_q) \right]^2} \frac{1}{1 + r_c(x_{p+q})} \right\}. \end{aligned} \quad (\text{F.19})$$

Diagram 5: $\mathcal{D}_{AA}^{(3)}$:

The expression to compute reads

$$\mathcal{P}_{AA}^{(1)} \mathcal{D}_{AA}^{(3)} = -\frac{1}{2} \mathcal{P}_{AA}^{(1)} \left\{ \left[\Gamma_{AAAA}^{(4)}(p, -p, -q) \right]_{\mu\nu\rho\sigma}^{abcd} \left[(G \partial_t R_k G)_{AA}(-q) \right]_{\rho\sigma}^{cd} \right\}. \quad (\text{F.20})$$

We split the diagram into three terms and calculate the traces for each term separately, organized according to their common Lorentz tensor structure.

Colour trace

The relevant colour traces are

$$\begin{aligned}\delta^{ab} (f^{ade} f^{bce} + f^{ace} f^{bde}) \delta^{cd} &= 2C_2(A) d_A \\ \delta^{ab} (f^{ade} f^{bce} - f^{abe} f^{cde}) \delta^{cd} &= C_2(A) d_A \\ \delta^{ab} (f^{ace} f^{bde} + f^{abe} f^{cde}) \delta^{cd} &= C_2(A) d_A.\end{aligned}\tag{F.21}$$

Colour trace

The relevant Lorentz traces are

$$\begin{aligned}\Pi_{\mu\nu}^\perp(p) \Pi_{\rho\sigma}^\perp(q) \delta_{\mu\nu} \delta_{\rho\sigma} &= (d-1)^2 \\ -\Pi_{\mu\nu}^\perp(p) \Pi_{\rho\sigma}^\perp(q) \delta_{\mu\rho} \delta_{\nu\sigma} &= -\left(d-2 + \frac{(p \cdot q)^2}{p^2 q^2}\right) \\ -\Pi_{\mu\nu}^\perp(p) \Pi_{\rho\sigma}^\perp(q) \delta_{\mu\sigma} \delta_{\nu\rho} &= -\left(d-2 + \frac{(p \cdot q)^2}{p^2 q^2}\right).\end{aligned}\tag{F.22}$$

Result

Putting everything together, we obtain

$$\begin{aligned}\mathcal{P}_{AA}^{(1)} \mathcal{D}_{AA}^{(3)} &= -\frac{C_2(A)}{d-1} \int_q \left\{ \frac{\lambda_{AAAA}(p, -p, -q)}{Z_A(q)} \left(3 + d(d-3) - \frac{(p \cdot q)^2}{p^2 q^2} \right) q^2 \right. \\ &\quad \left. \frac{\partial_t r_A(x_q) - \eta_A(q) r_A(x_q)}{\left(q^2 [1 + r_A(x_q)] + m_A^2 \right)^2} \right\}.\end{aligned}\tag{F.23}$$

Remarks:

All diagrams are proportional to $C_2(A)\alpha_S$, hence the dependence on the gauge group can be absorbed into a rescaling of the strong coupling constant.

F.4. Regulators

Here we discuss the choice of the propagator dressings in Yang-Mills theory. This discussion is taken from [54]. The respective choice has been used in [54, 55, 56].

In the functional renormalisation group, the choice of the regulator, together with the choice of the cutoff-independent parts of the initial effective action corresponds to defining a renormalisation scheme, for a more detailed discussion see [9]. Moreover, to any given order of a given approximation scheme there exist optimised regulators that lead to the most rapid convergence of the results, hence minimising the systematic error, see [175, 15, 9]. For recent extensions and applications relevant for the present work see [18, 174, 18]. In the present work we use

$$\begin{aligned}R_{k,\mu\nu}^{ab}(p) &= \tilde{Z}_{A,k} r(p^2/k^2) p^2 \delta^{ab} \Pi_{\mu\nu}^\perp(p), \\ R_k^{ab}(p) &= \tilde{Z}_{c,k} r(p^2/k^2) p^2 \delta^{ab},\end{aligned}\tag{F.24}$$

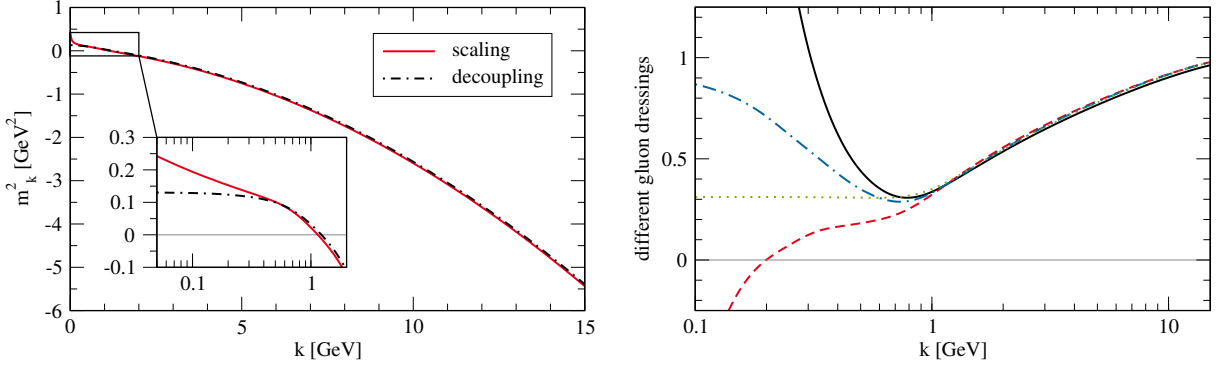


Figure F.3.: Left: Gluon mass parameter $m_k^2 = \Gamma_{AA,k}^{(2)}(p = 0)$ over k . Right: Possible choices for the scaling prefactor in the gluon regulator: $Z_{A,k}(k)$ (black, solid), $\bar{Z}_{A,k}(k)$ (red, dashed), $\hat{Z}_{A,k}(k)$ (blue, dot-dashed) and $\tilde{Z}_{A,k}$ (green, dotted) as defined in (F.26) and (F.28). Independence of the results from the above choice has been checked explicitly.

for the gluon and the ghost fields, respectively. For the shape function we choose a smooth version of the Litim or flat regulator [175]:

$$r(x) = \left(\frac{1}{x} - 1\right) \cdot \frac{1}{1 + e^{\frac{x-1}{a}}}, \quad (\text{F.25})$$

where we set $a = 0.02$. It has been argued in [9] that smooth versions of the flat regulator satisfy the functional optimisation criterion put forward there.

In ?? we multiply the regulators with scaling factors \tilde{Z} , related to the corresponding wave function renormalisations of the gluon and ghost fields

$$\begin{aligned} \tilde{Z}_{A,k} &:= Z_{A,k}((k^n + \bar{k}^n)^{1/n}), \\ \tilde{Z}_{c,k} &:= Z_{c,k}(k), \end{aligned} \quad (\text{F.26})$$

where we choose $n \approx 6$ and $\bar{k} \approx 1$ GeV. The cutoff scale running of \tilde{Z}_A is held constant below scales of about 1 GeV as the gluon wave function renormalisation $Z_{A,k}(p \approx k)$ diverges for $k \rightarrow 0$. Separating the tensor structure by

$$[\Gamma_{AA}^{(2)}]_{\mu\nu}^{ab}(p) =: \Gamma_{AA,k}^{(2)}(p) \delta^{ab} \Pi_{\mu\nu}^\perp(p), \quad (\text{F.27})$$

we parameterise $\Gamma_{AA,k}^{(2)}(p)$ by

$$\begin{aligned} \Gamma_{AA,k}^{(2)}(p) &=: Z_{A,k}(p) \cdot p^2 \\ &=: \bar{Z}_{A,k}(p) \cdot p^2 + m_k^2 \\ &=: \hat{Z}_{A,k}(p) \cdot (p^2 + m_k^2), \end{aligned} \quad (\text{F.28})$$

where we define $m_k^2 := \Gamma_{AA,k}^{(2)}(0)$ to guarantee the uniqueness of $\hat{Z}_{A,k}$. We see that these choices differ considerably below 1 GeV. For more details see Figure F.3 (right panel). In particular the naive choice $Z_{A,k}$ diverges since it carries the gluon mass gap. Consequently, we freeze $Z_{A,k}$ at a scale \bar{k} close to 1 GeV. We have checked explicitly that varying the value of \bar{k} and n has no influence on our results.

F.4.1. BRST transformation of the cutoff term

Here we consider (minus) the right hand side of (5.143),

$$\langle \mathfrak{s} \Delta S_k \rangle + \frac{\delta \Gamma_k}{\delta Q} \cdot \frac{\delta \Delta S_k}{\delta \Phi} = \langle \mathfrak{s} \Delta S_k \rangle + \mathfrak{s}_\Gamma \Delta S_k . \quad (\text{F.29})$$

where

$$\mathfrak{s}_\Gamma \Phi_i = \frac{\delta \Gamma_k}{\delta Q^i} = -\frac{\delta W_k}{\delta Q^i} , \quad (\text{F.30})$$

see (5.139). This leads us to

$$\langle (\mathfrak{s} \Phi_i) R^{ij} \Phi_j \rangle + (\mathfrak{s}_\Gamma \Phi_i) R^{ij} \Phi_j = \frac{\delta}{\delta Q^i} \langle R^{ij} \Phi_j \rangle = R^{ij} \frac{\delta}{\delta J^j} \frac{\delta}{\delta Q^i} W_k[J, Q] , \quad (\text{F.31})$$

where we have used (F.30) twice. We have also used, that the derivatives w.r.t. to J_j and Q_i , that are contracted with the regulator R^{ij} , commute. Now we use (F.30) again, and arrive at

$$\langle (\mathfrak{s} \Phi_i) R^{ij} \Phi_j \rangle + (\mathfrak{s}_\Gamma \Phi_i) R^{ij} \Phi_j = -R^{ij} \frac{\delta}{\delta J^j} \frac{\delta \Gamma_k[\Phi, Q]}{\delta Q^i} = -R^{ij} G_{jl} \frac{\delta^2 \Gamma_k[\Phi, Q]}{\delta \Phi_l \delta Q^i} , \quad (\text{F.32})$$

where we have used (1.12) for rewriting $\delta/\delta J$ as $G \cdot \delta/\delta \Phi$.

F.5. Wegner-Wilson loop

It is left to determine the operator $O_{q\bar{q}}$ as well as the underlying symmetry behind the confinement-deconfinement phase transition in pure Yang-Mills, as well as its breaking by dynamical quarks. To that end let us first consider an electron-positron pair, which is created at some initial time, pulled apart, kept at some distance L and then is annihilated, this describes a path C in space-time, see Figure F.4. The related free energy is described by a path integral, where the current J_μ of the worldlines of the $e^+ e^-$ pair is coupled to the photon field A_μ with

$$\int_x J_\mu A_\mu = -i e \left(\int_{t_0}^{t_1} d\tau [A_0(t, \vec{x}) - A_0(t, \vec{y})] + \int_{\vec{x}}^{\vec{y}} d\vec{z} [\vec{A}(t_1, \vec{x}) - \vec{A}(t_0, \vec{y})] \right) , \quad (\text{F.33})$$

with the worldline current

$$J_\mu(x) = -i e \int_C dz_\mu \delta(z - x) . \quad (\text{F.34})$$

The global sign in the current is pure convention and is related to that in the covariant derivative, in our case we have $D_\mu = \partial_\mu - i g A_\mu$, see ??.

In conclusion the source term (or operator of such a static electron-positron pair) is given by

$$\mathcal{W}_C[A] = e^{\int_x J_\mu A_\mu} = \underbrace{e^{-i e \int_C dz_\mu A_\mu(z)}}_{\text{Wegner-Wilson Loop}} . \quad (\text{F.35})$$

The Wegner-Wilson loop in QED has a very simple interpretation which we shall discuss briefly. Consider a closed path C that is the boundary of an area \mathcal{A} . Then the integral in the exponent can be rewritten with Stokes' theorem as

$$e \int_{C=\partial\mathcal{A}} dz_\mu A_\mu(z) = e \frac{1}{2} \int_{\mathcal{A}} dx_\mu dy_\nu F_{\mu\nu} . \quad (\text{F.36})$$

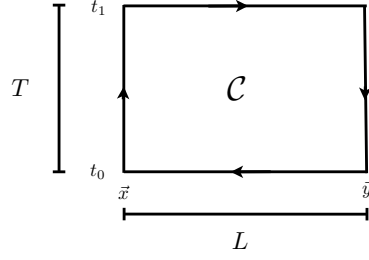


Figure F.4.: e^+e^- pair.

Accordingly, the phase in the Wegner-Wilson loop simply is the flux through the area \mathcal{A} with the boundary C . This is an observable quantity and is gauge invariance is evident from the flux representation (F.36). In the gauge field representation the gauge invariance of (F.35) follows with the $U(1)$ gauge transformations $U = \exp i\omega \in U(1)$ of $A_\mu \rightarrow A_\mu + 1/e \partial_\mu \omega$ with,

$$\mathcal{W}_C[A^U] = e^{-ie \int_C dz_\mu A_\mu^U(z)} = e^{-ie \int_C dz_\mu (A_\mu(z) + \frac{1}{e} \partial_\mu \omega)} = e^{-ie \int_C dz_\mu A_\mu(z)}, \quad (\text{F.37})$$

where we have used that $\int_C dz_\mu \partial_\mu \omega = 0$. Note also that an open Wilson line related to a path from the position x to the position y is a *parallel transporter* that transports gauge transformations from the position x to y ,

$$\mathcal{W}_{C_{x,y}}[A] = e^{-ie \int_{C_{x,y}} dz_\mu A_\mu(z)}, \quad \text{with} \quad \mathcal{W}_{C_{x,y}}[A^U] = U(x) \mathcal{W}_{C_{x,y}}[A] U^\dagger(y), \quad (\text{F.38})$$

This allows to define gauge-invariant correlation functions of e.g. fermionic fields ψ such as

$$\langle \bar{\psi}(x) \mathcal{W}_{C_{x,y}}[A] \psi(y) \rangle. \quad (\text{F.39})$$

In the case with dynamical electrons (F.39) describes a e^+e^- pair.

The above definitions and relations extend straightforwardly to non-Abelian gauge groups. The only change comes from the fact that now the gauge field is matrix valued and the simple exponential of $i g \int dz_\mu A_\mu$ does not have the necessary transformation properties (F.38) and the closed loop would fail to be gauge invariant. This situation is similar to that of defining the time-evolution operator in quantum mechanics and quantum field theory (S-matrix) on the basis of a Hamiltonian operator \hat{H} . There the resolution is to resort to time-ordering. In the present case we resort to path ordering which then transports the gauge transformation along the path. We define

$$U_{C_{x,y}} = \mathcal{P} e^{-ig \int_{C_{x,y}} dz_\mu A_\mu(z)}, \quad \text{with} \quad U_{C_{x,y}}[A^U] = U(x) U_{C_{x,y}} U^\dagger(y), \quad U(x) \in SU(N_c). \quad (\text{F.40})$$

The loop $U_C \in SU(N_c)$ is a group element and the transformation property under gauge transformation of A_μ , (5.7), originates in the path ordering defined with

$$\mathcal{P} A_{\mu_1}(x(s_1)) \cdots A_{\mu_n}(x(s_n)) = A_{\mu_{\sigma(1)}}(x(s_{\sigma(1)})) \cdots A_{\mu_{\sigma(n)}}(x(s_{\sigma(n)})), \quad \text{with} \quad s_{\sigma(1)} \leq s_{\sigma(2)} \leq \cdots \leq s_{\sigma(n)}. \quad (\text{F.41})$$

In (F.41) $s \in [0, 1]$ is an isomorphic (invertible) parameterisation $x(s)$ of the given path $C_{x,y}$ with $x(0) = x$ and $x(1) = y$. For integrals this leads to the relations well-known from the time ordering, the simplest one being that for a product of two integrals,

$$\frac{1}{2} \mathcal{P} \left[\int_x^y dz_\mu A_\mu(z) \int_x^y dz'_\nu A_\nu(z') \right] = \int_x^y dz_\mu A_\mu(z) \int_z^y dz'_\nu A_\nu(z'). \quad (\text{F.42})$$

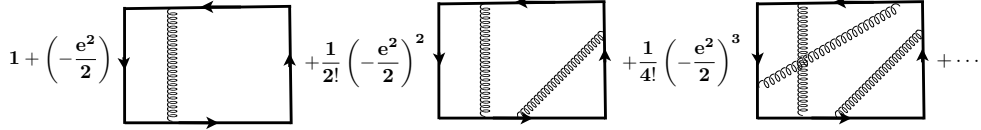


Figure F.5.: Perturbative expansion of the Wilson loop expectation value for e^+e^- .

Higher products follow similarly. Due to the path ordering derivatives of $U_{C_{x,y}}$ w.r.t. x or y pull down a gauge field to the left or to the right respectively.

$$\partial_\mu^x U_{C_{x,y}} = i g A_\mu(x) U_{C_{x,y}}, \quad \partial_\mu^y U_{C_{x,y}} = U_{C_{x,y}} (-i) g A_\mu(y). \quad (\text{F.43})$$

With these properties the covariant derivative can be simply expressed as a parallel transport of the partial derivative, to wit

$$U_{C_{x,y}} \partial_\mu^x U_{C_{x,y}}^\dagger = \partial_\mu^x - igA_\mu(x). \quad (\text{F.44})$$

The property (F.44) can be used to get a solution of the Dirac equation in terms of a phase factor \mathcal{W}_C and the solution of the free dirac equation ψ_0 . This is discussed in detail later for the static finite temperature case.

In summary this leads us to the definition of the expectation value of a quark–anti-quark pair in QCD with

$$\langle \bar{q}(x) \mathcal{W}_{C_{x,y}}[A] q(y) \rangle, \quad (\text{F.45})$$

with the Wilson line

$$\mathcal{W}_{C_{x,y}}[A] = \mathcal{P} e^{-i g \int_{C_{x,y}} A_\mu(z) dz_\mu}, \quad (\text{F.46})$$

where \mathcal{P} is the path ordering operator.

F.6. Wegner-Wilson loop in QED

For its computation let us first discuss the far simpler case of an electron-positron pair e^+e^- . Then the static potential is the standard Coulomb potential. Indeed in the static limit there is no self-interaction of the photon and the expectation value of the Wilson loop is simply given by the sum of boxes with n photon exchanges from positions x_i to y_i where one integrates over x_i and y_i on the contour $C[L, T]$. This is depicted in Figure F.5.

In other words we have

$$W[L, T] = e^{-\frac{e^2}{2} \int_{C[L,T]} dx_\mu \int_{C[L,T]} dy_\nu \langle A_\mu(x) A_\nu(y) \rangle_{\text{sub}}}, \quad (\text{F.47})$$

where we have used that $\langle A_{\mu_1} \cdots A_{\mu_{n+1}} \rangle = 0$. The subscript $\langle \cdots \rangle_{\text{sub}}$ refers to the necessary subtraction of infinite selfenergies related to close loops with endpoints $x = y$. Moreover, all correlation functions decay in products of two-point functions (Wick-theorem), schematically we have $\langle A_1 \cdots A_{2n} \rangle = \langle A_1 A_2 \rangle \cdots \langle A_{2n-1} A_{2n} \rangle + \cdots$, and there are $(2n-1)(2n-3)\cdots$ combinations. Upon contour integration all combinations give the same contribution and overall we have the n th order term in the propagator

$$\frac{(2n-1)(2n-3)\cdots}{(2n)!} 2^n \left(-\frac{e^2}{2}\right)^n \left(\int_C dx_\mu \int_C dy_\nu \langle A_\mu(x) A_\nu(y) \rangle \right)^n = \frac{1}{n!} \left(-\frac{e^2}{2} \int_C dx_\mu \int_C dy_\nu \langle A_\mu(x) A_\nu(y) \rangle \right)^n, \quad (\text{F.48})$$

for a general contour C , leading to the Gaussian expression (F.47). This leaves us with the task of computing

$$\begin{aligned}
\int_C dx_\mu \int_C dy_\nu \langle A_\mu(x) A_\nu(y) \rangle &= \int_C dx_\mu \int_C dy_\nu \int \frac{d^4 p}{(2\pi)^4} \frac{1}{p^2} \left(\delta_{\mu\nu} - (1-\xi) \frac{p_\mu p_\nu}{p^2} \right) e^{ip(x-y)} \\
&= \int_C dx_\mu \int_C dy_\mu \int \frac{d^4 p}{(2\pi)^4} \frac{1}{p^2} e^{ip(x-y)} \\
&= \int_C dx_\mu \int_C dy_\mu \frac{1}{4\pi^2} \frac{1}{(x-y)^2}.
\end{aligned} \tag{F.49}$$

To be explicit, we picked a covariant gauge in (F.49). However, we have already proven that the *closed* Wilson line is gauge invariant which now is explicit as the ξ -dependent term drops out with the help of

$$\int_C dx_\mu p_\mu e^{ipx} = -i \int_C dx_\mu \partial_\mu^x e^{ipx} = 0, \tag{F.50}$$

which eliminates all longitudinal contributions for closed loops. Note that this is not valid for open Wilson lines. Finally we are interested in the large T -limit in (7.7) where we have

$$\begin{aligned}
V_{e^+e^-}(L) &= - \lim_{T \rightarrow \infty} \frac{1}{T} \log W[L, T] = \lim_{T \rightarrow \infty} \frac{1}{T} \frac{e^2}{2} \lim_{T \rightarrow \infty} \int_{C[L,T]} dx_\mu \int_{C[L,T]} dy_\mu \left(\frac{1}{4\pi^2} \frac{1}{(x-y)^2} \right)_{\text{sub}} \\
&= - \lim_{T \rightarrow \infty} \frac{1}{T} e^2 \lim_{T \rightarrow \infty} \int_{t_0}^{t_1} dx_0 \int_{t_0}^{t_1} dy_0 \left(\frac{1}{4\pi^2} \frac{1}{(x_0-y_0)^2 + L^2} \right) \\
&= - \lim_{T \rightarrow \infty} \frac{1}{T} \frac{e^2}{4\pi} \lim_{T \rightarrow \infty} \int_{t_0}^{t_1} dx_0 \int_{t_0-x_0}^{t_1-x_0} dy_0 \left(\frac{1}{\pi} \frac{1}{y_0^2 + L^2} \right) \\
&= - \lim_{T \rightarrow \infty} \frac{1}{T} 2 \frac{e^2}{4\pi} \int_0^T dx_0 \arctan \left(\frac{x_0}{L} \right) \\
&= - \frac{e^2}{4\pi} \frac{1}{L}.
\end{aligned} \tag{F.51}$$

Equation (F.51) is the Coulomb potential as expected.

F.7. Details on the background field approach

In the background field approach the effective action has the following integro-differential path integral representation which facilitates the access to important properties,

$$e^{-\Gamma[\bar{A}, a]} = \int D\hat{a} \Delta_{\mathcal{F}}[\bar{A}, \hat{a} + a] \delta[\bar{D}_\mu(\hat{a}_\mu + a)] e^{-S_{\text{YM}}[A+\hat{a}] + \int_x \frac{\delta\Gamma[\bar{A}, a]}{\delta a^\mu} \hat{a}_\mu}, \quad J = \frac{\delta\Gamma[\bar{A}, a]}{\delta a}, \quad a = \langle \hat{a} \rangle. \tag{F.52}$$

where $\hat{A} = \bar{A} + \hat{a}$, $\bar{D} = D(\bar{A})$, $D = D(A)$ and we restricted ourselves to *Landau-deWitt gauge* ($\xi = 0$) with the background gauge fixing condition

$$\bar{D}_\mu \hat{a}_\mu = 0, \quad \longrightarrow \quad \mathcal{M}[\bar{A}, \hat{a} + a] = -\bar{D}_\mu D_\mu, \quad \Delta_{\mathcal{F}}[\bar{A}, \hat{a} + a] = \det \mathcal{M}[\bar{A}, \hat{a} + a]. \quad (\text{F.53})$$

see (7.45). A gauge invariant effective action is defined by

$$\Gamma[A] = \Gamma[A, 0], \quad (\text{F.54})$$

see (7.51). Inserting the relation between the a -derivative of Γ and the current J in (F.52) as well as using $\Gamma = \int_x J_\mu a_\mu - \log Z$ we arrive at the standard path integral expression for $Z[J]$ in the gauge (F.53). First we note that the effective action, evaluated on the equation of motion for the fluctuation field a ,

$$\frac{\delta \Gamma[\bar{A}, a]}{\delta a_\mu} \Big|_{a=a_{\text{EoM}}} = 0 \quad (\text{F.55})$$

does not depend on the background field: the effective action $\Gamma[\bar{A}, a_{\text{EoM}}]$ is given by (F.52) without the source term. Then the path integral in (F.52) reduces to

$$e^{-\Gamma[\bar{A}, a_{\text{EoM}}]} = \int D\hat{a}_{\text{gf}} e^{-S_{\text{YM}}[A + \hat{a}_{\text{gf}}]}. \quad (\text{F.56})$$

Even though the measure depends on the background field via the gauge fixing, the integration leads to \bar{A} -independent result as the action S_{YM} is gauge invariant. Therefore, (F.56) already entails that the two-field effective action reduces to the gauge invariant effective action in (F.54) on the EoM for the fluctuation field,

$$\Gamma[\bar{A}, a_{\text{EoM}}(\bar{A})] = \Gamma[A = \bar{A} + a_{\text{EoM}}(\bar{A})]. \quad (\text{F.57})$$

Accordingly we have

$$\frac{\delta \Gamma[\bar{A}, a_{\text{EoM}}(\bar{A})]}{\delta \bar{A}} = \frac{\delta}{\delta \bar{A}} \Big|_{a_{\text{EoM}}} \Gamma[\bar{A}, a_{\text{EoM}}] = 0. \quad (\text{F.58})$$

The first relation in (F.58) follows with (F.55), the second from the \bar{A} -independence of the integration in (F.56). In conclusion, a solution to the EoM of a also is one of \bar{A} . Moreover, such a solution is equivalent to solving the EoM for the gauge invariant effective action $\Gamma[A]$,

$$\frac{\delta \Gamma[A]}{\delta A} \Big|_{A=A_{\text{EoM}}} = 0, \quad \text{with} \quad a = 0. \quad (\text{F.59})$$

F.8. Perturbative Polyakov loop potential

As a preparation for the full computation we go through the perturbative computation. This already reveals the main mechanism we need for the access of the confinement-deconfinement phase transition. This computation has been done independently in [101] and [102] in 1980 (published 81). The potential is often called the Weiss potential.

For the explicit computation we restrict ourselves to $SU(2)$. The result does not depend on the gauge fixing parameter ξ and we choose $\xi = 1$, Feynman gauge, in order to facilitate the computation. Then the Lorentz part of the trace in the gauge field loop can be performed immediately, leading to a factor four for the four polarisations of a vector field. We have

$$V_{\text{pol}}(A_0) \simeq 4 * \frac{1}{2} \text{Tr} \ln(-D_\rho^2) - 2 * \frac{1}{2} \text{Tr} \ln(-D_\rho^2) = 2 \frac{1}{2} \text{Tr} \ln(-D_\rho^2), \quad (\text{F.60})$$

where we have made explicit the multiplicities of gluon and ghost, and we dropped the normalisation. The gluon dominates and the final result is twice that of one polarisation, which accounts for the two physical polarisations of the gluon. This is an expected property as we compute a gauge invariant potential that should reflect the fact that we only have two physical polarisations, and the gauge fixing is only a means to finally compute gauge invariant quantities. Now we use that we can diagonalise the operator D_ρ^2 in the adjoint representation in the algebra. The color eigenfunctions and eigenvalues in the adjoint representation are given by

$$\frac{g\beta}{2\pi} A_0^{\text{ad}} |\varphi_n^{\text{ad}}\rangle = \nu_n^{\text{ad}} |\varphi_n^{\text{ad}}\rangle, \quad n \in 1, \dots, N_c^2 - 1, \quad (\text{F.61})$$

and

$$SU(2) : \nu_n^{\text{ad}} \in (0, \pm\varphi), \quad SU(3) : \nu_n^{\text{ad}} \in \left(0, 0, \pm\varphi_3, \pm\frac{\varphi_3 \pm \sqrt{3}\varphi_8}{2}\right). \quad (\text{F.62})$$

Note that the eigenvalues of T_{ad}^3 are ± 1 , while they are $\pm 1/2$ in the fundamental representation. The relative factor 1/2 reflects the sensitivity to center transformations in the fundamental representation and the insensitivity in the adjoint representation. Performing the trace in (F.60) in terms of the eigenfunctions $|\varphi_n\rangle$ and momentum modes, we arrive at

$$V_{\text{Pol}}(A_0) \simeq 2[V_{\text{mode}}(\varphi) + V_{\text{mode}}(-\varphi)], \quad (\text{F.63})$$

with V_{Pol} being $1/2\text{Tr} \ln(-D^2)$, where the gauge field is substitute by one eigenmode,

$$\begin{aligned} V_{\text{mode}}(\varphi) &= \frac{T}{2} \sum_{n \in \mathbb{Z}} \int \frac{d^3 p}{(2\pi)^3} \left\{ \ln \frac{(2\pi T)^2(n + \varphi)^2 + \vec{p}^2}{(2\pi T)^2 n^2 + \vec{p}^2} \right\} \\ &= \frac{T}{4\pi^2} \sum_{n \in \mathbb{Z}} \int_0^\infty dp p^2 \left\{ \ln \frac{(2\pi T)^2(n + \varphi)^2 + p^2}{(2\pi T)^2 n^2 + p^2} \right\}, \end{aligned} \quad (\text{F.64})$$

where the denominator in the logarithm in (F.64) is a normalisation of the mode potential at vanishing φ : $V_{\text{mode}}(0) = 0$. The sum in (F.64) can be performed analytically by taking first a derivative w.r.t. p^2 and then using contour integrals. It results in

$$V_{\text{mode}}(\varphi) = \frac{T}{4\pi^2} \int_0^\infty dp p^2 \left\{ \left[\sum_{\pm} \ln \sinh \frac{\beta p \pm 2\pi i \varphi}{2} \right] - 2 \ln \sinh \frac{\beta p}{2} \right\}. \quad (\text{F.65})$$

Now we use that

$$\begin{aligned} \sum_{\pm} \ln \sinh \frac{\beta p \pm 2\pi i \varphi}{2} - 2 \ln \sinh \frac{\beta p}{2} &= \sum_{\pm} \ln(1 - e^{-\beta p \pm 2\pi i \varphi}) - 2 \ln(1 - e^{-\beta p}) \\ &= \sum_{\pm} \sum_{n=1}^\infty \frac{1}{n} e^{-\beta p n} (e^{\pm 2\pi i n \varphi} - 1). \end{aligned} \quad (\text{F.66})$$

In (F.66) we have pulled out a factor $\ln \exp(\beta p \pm 2\pi i \varphi)/2 = (\beta p \pm 2\pi i \varphi)/2$ from the $\ln \sinh$ -terms with φ , and $2 \ln \exp \beta p / 2 = \beta p$ from the $\ln \sinh$ -term in the normalisation. These terms cancel each other and we are led to the right hand side of (F.66). Then we have expanded the logarithms in a Taylor expansion

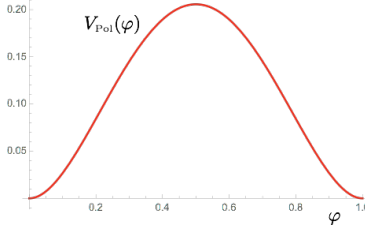


Figure F.6.: One loop Polyakov loop potential for $SU(2)$.

in the exponentials. In summary this leads us to

$$\begin{aligned} V_{\text{mode}}(\varphi) &= \frac{T}{4\pi^2} \int_0^\infty dp p^2 \sum_{\pm} \sum_{n=1}^\infty \frac{1}{n} e^{-\beta pn} (e^{\pm 2\pi i n \varphi} - 1) \\ &= \frac{T^4}{\pi^2} \sum_{n=1}^\infty \frac{1}{n^4} (\cos 2\pi n \varphi - 1). \end{aligned} \quad (\text{F.67})$$

The sum in (F.67) is gain easily performed with methods of complex analysis and we arrive at

$$\beta^4 V_{\text{mode}}(\varphi) = \frac{\pi^2}{48} \left[4 \left(\tilde{\varphi} - \frac{1}{2} \right)^2 - 1 \right]^2, \quad \tilde{\varphi} = \varphi \bmod 1, \quad (\text{F.68})$$

where we have devided out the trivial dimensional thermal factor T^4 . Inserting (F.68) in (F.63) for the Polyakov loop potential we are led to

$$\beta^4 V_{\text{pol}}(A_0) = \frac{\pi^2}{12} \left[4 \left(\tilde{\varphi} - \frac{1}{2} \right)^2 - 1 \right]^2, \quad (\text{F.69})$$

for $SU(2)$, while for $SU(3)$ the potential is given by

$$V_{\text{pol}}(A_0) = \sum_{n=1}^8 V_{\text{mode}}(\nu_n), \quad (\text{F.70})$$

with the eigenvalues ν_n in (F.62). We have plotted the $SU(2)$ potential in Figure F.6 as it has a very simple form which carries already the relevant information. The potential has minima at $\varphi = 0, 1$ and a maximum at $\varphi = 1/2$. For the minima the Polyakov loop variable $L[A_0]$ takes the value ± 1 , the maximum is the center-symmetric value $L[A_0] = 0$. This structure is also present for all $SU(N)$ -theories and originates in the -necessary- center symmetry of the potential. The center transformation in $SU(2)$ is given by

$$\varphi \rightarrow 1 - \varphi, \quad (\text{F.71})$$

which maps $L[\varphi = 0] = 1 \rightarrow L[\varphi = 1] = -1$ and vice versa, this comes via the multiplication of the Polyakov line $P(\vec{x})$ with the center element $-\mathbb{I}$. We conclude that in perturbation theory the potential has its minimum at the maximally center-breaking values, the theory is in the center-broken phase. At large temperatures perturbation theory is valid and quantum fluctuations are small: the fluctuating gauge field is close to $A_0 = 0$. This leads to

$$\lim_{T \rightarrow \infty} L[\langle A_0 \rangle] = 1. \quad (\text{F.72})$$

In turn, for small temperatures the potential should exhibit a minimum at $\varphi = 1/2$. Interestingly, this is achieved within the one loop computation if the gluon contributions are switched off, and the ghost contribution is left.

Finally we come back to the normalisation of $V_{\text{pol}}(A_0)$ in (7.64). We have normalised it such that $V_{\text{pol}}(A_0) = 0$. However, if we choose the normalisation as

$$\mathcal{N} = \left[\frac{1}{2} \text{Tr} \ln G_A^{-1}(0) - \text{Tr} G_c^{-1}(0) \right]_{T=0}, \quad (\text{F.73})$$

the value of the effective potential simply is the thermal pressure of the theory. The difference between (F.73) and that chosen in (F.64) for the mode potential is given by

$$\Delta\mathcal{N} = 2(N_c^2 - 1) \left[\frac{T}{2} \sum_{n \in \mathbb{Z}} \int \frac{d^3 p}{(2\pi)^3} \ln \left[(2\pi T)^2 n^2 + \vec{p}^2 \right] - \int \frac{d^4 p}{(2\pi)^4} \ln p^2 \right] = -p_{A,\text{SB}}, \quad (\text{F.74})$$

with

$$p_{A,\text{SB}} = \frac{\pi^4 T^4}{45} (N_c^2 - 1). \quad (\text{F.75})$$

Equation (F.74) is nothing but (minus) the Stefan-Boltzmann pressure of a $SU(N_c)$ gauge theory, see (F.75) for the scalar case. It is the scalar pressure times the number of physical modes: two physical transversal polarisations times the number of color modes, $(N_c^2 - 1)$, leading to $2(N_c^2 - 1)p_{\phi,\text{SB}}$. This leads us to our final result, the Weiss potential [101, 102],

$$\beta^4 V_{\text{pol}}(A_0) = \frac{\pi^2}{12} \left[4 \left(\tilde{\varphi} - \frac{1}{2} \right)^2 - 1 \right]^2 - \frac{\pi^4}{45} (N_c^2 - 1). \quad (\text{F.76})$$

G. Quantum Gravity appendices

G.1. Heat-Kernel techniques

We want to evaluate the trace of a function that depends on the Laplace operator on a curved background. The function can depend on couplings and background curvature, but for now we assume that it does not depend on covariant derivatives.

In general such a trace can be defined as sum/integral over the eigenvalues of the Laplace operator,

$$\text{Tr}f(\Delta) = N \sum_{\ell} \rho(\ell) f(\lambda(\ell)). \quad (\text{G.1})$$

Here $\lambda(\ell)$ are the spectral values, $\rho(\ell)$ are the multiplicities or the spectral density and N is some normalisation factor. The most standard example is the flat background where (G.1) turns into a standard momentum integral. For non-flat backgrounds a standard example is the four-sphere with constant background curvature $r = \frac{\bar{R}}{k^2} > 0$. There the spectrum of the scalar Laplacian is discrete and the spectral values and the multiplicities are given by

$$\lambda(\ell) = \frac{\ell(3+\ell)}{12}r, \quad \rho(\ell) = \frac{(2\ell+3)(\ell+2)!}{6\ell!}. \quad (\text{G.2})$$

The spectrum is discrete and ℓ takes integer values $\ell \geq 0$. The normalisation N is the inverse volume of the four sphere $N = V^{-1} = \frac{k^4 r^2}{384\pi^2}$. In summary, we can evaluate (G.1) for constant positive curvature in terms of an infinite series

$$\text{Tr}f(\Delta) = \frac{k^4 r^2}{384\pi^2} \sum_{\ell=0}^{\infty} \frac{(2\ell+3)(\ell+2)!}{6\ell!} f\left(\frac{\ell(3+\ell)}{12}r\right), \quad (\text{G.3})$$

which is called the spectral sum. This sum converges rather fast for large r , but convergence becomes exponentially slow in the limit $r \rightarrow 0$. When the curvature is negative similar formulas hold, but the spectrum of the Laplacian is continuous. The resulting integrals are called spectral integrals.

The heat-kernel method can be understood as curvature expansion about the flat background. Hence it allows for precise results for small values of the curvature, but it is hard to access the large curvature regime. The master formula for the heat-kernel techniques is

$$\text{Tr}f(\Delta) = \frac{1}{(4\pi)^{\frac{d}{2}}} \left[B_0(\Delta) Q_2[f(\Delta)] + B_2(\Delta) Q_1[f(\Delta)] \right] + O(\bar{R}^2), \quad (\text{G.4})$$

where the B_n are the heat-kernel coefficients of the Laplace operator Δ and the Q_n are defined by

$$Q_n[f(x)] = \frac{1}{\Gamma(n)} \int dx x^{n-1} f(x). \quad (\text{G.5})$$

In the following we show where this formula comes from and how it is used. A very common derivation uses the Laplace transformation

$$f(\Delta) = \int_0^{\infty} ds e^{-s\Delta} \tilde{f}(s). \quad (\text{G.6})$$

Applying this to (G.1) leads to

$$\mathrm{Tr}f(\Delta) = \int_0^\infty ds \tilde{f}(s) \mathrm{Tr} e^{-s\Delta}, \quad (\text{G.7})$$

where the last term is precisely the trace of the heat-kernel. For this trace the expansion is well established

$$\mathrm{Tr} e^{-s\Delta} = \frac{1}{(4\pi)^{\frac{d}{2}}} \sum_{n=0}^{\infty} s^{\frac{n-d}{2}} B_n(\Delta), \quad (\text{G.8})$$

and the coefficients B_n are again the heat-kernel coefficients as in (G.4). [Add reference!] Using this on (G.7) results in

$$\begin{aligned} \mathrm{Tr}f(\Delta) &= \frac{1}{(4\pi)^{\frac{d}{2}}} \sum_{n=0}^{\infty} B_n(\Delta) \int_0^\infty ds s^{\frac{n-d}{2}} \tilde{f}(s) \\ &= \frac{1}{(4\pi)^{\frac{d}{2}}} \sum_{n=0}^{\infty} \frac{1}{\Gamma(\frac{d-n}{2})} B_n(\Delta) \int_0^\infty dt t^{\frac{d-n}{2}-1} f(t) \\ &= \frac{1}{(4\pi)^{\frac{d}{2}}} \sum_{n=0}^{\infty} B_n(\Delta) Q_{\frac{d-n}{2}}[f(t)] \end{aligned} \quad (\text{G.9})$$

Here we have used the relation $\int_s s^{-x} \tilde{f}(s) = \frac{1}{\Gamma(x)} \int_z z^{x-1} f(z)$ [Should we show this relation?] and further used the definition of Q_n , see (G.5). Equation (G.9) is almost the same as (G.4). These reformulations have brought us the advantage that we have separated the dependences of the function f and of the Laplace operator Δ . The $Q_n[f]$ are in general easy to determine either numerically or even analytically. So we are only left with the task of determining the heat-kernel coefficients $B_k(\Delta)$. This has already been done for many different Laplacians and we want to display a few examples here.

First of all, the odd coefficients B_{2n+1} are zero. Furthermore they are usually expressed as

$$B_n(\bar{\Delta}) = \int d^d x \sqrt{\bar{g}} \mathrm{tr} b_n(\bar{\Delta}). \quad (\text{G.10})$$

If we choose the sphere as background the coefficients b_n simplify and we display them in Table G.1.

	TT	TV	S
$\mathrm{tr} b_0$	5	3	1
$\mathrm{tr} b_2$	$-\frac{5}{6}R$	$\frac{1}{4}R$	$\frac{1}{6}R$

Table G.1.: Heat kernel coefficients for transverse-traceless tensors (TT), transverse vectors (TV) and scalars (S) on S^4 .

G.2. Graviton propagator

G.2.1. York decomposition & curved background

We present here the graviton propagator in the York decomposition a maximally symmetric background in the gauge $\alpha = \beta = 0$. Recall that the York-decomposition for the graviton is given by

$$h_{\mu\nu} = h_{\mu\nu}^{\text{TT}} + 2\bar{\nabla}_{(\mu}\xi_{\nu)} + \left(\bar{\nabla}_\mu \bar{\nabla}_\nu - \frac{\bar{g}_{\mu\nu}}{d} \bar{\nabla}^2 \right) \sigma + \frac{1}{d} \bar{g}_{\mu\nu} h. \quad (\text{G.11})$$

With the field redefinitions according to [354, 355, 356]

$$\xi^\mu \rightarrow \frac{1}{\sqrt{\bar{\Delta} - \frac{\bar{R}}{4}}} \xi^\mu, \quad \sigma \rightarrow \frac{1}{\sqrt{\bar{\Delta}^2 - \bar{\Delta} \frac{\bar{R}}{3}}} \sigma, \quad (\text{G.12})$$

we cancel the non-trivial Jacobians and achieve that all field modes have the same mass dimension. The other field modes are not redefined. Then, with $g = \bar{g}$ the graviton two-point function has the shape

$$\begin{aligned} \Gamma_{hh}^{(2)} &= \begin{pmatrix} \Gamma_{h^{\text{TT}}h^{\text{TT}}}^{(2)} & 0 & 0 & 0 \\ 0 & \Gamma_{\xi\xi}^{(2)} & 0 & 0 \\ 0 & 0 & \Gamma_{h^{\text{Tr}}h^{\text{Tr}}}^{(2)} & \frac{1}{2}\Gamma_{h^{\text{Tr}}\sigma}^{(2)} \\ 0 & 0 & \frac{1}{2}\Gamma_{\sigma h^{\text{Tr}}}^{(2)} & \Gamma_{\sigma\sigma}^{(2)} \end{pmatrix} \\ &= \frac{Z_h}{32\pi} \begin{pmatrix} \Delta - 2\Lambda + \frac{2}{3}R & 0 & 0 & 0 \\ 0 & \frac{2}{\alpha}\Delta - 4\Lambda + \left(1 - \frac{1}{2\alpha}\right)R & 0 & 0 \\ 0 & 0 & \left(\frac{\beta^2}{8\alpha} - \frac{3}{8}\right)\Delta + \frac{\Lambda}{2} & \left(\frac{\beta}{\alpha} - 1\right)\frac{3}{8}\sqrt{\Delta^2 - \Delta\frac{R}{3}} \\ 0 & 0 & \left(\frac{\beta}{\alpha} - 1\right)\frac{3}{8}\sqrt{\Delta^2 - \Delta\frac{R}{3}} & \left(\frac{3}{\alpha} - 1\right)\frac{3}{8}\Delta - \frac{3}{2}\Lambda + \left(1 - \frac{1}{\alpha}\right)\frac{3}{8}R \end{pmatrix}. \end{aligned} \quad (\text{G.13})$$

Its inverse is given by

$$\left[\frac{1}{\Gamma^{(2)}} \right]_{hh} = \begin{pmatrix} G_{h^{\text{TT}}h^{\text{TT}}} & 0 & 0 & 0 \\ 0 & G_{\xi\xi} & 0 & 0 \\ 0 & 0 & G_{h^{\text{Tr}}h^{\text{Tr}}} & \frac{1}{2}G_{h^{\text{Tr}}\sigma} \\ 0 & 0 & \frac{1}{2}G_{\sigma h^{\text{Tr}}} & G_{\sigma\sigma} \end{pmatrix} \quad (\text{G.14a})$$

with $G_{\sigma h^{\text{Tr}}} = G_{h^{\text{Tr}}\sigma}$, and

$$\begin{aligned}
G_{h^{\text{TT}}h^{\text{TT}}} &= \frac{1}{\Delta + \frac{2R}{3} - 2\Lambda}, \\
G_{\xi\xi} &= \frac{\alpha}{2\Delta - (2 - \alpha)R - 4\alpha\Lambda}, \\
G_{h^{\text{Tr}}h^{\text{Tr}}} &= \frac{8(-\alpha R + R + (\alpha - 3)\Delta + 4\alpha\Lambda)}{(\beta - 3)^2\Delta^2 - 4(-\beta^2 + 2\alpha + 3)\Lambda\Delta + 16\alpha\Lambda^2 + R((- -\beta^2 + 2\beta + 2\alpha - 3)\Delta - 4(\alpha - 1)\Lambda)}, \\
G_{h^{\text{Tr}}\sigma} &= -\frac{16(\alpha - \beta)\sqrt{\Delta^2 - \frac{R\Delta}{3}}}{(\beta - 3)^2\Delta^2 - 4(-\beta^2 + 2\alpha + 3)\Lambda\Delta + 16\alpha\Lambda^2 + R((- -\beta^2 + 2\beta + 2\alpha - 3)\Delta - 4(\alpha - 1)\Lambda)}, \\
G_{\sigma\sigma} &= \frac{8(-\Delta\beta^2 + 3\alpha\Delta - 4\alpha\Lambda)}{3((\beta - 3)^2\Delta^2 - 4(-\beta^2 + 2\alpha + 3)\Lambda\Delta + 16\alpha\Lambda^2 + R((- -\beta^2 + 2\beta + 2\alpha - 3)\Delta - 4(\alpha - 1)\Lambda))}. \tag{G.14b}
\end{aligned}$$

In the limit $\alpha \rightarrow 0$ this simplifies tremendously to

$$\begin{aligned}
G_{h^{\text{TT}}h^{\text{TT}}} &= \frac{1}{\Delta + \frac{2R}{3} - 2\Lambda}, \\
G_{\xi\xi} &= 0, \\
G_{h^{\text{Tr}}h^{\text{Tr}}} &= -\frac{8(R - 3\Delta)}{R((\beta^2 - 2\beta + 3)\Delta - 4\Lambda) - \Delta(\Delta(\beta - 3)^2 + 4(\beta^2 - 3)\Lambda)}, \\
G_{h^{\text{Tr}}\sigma} &= -\frac{16\beta\sqrt{\Delta^2 - \frac{R\Delta}{3}}}{R((\beta^2 - 2\beta + 3)\Delta - 4\Lambda) - \Delta(\Delta(\beta - 3)^2 + 4(\beta^2 - 3)\Lambda)}, \\
G_{\sigma\sigma} &= \frac{8\beta^2\Delta}{3(R((\beta^2 - 2\beta + 3)\Delta - 4\Lambda) - \Delta(\Delta(\beta - 3)^2 + 4(\beta^2 - 3)\Lambda))}. \tag{G.14c}
\end{aligned}$$

The further choice $\beta = 0$ reduces the propagator to two dynamical degrees of freedom, the transverse traceless mode and the trace mode. Both the transverse vector mode and the scalar mode have disappeared,

$$G_{h^{\text{TT}}h^{\text{TT}}} = \frac{1}{\Delta + \frac{2R}{3} - 2\Lambda}, \quad G_{h^{\text{Tr}}h^{\text{Tr}}} = -\frac{8}{3}\frac{1}{\Delta - \frac{4}{3}\Lambda}, \quad G_{\xi\xi} = G_{h^{\text{Tr}}\sigma} = G_{\sigma\sigma} = 0. \tag{G.14d}$$

In the presence of the regulator the regularised propagator is given by $1/(\Gamma^{(2)} + R_k)$. Various forms have been used in the literature, in the fluctuation computations discussed in the present work we choose regulators

$$R_k = \Gamma_k^{(2)} \Big|_{R=0, \Lambda=0} r_k(x), \quad x = -\frac{\Delta}{k^2}. \tag{G.15}$$

Another choice being used frequently in the background approximation is

$$\Gamma^{(2)} + R_k = \Gamma^{(2)}(\Delta \rightarrow \Delta[1 + r_k(x)]), \tag{G.16}$$

For $\alpha = 0 = \beta$ both choices lead to the regularised propagators (at $\Phi = 0$)

$$G_{hh} = \left[\frac{1}{\Gamma^{(2)} + R_k} \right]_{hh} = \frac{32\pi}{Z_h k^2} \begin{pmatrix} \frac{1}{x[1+r_k(x)]+\mu+\frac{2}{3}r} & 0 & 0 & 0 \\ 0 & 0 & 0 & 0 \\ 0 & 0 & \frac{-\frac{8}{3}}{p^2[1+r_k(x)]+\frac{2}{3}\mu} & 0 \\ 0 & 0 & 0 & 0 \end{pmatrix}, \quad (\text{G.17})$$

where we have used the dimensionless quantities

$$x = -\frac{\Delta}{k^2}, \quad \mu = -\frac{2\Lambda}{k^2}, \quad r = \frac{R}{k^2}. \quad (\text{G.18})$$

G.2.2. Stelle decomposition & flat background

On a flat background it is simple to give explicit expressions for the projection operators. All projection operators are constructed from the transversal and the longitudinal projection operator

$$\Pi_{\mu\nu}^T = \delta_{\mu\nu} - \frac{P_\mu P_\nu}{p^2}, \quad \Pi_{\mu\nu}^L = \frac{P_\mu P_\nu}{p^2}. \quad (\text{G.19})$$

The four projection operators that span the space of symmetric rank four tensors are

$$\begin{aligned} \Pi_{\mu\nu\rho\sigma}^{(2)} &= \frac{1}{2} \left(\Pi_{\mu\rho}^T \Pi_{\nu\sigma}^T + \Pi_{\mu\sigma}^T \Pi_{\nu\rho}^T \right) - \frac{1}{3} \Pi_{\mu\nu}^T \Pi_{\rho\sigma}^T, \\ \Pi_{\mu\nu\rho\sigma}^{(1)} &= \frac{1}{2} \left(\Pi_{\mu\rho}^T \Pi_{\nu\sigma}^L + \Pi_{\mu\sigma}^T \Pi_{\nu\rho}^L + \Pi_{\nu\rho}^T \Pi_{\mu\sigma}^L + \Pi_{\nu\sigma}^T \Pi_{\mu\rho}^L \right), \\ \Pi_{\mu\nu\rho\sigma}^{(0-s)} &= \frac{1}{3} \Pi_{\mu\nu}^T \Pi_{\rho\sigma}^T, \\ \Pi_{\mu\nu\rho\sigma}^{(0-w)} &= \Pi_{\mu\nu}^L \Pi_{\rho\sigma}^L. \end{aligned} \quad (\text{G.20})$$

together with the mixing operators of the spin-0 modes

$$\Pi_{\mu\nu\rho\sigma}^{(0-sw)} = \frac{1}{\sqrt{3}} \Pi_{\mu\nu}^T \Pi_{\rho\sigma}^L, \quad \Pi_{\mu\nu\rho\sigma}^{(0-ws)} = \frac{1}{\sqrt{3}} \Pi_{\mu\nu}^L \Pi_{\rho\sigma}^T. \quad (\text{G.21})$$

$$\Gamma_{hh}^{(2)} = \frac{Z_h}{64\pi} \begin{pmatrix} 2(\mu_h k^2 + p^2) & 0 & 0 & 0 \\ 0 & 2\left(\mu k^2 + \frac{p^2}{\alpha}\right) & 0 & 0 \\ 0 & 0 & p^2\left(\frac{3}{\alpha} - 4\right) - \mu k^2 & -\sqrt{3}\left(\mu k^2 + \frac{p^2}{\alpha}\right) \\ 0 & 0 & -\sqrt{3}\left(\mu k^2 + \frac{p^2}{\alpha}\right) & \mu k^2 + \frac{p^2}{\alpha} \end{pmatrix}. \quad (\text{G.22})$$

G.3. Details of the fluctuation computation in pure gravity

G.4. Approximations of the stability matrix

The stability matrix B is defined as the Jacobi matrix of the flow equations for all couplings α_i . It is given by

$$B_{ij} = \partial_{\alpha_j} \partial_t \alpha_i . \quad (\text{G.23})$$

The critical exponents of a fixed point are defined as minus the eigenvalues of the stability matrix evaluated at this fixed point. In our setup, the stability matrix is infinite dimensional since it is spanned by all couplings λ_n and $g_n(p^2)$. Note that one momentum dependent coupling alone is enough to render the stability matrix infinite dimensional.

In this dissertation, only couplings up to order six appear in the flow. We furthermore do not resolve the full momentum dependence of the couplings. Thus, we have already rendered the stability matrix finite. Nevertheless, the full stability matrix is not known since the flows of the fifth- and sixth order couplings are unknown and depend itself on further higher couplings. In consequence, we have to make an approximation of the stability matrix to obtain the critical exponents. Note that we also have to make an approximation of the flow itself to close it. Naturally, these approximations are related.

We next present two different approximations of the stability matrix. We further argue that these approximations should give approximately the same values for the most relevant critical exponents if the expansion scheme is well converged. In almost all chapters of this dissertation we use the first approximation. In ?? we compare both methods.

The approximation of the flow is related to its closure and describes how the higher-order couplings are identified with the lower ones. We call this process identification scheme and denote it by $|_{\text{id.}}$. The two different approximations of the stability matrix are distinguished by the sequence of taking the derivatives and applying this identification scheme. In the first approximation, the identification is performed *before* taking the derivatives:

$$\bar{B}_{ij} = \partial_{\alpha_j} (\partial_t \alpha_i |_{\text{id.}}) . \quad (\text{G.24})$$

The critical exponents that correspond to this approximation represent the critical exponents that belong to the computed phase diagram of the theory.

In the second approximation, the identification is performed *after* taking the derivatives

$$\tilde{B}_{ij} = (\partial_{\alpha_j} \partial_t \alpha_i) |_{\text{id.}} . \quad (\text{G.25})$$

This approximation is more closely related to the full stability matrix in the sense that it respects the fact that the higher couplings in the full system do not coincide with the lower ones. Note that these two different approximations only differ if we choose a non-trivial identification scheme, i.e. if the higher-order couplings are functions of the lower ones.

If the expansion scheme is well converged, then the contributions of the higher couplings to the flow of the lower couplings are small, e.g. $(\partial_{\lambda_{n_{\max}+2}} \lambda_{n_{\max}}) |_{\text{FP}} \approx 0$. In this case, the most relevant eigenvalues of the stability matrices \bar{B} and \tilde{B} coincide approximately. The stabilisation of the most relevant eigenvalues was also observed in an expansion in R^n in [192]. In consequence, a huge deviation in the most relevant eigenvalues of both approximations would clearly indicate a lack of convergence. For this reason, we use the comparison of the different approximations as a first check of convergence.

G.5. Background couplings

In this Appendix we present the flow equations for the background couplings \bar{g} and $\bar{\lambda}$. They are in particular interesting in the limit $k \rightarrow 0$ where they become observables. In this limit, the regulator term

Identification scheme	μ^*	λ_3^*	λ_4^*	g_3^*	g_4^*	$\bar{\theta}_i$	$\tilde{\theta}_i$
$g_{n>4} \rightarrow g_3, \lambda_{n>4} \rightarrow \lambda_3$	-0.48	0.092	0.0077	0.62	0.53	5.0	$1.3 \pm 3.4i$
						4.2	$-0.62 \pm 1.8i$
						-4.7	-9.3
$g_{n>4} \rightarrow g_4, \lambda_{n>4} \rightarrow \lambda_3$	-0.45	0.12	0.028	0.83	0.57	4.7	$2.0 \pm 3.1i$
						5.0	$0.37 \pm 2.4i$
						-2.9	-8.0
						-5.6	-7.9
$g_{n>4} \rightarrow g_4, \lambda_{n>4} \rightarrow \lambda_4$	physical UV fixed point not found						
$g_{n>4} \rightarrow g_4, \lambda_6 \rightarrow \lambda_4, \lambda_5 \rightarrow \lambda_3$	-0.49	0.086	0.027	0.64	0.56	8.7	$1.4 \pm 3.7i$
						5.0	$-0.46 \pm 2.0i$
						-4.3	-11
						-5.5	-11

Table G.2.: Properties of the UV fixed point for different identification schemes, i.e. different closures of the flow equations, see App. G.6. The flow equations are computed with momentum dependent anomalous dimensions η_{ϕ_i} and bilocally projected Newton's couplings $g_n(k^2)$. The critical exponents $\bar{\theta}_i$ and $\tilde{\theta}_i$ stem from two approximation of the stability matrix, see App. G.4. An attractive UV fixed point is found in most identification schemes with mildly varying fixed point values. In the first approximation of the stability matrix we always find three attractive directions, while in the second approximation of the stability matrix we find one or three attractive directions, since the real part of one complex pair of eigenvalues is quite close to zero. These results suggest that the present system is rather stable under change of the closure of the flow equations. In the case of the single identification without a physical UV fixed point we found that it had in fact just vanished in the complex plane.

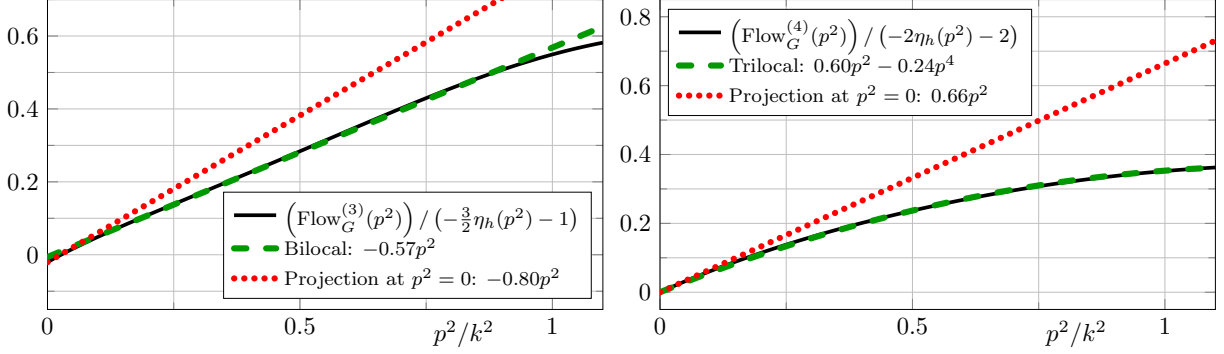


Figure G.1.: Fit of a local momentum projection at $p^2 = 0$ to the momentum dependence of the flow of the graviton three-point function (left) and the graviton four-point function (right) divided by $(-\frac{n}{2}\eta_h(p^2) - n + 2)$ as defined in (10.53). The flows are evaluated at $(\mu, \lambda_3, \lambda_4, g_3, g_4) = (-0.4, 0.1, -0.1, 0.7, 0.5)$ and $\lambda_6 = \lambda_5 = \lambda_3$ as well as $g_6 = g_5 = g_4$, i.e. the same values as in Figure 10.3 where a non-local momentum projection was used. In comparison to the non-local momentum projection, the local momentum projection does *not* capture the correct momentum dependence in the whole momentum range $0 \leq p^2 \leq k^2$ since it is sensitive to local momentum fluctuations. Furthermore, it is technically very challenging to project on the p^4 -term due to IR singularities. Note again that the constant parts of the flows are irrelevant for the beta functions since they are extracted from a different tensor projection.

vanishes by construction and diffeomorphism invariance is restored, which implies that these couplings can be interpreted as physical observables only for vanishing k .

For notational convenience we reintroduce the coupling $\lambda_2 = -\mu/2$. Following [356], we compute the flow of the background couplings with a curvature expansion on an Einstein space. We use a York-decomposition [171, 357] and field redefinitions [354, 355] to cancel the non-trivial Jacobians. The resulting flow equations are given by

$$\partial_t \bar{g} = 2\bar{g} - \bar{g}^2 f_{R^1}(\lambda_2; \eta_\phi), \quad \partial_t \bar{\lambda} = -4\bar{\lambda} + \bar{\lambda} \frac{\partial_t \bar{g}}{\bar{g}} + \bar{g} f_{R^0}(\lambda_2; \eta_\phi), \quad (\text{G.26})$$

where the functions f_{R^0} and f_{R^1} read

$$f_{R^0}(\lambda_2; \eta_\phi) = \frac{1}{24\pi} \left(\frac{(10 - 8\lambda_2)(6 - \eta_h(k^2))}{1 - 2\lambda_2} - 8(6 - \eta_c(k^2)) \right), \quad (\text{G.27})$$

$$f_{R^1}(\lambda_2; \eta_\phi) = \frac{1}{24\pi} \left(\frac{93 + 204\lambda_2 - 300\lambda_2^2 - \eta_h(k^2)(17 + 36\lambda_2 - 60\lambda_2^2)}{3(1 - 2\lambda_2)^2} + 10(5 - \eta_c(k^2)) \right).$$

In consequence the fixed point equations for the background couplings are given by

$$\bar{g}^* = \frac{2}{f_{R^1}(\lambda_2^*, \eta_\phi^*)}, \quad \bar{\lambda}^* = \frac{f_{R^0}(\lambda_2^*, \eta_\phi^*)}{2f_{R^1}(\lambda_2^*, \eta_\phi^*)}. \quad (\text{G.28})$$

Note that the background couplings are non-dynamical, i.e. they do not influence any other coupling. Furthermore, the background couplings only depend on the couplings of the two-point function. Hence only the graviton mass parameter μ (or equivalently λ_2) and the anomalous dimensions η_h and η_c directly affect them.

G.6. Dependence on the identification scheme

The flow of each n -point function depends on the couplings of the $(n+1)$ -point function and the $(n+2)$ -point function, see also [Figure 10.2](#). For the highest couplings, we consequently do not have a flow equation at hand. In our setup, these are the couplings of the five- and six-point function, i.e. λ_5 , λ_6 , g_5 , and g_6 . In order to close the flow of our system, we need to make an ansatz for these higher order couplings. A natural choice is one that is close to diffeomorphism invariance, i.e. to identify these couplings with a lower order coupling.

In our setup, there are two lower order couplings that correspond to a (partly) diffeomorphism invariant identification scheme, e.g. λ_5 can be identified with λ_3 or λ_4 . In a well converged expansion scheme, the details of the identification should not matter and lead to similar results. In this section, we compare the results for different identification schemes in order to evaluate the stability of our expansion scheme.

The properties of the non-trivial UV fixed point for different identifications schemes are displayed in [Table G.2](#). In all identification schemes except for the identification $g_{n>4} \rightarrow g_4$ and $\lambda_{n>4} \rightarrow \lambda_4$ we find an attractive UV fixed point. In this case we can see that the fixed point has just vanished in the complex plane. For all other identifications we observe that the fixed point values and the critical exponents vary mildly. Especially the number of attractive directions is consistently three with the first approximation to the stability matrix, c.f. [App. G.4](#). With the second approximation the number of attractive directions varies from one to three since the real part of one complex conjugated pair is close to zero.

In conclusion, this analysis suggests that our system is rather stable with respect to different identification schemes. Only one particular identification scheme has led to the disappearance of the attractive UV fixed point. This constitutes further support for our results in [subsection 10.7.2](#), where we found that our full system is very stable with respect to the identification of g_5 and g_6 .

G.7. Possible issues of a local momentum projection

In this section we want to point out some possible issues of a local momentum projection. A local momentum projection is for example a derivative expansion about a certain momentum, usually $p = 0$. The full solution of a flow equation includes a full resolution of the momentum dependence of all vertex flows. For higher n -point functions this task is computationally extremely challenging due to the high number of momentum variables. We have already argued in [subsection 10.6.2](#) that this task can be tremendously simplified with a symmetric momentum configuration. We have further shown in [subsection 10.6.3](#) that the quantity $\text{Flow}_G^{(n)} / (-\frac{n}{2}\eta_h(p^2) - n + 2)$ is polynomial in p^2 , at least for $n = 3, 4$. Thus it is possible to consistently project on each coefficient of this polynomial in the whole momentum range $0 \leq p^2 \leq k^2$ by employing a non-local momentum projection. In contrast, a local momentum projection scheme does not capture the correct momentum dependence over the whole momentum range $0 \leq p^2 \leq k^2$ in general since it is sensitive to local momentum fluctuations. Furthermore, it is very challenging to project on the p^4 coefficient or even higher momentum order coefficients due to IR singularities. All these statements are explicitly exemplified in [Figure G.1](#).

On the other hand, the local momentum projection at $p = 0$ has the advantage that it allows for analytic flow equations, as discussed in [App. G.9](#). Analytic flow equations are more easily evaluated in the whole theory space, but, as the discussion above suggests, one should be be mindful of the fact that they easily introduce a large error.

We use the analytic flow equations in [section 10.8](#) precisely for the reason that they can easily be evaluated in the whole theory space. Thus we show now that the fixed point properties in this analytic system are qualitatively similar to the full system, despite the error that is introduced by the analytic equations. The properties of the UV fixed point for different approximations are displayed in [Table G.3](#). Truncation 1 corresponds to our full system, i.e. with momentum dependent anomalous dimensions and bilocally evaluated gravitational couplings. Truncation 4 corresponds to the system used in [section 10.8](#), i.e.

Trunc.	μ^*	λ_3^*	λ_4^*	g_3^*	g_4^*		$\bar{\theta}_i$		
							$\tilde{\theta}_i$		
1	−0.45	0.12	0.028	0.83	0.57	4.7	$2.0 \pm 3.1i$	−2.9	−8.0
						5.0	$0.37 \pm 2.4i$	−5.6	−7.9
2	−0.41	0.076	0.0055	0.71	0.53	4.0	$1.5 \pm 3.6i$	−3.1	−6.0
						3.9	$0.38 \pm 4.4i$	−2.3	−6.6
3	−0.37	0.049	0.0055	1.1	0.83	7.3	$1.7 \pm 2.1i$	−3.0	−6.8
						7.2	$−0.32 \pm 2.7i$	−4.7	−6.8
4	−0.23	−0.060	−0.11	0.64	0.55	3.0	$1.9 \pm 1.6i$	−1.7	−3.4
						2.2	$0.50 \pm 1.7i$	−1.5	$± 0.88i$

Table G.3.: Properties of the UV fixed points for different approximations. In the truncations 3 and 4, we set $\eta_{\phi_i} = 0$, while in the truncations 1 and 2 we use momentum dependent anomalous dimensions. In truncations 2 and 4, the couplings $g_{3,4}$ are computed via a derivative expansion at $p^2 = 0$, while in the truncations 1 and 3 the couplings $g_{3,4}(k^2)$ are evaluated with a bilocal projection between $p^2 = 0$ and $p^2 = k^2$. The quality of the truncation decreases from 1 to 4. The fixed point values are obtained with the identification scheme $\lambda_{n>4} = \lambda_3$ and $g_{n>4} = g_4$. The critical exponents $\bar{\theta}_i$ and $\tilde{\theta}_i$ stem from two approximation of the stability matrix see App. G.4. The fixed point properties from different approximations are qualitatively very similar. In particular, all fixed points exhibit three relevant directions when the first approximation of the stability matrix is used. Using the second approximation of the stability matrix also results in three relevant directions in three out of four cases.

without anomalous dimensions and with gravitational couplings from a derivative expansion. Truncation 2 and 3 are in between those truncations, i.e. with anomalous dimension but gravitational couplings from a derivative expansion and without anomalous dimensions but with bilocally evaluated gravitational couplings, respectively.

We observe that the UV fixed point exists in all truncations, and that the properties of this fixed point vary mildly. The fixed point values are all located within a small region, with the exception of our simplest truncation. There, the couplings λ_3 and λ_4 have a different sign compared to the other truncations. Considering the critical exponents we always find three attractive directions with the first approximation of the stability matrix and in three out of four cases with the second approximation of the stability matrix. These results suggest that it is an acceptable approximation to use the analytic flow equations if one is only interested in the qualitative behaviour of the system.

G.8. Derivation of flow equations

We obtain the flow equations for the individual coupling constants by projecting onto the flow of the graviton n -point functions, as explained in ??.

The equations for the graviton mass parameter μ and for the graviton anomalous dimension η_h are extracted from the transverse-traceless part of the flow of the graviton two-point function. For $p^2 = 0$, we obtain the flow of the graviton mass parameter

$$\partial_t \mu = (\eta_h(0) - 2)\mu + \frac{32\pi}{5} \text{Flow}_{\text{TT}}^{(hh)}(0). \quad (\text{G.29})$$

We obtain an equation for the graviton anomalous dimension by evaluating the flow of the graviton two-point function bilocally at p^2 and $-\mu k^2$

$$\eta_h(p^2) = \frac{32\pi}{5(p^2 + \mu k^2)} \left(\text{Flow}_{\text{TT}}^{(hh)}(-\mu k^2) - \text{Flow}_{\text{TT}}^{(hh)}(p^2) \right). \quad (\text{G.30})$$

The ghost anomalous dimension is obtained from the transverse ghost two-point function

$$\eta_c(p^2) = -\frac{\text{Flow}_{\text{T}}^{(\bar{c}c)}(p^2)}{3p^2}. \quad (\text{G.31})$$

In case of the higher order couplings, we employ the projection operators described in [subsection 10.6.2](#). For the couplings λ_n , this leads to

$$\partial_t \lambda_n = \left(\frac{n}{2} \eta_h(0) + (n-4) - \frac{n-2}{2} \frac{\partial_t g_n}{g_n} \right) \lambda_n + \frac{g_n^{1-\frac{n}{2}}}{C^{\Lambda_n}} \text{Flow}_{\Lambda_n}^{(n)}(0), \quad (\text{G.32})$$

where the projection dependent constant is defined via $C^{\Lambda_n} = \Pi_{\Lambda_n} \circ \Pi_{\text{TT}}^n \circ \mathcal{T}^{(n)}(0; 1)$. Here, \circ denotes the pairwise contraction of indices.

As discussed in [??](#), the gravitational couplings $g_n(p^2)$ are momentum dependent. In order to simplify the computation we make an approximation of the full momentum dependence. This approximation exploits the fact that the flows are peaked at $p^2 = k^2$ and consequently we set the feed back on the right-hand side of the flow equation to $g_n(p^2) \approx g_n(k^2)$. This closes the flow equation for $g_n(k^2)$ and thus we only solve this equation. The easiest way to obtain the flow equation for $g_n(k^2)$ is a bilocal projection at $p^2 = 0$ and $p^2 = k^2$. For $g_4(k^2)$ we obtain

$$\begin{aligned} \partial_t g_4(k^2) &= 2g_4(k^2) + 2\eta_h(k^2)g_4(k^2) - C_4 g_4(k^2)\lambda_4(\eta_h(k^2) - \eta_h(0)) \\ &\quad + C_{p^2}^{G_4-1} (\text{Flow}_G^{(4)}(k^2) - \text{Flow}_G^{(4)}(0)). \end{aligned} \quad (\text{G.33})$$

The derivation of this equation is based on the assumption that λ_4 is small.

In [subsection 10.6.6](#) we have laid out a strategy to disentangle contributions from different tensor structures, in particular those of R and R^2 . The flow equations for the g_n are obtained by a projection onto the p^2 part of $\text{Flow}_G^{(n)}$ divided by $(-\frac{n}{2}\eta_h(p^2) - n + 2)$, see [subsection 10.6.3](#) and [subsection 10.6.6](#). The graviton three-point function is at most quadratic in the external momentum, and consequently it is again enough to use a bilocal projection at $p^2 = 0$ and $p^2 = k^2$. Consequently, the flow equation for g_3 is quantitatively equivalent to the previous one if λ_3 is small. The graviton four-point function, on the other hand, has p^4 as its highest momentum power, and thus we use a trilocal momentum projection at $p^2 = 0$,

$p^2 = k^2/2$, and $p^2 = k^2$. The flow equations of g_3 and g_4 are then given by

$$(1 + \eta_3) \partial_t g_3 = 2g_3 - 2g_3 C_3 (\partial_t \lambda_3 + 2\lambda_3) \left(\frac{1}{\frac{3}{2}\eta_h(k^2) + 1} - \frac{1}{\frac{3}{2}\eta_h(0) + 1} \right) \\ + \frac{2}{C_{p^2}^{G_3} \sqrt{g_3}} \left(\frac{\text{Flow}_G^{(3)}(k^2)}{\frac{3}{2}\eta_h(k^2) + 1} - \frac{\text{Flow}_G^{(3)}(0)}{\frac{3}{2}\eta_h(0) + 1} \right), \quad (\text{G.34})$$

$$(1 + \eta_4) \partial_t g_4 = 2g_4 - g_4 C_4 (\partial_t \lambda_4 + 2\lambda_4) \left(-\frac{1}{\eta_h(k^2) + 1} + \frac{4}{\eta_h(k^2/2) + 1} - \frac{3}{\eta_h(0) + 1} \right) \\ + \frac{1}{C_{p^2}^{G_4}} \left(-\frac{\text{Flow}_G^{(4)}(k^2)}{\eta_h(k^2) + 1} + 4 \frac{\text{Flow}_G^{(4)}(k^2/2)}{\eta_h(k^2/2) + 1} - 3 \frac{\text{Flow}_G^{(4)}(0)}{\eta_h(0) + 1} \right), \quad (\text{G.35})$$

$$\eta_3 = \frac{C_3 \lambda_3 - \frac{3}{2}\eta_h(k^2)}{\frac{3}{2}\eta_h(k^2) + 1} - \frac{C_3 \lambda_3}{\frac{3}{2}\eta_h(0) + 1}, \\ \eta_4 = \frac{-3C_4 \lambda_4}{\eta_h(0) + 1} + 4 \frac{C_4 \lambda_4 - \frac{1}{2}\eta_h(k^2/2)}{\eta_h(k^2/2) + 1} - \frac{C_4 \lambda_4 - \eta_h(k^2)}{\eta_h(k^2) + 1}.$$

The constants C are implicitly defined via $\Pi_{G_n} \circ \Pi_{\text{TT}}^n \circ \mathcal{T}^{(n)}(p^2; \Lambda_n) = C_{\Lambda_n}^{G_n} \Lambda_n + C_{p^2}^{G_n} p^2$, and we use the abbreviation $C_n = C_{\Lambda_n}^{G_n}/C_{p^2}^{G_n}$. Note that the constants η_n are chosen in such a way that $\eta_n = 0$ for vanishing anomalous dimensions.

Analogously, we can obtain a flow equation for the R^2 coupling of the graviton four-point function ω_4 by using a trilocal momentum projection, as explained in subsection 10.6.6. We evaluate the flows at the same momenta as for the trilocal flow equation of g_4 . The equation for ω_4 then reads

$$(1 + \eta_\omega) \partial_t \omega_4 = 2\omega_4 - \frac{C_{\Lambda_4}^{G_4}}{C_{\Omega_4}^{G_4}} (\partial_t \lambda_4 + 2\lambda_4) \left(\frac{1}{\eta_h(k^2) + 1} - \frac{2}{\eta_h(k^2/2) + 1} + \frac{1}{\eta_h(0) + 1} \right) \\ - \frac{\partial_t g_4}{g_4} \left(\frac{C_{\Lambda_4}^{G_4} \lambda_4 + C_{p^2}^{G_4} + C_{\Omega_4}^{G_4} \omega_4}{\eta_h(k^2) + 1} - 2 \frac{C_{\Lambda_4}^{G_4} \lambda_4 + \frac{1}{2}C_{p^2}^{G_4} + \frac{1}{4}C_{\Omega_4}^{G_4} \omega_4}{\eta_h(k^2/2) + 1} + \frac{C_{\Lambda_4}^{G_4} \lambda_4}{\eta_h(0) + 1} \right) \\ + \frac{1}{C_{\Omega_4}^{G_4} g_4} \left(\frac{\text{Flow}_G^{(4)}(k^2)}{\eta_h(k^2) + 1} - 2 \frac{\text{Flow}_G^{(4)}(k^2/2)}{\eta_h(k^2/2) + 1} + \frac{\text{Flow}_G^{(4)}(0)}{\eta_h(0) + 1} \right), \\ \eta_\omega = \frac{\eta_h(k^2/2)}{\eta_h(k^2/2) + 1} - \frac{2\eta_h(k^2)}{\eta_h(k^2) + 1}. \quad (\text{G.36})$$

The constants C are again defined via the contraction $\Pi_{G_n} \circ \Pi_{\text{TT}}^n \circ \mathcal{T}^{(n)}(p^2; \Lambda_n) = C_{\Lambda_n}^{G_n} \Lambda_n + C_{p^2}^{G_n} p^2 + C_{\Omega_n}^{G_n} \Omega_4 p^4$. Again, η_ω is defined with $\eta_\omega = 0$ for vanishing anomalous dimensions.

In the previous paragraphs we introduced abbreviations for constants that arise from the projection scheme. The explicit values of these constants are:

$$C^{\Lambda_3} = \frac{5}{192\pi^2}, \quad C^{\Lambda_4} = \frac{371881}{6718464\pi^2}, \quad C_{\Omega_4}^{G_4} = -\frac{96203921}{1632586752\pi^2}, \\ C_{\Lambda_4}^{G_4} = \frac{222485}{60466176\pi^2}, \quad C_{p^2}^{G_4} = \frac{6815761}{544195584\pi^2}, \quad C_4 = \frac{C_{\Lambda_4}^{G_4}}{C_{p^2}^{G_4}} = \frac{2002365}{6815761}, \\ C_{\Lambda_3}^{G_3} = -\frac{9}{4096\pi^2}, \quad C_{p^2}^{G_3} = \frac{171}{32768\pi^2}, \quad C_3 = \frac{C_{\Lambda_3}^{G_3}}{C_{p^2}^{G_3}} = -\frac{8}{19}. \quad (\text{G.37})$$

For analytic flow equations for the gravitational couplings g_n , which are significantly less accurate, see App. G.7, we have to apply a partial derivative with respect to p^2 and evaluate the result at $p^2 = 0$. The resulting equations are given by

$$\partial_t g_n = 2g_n + \frac{ng_n}{n-2} (\eta_h(0) + C_n \lambda_n \eta'_h(0)) + \frac{2}{n-2} \frac{g_n^{2-\frac{n}{2}}}{C_{p^2}^{G_n}} \text{Flow}_G^{(n)}(0), \quad (\text{G.38})$$

where ' denotes the dimensionless derivative with respect to p^2 . These equations remain completely analytic if we use a Litim-shaped regulator [175] and approximate the anomalous dimensions as constant, $\eta_\phi(q^2) \approx \text{const.}$

G.9. Analytic flow equations

All analytic flow equations are derived at $p^2 = 0$ (see e.g. (G.38)) and with a Litim-shaped regulator [175]. The anomalous dimensions in the momentum integrals are approximated as constant, i.e. $\eta_{\phi_i}(q^2) \approx$

$\eta_{\phi_i}(k^2)$. The analytic flow equations are then given by

$$\begin{aligned}
\partial_t \mu &= (\eta_h(0) - 2)\mu + \frac{1}{12\pi} \frac{g_4}{(1+\mu)^2} (3(\eta_h - 8) - 8\lambda_4(\eta_h - 6)) \\
&\quad - \frac{1}{180\pi} \frac{g_3}{(1+\mu)^3} (21(\eta_h - 10) - 120\lambda_3(\eta_h - 8) + 320\lambda_3^2(\eta_h - 6)) + \frac{g_3}{5\pi}(\eta_c - 10) \\
\partial_t \lambda_3 &= \left(\frac{3}{2}\eta_h(0) - 1 - \frac{1}{2} \frac{\partial_t g_3}{g_3} \right) \lambda_3 - \frac{1}{8\pi} \frac{g_3^{-\frac{1}{2}} g_5^{\frac{3}{2}}}{(1+\mu)^2} ((\eta_h - 8) - 4\lambda_5(\eta_h - 6)) \\
&\quad - \frac{1}{6\pi} \frac{g_4}{(1+\mu)^3} (3\lambda_4(\eta_h - 8) - 16\lambda_3\lambda_4(\eta_h - 6)) - \frac{g_3}{10\pi}(\eta_c - 12) \\
&\quad + \frac{1}{240\pi} \frac{g_3}{(1+\mu)^4} (11(\eta_h - 12) - 72\lambda_3(\eta_h - 10) + 120\lambda_3^2(\eta_h - 8) - 80\lambda_3^3(\eta_h - 6)) \\
\partial_t \lambda_4 &= \left(2\eta_h(0) - \frac{\partial_t g_4}{g_4} \right) \lambda_4 + \frac{1}{13387716\pi} \left(\frac{1}{2} \frac{g_6^2 g_4^{-1}}{(1+\mu)^2} (-4472787(\eta_h - 8) + 1639004\lambda_6(\eta_h - 6)) \right. \\
&\quad + \frac{1}{15} \frac{g_4}{(1+\mu)^3} (5066361(\eta_h - 10) - 22517160\lambda_4(\eta_h - 8) + 283174360\lambda_4^2(\eta_h - 6)) \\
&\quad + \frac{2}{15} \frac{g_3^{\frac{1}{2}} g_5^{\frac{3}{2}} g_4^{-1}}{(1+\mu)^3} (3940503(\eta_h - 10) - 60(187643\lambda_3 - 1303286\lambda_5)(\eta_h - 8) \\
&\quad \quad + 417051520\lambda_3\lambda_5(\eta_h - 6)) \\
&\quad + \frac{2}{5} \frac{g_3}{(1+\mu)^4} (-1313501(\eta_h - 12) + 3377574(2\lambda_3 + \lambda_4)(\eta_h - 10) \\
&\quad \quad - 15011440(\lambda_3 + 2\lambda_4)\lambda_3(\eta_h - 8) + 45442920\lambda_3^2\lambda_4(\eta_h - 6)) \\
&\quad + \frac{1}{5} \frac{g_3^2 g_4^{-1}}{(1+\mu)^5} (2874147(\eta_h - 14) - 20879816\lambda_3(\eta_h - 12) + 36027456\lambda_3^2(\eta_h - 10) \\
&\quad \quad + 88161840\lambda_3^3(\eta_h - 8) - 248160672\lambda_3^4(\eta_h - 6)) \\
&\quad \left. - \frac{10426288}{7} \frac{g_3^2}{g_4} (\eta_c - 14) \right) \\
\partial_t g_3 &= \left(2 + 3\eta_h(0) - \frac{8}{19} \eta'_h(0)\lambda_3 \right) g_3 + \frac{1}{19\pi} \left(\frac{g_3^{\frac{1}{2}} g_5^{\frac{3}{2}}}{(1+\mu)^2} \frac{47}{6}(\eta_h - 6) + \frac{g_3^2}{10} (53(\eta_c - 10) + 480) \right. \\
&\quad + \frac{g_3 g_4}{18(1+\mu)^3} (-45(\eta_h - 8) + 8(30\lambda_3 - 59\lambda_4)(\eta_h - 6) + 360\lambda_3\lambda_4(\eta_h - 4)) \\
&\quad + \frac{g_3 g_4}{(1+\mu)^4} 16(1 - 3\lambda_3)\lambda_4 - \frac{2g_3^2}{15(1+\mu)^5} (229 - 1780\lambda_3 + 3640\lambda_3^2 - 2336\lambda_3^3) \\
&\quad \left. - \frac{g_3^2}{80(1+\mu)^4} (147(\eta_h - 10) - 1860\lambda_3(\eta_h - 8) + 3380\lambda_3^2(\eta_h - 6) + 25920\lambda_3^3(\eta_h - 4)) \right) \\
\partial_t g_4 &= 2 \left(1 + \eta_h(0) + \frac{2002365}{6815761} \eta'_h(0)\lambda_4 \right) g_4 + \frac{2125764}{6815761\pi} \left(\frac{g_6^2}{(1+\mu)^2} \frac{32830375}{25509168}(\eta_h - 6) \right. \\
&\quad - \frac{g_4^2}{76527504(1+\mu)^3} (11305705(\eta_h - 8) + 61298276\lambda_4(\eta_h - 6) + 308793960\lambda_4^2(\eta_h - 4)) \\
&\quad - \frac{4g_4^2}{3188646(1+\mu)^4} (16061481 + 8(5355213\lambda_4 - 5610604)\lambda_4) \\
&\quad - \frac{g_3^{\frac{1}{2}} g_5^{\frac{3}{2}}}{19131876(1+\mu)^3} (-34242339(\eta_h - 8) + (86256922\lambda_3 - 7511302\lambda_5)(\eta_h - 6) \\
&\quad \quad - 4483422\lambda_3\lambda_5(\eta_h - 4)) \\
&\quad - \frac{g_3^{\frac{1}{2}} g_5^{\frac{3}{2}}}{(1+\mu)^4} (784609(17 - 32\lambda_3) - 8937232(4 - 9\lambda_3)\lambda_5) \\
&\quad + \frac{g_3 g_4}{90(1+\mu)^4} (323831781(\eta_h - 10) - (894383680\lambda_3 + 203187860\lambda_4)(\eta_h - 8) \\
&\quad \quad - (1296319430\lambda_3 - 1355312560\lambda_4)\lambda_3(\eta_h - 6) - 2929029840\lambda_3^2\lambda_4(\eta_h - 4)) \\
&\quad + \frac{g_3 g_4}{15(1+\mu)^5} (26769135(17 + 8\lambda_3(9\lambda_3 - 8)) \\
&\quad \quad - 2(353519805 + 4\lambda_3(742510961\lambda_3 - 514449355))\lambda_4) \\
&\quad + \frac{2g_3 g_4}{9(1+\mu)^4} (6783386859(\eta_h - 10) - (12157310900\lambda_3 + 457106270\lambda_4)(\eta_h - 8)
\end{aligned}$$

G.10. From asymptotic freedom to asymptotic safety

In this section, we provide our main line of reasoning for why matter fields, which are free or sufficiently weakly coupled in the UV – such as in asymptotic freedom – entail asymptotic safety in the full theory including gravity. Throughout, Yang-Mills theory serves as the principle example.

G.10.1. Yang-Mills coupled to gravity: the setup

Any correlation function approach to gravity works within an expansion of the theory about some generic metric. The necessity of gauge fixing in such an approach introduces a background metric into the approach. Hence, we use a background field approach in the gauge sector, giving us a setting with a combined background $\bar{g}_{\mu\nu}, \bar{A}_\mu^a$. Background independence is then ensured with the help of Nielsen or split Ward-Takahashi identities and the accompanying Slavnov-Taylor identities (STIs) for both the metric fluctuations and the gauge field fluctuations. The superfield ϕ comprises all fluctuations or quantum fields with

$$\begin{aligned} A_\mu &= \bar{A}_\mu + a_\mu, & g_{\mu\nu} &= \bar{g}_{\mu\nu} + \sqrt{G} h_{\mu\nu}, \\ \phi &= (h_{\mu\nu}, c_\mu, \bar{c}_\mu, a_\mu, c, \bar{c}) , \end{aligned} \quad (\text{G.40})$$

with the dynamical fluctuation graviton $h_{\mu\nu}$ and gauge field a_μ . In (G.40), c_μ and c are the gravity and Yang-Mills ghosts respectively. The classical Euclidean action of the Yang-Mills–gravity system is given by the sum of the gauge-fixed Yang-Mills and Einstein-Hilbert actions,

$$S_{\text{cl}}[\bar{g}, \bar{A}; \phi] = S_{\text{gauge}}[\bar{g}, \bar{A}; \phi] + S_{\text{gravity}}[\bar{g}, \bar{A}; \phi], \quad (\text{G.41})$$

where the two terms $S_{\text{gauge}} = S_A + S_{A,\text{gf}} + S_{A,\text{gh}}$ and $S_{\text{gravity}} = S_{\text{EH}} + S_{g,\text{gf}} + S_{g,\text{gh}}$ are the fully gauge fixed actions of Yang-Mills theory and gravity respectively. The Yang-Mills action reads

$$S_A[g, A] = \frac{1}{2} \int d^4x \sqrt{\det g} g^{\mu\mu'} g^{\nu\nu'} \text{tr} F_{\mu'\nu'} F_{\mu\nu}, \quad (\text{G.42})$$

where the trace in (G.42) is taken in the fundamental representation, and

$$F_{\mu\nu} = \frac{i}{g_s} [D_\mu, D_\nu], \quad D_\mu = \partial_\mu - ig_s A_\mu, \quad \text{tr} t^a t^b = \frac{1}{2}. \quad (\text{G.43})$$

The classical Yang-Mills action (G.42) only depends on the full fields g, A and induces gauge-field–graviton interactions via the determinant of the metric as well as the Lorentz contractions and derivatives. The gauge fixing is done in the background Lorentz gauge $\bar{D}_\mu a_\mu = 0$ with $\bar{D} = D_\mu(\bar{A})$. The gauge fixing and ghost terms read

$$\begin{aligned} S_{A,\text{gf}} &= \frac{1}{2\xi} \int d^4x \sqrt{\det \bar{g}} (\bar{g}^{\mu\nu} \bar{D}_\mu a_\nu)^2, \\ S_{A,\text{gh}} &= \int d^4x \sqrt{\det \bar{g}} \bar{g}^{\mu\nu} \bar{c} \bar{D}_\mu D_\nu c, \end{aligned} \quad (\text{G.44})$$

where we take the limit $\xi \rightarrow 0$. The gauge fixing and ghost terms only depend on the background metric and hence do not couple to the dynamical graviton $h_{\mu\nu}$. The Einstein-Hilbert action is given by

$$S_{\text{EH}} = \frac{1}{16\pi G} \int d^4x \sqrt{\det g} (2\Lambda - R(g)), \quad (\text{G.45})$$

with a linear gauge fixing F_μ and the corresponding ghost term,

$$S_{g,\text{gf}} = \frac{1}{2\alpha} \int d^4x \sqrt{\det \bar{g}} \bar{g}^{\mu\nu} F_\mu F_\nu, \\ S_{g,\text{gh}} = \int d^4x \sqrt{\det \bar{g}} \bar{g}^{\mu\mu'} \bar{g}^{\nu\nu'} \bar{c}_{\mu'} \mathcal{M}_{\mu\nu} c_\nu. \quad (\text{G.46})$$

with the Faddeev-Popov operator $\mathcal{M}_{\mu\nu}(\bar{g}, h)$ of the gauge fixing $F_\mu(\bar{g}, h)$. We employ a linear, de-Donder type gauge fixing,

$$F_\mu = \bar{\nabla}^\nu h_{\mu\nu} - \frac{1+\beta}{4} \bar{\nabla}_\mu h^\nu_\nu, \\ \mathcal{M}_{\mu\nu} = \bar{\nabla}^\rho (g_{\mu\nu} \nabla_\rho + g_{\rho\nu} \nabla_\mu) - \bar{\nabla}_\mu \nabla_\nu, \quad (\text{G.47})$$

with $\beta = 1$ and the limit $\alpha \rightarrow 0$, which is a fixed point of the ()RG flow [211].

G.10.2. Asymptotic freedom in Yang-Mills with gravity

Gauge theories with gauge group $U(N)$ or $SU(N)$ describe the electroweak and the strong interactions, and form the basis of the Standard Model of particle physics. A striking feature of non-Abelian gauge theories is asymptotic freedom, meaning that the theory is governed by a Gaussian fixed point in the ultraviolet, which implies that gluon interactions weaken for high energies and that perturbation theory is applicable. In fact, the great success of the Standard Model is possible only due to the presence of such a Gaussian fixed point, which allows us to neglect higher order operators in the high energy limit. The weakening of interactions is encoded in the energy dependence of the Yang-Mills coupling, which in turn is signalled by a strictly negative sign of the beta function. However, it is well known that fermions contribute with a positive sign to the running of the Yang-Mills coupling,

$$\frac{\beta_{\alpha_s}^{\text{1-loop}}}{\alpha_s^2} \equiv \mu \frac{\partial \alpha_s}{\partial \mu} \frac{1}{\alpha_s^2} = -\frac{1}{4\pi} \left(\frac{22}{3} N_c - \frac{4}{3} N_f \right), \quad (\text{G.48})$$

where we have displayed only the one-loop contributions with N_c and N_f denoting the number of colours and fermion flavours, and $\alpha_s = g_s^2/(4\pi)$. One can see that there is a critical number of fermion flavours $N_f^{\text{crit}} = \frac{11}{2} N_c$ above which the one-loop beta function changes sign. This implies that asymptotic freedom is lost. It has been noted recently that gauge theories with matter and without gravity may very well become asymptotically safe in their own right [358, 359, 360, 361, 362, 363].

Returning to gravity, it has been shown in [256, 364, 365, 366, 367, 368, 369, 203, 216] that graviton fluctuations lead to an additional negative term $\beta_{\alpha_s,h}$ in $\beta_{\alpha_s} \rightarrow \beta_{\alpha_s,a} + \beta_{\alpha_s,h}$ where $\beta_{\alpha_s,a}$ is the pure gauge theory contribution (G.48). The graviton contribution has a negative sign,

$$\beta_{\alpha_s,h} \leq 0. \quad (\text{G.49})$$

Because of the lack of perturbative renormalisability this term is gauge- and regularisation-dependent. However, it has been shown that it is always negative semi-definite, [203, 216], based on a kinematic identity related to diffeomorphism invariance. Hence, asymptotic freedom in Yang-Mills theories is assisted by graviton fluctuations. In the case of $U(1)$, they even trigger it. This result allows us to already get some insight into the coupled Yang-Mills–gravity system within a semi-analytic consideration in an effective theory spirit: In the present work we consider coupled Yang-Mills–gravity systems within an expansion of the pure gravity part in powers of the curvature scalar as well as taking into account the momentum dependence of correlation functions. In the Yang-Mills sub-sector we consider an expansion in $\text{tr } F^n$ and $(\text{tr } F^2)^n$, the lowest non-classical terms being

$$w_2 (\text{tr } F^2)^2, \quad v_4 \text{tr } F^4. \quad (\text{G.50})$$

Asymptotic freedom allows us to first integrate out the gauge field. This sub-system is well-described by integrating out the gauge field in a saddle point expansion within a one-loop approximation. Higher loop orders are suppressed by higher powers in the asymptotically free gauge coupling. This leads us to the effective action

$$\begin{aligned}\Gamma[\bar{g}, \bar{A}, \phi] = & S_{\text{gravity}}[\bar{g}; \phi] + S_{\text{gauge}}[\bar{g}, \bar{A}; \phi] \\ & - \frac{1}{2} \text{Tr} \ln \left[\Delta_1 \delta_{\mu\nu} + \left(1 - \frac{1}{\xi} \right) \nabla_\mu \nabla_\nu \right]_{k_a^{\text{IR}}}^{k_a^{\text{UV}}},\end{aligned}\quad (\text{G.51})$$

where Δ_1 represents the spin-one Laplacian and $k_a^{\text{IR}}, k_a^{\text{UV}}$ indicate diffeomorphism-preserving infrared and ultraviolet regularisations of the one-loop determinant. Most conveniently this is achieved by a proper-time regularisation, for a comprehensive analysis within the FRG framework see [28, 142]. In any case, both regularisations depend on the metric $g_{\mu\nu}$ and the respective scales $k_a^{\text{IR}}, k_a^{\text{UV}}$. The computation can be performed with standard heat-kernel methods.

The infrared sector of the theory is not relevant for the present discussion of the fate of asymptotic safety in the ultraviolet. Note also that Yang-Mills theory exhibits an infrared mass gap with the scale Λ_{QCD} due to its confining dynamics. In covariant gauges as used in the present work this mass gap results in a mass gap in the gluon propagator, for a treatment within the current FRG approach see [54, 55] and references therein. This dynamical gaping may be simulated here by simply identifying the infrared cutoff scale with Λ_{QCD} .

Moreover, even though integrating out the gauge field generates higher order terms such as (G.50) in the UV, they are suppressed by both, powers of the UV cutoff scale as well as the asymptotically free coupling. Accordingly, we drop the higher terms in the expansion of the Yang-Mills part of the effective action (G.51). Note that they are present in the full system as they are also generated by integrating out the graviton. This is discussed below.

It is left to discuss the pure gravity terms that are generated by ultraviolet gluon fluctuations in (G.51). They can be expanded in powers and inverse powers of the UV-cutoff scale $k_a = k_a^{\text{UV}}$. This gives an expansion in powers of the Ricci scalar R and higher order invariants. From the second line of (G.51) we are led to

$$\begin{aligned}(N_c^2 - 1) & \left[c_{g,a} k_a^2 \int d^4x \sqrt{\det g} (2c_{\lambda,a} k_a^2 - R) \right. \\ & + c_{R^2,a} \int d^4x \sqrt{\det g} (R^2 + z_a R_{\mu\nu}^2) \ln \frac{R + k_a^{\text{IR}}{}^2}{k_a^2} \\ & \left. + O\left(\frac{R^3}{k_a^2}\right), \right]\end{aligned}\quad (\text{G.52})$$

where we suppressed potential dependences on Δ_g and ∇_μ , in particular in the logarithmic terms. The logarithm also could contain further curvature invariants such as $R_{\mu\nu}^2$. In the spirit of the discussion of the confining infrared physics we may substitute $k_a^{\text{IR}} \rightarrow \Lambda_{\text{QCD}}$ in a full non-perturbative analysis. In (G.52), the coefficients $c_{g,a}, c_{\lambda,a}, c_{R^2,a}$ and z_a , are regularisation-dependent and lead to contributions to Newton's coupling, the cosmological constant, as well as generating an R^2 -term and potentially an $R_{\mu\nu}^2$ term. In the present Yang-Mills case, $c_{g,a}$ is positive for all regulators. For fermions and scalars, the respective coefficients $c_{g,\psi}, c_{g,\phi}$ are negative. In summary, this leaves us with an asymptotically free Yang-Mills action coupled to gravity with redefined couplings

$$\begin{aligned}G_{\text{eff}} &= \frac{G}{1 + (N_c^2 - 1)c_{g,a} k_a^2 G}, \\ \frac{\Lambda_{\text{eff}}}{G_{\text{eff}}} &= \frac{\Lambda}{G} + (N_c^2 - 1)c_{g,a} c_{\lambda,a} k_a^4.\end{aligned}\quad (\text{G.53})$$

The coupling parameters G, Λ should be seen as bare couplings of the Yang-Mills–gravity system and chosen such that the (renormalised) couplings $G_{\text{eff}}, \Lambda_{\text{eff}}$ are k_a independent. This corresponds to a standard renormalisation procedure (introducing the standard RG scale μ_{RG}) and leads to $G(N_c, k_a), \Lambda(N_c, k_a)$. Note that demanding k_a independence of the effective couplings also eliminates their N_c running. For example, for the effective Newton’s coupling

$$(N_c^2 - 1)\partial_{(N_c^2 - 1)} \ln G_{\text{eff}} = k_a^2 \partial_{k_a^2} \ln G_{\text{eff}} = 0, \quad (\text{G.54})$$

holds in a minimal subtraction scheme where the renormalisation scale μ_{RG} does not introduce further N_c -dependencies, most simply done with μ_{RG} -independent couplings G, Λ .

We also have to include $g_{R^2} R^2$ and $g_{R_{\mu\nu}^2} R_{\mu\nu}^2$ terms in the classical gravity action in order to renormalise also these couplings,

$$\begin{aligned} g_{R^2, \text{eff}} &= g_{R^2} + (N_c^2 - 1)c_{R^2, a} \ln \frac{k_a^{\text{IR}2}}{k_a^2}, \\ g_{R_{\mu\nu}^2, \text{eff}} &= g_{R_{\mu\nu}^2} + (N_c^2 - 1)c_{R^2, a} z_a \ln \frac{k_a^{\text{IR}2}}{k_a^2}. \end{aligned} \quad (\text{G.55})$$

Here, the minimal subtraction discussed above requires $g_{R^2}(N_c, \ln k_a/k_a^{\text{IR}})$ and $g_{R_{\mu\nu}^2}(N_c, \ln k_a/k_a^{\text{IR}})$. This leaves us with a theory, which includes all ultraviolet quantum effects of the Yang-Mills theory. Accordingly, in the ultraviolet its effective action (G.51) resembles the Einstein-Hilbert action coupled to the classical Yang-Mills action with appropriately redefined couplings. It also has R^2 and $R_{\mu\nu}^2$ terms. However, the latter terms are generated in any case by graviton fluctuations so there is no structural difference to standard gravity with the Einstein-Hilbert action coupled to the classical Yang-Mills.

The only relevant N_c dependence originates in the logarithmic curvature dependence of the marginal operators R^2 and $R_{\mu\nu}^2$ leading e.g. to

$$(N_c^2 - 1)c_{R^2, a} \int d^4x \sqrt{\det g} R^2 \ln \left(1 + \frac{R}{k_a^{\text{IR}2}} \right). \quad (\text{G.56})$$

These terms are typically generated by flows towards the infrared, for a respective computation in Yang-Mills theory see [370]. Such a running cannot be absorbed in the pure gravity part without introducing a non-local classical action. From its structure, the logarithmic running in (G.55) resembles the one of the strong coupling in many flavour QCD: the rôle of the gravity part here is taken by the gluon part in many flavour QCD and that of the Yang-Mills part here is taken by the many flavours. Accordingly, a fully conclusive analysis has to take into account these induced interactions. This is left to future work, here we concentrate on the Einstein-Hilbert part. The respective truncation to matter-gravity systems have been studied at length in the literature, and the arguments presented here fully apply. Note also that the current setup (and the results in the literature) can be understood as a matter-gravity theory, where the respective terms are removed by an appropriate classical gravity action that includes, e.g., $R^2 \ln R$ terms. The discussion of these theories is also linked to the question of unitary in asymptotically safe gravity. If we do not readjust the effective couplings within the minimal subtraction discussed above they show already the fixed point scaling to be expected in an asymptotically safe theory of quantum gravity, see (G.53) and (G.55). This merely reflects the fact that Yang-Mills theory has no explicit scales. If we only absorb the k_a running of the couplings while leaving open a general μ_{RG} dependence, the effective Newton’s coupling G_{eff} scales with $1/N_c^2$, while the effective cosmological constant scales with N_c^0 . In any case we have to use G_{eff} for the gravity scale in the Yang-Mills–gravity system instead of G . For example, the expansion of the full metric $g_{\mu\nu}$ in a background and a fluctuation then reads

$$g_{\mu\nu} = \bar{g}_{\mu\nu} + \sqrt{G_{\text{eff}}} h_{\mu\nu}, \quad (\text{G.57})$$

with the dimension-one field $h_{\mu\nu}$ in the $d = 4$ dimensional Yang-Mills–gravity system.

G.10.3. Asymptotic safety in gravity with Yang-Mills

It is left to integrate out graviton fluctuations on the basis of the combined effective action, where the pure gravity part is of the Einstein-Hilbert type. The couplings of the pure gravity sector, in particular, Newton's coupling and the cosmological constant only receive quantum contributions from pure gravity diagrams, while pure gauge and gauge-graviton couplings only receive contributions from diagrams that contain at least one graviton line. This system is asymptotically safe in the pure gravity sector and assists asymptotic freedom for the minimal gauge coupling, see (G.48) and (G.49), and leads to graviton-induced higher-order coupling such as (G.50). In summary, we conclude that Yang-Mills–gravity systems are asymptotically safe. The flow of this system and its completeness is discussed in section 11.6.

The present analysis is also important for the evaluation of general matter-gravity systems: we have argued that asymptotic freedom of the Yang-Mills theory allows us to successively integrate out the degrees of freedom, starting first with the Yang-Mills sector. Evidently, this is also true for matter-gravity systems with free matter such as treated comprehensively, e.g., in [207] and [60]. In the former, fermions and scalars were found to be unstable for a large flavour numbers while in the latter fermions were shown to be stable. For scalars, the situation was inconclusive as the anomalous dimension of the graviton was exceeding an upper bound, $\eta_h < 2$, beyond which a regulator of the form $R_{h,k}(p^2) \propto Z_h R_{h,k}^{(0)}(p^2)$ with $R_{h,k}^{(0)}(0) = k^2$ is no longer a regulator with the cutoff scale k ,

$$\lim_{k \rightarrow \infty} R_{h,k}(0) \propto (k^2)^{1-\eta_h/2} \rightarrow 0, \quad \text{for } \eta_h > 2. \quad (\text{G.58})$$

This bound can be pushed to $\eta_h < 4$ but also this bound was exceeded, see [60]. While the differences in the stability analysis can be partially attributed to the different approximations in [207] and [60] (the former does not resolve the difference between background gravitons and fluctuation gravitons in the pure gravity sector), we come to conclude here, that both (and all similar ones) analyses lack the structure discussed above. This calls for a careful reassessment of the UV flows of matter-gravity systems also in the view of relative cutoff scales. The latter is since long a well-known problem in quantum field theoretical applications of the FRG, in particular, in boson-fermion systems. For example, in condensed matter systems it has been observed that exact results for the three-body scattering (STM), see [371], can only be obtained within a consecutive integrating out of degrees of freedom in local approximations. If identical cutoff scales are chosen, the three-body scattering only is described approximately. For a recent analysis of relative cutoff scales in multiple boson and boson-fermion systems, see [18].

In summary, the gravitationally coupled free-matter–gravity systems, Yang-Mills–gravity systems, or more generally asymptotically free gauge-matter–gravity systems are asymptotically safe, independent of the number of matter degrees of freedom if this holds for one degree of freedom or more generally if this holds for the minimal number of degrees of freedom that already has the most general interaction structure of the coupled theory. Phrased differently: simple large N scaling cannot destroy asymptotic safety, with N being the number of gauge-matter degrees of freedom.

We emphasise that the analysis of such a minimal system as defined above is necessary. It is not sufficient to rely on the fact that the matter or gauge part can be integrated out first as gravity necessarily induces non-trivial matter and gauge self-interactions at an asymptotically safe gravity fixed point [246, 213, 61, 204, 215]. If these self-interactions do not destroy asymptotic safety, the systems achieve asymptotic safety for a general number of matter or gauge fields by guaranteeing the ultraviolet dominance of graviton fluctuations.

With these results at hand, we can now ask the question whether a "relative scaling" of gravity vs matter cutoffs maintains the observed graviton dominance. A natural "scaling hierarchy" for the cutoff scales k_h in the gravity and k_a in the Yang-Mills sector is motivated by the following heuristic consideration: while gravity feels the effective Newton's coupling G_{eff} , and hence, graviton fluctuations and gravity scales should be measured in G_{eff} , the Yang-Mills field generates contributions to the (bare) Newton's

coupling G . Assuming that both are of a similar strength, this leads to

$$G_{\text{eff}} k_h^2 \simeq G k_a^2 \quad (\text{G.59})$$

for the respective cutoff scales. Interestingly though, under this hierarchy of scales, the N_c dependence of the coupled system disappears, and, within an appropriate fine-tuning of the relation (G.59), the fixed point values of Newton's coupling and the cosmological constant show no N_c dependence at all. Stated differently, a rescaling such as in (G.59) guarantees the dominance of graviton fluctuations over gauge or matter fluctuations as long as the gauge-matter system is asymptotically free. The phenomenon of graviton dominance as observed with identical cutoffs continues to be observed under a weighted rescaling (G.59).

We close this chapter with some remarks.

- (1) The naturalness of the rescaling (G.59) is finally decided by taking into account momentum or spectral dependencies of the correlation functions. This is at the root of the question of stability and instability of matter-gravity systems. It is here where the marginal, logarithmically running, terms such as (G.56) come into play. They are not affected by this rescaling, which also shows their direct physics relevance.
- (2) Within the above rescaling, the fixed point of the gravity-induced gauge couplings such as w_2 and v_4 , see (G.50), are of order g^{*4} of the pure gravity fixed point coupling g^* . Note however, that this value can be changed by readjusting the rescaling (G.59).
- (3) Note that within the dynamical re-adjustment of the scales the fixed point Newton's coupling gets weak, $g^* \propto 1/N_c^2$. In other words, gravity dominates by getting weak. This is in line with the weak-gravity scenario advocated recently [214, 204, 215]. However, its physical foundation is different.
- (4) For a sufficiently large truncation, the theory should be insensitive to a relative rescaling of the cutoff scales k_{gravity} and k_{matter} and to other changes of the regularisation scheme. This is partially investigated in section 11.6. Moreover, in all of the following RG computations we do not resort to the rescaling (G.59) but use identical cutoff scales $k_{\text{gravity}} = k_{\text{matter}}$.

In the following analysis, we will refer to the present chapter for an evaluation of our results.

G.11. Computational Details for Yang-Mills gravity

G.11.1. Regulators

In the present work we use the optimised or flat regulator [175, 15, 176, 177] for all field modes. Specifically, the superfield regulator at $\bar{g} = 1\mathbb{I}$ and $\bar{A} = 0$ with flat Euclidean background metric is given by

$$\begin{aligned} R_k^{ij}(p) &= \delta^{ij} \left. \Gamma^{(\phi_i \phi_i^*)}(p) \right|_{\mu=0} r_{\phi_i}(p^2/k^2), \\ r(x) &= \left(\frac{1}{x} - 1 \right) \theta(1-x). \end{aligned} \quad (\text{G.60})$$

Here, ϕ^* is the dual superfield with $\phi^* = (h_{\mu\nu}, -\bar{c}_\mu, c_\mu, A_\mu, -\bar{c}, c)$. The regulator (G.60) is diagonal in field space keeping in mind the symplectic metric and allows for analytic expressions of the flow [252]. For the general scaling analysis we also discuss more general regulators, in particular, we refer to the exponential regulator with

$$r(x) = \frac{1}{\exp(x) - 1}, \quad (\text{G.61})$$

and to the sharp cutoff regulator with

$$r(x) = \frac{1}{\theta(x-1)} - 1. \quad (\text{G.62})$$

These regulators and variants thereof can be used to scan the space of cutoff functions [372, 373].

G.11.2. Regulator dependence of the gluon contribution to the graviton mass parameter

The coefficient $c_{\mu,a}$, which parameterises the gluon contribution to the graviton mass parameter, is given by

$$\begin{aligned} c_{\mu,a} &= -\frac{\text{Flow}_a^{(2h)}(p^2 = 0)}{g(N_c^2 - 1)} \\ &= \frac{1}{3\pi} \int \frac{dx x \dot{r}_h(x)}{(1 + r_h(x))^2} \left(\frac{4}{1 + r_h(x)} - 3 \right), \end{aligned} \quad (\text{G.63})$$

with $x = \frac{q^2}{k^2}$, $\eta_a = 0$ on the right-hand side and where the angular integration was already performed. We now use that

$$k \partial_k r_h(k, x) = k \frac{\partial x}{\partial k} \partial_x r_h(k, x) = -2x \partial_x r_h(k, x), \quad (\text{G.64})$$

and consequently we get

$$\begin{aligned} c_{\mu,a} &= -\frac{2}{3\pi} \int dx x^2 \left(\partial_x \left(\frac{2}{(1 + r_h(x))^2} - 2 \right) \right. \\ &\quad \left. - \partial_x \left(\frac{3}{1 + r_h(x)} - 3 \right) \right), \end{aligned} \quad (\text{G.65})$$

where we added zeros in order to perform the partial integration without boundary terms. The result after partial integration is

$$c_{\mu,a} = \frac{4}{3\pi} \int dx x \frac{r_h(x)(r_h(x) - 1)}{(1 + r_h(x))^2}. \quad (\text{G.66})$$

We have evaluated this integral for different types of regulator shape functions. The results are displayed in [Table G.4](#). The flat regulator evaluates this integral to zero, while exponential regulators give a positive sign and step-like or sharp regulators even give a negative sign. The usual expectation is that the regulator changes the size of a contribution but not its sign. In this case, however, two diagrams cancel each other approximately and by changing the regulator, we shift the weights between these two diagrams. Thus, any sign of this contribution is possible.

G.11.3. Inhomogeneous Fredholm integral equations of the second kind

In this Appendix, we discuss methods to solve Fredholm integral equations on the example of the gluon anomalous dimension

$$\eta_a(p^2) = f(p^2) + g \int \frac{d^4 q}{(2\pi)^4} K(p, q, \mu, \eta_h) \eta_a(q^2), \quad (\text{G.67})$$

see [subsection 11.3.2](#). Fredholm integral equations of the second kind are a well-known topic in pure and applied mathematics and there are several methods in order to solve such equations. A straightforward numerical solution is the so-called Nystroem method that is based on discretisation of the integral

Regulator	$c_{\mu,a}$
$r(x) = \frac{1}{\exp(x)-1}$	-0.21
$r(x) = \frac{1}{x} \exp(-x^2)$	-0.027
$r(x) = (\frac{1}{x} - 1)\Theta(1-x)$	0
$r(x) = \frac{1}{x}\Theta(1-x)$	0.034
$r(x) = \frac{10}{x}\Theta(1-x)$	0.17
$r(x) = \frac{1}{\Theta(x-1)} - 1$	$\frac{2}{3\pi} \approx 0.21$

Table G.4.: Gluon contribution to the graviton mass parameter for different regulators. Remarkably, the contribution does not only change in size but also its sign.

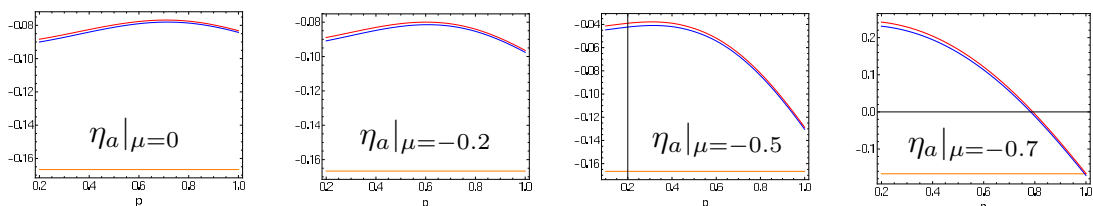


Figure G.2.: Shown is the momentum dependence of the graviton contribution to the gluon anomalous dimension η_a for different values of the graviton mass parameter $\mu = 0, -0.2, -0.5$, and -0.7 (from left to right). In each case, starting with a flat trial function (orange), a fast convergence from first (blue) to second (red) order in the iteration (G.69) is observed ($g = 0.5$ and $\eta_h = 0.5$).

operator with quadratures on N points. By doing so, one obtains Riemann sums that reduce to a system of N linear equations. Moreover, if there exist a solution to (G.67), it can be shown by the general theory of such equations that it is unique and the discretised version converges towards this solution in the limit $N \rightarrow \infty$. Another method that comes along with less numerical effort are iterative solutions based on the resolvent formalism and the Liouville-Neumann series. The basic idea of this approach is as follows. In order to get a feeling for such integral equations, we observe that for $g = 0$, the unique solution to (G.67) is trivially given by the inhomogeneity $f(p^2)$. Hence, if g is small in some sense, it seems reasonable that $f(p^2)$ is at least a good zeroth order approximation to the full solution $\eta_a(p^2)$, i.e.

$\eta_a(p^2) \approx \eta_{a,0}(p^2) \equiv f(p^2)$. In a first iteration step, we substitute $\eta_{a,0}(q^2)$ for $\eta_a(q^2)$ under the integral on the right-hand side of the integral equation (G.67),

$$\eta_{a,1}(p^2) = f(p^2) + g \int \frac{d^4 q}{(2\pi)^4} K(p, q, \mu, \eta_h) \eta_{a,0}(q^2). \quad (\text{G.68})$$

In this spirit we can construct iteratively a sequence $(\eta_{a,i}(p^2))_{i \in \mathbb{N}}$ with

$$\eta_{a,i+1}(p^2) = f(p^2) + g \int \frac{d^4 q}{(2\pi)^4} K(p, q, \mu, \eta_h) \eta_{a,i}(q^2). \quad (\text{G.69})$$

The convergence properties depend on the kernel K and the coupling constant g . We observe that due to the regulator structure, the kernel K is proportional to $r_a(q^2)$. Therefore, the kernel is integrable with respect to the loop momentum q . For the sake of simplicity, we will assume in the following a flat regulator $r_a(q^2) \sim \theta(1 - q^2)$, where q is the dimensionless momentum. The discussion can be generalised straightforwardly to arbitrary regulators. With a flat regulator, we write $K(p, q) =: \theta(1 - q^2) \check{K}(p, q)$. As a consequence, the integral in the Fredholm equation is defined on the domain $[0, 1]$, and in all equations, K is substituted by \check{K} . Moreover, we define the angular averaged kernel

$$\langle \check{K} \rangle_\Omega(p, q, \mu, \eta_h) := \int_{S^3} \frac{d\Omega}{(2\pi)^4} \check{K}(p, q, x, \mu, \eta_h), \quad (\text{G.70})$$

where $d\Omega$ is the canonical measure on the three sphere. The kernel $\langle \check{K} \rangle_\Omega$ can be normed, in particular, it exists its 2-norm with respect to the first two arguments

$$\|\langle \check{K} \rangle_\Omega\|_2 := \left(\int_0^1 \int_0^1 d\Omega \int_0^1 dq dp |\langle \check{K} \rangle_\Omega(p, q, \mu, \eta_h)|^2 \right)^{1/2} \quad (\text{G.71})$$

It can then be shown that the sequence $(\eta_i(p^2))_{i \in \mathbb{N}}$ converges towards the full solution, i.e.,

$$\lim_{i \rightarrow \infty} \eta_{a,i}(p^2) = \eta_a(p^2), \quad (\text{G.72})$$

if the kernel is bounded as

$$|g| \|\langle \check{K} \rangle_\Omega\|_2 < 1. \quad (\text{G.73})$$

The solution can then be written as a Liouville-Neumann series according to

$$\eta_a(p^2) = f(p^2) + g \int_{\mathbb{R}^4} \frac{d^4 q}{(2\pi)^4} R(p, q, \mu, \eta_h, g) f(q^2), \quad (\text{G.74})$$

with the resolvent kernel

$$R(p, q, \mu, \eta_h, g) = \sum_{i=1}^{\infty} g^{i-1} K_i(p, q, \mu, \eta_h), \quad (\text{G.75})$$

where K_i are the iterated kernels given by

$$\begin{aligned} K_i(p, q, \mu, \eta_h) &= \int \int \cdots \int \frac{d^4 q_1}{(2\pi)^4} \frac{d^4 q_2}{(2\pi)^4} \cdots \frac{d^4 q_{i-1}}{(2\pi)^4} \\ &\times K(p, q_1, \mu, \eta_h) K(q_1, q_2, \mu, \eta_h) \times \dots \\ &\times K(q_{i-1}, q, \mu, \eta_h). \end{aligned} \quad (\text{G.76})$$

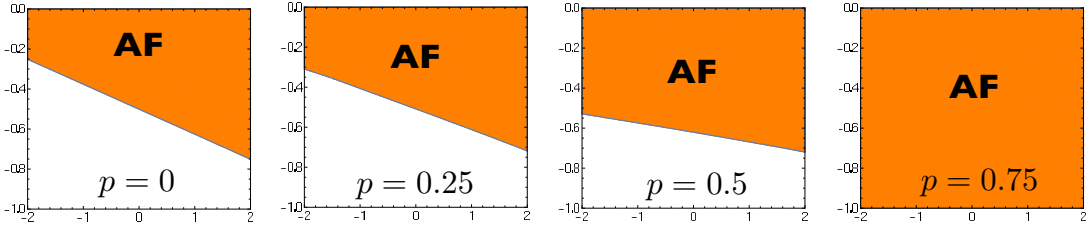


Figure G.3.: In the plane of the graviton anomalous dimension (η_h^* , lower axis) and the graviton mass parameter μ^* , the region with asymptotic freedom (AF) is coloured (orange) corresponding to a positive sign of the gluon anomalous dimension η_a . Moreover, the gluon anomalous dimension is determined from a momentum derivative evaluated at different momenta $p = 0, 0.25, 0.5$, and 0.75 (from left to right). The domain with asymptotic freedom consistently grows as soon as momenta of order of the RG scale are adopted.

By truncating the resolvent series at some finite order i_0 , one obtains an approximate solution to the integral equation. If the bound (G.73) is satisfied, the Liouville-Neumann series converges for any smooth initial choice $\eta_{a,0}$. One can also choose zeroth iterations that are different from the inhomogeneity $f(p^2)$. It is clear that convergence properties depend on the initial choice. For instance, if one has the correct guess for the full solution and uses this as a starting point for the iteration, then one finds $\eta_{a,0} = \eta_{a,1}$, and one can conclude that the exact solution has been found. Additionally, there are improved iteration schemes that increase the radius of convergence significantly. In [374], it has been proven that it exists a parameter $c \in \mathbb{R}$, such that the iteration prescription

$$\begin{aligned} \eta_{a,i+1}(p^2) &= (1 - c)f(p^2) + c\eta_{a,i}(p^2) \\ &\quad + (1 - c)g \int \frac{d^4q}{(2\pi)^4} K(p, q, \mu, \eta_h) \eta_{a,i}(q^2) \end{aligned} \tag{G.77}$$

has a radius of convergence that is larger than the one of the standard Liouville-Neumann series, which is obtained from the improved iterations with $c = 0$.

The convergence in the present system is analysed in Figure G.2. We plot $\eta_a(p^2)$ for some specific parameter values. All these plots are obtained for $g = 0.5$; however, we stress that the sign of η_a does not depend on this choice as the result is a power series in g . We investigate the iterations, where we have always assumed a constant function $\eta_{a,0} = \text{const}$ as a first approximation. We then plot the first, second, and third order and find rapid convergence in all cases, which is expected as we have checked that the kernel in (11.42) generates a very large radius of convergence. The third iteration is for this choice of $\eta_{a,0}$ not even visible any more, since the corresponding curve lies exactly on top of the second iteration.

G.11.4. Sign of the gluon anomalous dimension

In this Appendix, we discuss the stability of the sign of the gluon anomalous dimension. As discussed in section 11.3, we need a negative sign in order to obtain asymptotic freedom in the gauge sector. This directly corresponds to the demand that the gravity contributions to the gluon anomalous dimension should be negative. In the App. G.11.3 we discussed the full momentum dependent solution of $\eta_a(p^2)$. We further argued in section 11.3 that the sign at $p^2 = k^2$ is the decisive one for the Yang-Mills beta function. In the following sections, we present different approximations to the gluon anomalous dimension, and how stable the sign is within these approximations.

G.11.5. Derivative at vanishing momentum

The simplest approximation is to assume a momentum independent anomalous dimension and to obtain an equation for η_a with a derivative at $p^2 = 0$. The equation for η_a is then given by

$$\eta_{a,h} = -\partial_{p^2} \text{Flow}_h^{(AA)} \Big|_{p^2=0}. \quad (\text{G.78})$$

We obtain the analytic result

$$\eta_{a,h} = -\frac{g}{8\pi} \left(\frac{8 - \eta_a}{1 + \mu} - \frac{4 - \eta_h}{(1 + \mu)^2} \right), \quad (\text{G.79})$$

which is identical to the η_a in the UV if the gauge sector is asymptotically free. Therefore, assuming a fixed point in the gravitational sector, we are left with the ultraviolet limit

$$\eta_a^* = \frac{g^*}{1 - \frac{g^*}{8\pi(1+\mu^*)}} \left(\frac{4 + 8\mu^* + \eta_h^*}{8\pi(1 + \mu^*)^2} \right). \quad (\text{G.80})$$

This function changes sign at the critical value

$$\mu_{\text{crit}}^* = -\frac{1}{8}(4 + \eta_h^*). \quad (\text{G.81})$$

Moreover, there is a pole at $\mu^* = -1 + \frac{g^*}{8\pi}$ with another sign change for the regimes to the left and to the right of the pole. However, this sign change at the pole can be neglected, as usual fixed point values of g are $O(1)$. For fixed point values of this order, the pole is located at $\mu^* \approx -0.96$, which in turn is a fixed point value that is very unusual. Therefore, we assume the overall prefactor in (G.80) to be positive. Then, $\eta_a^* \geq 0$ for $\mu^* \leq -\frac{1}{8}(4 + \eta_h^*)$. This agrees with previous computations in the background field approximation, where $\eta_h^* = -2$ and $\mu = -2\lambda$, and consequently, $\lambda_{\text{crit}}^* = \frac{1}{8}$ [203]. In our more general case, the anomalous dimension of the graviton is not fixed by the fixed point condition for Newton's coupling. The fixed point value for the graviton mass parameter where the gravitational contribution changes sign is plotted against the graviton anomalous dimension in the left panel of Figure G.3. There are some bounds on anomalous dimensions for well-defined theories. From previous results [58, 59, 29, 60, 158, 62], we know that typical fixed point values are roughly given by $\eta_h \approx 1$ and $\mu \approx -0.6$, which is just at the critical value where asymptotic freedom is lost.

We conclude that in this simplest approximation the stability of asymptotic freedom is not guaranteed, but depends strongly on subtle effects in the gravity sector. In the following, we investigate how this picture changes in more elaborate approximations and specifications.

G.11.6. Derivative at non-vanishing momentum

We now generalise the procedure from the previous section and use a derivative at finite momentum. The equation for η_a is then given by

$$\eta_{a,h} = -\partial_{p^2} \text{Flow}_h^{(AA)} \Big|_{p=\alpha k}. \quad (\text{G.82})$$

For such derivatives the results are only numerical. In Figure G.3 we show the results for $\alpha = \frac{1}{4}, \frac{1}{2}, \frac{3}{4}$. We again display the sign of the gluon anomalous dimension in the (μ^*, η_h^*) plane. We find the encouraging result that the area, which does not support asymptotic freedom in the gauge sector is getting smaller with an increasing α . With a derivative at $p^2 = k^2$, the region has completely disappeared from the investigated area. We conclude that with this generalised derivation of the gluon anomalous dimension, asymptotic freedom is supported in the whole important parameter region of gravity.

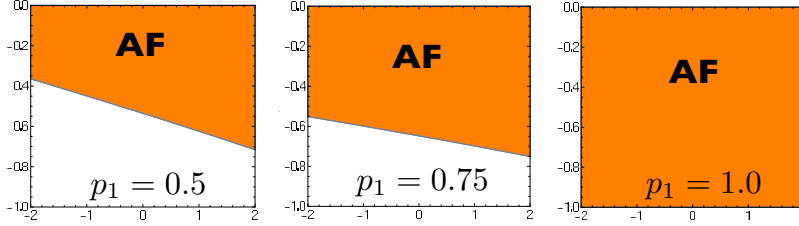


Figure G.4.: Same as Figure G.3, except that the gluon anomalous dimension is determined from a finite difference derivative (G.83) with $p_2 = 0$ and various momenta $p_1 = \frac{1}{2}, \frac{3}{4}, 1$ (from left to right). The domain with asymptotic freedom consistently grows with growing $p_1 - p_2$ of the order of the RG scale, fully consistent with Figure G.2.

G.11.7. Finite differences

A further generalisation of the procedure from the previous sections is to derive the gluon anomalous dimension by a finite difference. In this case, we define η_a to be momentum dependent. It is then given by

$$\eta_{a,h}(p^2) = -\frac{\text{Flow}_h^{(AA)}(p^2) - \text{Flow}_h^{(AA)}(0)}{p^2}. \quad (\text{G.83})$$

The corresponding results are presented in Figure G.4 for $p = \frac{1}{2}, \frac{3}{4}, 1$. The results are very similar to the ones with the derivative definition at non-vanishing momentum. The gluon anomalous dimension is negative and supports asymptotic freedom if we evaluate it at $p^2 = k^2$. This is also the approximation for η_a that we utilise throughout this work and also Figure 11.6 is computed with this approximation.

G.11.8. Scaling equations

In this Appendix, we augment the analysis from section 11.6 by providing scaling equations for all couplings. In particular, we are lifting the identification (11.26). Here we extract the fixed point scaling from a flat regulator choice and utilise a reparameterisation of the flow equations that minimises the occurrence of factors of $1 + \mu$. Moreover, in the previous chapter, we have utilised projections on gravitational couplings g_n and g_{aah} within a finite difference construction. In the literature, projections with derivatives at vanishing momentum, $p^2 = 0$, are often used. It has been argued in [58, 59, 29, 60, 158, 62, 204] that this definition has large ambiguities at $p^2 = 0$, which limits its applicability. Still, it has the charm of providing analytic flows and fixed point equations and hence facilitating the access to the current analysis.

The structure of the flow and fixed point equations is more apparent if we absorb $1/(1 + \mu)$ -factors in the gravitational couplings with

$$\begin{aligned} \bar{g}_n &= g_n \left(\frac{1}{1 + \mu} \right)^{\gamma_n}, & \bar{g}_{\bar{c}ch^n} &= g_{\bar{c}ch^n} \left(\frac{1}{1 + \mu} \right)^{\gamma_c}, \\ \bar{g}_{a^n h^m} &= g_{a^n h^m} \left(\frac{1}{1 + \mu} \right)^{\gamma_a}, \end{aligned} \quad (\text{G.84a})$$

with the scaling coefficients

$$\gamma_n = \frac{n}{n - 2}, \quad \gamma_a = \gamma_c = 1, \quad (\text{G.84b})$$

and μ, λ_n are not rescaled. This removes all potentially singular factors $1/(1 + \mu)$ -factors in the diagrams that stem from the respective powers of the graviton propagators in the loops. It still leaves us with

contributions proportional to $1/(1 + \mu)$ due to the projection procedure with derivatives at $p^2 = 0$ and due to regulator insertions. The rescaling power of $1/(1 + \mu)$ varies between $1/(1 + \mu)^3$ for the lowest coupling g_3 and $1/(1 + \mu)$ for $g_{n \rightarrow \infty}$.

In the following equations we identify blocks of gravitational couplings: as before all gravitational self-couplings $\bar{g}_n, \bar{g}_{\bar{c}ch^n}$ are identified with \bar{g}_3 and all λ_n are identified with λ_3 . Additionally, we identify all Yang-Mills–gravity interactions \bar{g}_{aah^n} with \bar{g}_{aah} . This leads us to

$$\bar{g}_n = \bar{g}_3 = \bar{g}, \quad \lambda_{n>2} = \lambda_3, \quad (\text{G.85a})$$

for the pure gravity couplings and

$$\bar{g}_{\bar{c}ch^n} = \bar{g}_c, \quad \bar{g}_{aah^n} = \bar{g}_a, \quad (\text{G.85b})$$

for the ghost-graviton and gluon-graviton couplings. We emphasise that G.85 and G.84a imply

$$g_n = g_3(1 + \mu)^{\gamma_3 - \gamma_n}, \quad (\text{G.86})$$

with $\gamma_3 > \gamma_n$. Eq.(G.86) seemingly entails the irrelevance of the lower order couplings g_n for $\mu \rightarrow -1$. However, the lower order couplings contribute to diagrams with more graviton propagators. In combination, this leads to a uniform scaling of all diagrams as expected in a scaling limit. Note that the scaling analysis can also be performed if removing the approximation G.85. It leads to an identical scaling $\bar{g}_n \sim \bar{g}_3$ and $\bar{g}_{aah^n} \sim \bar{g}_{aah}$. The discussion of such a full analysis is deferred to future work.

Here, we are only interested in the relative scaling between the pure gravity and Yang-Mills gravity diagrams, and simply discuss the structure of these equations. To that end, we use the analytic pure gravity equations derived in [29, 62] expressed with the rescaled couplings G.84. We also use the identification G.85, and additionally, we suppress the ghost contribution for simplicity. The ghost contribution comes with the same power in $1 + \mu$ as the gluon contribution. The analysis is facilitated by only using positive coefficients c_i, d_i , making the relative signs of the different terms apparent. In general the sign of some of these coefficients depends on λ_3 , and we define them such that they are positive at $\lambda_3 = 0$. The explicit values for the coefficients is provided in App. G.11.10. Within this notation, all factors $1/(1 + \mu)$ in the loops are absorbed in the couplings except the one, which comes from external momentum derivatives of propagators, $\partial_{p^2}G$, due to the projection procedure or from regulator insertions. In summary, we are led to

$$\begin{aligned} \dot{\mu} &= -(2 - \eta_h)\mu - \bar{g} \left[c_{\mu,h} + (1 + \mu)(N_c^2 - 1)c_{\mu,a} \frac{\bar{g}_a}{\bar{g}} \right], \\ \dot{\bar{g}} &= (2 + 3\bar{\eta}_h)\bar{g} \\ &\quad - \bar{g}^2 \left[\frac{c_{\bar{g},h}}{1 + \mu} + \frac{d_{\bar{g},h}}{(1 + \mu)^2} + (N_c^2 - 1)c_{\bar{g},a} \left(\frac{\bar{g}_a}{\bar{g}} \right)^{\frac{3}{2}} \right], \\ \dot{\lambda}_3 &= - \left(1 + \frac{\partial_t \bar{g}}{2\bar{g}} - \frac{3}{2}\bar{\eta}_h \right) \lambda_3 \\ &\quad + \bar{g} \left[\frac{c_{\lambda_3,h}}{1 + \mu} + (N_c^2 - 1)c_{\lambda_3,a} \left(\frac{\bar{g}_a}{\bar{g}} \right)^{\frac{3}{2}} \right], \end{aligned} \quad (\text{G.87a})$$

for the pure gravity couplings. Here, the term $d_{\bar{g},h}/(1 + \mu)^2$ stems from the $\partial_{p^2}G$ contributions, and all coefficients c, d from graviton loops depend on λ_3 with $c(0), d(0) > 0$. The ghost-graviton and the

gauge-graviton coupling have the flows

$$\begin{aligned}\dot{\bar{g}}_a &= (2 + 2\eta_a + \bar{\eta}_h) \bar{g}_a - \bar{g}_a^2 \left[-c_{\bar{g}_a,a} + \frac{d_{\bar{g}_a,a}}{1+\mu} \right. \\ &\quad \left. + \left(c_{\bar{g}_a,h} - \frac{d_{\bar{g}_a,h}}{1+\mu} \right) \left(\frac{\bar{g}}{\bar{g}_a} \right)^{\frac{1}{2}} \right]. \\ \dot{\bar{g}}_c &= (2 + 2\eta_c + \bar{\eta}_h) \bar{g}_c - \bar{g}_c^2 \left[c_{\bar{g}_c,c} + \frac{d_{\bar{g}_c,c}}{1+\mu} \right. \\ &\quad \left. + \left(c_{\bar{g}_c,h} + \frac{d_{\bar{g}_c,h}}{1+\mu} \right) \left(\frac{\bar{g}}{\bar{g}_c} \right)^{\frac{1}{2}} \right].\end{aligned}\tag{G.87b}$$

Here, the d terms originate from the diagram with a regularised graviton line, $(G\partial_t R_k G)^{(hh)}$. The coefficients $c_{i,h}$ and $d_{i,h}$ are λ_3 dependent as they receive contributions from the diagram with a three-graviton vertex. The signs are chosen such that $c_{i,h}(0), d_{i,h}(0) > 0$. The coefficients and the signs in the flow equation for \bar{g}_c were not derived in this work.

The rescaled graviton anomalous dimension $\bar{\eta}_h$ reads

$$\bar{\eta}_h = -\frac{\partial_t [Z_h(1+\mu)]}{Z_h(1+\mu)} = \eta_h - \frac{\dot{\mu}}{1+\mu},\tag{G.88}$$

which includes the scale dependence of the full dressing of the graviton propagator including the mass parameter. The set of anomalous dimensions is given by

$$\begin{aligned}\eta_h &= \bar{g} \left[c_{\eta_h,h} + \frac{d_{\eta_h,h}}{1+\mu} + (N_c^2 - 1)c_{\eta_h,a} \frac{\bar{g}_a}{\bar{g}} \right], \\ \eta_c &= -\bar{g} \left[c_{\eta_c,h} + \frac{d_{\eta_c,h}}{1+\mu} \right], \quad \eta_a = -\bar{g}_a \left[c_{\eta_a,h} - \frac{d_{\eta_a,h}}{1+\mu} \right],\end{aligned}\tag{G.89}$$

and completes the set of flow equations. Again, the graviton contributions to η_h have a λ_3 dependence with $c_{\eta_h,h}(0), d_{\eta_h,h}(0) > 0$. All other coefficients do not carry a λ_3 dependence. Note also that the $\partial_t \mu / (1+\mu)$ terms in the scaling terms on the right-hand side of G.87 come from the normalisation of the \bar{g} 's with powers of $1/(1+\mu)$. In the \bar{g}_n flows this term is $n/(n-2)\partial_t \mu / (1+\mu)$ derived from the rescaling G.84a. For the ghost-gravity and gauge gravity couplings, it is always the term $\partial_t \mu / (1+\mu)$ derived from G.84.

G.11.9. Flow equations

Here, we recall the results for the pure gravity flow for μ , g_3 , and λ_3 derived in [29, 62], add the derived gluon contributions, and formulate them in terms of the rescaled couplings

$$\begin{aligned}\bar{g}_n &= g_n \left(\frac{1}{1+\mu} \right)^{\frac{n}{n-2}}, & \bar{g}_c &= g_c \left(\frac{1}{1+\mu} \right), \\ \bar{g}_a &= g_a \left(\frac{1}{1+\mu} \right), & \bar{\eta}_h &= \eta_h - \frac{\dot{\mu}}{1+\mu},\end{aligned}\tag{G.90}$$

see App. G.11.8 and G.84 for details. In order to show the interrelation of the different couplings we keep all dependences on the higher couplings \bar{g}_n . The flow equations are given by

$$\begin{aligned}
\partial_t \mu &= -(2 - \eta_h) \mu + \frac{\bar{g}_3}{180\pi} [21(10 - \eta_h) - 120\lambda_3(8 - \eta_h) + 320\lambda_3^2(6 - \eta_h)] \\
&\quad - \frac{\bar{g}_4}{12\pi} [3(8 - \eta_h) - 8\lambda_4(6 - \eta_h)] - (1 + \mu) \frac{\bar{g}_c}{5\pi} (10 - \eta_c) + (1 + \mu) (N_c^2 - 1) \frac{\bar{g}_a \eta_a}{60\pi}, \\
\partial_t \lambda_3 &= -\left(1 + \frac{\partial_t \bar{g}_3}{2\bar{g}_3} - \frac{3}{2}\bar{\eta}_h\right) \lambda_3 + \bar{g}_3 \left\{ -\frac{1}{1 + \mu} \frac{1}{240\pi} [11(12 - \eta_h) - 72\lambda_3(10 - \eta_h) + 120\lambda_3^2(8 - \eta_h) - 80\lambda_3^3(6 - \eta_h)] \right. \\
&\quad + \frac{1}{6\pi} \frac{1}{1 + \mu} \frac{\bar{g}_4}{\bar{g}_3} [3\lambda_4(8 - \eta_h) - 16\lambda_3\lambda_4(6 - \eta_h)] + \frac{1}{8\pi} \frac{1}{1 + \mu} \left(\frac{\bar{g}_5}{\bar{g}_3}\right)^{\frac{3}{2}} [(8 - \eta_h) - 4\lambda_5(6 - \eta_h)] \\
&\quad \left. + \frac{1}{10\pi} \left(\frac{\bar{g}_c}{\bar{g}_3}\right)^{\frac{3}{2}} (12 - \eta_c) + \frac{1}{60\pi} (N_c^2 - 1) \left(\frac{\bar{g}_a}{\bar{g}_3}\right)^{\frac{3}{2}} (3 - \eta_a) \right\}, \\
\partial_t \bar{g}_3 &= (2 + 3\bar{\eta}_h) \bar{g}_3 - \frac{\bar{g}_3^2}{19\pi} \left\{ \frac{1}{(1 + \mu)^2} \frac{2}{15} [229 - 1780\lambda_3 + 3640\lambda_3^2 - 2336\lambda_3^3] \right. \\
&\quad - \frac{1}{1 + \mu} \frac{1}{80} [147(10 - \eta_h) - 1860\lambda_3(8 - \eta_h) + 3380\lambda_3^2(6 - \eta_h) + 25920\lambda_3^3(4 - \eta_h)] \\
&\quad - \frac{1}{1 + \mu} \frac{\bar{g}_4}{\bar{g}_3} \left[\frac{1}{18} [45(8 - \eta_h) - 8(30\lambda_3 - 59\lambda_4)(6 - \eta_h) - 360\lambda_3\lambda_4(4 - \eta_h)] + \frac{16}{1 + \mu} (1 - 3\lambda_3) \lambda_4 \right] \\
&\quad \left. + \frac{1}{1 + \mu} \frac{47}{6} \left(\frac{\bar{g}_5}{\bar{g}_3}\right)^{\frac{3}{2}} (6 - \eta_h) + \left(\frac{\bar{g}_c}{\bar{g}_3}\right)^{\frac{3}{2}} \left[\frac{50 - 53\eta_c}{10} \right] + (N_c^2 - 1) \left(\frac{\bar{g}_a}{\bar{g}_3}\right)^{\frac{3}{2}} \left[\frac{133 + \eta_a}{30} \right] \right\}, \\
\partial_t \bar{g}_a &= (2 + 2\eta_a + \bar{\eta}_h) \bar{g}_a - \frac{\bar{g}_a^2}{30\pi} \left\{ -\frac{100 - 13\eta_a}{2} + \frac{13(5 - \eta_h)}{\mu + 1} \right. \\
&\quad \left. + \left(\frac{\bar{g}_3}{\bar{g}_a}\right)^{\frac{1}{2}} \left(\frac{330 - 640\lambda_3 - \eta_a(33 - 80\lambda_3)}{12} + \frac{-15 + 400\lambda_3 - \eta_h(80\lambda_3 - 6)}{3(\mu + 1)} \right) \right\}, \tag{G.91}
\end{aligned}$$

and the anomalous dimension read

$$\begin{aligned}
\eta_h &= \frac{\bar{g}_3}{4\pi} \left(\frac{\bar{g}_4}{\bar{g}_3} (6 - \eta_h) - \frac{6(8 - \eta_h) + 8(6 - \eta_h)\lambda_3 - 36(4 - \eta_h)\lambda_3^2}{9} + \frac{17 + 8\lambda_3(9\lambda_3 - 8)}{3(1 + \mu)} - \frac{\bar{g}_c}{\bar{g}_3} \eta_c + (N_c^2 - 1) \frac{\bar{g}_a}{\bar{g}_3} \frac{1 + \eta_a}{3} \right), \\
\eta_c &= -\frac{\bar{g}_c}{9\pi} \left(\frac{8 - \eta_h}{1 + \mu} + 8 - \eta_c \right), \quad \eta_a = -\frac{\bar{g}_a}{8\pi} \left(8 - \eta_a - \frac{4 - \eta_h}{1 + \mu} \right). \tag{G.92}
\end{aligned}$$

The two terms in the flow equation for \bar{g}_3 proportional to $1/(1 + \mu)^2$ and the term in η_h proportional to $1/(1 + \mu)$ signal the derivative expansion at $p^2 = 0$. This is the price to pay for an analytic flow equation. On the other hand the terms proportional to $1/(1 + \mu)$ in \bar{g}_a , η_a and η_c come from a regulator insertion in a graviton propagator compared to a ghost or gluon propagator.

The computation of these flow equations involves contractions of very large tensor structures. These contractions are computed with the help of the symbolic manipulation system *FORM* [193, 194]. We furthermore employ specialised Mathematica packages. In particular, we use *xPert* [195] for the generation of vertex functions, and the *FormTracer* [197] to trace diagrams.

G.11.10. Coefficients in the scaling equations

The coefficients in the scaling equations in App. G.11.8 are given here in the approximation G.85. We assume that the anomalous dimensions satisfy $|\eta| \leq 2$: they should not dominate the scaling of the regulator. While the upper bound $\eta \leq 2$ is a (weak) consistency bound for the regulator, for a detailed

discussion, see [60], the lower one can be seen as a (weak) consistency bound on the propagators. For $\eta < -2$, they cease to be well-defined as Fourier transforms of space-time correlations functions (if they scale universally down to vanishing momenta). For simplicity, we display the coefficients with $\lambda_3 = 0$. Note that all coefficients are defined such that they are always positive. All coefficients can be directly read off from the equations (G.91) and (G.92).

We get the coefficients $c_{\mu,h}$ and $c_{\mu,a}$ in the fixed point equation of the mass parameter μ are given by

$$c_{\mu,h} = \frac{17}{6\pi} - \frac{2}{15\pi}\eta_h - \frac{1}{5\pi}\eta_c, \quad c_{\mu,a} = -\frac{1}{60\pi}\eta_a. \quad (\text{G.93})$$

Note that the second coefficient is positive since $\eta_a < 0$. The coefficients $c_{\bar{g},h}$ and $c_{\bar{g},a}$ in the fixed point equation of the pure gravity coupling \bar{g} read

$$\begin{aligned} c_{\bar{g},h} &= \frac{47}{57\pi} - \frac{53}{190\pi}\eta_h - \frac{37}{190\pi}\eta_c, & d_{\bar{g},h} &= \frac{598}{285\pi}, \\ c_{\bar{g},a} &= \frac{7}{30\pi} + \frac{1}{570\pi}\eta_a, \end{aligned} \quad (\text{G.94})$$

while the coefficients $c_{\lambda_3,h}$ and $c_{\lambda_3,a}$ in the fixed point equation of the coupling λ_3 are given by

$$\begin{aligned} c_{\lambda_3,h} &= \frac{33}{20\pi} - \frac{19}{240\pi}\eta_h - \frac{1}{10\pi}\eta_c, \\ c_{\lambda_3,a} &= \frac{3}{60\pi} - \frac{1}{60\pi}\eta_a. \end{aligned} \quad (\text{G.95})$$

Furthermore, the coefficient $c_{\bar{g}_a}$ in the fixed point equation for the two-gluon–graviton coupling \bar{g}_a reads

$$\begin{aligned} c_{\bar{g}_a,a} &= \frac{5}{3\pi} - \frac{13}{60\pi}\eta_a, & d_{\bar{g}_a,a} &= \frac{13}{6\pi} - \frac{13}{30\pi}\eta_h, \\ c_{\bar{g}_a,h} &= \frac{11}{12\pi} - \frac{11}{120\pi}\eta_a, & d_{\bar{g}_a,h} &= \frac{1}{6\pi} - \frac{1}{15\pi}\eta_h. \end{aligned} \quad (\text{G.96})$$

We also summarise the coefficients of the anomalous dimensions, to wit

$$\begin{aligned} c_{\eta_h,h} &= \frac{1}{6\pi} - \frac{1}{12\pi}\eta_h - \frac{1}{4\pi}\eta_c, & d_{\eta_h,h} &= \frac{17}{12\pi}, \\ c_{\eta_h,a} &= \frac{1}{12\pi} + \frac{1}{12\pi}\eta_a, & & \\ c_{\eta_c} &= \frac{8}{9\pi} - \frac{1}{9\pi}\eta_c, & d_{\eta_c} &= \frac{8}{9\pi} - \frac{1}{9\pi}\eta_h, \\ c_{\eta_a} &= \frac{1}{\pi} - \frac{1}{8\pi}\eta_a, & d_{\eta_a} &= \frac{1}{2\pi} - \frac{1}{8\pi}\eta_h. \end{aligned} \quad (\text{G.97})$$

G.12. Quantum Improved Schwarzschild-(A)dS and Kerr-(A)dS Space-times

G.12.1. Choice of Scale Identification

Here we motivate our choice for $k(r)$ in (12.17). Inserting the general parametrisation $k(r) = \xi/D(r)$, into (G.113), we are left with

$$\begin{aligned} f(r) &= 1 - \frac{2M}{r} \frac{g(r)D^2(r)}{\xi^2} - \frac{r^2}{3} \frac{\lambda(r)\xi^2}{D^2(r)} \\ &\stackrel{\text{UV}}{\approx}_{r \rightarrow 0} 1 - \frac{2M}{r} \frac{g_* D^2(r)}{\xi^2} - \frac{r^2}{3} \frac{\lambda_* \xi^2}{D^2(r)}, \\ \Delta_r &\stackrel{\text{UV}}{\approx}_{r \rightarrow 0} (r^2 + a^2) \left(1 - \frac{r^2}{3} \frac{\lambda_* \xi^2}{D^2(r)} \right) - \frac{2M}{r} \frac{g_* D^2(r)}{\xi^2}. \end{aligned} \quad (\text{G.98})$$

The numerical values of g_* and λ_* depend on the particular RG-trajectory and parametrisation we have chosen and therefore cannot be physical observables. However, the product $g_*\lambda_*$ is an observable and hence independent of the particular choice of the RG-trajectory. Its magnitude turns out to be $g_*\lambda_* \approx 0.1$, e.g. in [235, 62]. In this light, we have two choices for ξ in order to make (G.98) solely dependent on $g_*\lambda_*$,

$$\xi^2 = g_* \quad \text{or} \quad \xi^2 = \frac{1}{\lambda_*}. \quad (\text{G.99})$$

Thus, in (12.17) we have chosen the second of the two equivalent options. Varying ξ for a fixed geometry (G_0, Λ_0, m, a) , which is effectively done also in the quantum Kretschmann scenario by introducing χ , turns out to have only a weak impact on the position of the inner horizon. Since it is typically located at small radii, we recall from Table G.5, that varying ξ mildly modifies the UV-limit. Furthermore, we have an upper limit $\chi < (3/8)^{1/4}$.

G.12.2. Killing Horizons

In this section, we review the formal proof that every zero of $\Delta_r(r)$ in (12.19) is a Killing horizon. This implies that a constant surface gravity and thereby a temperature can be associated to each horizon. The Schwarzschild-(A)dS case is automatically contained by taking $a \rightarrow 0$.

Starting from the Kerr-(A)dS metric (12.19), assume that $\Delta_r(r)$ has j positive roots, i.e. can be written as

$$\Delta_r(r) = \prod_{i=0}^j (r - r_i) \quad \text{with} \quad 0 \leq r_0 \leq r_1 < \dots < r_j. \quad (\text{G.100})$$

The horizons are the hypersurfaces $r = r_i = \text{const.}$ Since the space-time is axisymmetric and stationary, we have two commuting Killing vector fields: $\left(\frac{\partial}{\partial t}\right)^a$ is stationary, at least in some region of the space-time, and $\left(\frac{\partial}{\partial \phi}\right)^a$ manifests the symmetry axis. We now have to construct a Killing vector field ξ^a , that is normal to, and null on these horizon hypersurfaces. The most general form for ξ^a would be a linear combination of both Killing vector fields,

$$\xi^a = \left(\frac{\partial}{\partial t}\right)^a + \alpha \left(\frac{\partial}{\partial \phi}\right)^a, \quad (\text{G.101})$$

with a constant α . We will fix this constant later by requiring that ξ^a should vanish at the horizons. But first, we must change from Boyer-Lindquist coordinates (12.19), to coordinates that leave the metric regular at the horizons. Such coordinates are induced by the principal null directions of the space-time. The Kerr-(A)dS space-time is of algebraic type D, thus admits two distinct principal null directions,

referred to as ingoing and outgoing. They can be represented in Boyer-Lindquist coordinates by the following vectors,

$$n_\pm^\mu = \left(\frac{r^2 + a^2}{\Delta_r} \Xi, \pm 1, 0, \frac{a}{\Delta_r} \Xi \right), \quad (\text{G.102})$$

where $+1$ is outgoing and -1 ingoing. They now induce outgoing and ingoing coordinates, being the Kerr-(A)dS counterparts of Kerr-coordinates in flat space. We will select the outgoing version, but in principle we could also work with ingoing ones. The outgoing Kerr-(A)dS coordinates (v, χ) are defined as,

$$\begin{aligned} dv &= dt + \Xi \frac{r^2 + a^2}{\Delta_r} dr \\ d\chi &= d\phi + \Xi \frac{a}{\Delta_r} dr. \end{aligned} \quad (\text{G.103})$$

Inserting these back into (12.19), leaves us with the metric in terms of Kerr-(A)dS coordinates (v, r, θ, χ) ,

$$\begin{aligned} ds^2 &= -\frac{1}{\rho^2 \Xi^2} (\Delta_r - \Delta_\theta a^2 \sin^2 \theta) dv^2 + \frac{2}{\Xi} dv dr \\ &\quad - \frac{2a \sin^2 \theta}{\rho^2 \Xi^2} ((r^2 + a^2) \Delta_\theta - \Delta_r) dv d\chi \\ &\quad - \frac{2a \sin^2 \theta}{\Xi} d\chi dr + \frac{\sin^2 \theta}{\rho^2 \Xi^2} (\Delta_\theta (r^2 + a^2)^2 \\ &\quad - \Delta_r a^2 \sin^2 \theta) d\chi^2 + \frac{\rho^2}{\Delta_\theta} d\theta^2. \end{aligned} \quad (\text{G.104})$$

One can check that (G.104) reduces to Kerr coordinates for $\Lambda = 0$. The Killing vector field ξ^a now reads

$$\xi^a = \left(\frac{\partial}{\partial v} \right)^a + \alpha \left(\frac{\partial}{\partial \chi} \right)^a. \quad (\text{G.105})$$

Requiring that ξ^a is null on the horizons $r = r_i$ yields

$$\begin{aligned} \xi^2|_{r=r_i} &= [g_{vv} + 2\alpha g_{v\chi} + \alpha^2 g_{\chi\chi}]_{r=r_i} \\ &= \frac{\Delta_\theta \sin^2 \theta}{\rho_i^2 \Xi^2} [a - \alpha(r_i^2 + a^2)]^2 \stackrel{!}{=} 0 \end{aligned} \quad (\text{G.106})$$

and therefore

$$\alpha = \frac{a}{r_i^2 + a^2}. \quad (\text{G.107})$$

Thus, we have found a family of vector fields $(\xi^a)_i$, being null at one horizon at a time. In order to show that the hypersurfaces $r = r_i$ are Killing horizons, it remains to be checked if ξ^a is hypersurface orthogonal, i.e. $\xi_a = \xi_\mu dx^\mu \sim dr$ evaluated at the horizon,

$$(\xi)_a|_{r=r_i} = [g_{\mu\nu} \xi^\nu dx^\mu]_{r=r_i} = \frac{1}{\Xi} \left(1 - \frac{a^2 \sin^2 \theta}{r_i^2 + a^2} \right) dr, \quad (\text{G.108})$$

with all other components vanishing. In summary, we are able to construct a Killing vector field ξ^a which is null on, and normal to each horizon hypersurface $r = r_i$, and hence have shown that the horizons corresponding to the roots of Δ_r are indeed Killing horizons.

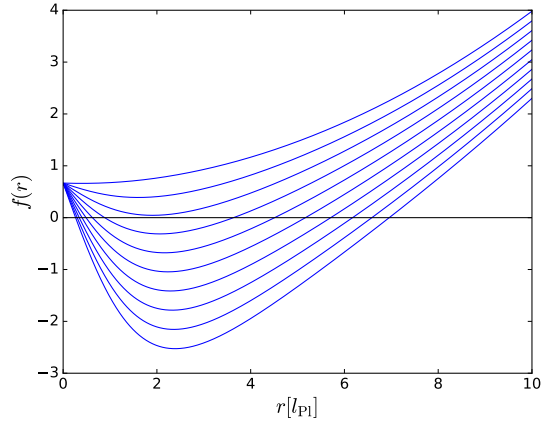


Figure G.5.: $f(r)$ from (12.18) based on the linear matching for increasing mass from top to bottom, with $\Lambda_0 = -0.1, M = 0.1, 1, 2, 3, 4, 5, 6, 7, 8, 9, 10M_{\text{Pl}}$.

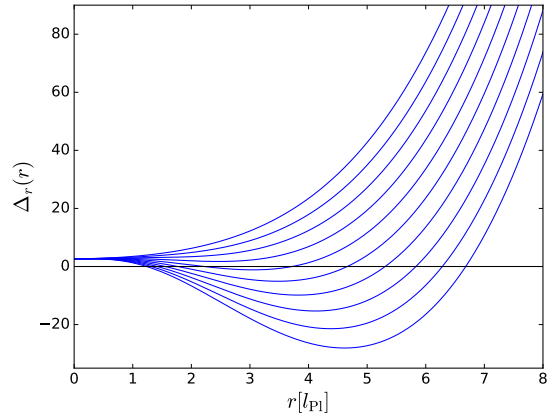


Figure G.6.: $\Delta_r(r)$ from (12.20) based on the linear matching for increasing mass from top to bottom, with $\Lambda_0 = -0.1, a = 2$ and $M = 0.1, 1, 2, 3, 4, 5, 6, 7, 8, 9, 10M_{\text{Pl}}$.

G.12.3. Other Matchings

Linear Matching

The simplest scaling is based on a dimensional analysis,

$$D_{\text{Lin}}(r) = r , \quad (\text{G.109})$$

which has already been adopted for instance in [297]. In the case of an identically vanishing cosmological coupling, is the IR-limit of the classical proper distance along a radial path [305]. But this matching does not take physical scales of the underlying space-time into account, for instance the black hole scales given by M & a , or scales induced by the gravitational or the cosmological coupling. Nevertheless, this function already gives rise to many phenomena observed for more complicated choices and hence can serve as a toy model.

Proper Distances

We can also use the proper distance along a curve C in space-time to specify $D(r)$,

$$D(r) = D_{\text{prop}} = \int_C \sqrt{|g_{\mu\nu} dx^\mu dx^\nu|} . \quad (\text{G.110})$$

This definition is diffeomorphism invariant and encodes the space-time structure, since the gravitational and cosmological coupling typically appear in the metric. In most cases in the literature, e.g. [335, 305, 334], the gravitational as well as cosmological coupling have been fixed to be constants, for instance the IR-values Λ_0 and G_0 . However, since the FRG-flow generically gives rise to running couplings, it is more natural and consequent to consider this running also in the above integral, thus $G \rightarrow G(r)$ and $\Lambda \rightarrow \Lambda(r)$. In the following, this quantum improvement procedure of proper distances is extended to Schwarzschild- and Kerr-(A)dS geometries. We will provide expressions for the proper distance along a radial path and along the geodesic of a radially infalling observer, both for constant, as well as running G and Λ . Additionally, the UV-limit of each proper distance is obtained, cf. [Table G.5](#).

Radial Path Inspired by the symmetry of the space-time, we first take the following radial path from 0 to r as integration contour C in [\(G.110\)](#),

$$\begin{aligned} C_{\text{Schw-(A)dS}} : \quad dt &= d\Omega = 0 , \\ C_{\text{Kerr-(A)dS}} : \quad dt &= d\phi = d\theta = 0 \quad \text{and} \quad \theta = \pi/2 . \end{aligned} \quad (\text{G.111})$$

The restriction to the equatorial plane in the Kerr case is done for the sake of simplicity. Driven by the results of [299] for the flat Kerr geometry, we assume that the varying θ will not alter our results qualitatively. Applying the above integration paths to [\(G.110\)](#) yields,

$$\begin{aligned} D_{\text{Sch}}(r) &= \int_0^r d\tilde{r} \sqrt{|g_{\tilde{r}\tilde{r}}|} = \int_0^r d\tilde{r} \frac{1}{\sqrt{|f(\tilde{r})|}} , \\ D_{\text{Kerr}}(r) &= \int_0^r d\tilde{r} \sqrt{|g_{\tilde{r}\tilde{r}}|} = \int_0^r d\tilde{r} \sqrt{\frac{\tilde{r}^2}{|\Delta_r(\tilde{r})|}} , \end{aligned} \quad (\text{G.112})$$

with the lapse functions

$$\begin{aligned} f(r) &= 1 - \frac{2GM}{r} - \frac{\Lambda}{3}r^2 \quad \text{and} \\ \Delta_r(r) &= (r^2 + a^2) \left(1 - \frac{\Lambda}{3}r^2\right) - 2MGr . \end{aligned} \quad (\text{G.113})$$

In the following, this scenario with constant G and Λ will be referred to as *classical radial path*, because the space-time underlying the integral is a classical black hole geometry with a cosmological constant. Alternatively, we account for the running of the couplings already in the proper distance, referred to as *quantum radial path* with $G = G(r)$ and $\Lambda = \Lambda(r)$ in the above integrals. This turns [\(G.112\)](#) into integral equations for $D(r)$, which can be transformed into a differential equation by taking a derivative with respect to r . One can then easily see that the derivative of $D(r)$ diverges at every horizon, where $f(r)$ and $\Delta(r)$ vanish. Using the fixed point behaviour of G and Λ in the UV, these differential equations read for

small r ,

$$D'_{\text{sch,qu}}(r) = \frac{1}{\sqrt{\left| 1 - 2Mg_*\lambda_* \frac{D_{\text{sch,qu}}^2(r)}{r} - \frac{r^2}{3D_{\text{sch,qu}}^2(r)} \right|}},$$

$$D'_{\text{kerr,qu}}(r) = \frac{1}{\sqrt{\left| 1 + \frac{a^2}{r^2} - \frac{r^2}{3D_{\text{kerr,qu}}^2(r)} - \frac{a^2}{3D_{\text{kerr,qu}}^2(r)} \right|}}. \quad (\text{G.114})$$

Both classical matchings as well as the one for the quantum Schwarzschild scenario monotonously increase and satisfy $D(r \rightarrow 0) = 0$, as can be seen from the numerical results in [Figure G.9](#). In contrast, the proper distance is identically zero in the quantum Kerr scenario, see [\(G.118\)](#).

It turns out (cf. [section 12.8](#)), that the expression for the Hawking temperature in a quantum improved space-time contains terms proportional to the derivative of $D(r)$, hence using the above construction for the proper distance leads to diverging Hawking temperatures at all horizons. Therefore, in the following we also discuss the proper distance induced by the eigentime of a radially infalling observer, where this feature is absent.

Radial Timelike Geodesic The eigentime τ of an observer, initially at rest at R and falling along a radial timelike geodesic into the singularity, can also be used to identify the momentum cut-off scale with a length scale by setting $D(r) = \tau(r)$. Derived in appendix [G.12.6](#), the eigentime for the Schwarzschild-(A)dS scenario reads

$$D(R) = \int_0^R dr \frac{1}{\sqrt{|E^2 - f(r)|}}, \quad (\text{G.115})$$

with $E = f(R)$ for an observer initially starting at rest. It is worth noting that for $E = 0$, the integral reduces to the one in [\(G.112\)](#). By fixing E , we equivalently specify the maximal distance R of the observer from the origin. Independent on the particular value of E , the proper distance again exhibits poles if $E^2 - f(r) = 0$, now shifted by E^2 away from the horizons. Once more, [\(G.115\)](#) gives rise to two different proper distances, referred to as either *classical* or *quantum geodesic*, depending on whether the underlying space-time is based on the constant or running versions of G and Λ . The analogous expression for the proper distance induced by a radial geodesic in the Kerr-(A)dS scenario reads (see appendix [G.12.7](#))

$$D(R) = \int_0^R dr \frac{r^2}{\sqrt{|E^2 \Xi^2 [(r^2 + a^2)^2 - a^2 \Delta_r] - r^2 \Delta_r|}},$$

$$(G.116)$$

$$E^2 = E^2(R) = \frac{R^2 \Delta_R}{\Xi^2 [(R^2 + a^2)^2 - a^2 \Delta_R]},$$

and reduces to [\(G.112\)](#) for $E = 0$. Again, we achieved that there are no poles at the horizons. Once more, we have two versions depending on whether G and Λ are running or not. The numerical results can be found in [Figure G.10](#), however, the proper distance in the quantum Kerr scenario is again identically zero.

G.12.4. Shape and Divergences of Proper Distances

As can be seen from [Figure G.9-G.11](#), all functions $D(r)$ are monotonously increasing, some proper distances display a rapid increase. In order to understand these jumps and possible divergences, we

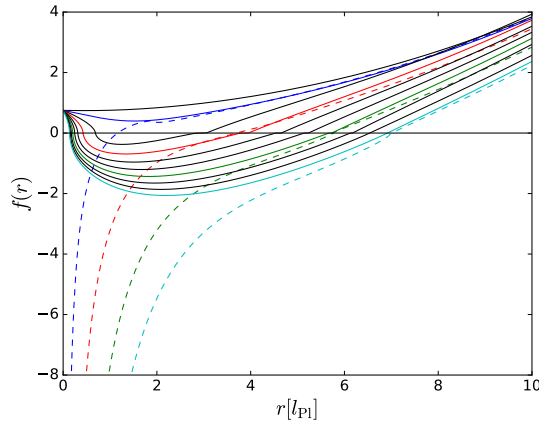


Figure G.7.: $f(r)$ based on the radial path matching for increasing mass from top to bottom. Results, where $D(r)$ is computed consistently in a quantum improved space-time, are shown in solid, the dashed curves are the ones with a classically computed $D(r)$. With parameters $\Lambda_0 = -0.1$ and $M = 0.1, 1, 2, 3, 4, 5, 6, 7, 8, 9, 10M_{\text{Pl}}$. Curves of the same mass have the same colour.

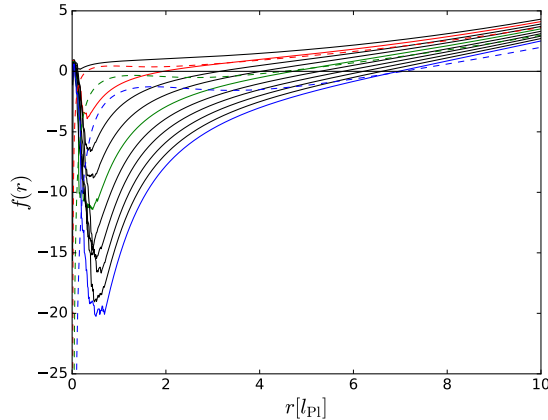


Figure G.8.: $f(r)$ based on the radial geodesic matching for increasing mass from top to bottom. Results, where $D(r)$ is computed consistently in a quantum improved space-time, are shown in solid, the dashed curves are the ones with a classically computed $D(r)$. With parameters $\Lambda_0 = -0.1$ and $M = 0.1, 1, 2, 3, 4, 5, 6, 7, 8, 9, 10M_{\text{Pl}}$. Curves of the same mass have the same colour.

	Kretschmann		Radial Path		Geodesic Path	
	classic	quantum	classic	quantum	classic	quantum
Schwarzschild	$\frac{1}{3^{1/4} 2\chi \sqrt{MG_0}} r^{3/2}$	$\left(\frac{\chi^{-4}-8/3}{48M^2(g_*\lambda_*)^2}\right)^{1/8} r^{3/4}$	$\frac{2}{3\sqrt{2G_0M}} r^{3/2}$	$\frac{2}{\sqrt{3}} r$	$\frac{\pi}{2\sqrt{2G_0M}} r^{3/2}$	$\left(\frac{67}{18Mg_*\lambda_*}\right)^{1/4} r^{3/4}$
			$\frac{r^2}{2a}$	0	$\frac{\pi}{4a} r^2$	0

Table G.5.: UV-limits ($r \rightarrow 0$) of $D(r)$ for all investigated matchings.

have to look at the integral expressions for each proper distance (G.112), (G.115), and (G.116). The expression $h(r)$ under each square root can become zero, and if $h(r)$ has just a single root at $r = r_0 < R$, the corresponding pole is integrable, causing a jump in the proper distance,

$$\begin{aligned} D(R) &= \int_0^R dr \frac{1}{\sqrt{h(r)}} = \int_0^R dr \frac{1}{\sqrt{(r - r_0)\tilde{h}(r)}} \\ &\sim \int_0^R dr (r - r_0)^{-1/2}, \end{aligned} \tag{G.117}$$

where $\tilde{h}(r)$ has no root at $r = r_0$. However, once the multiplicity of r_0 is larger than one, the pole is not integrable anymore and $D(r)$ exhibits a divergence at $r = r_0$. In any case, $D'(r)$ is diverging for the radial path proper distances, even at integrable poles of $D(r)$, as can be seen from (G.114). In case of the classical radial path, the position of these poles has no direct physical significance, however in the quantum case, the poles are located precisely at the horizons, because then, the function $h(r)$ is nothing other than the horizon condition. Thus, for extremal black holes when at least two horizons coincide, the quantum proper distance along a radial path is ill-defined. $D'(r)$ is always diverging at the horizons leading to a diverging Hawking temperature of the horizon, as is shown in section 12.8.

For this reason, we introduce the scenario with an infalling observer along a timelike, radial geodesic, in order to remove these problems, only due to the poor choice of the function $h(r)$ and absent in all other scenarios. However, it turns out, that in both proper distance scenarios for Kerr-(A)dS with an underlying quantum space-time, the proper distance must vanish identically, in order to satisfy the condition $D(0) = 0$. For instance, this can be seen by solving (G.114) in the limit $r \rightarrow 0$, satisfying the boundary condition $D(0) = \epsilon$, yielding

$$D_{\text{rad,UV}}^{\text{kerr}}(r) = \frac{\epsilon}{a\sqrt{3}} \left(\sqrt{r^2 + a^2} + r \right)^{\sqrt{3}}. \tag{G.118}$$

Therefore, the solution vanishes identically in the limit $\epsilon \rightarrow 0$, which is confirmed also for the full, numerical solution of (G.112). The same behaviour is found for Kerr-(A)dS, when the scale matching is based on the geodesic in a quantum-improved space-time.

G.12.5. UV-limits of $D(r)$

For statements about the curvature near the singularity and also for the construction of the Penrose diagrams, the UV-limit for each proper distance is needed.

The leading order behaviour in the UV for the classical proper distances, i.e. constant G_0 and Λ_0 , can be obtained from (G.112), (G.115) and (G.116) by approximating the integral in the limit $r \rightarrow 0$. For the identification based on the classical Kretschmann scalar (12.22), the UV-behaviour can easily be read off from (12.23).

In the quantum versions, the leading order of the proper distance in the UV-limit can be obtained by assuming a power law behaviour of the form $D(r) = A r^\alpha$, with constants $A > 0$ and $\alpha > 0$ in order to satisfy the boundary condition $D(0) = 0$. The constants A and α can be determined by inserting this ansatz back into the above equations, now being an integral, differential or functional equation respectively. All scenarios display monotonously increasing functions satisfying $D(0) = 0$, apart from the quantum proper distance expressions for Kerr. They are identically zero, as an iterative algorithm for solving the integral equations shows.

For each scenario, the analytical UV-expression is listed in Table G.5. The numerical results for $D(r)$ are shown in Figure G.9, Figure G.10, Figure G.11. Furthermore, the leading order exponent α can be

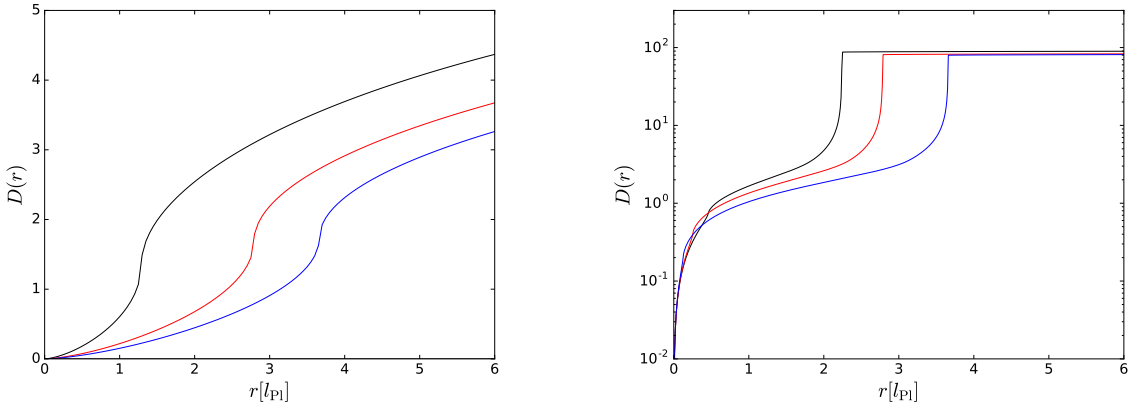


Figure G.9.: Left: proper distance along a radial path through a classical Schwarzschild-AdS space-time for three different masses $M = 1, 5, 10 M_{\text{Pl}}$. Right: the same for a quantum Schwarzschild-AdS space-time.

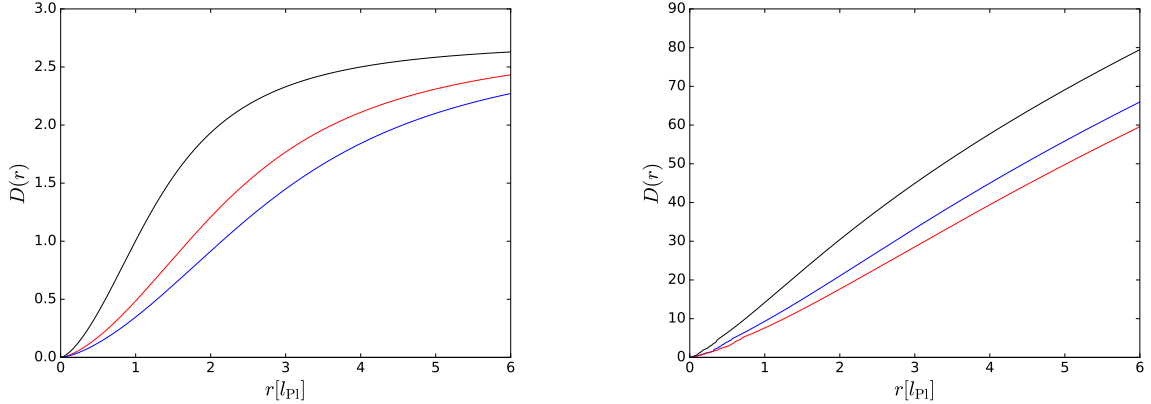


Figure G.10.: Left: proper distance along a radial geodesic through a classical Schwarzschild-AdS space-time for three different masses $M = 1, 5, 10 M_{\text{Pl}}$. Right: the same for a quantum Schwarzschild-AdS space-time.

extracted numerically from the slope of the linear relation between the proper distance $D(r) = A r^\alpha$ and its integral function $\mathcal{D}(r) = \frac{A}{\alpha+1} r^{\alpha+1}$:

$$\frac{\mathcal{D}(r)}{D(r)} = \frac{r}{\alpha + 1}. \quad (\text{G.119})$$

This cross-check confirms agreement between numerical exponent and the one found analytically in Table G.5.

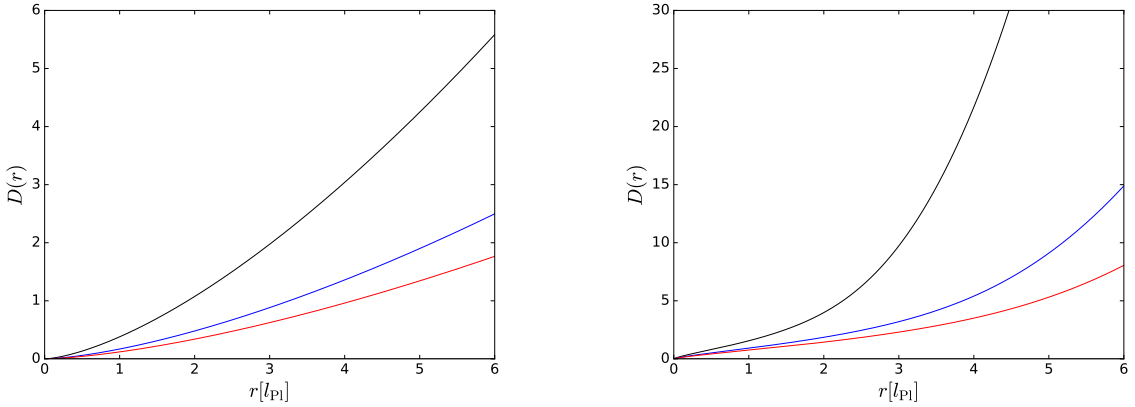


Figure G.11.: Function $D(r)$ in classical Kretschmann matching (left) and for quantum Kretschmann scenario (right) for three different masses $M = 1, 5, 10 M_{\text{Pl}}$.

G.12.6. Eigentime of an Inflating Observer in a Schwarzschild-(A)dS Geometry

Another physically well-motivated choice for the integration path in (G.110) is the curve determined by an observer some distance away from the black hole, falling into the black hole along a radial timelike geodesic. Because the observer's four-velocity u^a is conserved along geodesics, we normalise it to be

$$-1 \stackrel{!}{=} u_a u^a . \quad (\text{G.120})$$

Furthermore, we can choose the coordinate system such that the motion takes place only in the equatorial plane $\theta = \pi/2$. Using (12.18), the normalisation condition of the four-velocity in the equatorial plane reads:

$$-f(r) t^2 + \frac{\dot{r}^2}{f(r)} + r^2 \dot{\phi}^2 = -1 , \quad (\text{G.121})$$

where (\cdot) denotes the derivative with respect to the eigentime τ . We have also conserved quantities E and L corresponding to the Killing vector fields $\xi^a = \left(\frac{\partial}{\partial t}\right)^a$ and $\psi^a = \left(\frac{\partial}{\partial \phi}\right)^a$:

$$E = -g_{ab} \xi^a u^b = f(r) \dot{t} , \quad (\text{G.122})$$

$$L = g_{ab} \psi^a u^b = r^2 \dot{\phi} . \quad (\text{G.123})$$

However, for simplicity, we will choose an observer with $L = 0$. Inserting E and L back into (G.121) to eliminate \dot{t} and $\dot{\phi}$ leaves us with

$$E^2 = \dot{r}^2 + f(r) . \quad (\text{G.124})$$

This is a type of energy equation for the observer, at least in asymptotically flat spacetimes. We now have to specify the initial conditions for the observer. In the asymptotically flat spacetime, one usually places the observer initially at rest at $r = \infty$, still leaving E finite. However, we cannot do that in the case of a non-vanishing cosmological constant, because $f(r)$ is diverging for $r \rightarrow \infty$. Therefore, we take rather an observer at rest ($\dot{r}^2 = 0$) at some finite distance R to determine E :

$$E^2 = f(R) . \quad (\text{G.125})$$

The proper distance is then given by the eigentime the observer needs to arrive at $r = 0$ after starting at R , i.e the integral over the eigentime along the geodesic:

$$D(R) = \int_0^R dr \frac{1}{\sqrt{|E^2 - f(r)|}} = \int_0^R dr \frac{1}{\sqrt{|f(R) - f(r)|}} . \quad (\text{G.126})$$

G.12.7. Eigentime of an Inflating Observer in a Kerr-(A)dS Geometry

Following the same procedure for a timelike geodesic in the equatorial plane in Kerr-(A)dS, given by the metric (12.19), the normalisation of the four-velocity is

$$-1 = g_{tt} \dot{t}^2 + g_{\phi\phi} \dot{\phi}^2 + 2g_{t\phi} \dot{t}\dot{\phi} + g_{rr} \dot{r}^2 , \quad (\text{G.127})$$

whereas the conserved quantities induced by the Killing vector fields $\xi^a = \left(\frac{\partial}{\partial t}\right)^a$ and $\psi^a = \left(\frac{\partial}{\partial \phi}\right)^a$ read

$$E = -g_{ab} \xi^a u^b = -g_{tt} \dot{t} - g_{t\phi} \dot{\phi} , \quad (\text{G.128})$$

$$L = g_{ab} \psi^a u^b = g_{\phi\phi} \dot{\phi} + g_{t\phi} \dot{t} . \quad (\text{G.129})$$

Combining the equations and restricting again to $L = 0$ yields the following radial equation,

$$\dot{r}^2 = \frac{E^2 \Xi^2 [(r^2 + a^2)^2 - a^2 \Delta_r] - r^2 \Delta_r}{r^4} . \quad (\text{G.130})$$

Subsequently, we arrive at the proper distance in a Kerr-(A)dS geometry induced by an infalling observer in the equatorial plane, initially starting at rest at $r = R$ and falling towards the singularity at $r = 0$:

$$D(R) = \int_0^R dr \frac{r^2}{\sqrt{|E^2 \Xi^2 [(r^2 + a^2)^2 - a^2 \Delta_r] - r^2 \Delta_r|}} , \quad (\text{G.131})$$

where E is in this case then given by

$$E^2 = E^2(R) = \frac{R^2 \Delta_R}{\Xi^2 [(R^2 + a^2)^2 - a^2 \Delta_R]} . \quad (\text{G.132})$$

Bibliography

- [1] A. Wipf, Lect.Notes Phys. **864** (2013).
- [2] R. Alkofer and L. von Smekal, Phys. Rept. **353**, 281 (2001), hep-ph/0007355.
- [3] C. D. Roberts and S. M. Schmidt, Prog. Part. Nucl. Phys. **45**, S1 (2000), nucl-th/0005064.
- [4] C. S. Fischer, J.Phys.G **G32**, R253 (2006), hep-ph/0605173.
- [5] D. Binosi and J. Papavassiliou, Phys. Rept. **479**, 1 (2009), 0909.2536.
- [6] G. Eichmann, H. Sanchis-Alepuz, R. Williams, R. Alkofer, and C. S. Fischer, Prog. Part. Nucl. Phys. **91**, 1 (2016), 1606.09602.
- [7] C. S. Fischer, (2018), 1810.12938.
- [8] T. R. Morris, Prog. Theor. Phys. Suppl. **131**, 395 (1998), hep-th/9802039.
- [9] J. M. Pawłowski, Annals Phys. **322**, 2831 (2007), hep-th/0512261.
- [10] O. J. Rosten, Phys. Rept. **511**, 177 (2012), 1003.1366.
- [11] L. P. Kadanoff, Physics Physique Fizika **2**, 263 (1966).
- [12] K. G. Wilson, Phys.Rev. **B4**, 3174 (1971).
- [13] K. G. Wilson, Phys.Rev. **B4**, 3184 (1971).
- [14] F. J. Wegner and A. Houghton, Phys. Rev. **A8**, 401 (1973).
- [15] D. F. Litim, Phys. Rev. **D64**, 105007 (2001), hep-th/0103195.
- [16] D. F. Litim, JHEP **0111**, 059 (2001), hep-th/0111159.
- [17] I. Nandori, JHEP **04**, 150 (2013), 1208.5021.
- [18] J. M. Pawłowski, M. M. Scherer, R. Schmidt, and S. J. Wetzel, Annals Phys. **384**, 165 (2017), 1512.03598.
- [19] J. Braun, M. Leonhardt, and J. M. Pawłowski, (2018), 1806.04432.
- [20] J. Polchinski, Nucl.Phys. **B231**, 269 (1984).
- [21] C. Wetterich, Phys.Lett. **B301**, 90 (1993).
- [22] K. Symanzik, Springer Tracts Mod.Phys. **57**, 222 (1971).
- [23] K. Symanzik, Commun.Math.Phys. **23**, 49 (1971).
- [24] M. Bonini, M. D'Attanasio, and G. Marchesini, Nucl. Phys. **B409**, 441 (1993), hep-th/9301114.
- [25] U. Ellwanger, Z. Phys. **C62**, 503 (1994), hep-ph/9308260.

- [26] T. R. Morris, Int. J. Mod. Phys. **A**9, 2411 (1994), hep-ph/9308265.
- [27] C. Becchi, (1996), hep-th/9607188.
- [28] D. F. Litim and J. M. Pawłowski, Phys. Rev. **D**66, 025030 (2002), hep-th/0202188.
- [29] N. Christiansen, B. Knorr, J. Meibohm, J. M. Pawłowski, and M. Reichert, Phys. Rev. **D**92, 121501 (2015), 1506.07016.
- [30] D. F. Litim, J. M. Pawłowski, and L. Vergara, (2006), hep-th/0602140.
- [31] J. P. Blaizot, R. Mendez Galain, and N. Wschebor, Phys. Lett. **B**632, 571 (2006), hep-th/0503103.
- [32] J.-P. Blaizot, R. Mendez-Galain, and N. Wschebor, Phys. Rev. **E**74, 051116 (2006), hep-th/0512317.
- [33] J.-P. Blaizot, R. Mendez-Galain, and N. Wschebor, Phys. Rev. **E**74, 051117 (2006), hep-th/0603163.
- [34] D. F. Litim and J. M. Pawłowski, Phys. Rev. **D**66, 025030 (2002), hep-th/0202188.
- [35] T. Papenbrock and C. Wetterich, Z.Phys. **C**65, 519 (1995), hep-th/9403164.
- [36] U. Ellwanger, Z.Phys. **C**76, 721 (1997), hep-ph/9702309.
- [37] M. Pernici and M. Raciti, Nucl. Phys. **B**531, 560 (1998), hep-th/9803212.
- [38] P. Kopietz, Nucl. Phys. **B**595, 493 (2001), hep-th/0007128.
- [39] A. Codello, M. Demmel, and O. Zanusso, (2013), 1310.7625.
- [40] A. Codello, M. Safari, G. P. Vacca, and O. Zanusso, Eur. Phys. J. **C**78, 30 (2018), 1705.05558.
- [41] J. Berges, AIP Conf. Proc. **739**, 3 (2005), hep-ph/0409233.
- [42] J.-P. Blaizot, J. M. Pawłowski, and U. Reinosa, Phys. Lett. **B**696, 523 (2011), 1009.6048.
- [43] M. E. Carrington, Phys. Rev. **D**87, 045011 (2013), 1211.4127.
- [44] N. Dupuis, Phys. Rev. **B**89, 035113 (2014), 1310.4979.
- [45] M. E. Carrington, W.-J. Fu, D. Pickering, and J. W. Pulver, Phys. Rev. **D**91, 025003 (2015), 1404.0710.
- [46] M. E. Carrington *et al.*, Phys. Rev. **D**97, 036005 (2018), 1711.09135.
- [47] A. A. Katanin, Phys. Rev. B **70**, 115109 (2004).
- [48] P. Kopietz, L. Bartosch, and F. Schutz, *Introduction to the functional renormalization group* (Lect. Notes Phys., 2010).
- [49] K. Veschgini and M. Salmhofer, Phys. Rev. **B**88, 155131 (2013), 1306.4346.
- [50] A. A. Katanin, ArXiv e-prints (2016), 1604.01702.
- [51] F. B. Kugler and J. von Delft, ArXiv e-prints (2018), 1807.02898.
- [52] M. Mitter, J. M. Pawłowski, and N. Strodthoff, Phys. Rev. **D**91, 054035 (2015), 1411.7978.

- [53] J. Braun, L. Fister, J. M. Pawłowski, and F. Rennecke, Phys. Rev. **D94**, 034016 (2016), 1412.1045.
- [54] A. K. Cyrol, L. Fister, M. Mitter, J. M. Pawłowski, and N. Strodthoff, Phys. Rev. **D94**, 054005 (2016), 1605.01856.
- [55] A. K. Cyrol, M. Mitter, J. M. Pawłowski, and N. Strodthoff, Phys. Rev. **D97**, 054006 (2018), 1706.06326.
- [56] A. K. Cyrol, M. Mitter, J. M. Pawłowski, and N. Strodthoff, Phys. Rev. **D97**, 054015 (2018), 1708.03482.
- [57] L. Corell, A. K. Cyrol, M. Mitter, J. M. Pawłowski, and N. Strodthoff, (2018), 1803.10092.
- [58] N. Christiansen, D. F. Litim, J. M. Pawłowski, and A. Rodigast, Phys. Lett. **B728**, 114 (2014), 1209.4038.
- [59] N. Christiansen, B. Knorr, J. M. Pawłowski, and A. Rodigast, Phys. Rev. **D93**, 044036 (2016), 1403.1232.
- [60] J. Meibohm, J. M. Pawłowski, and M. Reichert, Phys. Rev. **D93**, 084035 (2016), 1510.07018.
- [61] J. Meibohm and J. M. Pawłowski, Eur. Phys. J. **C76**, 285 (2016), 1601.04597.
- [62] T. Denz, J. M. Pawłowski, and M. Reichert, Eur. Phys. J. **C78**, 336 (2018), 1612.07315.
- [63] N. Christiansen, K. Falls, J. M. Pawłowski, and M. Reichert, Phys. Rev. **D97**, 046007 (2018), 1711.09259.
- [64] A. Eichhorn, P. Labus, J. M. Pawłowski, and M. Reichert, SciPost Phys. **5**, 031 (2018), 1804.00012.
- [65] A. Eichhorn, S. Lippoldt, J. M. Pawłowski, M. Reichert, and M. Schiffer, (2018), 1810.02828.
- [66] L. Fister, *On the Phase Diagram of QCD with Dynamical Quarks*, PhD thesis, Heidelberg U., 2012.
- [67] J. M. Pawłowski and F. Rennecke, Phys. Rev. **D90**, 076002 (2014), 1403.1179.
- [68] N. Tetradis and D. F. Litim, Nucl. Phys. **B464**, 492 (1996), hep-th/9512073.
- [69] A. Katsis and N. Tetradis, Phys. Lett. **B780**, 491 (2018), 1801.07659.
- [70] N. Mermin and H. Wagner, Phys.Rev.Lett. **17**, 1133 (1966).
- [71] P. Hohenberg, Phys.Rev. **158**, 383 (1967).
- [72] F. Lamprecht, Confinement in polyakov-gauge and flow equations for dynamical degrees of freedom, Master's thesis, Heidelberg University, 2007.
- [73] A. Codello and G. D'Odorico, Phys.Rev.Lett. **110**, 141601 (2013), 1210.4037.
- [74] N. O. Defenu, A. Trombettoni, I. Nándori, and T. Enss, Phys. Rev. **B96**, 174505 (2017), 1706.00618.
- [75] F. Isaule, M. C. Birse, and N. R. Walet, Phys. Rev. **B98**, 144502 (2018), 1806.10373.
- [76] S. R. Coleman and E. J. Weinberg, Phys. Rev. **D7**, 1888 (1973).

- [77] Particle Data Group, C. Patrignani *et al.*, Chin. Phys. **C40**, 100001 (2016).
- [78] J. R. Pelaez, Phys. Rept. **658**, 1 (2016), 1510.00653.
- [79] W.-j. Fu, J. M. Pawłowski, F. Rennecke, and B.-J. Schaefer, Phys. Rev. **D94**, 116020 (2016), 1608.04302.
- [80] K. G. Wilson and J. B. Kogut, Phys. Rept. **12**, 75 (1974).
- [81] J. Braun, H. Gies, and D. D. Scherer, Phys.Rev. **D83**, 085012 (2011), 1011.1456.
- [82] A. M. Jaffe and E. Witten, (2000).
- [83] R. F. Streater and A. S. Wightman, *PCT, spin and statistics, and all that* (, 1989).
- [84] K. Osterwalder and R. Schrader, Commun. Math. Phys. **42**, 281 (1975).
- [85] C. Ford, U. Mitreuter, T. Tok, A. Wipf, and J. Pawłowski, Annals Phys. **269**, 26 (1998), hep-th/9802191.
- [86] J. Braun, H. Gies, and J. M. Pawłowski, Phys. Lett. **B684**, 262 (2010), 0708.2413.
- [87] F. Marhauser and J. M. Pawłowski, (2008), 0812.1144.
- [88] L. Fister and J. M. Pawłowski, Phys. Rev. **D88**, 045010 (2013), 1301.4163.
- [89] C. S. Fischer, A. Maas, and J. M. Pawłowski, Annals Phys. **324**, 2408 (2009), 0810.1987.
- [90] J. C. Taylor, Nucl. Phys. **B33**, 436 (1971).
- [91] A. Sternbeck, E. M. Ilgenfritz, M. Müller-Preussker, A. Schiller, and I. L. Bogolubsky, PoS LAT2006, 076 (2006), hep-lat/0610053.
- [92] C. Becchi, A. Rouet, and R. Stora, Annals Phys. **98**, 287 (1976).
- [93] I. Tyutin, (1975), 0812.0580.
- [94] M. Henneaux and C. Teitelboim, *Quantization of gauge systems* (Princeton University Press, Princeton, 1992), Princeton, USA: Univ. Pr. (1992) 520 p.
- [95] H. Gies and C. Wetterich, Phys.Rev. **D65**, 065001 (2002), hep-th/0107221.
- [96] H. Gies and C. Wetterich, Phys.Rev. **D69**, 025001 (2004), hep-th/0209183.
- [97] J. Braun, Eur. Phys. J. **C64**, 459 (2009), 0810.1727.
- [98] S. Floerchinger and C. Wetterich, Phys.Lett. **B680**, 371 (2009), 0905.0915.
- [99] S. Floerchinger, Eur. Phys. J. **C69**, 119 (2010), 1001.4497.
- [100] J. Braun, M. Leonhardt, and M. Pospiech, Phys. Rev. **D96**, 076003 (2017), 1705.00074.
- [101] D. J. Gross, R. D. Pisarski, and L. G. Yaffe, Rev.Mod.Phys. **53**, 43 (1981).
- [102] N. Weiss, Phys.Rev. **D24**, 475 (1981).
- [103] P. B. Arnold and L. G. Yaffe, Phys. Rev. **D52**, 7208 (1995), hep-ph/9508280.
- [104] A. Maas, J. M. Pawłowski, L. von Smekal, and D. Spielmann, (2011), 1110.6340.

- [105] A. Maas, private communication.
- [106] P. J. Silva, O. Oliveira, P. Bicudo, and N. Cardoso, Phys. Rev. **D89**, 074503 (2014), 1310.5629.
- [107] L. Fister and J. M. Pawłowski, (2013), 1302.1373.
- [108] T. K. Herbst, J. Luecker, and J. M. Pawłowski, (2015), 1510.03830.
- [109] C. Pagani, Phys. Rev. **D94**, 045001 (2016), 1603.07250.
- [110] J. M. Pawłowski, AIP Conf.Proc. **1343**, 75 (2011), 1012.5075.
- [111] J. M. Pawłowski, Nucl. Phys. **A931**, 113 (2014).
- [112] T. K. Herbst, J. M. Pawłowski, and B.-J. Schaefer, Phys.Lett. **B696**, 58 (2011), 1008.0081.
- [113] T. K. Herbst, J. M. Pawłowski, and B.-J. Schaefer, Phys. Rev. **D88**, 014007 (2013), 1302.1426.
- [114] F. Rennecke, Phys. Rev. **D92**, 076012 (2015), 1504.03585.
- [115] J. Braun, M. Leonhardt, and M. Pospiech, Phys. Rev. **D97**, 076010 (2018), 1801.08338.
- [116] W.-j. Fu, J. M. Pawłowski, and F. Rennecke, in preparation (2019).
- [117] S. Carroll, *Spacetime and Geometry: An Introduction to General Relativity* (Addison-Wesley, Reading, 2003).
- [118] H. W. Hamber, *Quantum gravitation: The Feynman path integral approach* (Springer, Berlin, 2009).
- [119] D. F. Litim and J. M. Pawłowski, Nucl.Phys.Proc.Suppl. **74**, 329 (1999), hep-th/9809023.
- [120] M. E. Peskin and D. V. Schroeder, *An Introduction to quantum field theory* (Addison-Wesley, Reading, 1995).
- [121] G. 't Hooft and M. Veltman, Annales Poincare Phys.Theor. **A20**, 69 (1974).
- [122] M. H. Goroff and A. Sagnotti, Phys. Lett. **160B**, 81 (1985).
- [123] M. H. Goroff and A. Sagnotti, Nucl. Phys. **B266**, 709 (1986).
- [124] A. E. M. van de Ven, Nucl. Phys. **B378**, 309 (1992).
- [125] S. Weinberg, General Relativity: An Einstein centenary survey, Eds. Hawking, S.W., Israel, W; Cambridge University Press , 790 (1979).
- [126] K. Gawedzki and A. Kupiainen, Phys.Rev.Lett. **55**, 363 (1985).
- [127] H. Gies, J. Jaeckel, and C. Wetterich, Phys. Rev. **D69**, 105008 (2004), hep-ph/0312034.
- [128] J.-M. Schwindt and C. Wetterich, Phys.Rev. **D81**, 055005 (2010), 0812.4223.
- [129] H. Gies and L. Janssen, Phys.Rev. **D82**, 085018 (2010), 1006.3747.
- [130] H. Gies and M. M. Scherer, Eur. Phys. J. **C66**, 387 (2010), 0901.2459.
- [131] H. Gies, S. Rechenberger, and M. M. Scherer, Eur. Phys. J. **C66**, 403 (2010), 0907.0327.
- [132] M. M. Scherer, H. Gies, and S. Rechenberger, Acta Phys.Polon.Supp. **2**, 541 (2009), 0910.0395.

- [133] H. Gies, Phys. Rev. **D68**, 085015 (2003), hep-th/0305208.
- [134] A. Codello and R. Percacci, Phys. Lett. **B672**, 280 (2009), 0810.0715.
- [135] R. Percacci and O. Zanusso, Phys. Rev. **D81**, 065012 (2010), 0910.0851.
- [136] M. Fabbrichesi, R. Percacci, A. Tonero, and O. Zanusso, Phys. Rev. **D83**, 025016 (2011), 1010.0912.
- [137] R. Flore, A. Wipf, and O. Zanusso, (2012), 1207.4499.
- [138] X. Calmet, Mod. Phys. Lett. **A26**, 1571 (2011), 1012.5529.
- [139] M. Fabbrichesi, R. Percacci, A. Tonero, and L. Vecchi, Phys. Rev. Lett. **107**, 021803 (2011), 1102.2113.
- [140] F. Bazzocchi, M. Fabbrichesi, R. Percacci, A. Tonero, and L. Vecchi, Phys. Lett. **B705**, 388 (2011), 1105.1968.
- [141] D. F. Litim and J. M. Pawłowski, JHEP **0209**, 049 (2002), hep-th/0203005.
- [142] D. F. Litim and J. M. Pawłowski, Phys. Lett. **B546**, 279 (2002), hep-th/0208216.
- [143] J. M. Pawłowski, (2003), hep-th/0310018.
- [144] I. Donkin and J. M. Pawłowski, (2012), 1203.4207.
- [145] M. Safari, Eur. Phys. J. **C76**, 201 (2016), 1508.06244.
- [146] I. H. Bridle, J. A. Dietz, and T. R. Morris, JHEP **03**, 093 (2014), 1312.2846.
- [147] J. A. Dietz and T. R. Morris, JHEP **04**, 118 (2015), 1502.07396.
- [148] T. R. Morris, JHEP **11**, 160 (2016), 1610.03081.
- [149] R. Percacci and G. P. Vacca, Eur. Phys. J. **C77**, 52 (2017), 1611.07005.
- [150] M. Safari and G. P. Vacca, JHEP **11**, 139 (2016), 1607.07074.
- [151] C. M. Nieto, R. Percacci, and V. Skrinjar, Phys. Rev. **D96**, 106019 (2017), 1708.09760.
- [152] E. Manrique and M. Reuter, Annals Phys. **325**, 785 (2010), 0907.2617.
- [153] E. Manrique, M. Reuter, and F. Saueressig, Annals Phys. **326**, 440 (2011), 1003.5129.
- [154] E. Manrique, M. Reuter, and F. Saueressig, Annals Phys. **326**, 463 (2011), 1006.0099.
- [155] A. Codello, G. D’Odorico, and C. Pagani, Phys. Rev. **D89**, 081701 (2014), 1304.4777.
- [156] D. Becker and M. Reuter, Annals Phys. **350**, 225 (2014), 1404.4537.
- [157] T. Henz, J. M. Pawłowski, and C. Wetterich, Phys. Lett. **B769**, 105 (2017), 1605.01858.
- [158] N. Christiansen, (2016), 1612.06223.
- [159] B. Knorr and S. Lippoldt, Phys. Rev. **D96**, 065020 (2017), 1707.01397.
- [160] N. Christiansen, D. F. Litim, J. M. Pawłowski, and M. Reichert, (2017), 1710.04669.

- [161] B. Knorr, (2017), 1710.07055.
- [162] J. Braun, L. M. Haas, F. Marhauser, and J. M. Pawłowski, Phys. Rev. Lett. **106**, 022002 (2011), 0908.0008.
- [163] J. Braun, A. Eichhorn, H. Gies, and J. M. Pawłowski, Eur.Phys.J. **C70**, 689 (2010), 1007.2619.
- [164] U. Reinosa, J. Serreau, M. Tissier, and N. Wschebor, Phys. Lett. **B742**, 61 (2015), 1407.6469.
- [165] M. Reuter, Phys. Rev. **D57**, 971 (1998), hep-th/9605030.
- [166] K. Falls, D. F. Litim, K. Nikolakopoulos, and C. Rahmede, (2016), 1607.04962.
- [167] N. Ohta, R. Percacci, and G. P. Vacca, Eur. Phys. J. **C76**, 46 (2016), 1511.09393.
- [168] N. Ohta, R. Percacci, and G. P. Vacca, Phys. Rev. **D92**, 061501 (2015), 1507.00968.
- [169] M. Demmel, F. Saueressig, and O. Zanusso, JHEP **08**, 113 (2015), 1504.07656.
- [170] S. Gonzalez-Martin, T. R. Morris, and Z. H. Slade, Phys. Rev. **D95**, 106010 (2017), 1704.08873.
- [171] J. York, James W., J.Math.Phys. **14**, 456 (1973).
- [172] C. S. Fischer and J. M. Pawłowski, Phys. Rev. **D80**, 025023 (2009), 0903.2193.
- [173] E. Mottola, Acta Phys. Polon. **B41**, 2031 (2010), 1008.5006.
- [174] D. Schnoerr, I. Boettcher, J. M. Pawłowski, and C. Wetterich, Annals Phys. **334**, 83 (2013), 1301.4169.
- [175] D. F. Litim, Phys.Lett. **B486**, 92 (2000), hep-th/0005245.
- [176] D. F. Litim, Int. J. Mod. Phys. **A16**, 2081 (2001), hep-th/0104221.
- [177] D. F. Litim and J. M. Pawłowski, JHEP **0611**, 026 (2006), hep-th/0609122.
- [178] K. S. Stelle, Gen. Rel. Grav. **9**, 353 (1978).
- [179] S. Floerchinger, (2011), 1112.4374.
- [180] K. Kamikado, N. Strodthoff, L. von Smekal, and J. Wambach, Eur.Phys.J. **C74**, 2806 (2014), 1302.6199.
- [181] R.-A. Tripolt, N. Strodthoff, L. von Smekal, and J. Wambach, Phys.Rev. **D89**, 034010 (2014), 1311.0630.
- [182] J. M. Pawłowski and N. Strodthoff, Phys. Rev. **D92**, 094009 (2015), 1508.01160.
- [183] N. Strodthoff, Phys. Rev. **D95**, 076002 (2017), 1611.05036.
- [184] A. Bonanno and M. Reuter, JHEP **0502**, 035 (2005), hep-th/0410191.
- [185] E. Manrique, S. Rechenberger, and F. Saueressig, Phys.Rev.Lett. **106**, 251302 (2011), 1102.5012.
- [186] J. Biemans, A. Platania, and F. Saueressig, Phys. Rev. **D95**, 086013 (2017), 1609.04813.
- [187] C. Wetterich, Phys. Lett. **B773**, 6 (2017), 1704.08040.
- [188] O. Lauscher and M. Reuter, Phys. Rev. **D66**, 025026 (2002), hep-th/0205062.

- [189] A. Codello, R. Percacci, and C. Rahmede, *Int. J. Mod. Phys. A* **23**, 143 (2008), 0705.1769.
- [190] P. F. Machado and F. Saueressig, *Phys. Rev. D* **77**, 124045 (2008), 0712.0445.
- [191] A. Codello, R. Percacci, and C. Rahmede, *Annals Phys.* **324**, 414 (2009), 0805.2909.
- [192] K. Falls, D. Litim, K. Nikolakopoulos, and C. Rahmede, (2013), 1301.4191.
- [193] J. A. M. Vermaasen, (2000), math-ph/0010025.
- [194] J. Kuipers, T. Ueda, J. A. M. Vermaasen, and J. Vollinga, *Comput. Phys. Commun.* **184**, 1453 (2013), 1203.6543.
- [195] D. Brizuela, J. M. Martin-Garcia, and G. A. M. Marugan, (2008), arXiv:0807.0824.
- [196] M. Q. Huber and J. Braun, *Comput. Phys. Commun.* **183**, 1290 (2012), 1102.5307.
- [197] A. K. Cyrol, M. Mitter, and N. Strodthoff, *Comput. Phys. Commun.* **219**, 346 (2017), 1610.09331.
- [198] H. A. Weldon, *Phys. Rev. D* **63**, 104010 (2001), gr-qc/0009086.
- [199] H. Gies and S. Lippoldt, *Phys.Rev. D* **89**, 064040 (2014), 1310.2509.
- [200] S. Lippoldt, *Phys. Rev. D* **91**, 104006 (2015), 1502.05607.
- [201] J.-E. Daum, U. Harst, and M. Reuter, *JHEP* **1001**, 084 (2010), 0910.4938.
- [202] U. Harst and M. Reuter, *JHEP* **05**, 119 (2011), 1101.6007.
- [203] S. Folkerts, D. F. Litim, and J. M. Pawłowski, (2011), 1101.5552.
- [204] N. Christiansen and A. Eichhorn, *Phys. Lett. B* **770**, 154 (2017), 1702.07724.
- [205] A. Eichhorn and F. Versteegen, *JHEP* **01**, 030 (2018), 1709.07252.
- [206] A. Eichhorn and H. Gies, *Phys. Rev. D* **81**, 104010 (2010), 1001.5033.
- [207] P. Donà, A. Eichhorn, and R. Percacci, *Phys. Rev. D* **89**, 084035 (2014), 1311.2898.
- [208] M. Demmel, F. Saueressig, and O. Zanusso, *Annals Phys.* **359**, 141 (2015), 1412.7207.
- [209] M. Demmel and A. Nink, *Phys. Rev. D* **92**, 104013 (2015), 1506.03809.
- [210] V. Branchina, K. A. Meissner, and G. Veneziano, *Phys.Lett. B* **574**, 319 (2003), hep-th/0309234.
- [211] D. F. Litim and J. M. Pawłowski, *Phys. Lett. B* **435**, 181 (1998), hep-th/9802064.
- [212] F. Freire, D. F. Litim, and J. M. Pawłowski, *Phys. Lett. B* **495**, 256 (2000), hep-th/0009110.
- [213] A. Eichhorn, *Phys.Rev. D* **86**, 105021 (2012), 1204.0965.
- [214] A. Eichhorn, A. Held, and J. M. Pawłowski, *Phys. Rev. D* **94**, 104027 (2016), 1604.02041.
- [215] A. Eichhorn and A. Held, *Phys. Rev. D* **96**, 086025 (2017), 1705.02342.
- [216] S. Folkerts, Diploma thesis, Heidelberg (2009).
- [217] P. Dona and R. Percacci, (2012), 1209.3649.
- [218] N. Christiansen, A. Eichhorn, and A. Held, *Phys. Rev. D* **96**, 084021 (2017), 1705.01858.

- [219] M. Pelaez, M. Tissier, and N. Wschebor, Phys. Rev. **D88**, 125003 (2013), 1310.2594.
- [220] A. C. Aguilar, D. Binosi, D. Ibañez, and J. Papavassiliou, Phys. Rev. **D89**, 085008 (2014), 1312.1212.
- [221] A. Blum, M. Q. Huber, M. Mitter, and L. von Smekal, Phys. Rev. **D89**, 061703 (2014), 1401.0713.
- [222] G. Eichmann, R. Williams, R. Alkofer, and M. Vujinovic, Phys. Rev. **D89**, 105014 (2014), 1402.1365.
- [223] K. Falls, D. F. Litim, K. Nikolakopoulos, and C. Rahmede, Phys. Rev. **D93**, 104022 (2016), 1410.4815.
- [224] M. R. Niedermaier, Phys. Rev. Lett. **103**, 101303 (2009).
- [225] M. Shaposhnikov and C. Wetterich, Phys. Lett. **B683**, 196 (2010), 0912.0208.
- [226] A. Eichhorn and A. Held, Phys. Lett. **B777**, 217 (2018), 1707.01107.
- [227] A. Eichhorn, Y. Hamada, J. Lumma, and M. Yamada, Phys. Rev. **D97**, 086004 (2018), 1712.00319.
- [228] A. Eichhorn and A. Held, Phys. Rev. Lett. **121**, 151302 (2018), 1803.04027.
- [229] J. Berges, N. Tetradis, and C. Wetterich, Phys. Rept. **363**, 223 (2002), hep-ph/0005122.
- [230] H. Gies, Lect.Notes Phys. **852**, 287 (2012), hep-ph/0611146.
- [231] B. Delamotte, (2007), cond-mat/0702365.
- [232] J. Braun, (2011), 1108.4449.
- [233] M. Niedermaier and M. Reuter, Living Rev.Rel. **9**, 5 (2006).
- [234] D. F. Litim, Phil.Trans.Roy.Soc.Lond. **A369**, 2759 (2011), 1102.4624.
- [235] M. Reuter and F. Saueressig, New J.Phys. **14**, 055022 (2012), 1202.2274.
- [236] R. Percacci, *An Introduction to Covariant Quantum Gravity and Asymptotic Safety*volume 3 of *100 Years of General Relativity* (World Scientific, 2017).
- [237] A. Bonanno and F. Saueressig, Comptes Rendus Physique **18**, 254 (2017), 1702.04137.
- [238] A. Eichhorn, Found. Phys. **48**, 1407 (2018), 1709.03696.
- [239] P. Donà, A. Eichhorn, P. Labus, and R. Percacci, Phys. Rev. **D93**, 044049 (2016), 1512.01589.
- [240] A. Eichhorn, S. Lippoldt, and V. Skrinjar, Phys. Rev. **D97**, 026002 (2018), 1710.03005.
- [241] A. Eichhorn, S. Lippoldt, and M. Schiffer, (2018), 1812.08782.
- [242] D. Brizuela, J. M. Martin-Garcia, and G. A. Mena Marugan, Gen. Rel. Grav. **41**, 2415 (2009), 0807.0824.
- [243] D. Benedetti, P. F. Machado, and F. Saueressig, Mod. Phys. Lett. **A24**, 2233 (2009), 0901.2984.
- [244] H. Gies, B. Knorr, S. Lippoldt, and F. Saueressig, Phys. Rev. Lett. **116**, 211302 (2016), 1601.01800.

- [245] G. P. De Brito, N. Ohta, A. D. Pereira, A. A. Tomaz, and M. Yamada, Phys. Rev. **D98**, 026027 (2018), 1805.09656.
- [246] A. Eichhorn and H. Gies, (2011), 1104.5366.
- [247] U. Ellwanger, M. Hirsch, and A. Weber, Z.Phys. **C69**, 687 (1996), hep-th/9506019.
- [248] ATLAS, CDF, CMS, D0, (2014), 1403.4427.
- [249] Particle Data Group, M. Tanabashi *et al.*, Phys. Rev. **D98**, 030001 (2018).
- [250] M. Reuter and F. Saueressig, Phys.Rev. **D65**, 065016 (2002), hep-th/0110054.
- [251] M. Reuter and H. Weyer, JCAP **0412**, 001 (2004), hep-th/0410119.
- [252] D. F. Litim, Phys. Rev. Lett. **92**, 201301 (2004), hep-th/0312114.
- [253] G. Narain and R. Percacci, Class. Quant. Grav. **27**, 075001 (2010), 0911.0386.
- [254] A. Eichhorn and S. Lippoldt, Phys. Lett. **B767**, 142 (2017), 1611.05878.
- [255] K. G. Falls, C. S. King, D. F. Litim, K. Nikolopoulos, and C. Rahmede, (2017), 1801.00162.
- [256] S. P. Robinson and F. Wilczek, Phys. Rev. Lett. **96**, 231601 (2006), hep-th/0509050.
- [257] A. Rodigast and T. Schuster, Phys. Rev. Lett. **104**, 081301 (2010), 0908.2422.
- [258] O. Zanusso, L. Zambelli, G. P. Vacca, and R. Percacci, Phys. Lett. **B689**, 90 (2010), 0904.0938.
- [259] K.-y. Oda and M. Yamada, Class. Quant. Grav. **33**, 125011 (2016), 1510.03734.
- [260] Y. Hamada and M. Yamada, JHEP **08**, 070 (2017), 1703.09033.
- [261] M. Gell-Mann and F. E. Low, Phys. Rev. **95**, 1300 (1954).
- [262] D. J. Gross and F. Wilczek, Phys. Rev. Lett. **30**, 1343 (1973).
- [263] H. D. Politzer, Phys. Rev. Lett. **30**, 1346 (1973).
- [264] A. Eichhorn, A. Held, and C. Wetterich, Phys. Lett. **B782**, 198 (2018), 1711.02949.
- [265] T. P. Cheng, E. Eichten, and L.-F. Li, Phys. Rev. **D9**, 2259 (1974).
- [266] B. Pendleton and G. G. Ross, Phys. Lett. **98B**, 291 (1981).
- [267] C. T. Hill, Phys. Rev. **D24**, 691 (1981).
- [268] C. Wetterich, Phys. Lett. **104B**, 269 (1981).
- [269] D. Buttazzo *et al.*, JHEP **12**, 089 (2013), 1307.3536.
- [270] W. E. Caswell, Phys. Rev. Lett. **33**, 244 (1974).
- [271] D. R. T. Jones, Nucl. Phys. **B75**, 531 (1974).
- [272] D. R. T. Jones, Phys. Rev. **D25**, 581 (1982).
- [273] M. Fischler and J. Oliensis, Phys. Lett. **119B**, 385 (1982).
- [274] M. E. Machacek and M. T. Vaughn, Nucl. Phys. **B222**, 83 (1983).

- [275] M. E. Machacek and M. T. Vaughn, Nucl. Phys. **B236**, 221 (1984).
- [276] D. Becker and M. Reuter, JHEP **1207**, 172 (2012), 1205.3583.
- [277] P. Fischer and D. F. Litim, Phys. Lett. **B638**, 497 (2006), hep-th/0602203.
- [278] A. Codello and O. Zanusso, Phys.Rev. **D83**, 125021 (2011), 1103.1089.
- [279] M. Reuter and H. Weyer, Phys. Rev. **D79**, 105005 (2009), 0801.3287.
- [280] M. Reuter and H. Weyer, Phys. Rev. **D80**, 025001 (2009), 0804.1475.
- [281] P. F. Machado and R. Percacci, Phys. Rev. **D80**, 024020 (2009), 0904.2510.
- [282] D. Litim and A. Satz, (2012), 1205.4218.
- [283] A. Bonanno and F. Guarnieri, Phys.Rev. **D86**, 105027 (2012), 1206.6531.
- [284] R. Percacci, New J.Phys. **13**, 125013 (2011), 1110.6758.
- [285] A. Codello, G. D’Odorico, C. Pagani, and R. Percacci, (2012), 1210.3284.
- [286] G. Vilkovisky, Nucl.Phys. **B234**, 125 (1984).
- [287] B. S. DeWitt, Quantum Field Theory and Quantum Statistics, Vol. 1, Batalin, I.A. (Ed.) et al. , 191 (1988).
- [288] S. Nagy, J. Krizsan, and K. Sailer, JHEP **1207**, 102 (2012), 1203.6564.
- [289] G. Vacca and L. Zambelli, Phys.Rev. **D83**, 125024 (2011), 1103.2219.
- [290] G. Vacca and L. Zambelli, Phys.Rev. **D86**, 085041 (2012), 1208.2181.
- [291] J.-E. Daum and M. Reuter, Phys.Lett. **B710**, 215 (2012), 1012.4280.
- [292] D. Benedetti and S. Speziale, JHEP **1106**, 107 (2011), 1104.4028.
- [293] U. Harst and M. Reuter, JHEP **1205**, 005 (2012), 1203.2158.
- [294] S. Rechenberger and F. Saueressig, (2012), 1212.5114.
- [295] E. Manrique and M. Reuter, Phys. Rev. **D79**, 025008 (2009), 0811.3888.
- [296] A. Nink and M. Reuter, (2012), 1208.0031.
- [297] A. Bonanno and M. Reuter, Phys. Rev. **D62**, 043008 (2000), hep-th/0002196.
- [298] Y.-F. Cai and D. A. Easson, JCAP **1009**, 002 (2010), 1007.1317.
- [299] M. Reuter and E. Tuiran, Phys. Rev. **D83**, 044041 (2011), 1009.3528.
- [300] A. Bonanno and M. Reuter, Phys. Rev. **D73**, 083005 (2006), hep-th/0602159.
- [301] R. Casadio, S. D. H. Hsu, and B. Mirza, Phys. Lett. **B695**, 317 (2011), 1008.2768.
- [302] K. Falls and D. F. Litim, Phys. Rev. **D89**, 084002 (2014), 1212.1821.
- [303] B. Koch, Phys.Lett. **B663**, 334 (2008), 0707.4644.
- [304] T. Burschil and B. Koch, Zh. Eksp. Teor. Fiz. **92**, 219 (2010), 0912.4517.

- [305] K. Falls, D. F. Litim, and A. Raghuraman, Int.J.Mod.Phys. **A***27*, 1250019 (2012), 1002.0260.
- [306] A. Bonanno, Phys.Rev. **D***85*, 081503 (2012), 1203.1962.
- [307] J. Hewett and T. Rizzo, JHEP **12**, 009 (2007), 0707.3182.
- [308] D. F. Litim and T. Plehn, Phys. Rev. Lett. **100**, 131301 (2008), 0707.3983.
- [309] E. Gerwick, D. Litim, and T. Plehn, Phys. Rev. **D***83*, 084048 (2011), 1101.5548.
- [310] B. Dobrich and A. Eichhorn, JHEP **1206**, 156 (2012), 1203.6366.
- [311] F. Bezrukov, M. Y. Kalmykov, B. A. Kniehl, and M. Shaposhnikov, JHEP **1210**, 140 (2012), 1205.2893.
- [312] C. Wetterich, Phys.Lett. **B***718*, 573 (2012), 1112.2910.
- [313] O. Lauscher and M. Reuter, JHEP **0510**, 050 (2005), hep-th/0508202.
- [314] M. Reuter and F. Saueressig, JHEP **1112**, 012 (2011), 1110.5224.
- [315] S. Rechenberger and F. Saueressig, Phys.Rev. **D***86*, 024018 (2012), 1206.0657.
- [316] A. Bonanno and M. Reuter, Phys. Rev. **D***65*, 043508 (2002), hep-th/0106133.
- [317] A. Bonanno and M. Reuter, Int. J. Mod. Phys. **D***13*, 107 (2004), astro-ph/0210472.
- [318] A. Bonanno and M. Reuter, Phys. Lett. **B***527*, 9 (2002), astro-ph/0106468.
- [319] E. Bentivegna, A. Bonanno, and M. Reuter, JCAP **0401**, 001 (2004), astro-ph/0303150.
- [320] M. Reuter and F. Saueressig, JCAP **0509**, 012 (2005), hep-th/0507167.
- [321] M. Reuter and H. Weyer, Phys.Rev. **D***70*, 124028 (2004), hep-th/0410117.
- [322] M. Reuter and H. Weyer, Int. J. Mod. Phys. **D***15*, 2011 (2006), hep-th/0702051.
- [323] A. Bonanno and M. Reuter, JCAP **0708**, 024 (2007), 0706.0174.
- [324] A. Bonanno and M. Reuter, J.Phys.Conf.Ser. **140**, 012008 (2008), 0803.2546.
- [325] S. Weinberg, Phys. Rev. **D***81*, 083535 (2010), 0911.3165.
- [326] S.-H. H. Tye and J. Xu, Phys.Rev. **D***82*, 127302 (2010), 1008.4787.
- [327] A. Contillo, Phys. Rev. **D***83*, 085016 (2011), 1011.4618.
- [328] A. Bonanno, A. Contillo, and R. Percacci, Class. Quant. Grav. **28**, 145026 (2011), 1006.0192.
- [329] M. Hindmarsh and I. D. Saltas, Phys.Rev. **D***86*, 064029 (2012), 1203.3957.
- [330] Y.-F. Cai and D. A. Easson, Phys.Rev. **D***84*, 103502 (2011), 1107.5815.
- [331] A. Contillo, M. Hindmarsh, and C. Rahmede, Phys.Rev. **D***85*, 043501 (2012), 1108.0422.
- [332] M. Hindmarsh, D. Litim, and C. Rahmede, JCAP **1107**, 019 (2011), 1101.5401.
- [333] A. Bonanno and M. Reuter, Phys. Rev. **D***60*, 084011 (1999), gr-qc/9811026.
- [334] B. Koch and F. Saueressig, Class. Quant. Grav. **31**, 015006 (2014), 1306.1546.

- [335] B. Koch and F. Saueressig, Int. J. Mod. Phys. A29, 1430011 (2014), 1401.4452.
- [336] A. Bonanno, B. Koch, and A. Platania, Class. Quant. Grav. **34**, 095012 (2017), 1610.05299.
- [337] H. Emoto, (2005), hep-th/0511075.
- [338] M. Niedermaier, Class. Quant. Grav. **24**, R171 (2007), gr-qc/0610018.
- [339] W. Dittrich and M. Reuter, *Effective Lagrangians in Quantum Electrodynamics* (Springer Verlag, 1985).
- [340] G. W. Gibbons and S. W. Hawking, Phys. Rev. D **15**, 2738 (1977).
- [341] E. J. Copeland, C. Rahmede, and I. D. Saltas, Phys. Rev. D **91**, 103530 (2015), 1311.0881.
- [342] B. Carter, Phys. Rev. **174**, 1559 (1968).
- [343] E. Hackmann, C. Lammerzahl, V. Kagramanova, and J. Kunz, Phys. Rev. D **81**, 044020 (2010), 1009.6117.
- [344] M. Dafermos, Commun. Math. Phys. **332**, 729 (2014), 1201.1797.
- [345] L. Modesto, Phys. Rev. D **70**, 124009 (2004), gr-qc/0407097.
- [346] B. Koch and I. Ramirez, Class. Quant. Grav. **28**, 055008 (2011), 1010.2799.
- [347] S. W. Hawking, Comm. Math. Phys. **43**, 199 (1975).
- [348] G. W. Gibbons and S. W. Hawking, Phys. Rev. D **15**, 2752 (1977).
- [349] S. Aretakis, Adv. Theor. Math. Phys. **19**, 507 (2015), 1206.6598.
- [350] P. Chen, Y. C. Ong, and D.-h. Yeom, Phys. Rept. **603**, 1 (2015), 1412.8366.
- [351] M. Buballa, Phys.Rept. **407**, 205 (2005), hep-ph/0402234.
- [352] K. Langfeld, (2003), hep-lat/0301007.
- [353] T. Heinzl, Nucl.Phys.Proc.Suppl. **54A**, 194 (1997), hep-th/9609055.
- [354] D. Dou and R. Percacci, Class. Quant. Grav. **15**, 3449 (1998), hep-th/9707239.
- [355] O. Lauscher and M. Reuter, Phys. Rev. D **65**, 025013 (2002), hep-th/0108040.
- [356] H. Gies, B. Knorr, and S. Lippoldt, Phys. Rev. D **92**, 084020 (2015), 1507.08859.
- [357] K. S. Stelle, Phys. Rev. D **16**, 953 (1977).
- [358] D. F. Litim and F. Sannino, JHEP **12**, 178 (2014), 1406.2337.
- [359] D. F. Litim, M. Mojaza, and F. Sannino, JHEP **01**, 081 (2016), 1501.03061.
- [360] A. D. Bond and D. F. Litim, Eur. Phys. J. C **77**, 429 (2017), 1608.00519.
- [361] A. D. Bond, G. Hiller, K. Kowalska, and D. F. Litim, JHEP **08**, 004 (2017), 1702.01727.
- [362] A. D. Bond and D. F. Litim, Phys. Rev. D **97**, 085008 (2018), 1707.04217.
- [363] A. D. Bond and D. F. Litim, Phys. Rev. Lett. **119**, 211601 (2017), 1709.06953.

- [364] A. R. Pietrykowski, Phys. Rev. Lett. **98**, 061801 (2007), hep-th/0606208.
- [365] D. J. Toms, Phys. Rev. **D76**, 045015 (2007), 0708.2990.
- [366] D. Ebert, J. Plefka, and A. Rodigast, Phys. Lett. **B660**, 579 (2008), 0710.1002.
- [367] Y. Tang and Y.-L. Wu, Commun. Theor. Phys. **54**, 1040 (2010), 0807.0331.
- [368] D. J. Toms, Nature **468**, 56 (2010), 1010.0793.
- [369] J. E. Daum, U. Harst, and M. Reuter, (2010), 1005.1488.
- [370] A. Eichhorn, H. Gies, and J. M. Pawłowski, Phys.Rev. **D83**, 045014 (2011), 1010.2153.
- [371] S. Diehl, H. C. Krahl, and M. Scherer, Phys. Rev. **C78**, 034001 (2008), 0712.2846.
- [372] D. F. Litim, Nucl. Phys. **B631**, 128 (2002), hep-th/0203006.
- [373] D. F. Litim, Phys.Rev. **D76**, 105001 (2007), 0704.1514.
- [374] H. Bückner *et al.*, Duke Mathematical Journal **15**, 197 (1948).